Investigation of Scale Effects on Propeller

Sheet and Tip Vortex Cavitation Based on Hybrid Simulation Methods

Moustafa Abdel-Maksoud
Institute for Fluid Dynamics and Ship Theory
Hamburg University of Technology

Fluiddynamik und Schiffstheorie

TUHH

Prof. Dr. Yücel Odabaşı

Prof. Dr. Yücel Odabaşı

Cavitation
- Free-stream turbulence
- Air content
- Surface roughness

Wake
- Scaling
- Quality
- Prediction

Pressure fluctuation
- Vibration excitation
- Propeller hull interaction
- Extrapolation

Ship motion
- Roll damping
- Stability
- Non-linear wave radiation

Prof. Dr. Yücel Odabaşı

ISTANBUL TECHNICAL UNIVERSITY LARGE CAVITATION TUNNEL (ITU-CAT)

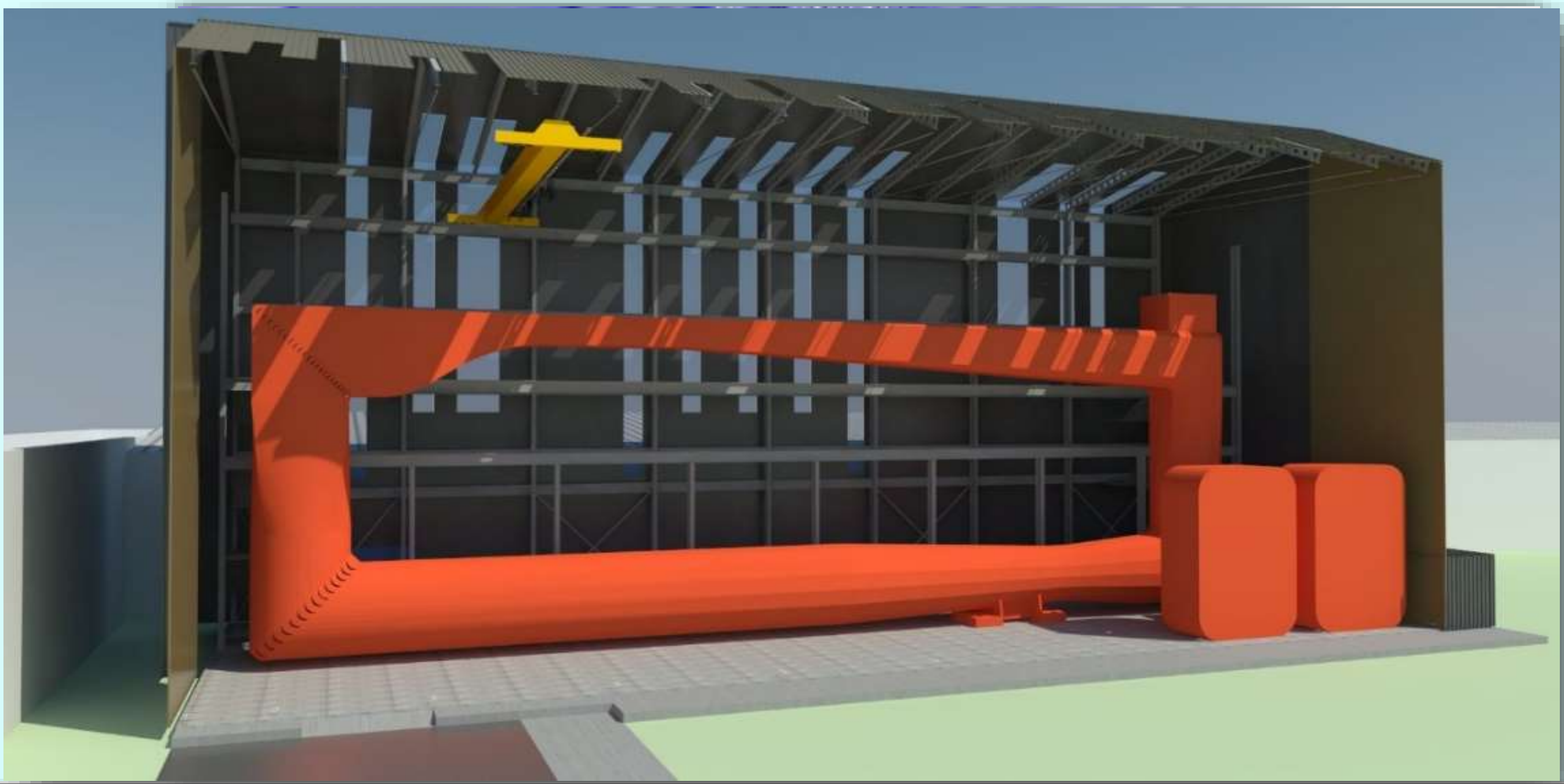

ISTANBUL TECHNICAL UNIVERSITY LARGE CAVITATION TUNNEL (ITU-CAT)

Tunnel max. water velocity 15 m/s

Test section: L=5.5m, B=1.5 m, H=1.2 m

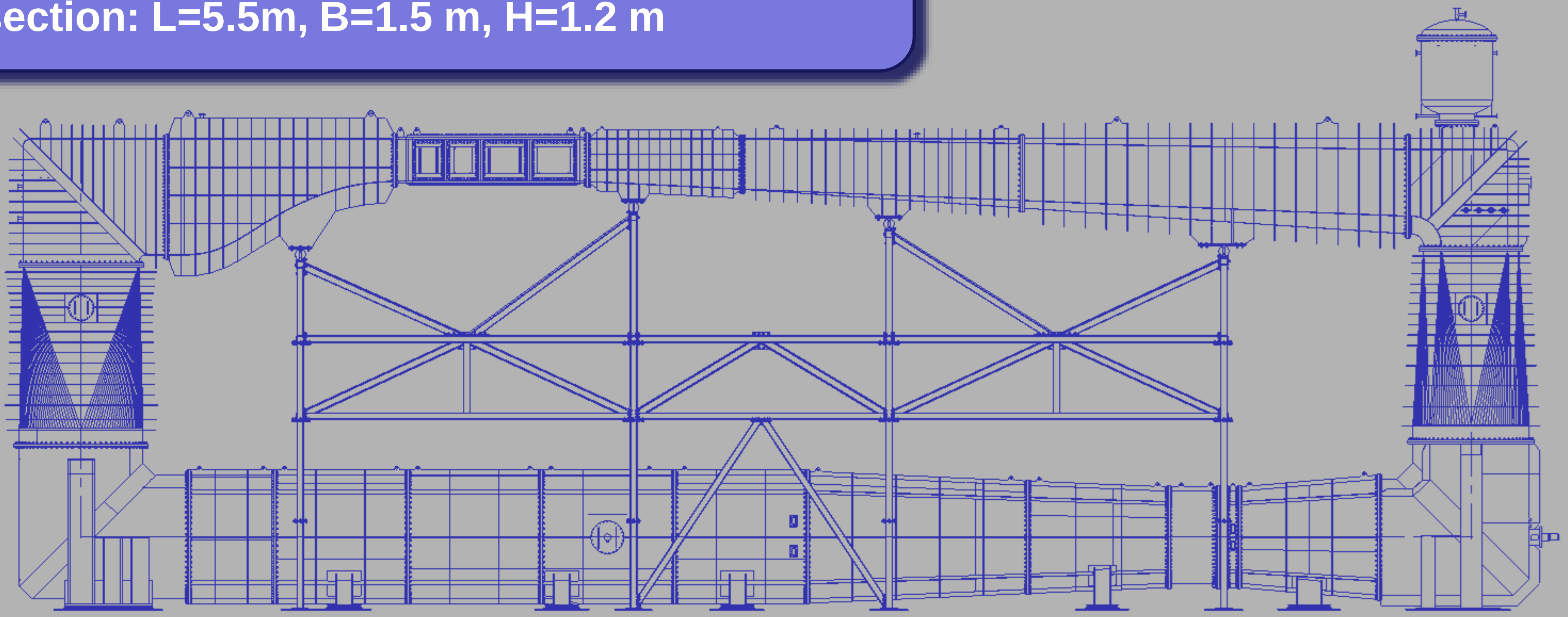

Outline

- **Tip vortex flow (**3D hydrofoil**)**
  - RANS-LES-simulations
  - Remeshed Vortex Particle Method

  - **Tip vortex flow cavitation**
  - Hybrid method
  - Pressure fluctuation
- **Conclusion**

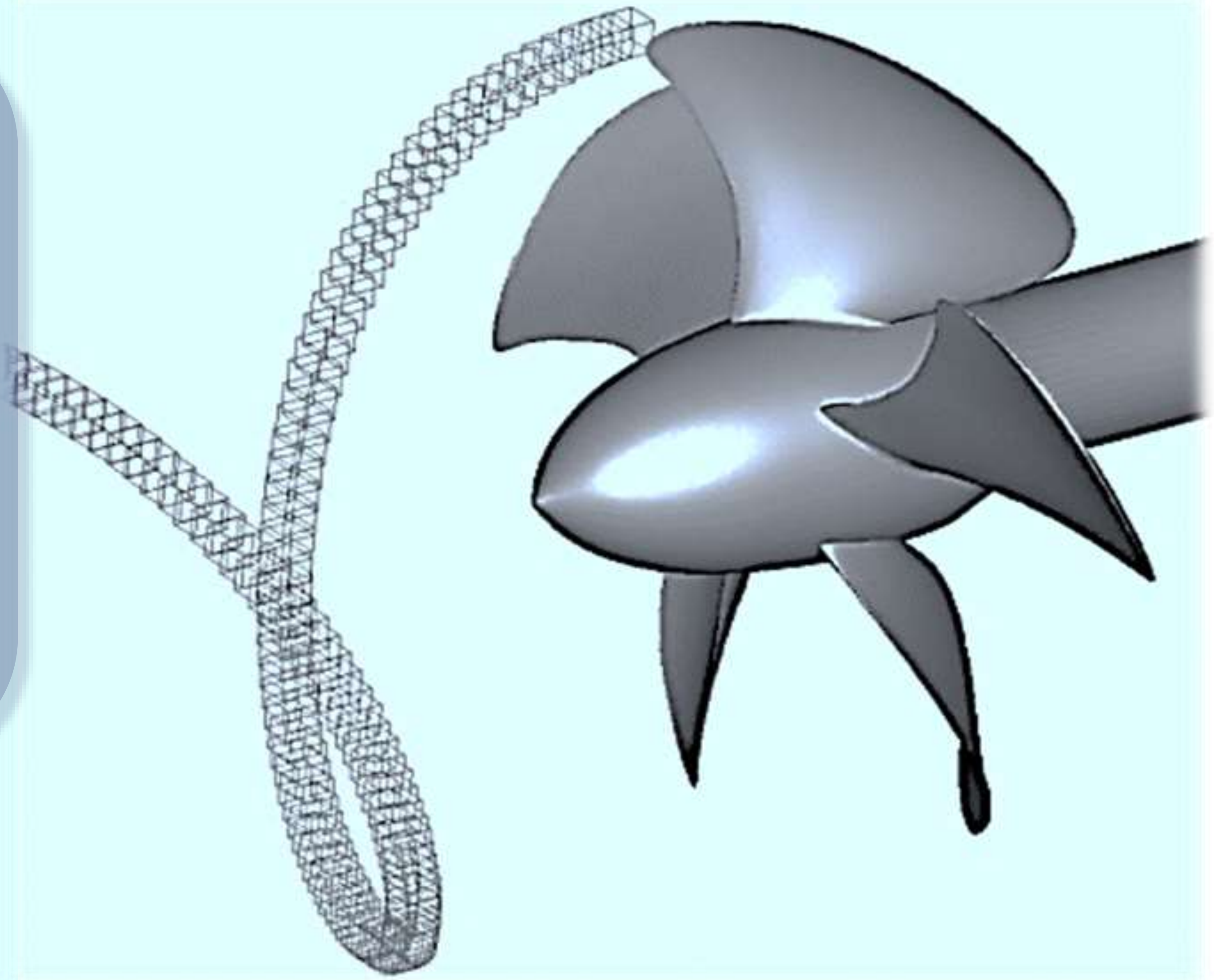

Outline

Sheet Cavitation

- **Cavitation modelling**
  - Euler-Lagrange model (E.L.)
  - Combined model (E.E.- E.L.)
- **Acoustic modelling**
- **Validation and application**
  - 2D Hydrofoil
  - Scale effects, sheet cavitation
  - PPTC-Propeller
- **Conclusion**

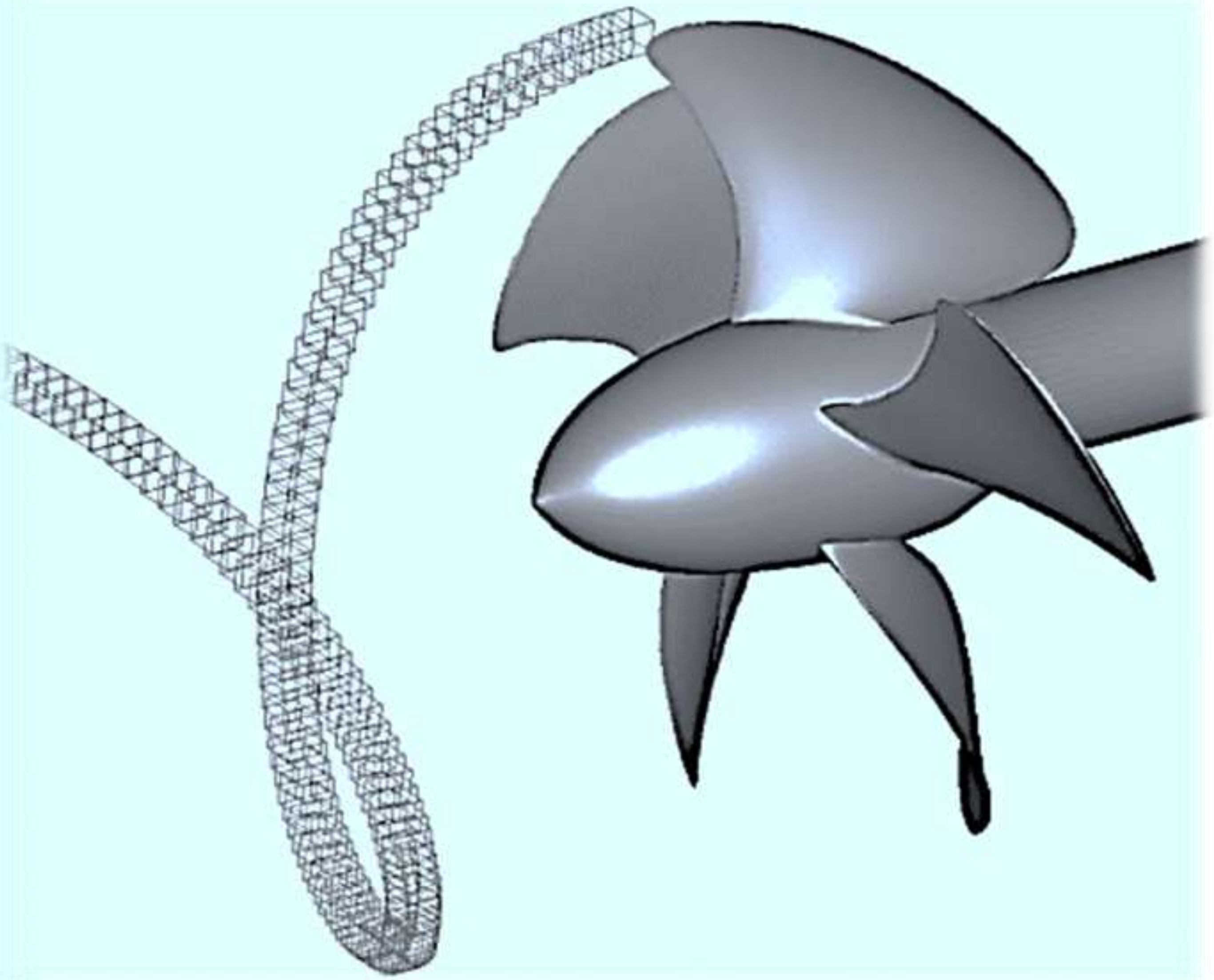

Sheet cavitation research at TUHH

BMWi, (German Federal Ministry for Economic Affairs)
Strong cooperation with the industry

- **KonKav I, KonKav II:** Water quality and scale effects
  - Partners:
  - HSVA: Mr. Chr. Johannsen,
  - SVA Potsdam: Mr. H.-J. Heinke,
  - University: URO, Prof. N. Damaschke

- **HiO-Cav: Improved tip vortex cavitation simulation**
  - Partners:
  - SVA Potsdam: Mr. H.-J. Heinke,
  - University: URO, Prof. N. Damaschke,
  - Industry: GMM, ThyssenKrupp, Piening

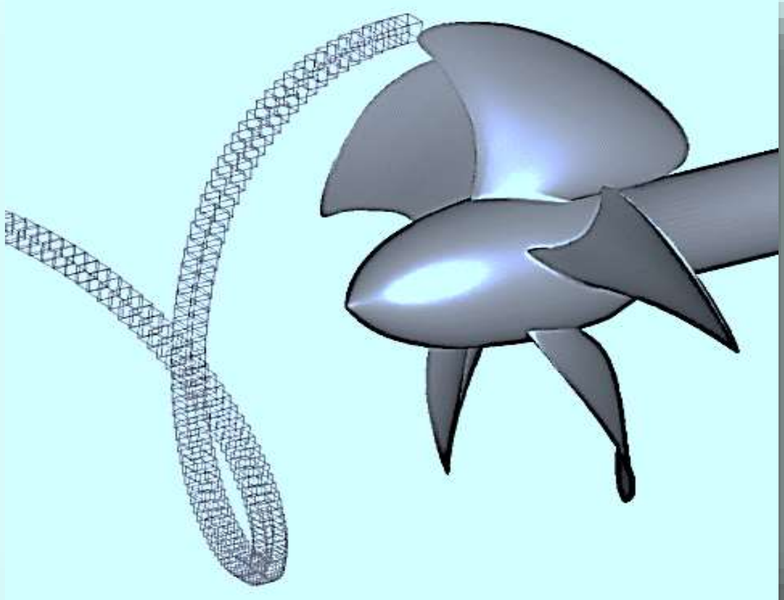

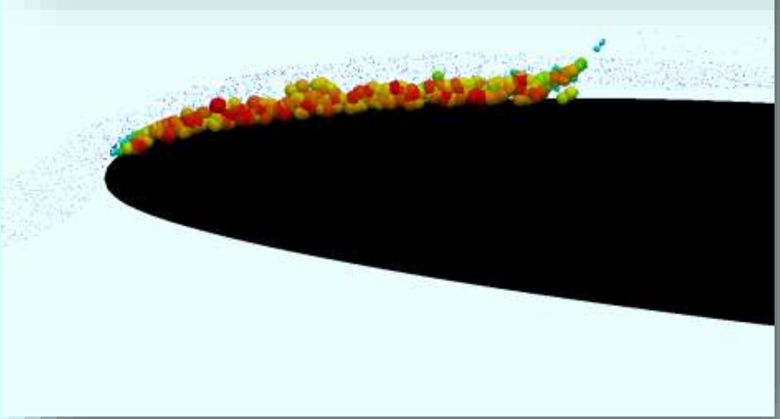

Cavitation research at TUHH

DFG (German Research Foundation)
Numerical investigation on concentrated vortical structures
Partner: URO, Prof. N. Kornev

German Navy
Investigation on the acoustic behaviour of marine propellers
Partner: HSVA

Experimental investigations

Mr. H.-J. Heinke and SVA Potsdam team
Mr. Chr. Johannsen and HSVA-team

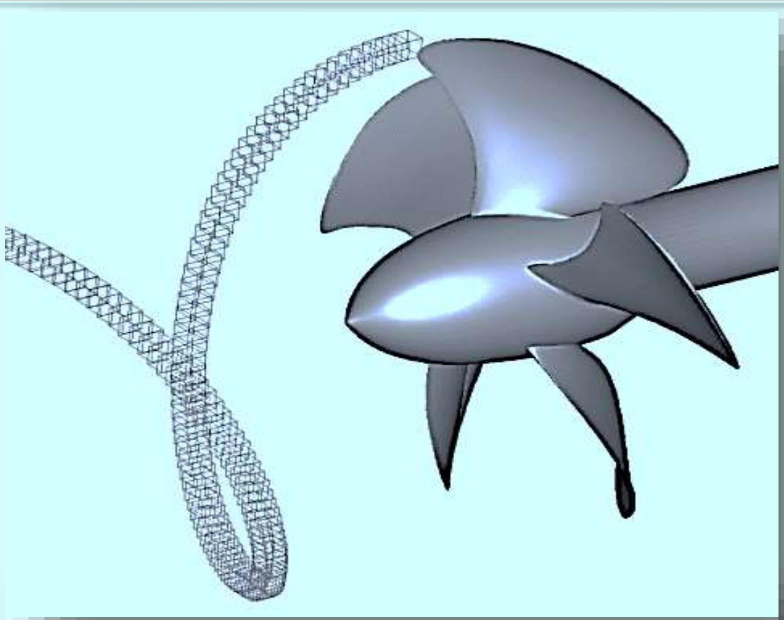

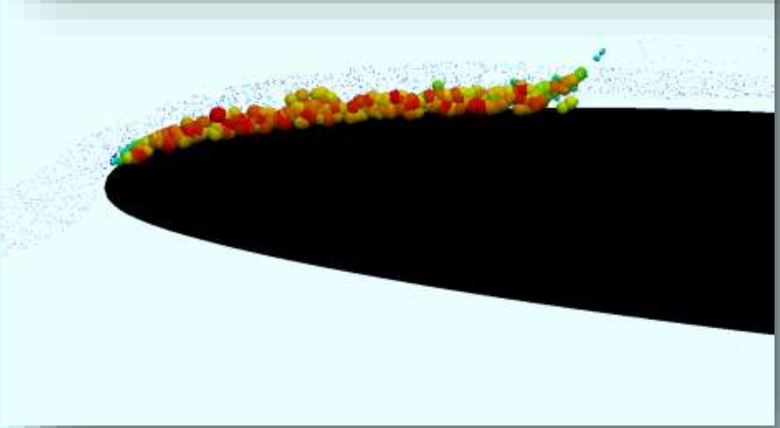

Cavitation research at TUHH

Contribution:

Prof. Nils Damaschke, Water quality measurements
Prof. Nikolai Kornev, Numerical simulation of vortical structures
Prof. Thomas Rung, Euler-Lagrange simulation

Dr. Sergey Yakubov, Euler-Lagrange simulation
Dr. Stephan Berger, Tip vortex and propeller induced pulses
Dr. Youjiang Wang, Numerical simulation of vortical structures
Dr. Ernst-August Weitendorf, Water quality on cavitation pattern

Patrick Schiller, Scale effects on sheet cavitation
Bahaddin Cankurt, Euler-Lagrange simulation, tip vortex cavit.
Roland Gosda, Scale effects on tip vortex cavitation
Dag Feder, Numerical simulation of vortical structures

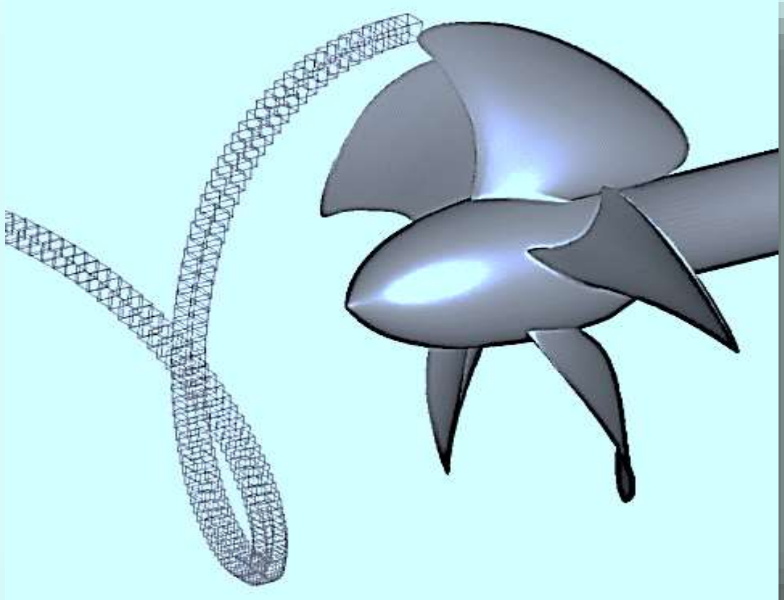

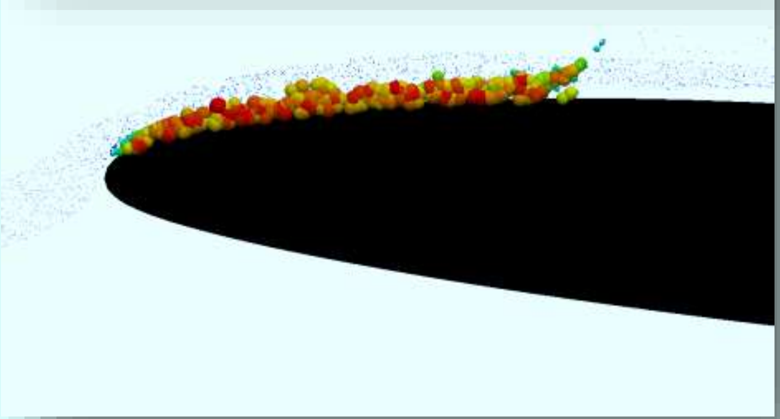

Complex vortical structure

NASA

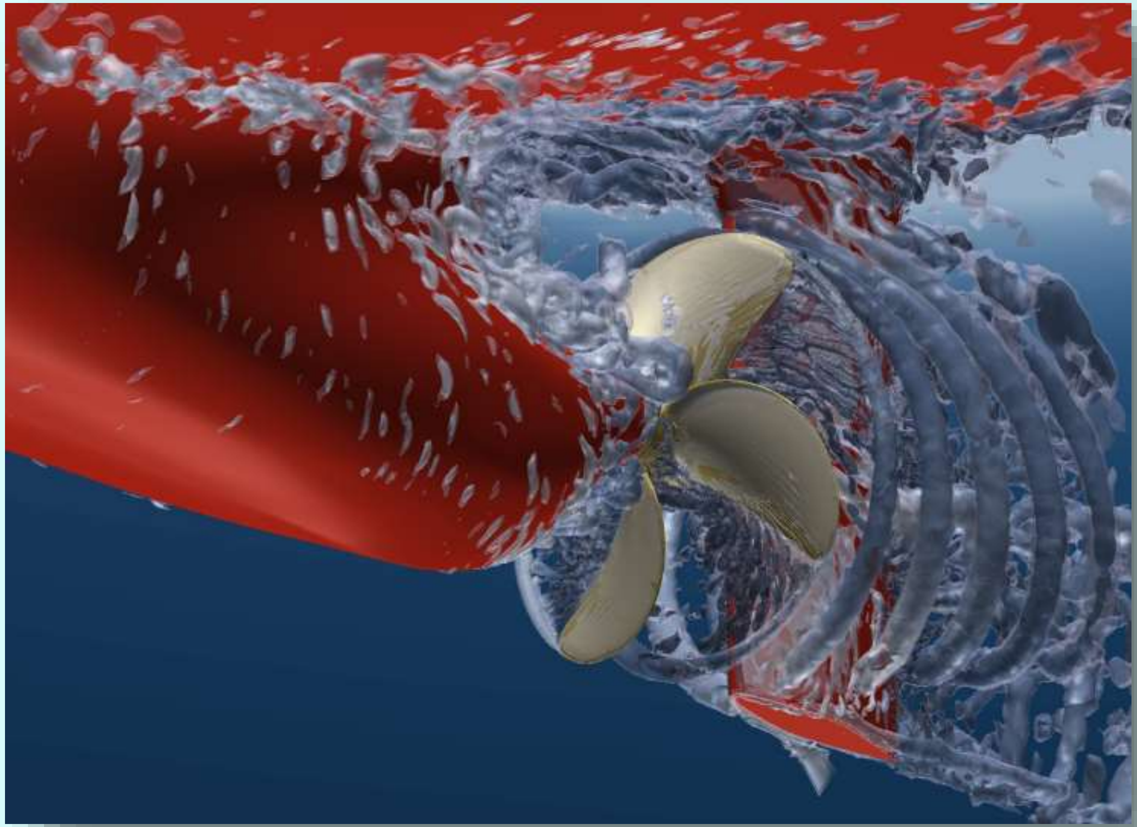

Tip vortex flow

Longevity: huge numerical diffusion

Contribution: Dag Feder

Numerical errors:

- Spatial resolution
- High-order discretisation (convection)
- Turbulence modelling (curvature)

Devenport

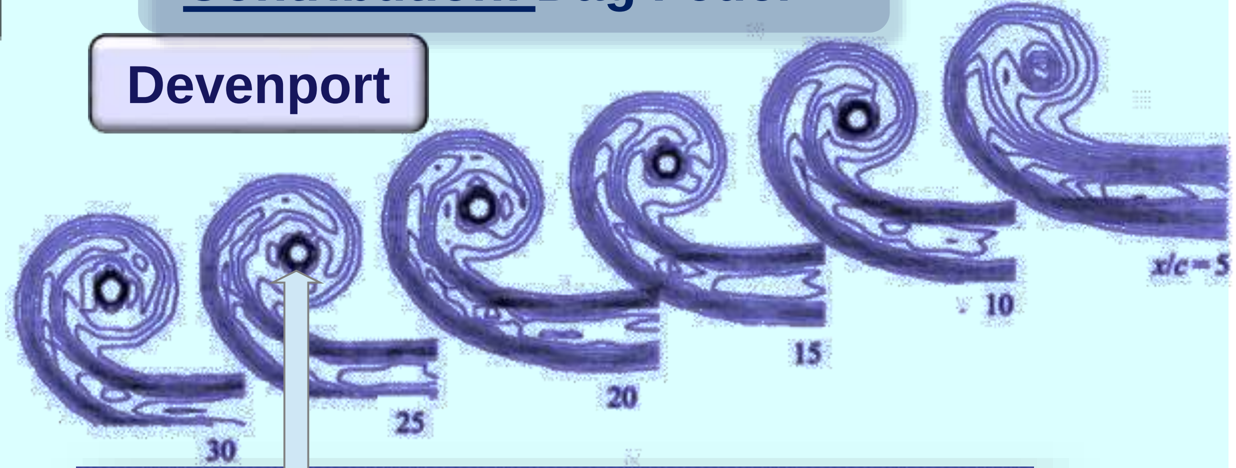

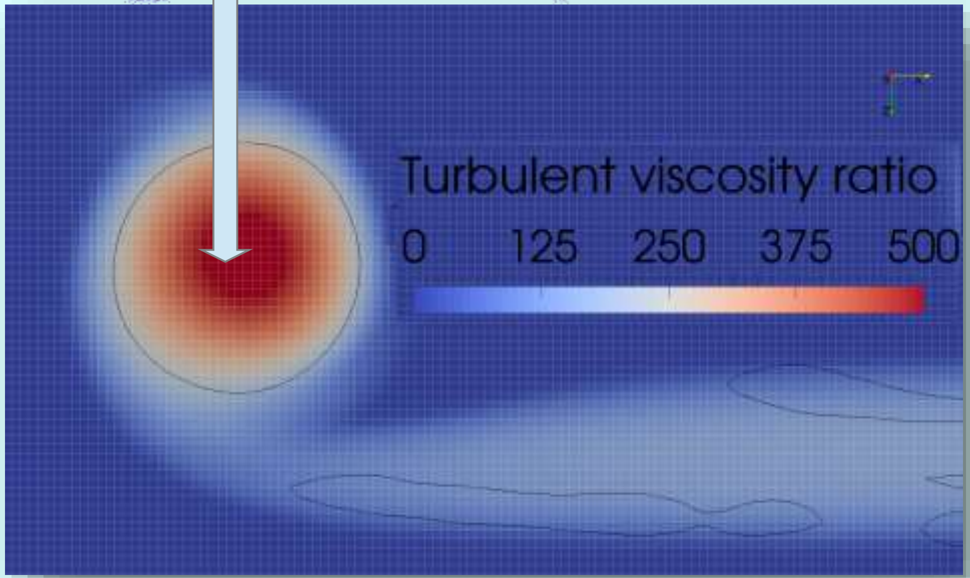

Approach

- AMR (near vortex cores)
- Vorticity Confinement: vortex reinforcement
- Consideration of laminar-like core (CC, RSM, DES)

Devenport - case

Wind tunnel experiment: trailing tip vortex

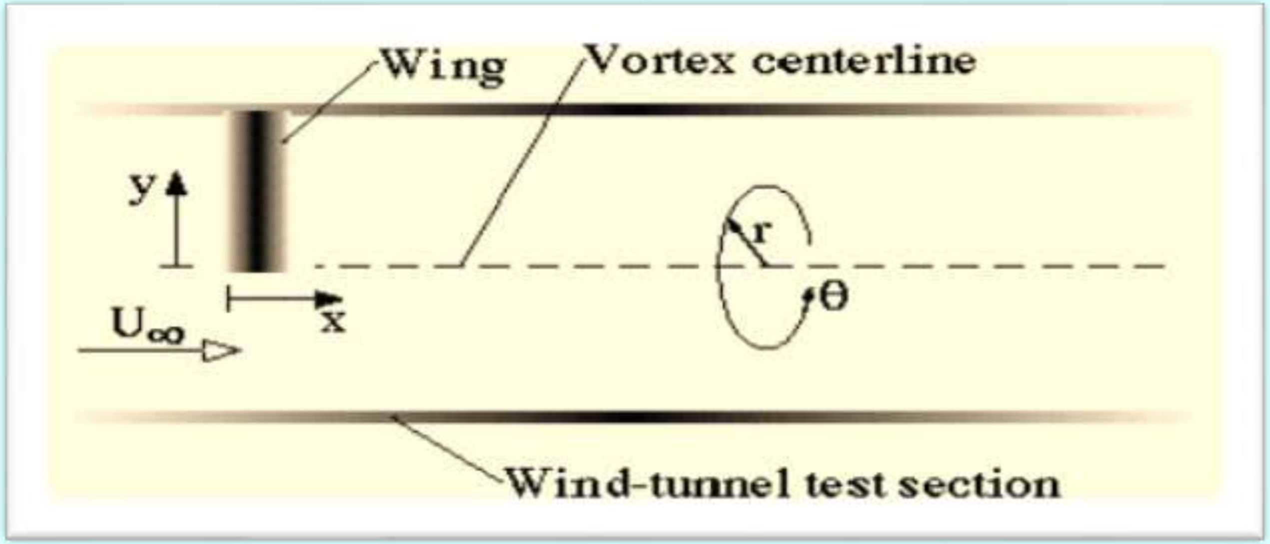

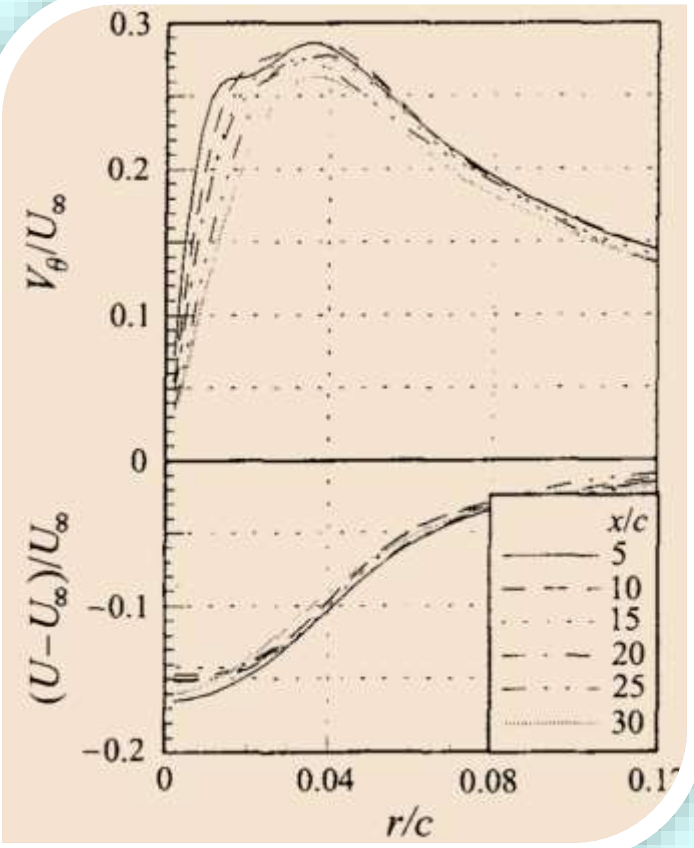

Measurements:
- Velocity profiles: axial, tangential
- Turbulence stress

Wandering motion: correction

Constant vortex core
Laminar flow in core

NACA0012, AOA= 5°, Re=5.10⁵

Devenport et al., 1996

Numerical setup

Solver: pimpleFoam, v3.0.1

Turbulence modelling

Hybrid RANS-LES: Spalart Allmaras-DDES

Wall treatment: low-Re

Cells: 4, 6, 20 M

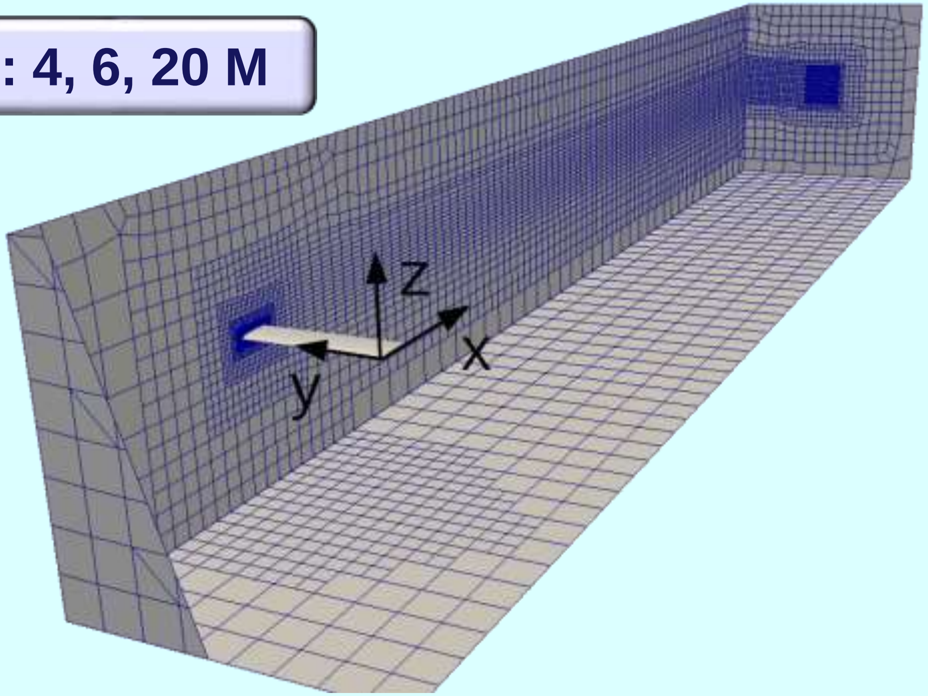

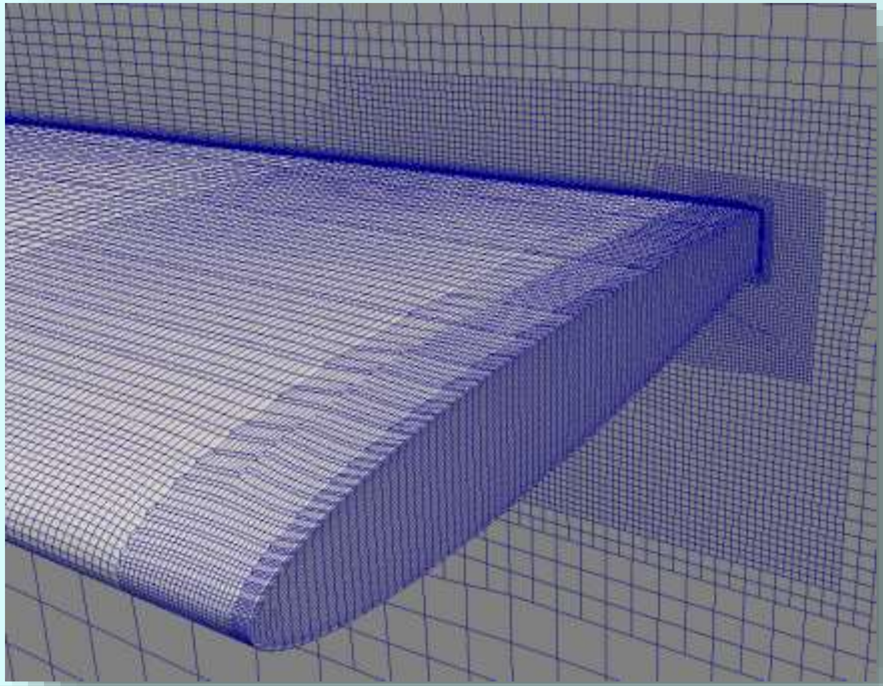

4/ 8/ 16 cells per vortex core

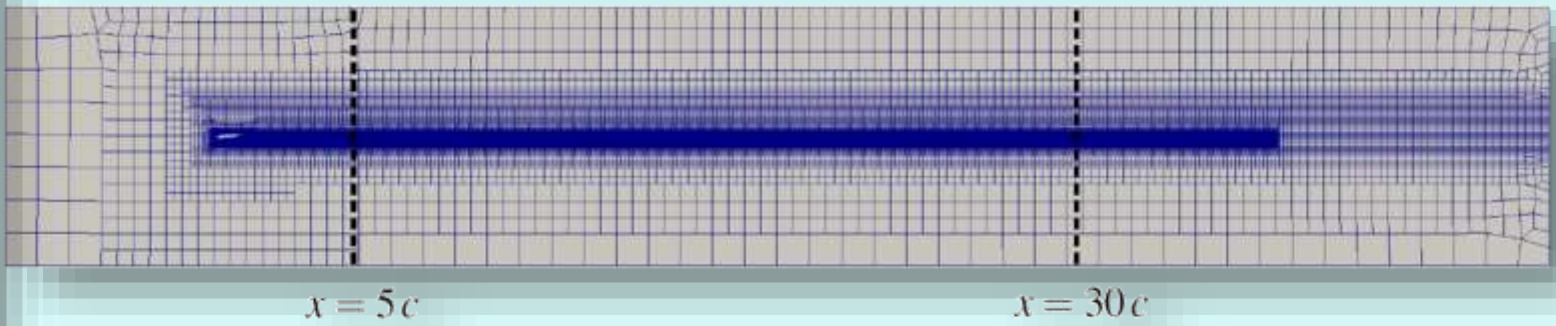

Results: reduced numerical diffusion

Core radius

- Exp.: constant
- Sim.: „convergence“
- VC: -10%

Peak tangential velocity

- Exp.: slight decrease
- Sim.: stronger decrease
- VC: +10…17%

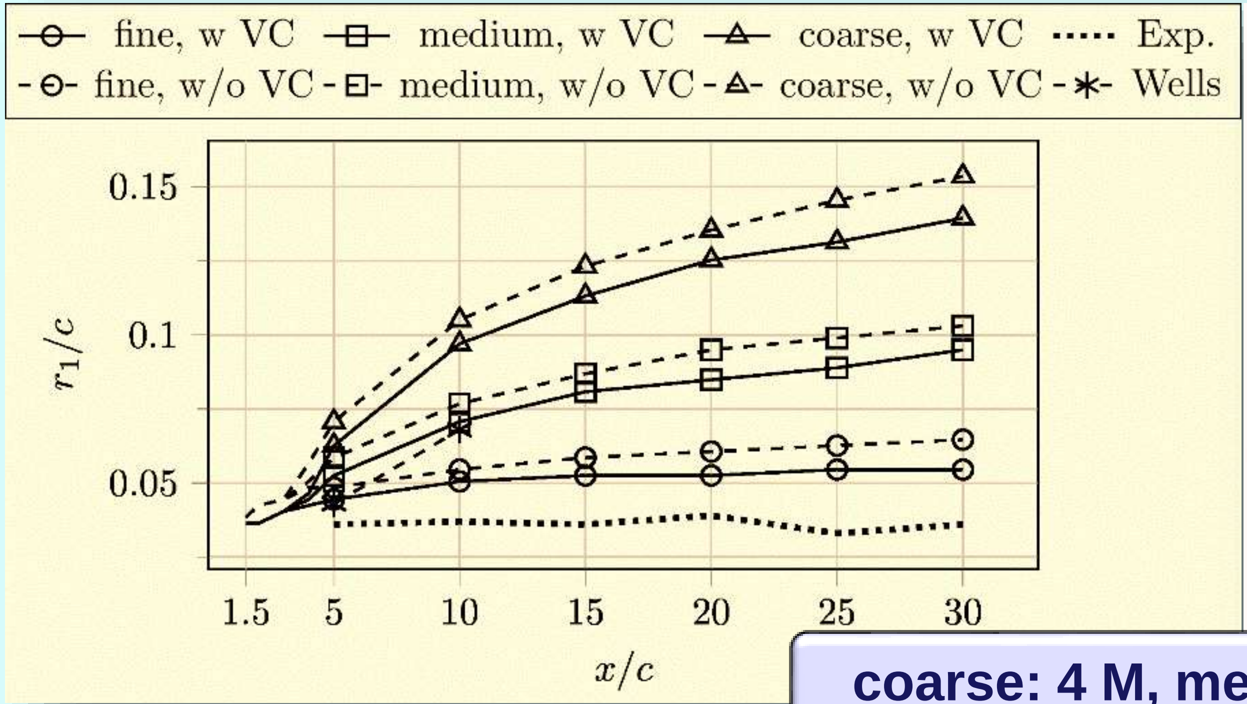

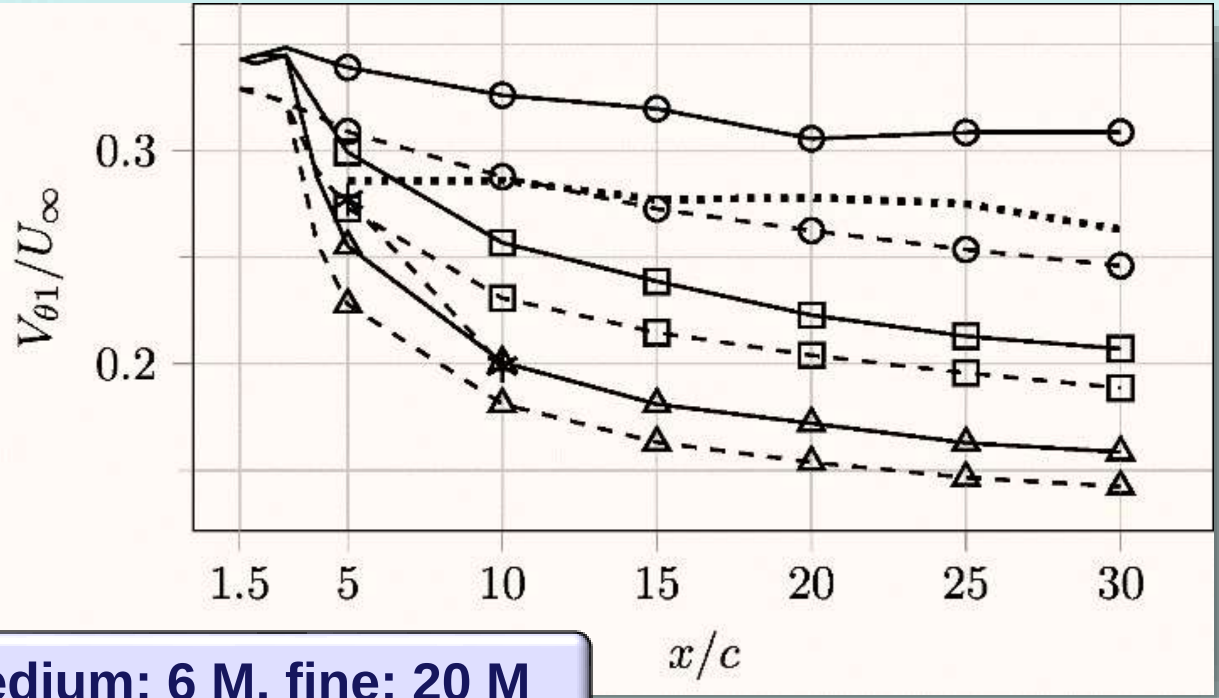

coarse: 4 M, medium: 6 M, fine: 20 M

Tip vortex flow

Remeshed Vortex Particle Method

Contribution: Dr. Youjiang Wang

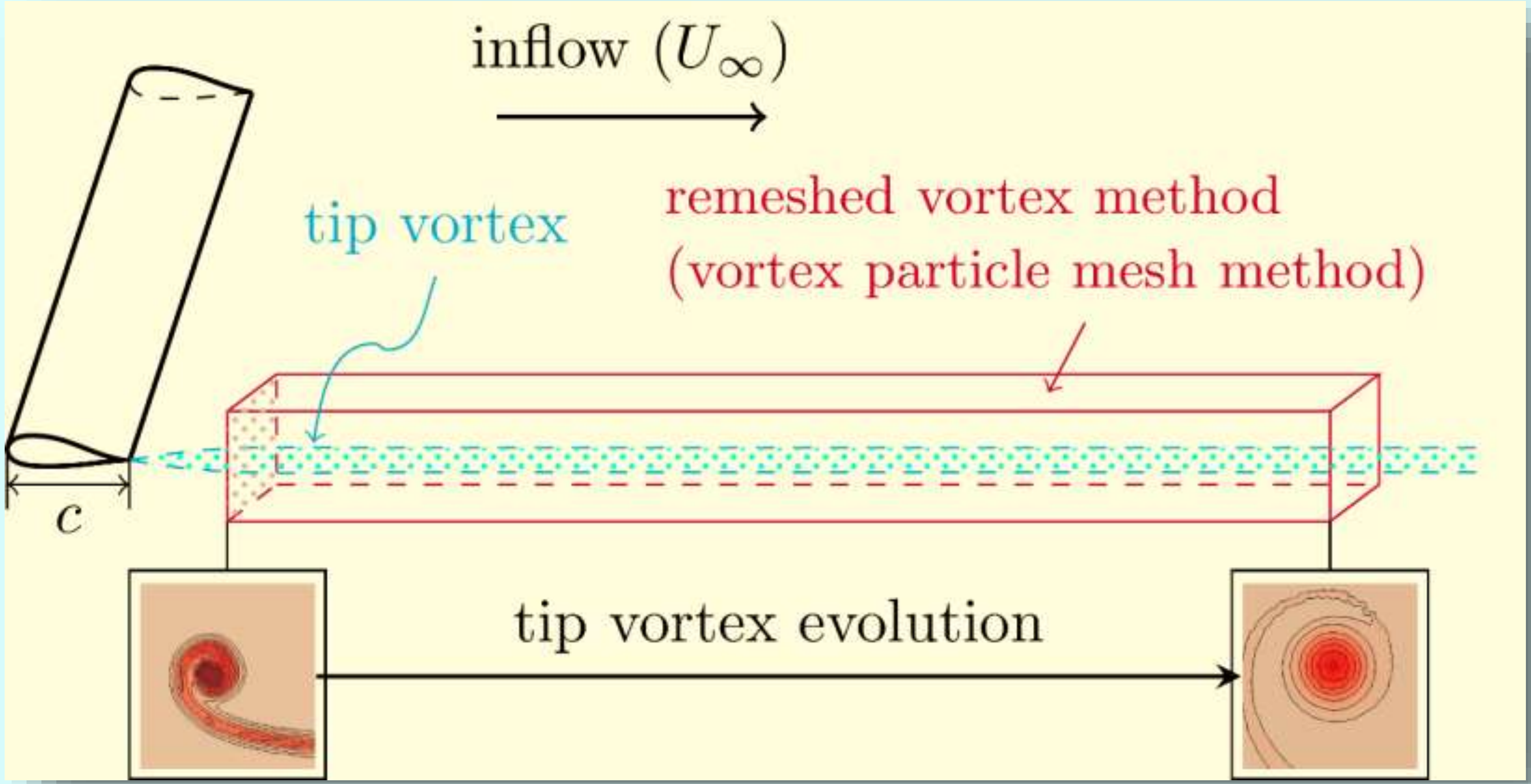

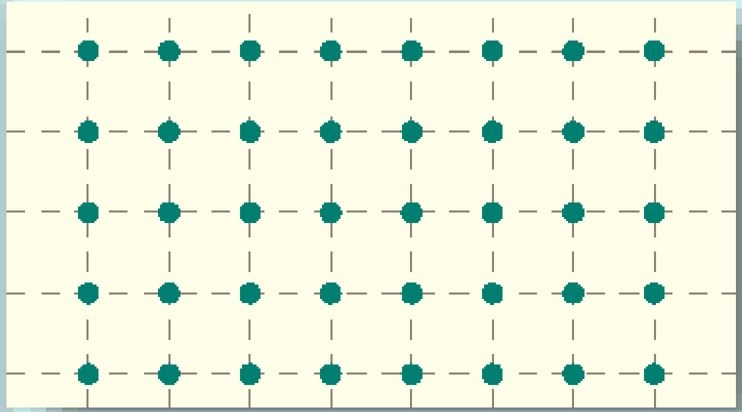

Particle distribution

Tip vortex flow

Remeshed Vortex Particle Method

Projection → $\nabla \cdot \omega = 0$ — On mesh

Calculate velocity — On mesh

Calculate stretching — On mesh

Advection — On particles

Paricle-to-mesh Interpolation

Viscous diffusion — On mesh

LES turbulence model — On mesh

iteration

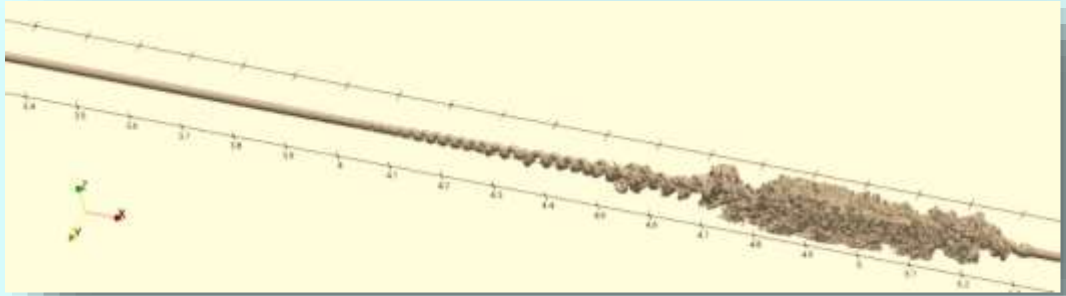

observed instability (iso-surface of vorticity)

Circumferential velocity

$\max(u_\theta/U_\infty)$

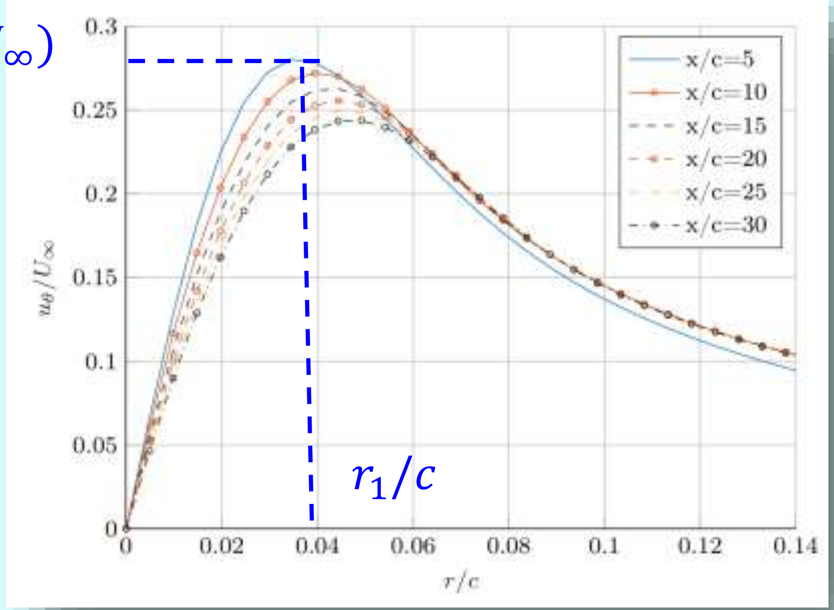

Tip vortex cavitation

Challenges

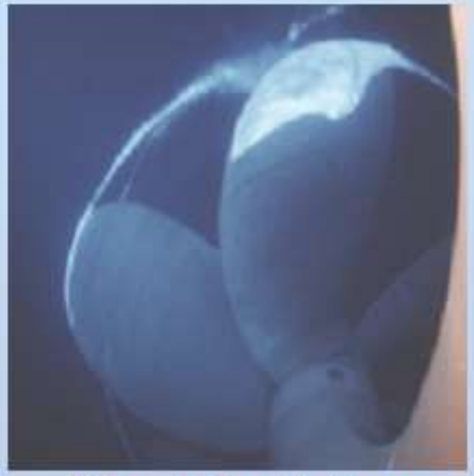

Sheet Cavitation

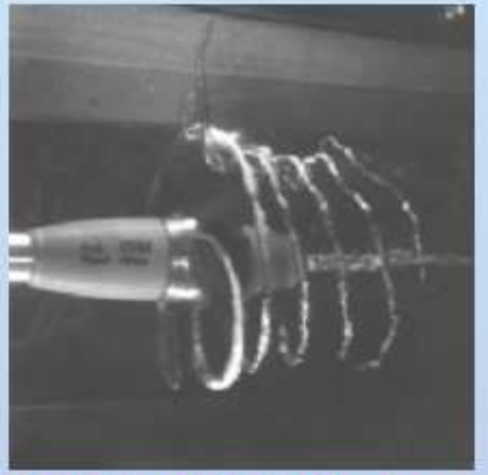

PHV and Hub Vortex

Tip Vortex with Nodes

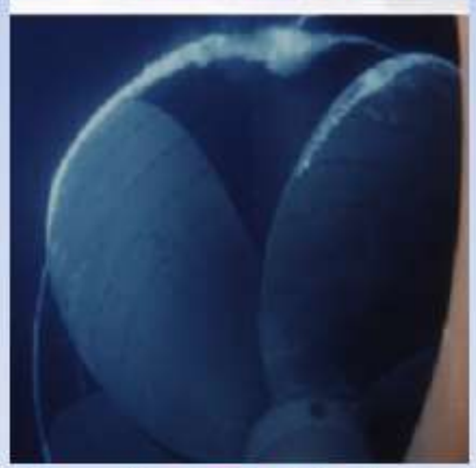

Bursting Tip Vortex

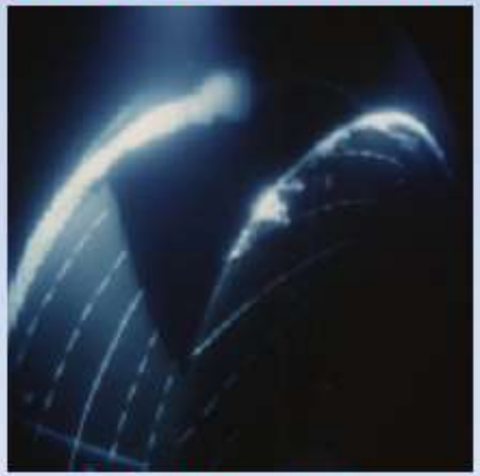

Cloud Cavitation

Cloud Cavitation

Challenges: strong interaction with the sheet cavitation

Tip vortex cavitation

Sheet cavitation

3D NACA 66_2 - 415 hydrofoil, $\alpha = 8$, $\sigma = 2.283$

Challenges: strong interaction with the sheet cavitation

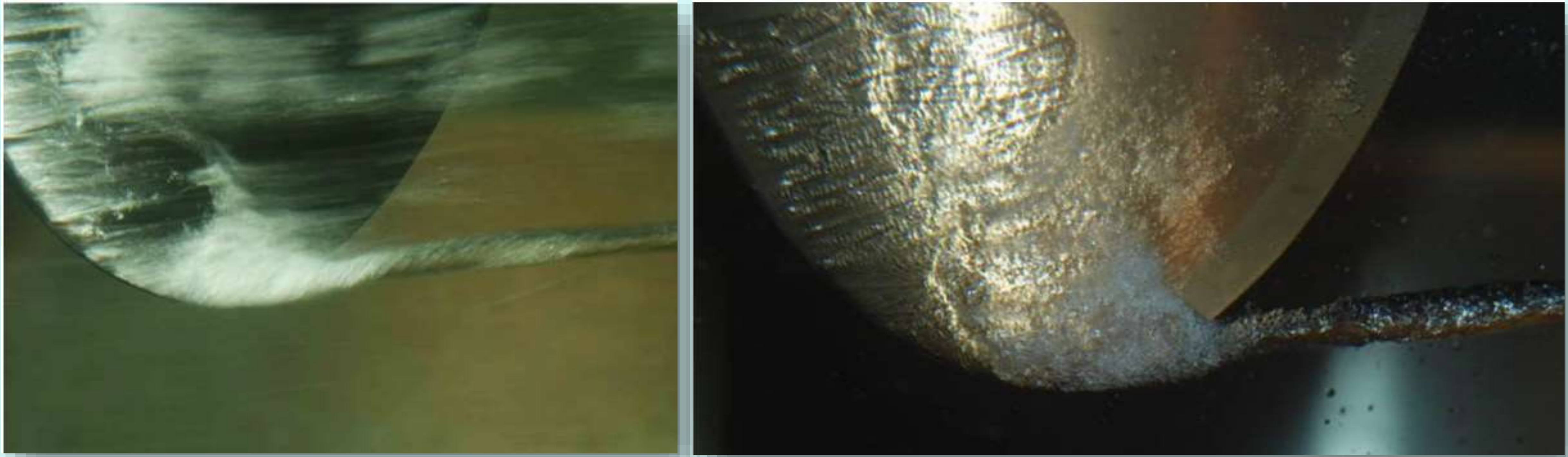

3D NACA 66_2 - 415 hydrofoil, α= 8, σ=2.283

H.-J. Heinke, H. Richter, Einfluss der Wassereigenschaften der Versuchsanlage K15A auf die Kavitation, SVA-report 4028, 2013.

Tip vortex cavitation, 3D NACA 66_2 - 415 hydrofoil

Experiment, SVA Potsdam

Contribution: Bahaddin Cankurt

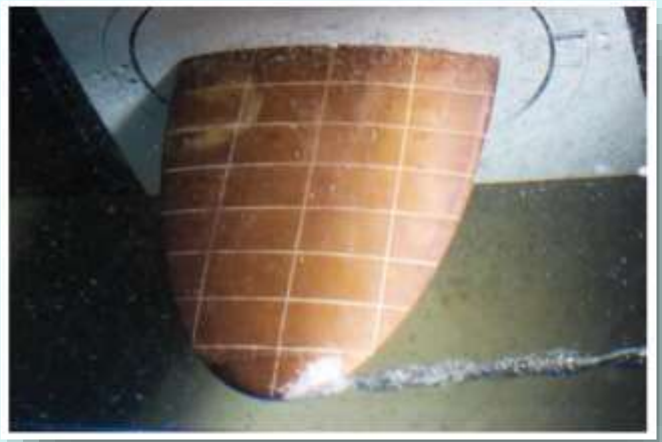

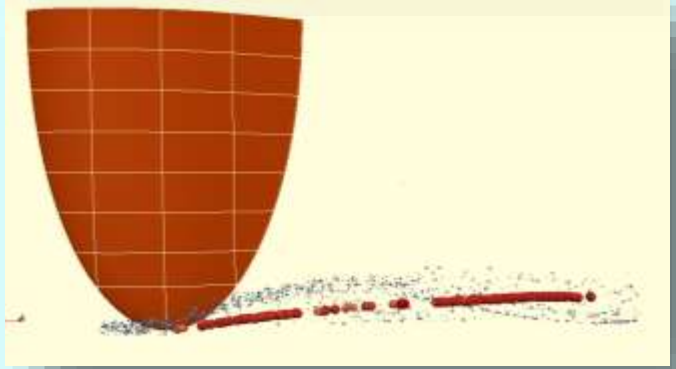

Simulation, TUHH

Modelling of tip vortex cavitation

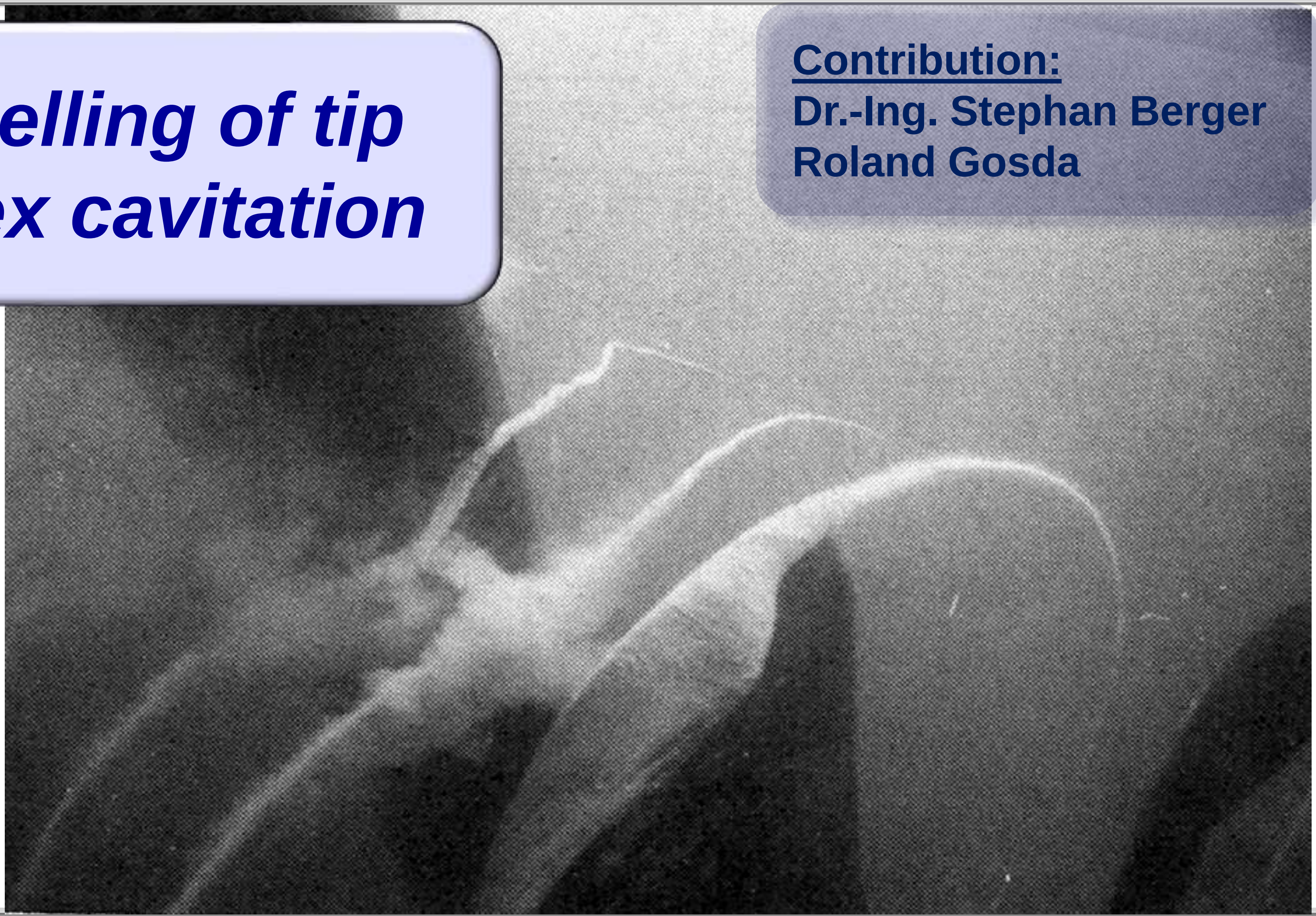

Contribution:
Dr.-Ing. Stephan Berger
Roland Gosda

Modelling of tip vortex cavitation

$$\hat{p}_c \propto \frac{\ddot{V}_c}{d}$$ — Cavitation

$q \gtrsim 2$ — Tip vortex cavitation (TVC)

Sheet cavitation (SC)

Lift effect

$q = 1 \dots 2$ — Displacement effect

$q f_b = q n n_b$ — Multiple of the blade frequency

$q = 1$ — first order

$q \geq 2$ — Higher order

Cavitating Propeller of a container ship; High speed-video: model-test SVA Potsdam

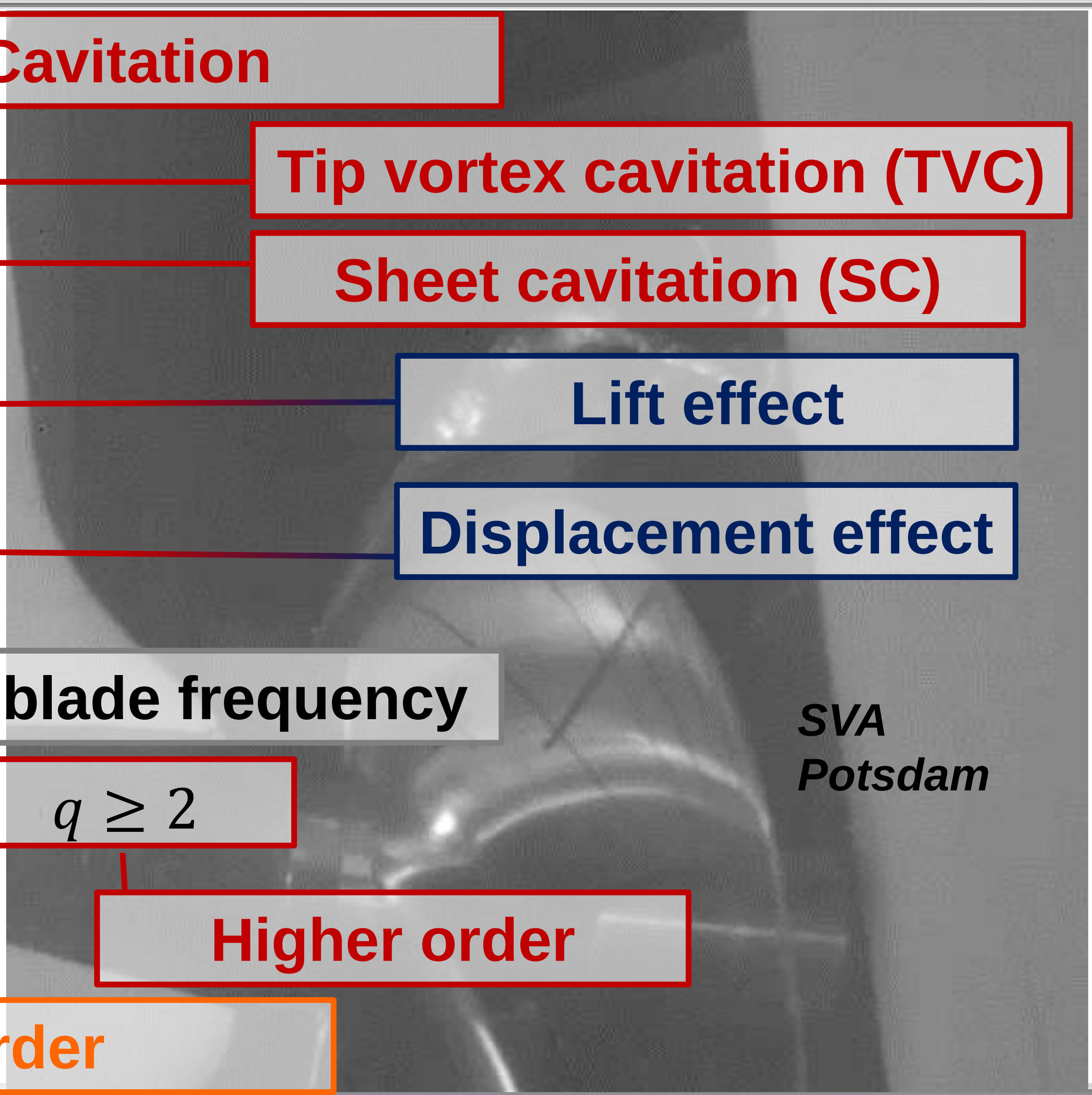

Modelling of tip vortex cavitation

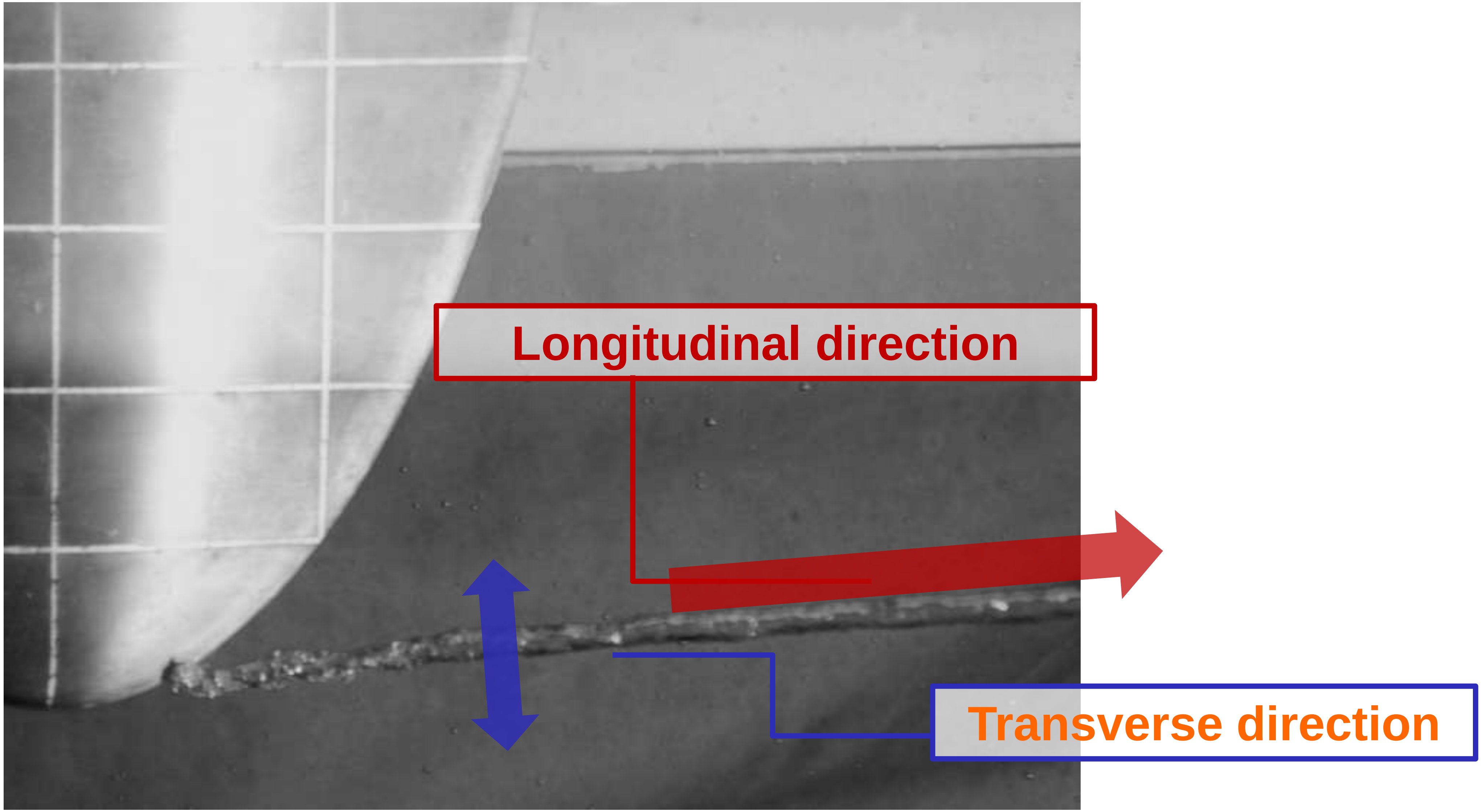

Simplifications and assumptions

- Neglect of the interaction between the segments (quasi 2-D)
- Circulation Γ_k^* of segment k increases from $\Gamma_{\text{ini}} = \gamma_{\text{ini}}\Gamma_b$ to Γ_b (due to rolling up process)

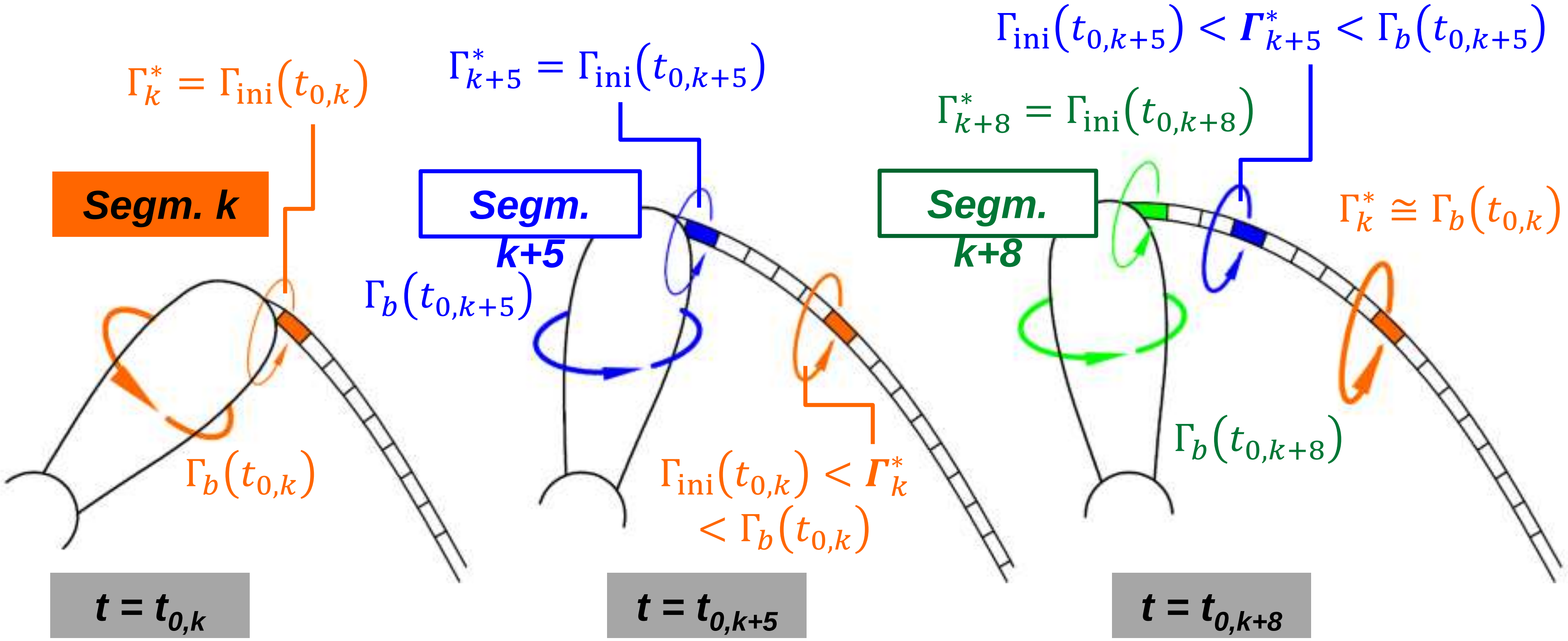

Calculation of the pressure disturbance by TVC

Superposition of the influences of all segments

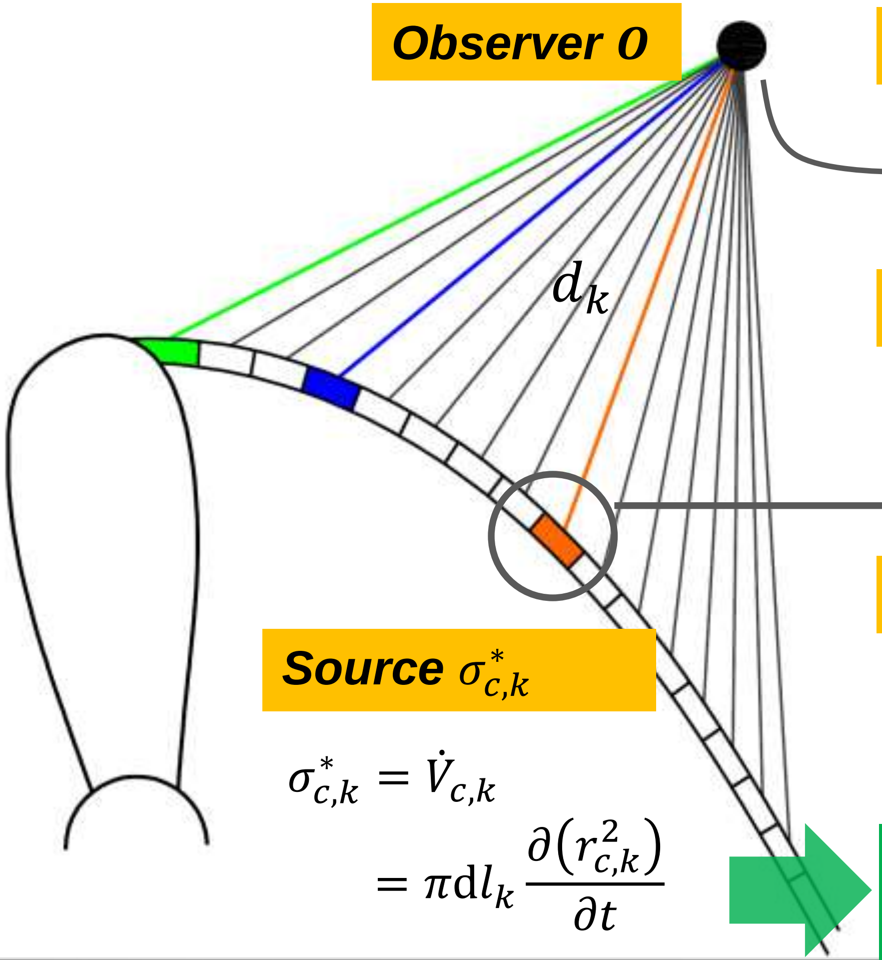

Induced potential in 0

$$\phi_k^* = -\frac{\sigma_{c,k}^*}{4\pi d_k}$$

Influences of all segments

$$\Phi_{\mathrm{TVC}} = \sum_k \phi_k^*$$

Linearized Bernoulli equation

$$p'_{\mathrm{TVC}} = -\rho B_f \frac{\partial \Phi_{\mathrm{TVC}}}{\partial t}$$

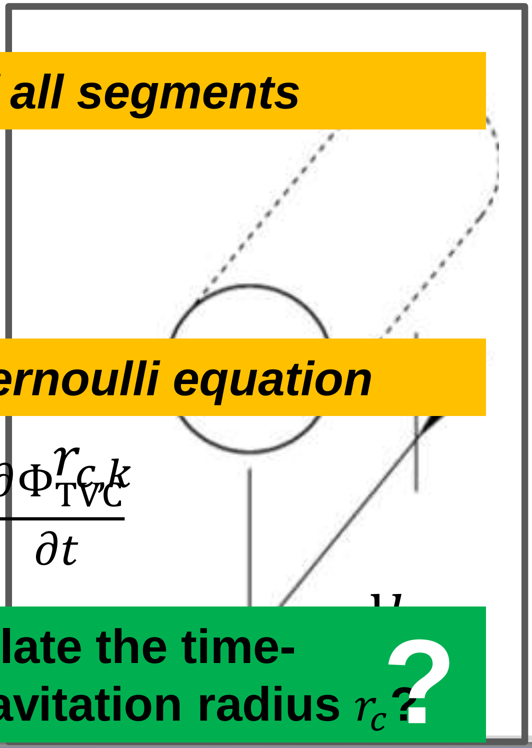

Source $\sigma_{c,k}^*$

$$\sigma_{c,k}^* = \dot{V}_{c,k} = \pi \mathrm{d}l_k \frac{\partial\left(r_{c,k}^2\right)}{\partial t}$$

How to calculate the time-dependent cavitation radius r_c?

Dynamics of a cavitating vortex segment

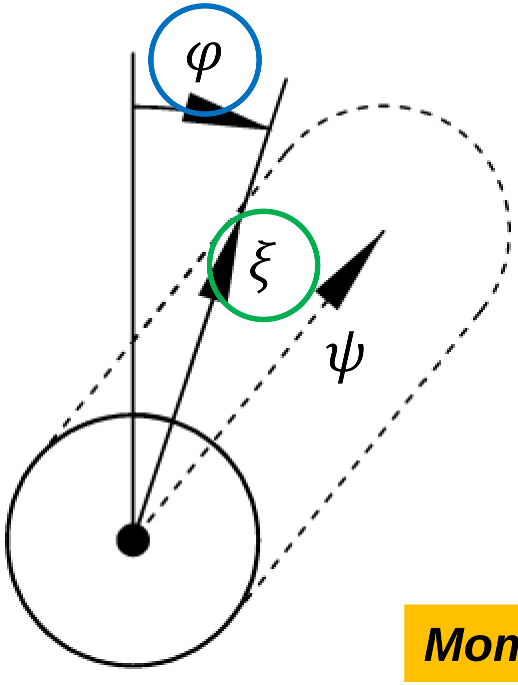

Assumptions

$$\rho, \mu = \text{const.}, \quad \frac{\partial}{\partial \varphi} = 0, \quad \frac{\partial}{\partial \psi} = 0$$

Continuity equation in cylindrical coordinates

$$\frac{1}{\xi}\frac{\partial(\xi u_\xi)}{\partial \xi} = 0$$

Momentum equations in cylindrical coordinates

radial ξ:

$$\rho\left(\frac{\partial u_\xi}{\partial t} + u_\xi \frac{\partial u_\xi}{\partial \xi} - \frac{u_\varphi^2}{\xi}\right) = -\frac{\partial p}{\partial \xi} + \mu \frac{\partial}{\partial \xi}\cancel{\left(\frac{1}{\xi}\frac{\partial(\xi u_\xi)}{\partial \xi}\right)}$$

tangential φ:

$$\rho\left(\frac{\partial u_\varphi}{\partial t} + u_\xi \frac{\partial u_\varphi}{\partial \xi} - \frac{u_\xi u_\varphi}{\xi}\right) = f_\varphi + \mu \frac{\partial}{\partial \xi}\left(\frac{1}{\xi}\frac{\partial(\xi u_\varphi)}{\partial \xi}\right)$$

Dynamics of a cavitating vortex segment

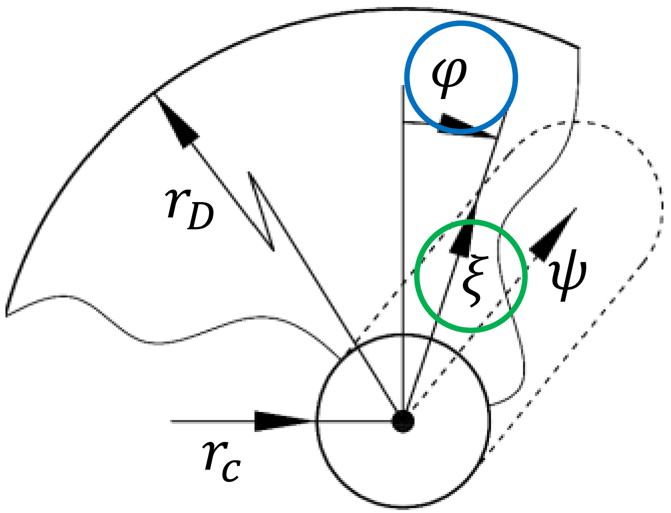

Kinematic relationship

$$2\pi r_c \dot{r}_c = 2\pi \xi u_\xi \quad \Leftrightarrow u_\xi = \frac{r_c \dot{r}_c}{\xi}$$

Momentum equations in terms of r_c

radial ξ:

$$\rho\left(\frac{\ddot{r}_c r_c + \dot{r}_c^2}{\xi} - \frac{\dot{r}_c^2 r_c^2}{\xi^3} - \frac{u_\varphi^2}{\xi}\right) = -\frac{\partial p}{\partial \xi}$$

tangential φ:

$$\rho\left(\frac{\partial u_\varphi}{\partial t} + \frac{r_c \dot{r}_c}{\xi}\left(\frac{\partial u_\varphi}{\partial \xi} - \frac{u_\varphi}{\xi}\right)\right) = f_\varphi + \mu \frac{\partial}{\partial \xi}\left(\frac{1}{\xi}\frac{\partial(\xi u_\varphi)}{\partial \xi}\right)$$

Integration of radial momentum equation from r_c to r_D

$$(\ddot{r}_c r_c + \dot{r}_c^2)\boxed{\ln\left(\frac{r_D}{r_c}\right)} + \frac{\dot{r}_c^2 r_c^2}{2}\left(\frac{1}{r_D^2} - \frac{1}{r_c^2}\right) = \frac{1}{\rho}(p_c - p_{\mathrm{vtx}})$$

Dynamics of a cavitating vortex segment

radial ξ:

$$(\ddot{r}_c r_c + \dot{r}_c^2)\ln\left(\frac{r_D}{r_c}\right) + \frac{\dot{r}_c^2 r_c^2}{2}\left(\frac{1}{r_D^2} - \frac{1}{r_c^2}\right) = \frac{1}{\rho}(p_c - p_{\mathrm{vtx}})$$

Balance of forces at the bubble surface:

$$p_c = p_v + p_{g0}\left(\frac{r_{c0}}{r_c}\right)^{2n} - 2\mu\frac{\dot{r}_c}{r_c} - \frac{S}{r_c}$$

Influence of the vortex (u_φ)

$$p_{\mathrm{vtx}}(r_c) = p_D - \rho\int_{r_c}^{r_D}\frac{u_\varphi^2}{\xi}\,\mathrm{d}\xi$$

tangential φ:

$$\rho\left(\frac{\partial u_\varphi}{\partial t} + \frac{r_c \dot{r}_c}{\xi}\left(\frac{\partial u_\varphi}{\partial \xi} - \frac{u_\varphi}{\xi}\right)\right) = f_\varphi + \mu\frac{\partial}{\partial \xi}\left(\frac{1}{\xi}\frac{\partial(\xi u_\varphi)}{\partial \xi}\right)$$

Numerical solution methods for the determination of $r_c(t)$

Formulation f1: coupled

Formulation f2: uncoupled

Solution method

Starting point: Radial and tangential momentum equation

$$\rho\left[(\ddot{r}_c r_c+\dot{r}_c^2)\ln\left(\frac{r_D}{r_c}\right)+\frac{\dot{r}_c^2 r_c^2}{2}\left(\frac{1}{r_D^2}-\frac{1}{r_c^2}\right)\right]=p_c-p_D+\rho\int_{r_c}^{r_D}\frac{u_\varphi^2}{\xi}\,\mathrm{d}\xi$$

$$\rho\left(\frac{\partial u_\varphi}{\partial t}+\frac{r_c\dot{r}_c}{\xi}\left(\frac{\partial u_\varphi}{\partial \xi}-\frac{u_\varphi}{\xi}\right)\right)=f_\varphi+\mu\frac{\partial}{\partial \xi}\left(\frac{1}{\xi}\frac{\partial(\xi u_\varphi)}{\partial \xi}\right)$$

Formulation f1

- Solve the radial *and* the tangential momentum equation
- Modelling of the circulation increase via source term

$$f_\varphi=\rho\frac{\partial\Gamma^*}{\partial t}\frac{1}{2\pi\xi}\left[1-\exp\left(\frac{-\beta\xi^2}{r_a^2}\right)\right]$$

Formulation f2

- Solve the radial momentum equation
- Utilizing a vortex model (Lamb-Oseen) for u_φ

$$u_\varphi=\frac{\Gamma^*}{2\pi\xi}\left[1-\exp\left(\frac{-\beta\xi^2}{r_a^2(t)}\right)\right]$$

- Vortex parameter: circulation Γ^* and viscous core radius r_a of the respective segment

Dynamic behaviour of a single vortex cavitation segment

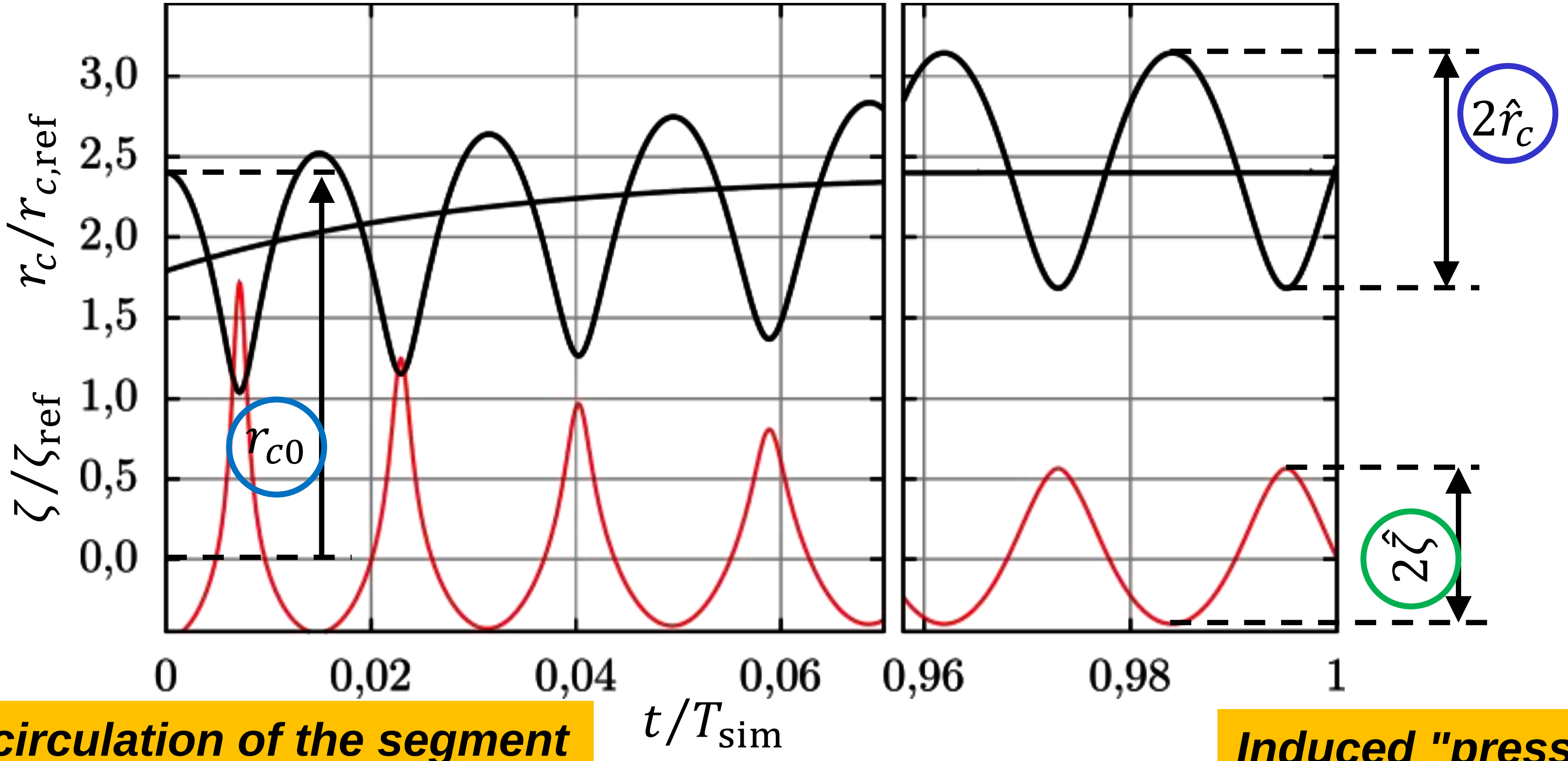

Increase in the circulation of the segment

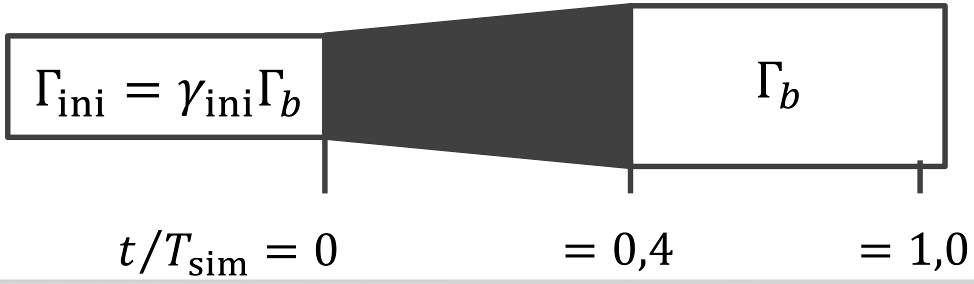

Induced "pressure" fluctuation:

$$\zeta = \frac{\partial^2 (r_c^2)}{\partial t^2}$$

Influence by sheet cavitation

Idea: Initialization of segments with half sheet cavitation thickness

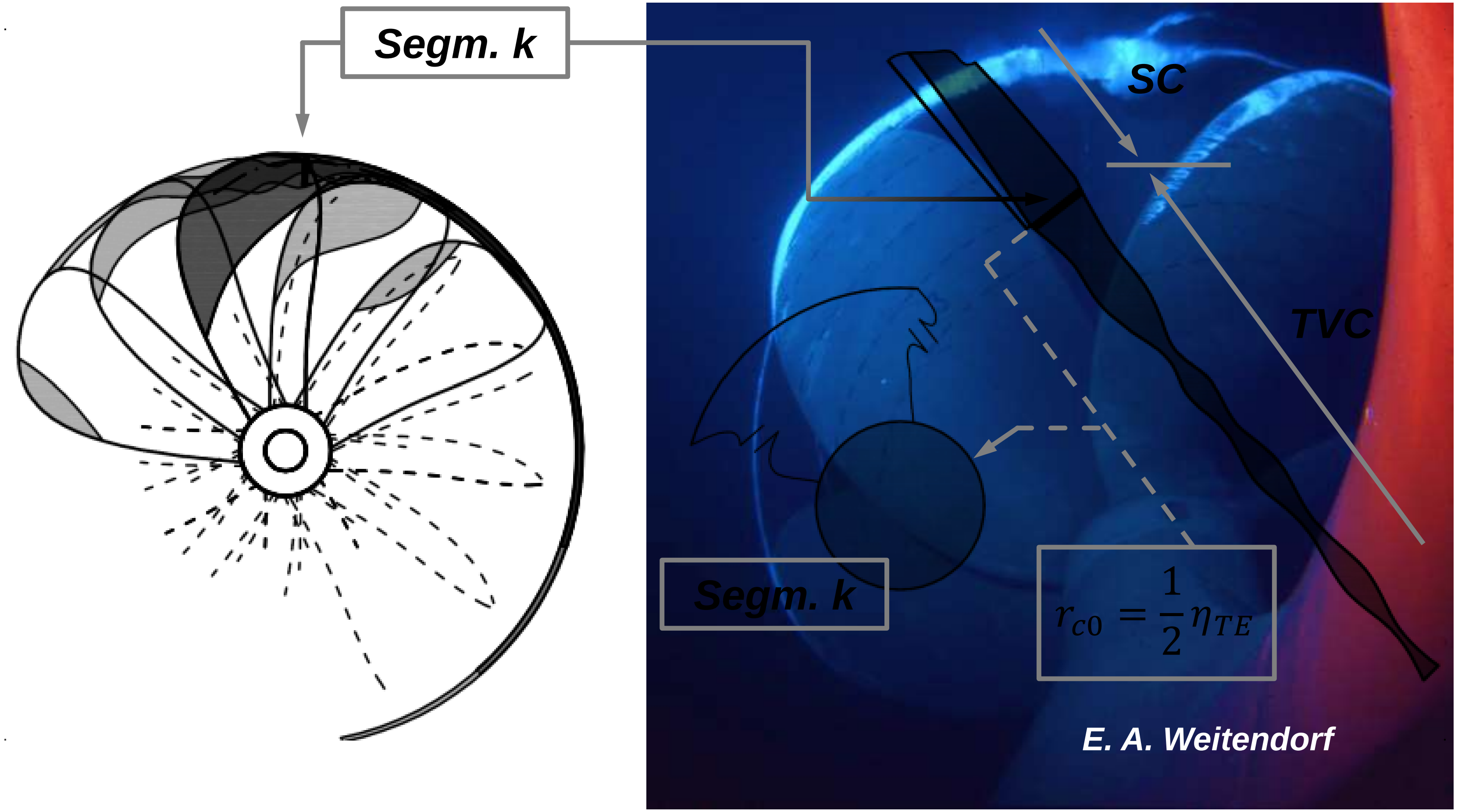

Hybrid simulation method

Contribution:
Dr.-Ing. Stephan Berger
Roland Gosda

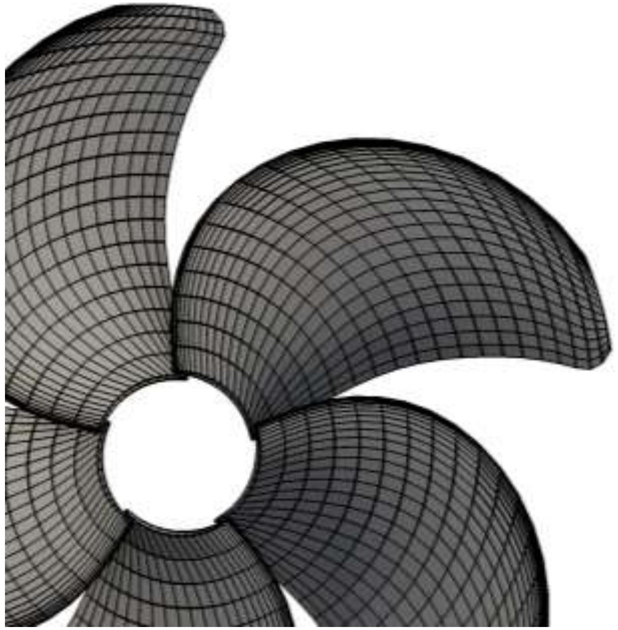

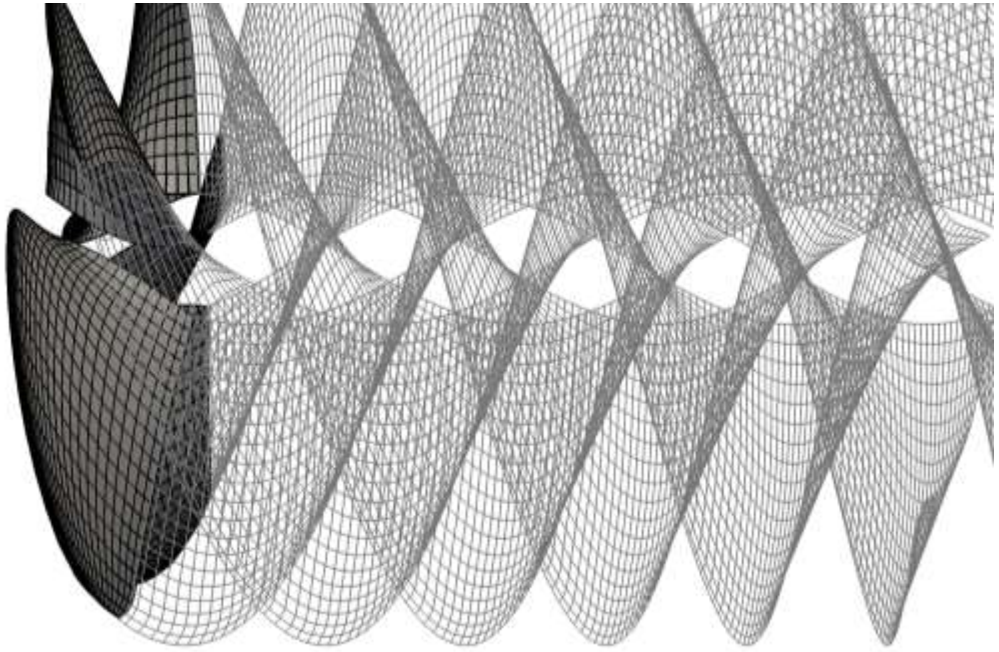

Overview

Combination of three different methods

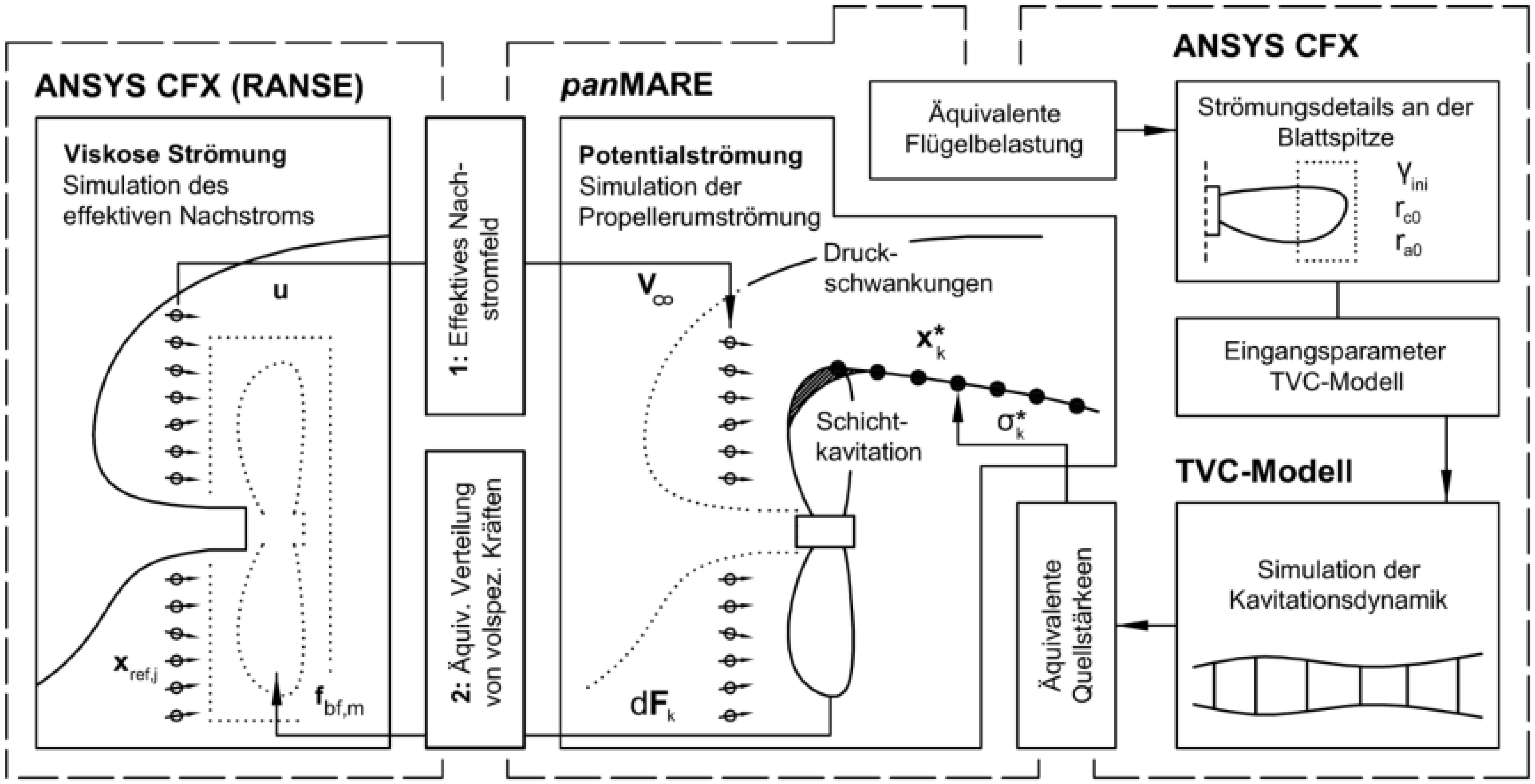

Determination of the TVC model parameters

RANSE investigations with ANSYS CFX for equivalent blade loads

Vortex structure

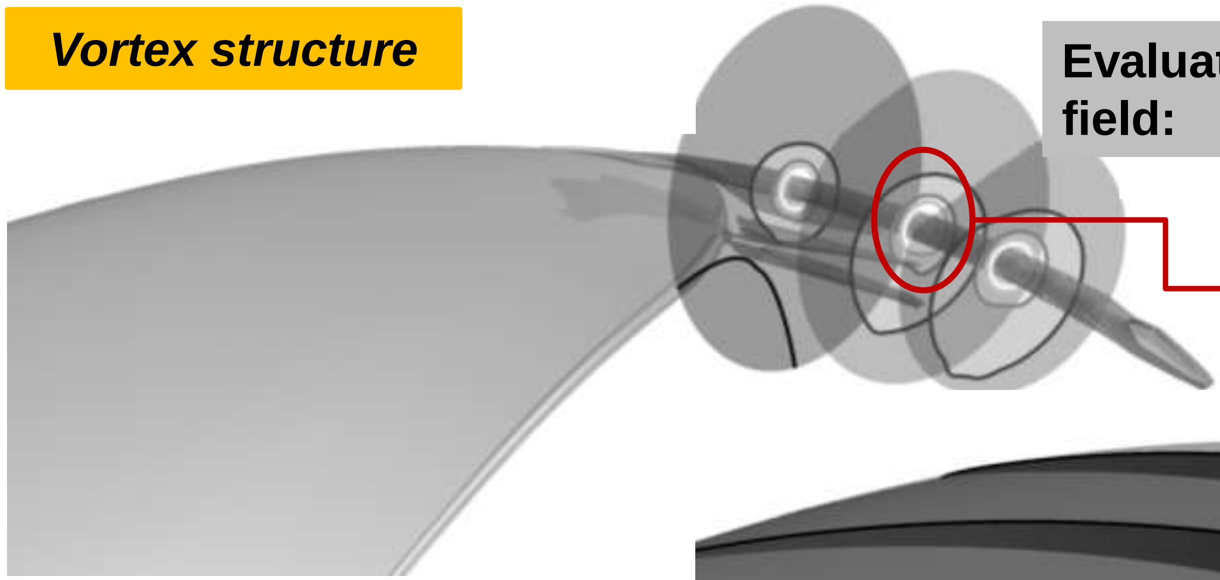

Evaluation of the velocity field:

$$r_a,\ \gamma_{ini} = \frac{\Gamma_{ini}}{\Gamma_b}$$

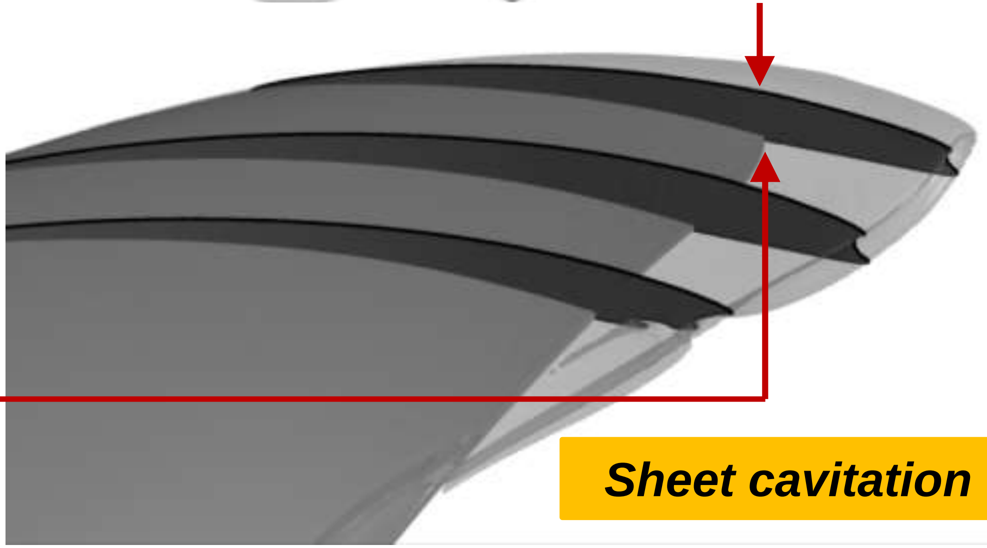

Initial cavitation radius:

$$r_{c0} = \frac{1}{2}\eta_{TE}$$

Sheet cavitation

Experimental Validation

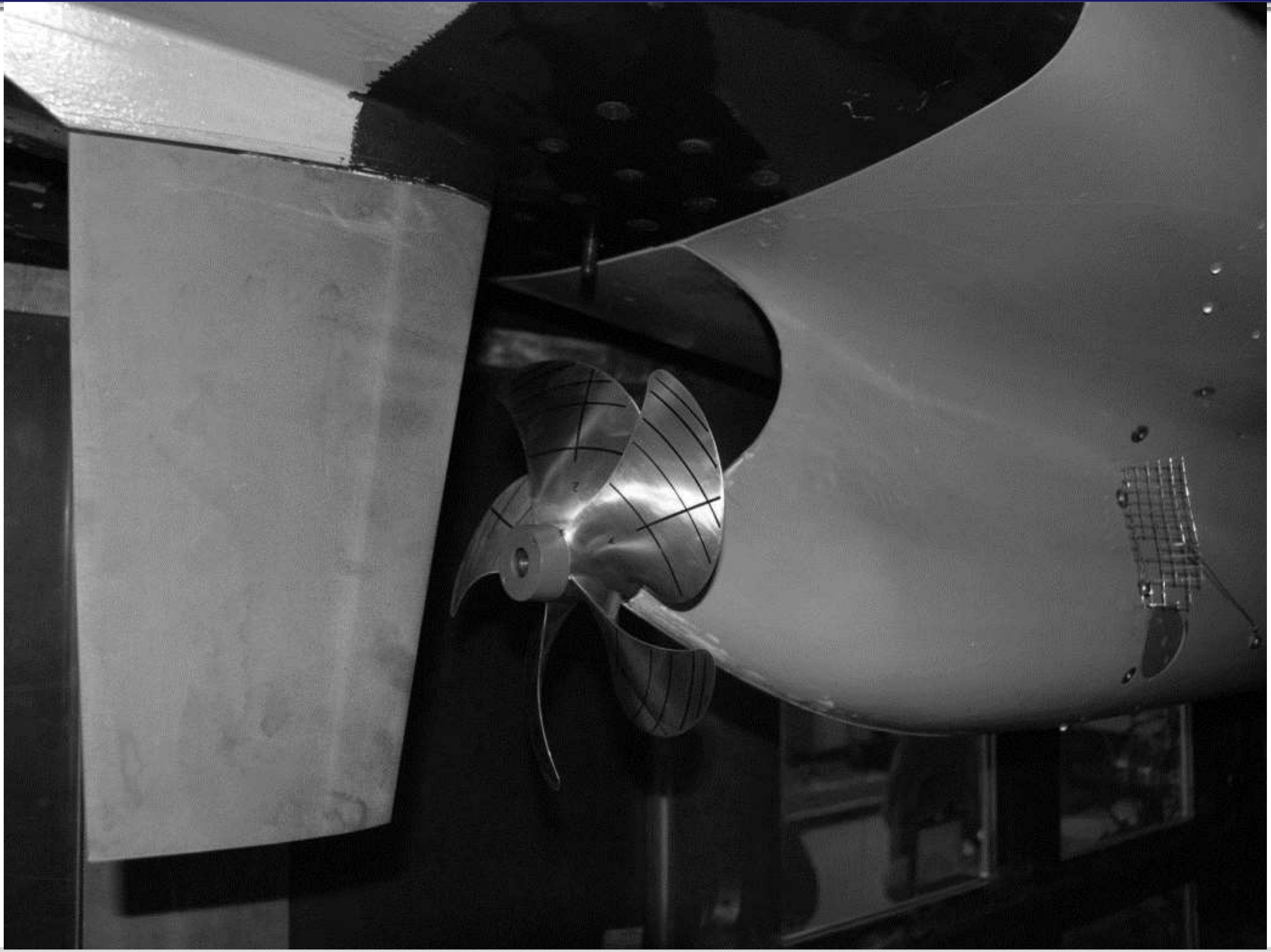

Experimental Validation

Ship C, propeller P00C

Parameter	Value
k_T	0,196
$\sigma_{n0,8}$	1,7
D	7,75 m
n	1,735 s^{-1}
V_S	23,18 kn
n_b	5

Full-scale wake

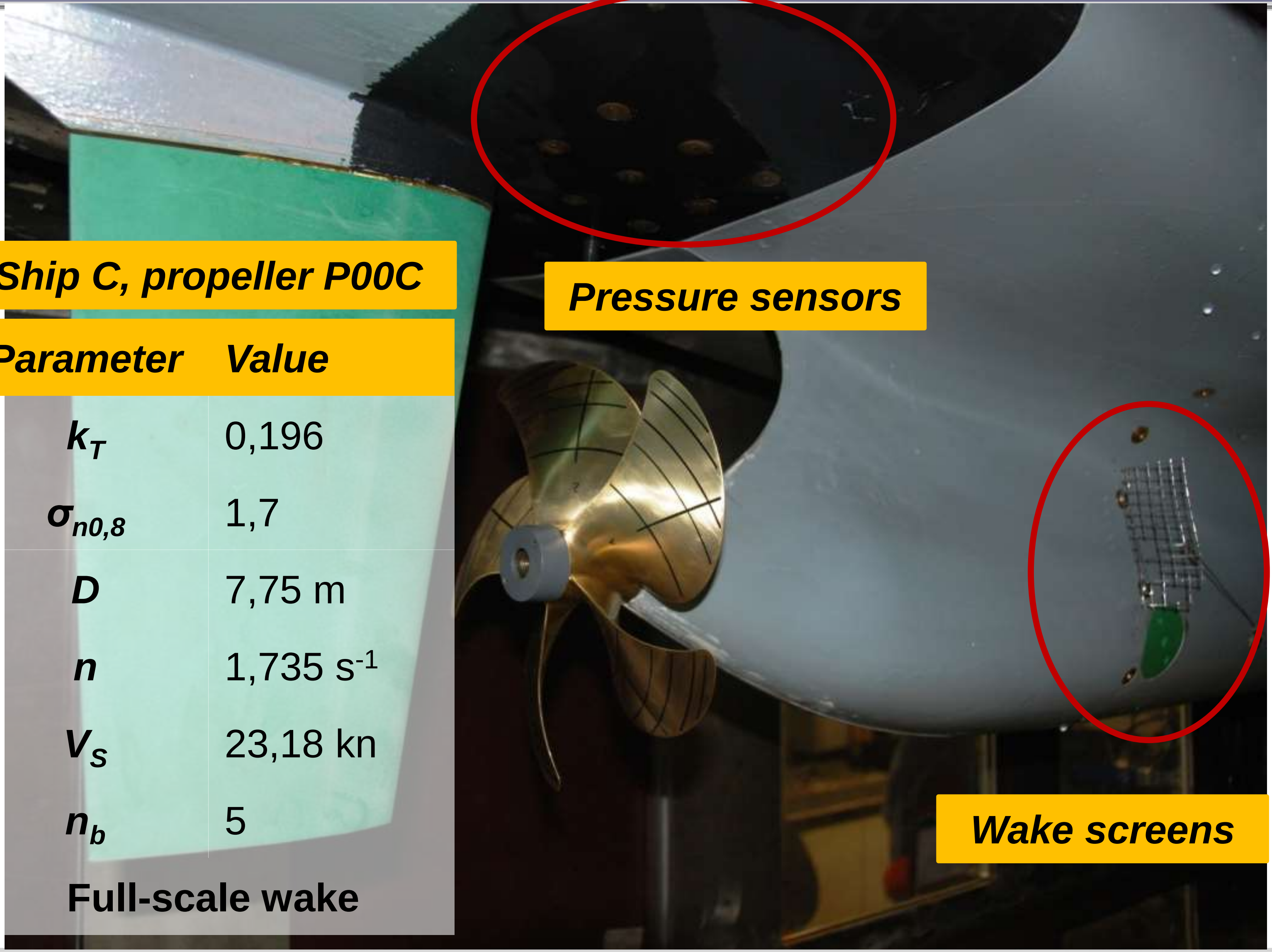

Numerical simulation

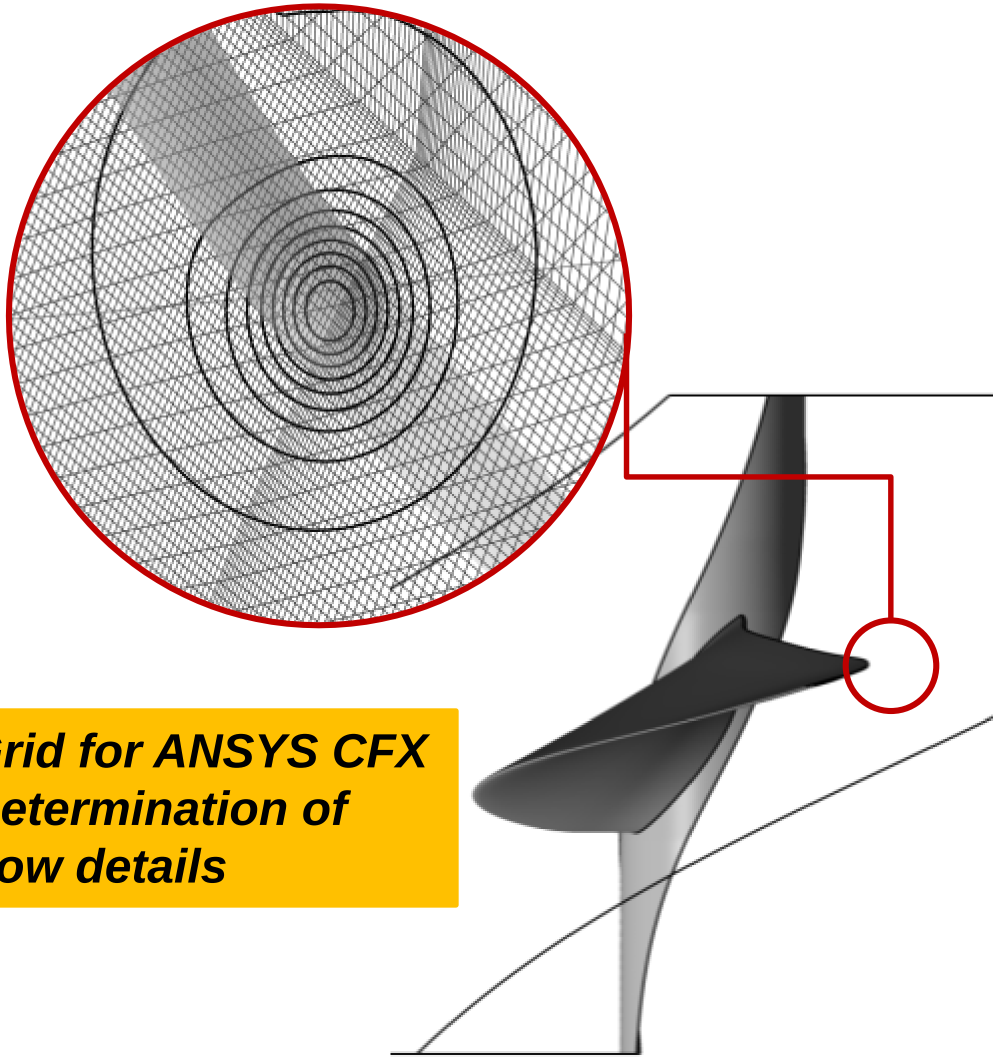

Grid for ANSYS CFX
Determination of flow details

Panelisation
panMARE

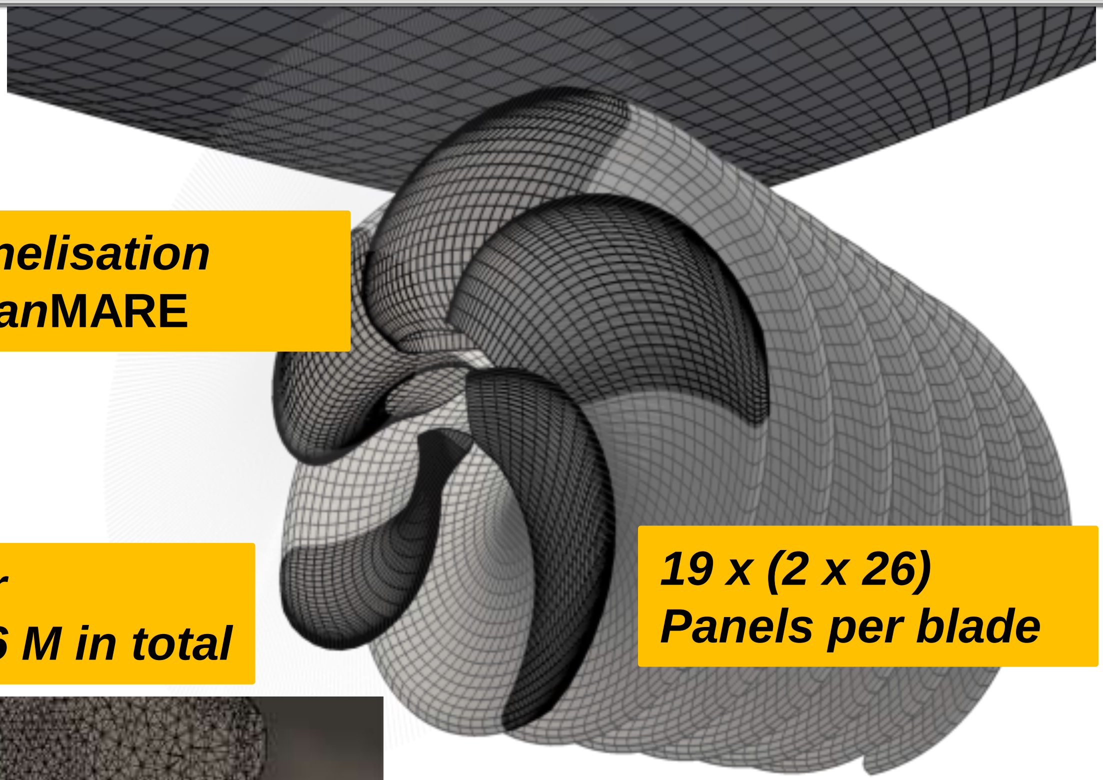

0,2 M C.V. for propeller; 5.6 M in total

19 x (2 x 26)
Panels per blade

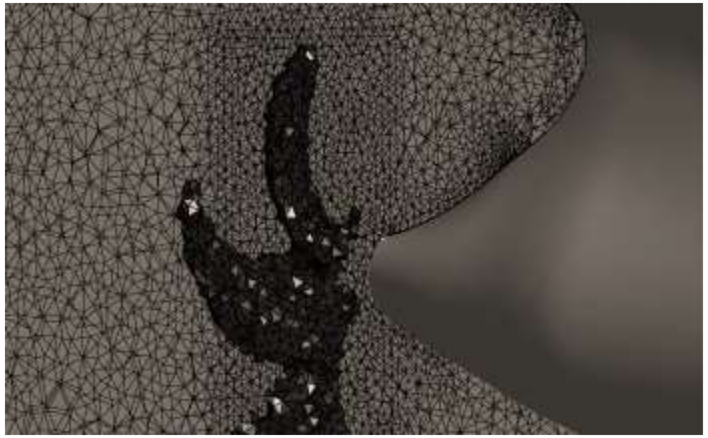

Grid for ANSYS CFX
Determination of the effective wake field

Experimental validation

Cavitation pattern

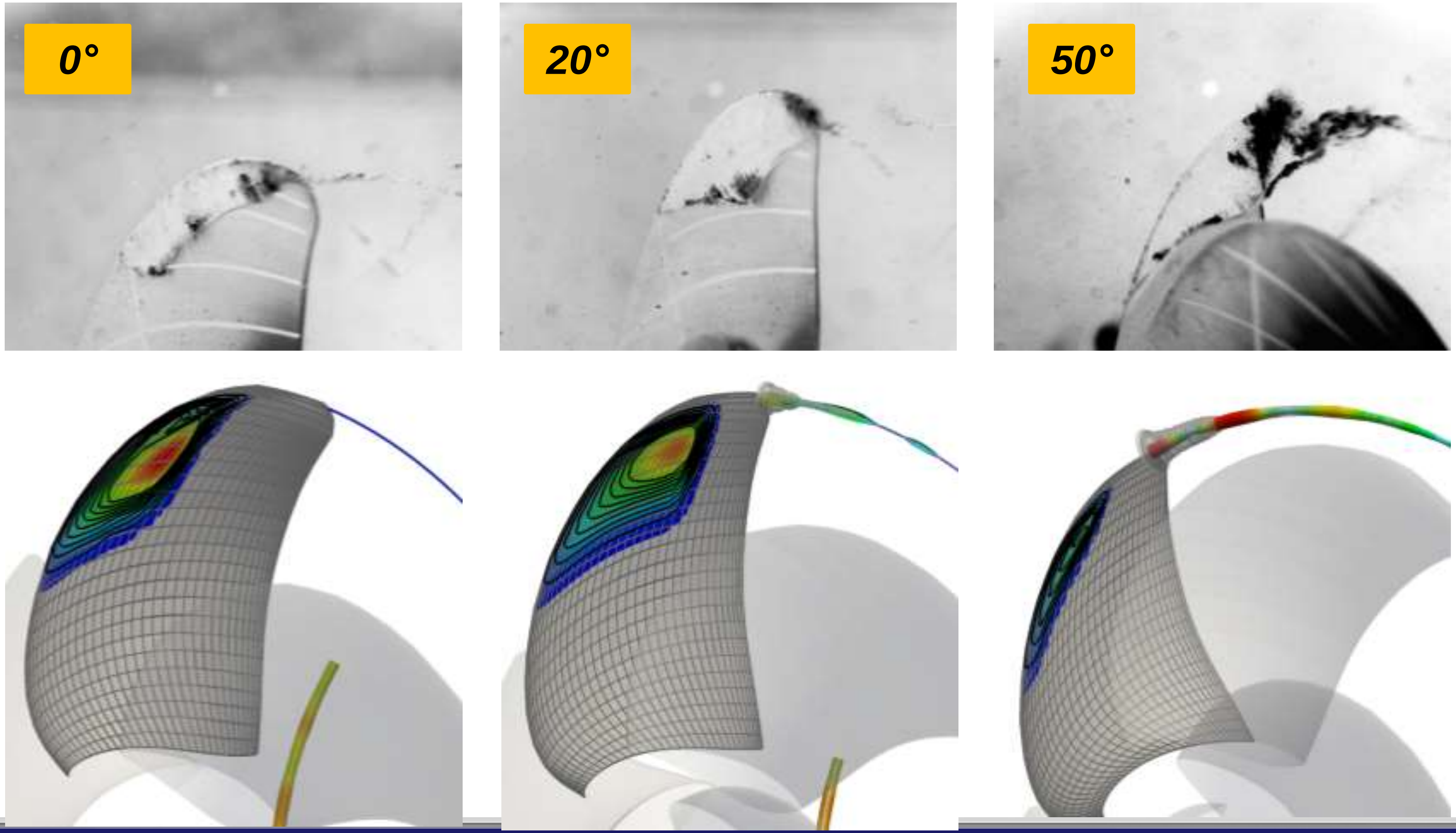

Behaviour of tip vortex cavitation

Bottom view

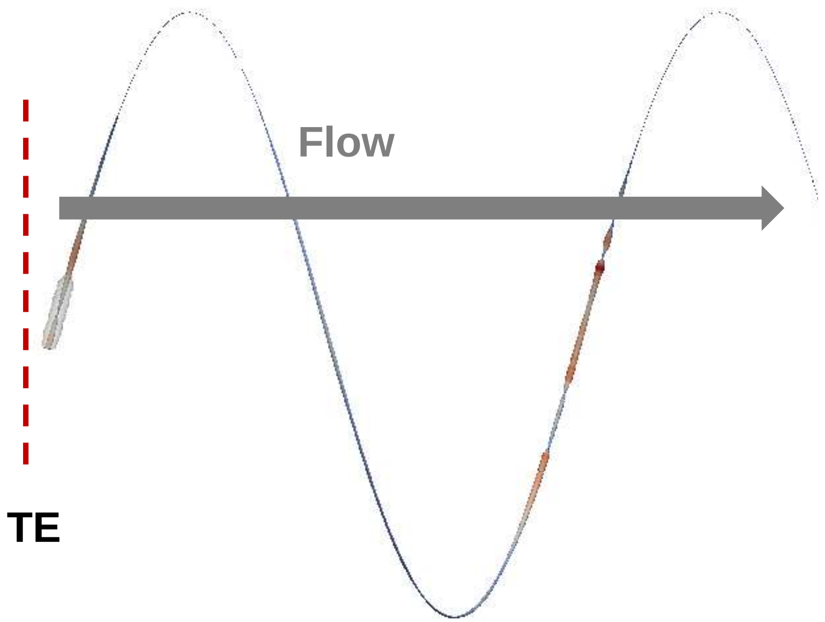

Experimental validation

Behaviour of tip vortex cavitation

Bottom view

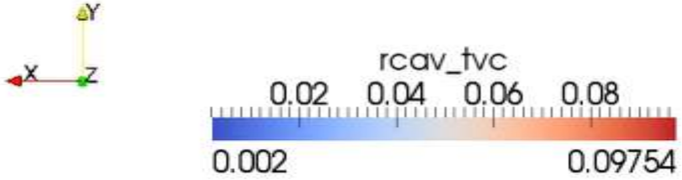

Rear view

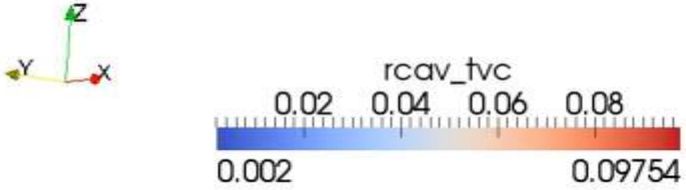

Experimental validation

Pressure fluctuations

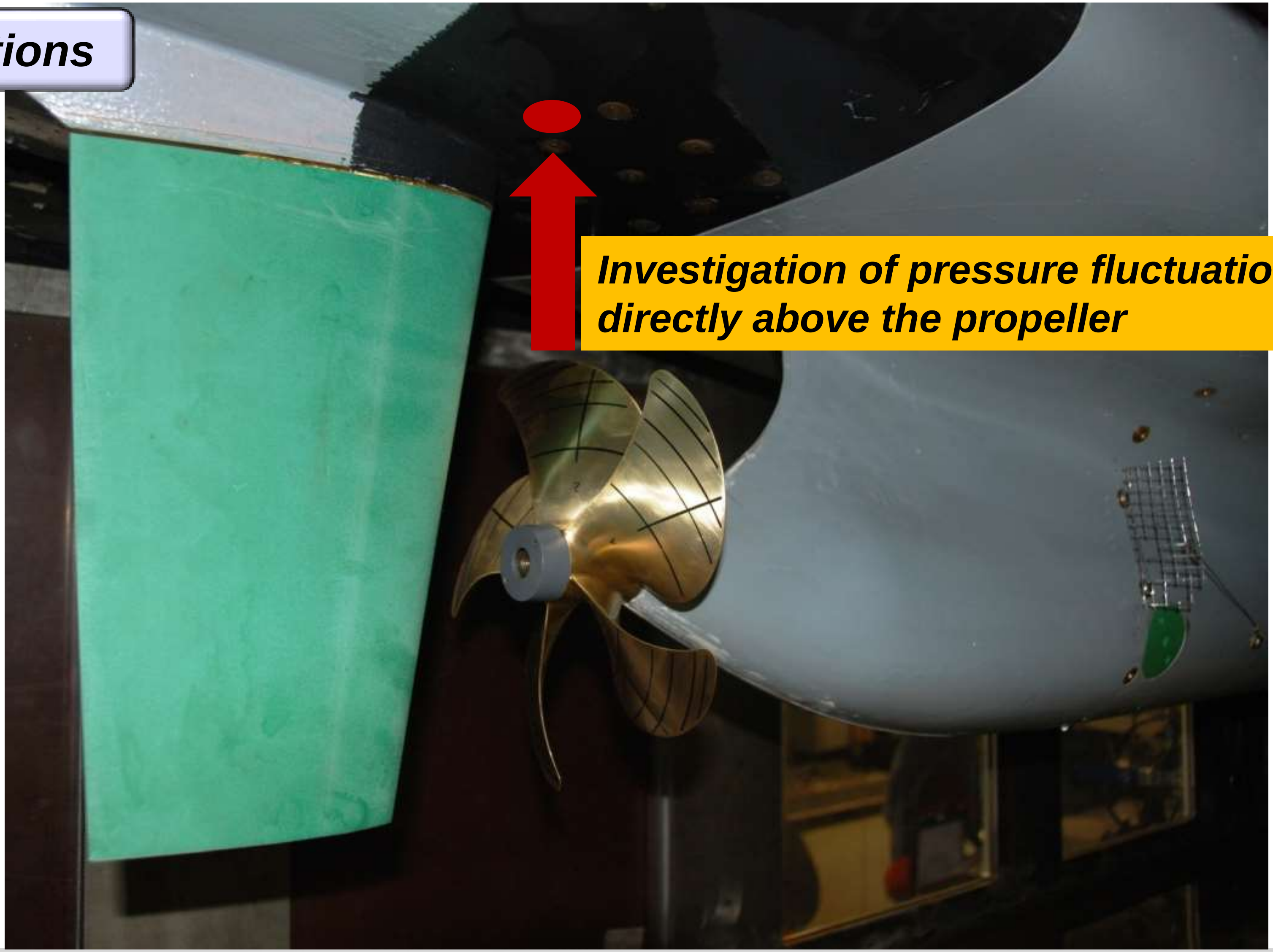

Investigation of pressure fluctuations directly above the propeller

Experimental validation

Pressure fluctuations

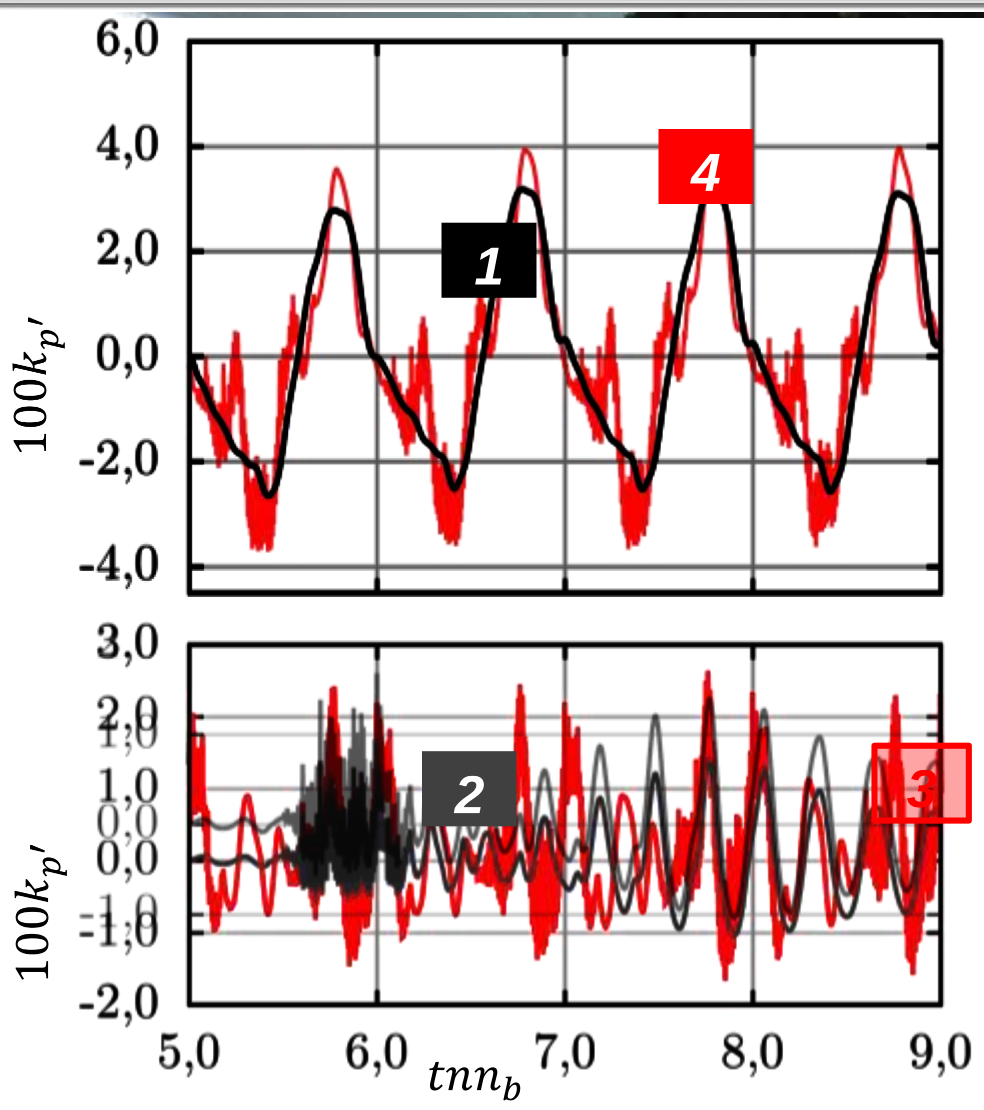

Pressure fluctuation coefficient

$$k_{p'} = \frac{p'}{\rho n^2 D^2}$$

Legend

	Simulation
1	Sheet cavitation
2	TVC, Blade
3	TVC, Propeller
4	Sheet cav. + TVC

Experimental validation

Pressure fluctuations

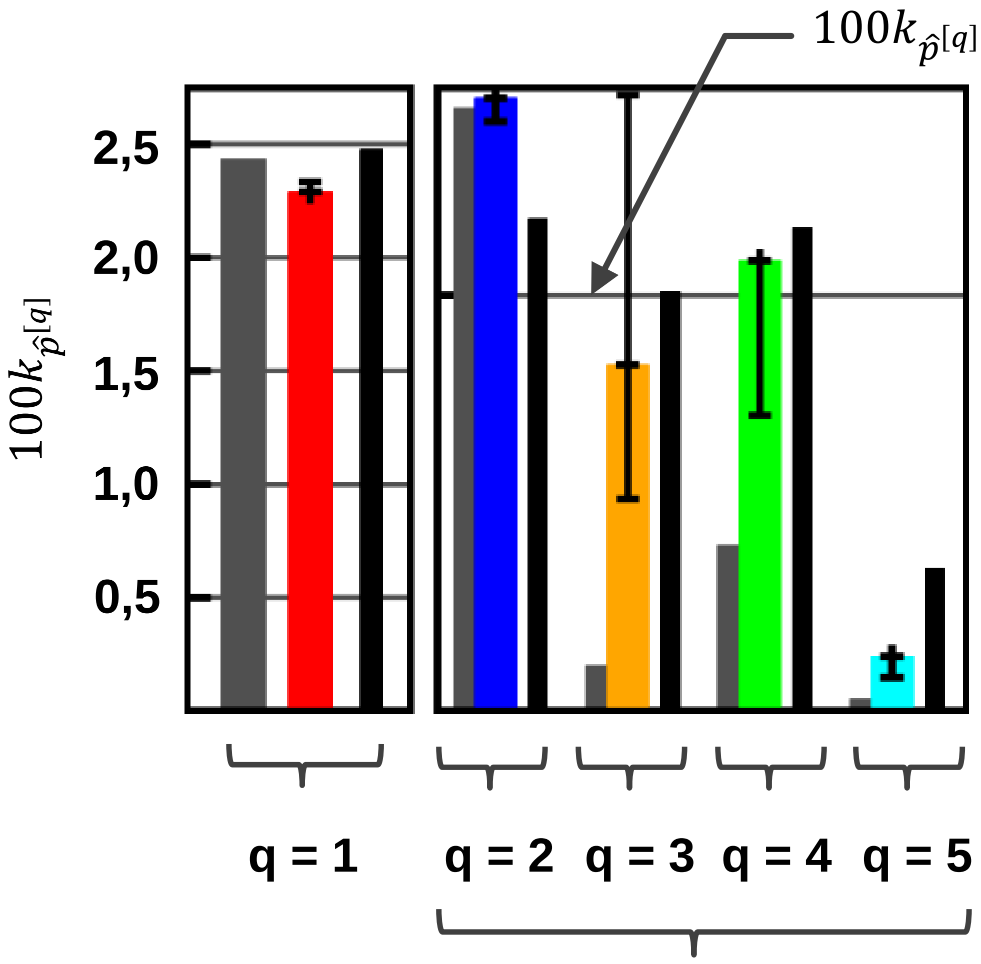

Higher order

Pressure fluctuation coefficient

$$k_{\hat{p}^{[q]}} = \frac{\hat{p}^{[q]}}{\rho n^2 D^2}$$

Legend

Experiment SVA Potsdam

Simulation

- **Sheet cav.**
- **+ TVC**

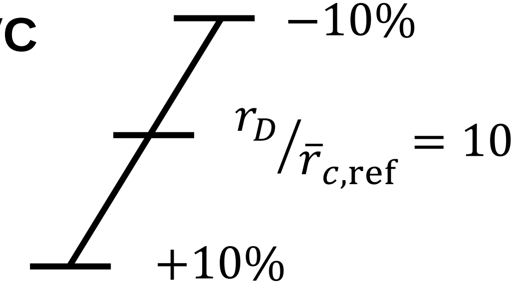

Experimental validation

Pressure fluctuations

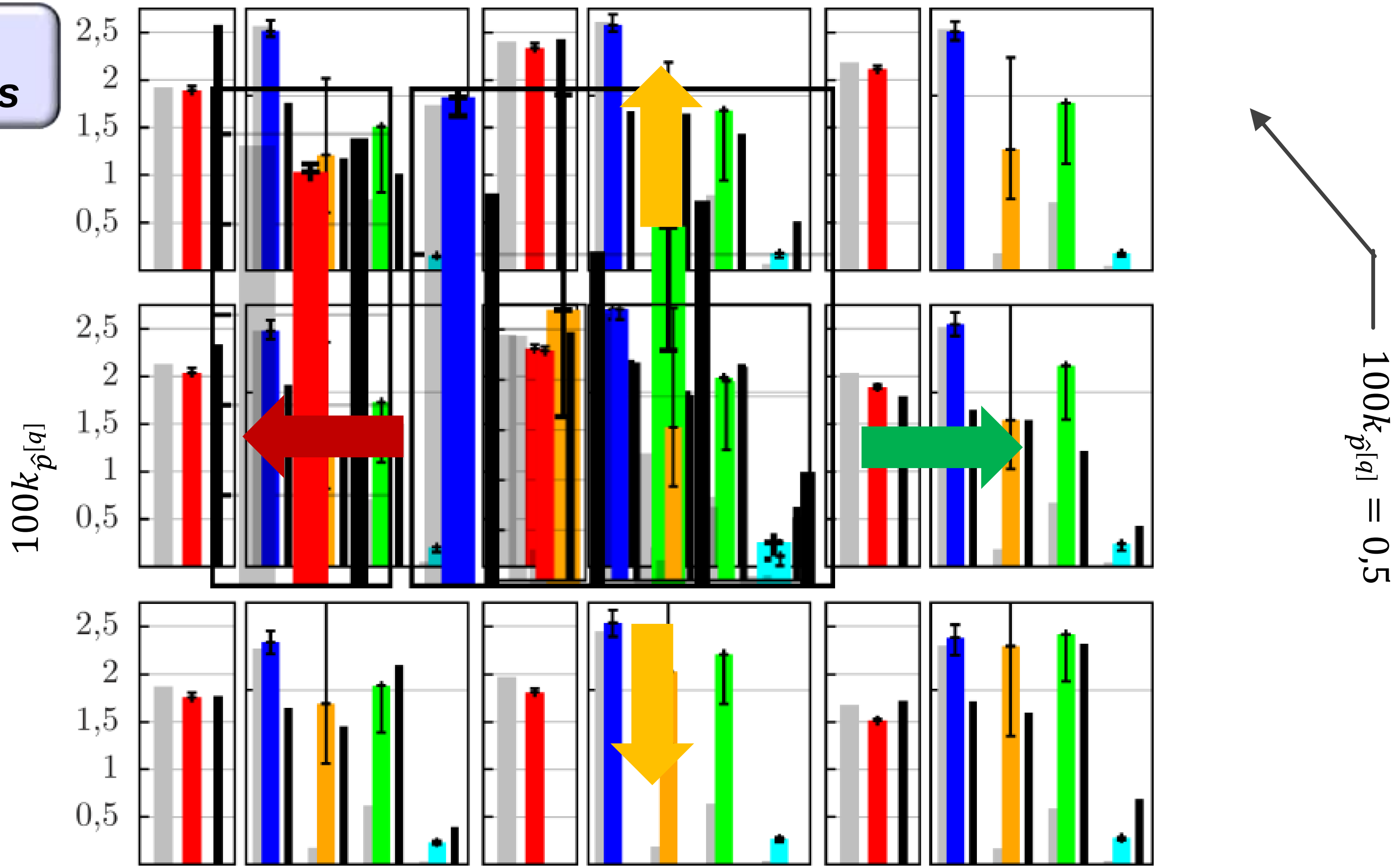

Experimental validation

Pressure fluctuations

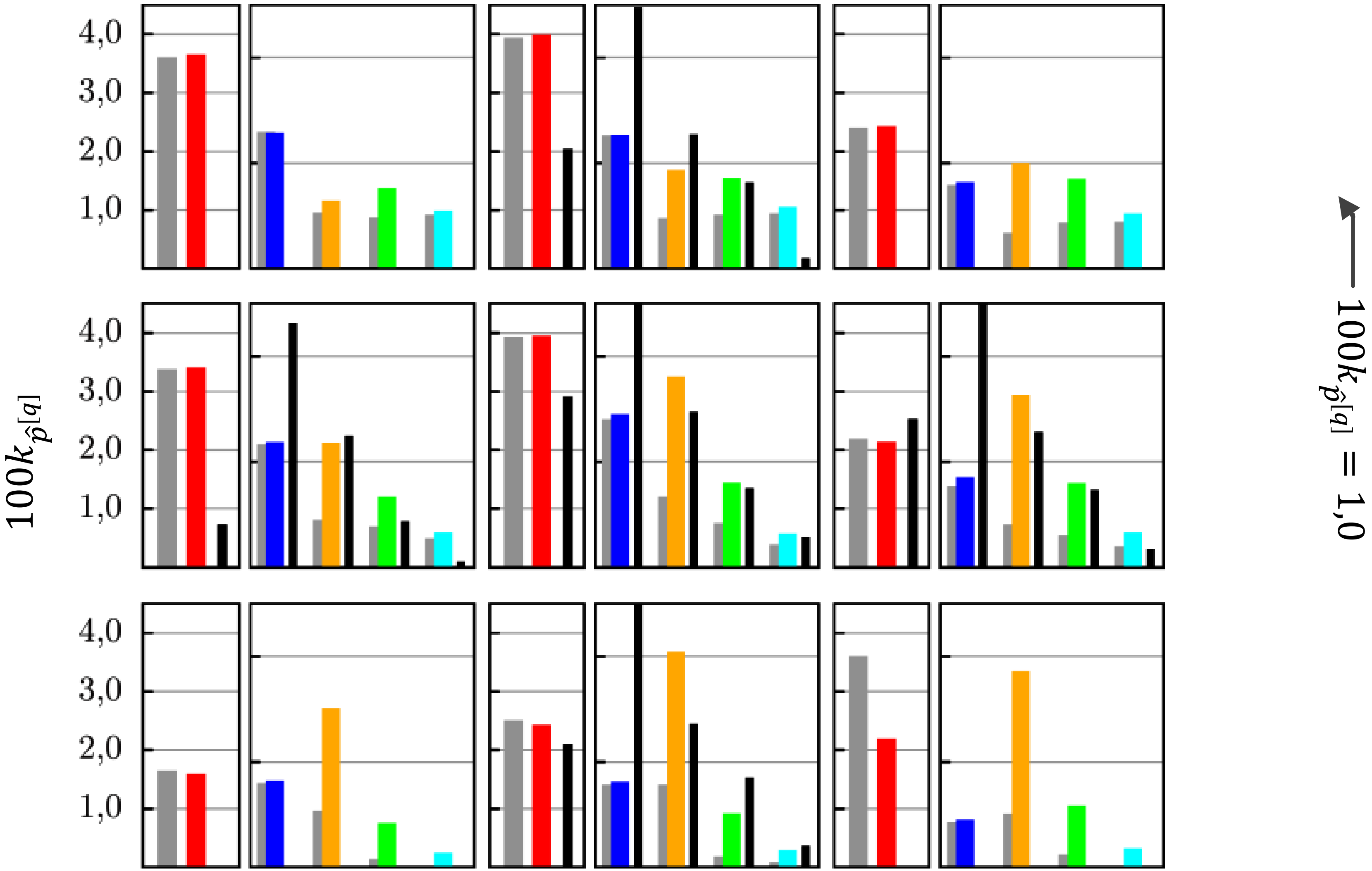

Conclusion and outlook

Conclusion and outlook

Development of a hybrid simulation method

- **Determination of the propeller load and modelling of sheet cavitation with *pan*MARE**
- **Modelling of TVC using a quasi 2-D-approach**
- **Simulation of effective wake field by using the coupling RANSE/*pan*MARE**

↓

Improved prediction of higher order pressure fluctuations

Conclusion and outlook

Further development

- **Elimination of the parameter r_D (outer radius of integration)**
- **Influence of the rudder**
- **Experimental investigation of the interaction between sheet and tip vortex cavitation**

Universität Rostock (2x)

Tip vortex is and stays a fascinating topic!

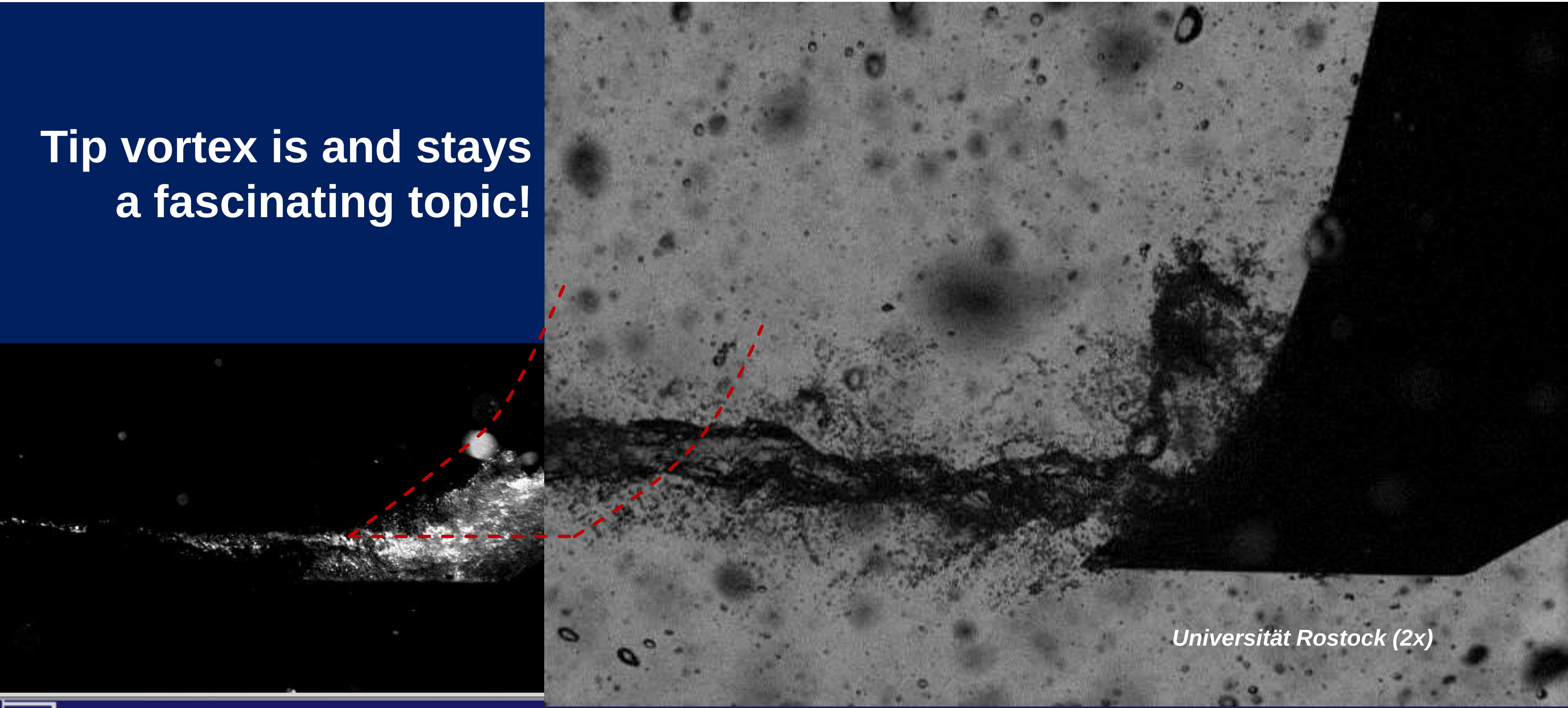

Motivation: Huge uncertainty in model tests

Cavity extent

Full Scale

- **Scale effects**
- **Test facility influence**
- **Water quality**

HYKAT

Weitendorf, E.-A. and Tanger, H., (1992), Cavitation correlation and nuclei investigation in two water tunnels- comparison in the HYKAT and the medium size tunnel, Cavitation, I mech I 1992-11, Mech. Eng. Publication Ltd, ISBN 0852988044.

Medium Tunnel

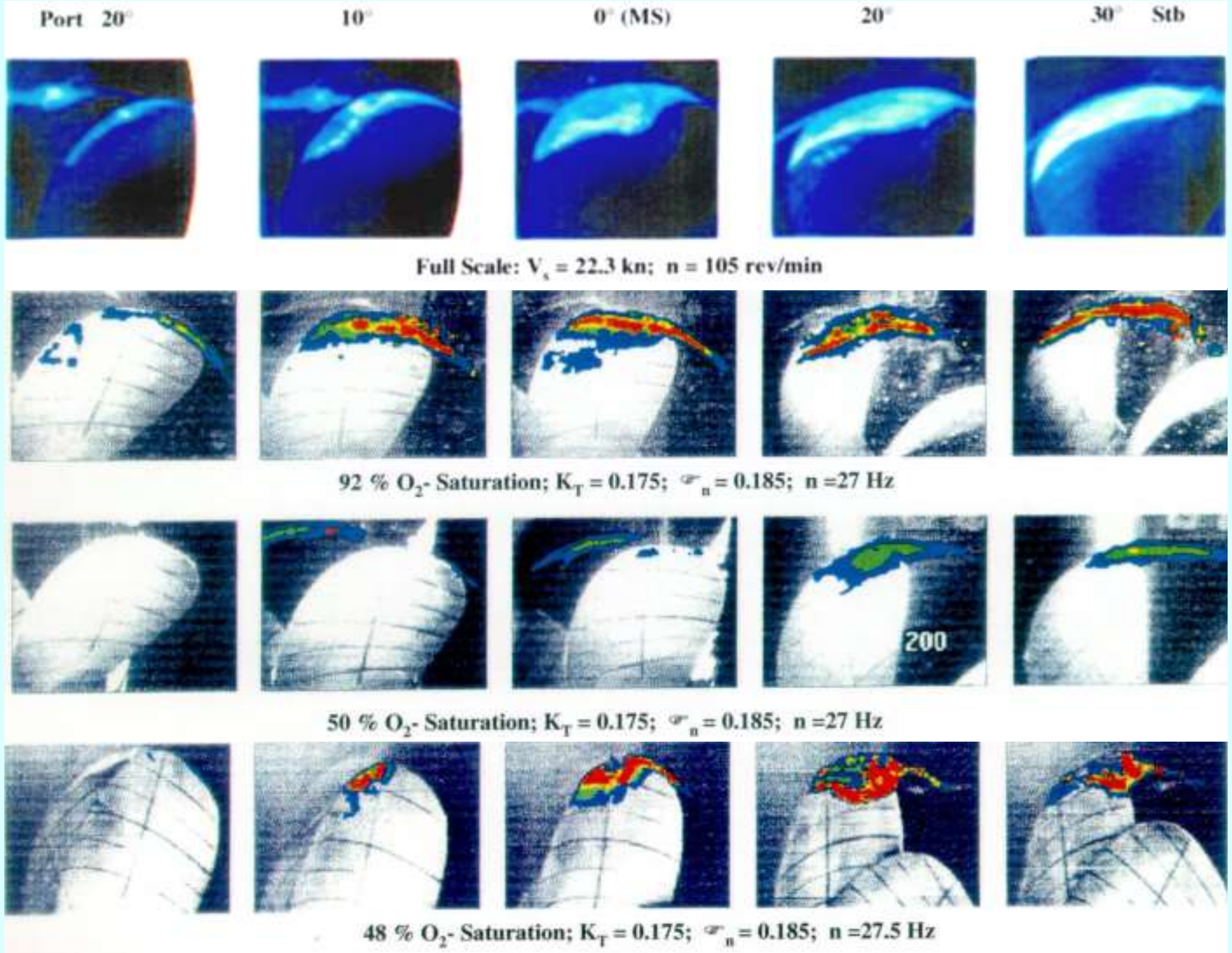

Unstable Cavitation (blue) Stable Cavitation (red)

Motivation: Huge uncertainty in model tests

Test facility influence and water quality

Time dependent HYKAT and K15A bubble concentrations c (20-230µm) with ship model for gassed and degassed O_2-saturations

Propeller loading
KT = 0.29; Cavitation number σn= 2.0

H.- J. Heinke, Chr. Johannsen, W. Kröger, P. Schiller, E.-A. Weitendorf, On Cavitation Nuclei in Water Tunnels, Proceedings of the 8th International Symposium on Cavitation CAV2012 – Paper No. 270 August 14-16, 2012, Singapore.

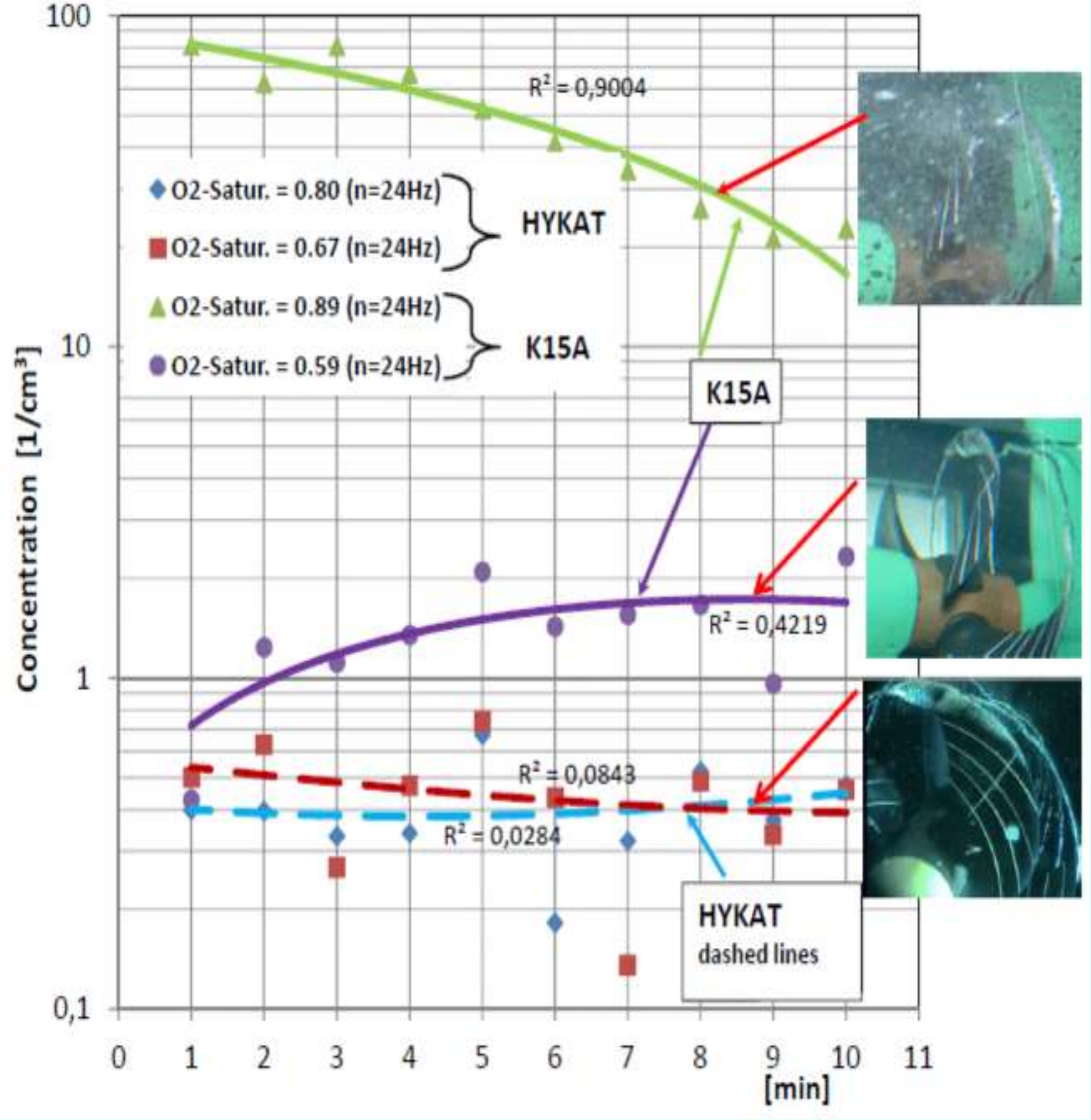

Motivation: Huge uncertainty in model tests

Water quality

Tunnel K15A without model
Oxygen saturation O_2 =77%

H.- J. Heinke, Chr. Johannsen, W. Kröger, P. Schiller, E.-A. Weitendorf, On Cavitation Nuclei in Water Tunnels, Proceedings of the 8th International Symposium on Cavitation CAV2012 – Paper No. 270 August 14-16, 2012, Singapore.

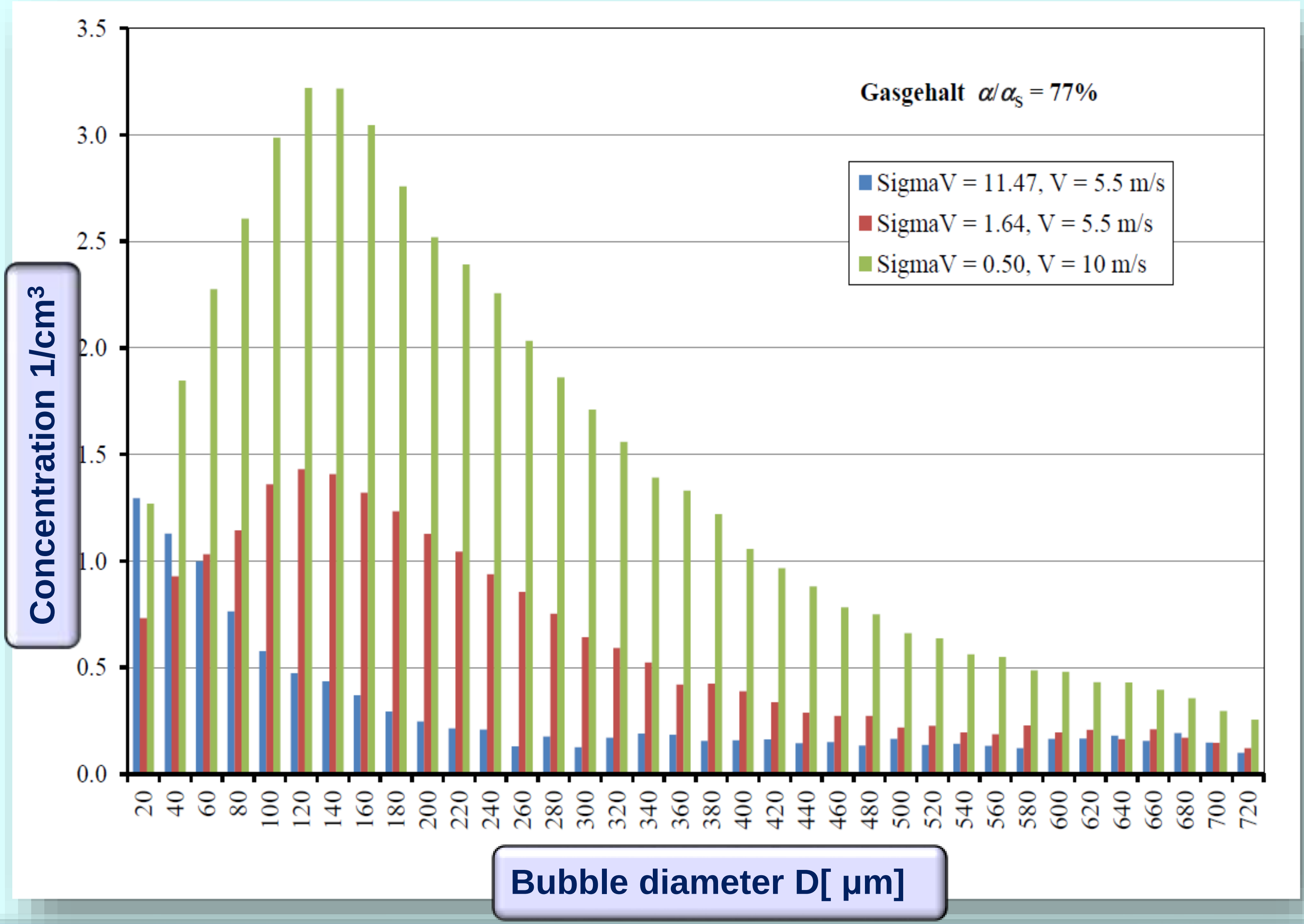

Motivation: Scale effects

Empirical relations for scale effects, A. Keller [Pasadena 2001]

Keller, Andreas Peter (2001) Cavitation Scale Effects - Empirically Found Relations and the Correlation of Cavitation Number and Hydrodynamic Coefficients,. : CAV 2001: Fourth International Symposium on Cavitation, June 20-23, 2001, California Institute of Technology, Pasadena, CA USA.

L_0, ν_0, V_0, S_0 respective reference values

***K_0* = Empirical constant depending on shape and cavitation type (!!)**

$$\sigma = \frac{P_\infty - P_V}{\frac{1}{2}\rho V_\infty^2}$$

Traditional cavitation number

$$\sigma_i = \sigma_0\left[1+\left(\frac{V_\infty}{V_0}\right)^2\right]$$

Velocity scale relation

$$\sigma_0 = k\left(\frac{L}{L_0}\right)^{1/2}$$

Size scale relation

$$k = K\left(\frac{\nu_0}{\nu}\right)^{1/4}$$

Viscosity scaling

$$K = K_0\left(1+K_0\frac{S}{S_0}\right)$$

Turbulence scaling

$$\sigma_i = K_0\left(\frac{L}{L_0}\right)^{1/2}\left(\frac{\nu_0}{\nu}\right)^{1/4}\left[1+\left(\frac{V_\infty}{V_0}\right)^2\right]\left(1+K_0\frac{S}{S_0}\right)$$

universal empirical scaling relation σ_i

Motivation

Main aim

Development and application of a cavitation model which can consider water quality and its influence on cavitation behaviour and pressure fluctuations.

⇒ Support for full scale prediction.

Main approaches to cavitation simulation

(1) **Eulerian**

(mass-transfer; (non-)unique kinematics)

(2) **Lagrangian**

(discrete particle tracking in Eulerian liquid)

Each has its drawbacks and benefits

(effort, accuracy, capability)

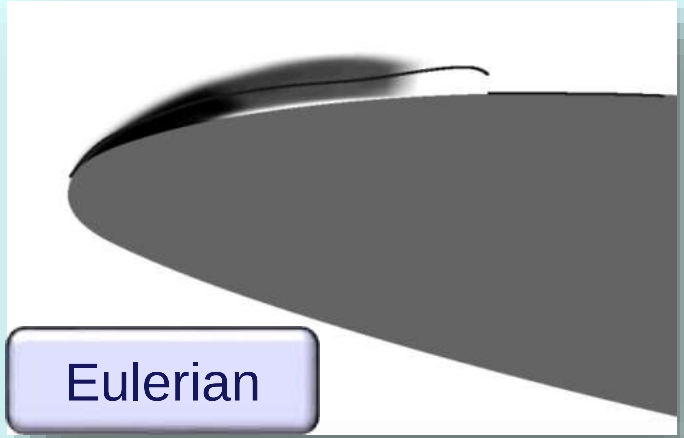

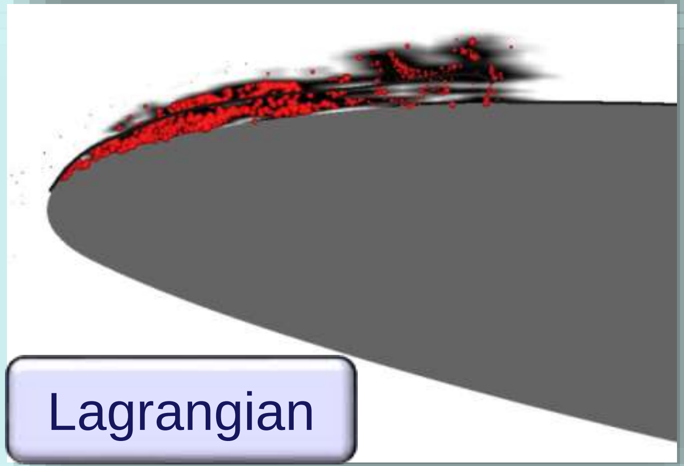

Computational framework

Fluid modelled as mixture of incompressible components

Liquid – vapour bubbles

- **Mixture governed by Navier-Stokes equations**

$$\frac{\partial(\rho U_i)}{\partial t} + U_k \frac{\partial(\rho U_i)}{\partial x_k} - \frac{\partial}{\partial x_k}\left(\tau_{ik} - p\delta_{ik}\right) - f_i = 0 \,, \qquad \frac{\partial \rho}{\partial t} + \frac{\partial(\rho U_k)}{\partial x_k} = 0$$

- **Eulerian mixture obtained from FreSCo+**
  - cell-centered finite volume; segregated algorithm
  - unstructured grids; 2nd order in space & time
  - modified SIMPLE scheme for pressure-velocity coupling
  - RANS/DES/LES turbulence models

Mixture properties (density and viscosity)

- **Computed from partial properties of fluid (l),** NCG, **vapour (v)**

$$r = a r_v + (1 - a) r_l \qquad a = \frac{V_v}{V_v + V_l}$$

$$m = a m_v + (1 - a) m_l$$

- **How to compute α ?**
  - Euler-Euler
  - Euler-Lagrange
  - combined Euler-Euler/Lagrange

Bubble is modelled as a sphere moving in the mixture

Contribution: Dr. Sergey Yakubov

Trajectory is described by the bubble-momentum equation

$$m^b \frac{dV_i}{dt} = \underbrace{\left(m^b - m^m\right) g_i}_{\text{Buoyancy}} + \underbrace{m^m \frac{dU_i}{dt}}_{\text{Fluid accel.}} - \underbrace{\frac{m^m}{2}\left(\frac{dV_i}{dt} - \frac{dU_i}{dt}\right)}_{\text{Added mass}} + \underbrace{F_i^D}_{\text{Drag}} + \underbrace{F_i^L}_{\text{Lift}} + \underbrace{F_i^V}_{\Delta\text{Vol.}}$$

… and thus follows it's
own directions

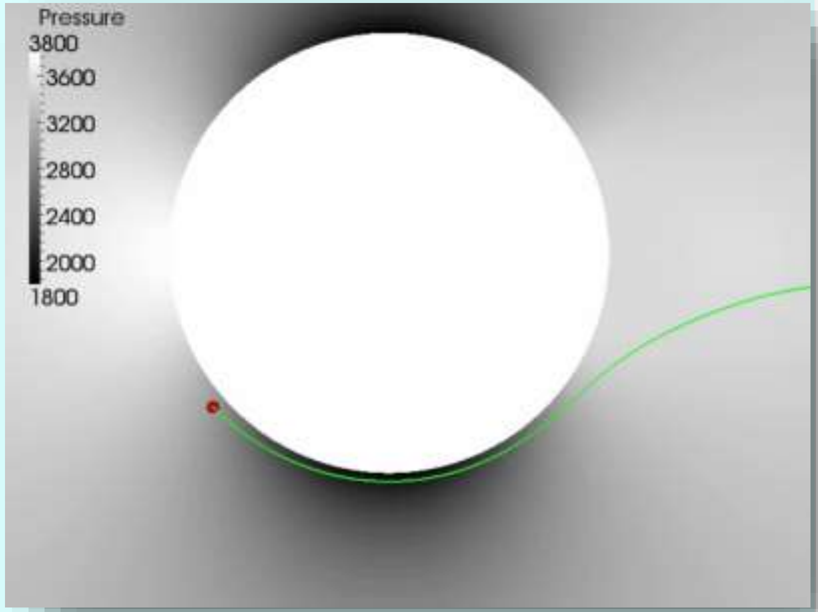

Bubble is modelled as a sphere moving in the mixture

Rayleigh-Plesset equation determines radius evolution

$$\ddot{R}R + \frac{3}{2}\dot{R}^2 = \frac{1}{\rho^m}\left[p^v - p^g - p^\infty - \frac{2\sigma}{R} - \frac{4\mu^m}{R}\dot{R}\right] - \frac{(U_i - V_i)^2}{4}$$

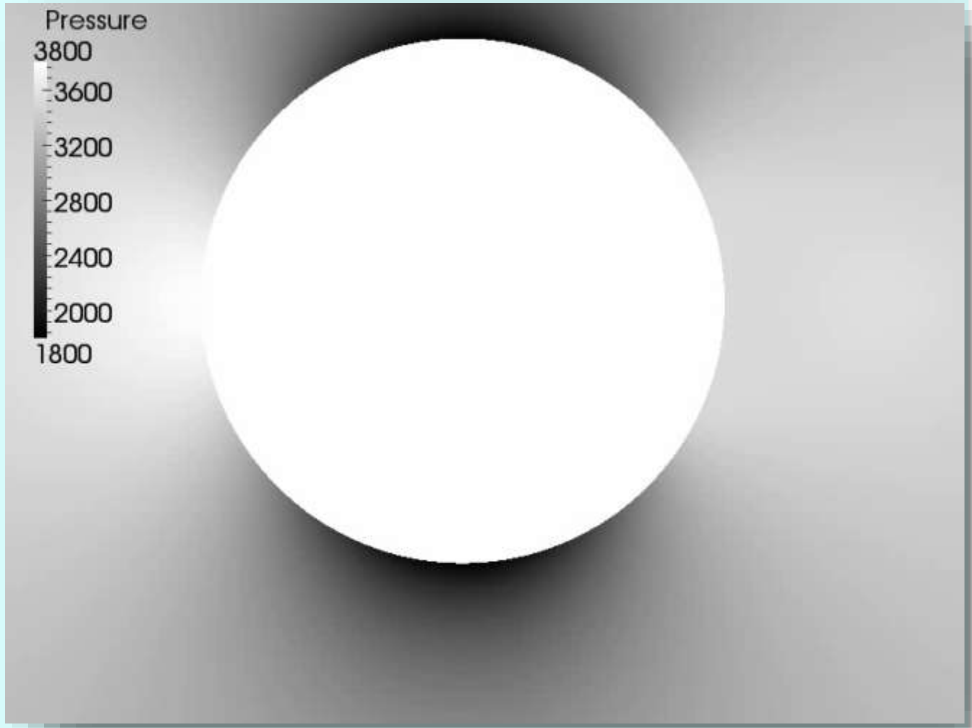

… which needs to be mapped to the mixture field

Cavitation modelling - Euler-Lagrange approach

Mapping bubbles to compute vapor volume fraction in cell

Procedure uses Gaussian interpolation

$$\boxed{\alpha_p = \sum_{i=1}^{n_b} \Omega(\mathbf{x}_p, \mathbf{x}_b) V_b}$$

$$\Omega(\mathbf{x}, \mathbf{x}_b) = \left[e^{-\frac{\sum_{k=1}^{3} (x_k - x_{b,k})^2}{2\sigma^2}} \right] \Bigg/ \left[\sum_{i=1}^{n} e^{-\frac{\sum_{k=1}^{3} (x_{i,k} - x_{b,k})^2}{2\sigma^2}} V_i \right]$$

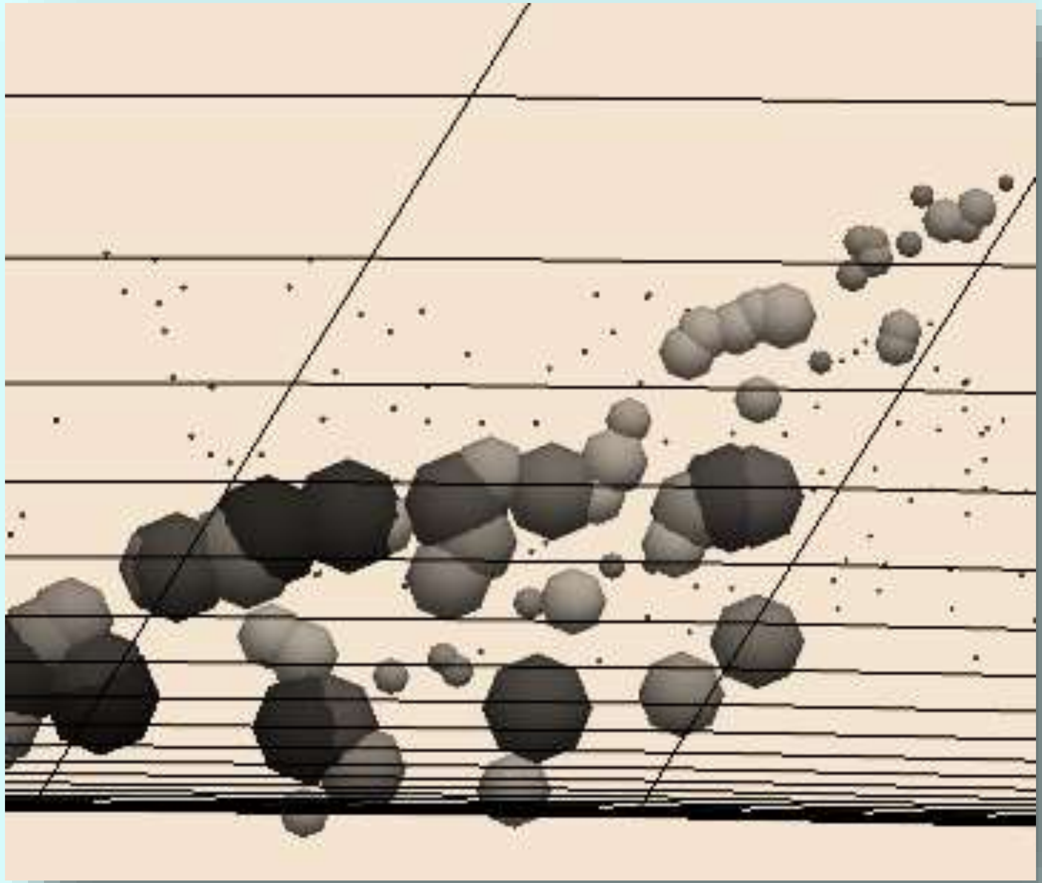

Cavitation modelling - Euler-Lagrange approach

Statistical nuclei initialization

- Statistical distribution obtained from experimental data
- Mimic different water qualities (different tunnels, ocean)

prescribe bubble spectrum

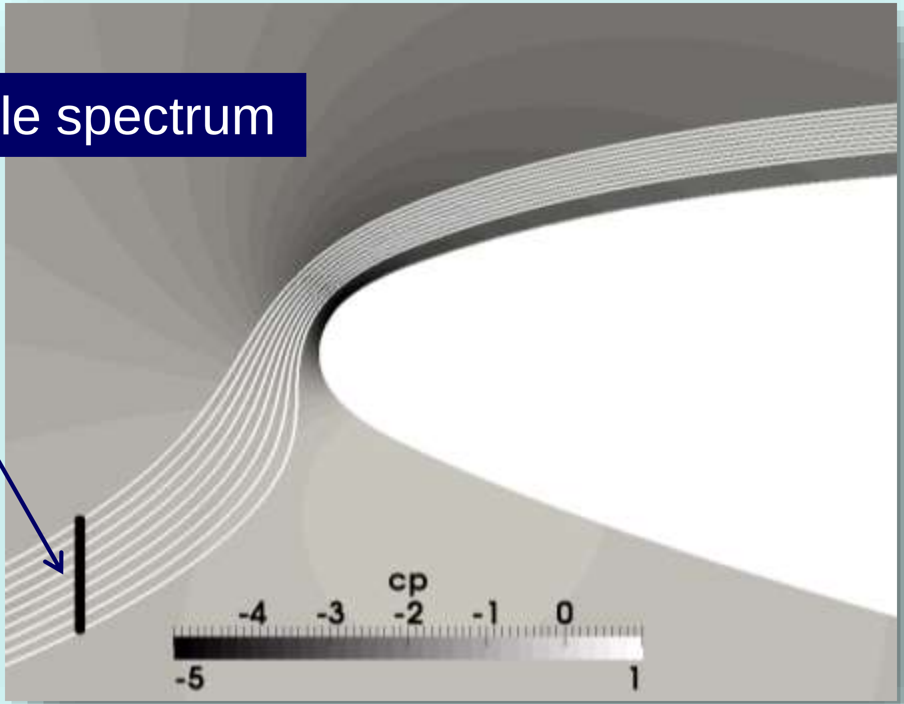

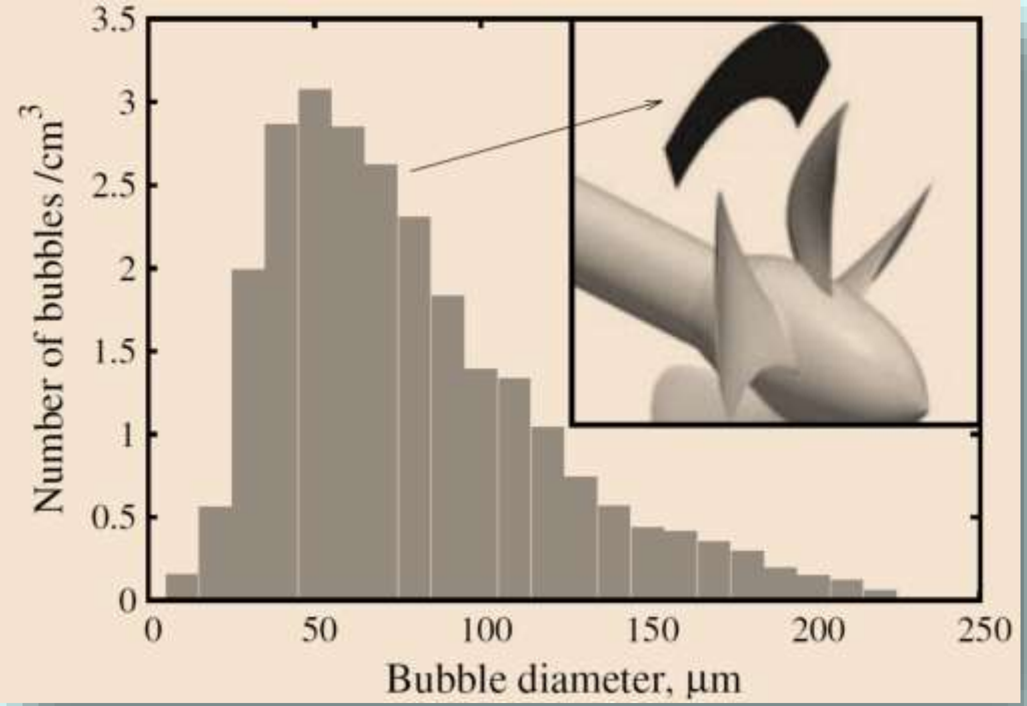

Cavitation modelling - combined approach

Euler-Euler

- Reasonable prediction of sheet cavitation
- Moderate computational effort
- Restricted to simplified dynamics, insensitive to water quality

Euler-Lagrange

- Full bubble dynamics, captures water quality effects
- Large computational effort

Euler-Euler can be used in large cavitation regions

Euler-Lagrange can be used in smaller regions of special interest (e.g. tip vortex) or for cavitation inception detection

Acoustic pressure from cavitating small bubbles

Contribution: Patrick Schiller

Bubble grows where $p_\infty < (p_v + p_g)$ and reaches its maximum after it passes the minimum pressure location.

It starts to collapse in increasing pressure, executes volume oscillations causing an acoustic signal.

Resulting acoustic pressure $P_{ac}(t)$ is proportional to acceleration of bubble volume

$$P_{ac} = \frac{\rho}{4\pi L} \frac{d^2 V_b}{dt^2}$$

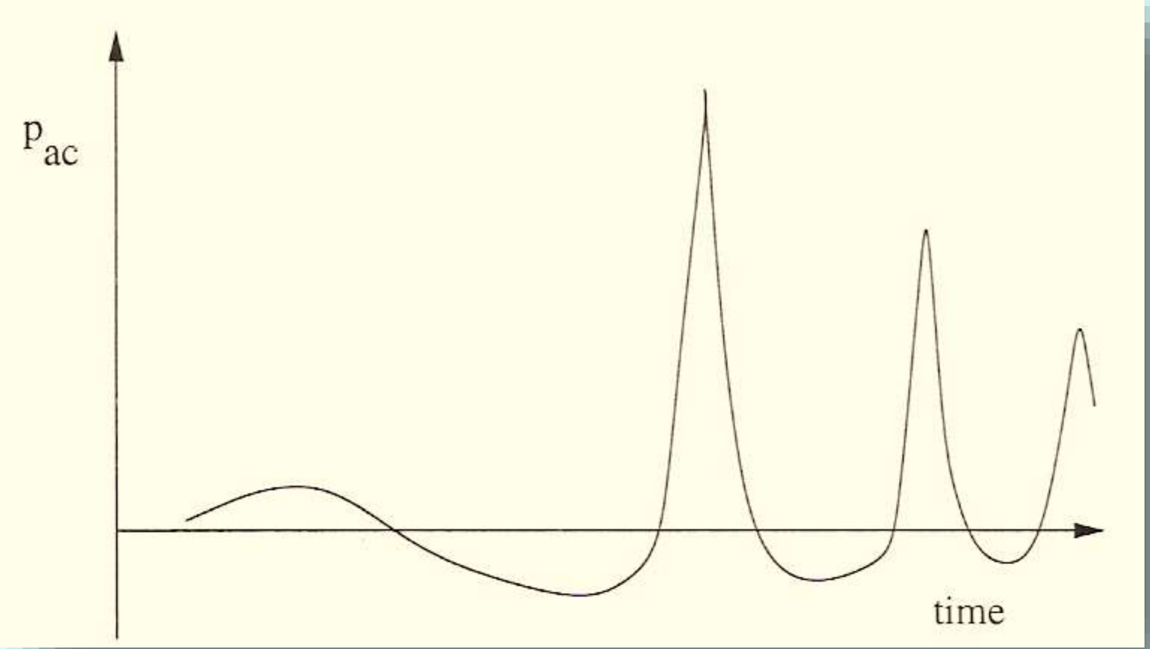

Typical time behaviour of $p_{ac}(t)$ for a cavitating single vapour bubble with non-condensable gas

Instantaneous acoustic pressure

Considering the delay time of a pressure signal caused by a bubble at a distance L from a fixed observer and the speed of sound in liquid.

$$t' = t - L/a$$

$$V_b\,(t') = \frac{4}{3}\pi R^3(t')$$

$$P_{ac}(t) = \frac{R(t')}{L}\rho\left(R(t')\ddot{R}(t') + 2\dot{R}(t')\right)$$

Already known through solution of Rayleigh-Plesset equation

$R = R(t')$, $\dot{R}(t') = \frac{d\,R(t')}{dt'}$ **and** $\ddot{R}(t') = \frac{d\,\dot{R}(t')}{dt'}$

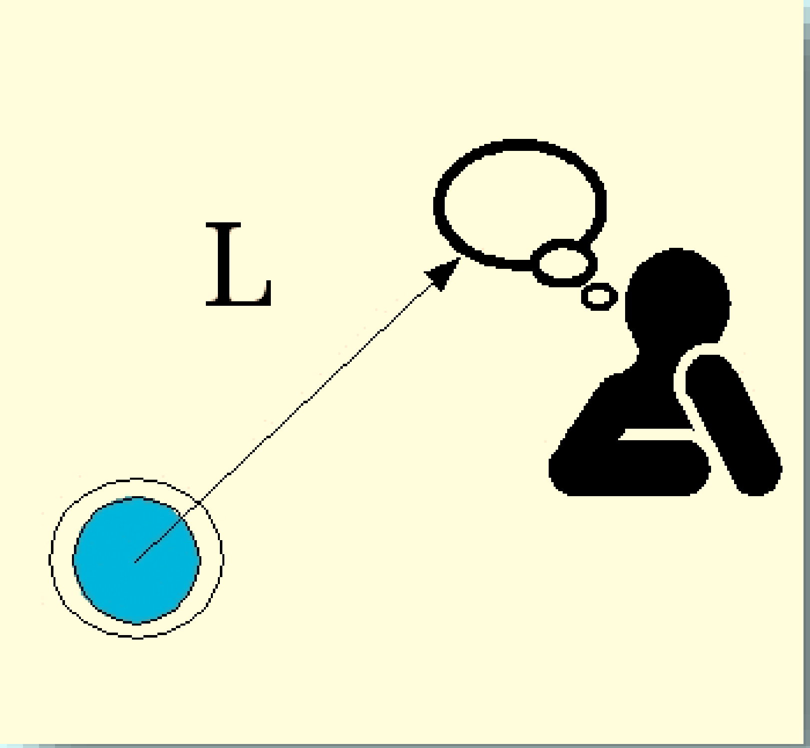

Time record of acoustic pressure

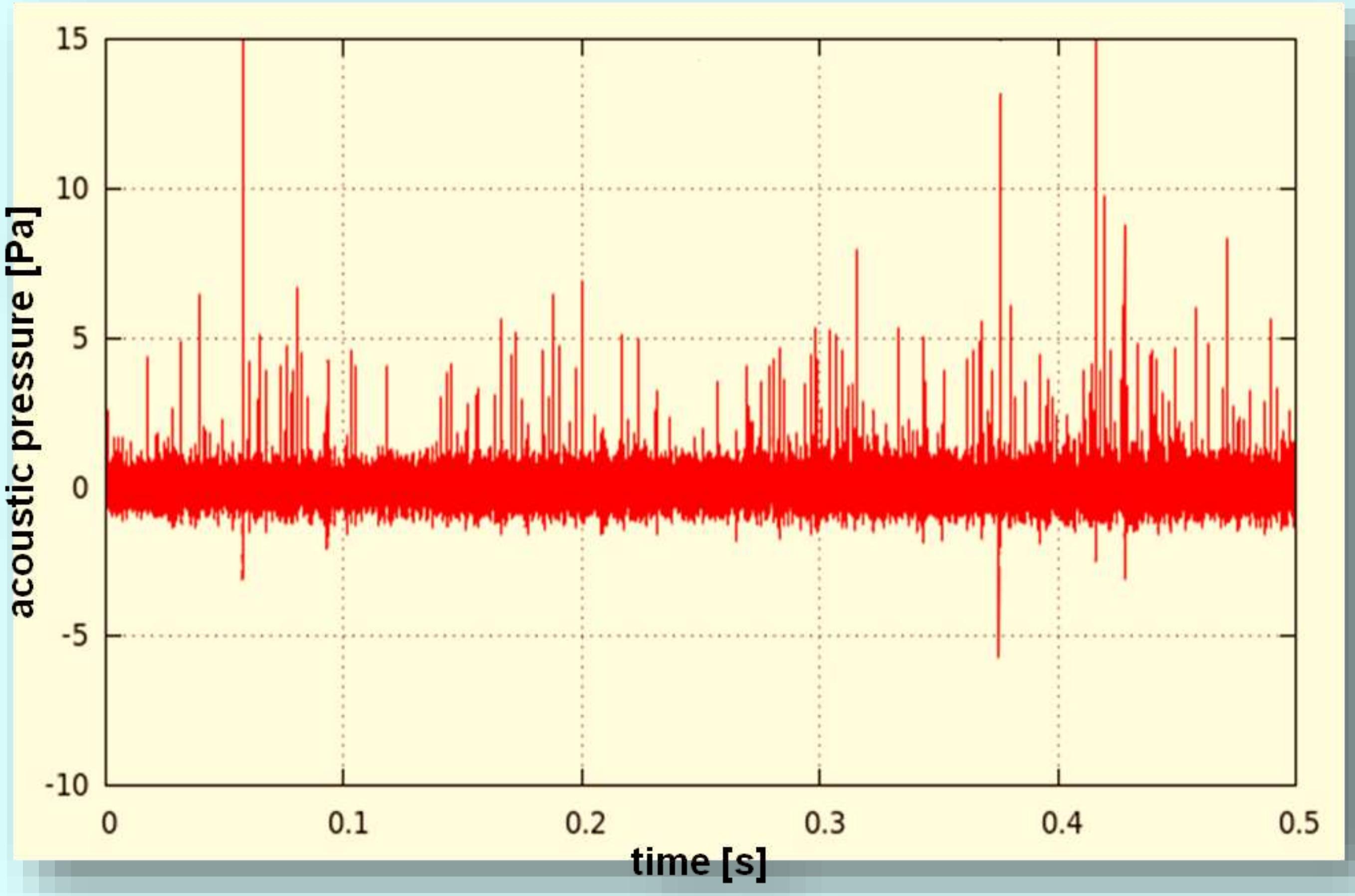

Acoustic pressure

FFT Analyses

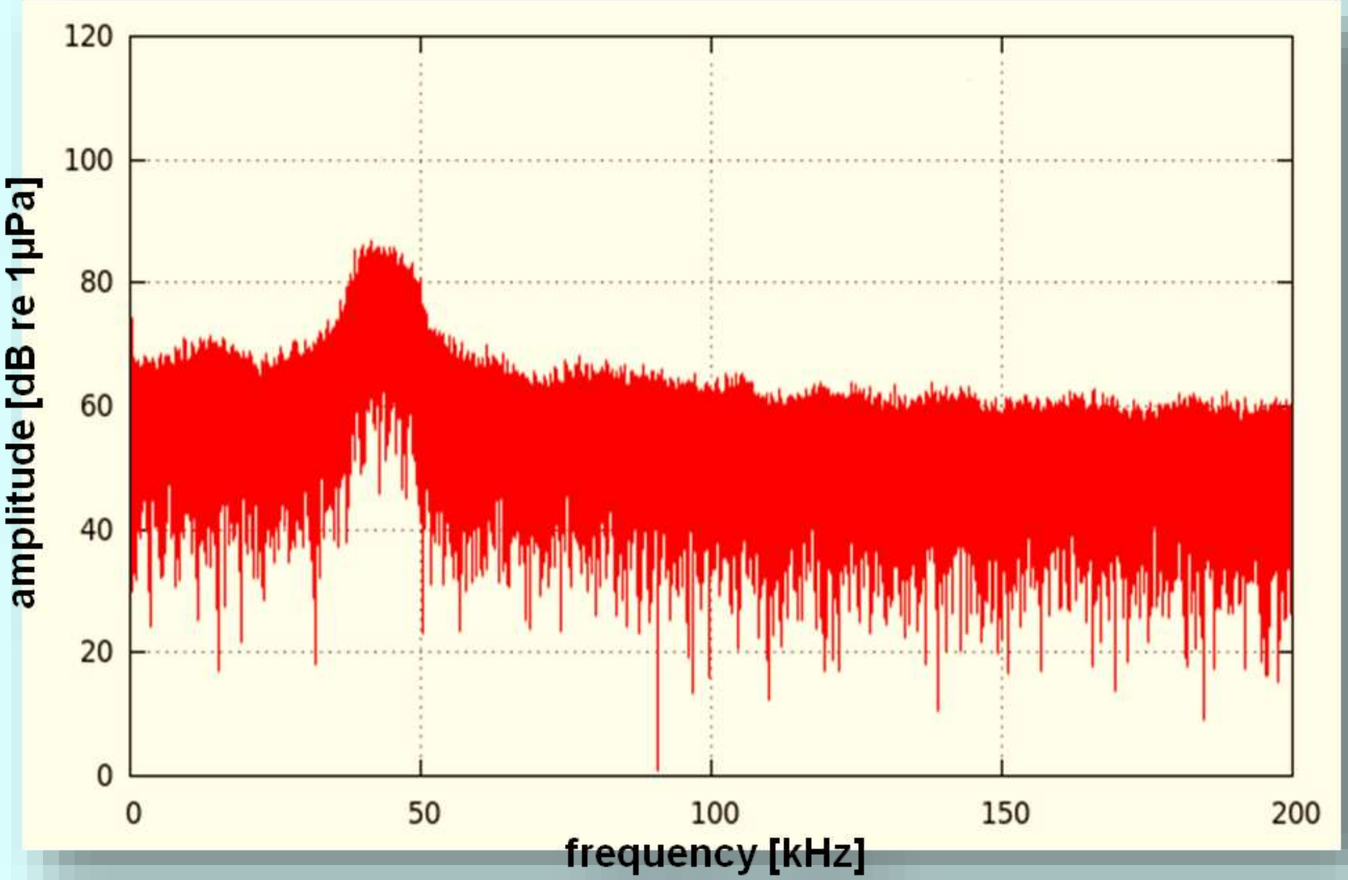

Cavitation nuclei characterization

Interferometric Particle Imaging (IPI-Technology)

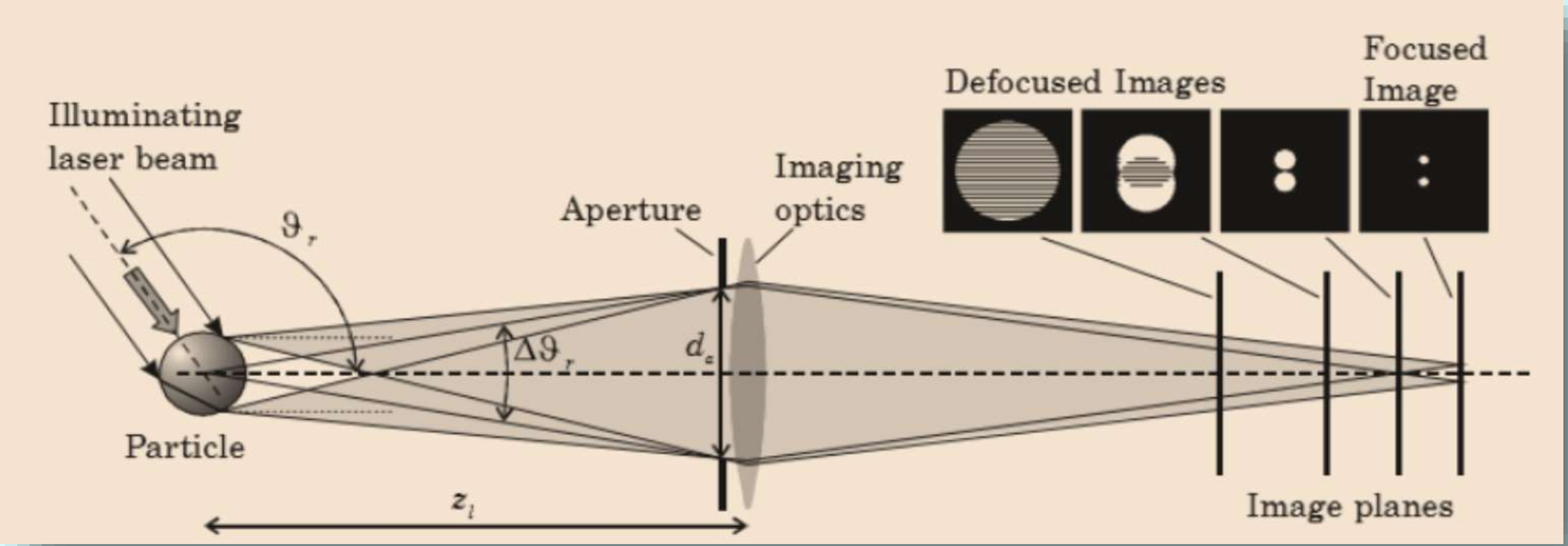

E. Ebert, A. Kleinwächter, R. Kostbade, and N. Damaschke, "Interferometric Particle Imaging for cavitation nuclei characterization in cavitation tunnels and in the wake flow," presented at the 17h Int. Symp. on Applications of Laser Techniques to Fluid Mechanics, Lisbon, Portugal, 2014.

Cavitation nuclei characterization

Interferometric Particle Imaging (IPI-Technology)

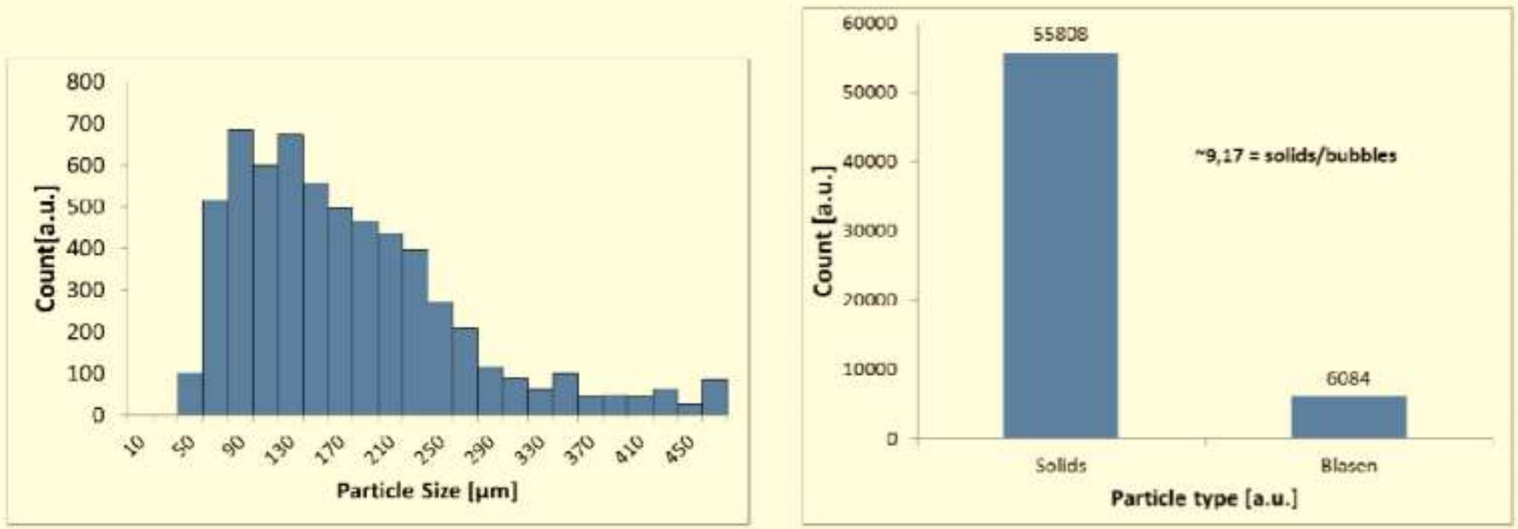

Measured particle size distribution

Particle classification

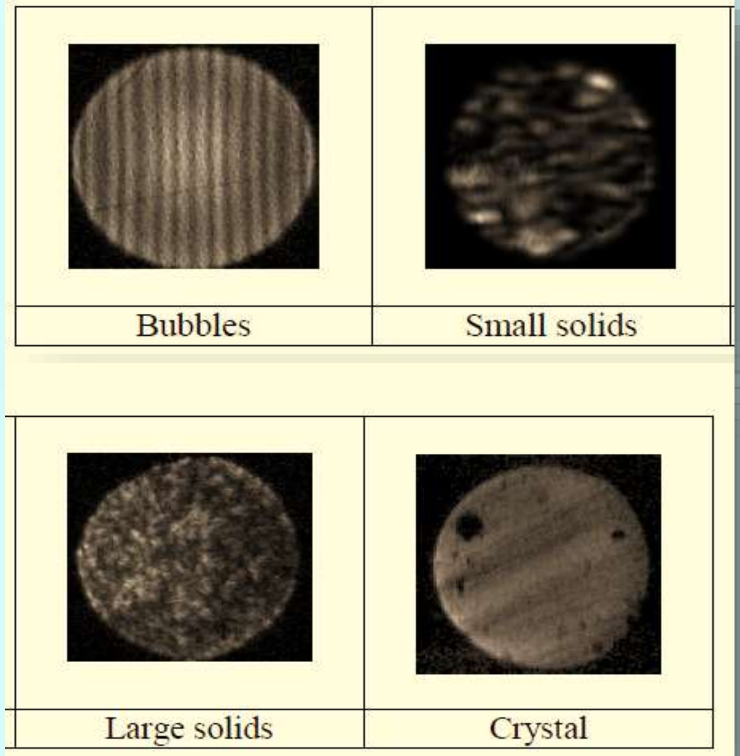

Examples of interference pattern from different particle types in a Gaussian laser beam

E. Ebert, A. Kleinwächter, R. Kostbade, and N. Damaschke, "Interferometric Particle Imaging for cavitation nuclei characterization in cavitation tunnels and in the wake flow," presented at the 17h Int. Symp. on Applications of Laser Techniques to Fluid Mechanics, Lisbon, Portugal, 2014.

Application and validation, sheet cavitation, for 2D NACA 66_2 - 415 a = 0.8

2D Test case:

- Chord length c = 0.2025 m
- NACA 66_2 - 415 a=0.8 hydrofoil
- Chord length c_0 = 0.2025 m

Measurements at SVA Potsdam in K15A cavitation tunnel during KonKav I project

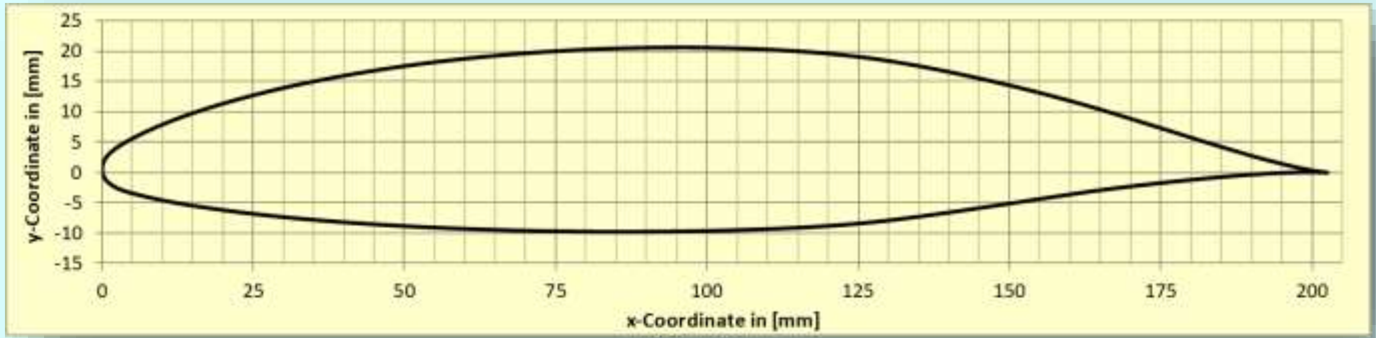

Cross section of NACA 66_2 - 415 a=0.8 hydrofoil

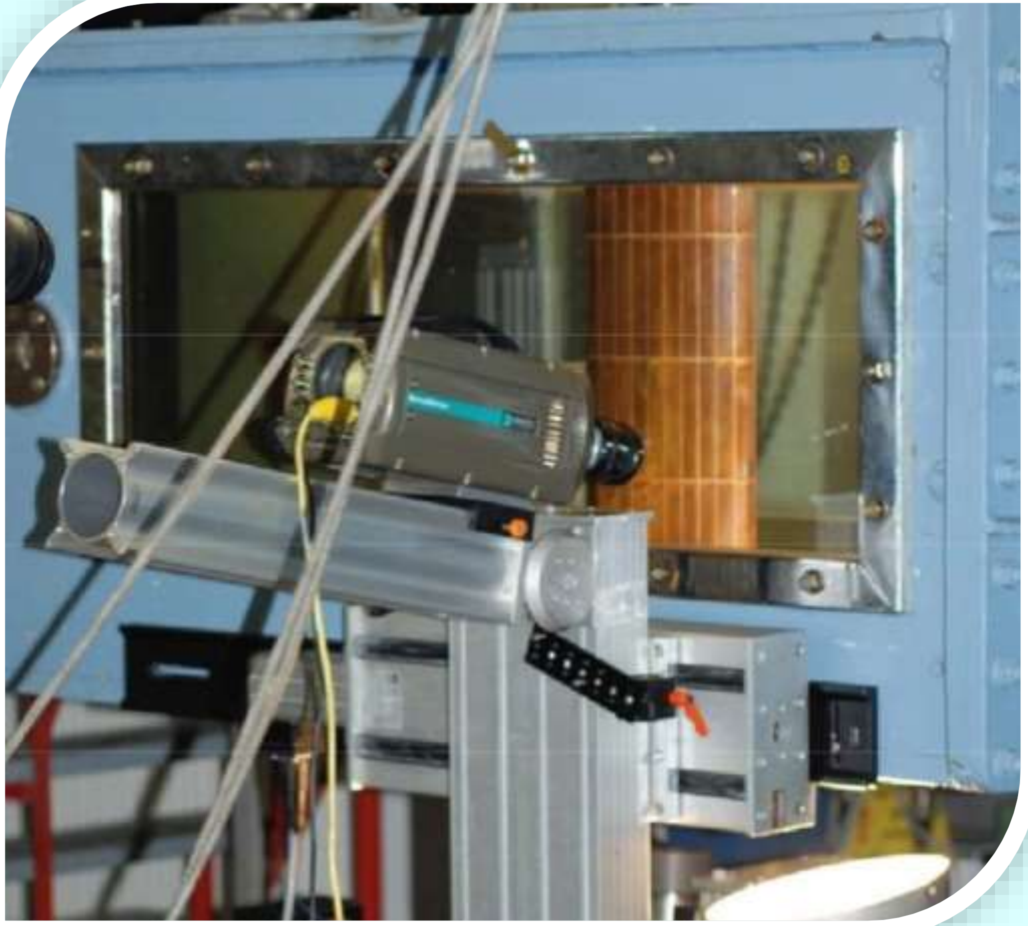

Sheet cavitation, 2D NACA 66_2 - 415 a = 0.8

2D Test case:

Contribution: Patrick Schiller

- Angle of attack = 15°
- Cavitation number σ = 3.00
- Approach velocity v = 5.5 m/s (Re = 1.1×10^6)

Quasi 3D grid with 50k cells (Y+ ~ 30)

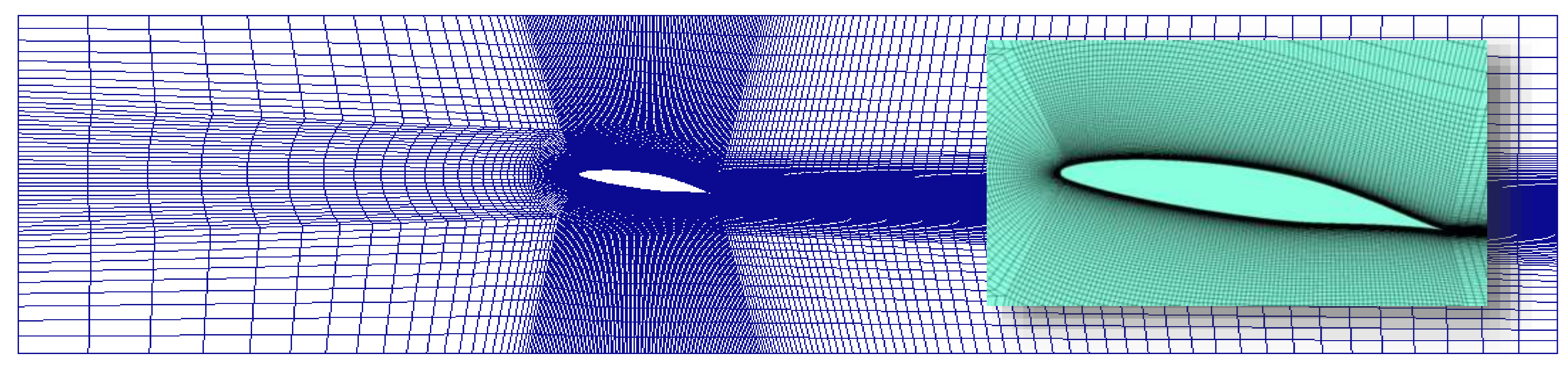

Sheet cavitation, 2D NACA 66_2 - 415 a = 0.8

Experimental results K15A

Sheet extent along suction side

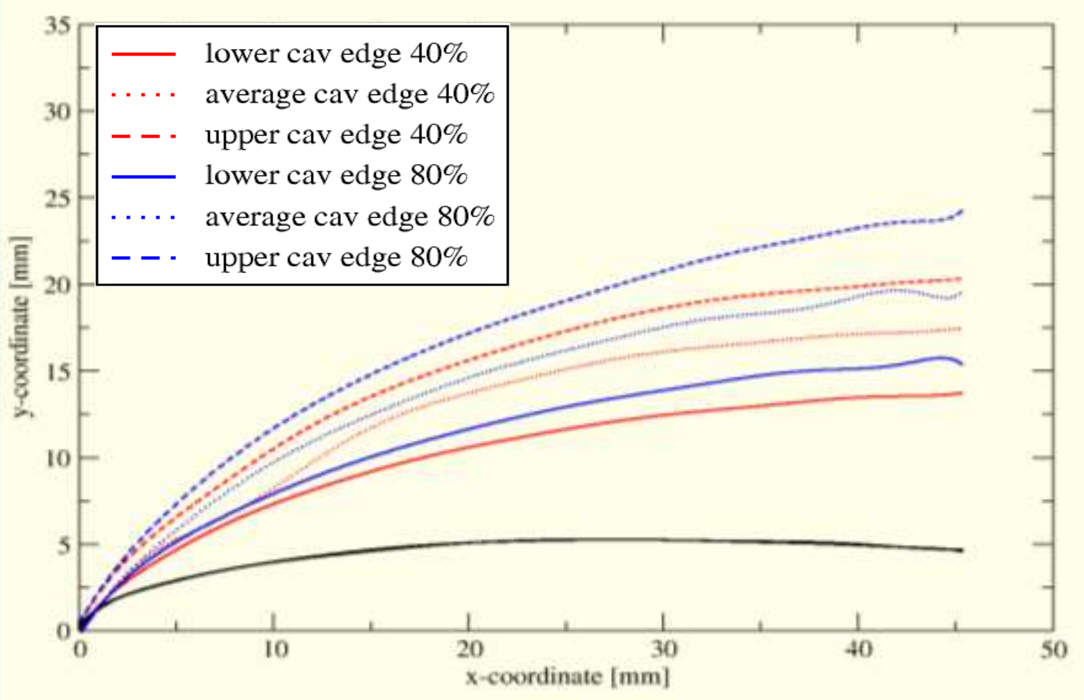

Cavitation sheet thickness

(shadow imaging)

Concentration vs. bubble diameter

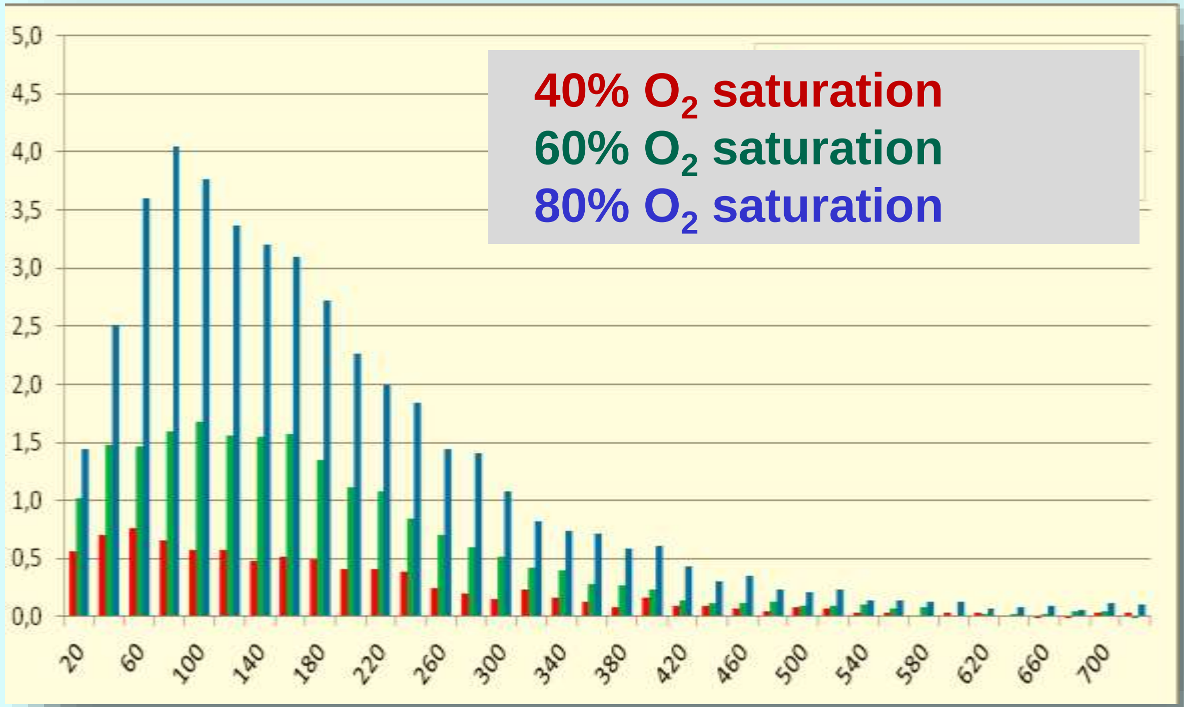

Measured bubble spectra

Application and validation for 2D NACA 66_2 - 415 a = 0.8

Simulation results

40% O_2

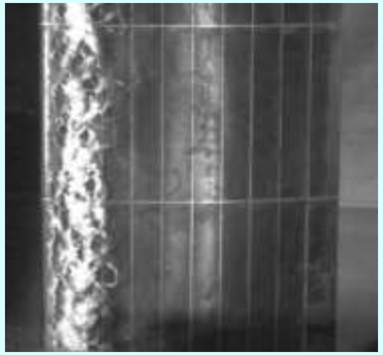

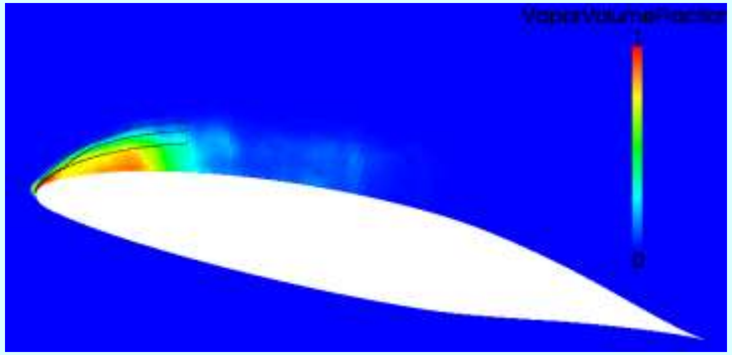

60% O_2

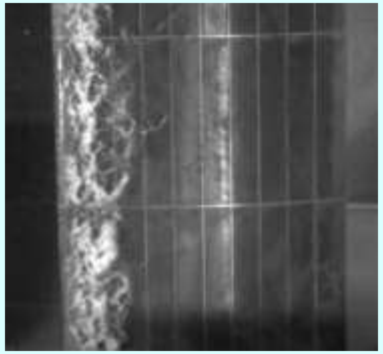

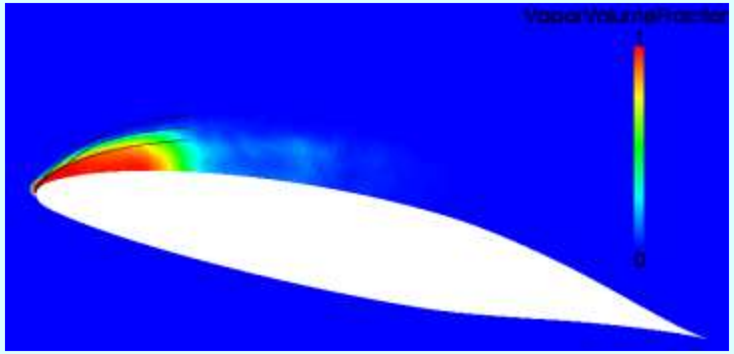

80% O_2

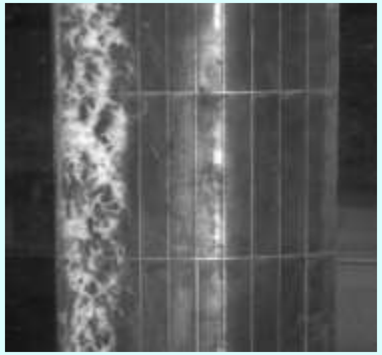

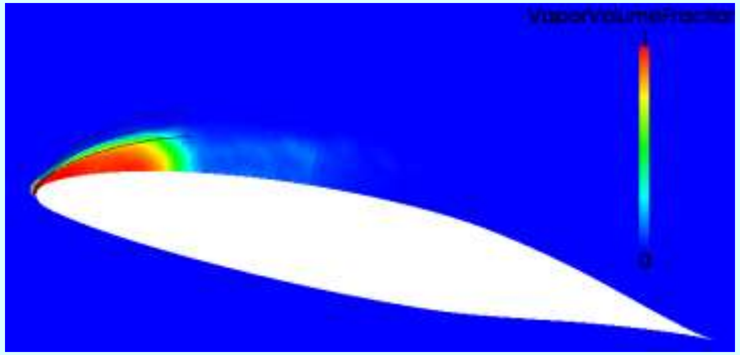

Scale effects

Velocity scale effect

Comparison of Euler-Euler (E.E.) and Euler-Lagrange Model (E.L.)

E.E. (Zwart)

E.L.

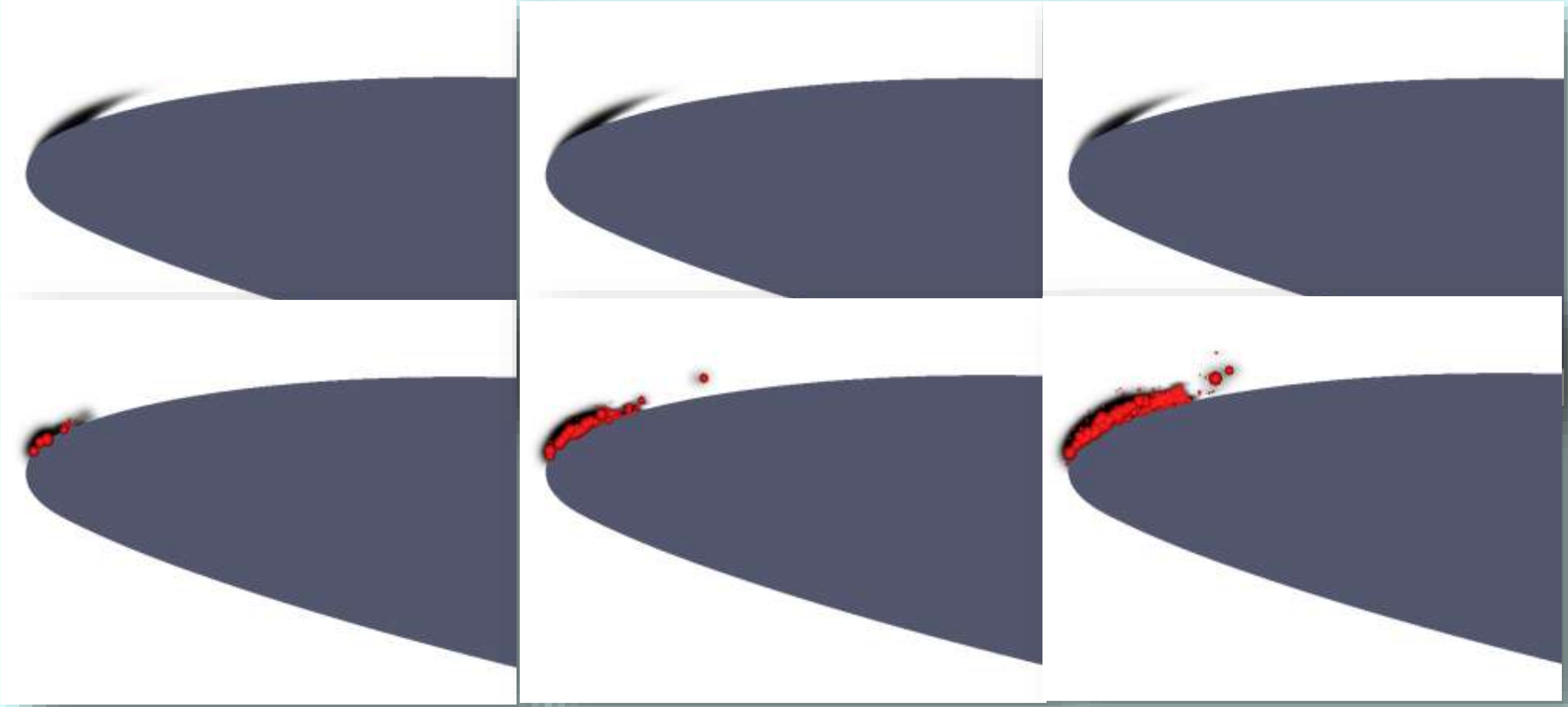

v = 2.75 m/s

v = 5.5 m/s

v = 11.0 m/s

Investigated scenarios

V [m/s]	0.917	1.833	2.75	5.5	8.25	11.0	13.75
p_∞ [Pa]	3561	7340	13644	47675	104394	183800	285894
D_{bubble} [µm]	247.20	177.47	139.76	91.00	70.09	58.10	50.19

Baseline case

1) Bubble diameter variation (baseline case)
2) Velocity variation (baseline case)
3) Velocity variation with re-adjusted bubble diameter

$$p_\infty = p_{g0}\left(\frac{R_0}{R}\right)^3 + p_v - \frac{2S}{R}$$

4) Chord length variation (baseline case)

Scale effects

Bubble diameter variation (baseline case)

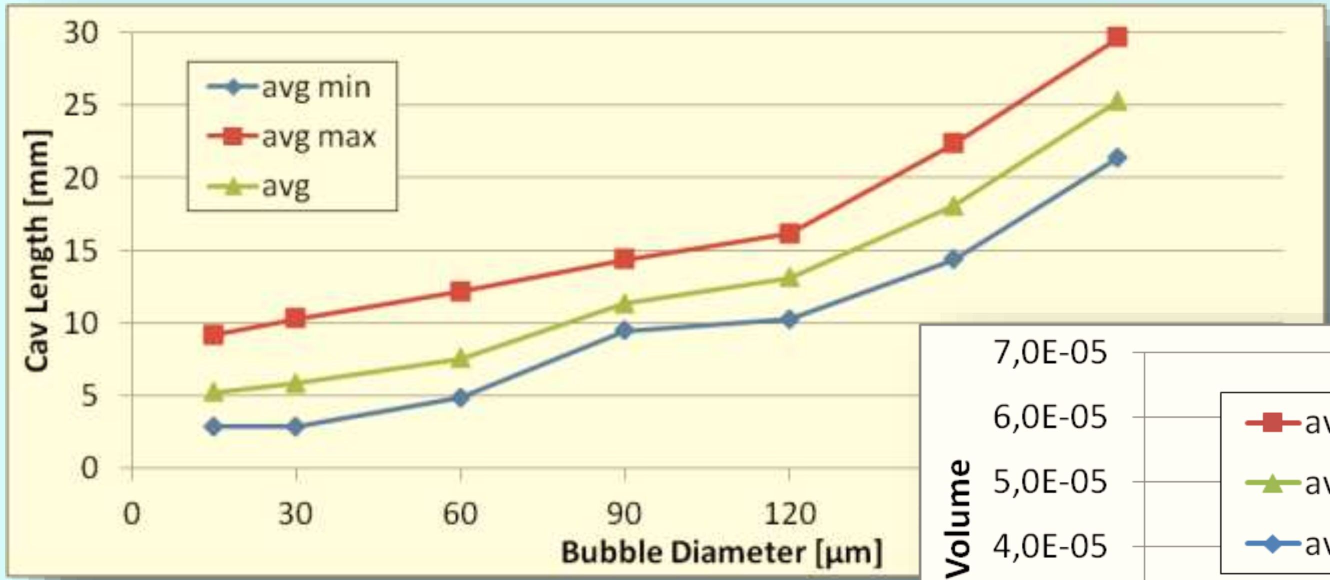

Cavitation length

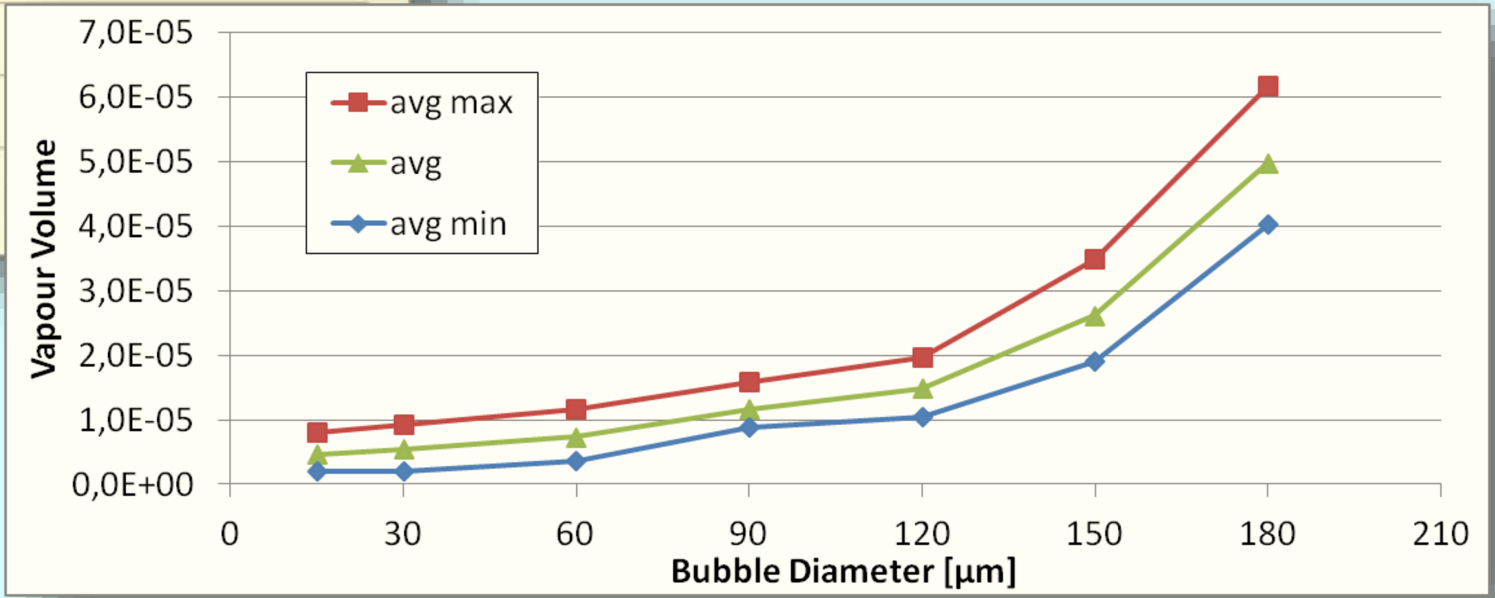

Vapour content

Scale effects

Variation of inflow velocity (bubble diameter = const. = 91mm)

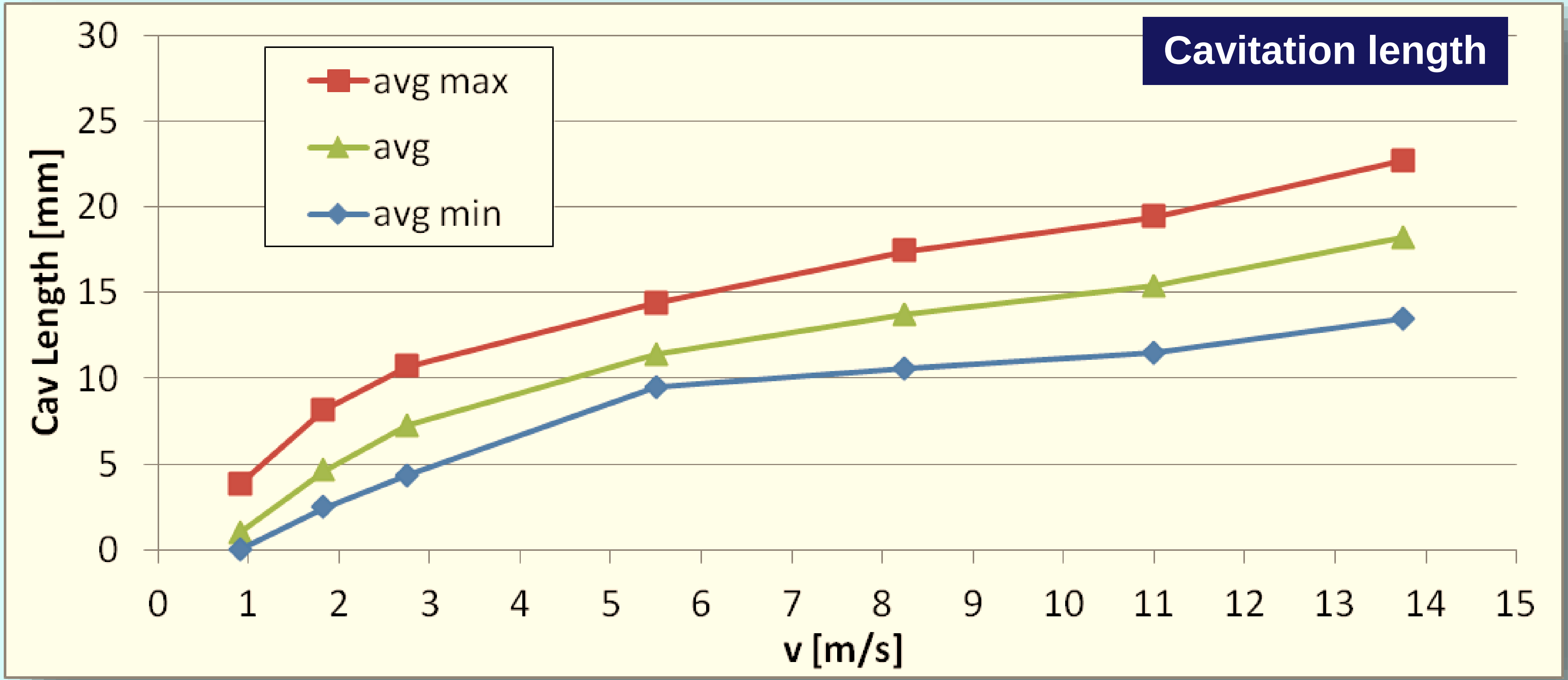

Variation of inflow velocity (adjusted bubble diameter)

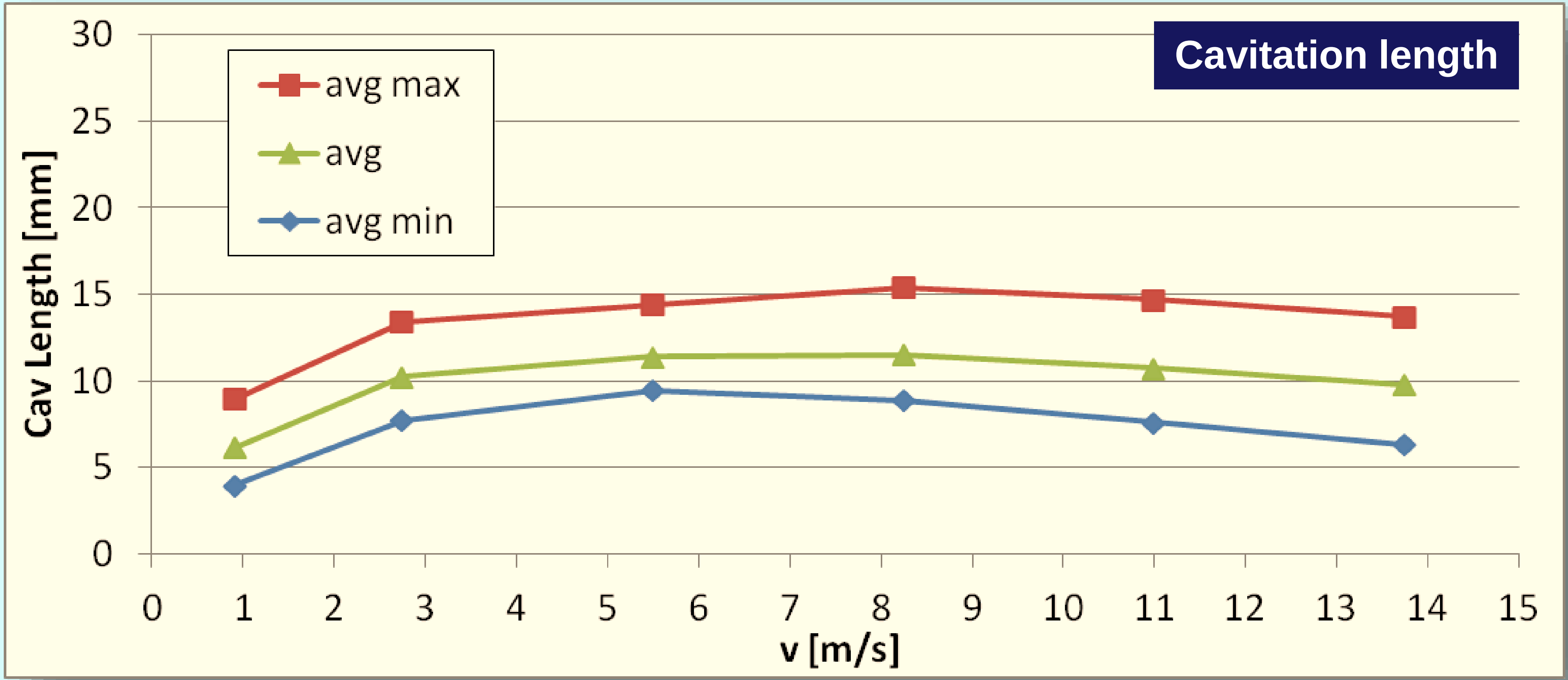

Simulation results – scale effects

Chord length variation (baseline case)

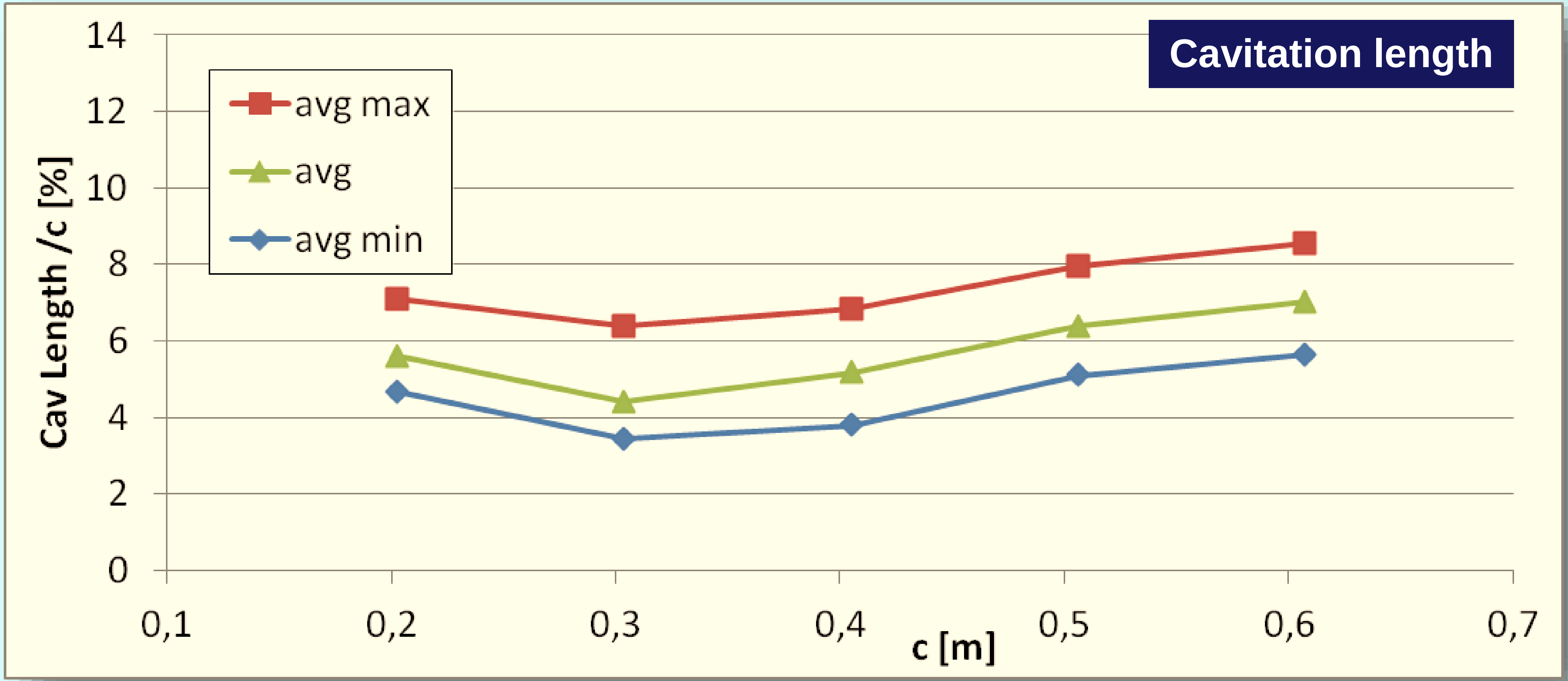

Chord length variation (Animation)

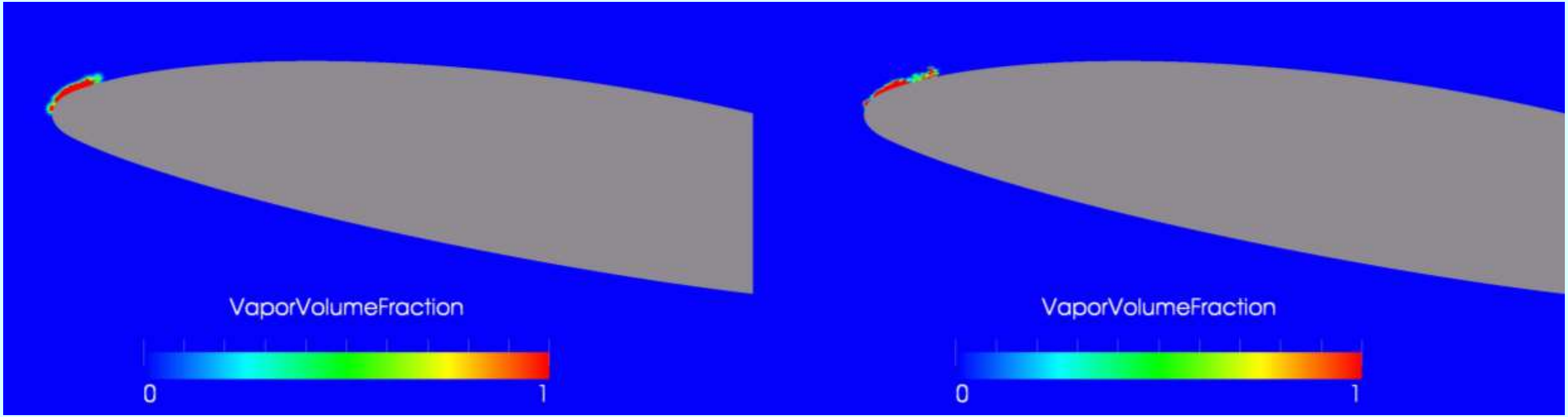

c = 0.303 m

c = 0.606 m

Acoustic cavitation inception study– scale effects

Flow field calculation

2D grid with 72k, y+ ≤ 1

Adjustment of ambient pressure for change of cavitation number σ

$$\sigma = \frac{p_\infty - p_v}{0.5 \cdot \rho \cdot v^2}$$

Frozen flow field used for Lagrange phase

Normalized pressure distribution

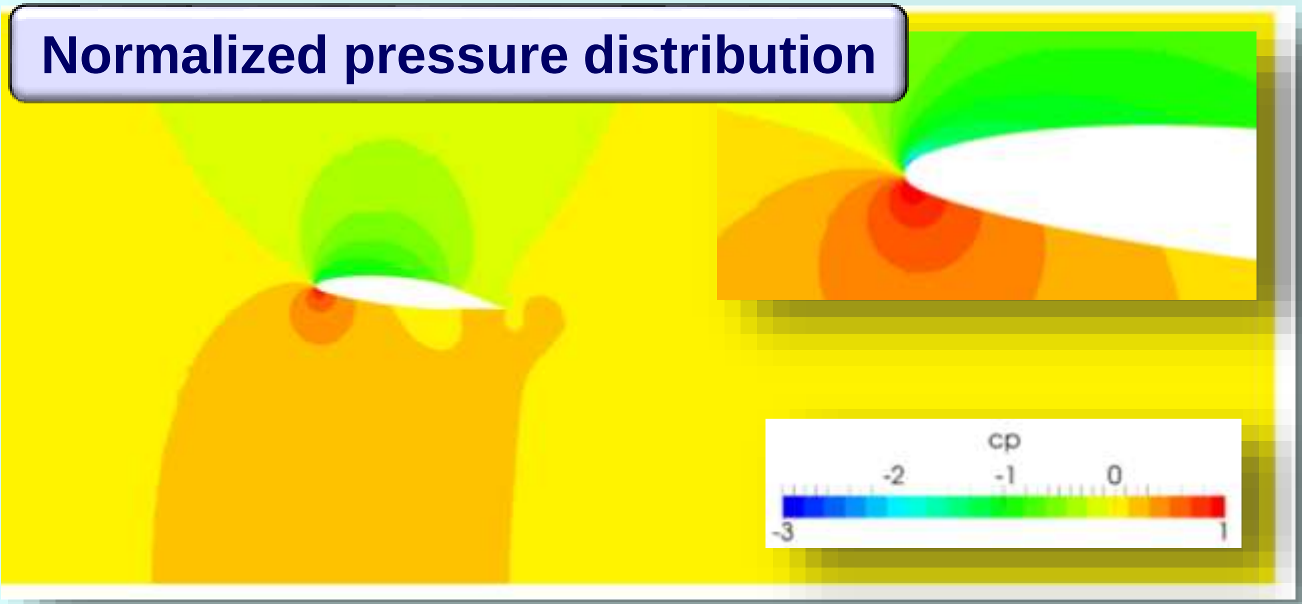

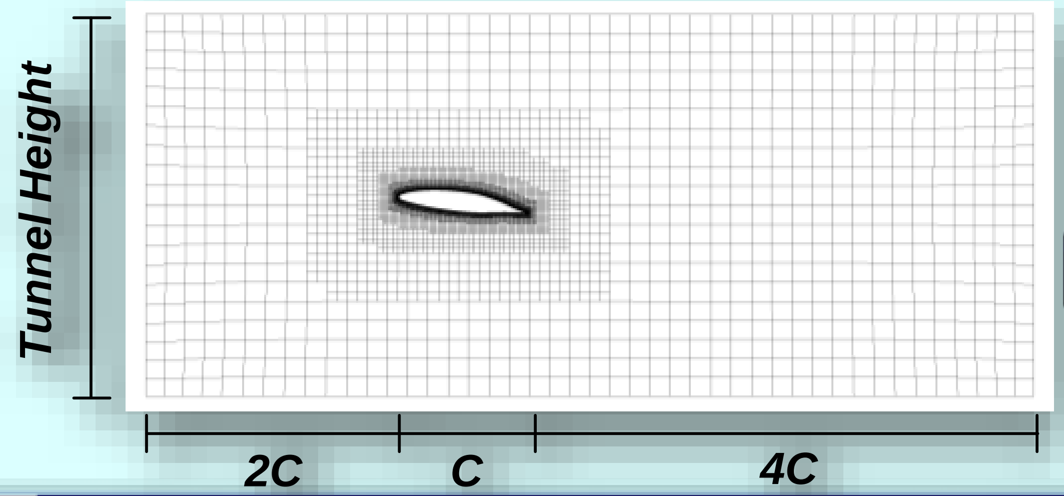

Numerical grid

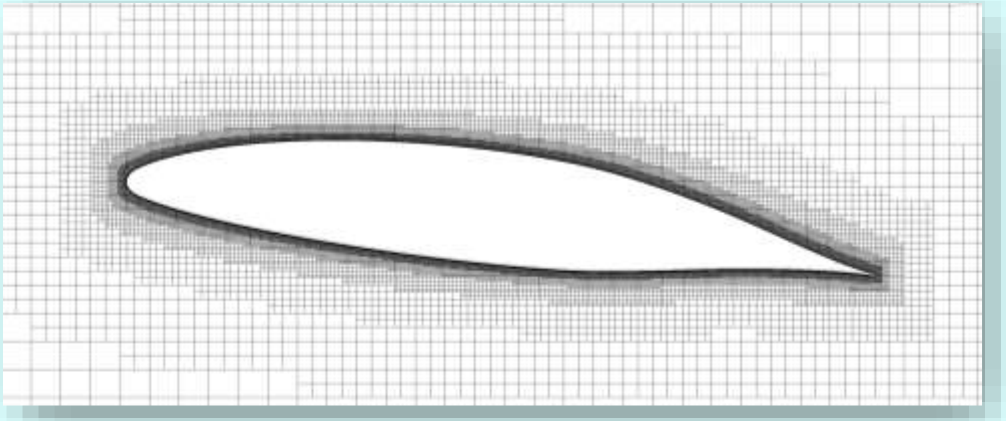

Simulation setup

Lagrange phase

Random bubble initialization in predefined area
Lagrange timestep 10^{-7} s
Bubble release every 10^{-4} s (Euler timestep)
Total simulation time 10 s

Acoustic

Recording frequency 1000 kHz
Recording position 1 m above leading edge
Acoustic cavitation inception criteria based on event rate
10 peaks/s over 10Pa (criterion 1)
50 peaks/s over 40Pa (criterion 2)

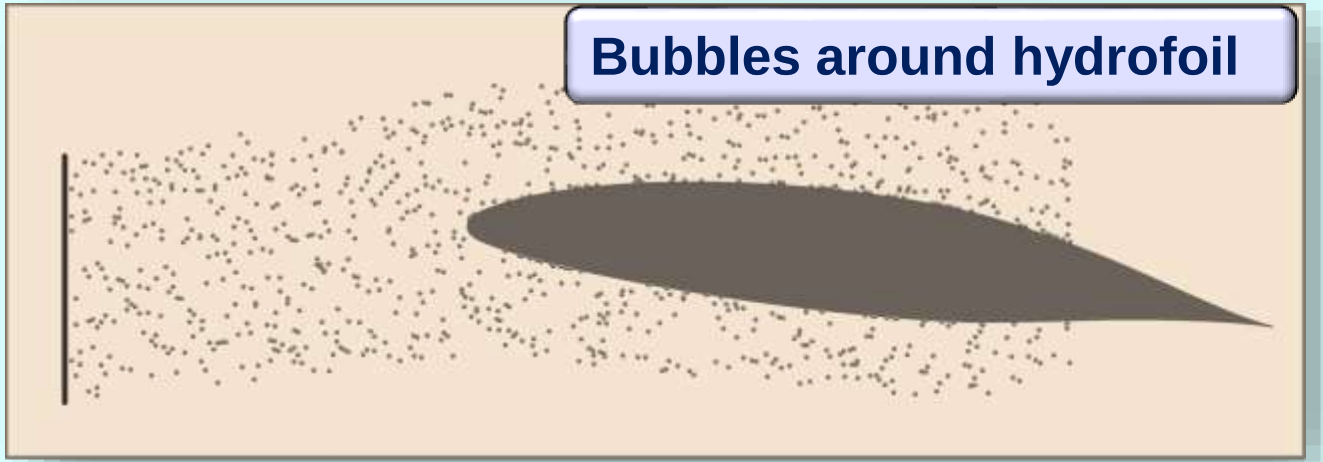

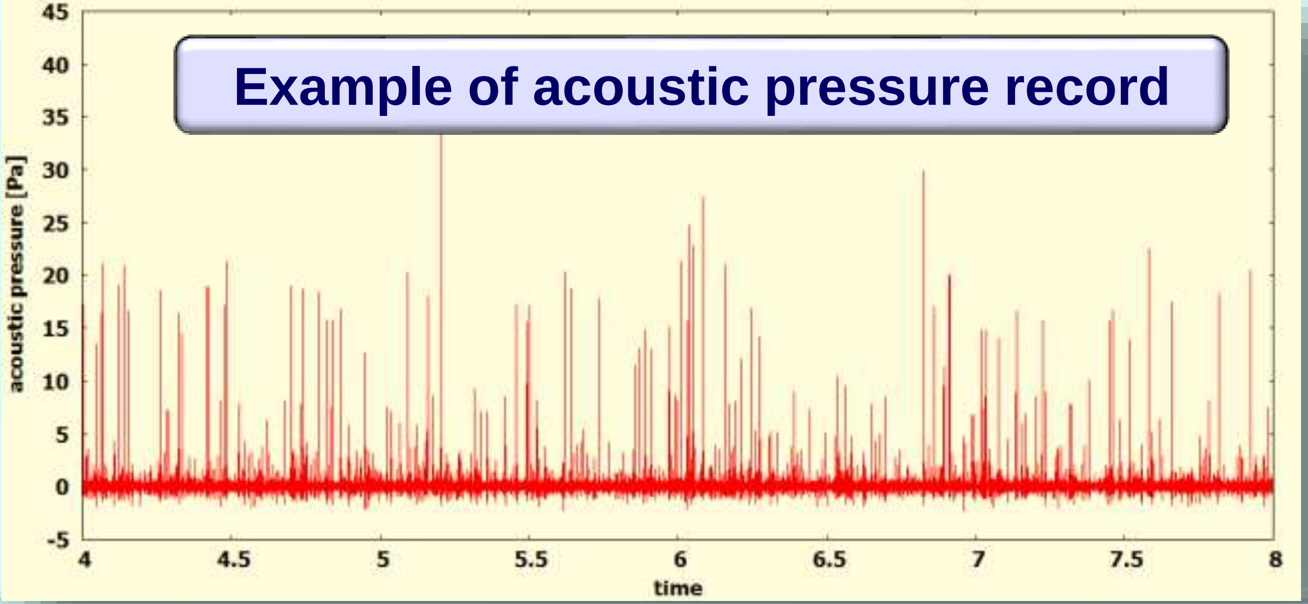

Simulation setup

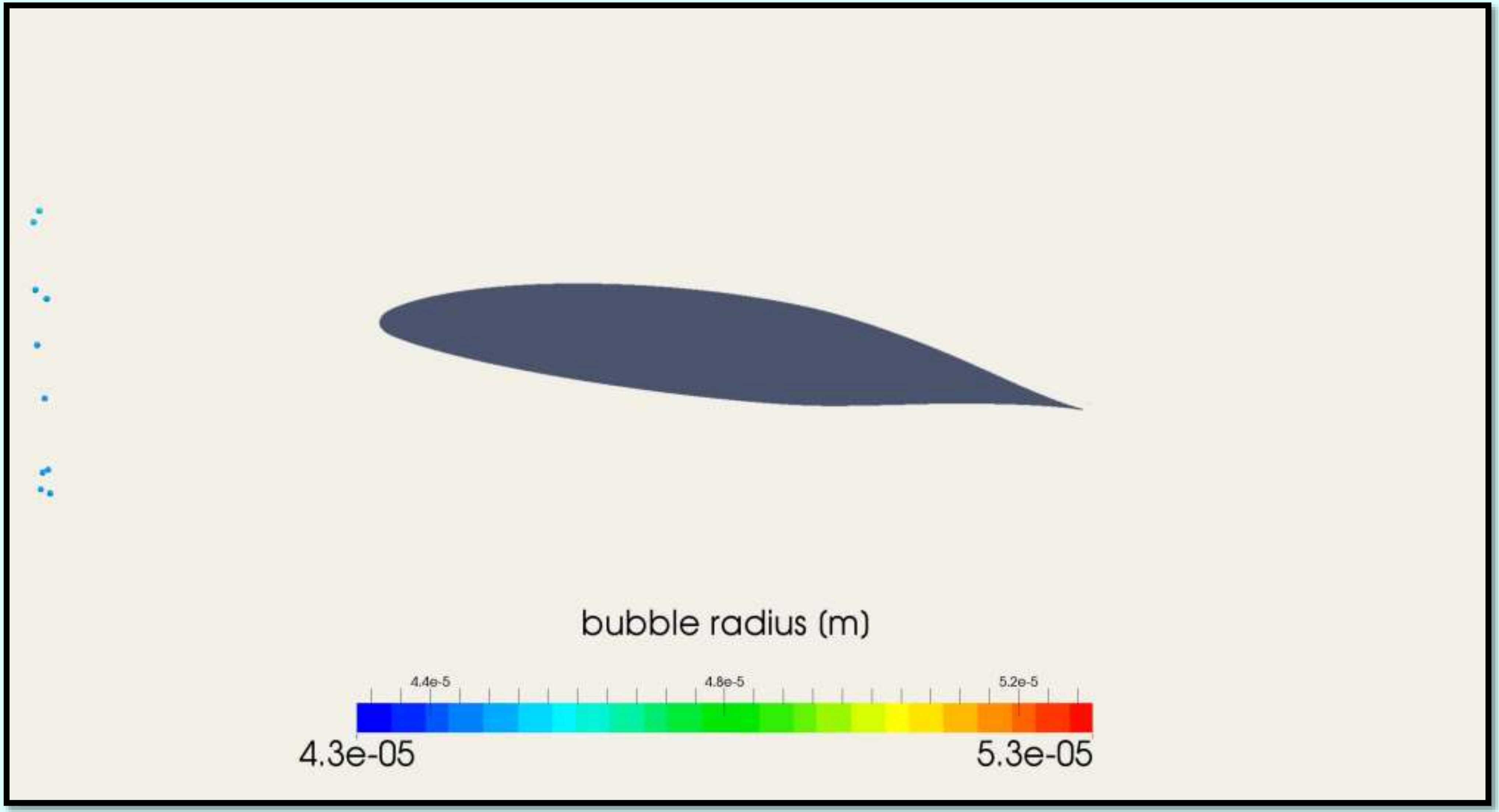

Acoustic cavitation inception study

Development of peak counts number over cavitation number

Characteristic curves for different scenarios

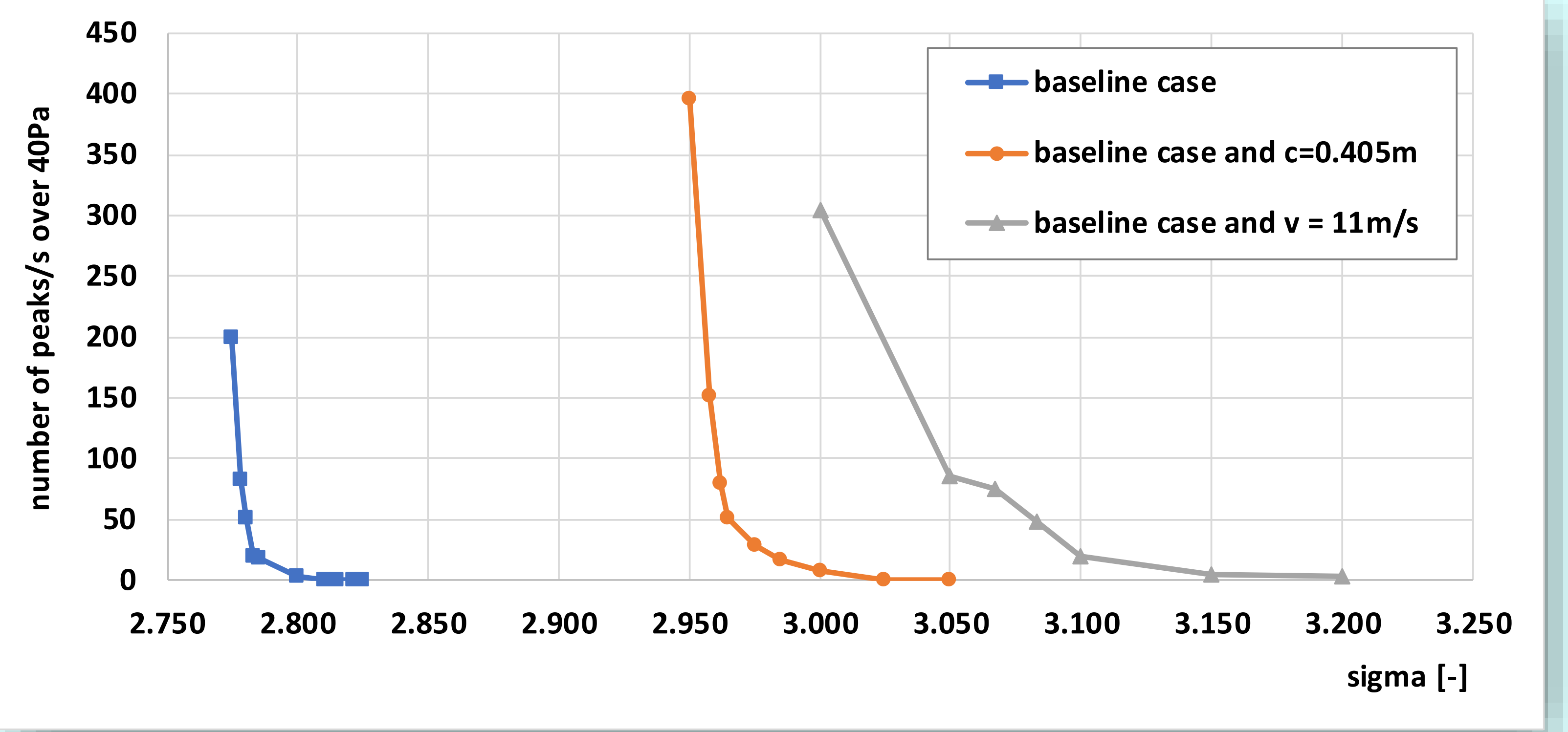

Acoustic cavitation inception number σ_{in} = intersection of characteristic curves with specified criterion

PPTC-Test case

Contribution: Dr. Sergey Yakubov

Test condition:

Advance coefficient:	1.01
Cavitation number based on n:	1.96
Thrust coefficient (non-cavitating):	0.38
Number of revolutions n:	21
Air content:	80% of saturation
Reynolds number at r/R=0.7	1.4×10^6

Application and validation for propeller flows

Full propeller grid

Domain $L_d = 7D$, $D_d = 4D$

12 million cells

Y+ ~ 30

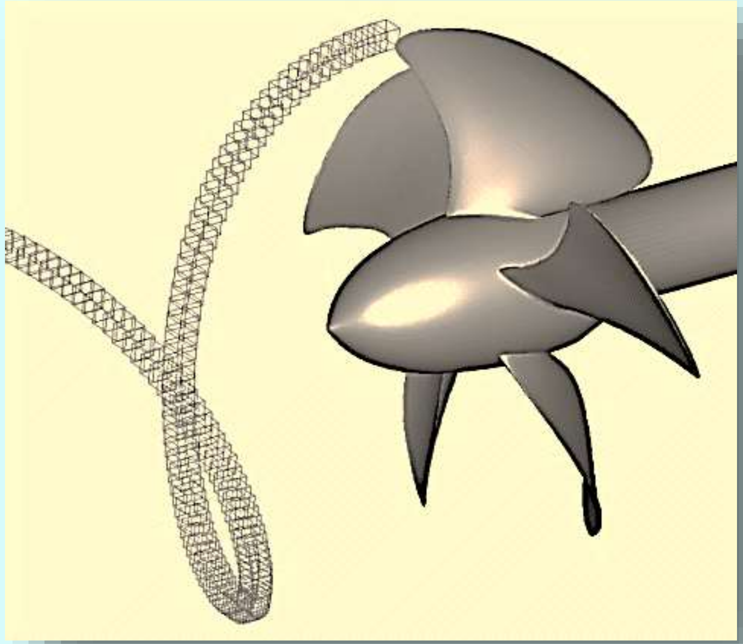

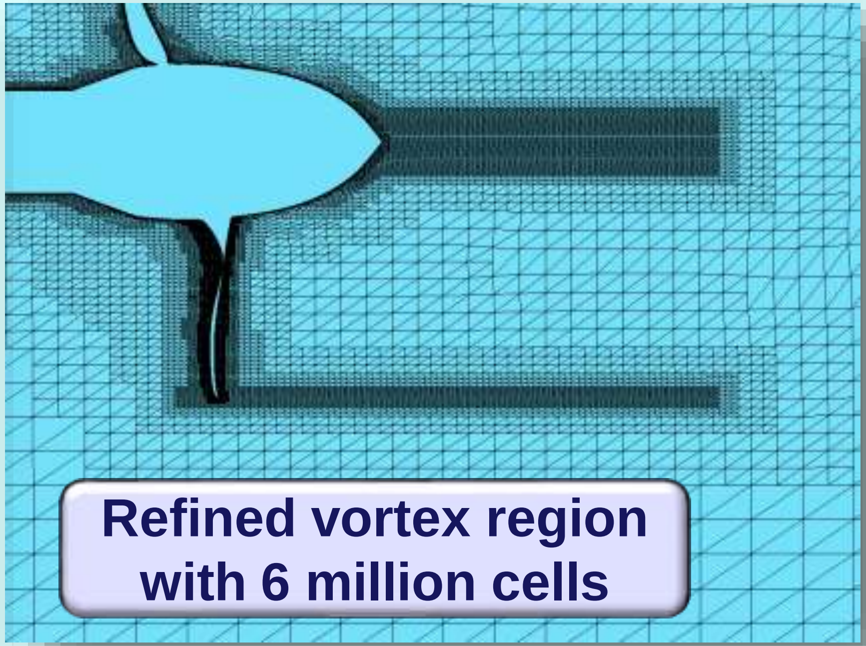

Computational model

RANS (k-ω model)

TVD-QUICK advection

Unsteady simulations with 360 time steps per revolution

Euler-Euler, Euler-Lagrange,

combined cavitation models

Simulation results – PPTC

Results

Vapour bubbles

Vapour vol. fraction 0.2

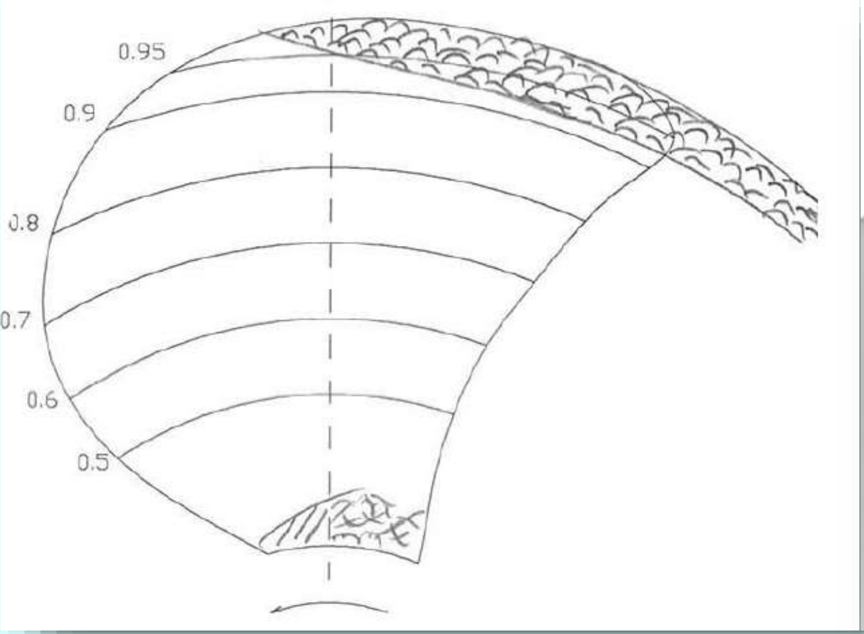

Experiment

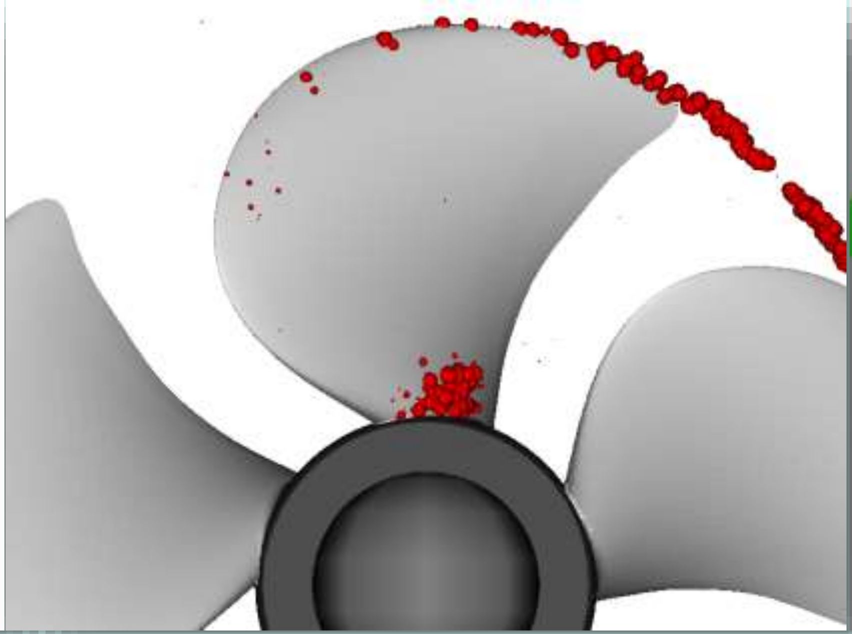

Euler-Lag. approach
(full sector)

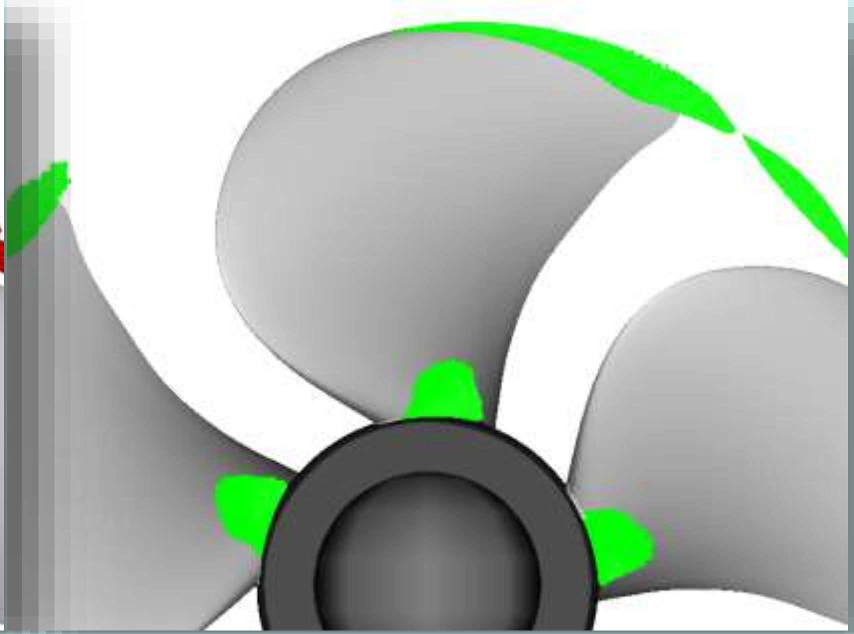

Euler-Euler

Simulation results – PPTC

Results

Vapour bubbles

Vapour vol. fraction 0.2

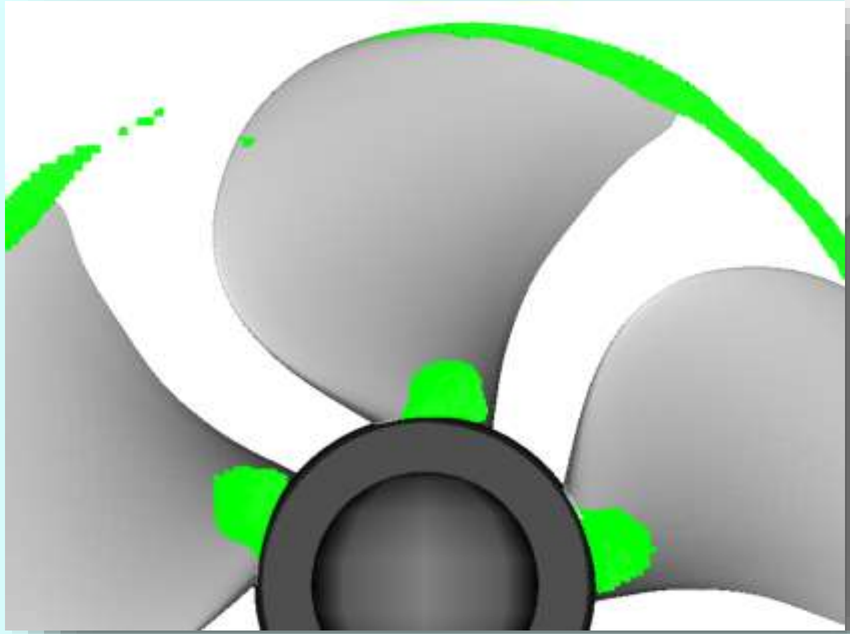

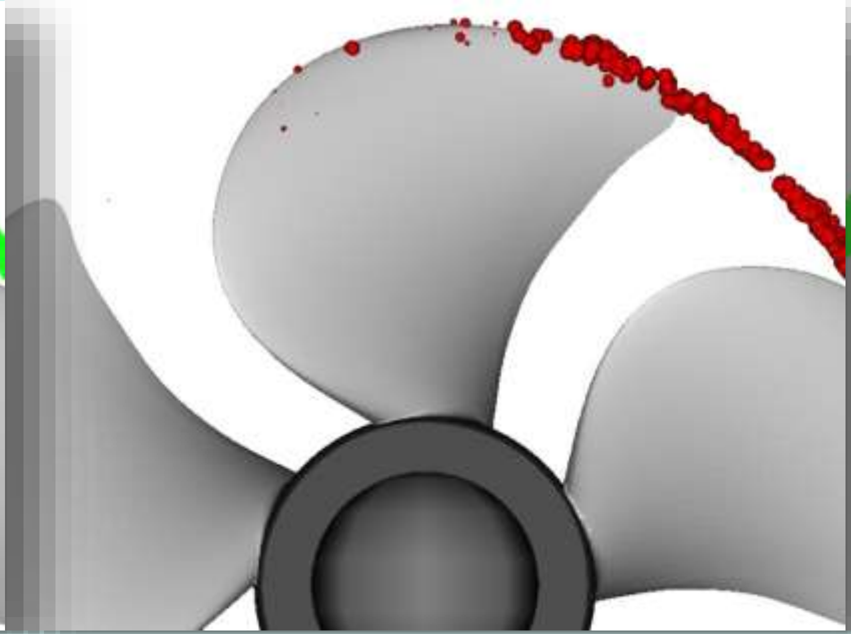

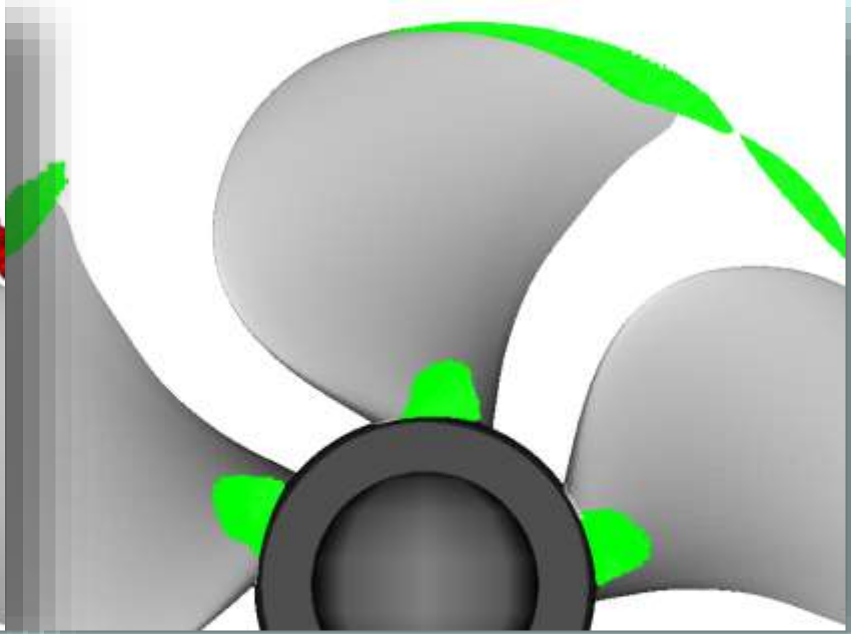

Combined approach

Euler-Lag. approach
(full sector)

Euler-Euler

Simulation results for different water quality

$k_T = 0.22$, $n = 28$ 1/s, $\sigma_n = 2.0$

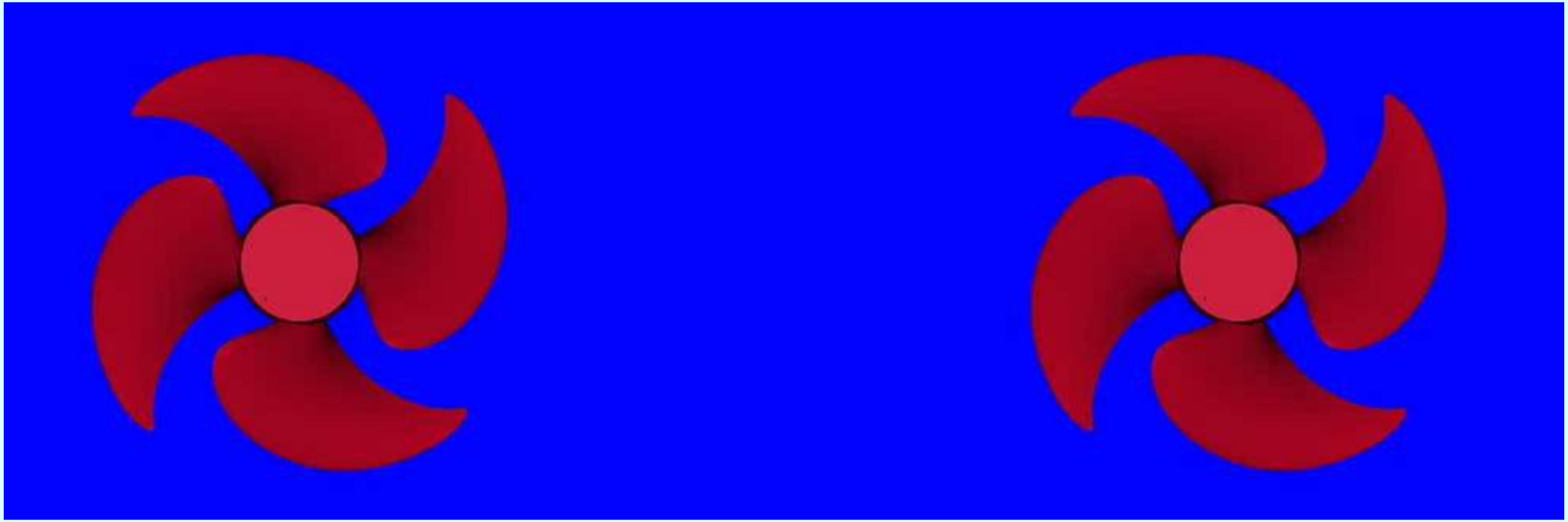

40% O_2 80% O_2

Main results

- **Predictive performance of Euler-Lagrange model encouraging**
  - Cavitation pattern
  - Pressure fluctuations
  - Acoustic cavitation inception
- **Euler-Lagrange displays benefits over Euler-Euler**
  - ability to capture scale effects
  - more comprehensive water model
  - more detailed bubble dynamics
  - less prone to model-coefficients
- **Combined model seems fair engineering approach**
- **Good platform for erosion studies**

FDS - Institute for Fluid Dynamics and Ship Theory

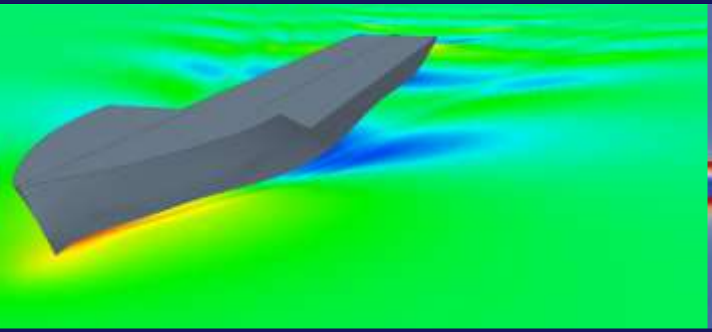
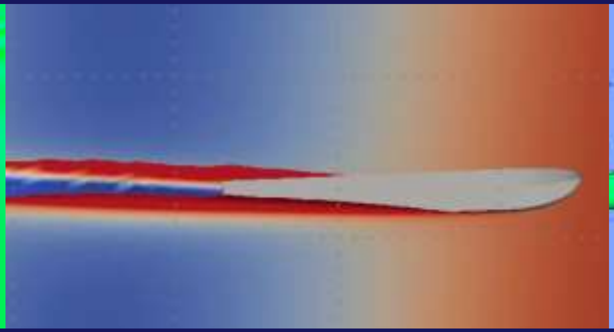
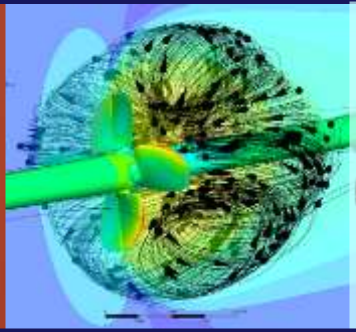
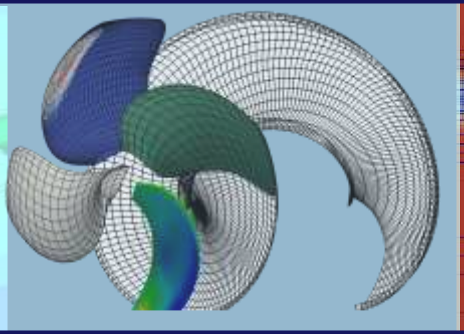
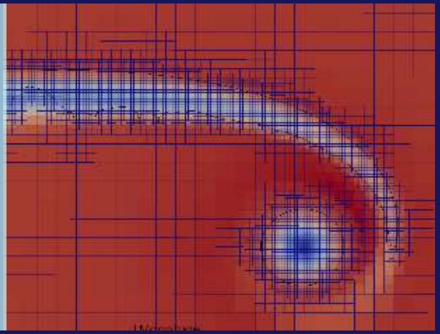

Fluiddynamik
und
Schiffstheorie

TUHH

NAVAL ARCHITECTURE AND MARINE ENGINEERING
UNIVERSITY of MICHIGAN ■ COLLEGE of ENGINEERING

Multi-functional Marine Structures: New Frontiers for Cavitating & Ventilating Flows?

Prof. Yin Lu (Julie) Young
Professor of Naval Architecture & Marine Engineering
Director of The Aaron Friedman Marine Hydrodynamics Laboratory

Collaborators:
Naval Surface Warfare Center, Carderock Division, USA
CNR INSEAN, Italy
Australian Maritime College, Australia
Defense Science Technology Group, Australia

Research Group

Prof. Casey Harwood

Dr. Deniz Akcabay

Ms. Yingqian Liao

Ms. Rachel Gouveia

Ms. Alexandra Damley-Strnad

Mr. Oscar Gonzalez Gallego

Why Multi-functional?

- Exploit advances in materials & manufacturing to drastically enhance performance, agility, functionality, and reliability
- Enable integrated sensing and control to facilitate autonomous operations and artificial intelligence
- Enable development of novel marine structures that can carry load, enable flow sensing and condition monitoring, increase fuel efficiency, harvest flow kinetic energy, etc

Special composite tape layering robot at *Aerocomposite-Ulyanovsk*

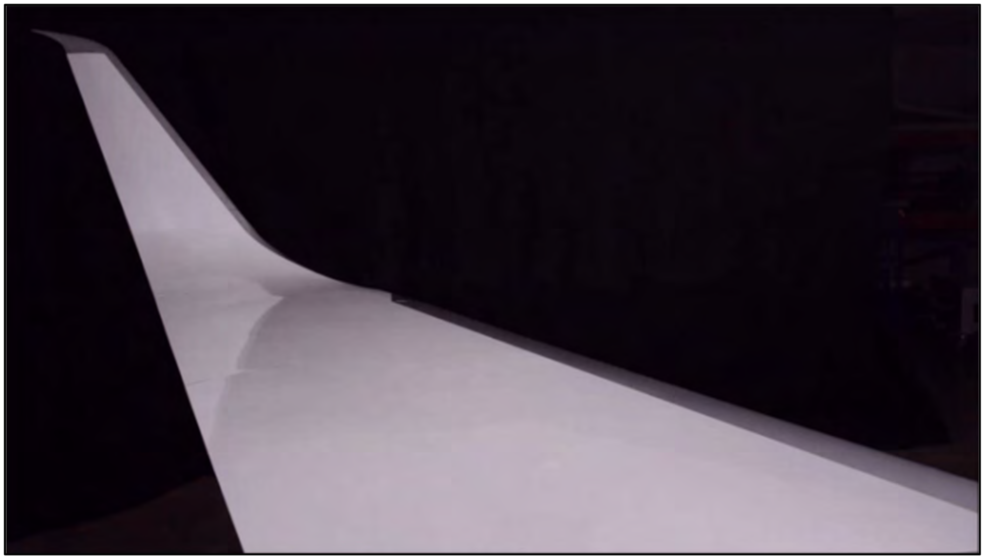

http://www.flxsys.com/

Biological Multi-functional Structure

MICHIGAN ENGINEERING
UNIVERSITY of MICHIGAN ■ COLLEGE of ENGINEERING

Fish = multi-functional composite lifting body that can not only generate thrust and perform rapid maneuvers, but also utilizes self-motion to detect obstacles, and uses flexible lifting surfaces and muscles for flow control

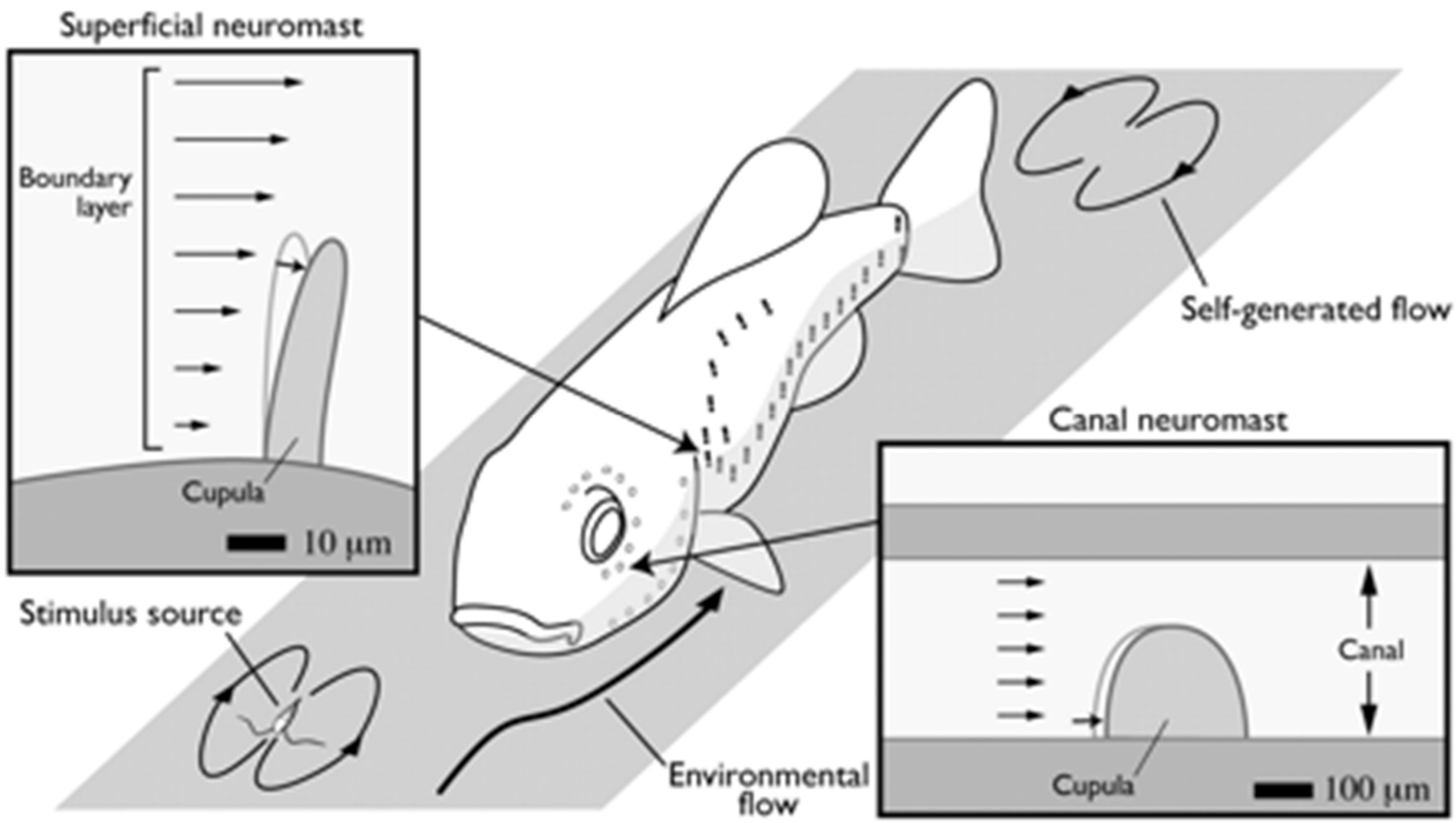

Superficial neuromasts (on the surface) – displacement sensors
Canal neuromasts (beneath the skin) – pressure gradient sensors

Dynamics of Cavitation

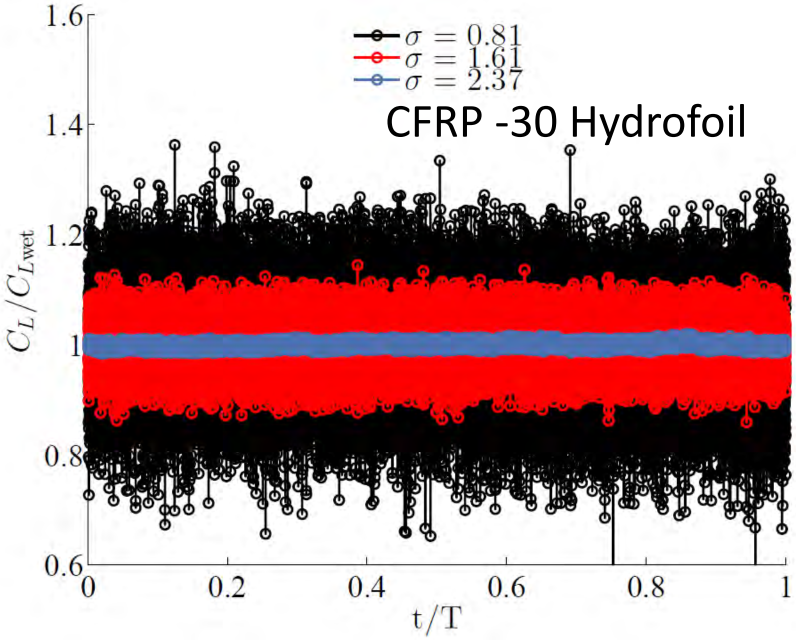

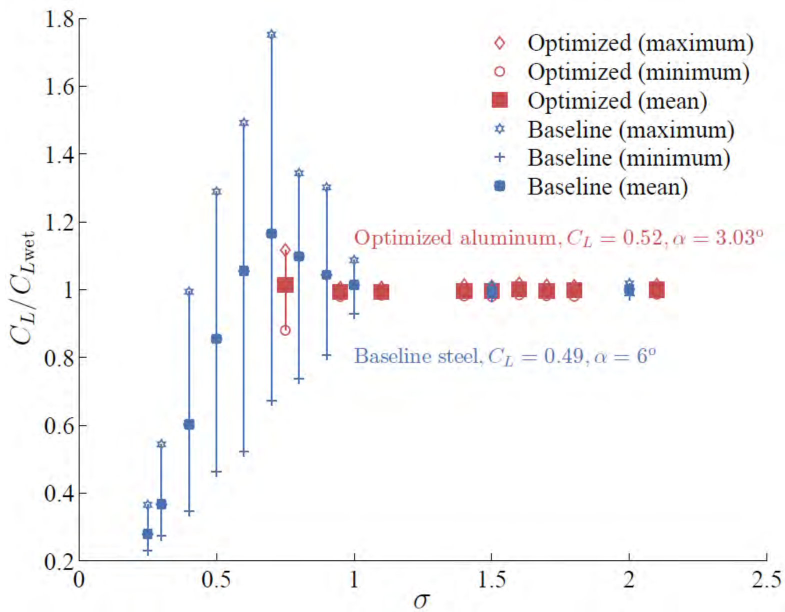

σ = 2.37

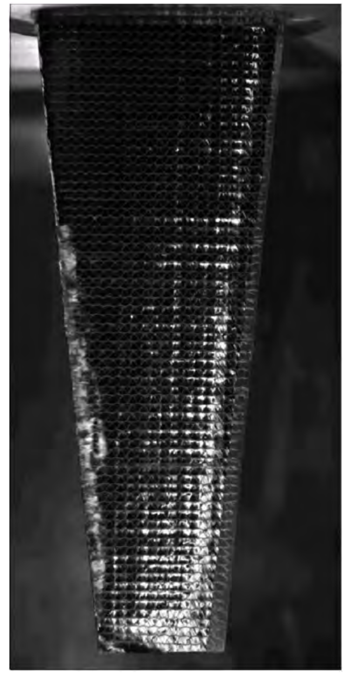

σ = 0.81

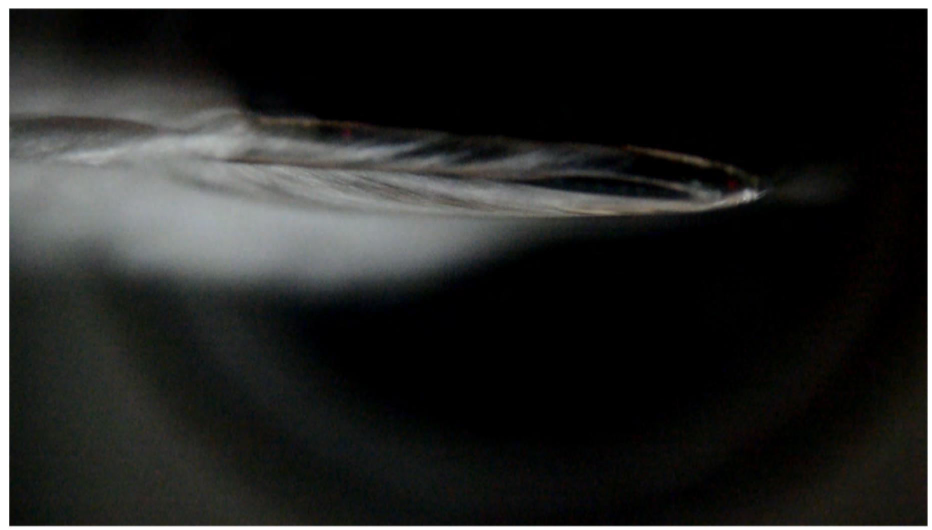

Dynamics of Ventilation

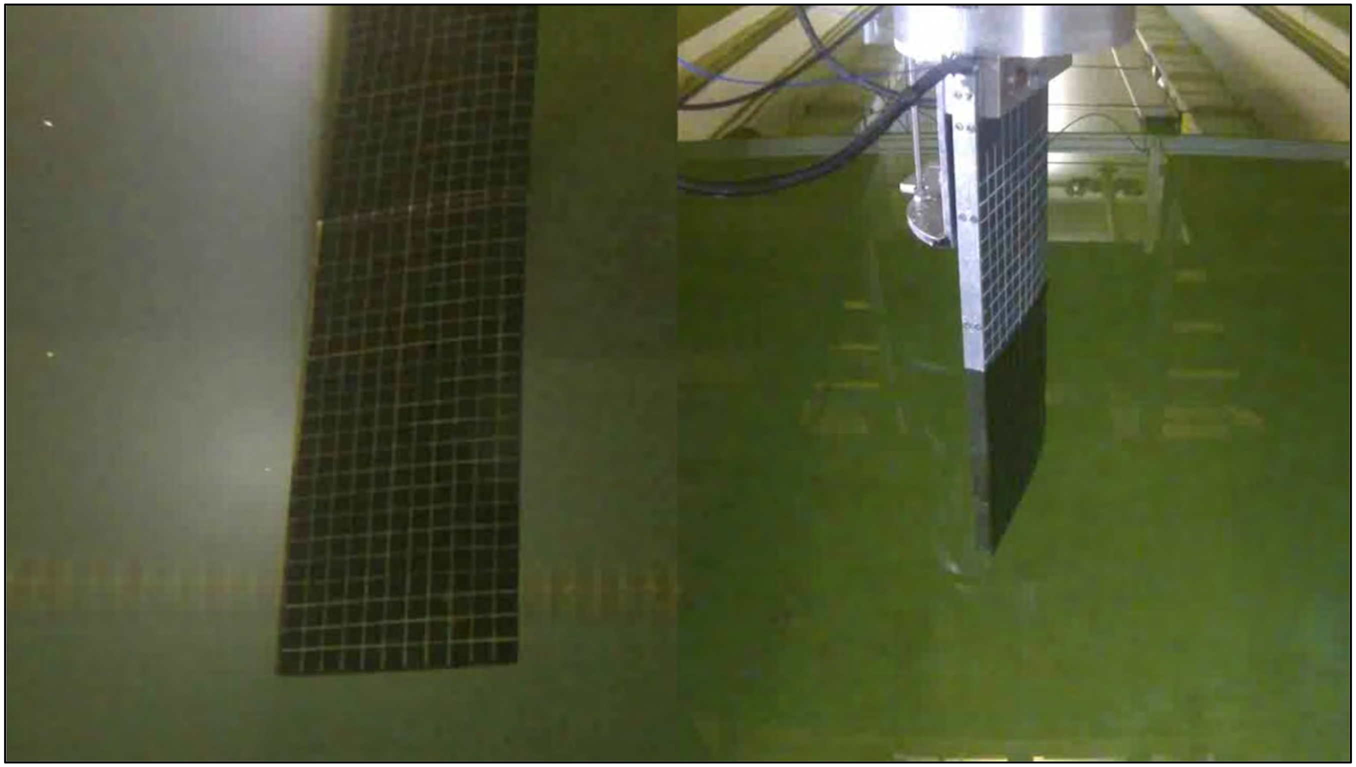

- Cavitation involves phase change between liquid and vapor
- Ventilation involves entrainment of gas to low pressure regions around the body

Source: Oracle Team USA

Ventilation Formation Mechanisms

MICHIGAN ENGINEERING
UNIVERSITY of MICHIGAN ▪ COLLEGE of ENGINEERING

1) C.M. Harwood, Y.L. Young, S.L. Ceccio, "Ventilated Cavities on a Surface-Piercing Hydrofoil at Moderate Froude Numbers: Cavity Formation, Elimination, and Stability," Journal of Fluid Mechanics, Vol. 800, pp. 5-56, 2016.
2) Y.L. Young, C.M. Harwood, F.M. Montero, J.C. Ward, and S.L. Ceccio, "Ventilation of Lifting Bodies: Review of the Physics and Discussion of Scaling Effects," Applied Mechanics Reviews, Vol. 69, 010801, 2017.

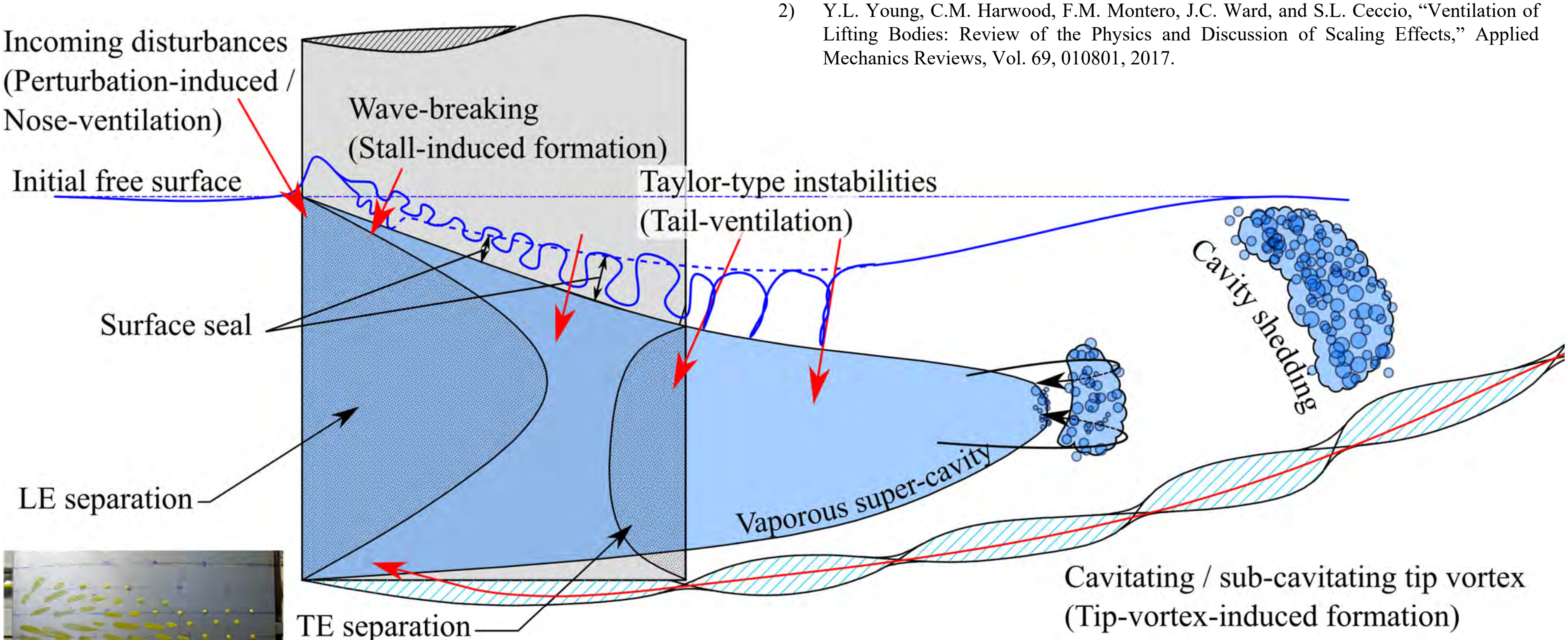

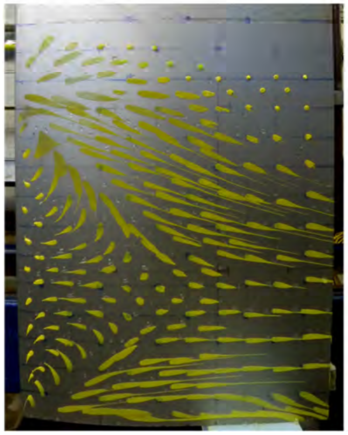

Natural ventilation develops when:
1. Local pressure is lower than the ambient pressure
2. Presence of flow separation
3. Path for air ingress

Tip-Vortex Ventilation & Impact

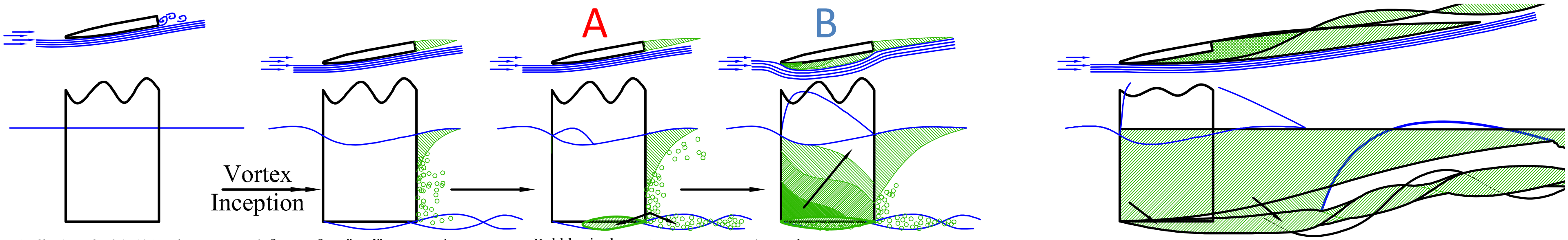

Fully Attached (FA) Regime: Flow is initially attached, with eddying separated wake (base pressure) behind TE

A free surface "seal" prevents ingress of air into regions of subatmospheric pressure. Bubbles from the base-cavity are entrained in the low-pressure core of the tip vortex.

Bubbles in the vortex core coalesce to form an aerated vortex at the tip of the foil.

Aerated vortex core moves upstream until it encounters a favorable pressure gradient. It then rapidly expands and propagates a cavity from the LE at the submerged tip toward the TE at the free surface.

Fully Ventilated (FV) regime: Stable supercavity is developed (closure of cavity occurs downstream of TE). Vortex core ingests air from cavity and becomes fully aerated.

$15°; Fn_h = 3.5; AR = 1$

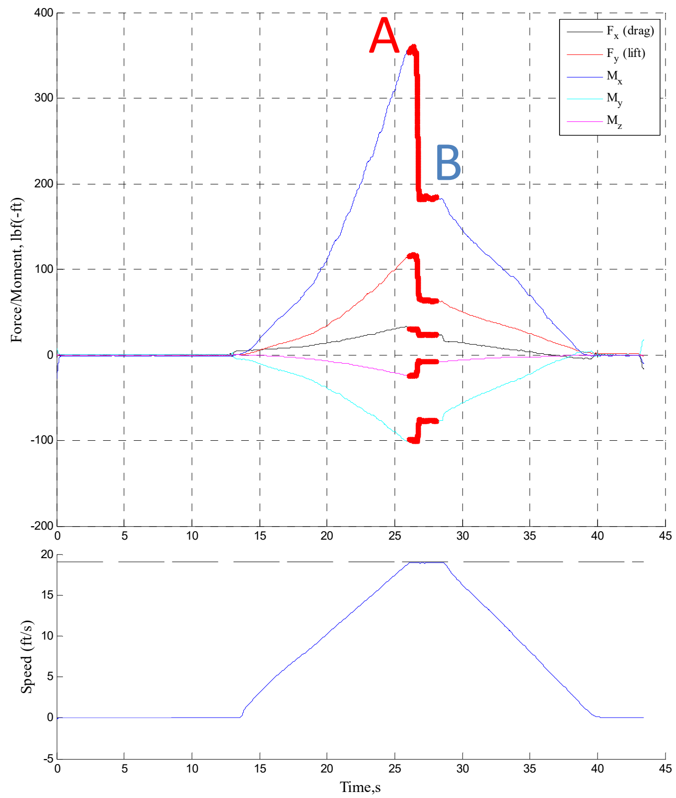

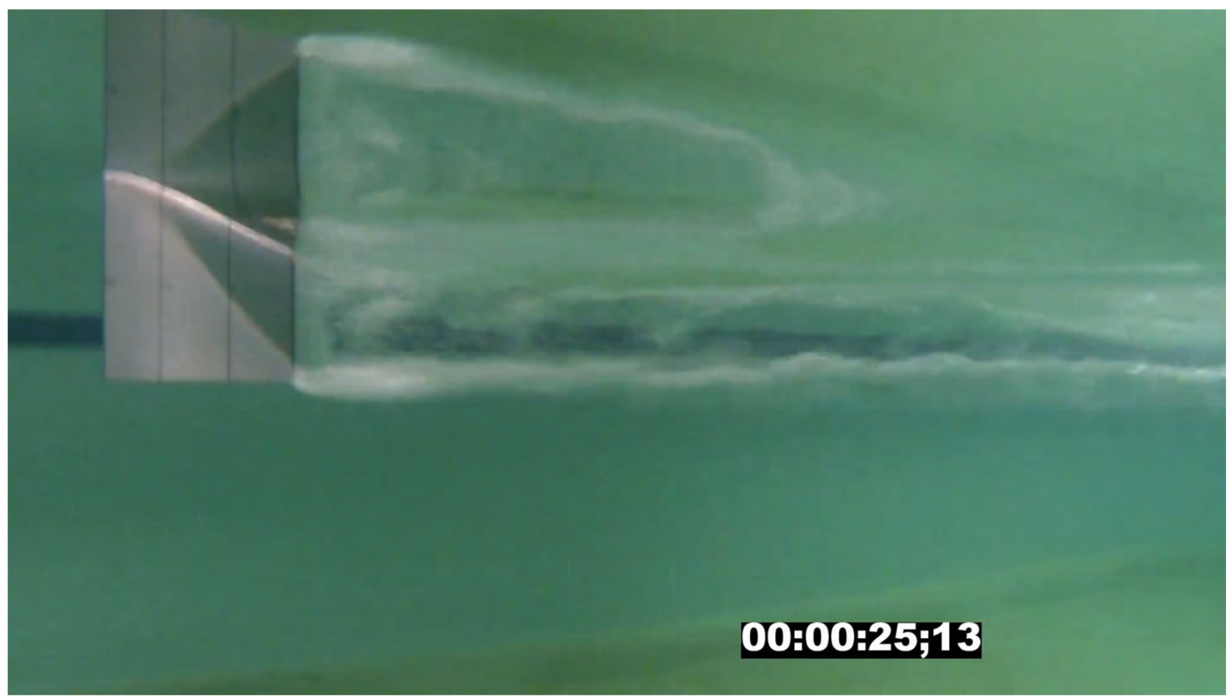

Perturbed Ventilation & Its Impact

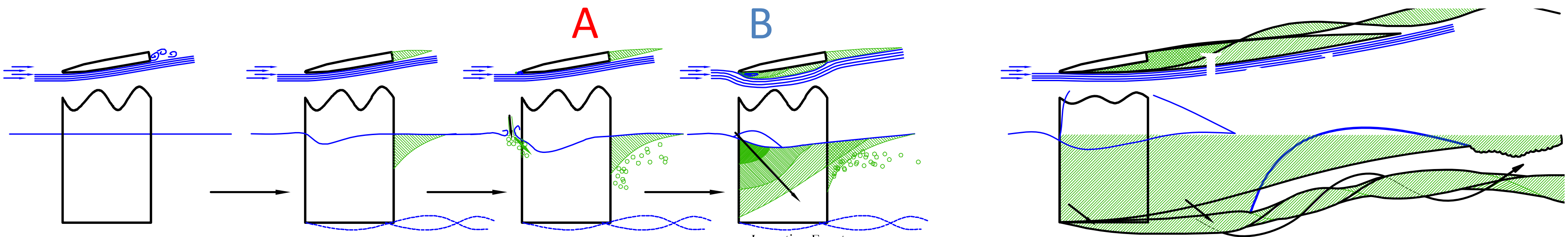

Fully Attached (FA) Regime: Flow is initially attached, with eddying separated wake (base pressure) behind TE

Low pressure near LE draws free surface down. Regions of subatmospheric pressures may exist, but the free surface forms a "seal" that prevents air-ingress.

Jet of air is injected at foil leading edge. This provides an air path and breaks the surface "seal."

Inception Event: Air is rapidly ingested into subatmospheric pressure zones, even after air jet is turned off. Cavity begins near LE at free surface and propagates toward TE at the submerged tip.

Fully Ventilated (FV) regime: Stable supercavity is developed (closure of cavity occurs downstream of TE). Bottom of cavity is rolled into the tip vortex, creating a fully-aerated vortex core

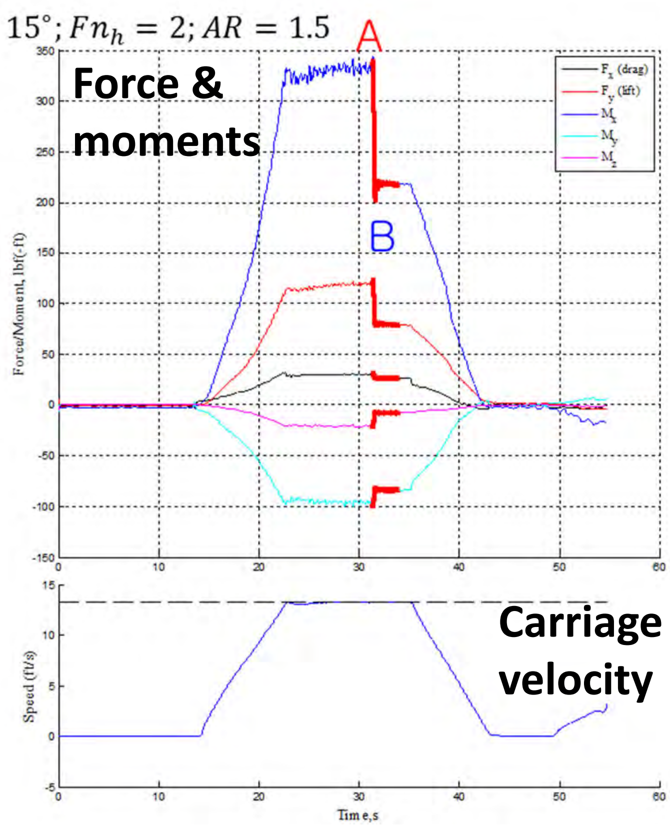

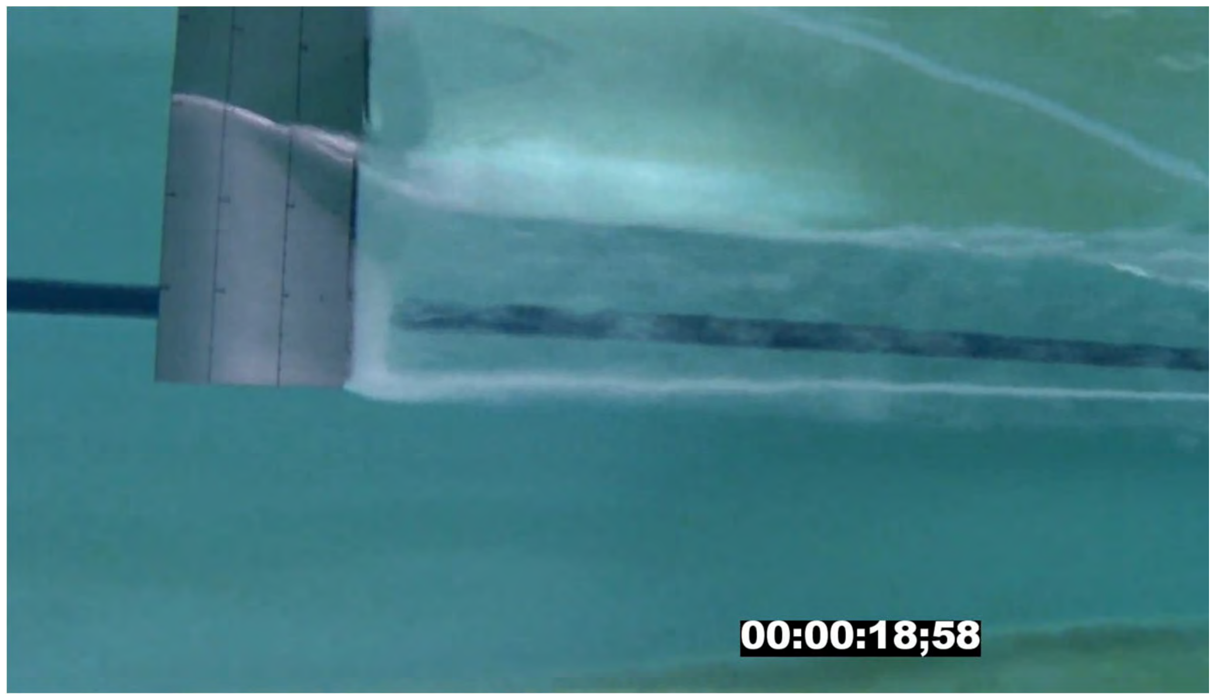

Video is playing at 1/6th the real speed

Cavitation-Induced Ventilation

MICHIGAN ENGINEERING
UNIVERSITY of MICHIGAN • COLLEGE of ENGINEERING

$\alpha = 5°,\ Fn_h = 2.25,\ AR_h = 1,\ \sigma_v = 0.35$

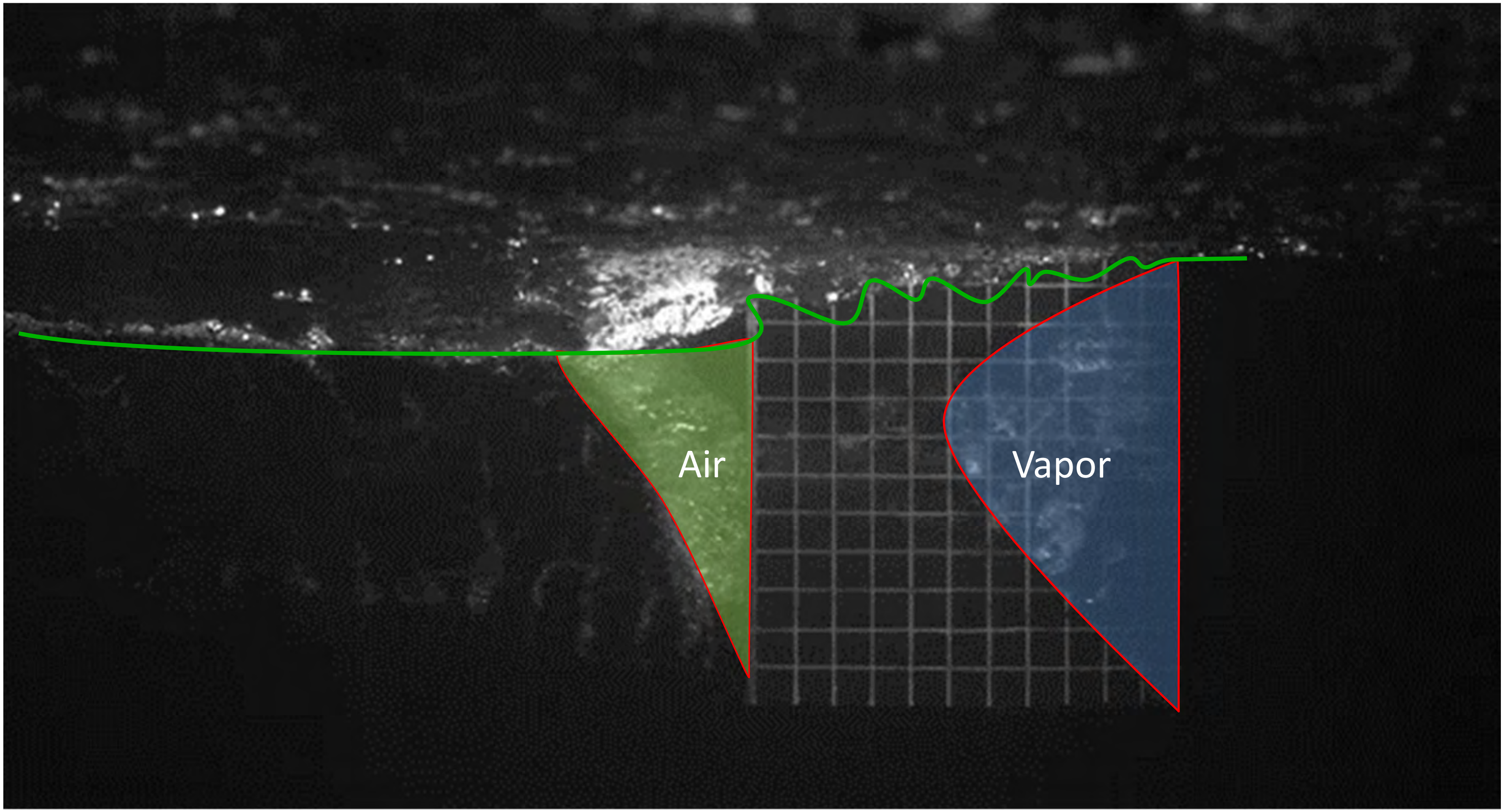

Video played back at 1/20th speed

Marine Technology Research Institute INSEAN

Cavitation & Ventilation Impact on Loads

- **Cavitation number**: $\boldsymbol{\sigma_c = \frac{P_\infty + \rho g h - P_C}{\frac{1}{2}\rho V^2} = \sigma_V + \frac{2}{{F_{n_h}}^2}; \ \sigma_V = \frac{P_\infty - P_V}{\frac{1}{2}\rho V^2}}$
  - P_C = cavity pressure; P_∞= free stream pressure ($P_\infty = P_0 + \rho g z$)
- **Ventilation:** filled with non-condensable gas (e.g. air)
  - $P_C = P_\infty$ (e.g. ambient pressure at free surface or 101.3 kPa in full-scale), σ_V=0, $\sigma_c = \frac{2}{{F_{n_h}}^2}$
- **Vaporous cavitation:** filled with water vapor
  - $P_C = P_V \approx 2\ kPa$

- The load coefficients for all 4 flow regimes can be collapse on to the same curve σ_c/α
- In general , as σ_c/α decreases, cavity length increases, and lift/thrust decreases.

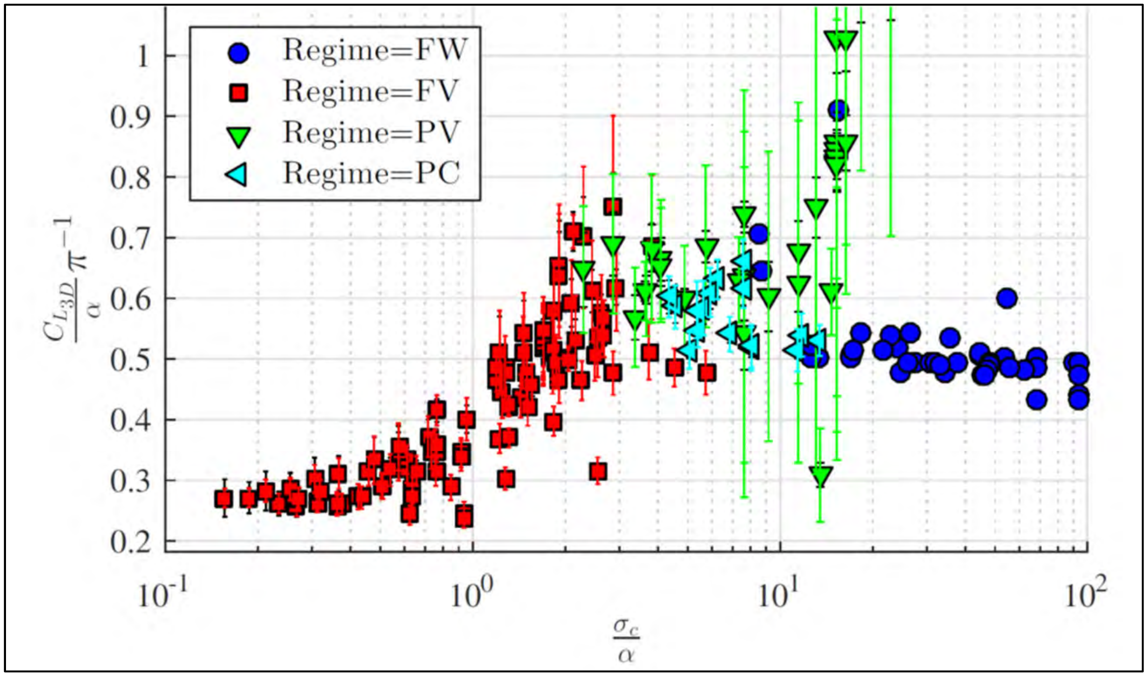

Ventilation Washout Condition

- The ventilated cavity washout condition is defined as when the cavity closure angle $\bar{\Phi} > 45°$, which creates an upstream component that destabilizes the cavity.

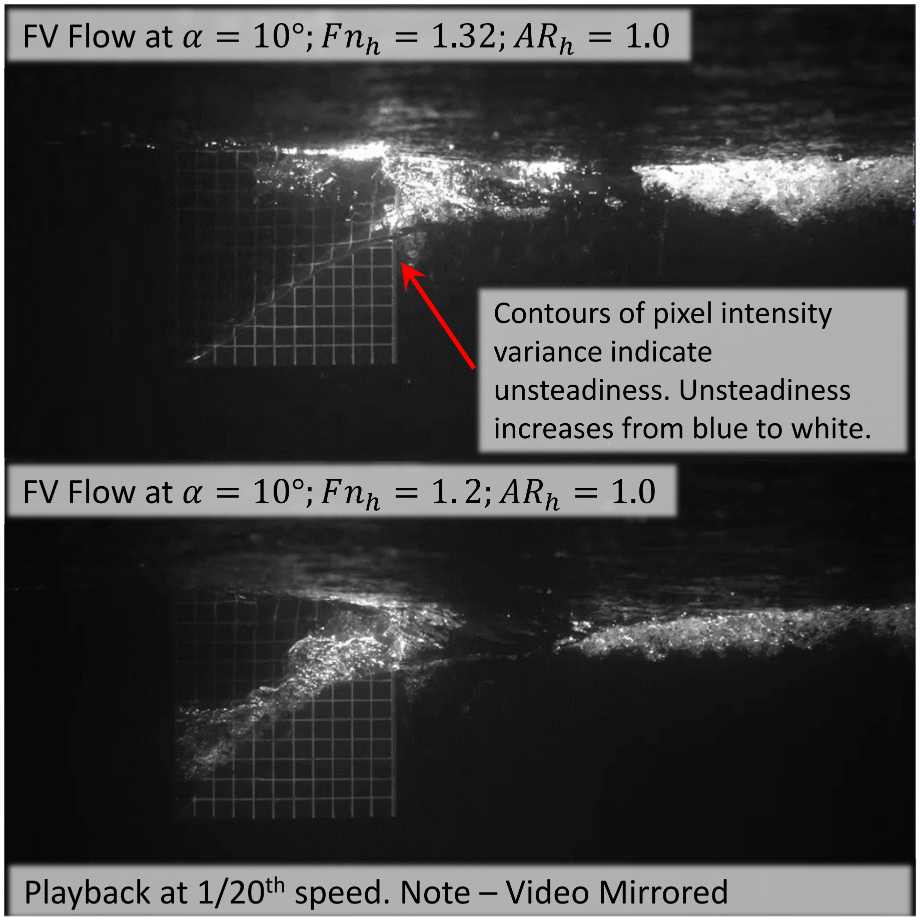

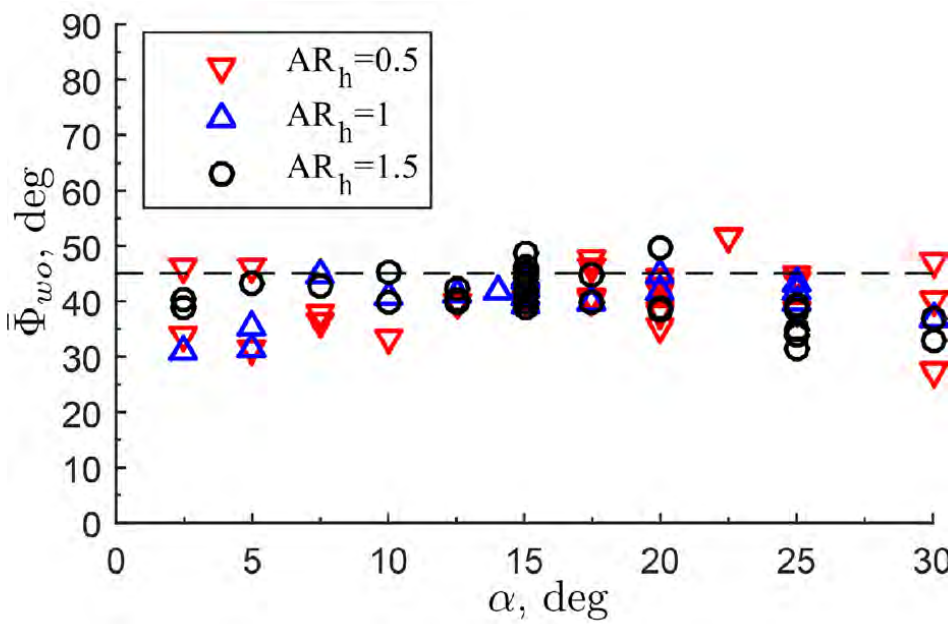

- Repeated tests at varied α, AR_h confirm the 45° criterion for cavity destabilization and washout.

Real-Time *In Situ* 3D Shape Sensing

MICHIGAN ENGINEERING
UNIVERSITY of MICHIGAN • COLLEGE of ENGINEERING

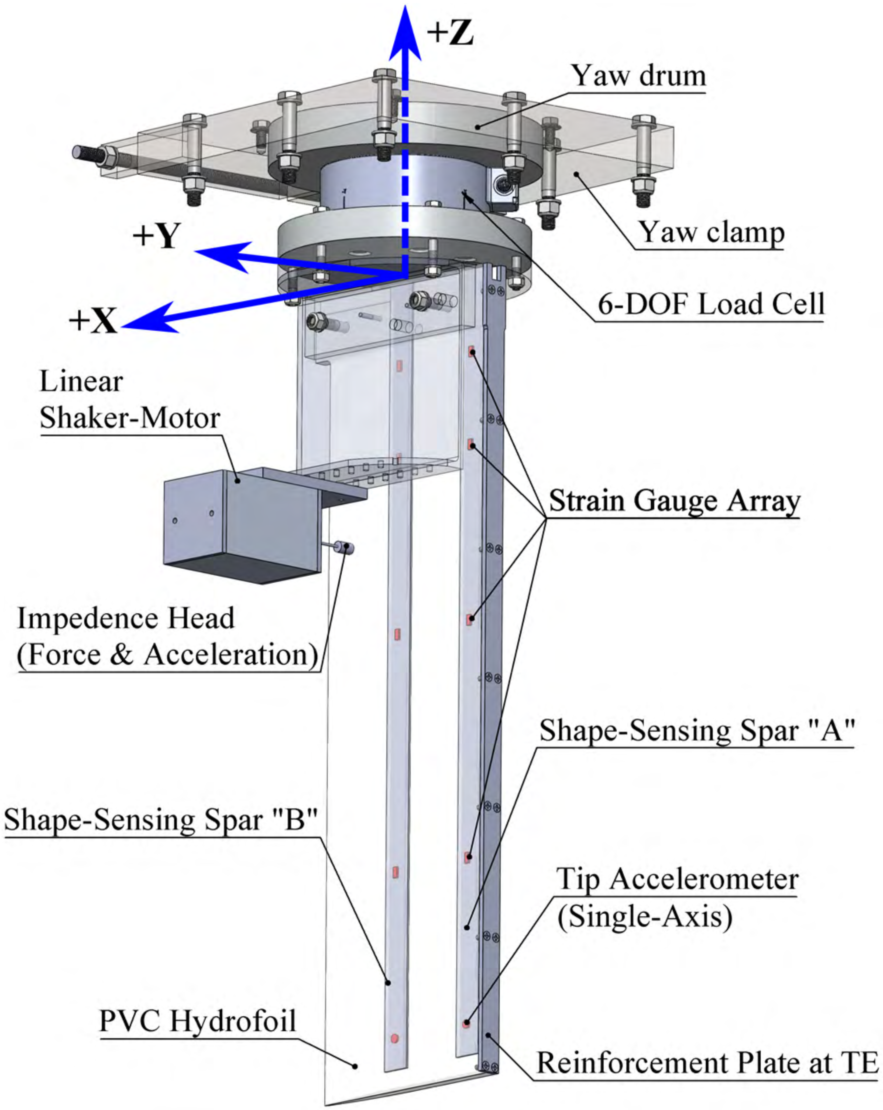

Use embedded strain sensors to determine the ***in situ*** 3-D deformations and vibration characteristics in **real-time**.

Influence of Ventilation on Dynamics

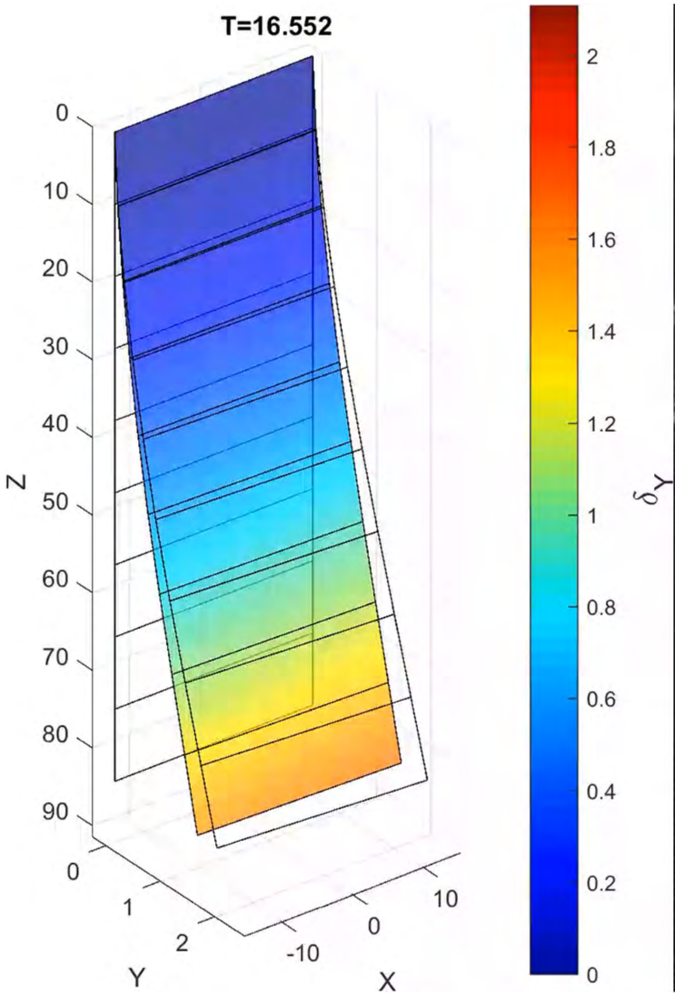

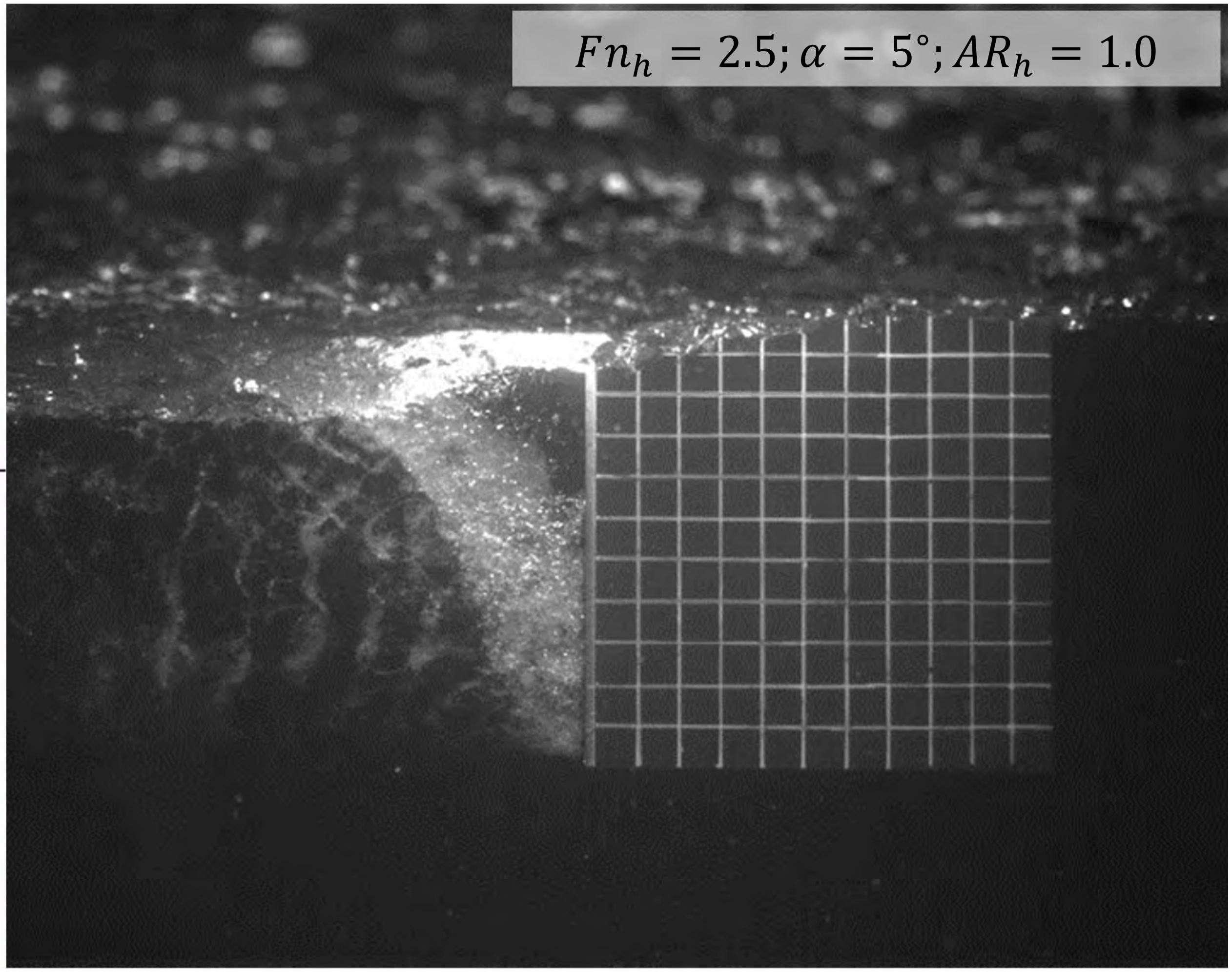

Video played back at $1/20^{th}$ speed

Use embedded sensors to determine the ***in situ*** 3-D deformations and vibration characteristics in complex multiphase flows.

Modeling of the Multiphase FSI Response

- General equation of motion:
- $\mathbf{M_S}\ddot{\mathbf{X}} + \mathbf{C_S}\dot{\mathbf{X}} + \mathbf{K_S}\mathbf{X} = \mathbf{F_{EX}}(\boldsymbol{t}) + \mathbf{F_{FL}}(\boldsymbol{t})$
- $\mathbf{F_{FL}}(\boldsymbol{t}) = \underbrace{-\left(\mathbf{M_{FL}}(\boldsymbol{t})\ddot{\mathbf{X}} + \mathbf{C_{FL}}(\boldsymbol{t})\dot{\mathbf{X}} + \mathbf{K_{FL}}(\boldsymbol{t})\mathbf{X}\right)}_{\text{Motion-induced (FSI) Forces}} + \underbrace{\mathbf{F_{sf,r}} + \mathbf{F_{uf,\boldsymbol{r}}}(\boldsymbol{t})}_{\text{Flow-induced (rigid body) forces}}$
- $(\mathbf{M_S} + \mathbf{M_{FL}}(\boldsymbol{t}))\ddot{\mathbf{X}} + (\mathbf{C_S} + \mathbf{C_{FL}}(\boldsymbol{t}))\dot{\mathbf{X}} + (\mathbf{K_S} + \mathbf{K_{FL}}(\boldsymbol{t}))\mathbf{X} =$

  $\mathbf{F_{EX}}(\boldsymbol{t}) + \mathbf{F_{sf,r}} + \mathbf{F_{uf,\boldsymbol{r}}}\ (\boldsymbol{t})$

How do fluid-to-solid force ratios vary with:

Submergence
Flow speed or Fn_h
Flow regime: FW, PC, PV or FV

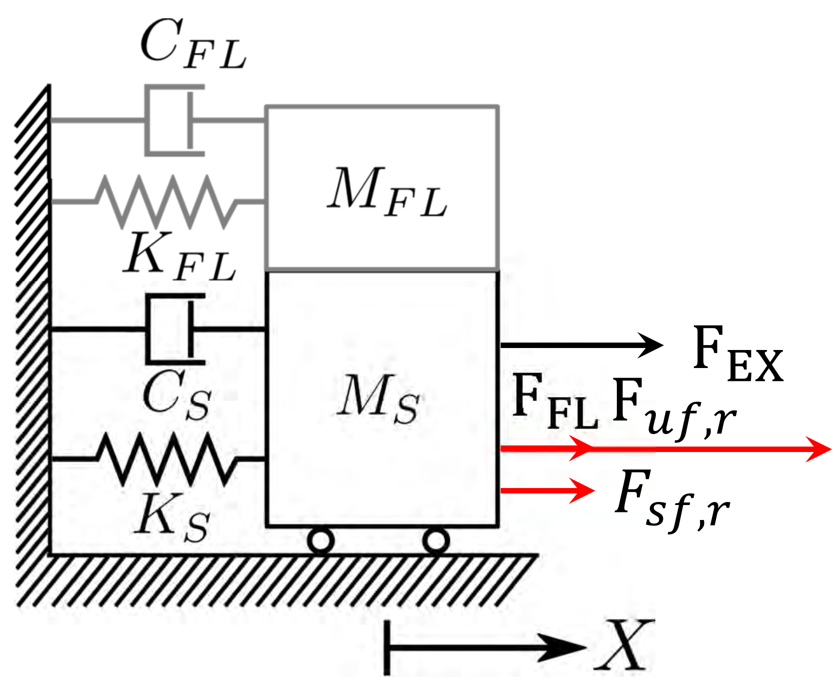

Influence of Submergence on Vibrations

MICHIGAN ENGINEERING
UNIVERSITY of MICHIGAN • COLLEGE of ENGINEERING

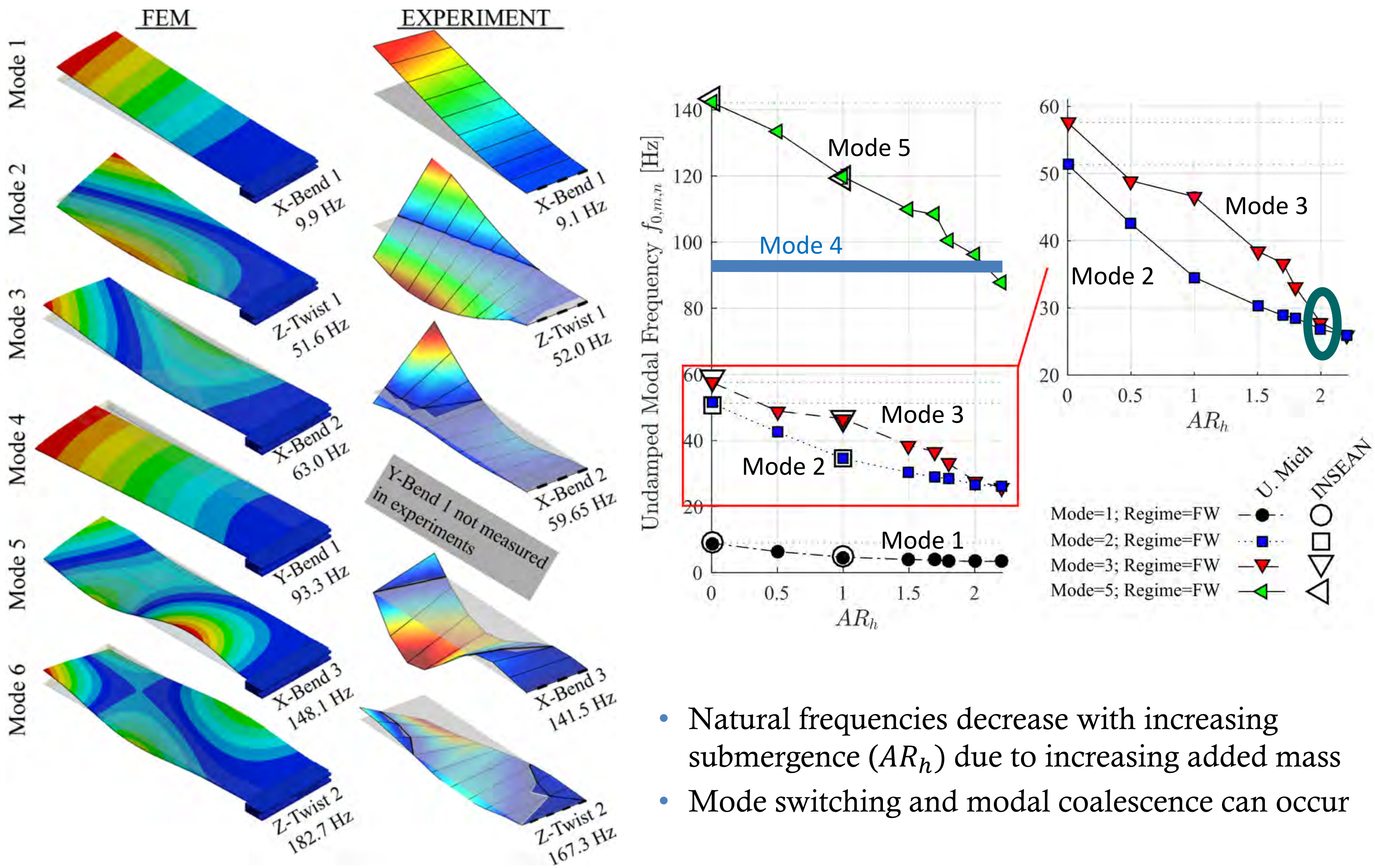

- Natural frequencies decrease with increasing submergence (AR_h) due to increasing added mass
- Mode switching and modal coalescence can occur

Influence of Ventilation on Vibrations

MICHIGAN ENGINEERING
UNIVERSITY of MICHIGAN • COLLEGE of ENGINEERING

- Natural frequencies vary with speed => potential for frequency coalescence at higher speeds
- Natural frequencies tend to increase with cavitation/ventilation b/c of lower added mass

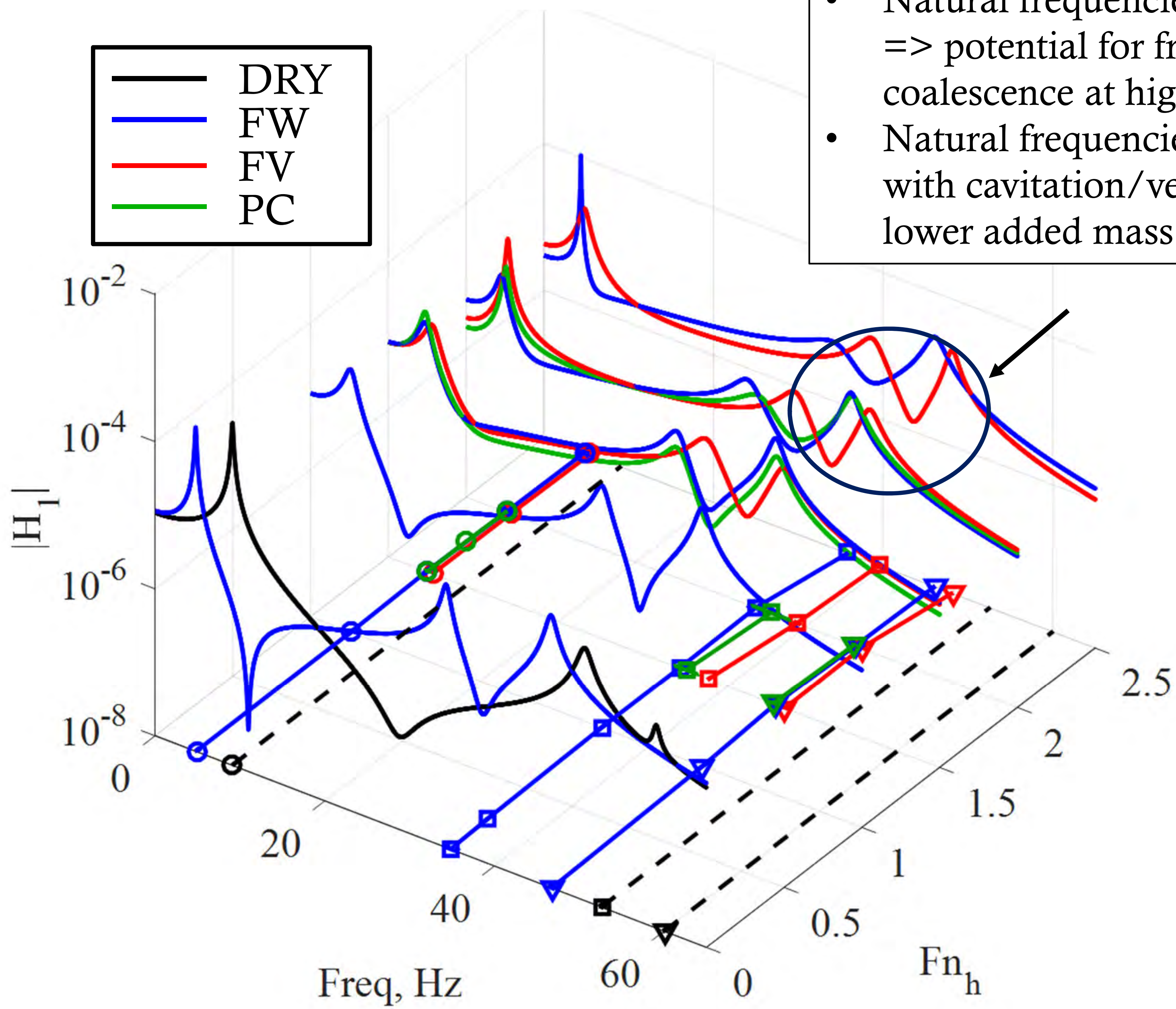

$AR_h = 1$

Waves & Ventilation Effect on Dynamics

MICHIGAN ENGINEERING
UNIVERSITY of MICHIGAN ▪ COLLEGE of ENGINEERING

Surface-Piercing Hydrofoil: $AR_h = 2, Fn_h = 1.5$

$\alpha = 5^o$ **(FW)**
$\zeta = 3$ cm
$f = 0.67$ hz
f_e=1.73 Hz

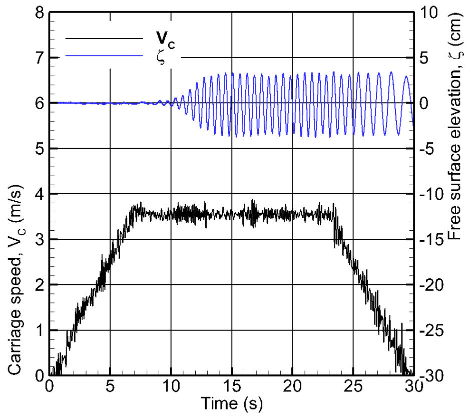

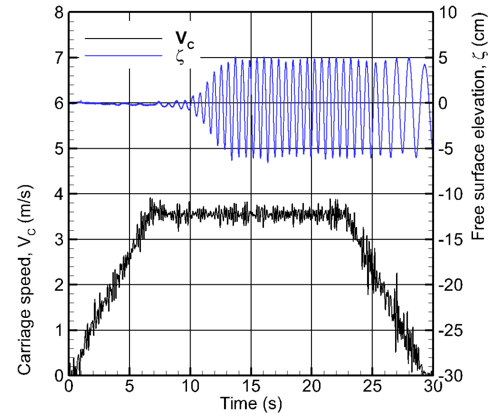

$\alpha = 20^o$ **(FV)**
$\zeta = 5$ cm
$f = 0.67$ hz
f_e=1.67 Hz

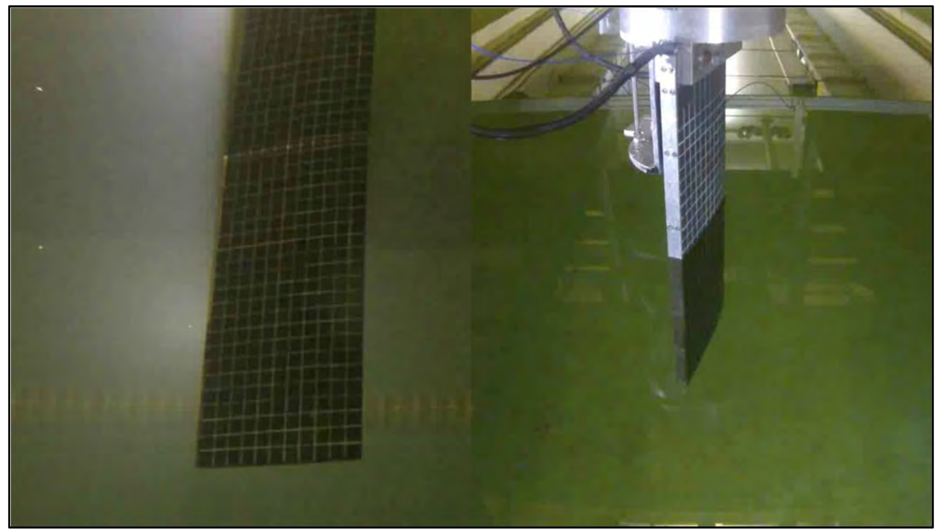

Impact of Frequency Coalescence

MICHIGAN ENGINEERING
UNIVERSITY of MICHIGAN • COLLEGE of ENGINEERING

Ventilation Effect on Load Coefficients: $AR_h = 2, Fn_h = 1.5$

α = 5° (FW, Calm Water) | α = 20° (FV, Calm Water)

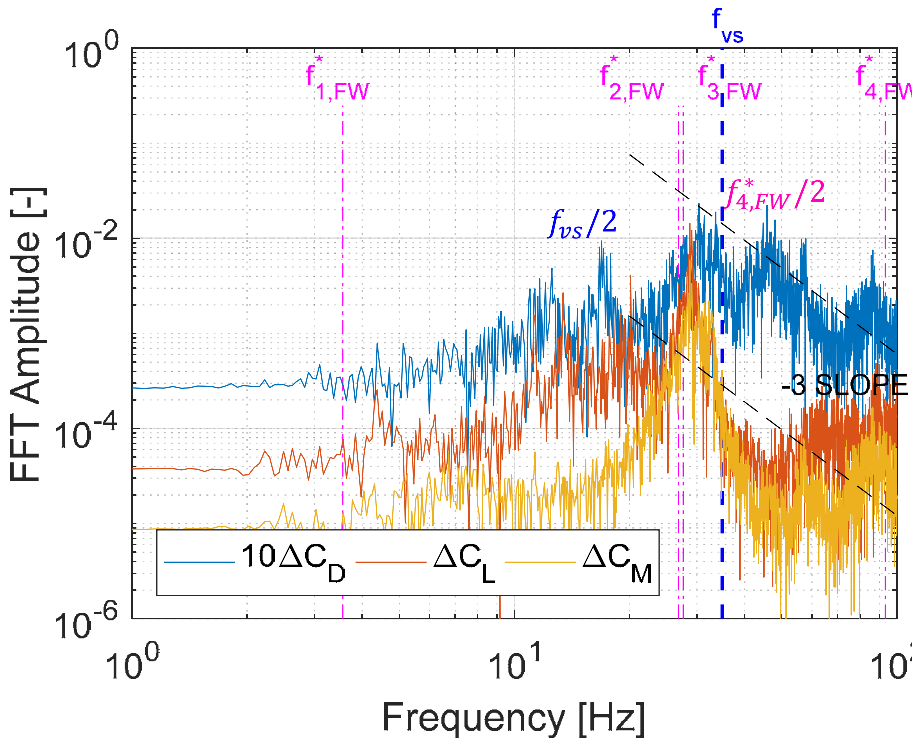

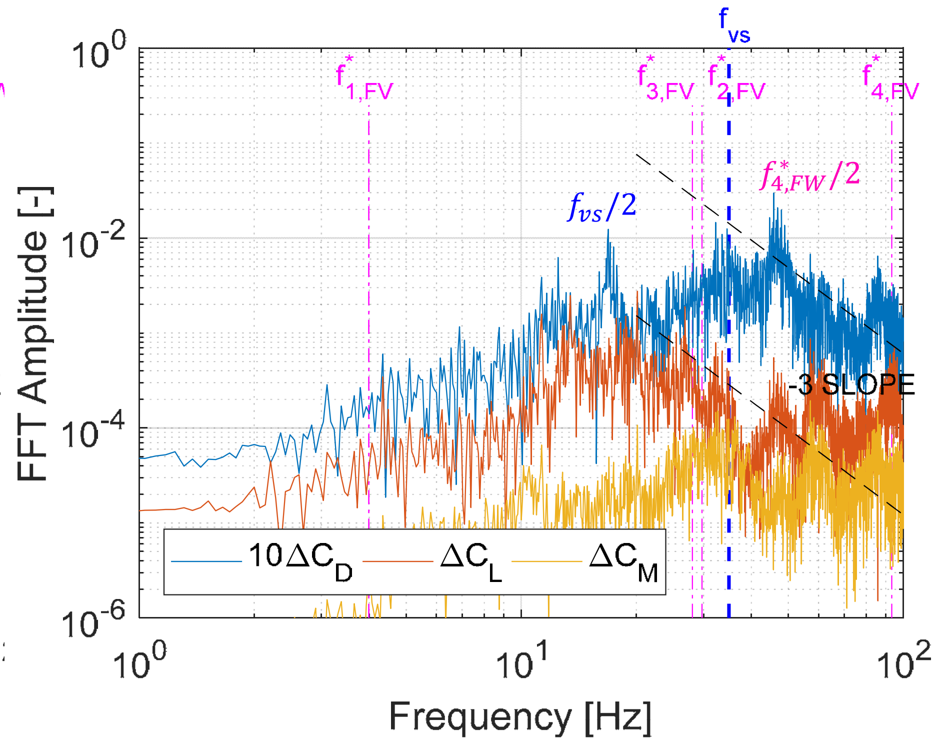

- In FW flow, modes 2 and 3 coalesced => significant dynamic load amplification near 27 Hz
- In FV flow, modes 2 and 3 separated => peak near 27 Hz reduced drastically

In Situ Hydroelastic Load Reconstruction

MICHIGAN ENGINEERING
UNIVERSITY of MICHIGAN • COLLEGE of ENGINEERING

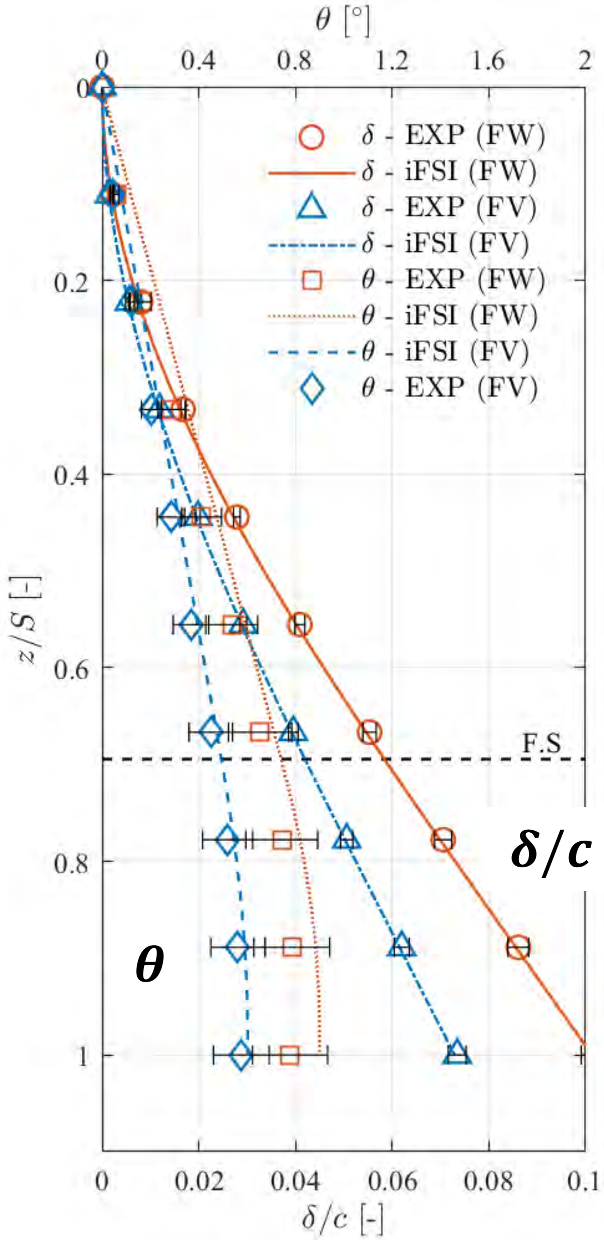

	EXP (FW)	iFSI (FW)	EXP (FV)	iFSI (FV)
α	10°	9.759°	10°	10.55°
AR_h	1.00	1.01	1.00	1.01
C_L	0.282	0.276	0.196	0.200
C_M	0.073	0.069	0.025	0.026

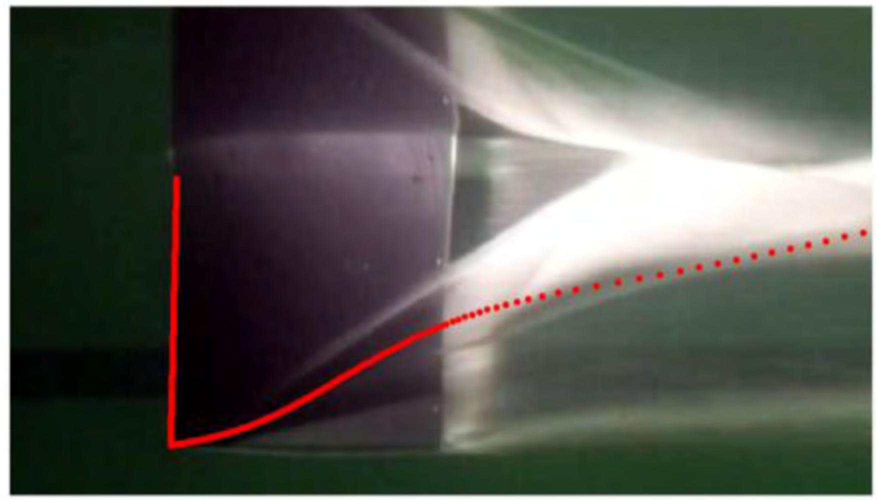

- Good agreement between predicted and actual operating conditions (α and AR_h), and resulting hydrodynamic load coefficients and deformations.
- CPU time: 0.7 s

Active Ventilation Inception Control

MICHIGAN ENGINEERING
UNIVERSITY of MICHIGAN ■ COLLEGE of ENGINEERING

$\alpha = 15^o; AR_h = 1; \pm 5.5$ **lbs exciting force**

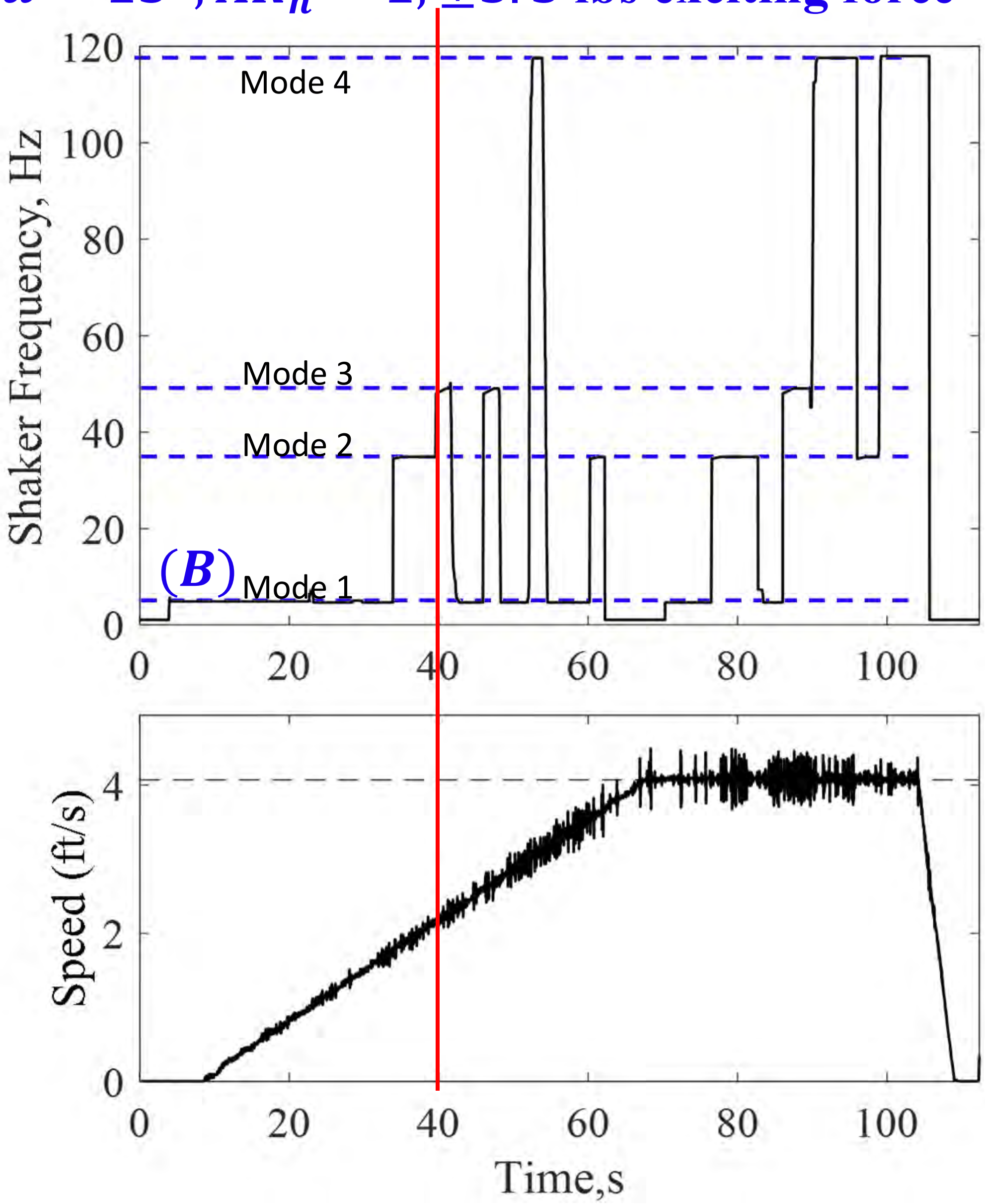

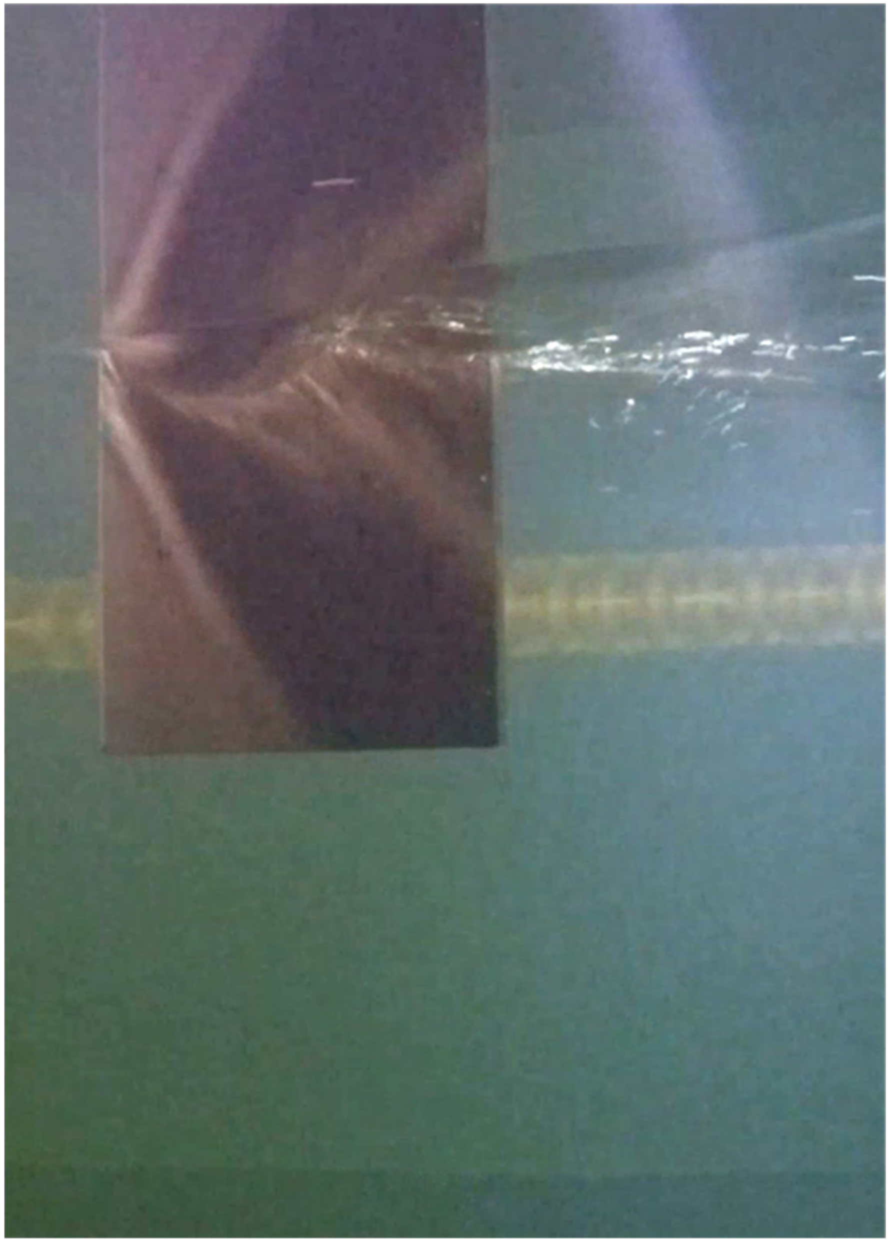

Why Lightweight Composites?

- Drastically expand design space by introducing material in addition to geometric parameters to modify the steady-state and dynamic performance, change stability boundaries, and control flow-induced vibrations and noise
- Improve fatigue performance & reduce life-cycle cost
- Enable *in situ* sensing and control => multi-functional!

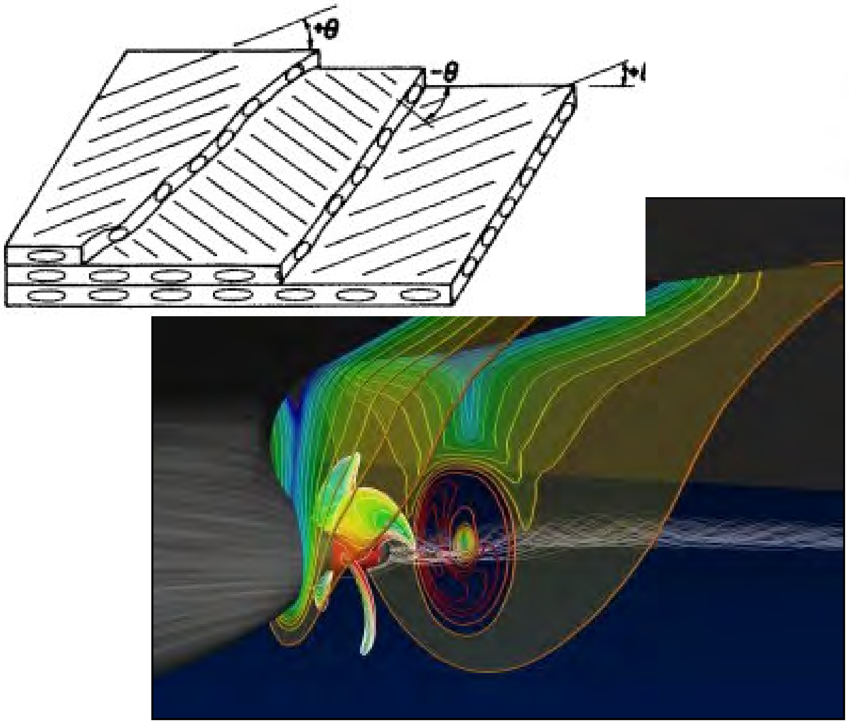

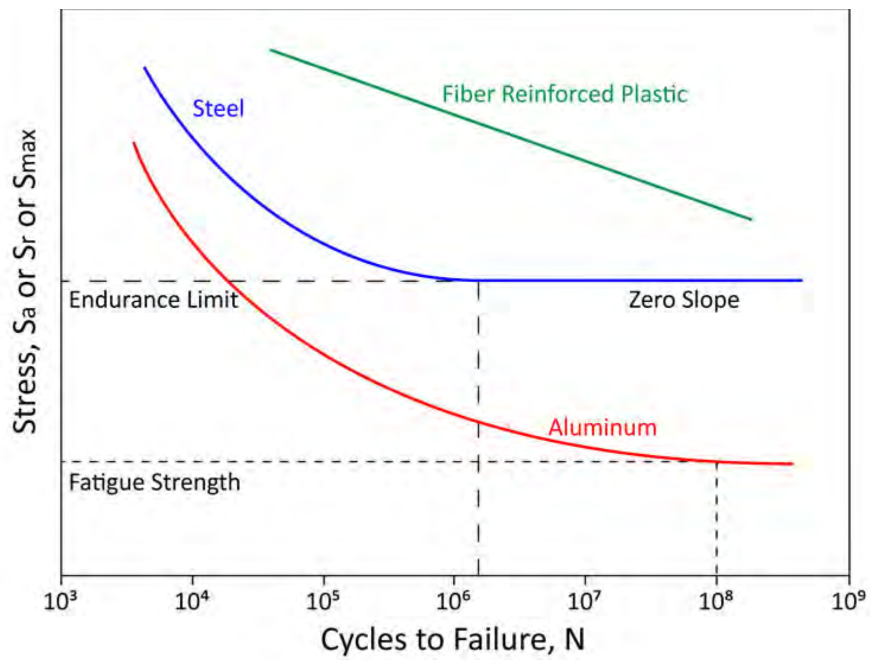

https://www.qualitymag.com/articles/94171-stress-life-fatigue-testing-basics

Tailoring of Material Anisotropy

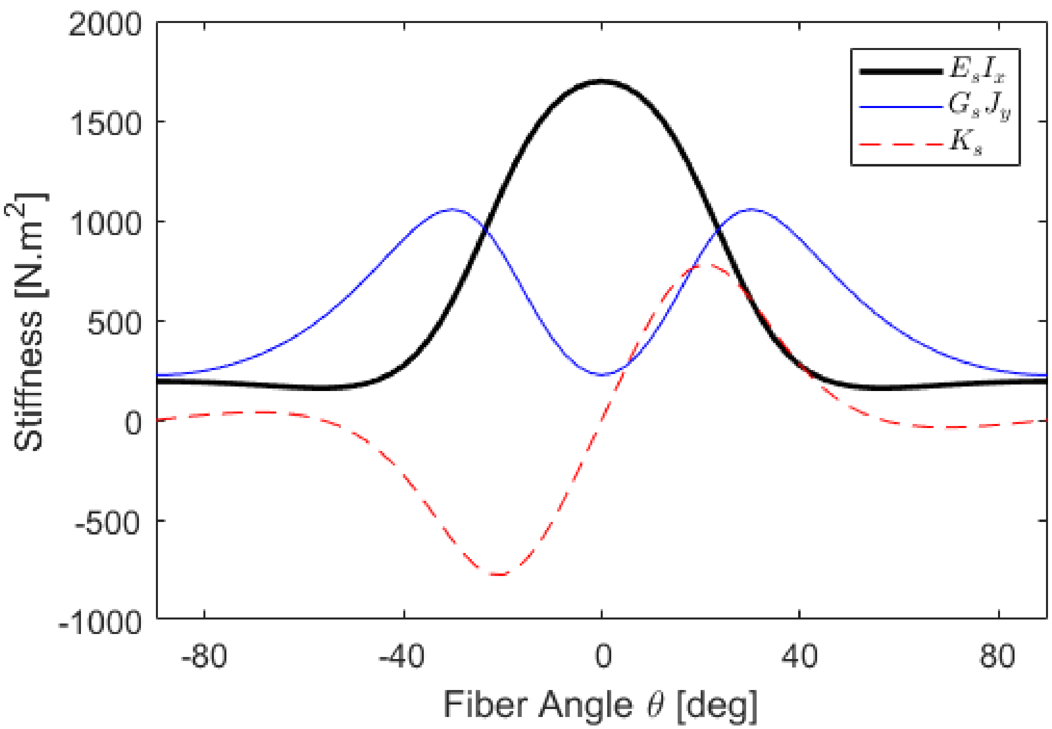

CFRP +30 CFRP 00 CFRP -30 SS

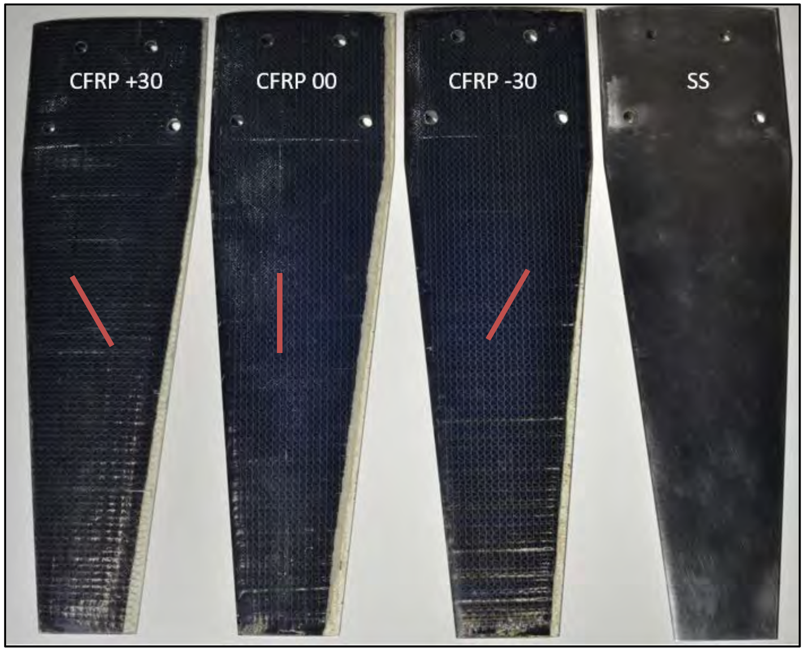

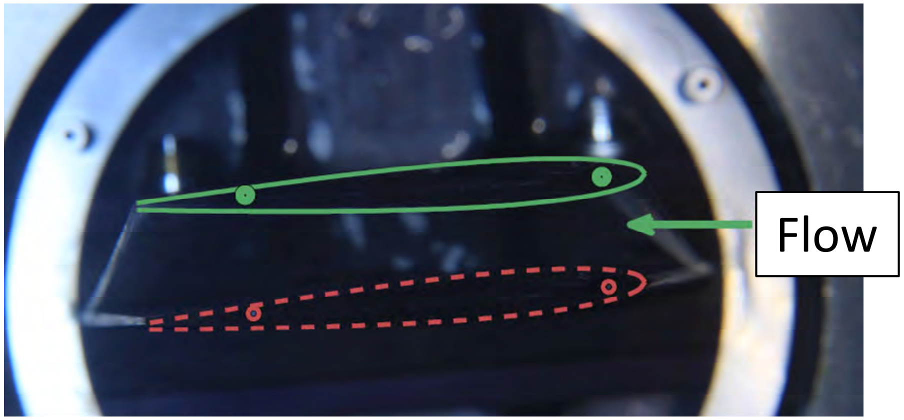

CFRP +30; δ_{tip} = 13.5 mm; θ_{tip} = -1.04°

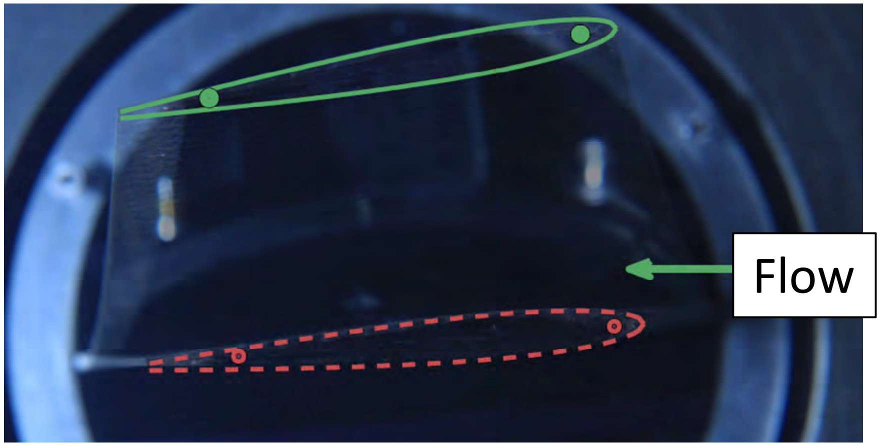

CFRP -30; δ_{tip} = 32.8 mm; θ_{tip} = 5.10°

Steady-State Anisotropic Response

$\alpha = 10^o$ & $Re = 10^6$

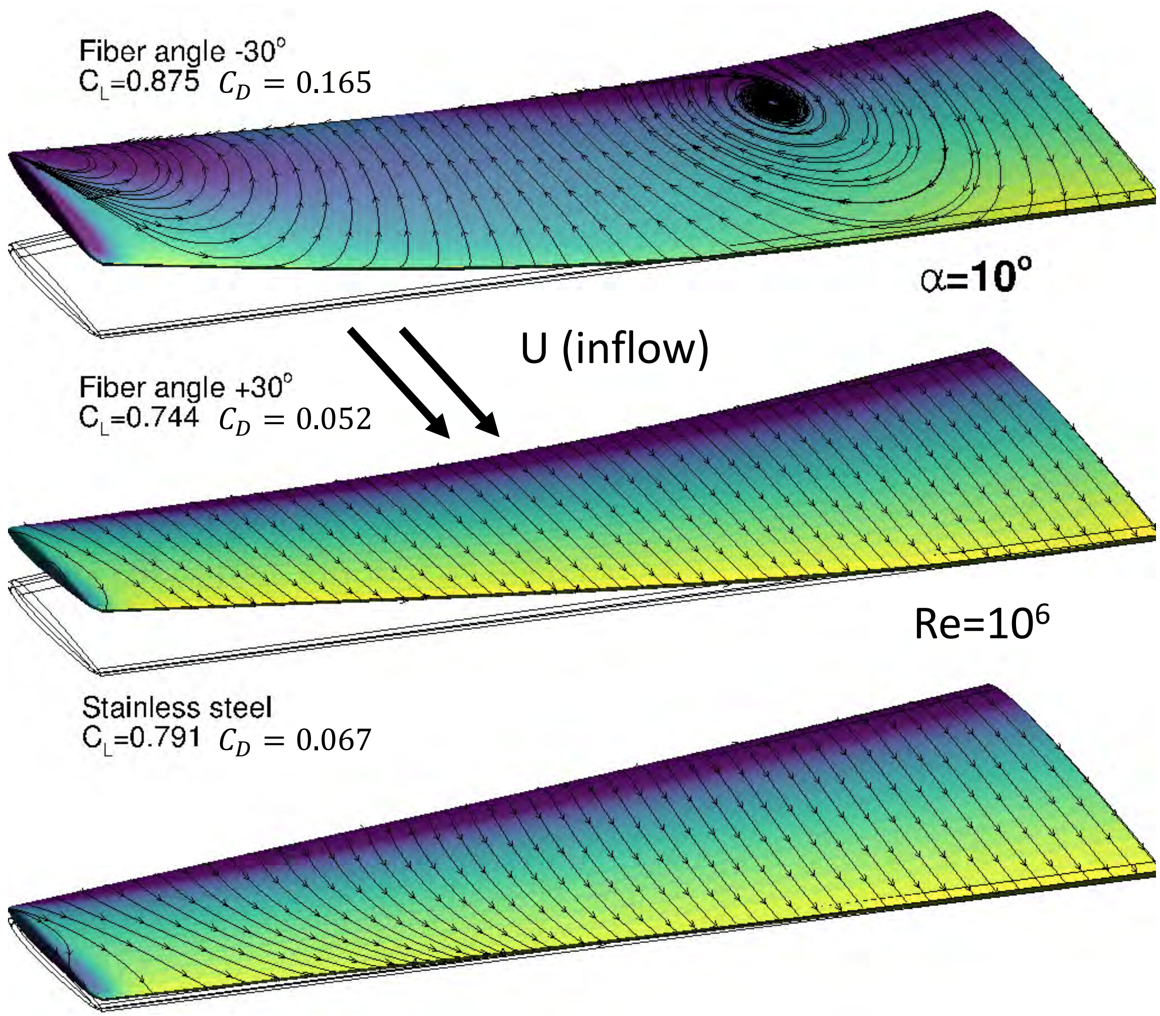

CFRP -30
Nose-up twist
Increased forces

CFRP +30
Nose-down twist
Reduced forces

SS
Rigid Reference

Bend-twist coupling caused by material anisotropy can drastically impact foil performance, including lift & drag, stall angle, and cavitation inception speed

Load Dependent & Anisotropic Response

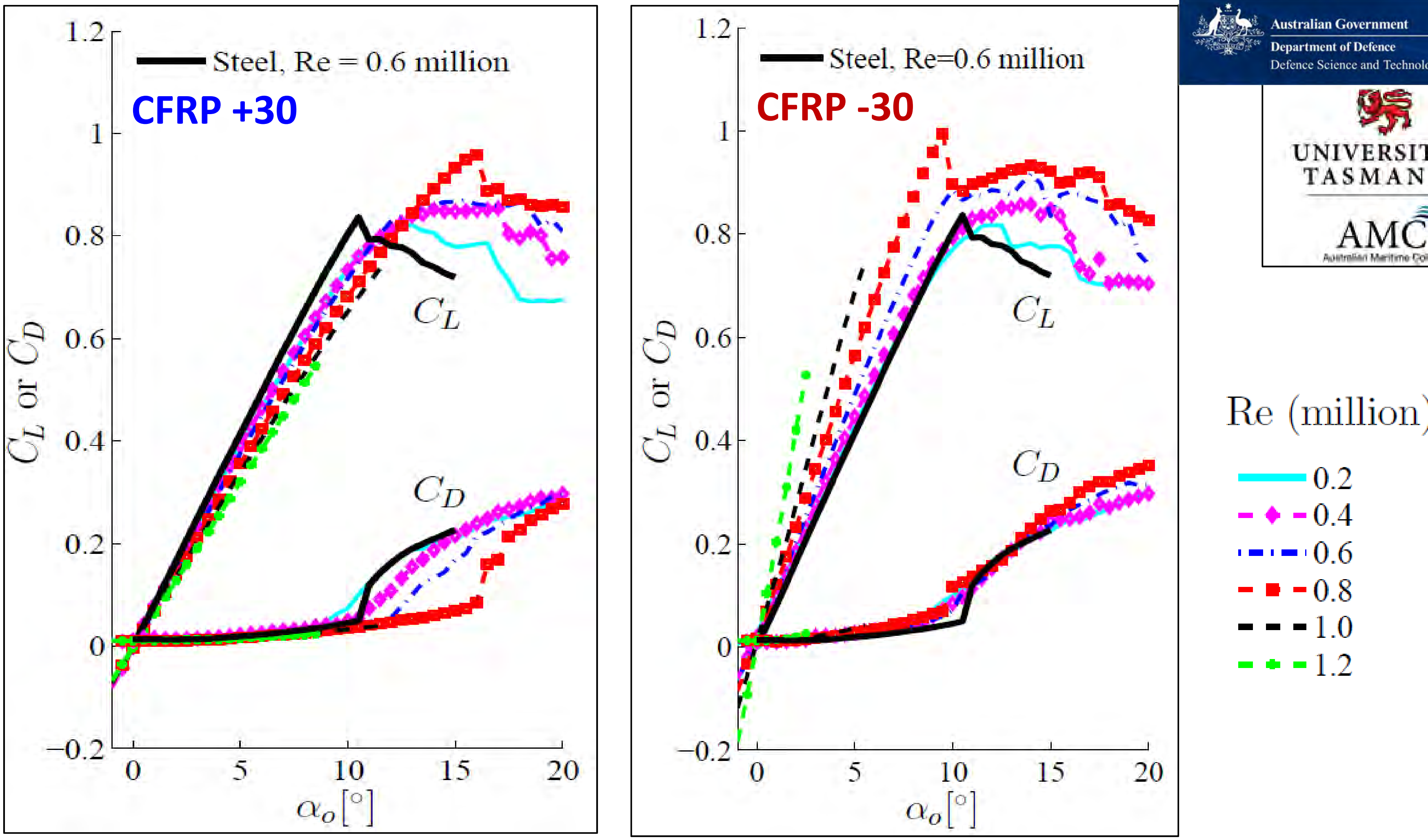

Experiment Result: Nose-down twist caused by material anisotropy of the CFRP +30 hydrofoil lead to decrease in lift & moment and delayed stall with increasing flow speed, while the opposite is true for the CFRP -30 hydrofoil.

Dry vs. Wet Mode Shapes

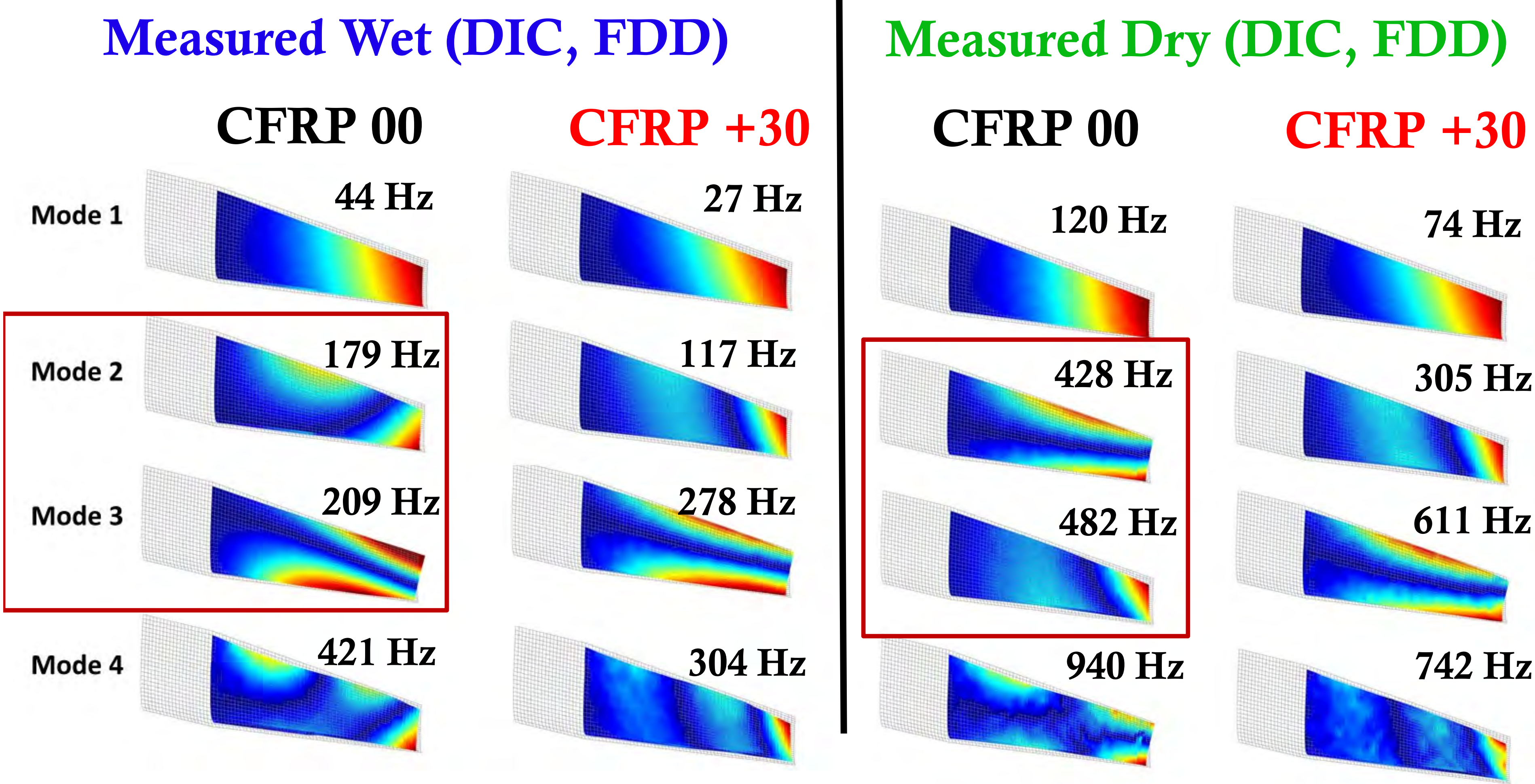

The dry and wet modes 2 and 3 switch order for the CFRP 00 hydrofoil because of higher added mass for the bending compared to pitching motions

Dry vs. Wet Natural Frequencies

MICHIGAN ENGINEERING
UNIVERSITY of MICHIGAN • COLLEGE of ENGINEERING

Australian Government
Department of Defence
Science and Technology

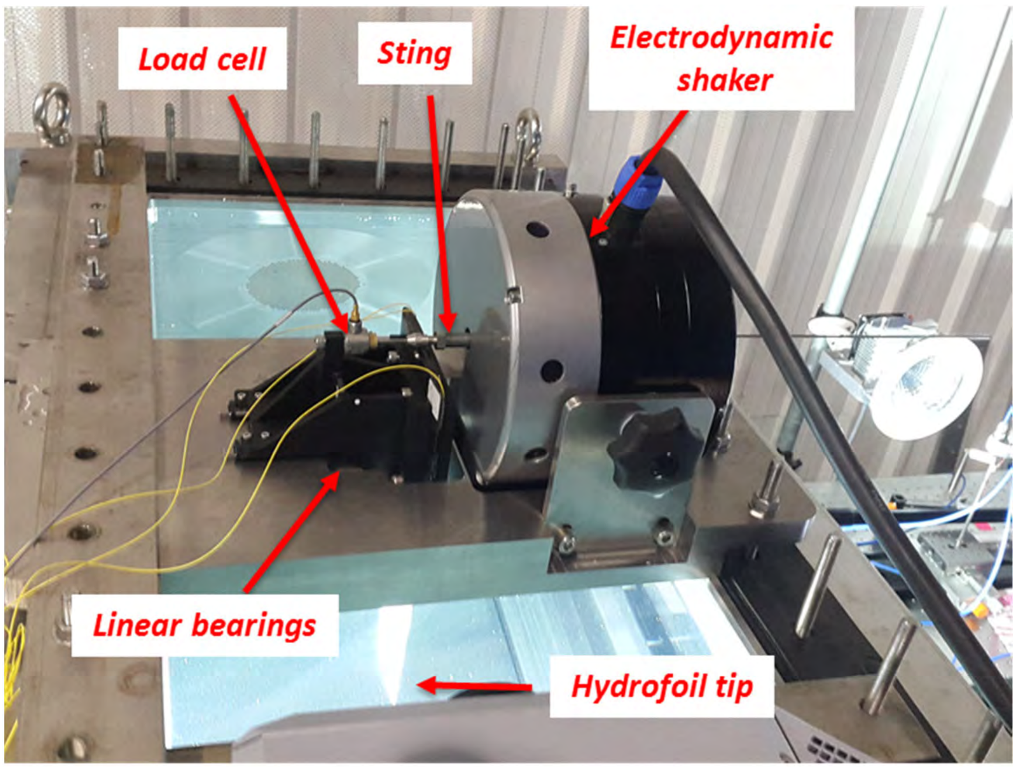

Test setup (Wet)

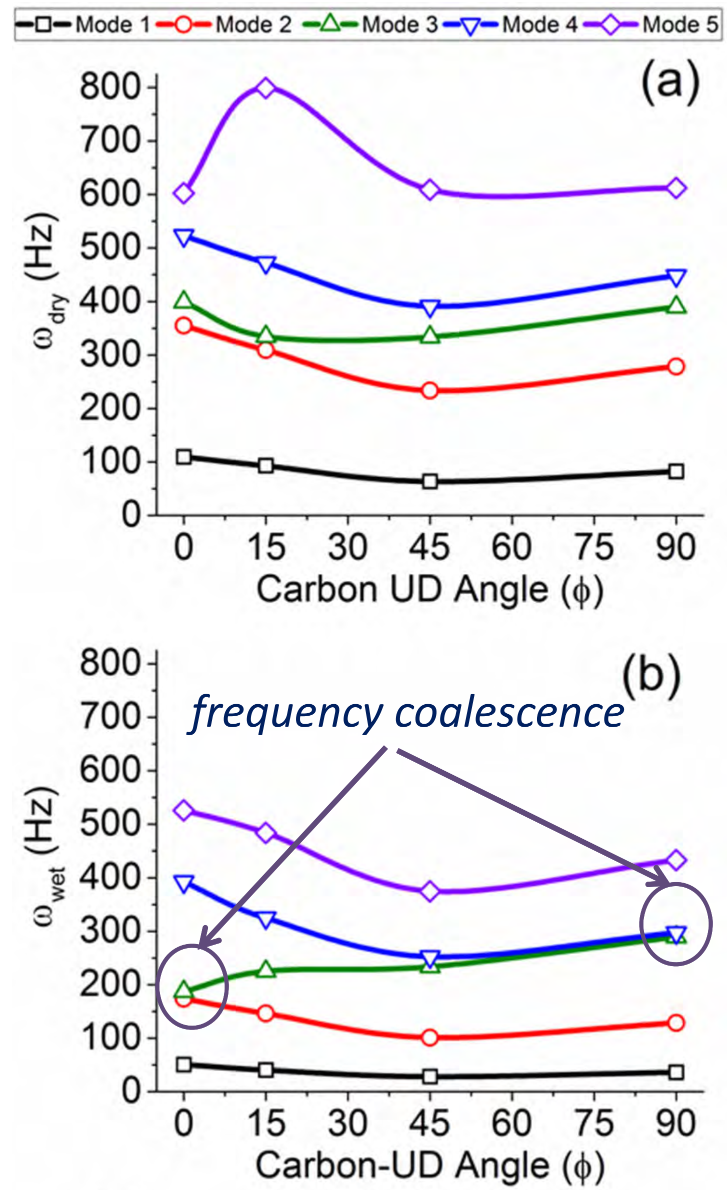

Cavity Pattern: Re=0.8e6, σ=0.66, α=6º

MICHIGAN ENGINEERING
UNIVERSITY of MICHIGAN • COLLEGE of ENGINEERING

Australian Government
Department of Defence
Defence Science and Technology Group

UNIVERSITY of TASMANIA
AMC
Australian Maritime College

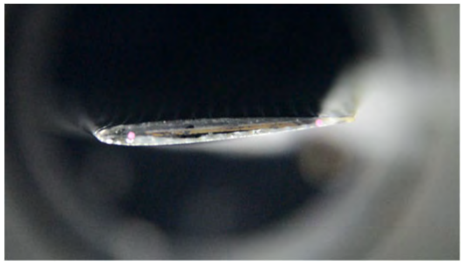

CFRP +30º Hydrofoil

CFRP -30º Hydrofoil

3D Cavitation Pattern: $\sigma = 0.6, \alpha_o = 6^o$

Observed

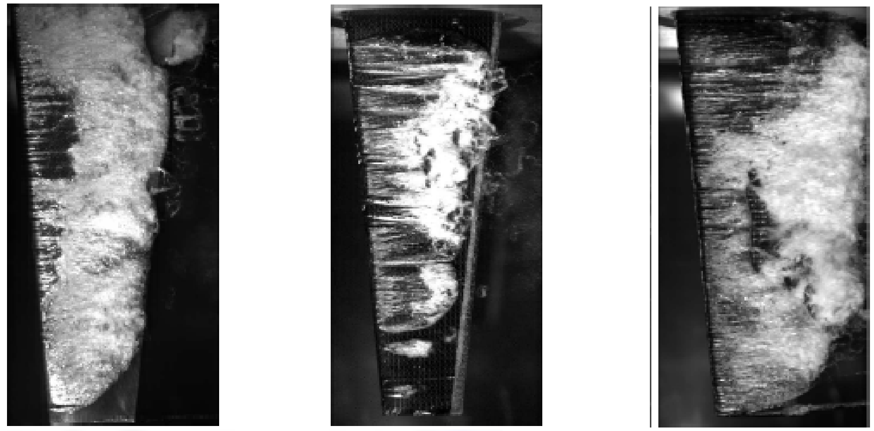

Predicted

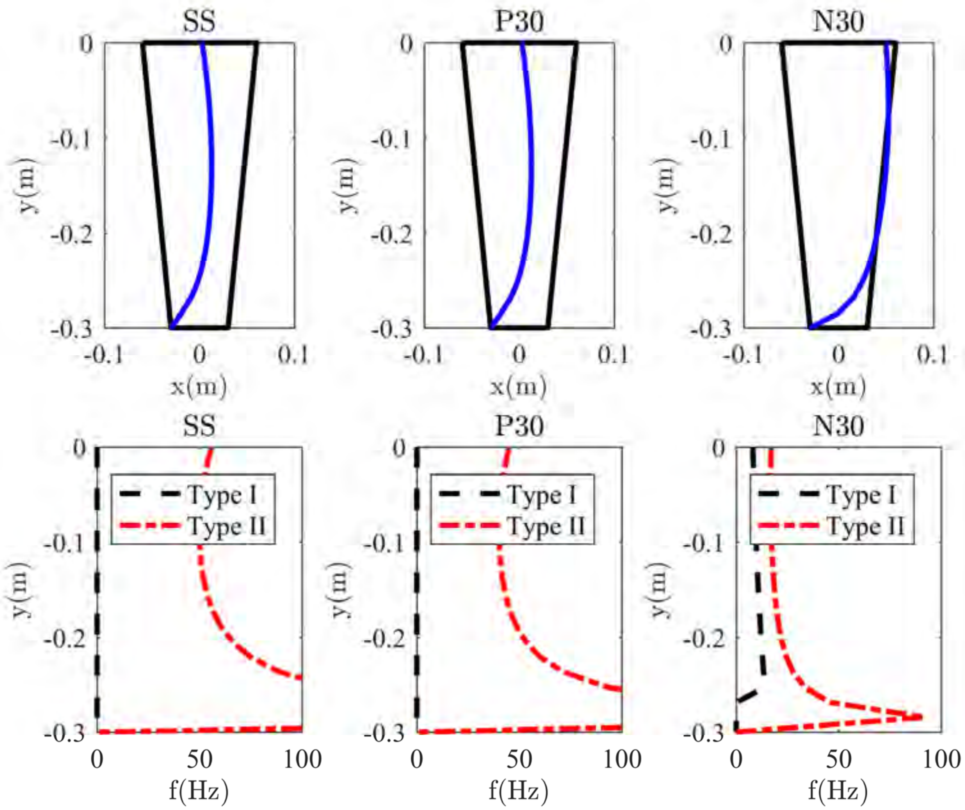

Type I shock-wave driven

$\mathrm{St}_1 = \frac{\mathrm{f}_1 \mathrm{c}}{\mathrm{U}} = 0.12 \quad (f_1 = 11\ \mathrm{Hz})$

for $0.75 \leq \frac{L_c}{c} \leq 1.75$

Type II re-entrant jet driven

$$\mathrm{St}_2 = \frac{\mathrm{f}_2 \mathrm{c}}{\mathrm{U}} = 0.0052\psi^3 + St_1$$

3D Cavitation Pattern: $\sigma = 0.25, \alpha_o = 6^o$

Observed

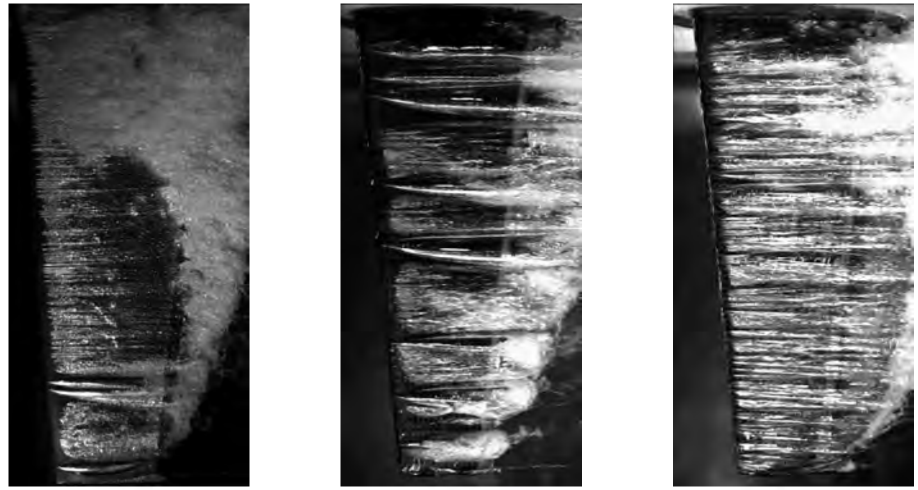

Predicted

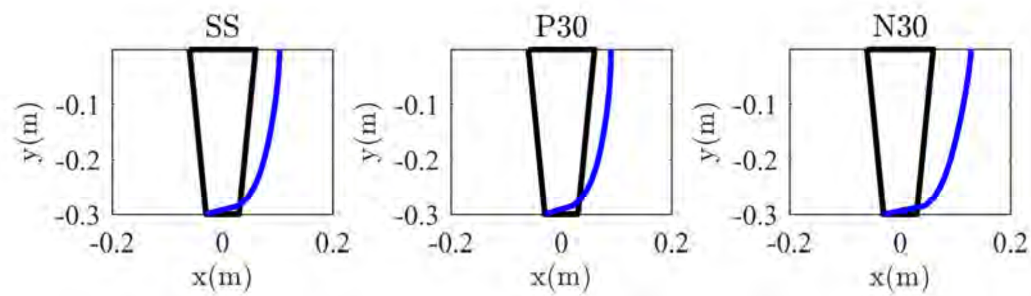

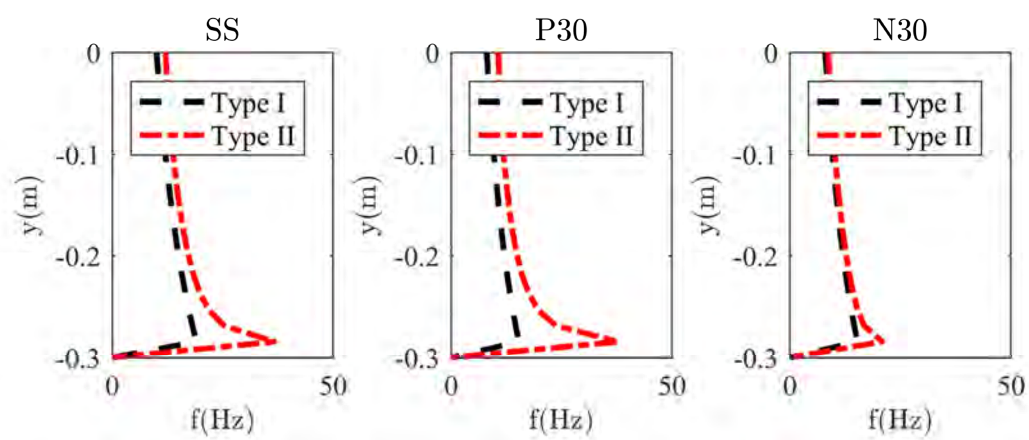

Both Type I and Type II shedding occur at $\sigma = 0.25$, and the cavity shedding frequencies nearly coincide.

Cavity Shedding Dynamics

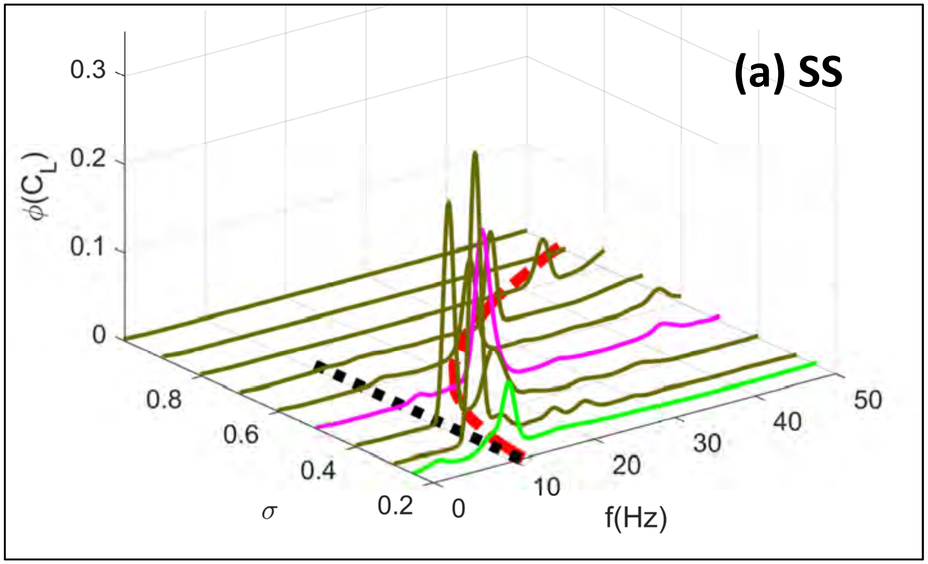

- The peaks of the lift frequency spectra generally fall along the Type I and Type II cavity shedding frequency curves, and the peaks are most intense when Types I and II cavity shedding occur simultaneously.
- Additional peaks near 30 Hz can be observed for the P30 & N30 hydrofoils, which corresponds to when the Type II cavity shedding frequency is near the foil's first wetted natural frequency.

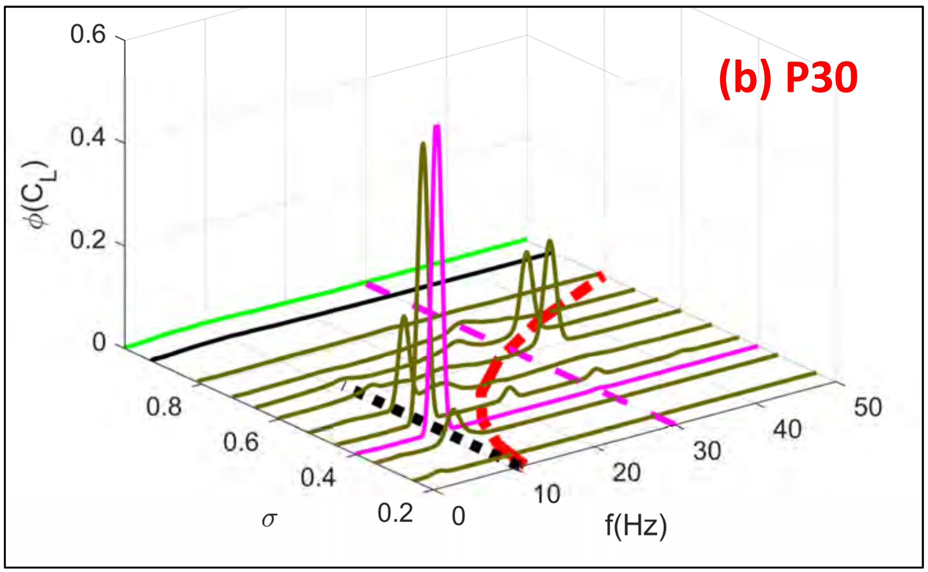

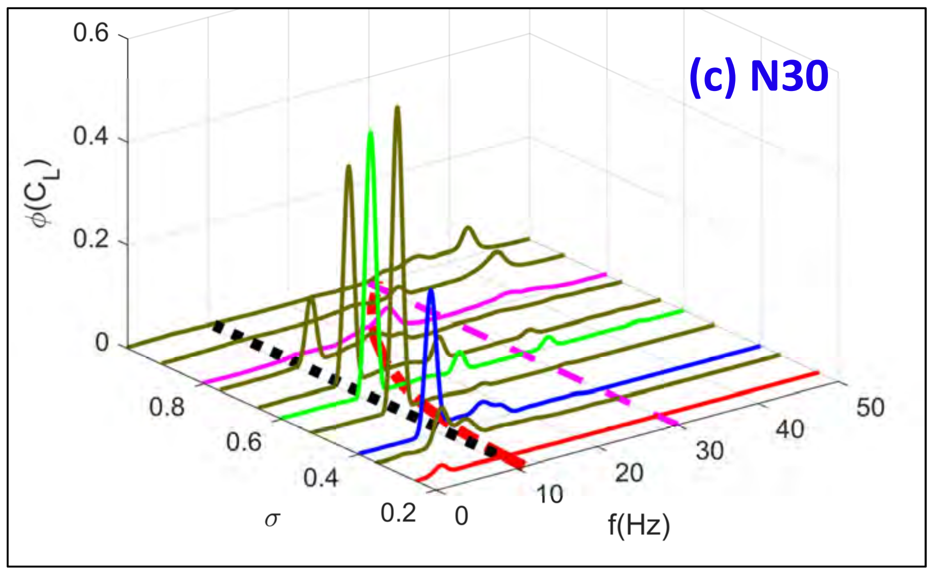

Composite Hydrofoil in FW Flow

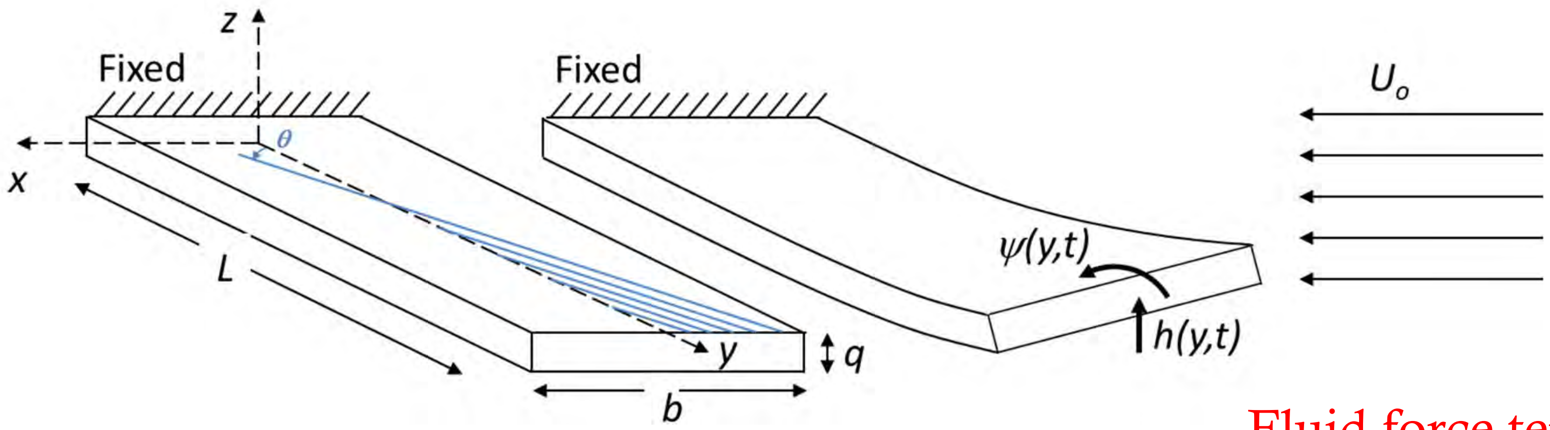

Fluid force terms

$$m_s \frac{\partial^2 h}{\partial t^2} - \boxed{m_s x_\alpha b \frac{\partial^2 \psi}{\partial t^2}} = -EI_s \frac{\partial^4 h}{\partial y^4} \boxed{-K_s \frac{\partial^3 \psi}{\partial y^3}} \boxed{-ab \frac{\partial^4 \psi}{\partial y^4}} + \boxed{F_z},$$

$$I_s^{E.A.} \frac{\partial^2 \psi}{\partial t^2} - \boxed{m_s x_\alpha b \frac{\partial^2 h}{\partial t^2}} = +GJ_s \frac{\partial^2 \psi}{\partial y^2} \boxed{+K_s \frac{\partial^3 h}{\partial y^3}} \boxed{-abEI_s \frac{\partial^4 h}{\partial y^4} - S_s \frac{\partial^4 \psi}{\partial y^4}} + \boxed{M_y}$$

Bend-twist coupling terms

Warping terms

Q: How to model the forces/moments due to the external flow?

- Use analytical potential flow model for balance of efficiency & accuracy
- Glauert's lifting line theory + Theodorsen's unsteady foil theory

Hydroelastic Model – w/o Sweep

Inviscid, Incompressible Flow Theory: Theodorsen (1935), Sears (1941)

- Assumes thin oscillating plate, small deformations
- Assumes wake parallel to inflow, no separation

$$\mathbf{M}_s\begin{pmatrix}\ddot{h}\\ \ddot{\psi}\end{pmatrix}+\mathbf{C}_s\begin{pmatrix}\dot{h}\\ \dot{\psi}\end{pmatrix}+\mathbf{K}_s\begin{pmatrix}h\\ \psi\end{pmatrix}=\begin{pmatrix}F_z^{\text{flow}}\\ M_y^{\text{flow}}\end{pmatrix}=\mathbf{F}_f^M+\mathbf{F}_f^C+\mathbf{F}_f^K,$$

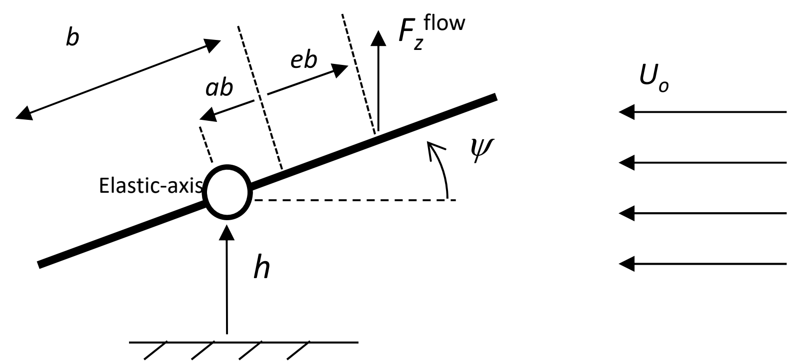

Fluid-added mass

$$\mathbf{F}_f^M=\rho_f\pi b^2\begin{pmatrix}-1 & -ba\\ -ba & -b^2\left(\frac{1}{8}+a^2\right)\end{pmatrix}\frac{\partial^2}{\partial t^2}\begin{pmatrix}h\\ \psi\end{pmatrix}$$

α_0 = Initial angle of attack

$a_0=\frac{dC_L}{d\alpha}$ = Slope of lift curve

$k=\frac{\omega b}{U_0}$ Reduced frequency

$\Omega(k)$: Theodorsen's function

Fluid-induced damping

$$\mathbf{F}_f^C=\tfrac{1}{2}\boxed{\rho_f U_0}(2b)\begin{pmatrix}-a_0\Omega(k) & \frac{b}{2}\left(2\pi+a_0(1-2a)\Omega(k)\right)\\ -ba_0(eb)\Omega(k) & -b^2(1-2a)\left(\pi-a_0(eb)\Omega(k)\right)\end{pmatrix}\frac{\partial}{\partial t}\begin{pmatrix}h\\ \psi\end{pmatrix}$$

Fluid stiffness forces

$$\mathbf{F}_f^K=\tfrac{1}{2}\boxed{\rho_f U_0^2}a_0(2b)\begin{pmatrix}0 & \Omega(k)\\ 0 & (eb)\Omega(k)\end{pmatrix}\begin{pmatrix}h\\ \psi+\alpha_0\end{pmatrix}$$

Fluid stiffness terms are positive, so they enhance plate motion

Validation – Root Locus Plot of an Airfoil

b=3 ft, a=-0.2, μ=20, $r_\alpha^{\,2}$=0.25, η_s=0.03
ω_h^{air}=10 rad/s, ω_ψ^{air}=25 rad/s,

$$\mu = m_s / \left(\rho_f \pi b^2 \right)$$

$$\eta = 2\,\mathrm{Im}(\omega)/\mathrm{Re}(\omega)$$

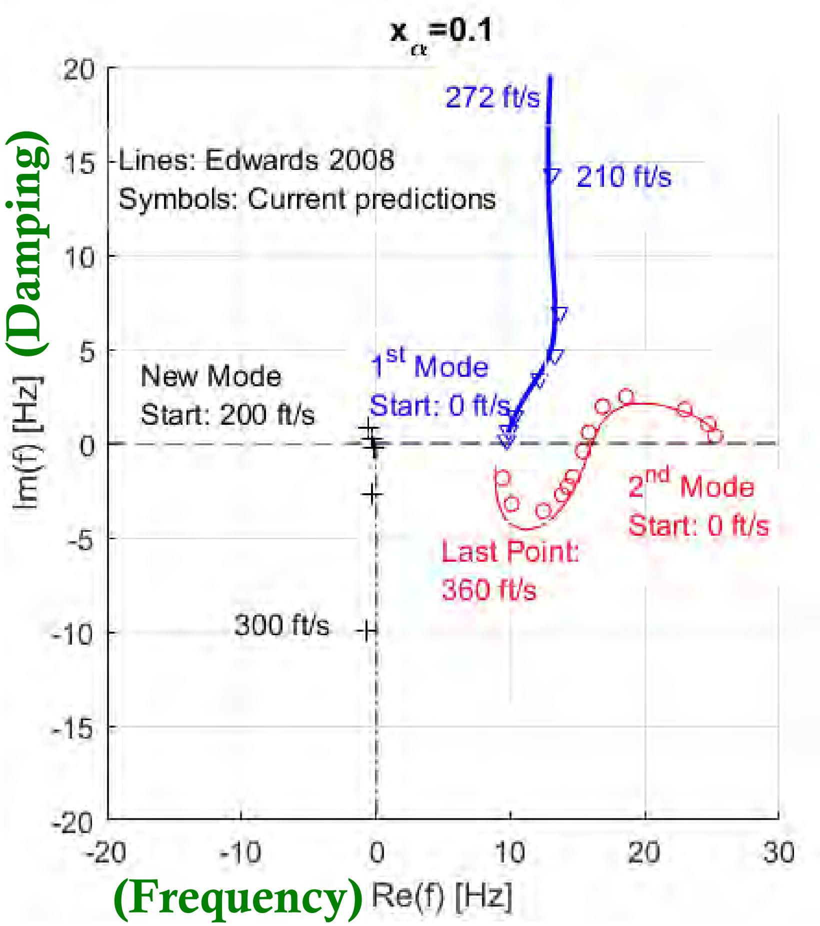

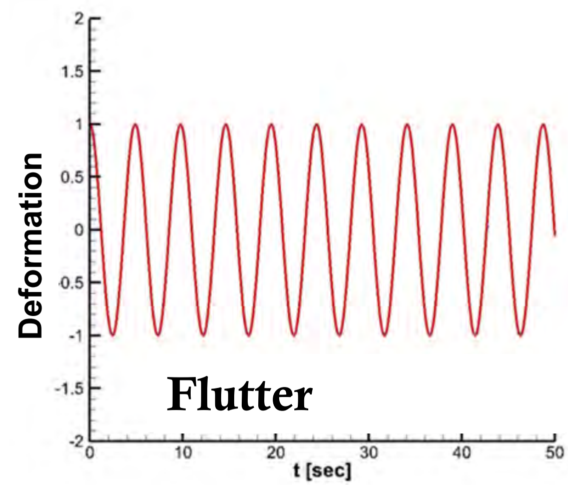

NASA

Good agreement with Edwards (2008), including emergence of "New Mode"

Composite Plate in Water

MICHIGAN ENGINEERING
UNIVERSITY of MICHIGAN • COLLEGE of ENGINEERING

Total damping loss factor $\eta = 2\,\mathrm{Im}(\omega)/\mathrm{Re}(\omega)$

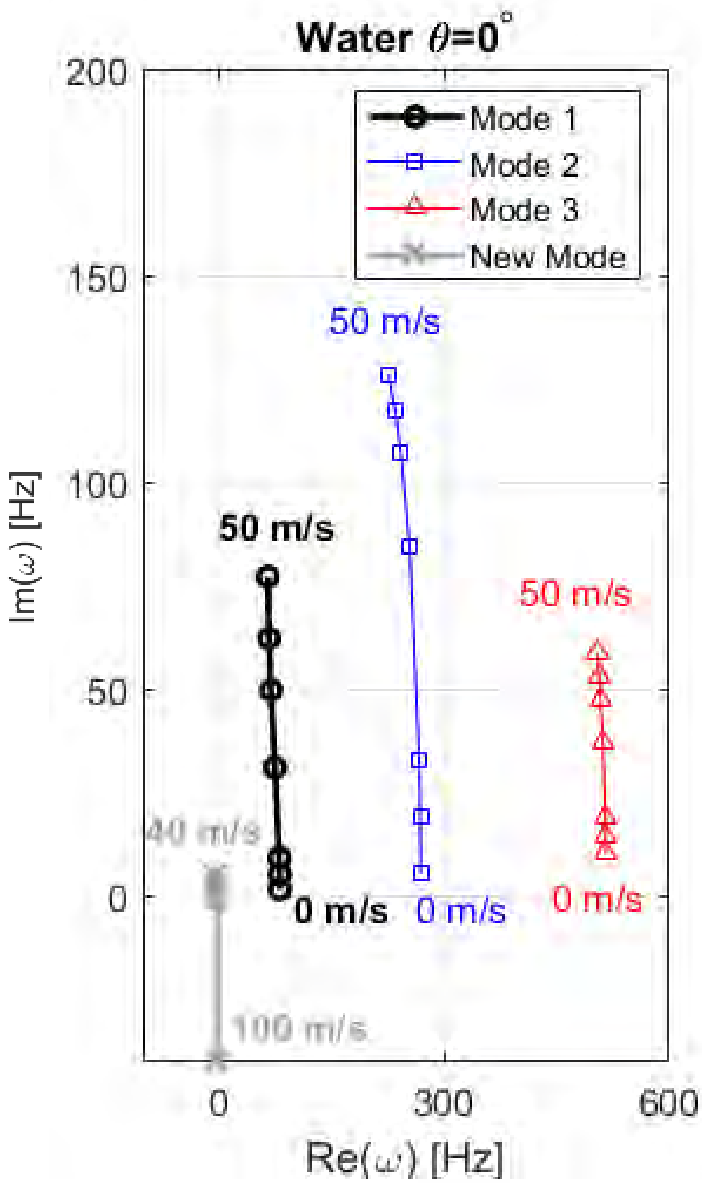

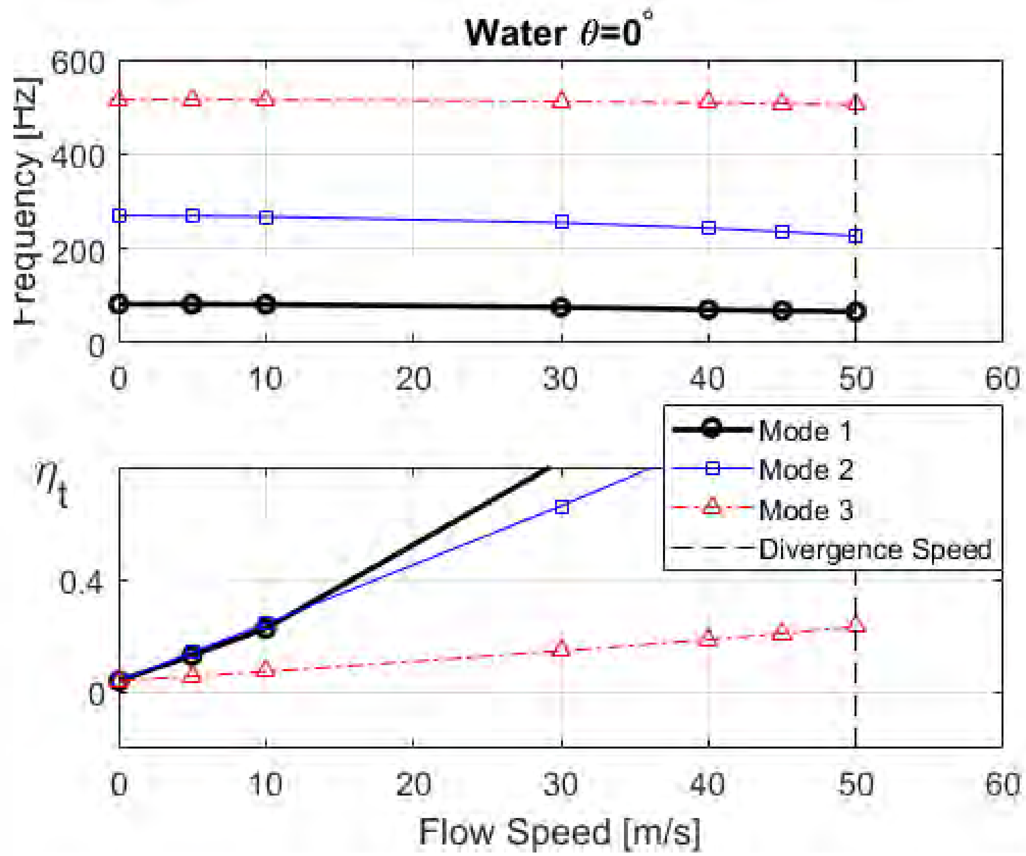

- The natural frequencies change slightly while the loss factors increase rapidly with increasing U.
- The new mode emerges at high speeds b/c of the circulatory terms $C_f \sim \rho_f U$ & $K_f \sim \rho_f U^2$.

Composite Plate in Water

MICHIGAN ENGINEERING
UNIVERSITY of MICHIGAN • COLLEGE of ENGINEERING

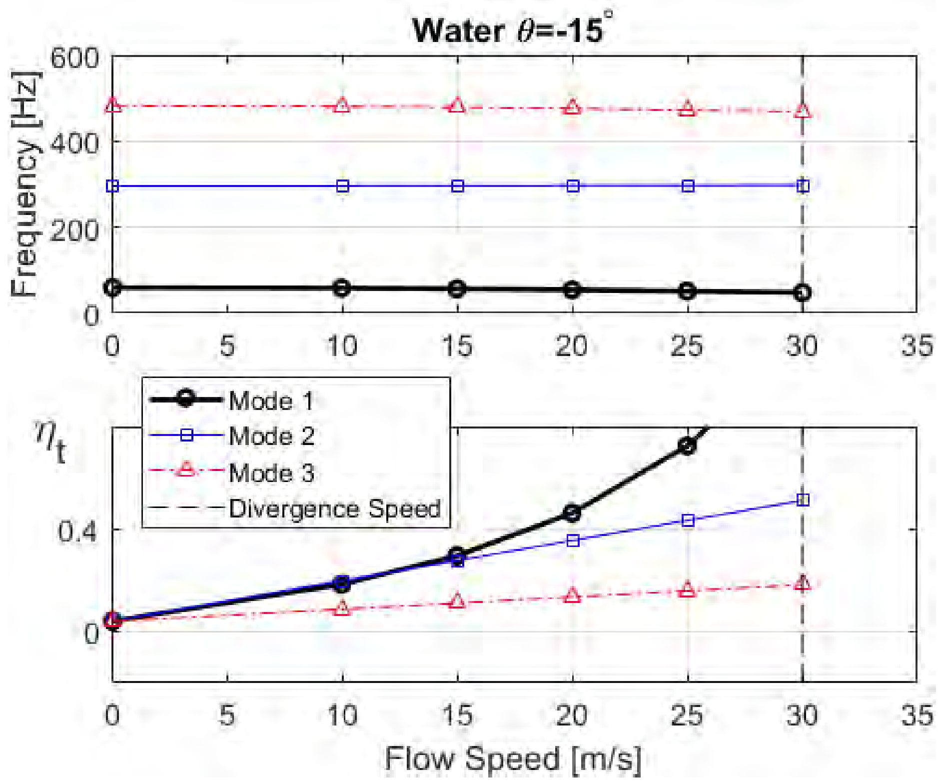

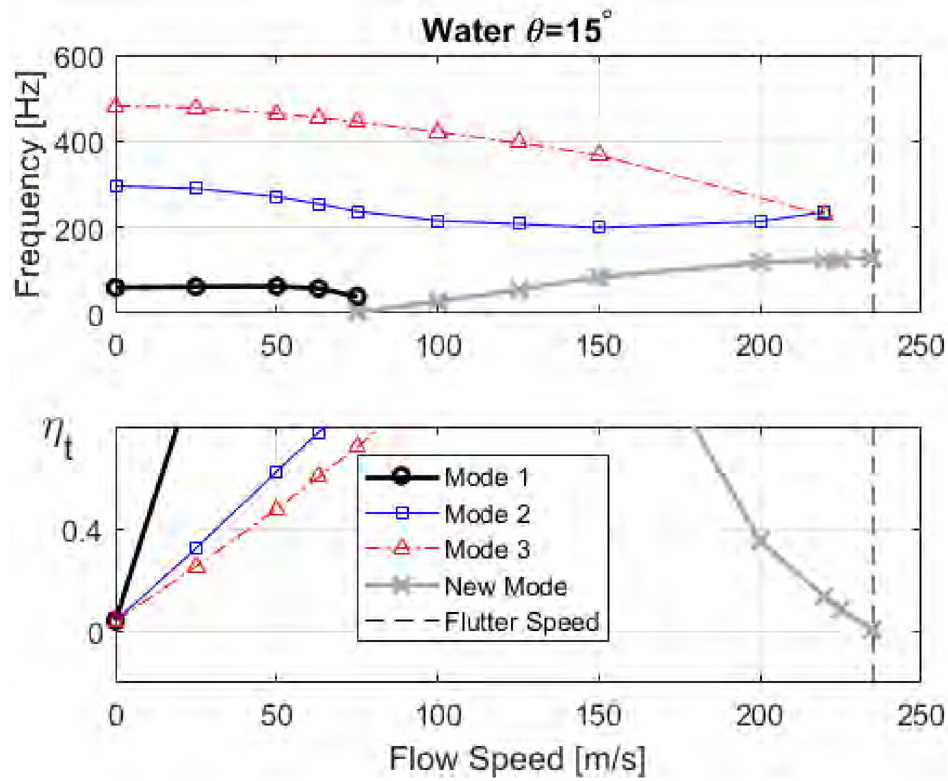

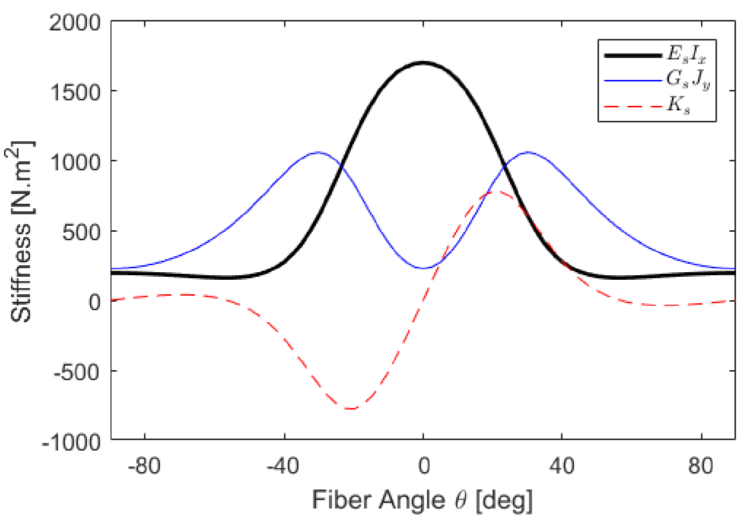

- Differences between $\theta = -15^o$ and $\theta = 15^o$ is due solely to the opposite sign of the material bend-twist coupling K_s, and its interaction with the fluid force terms.
- New mode emerges at 50 m/s, & becomes real at 74 m/s => vibrations at frequency much lower than the still water fundamental frequency.

Composite Plate in Water

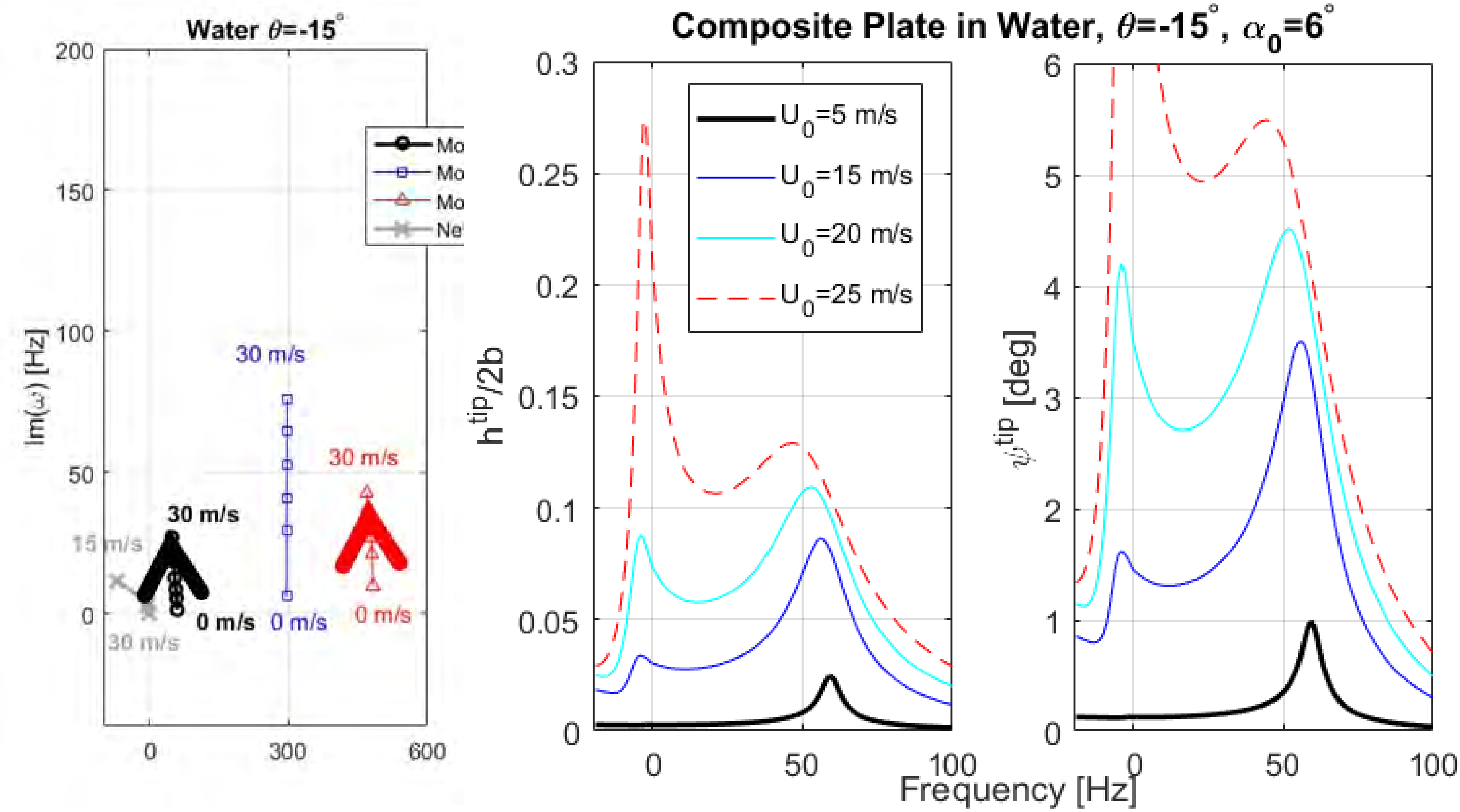

The new mode will cause rapid rise in the steady-state deformations with speed b/c the fluid disturbing force exceeds the solid elastic restoring force, but the flow-induced motions will be rapidly damped out until $U_o = U_D$.

Critical Speeds in Air vs. Water Water

MICHIGAN ENGINEERING
UNIVERSITY of MICHIGAN ■ COLLEGE of ENGINEERING

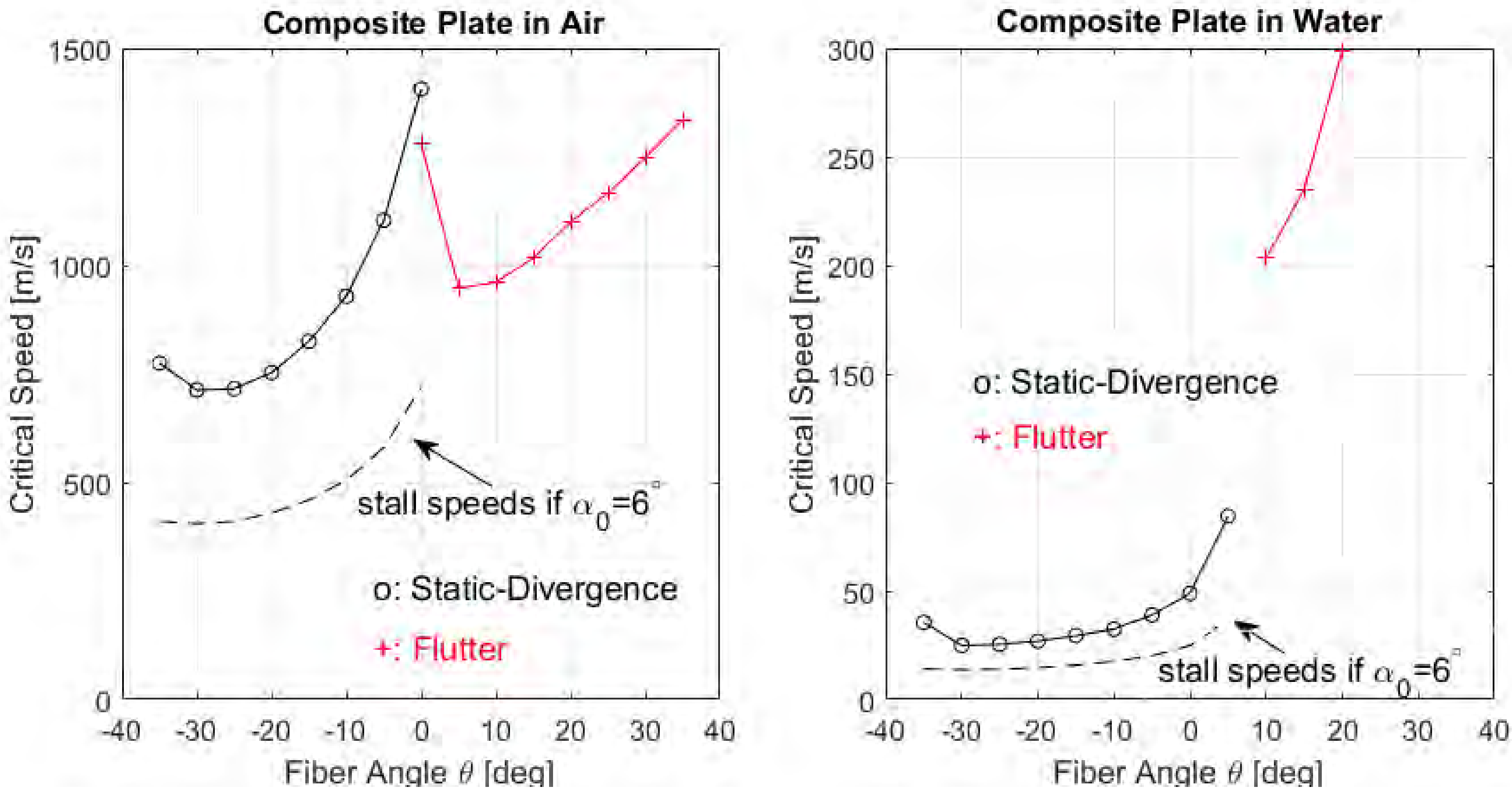

- Critical speed and governing instability mechanism change with θ and ρ_f.
- Flutter is more critical for $\theta > 0$, static-divergence is more critical for $\theta < 0$.
- Critical speed is much lower in water compared to in air because of higher ρ_f.
- Stall, cavitation, ventilation, and material failure can happen before static-divergence or flutter.

Multi-disciplinary Design Optimization

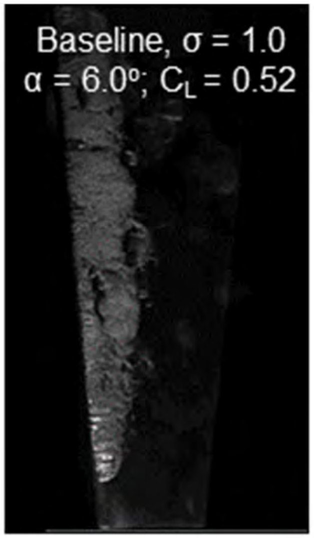

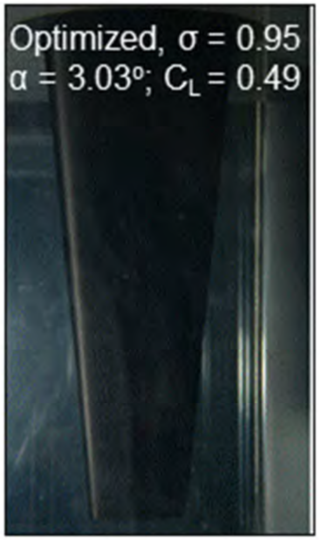

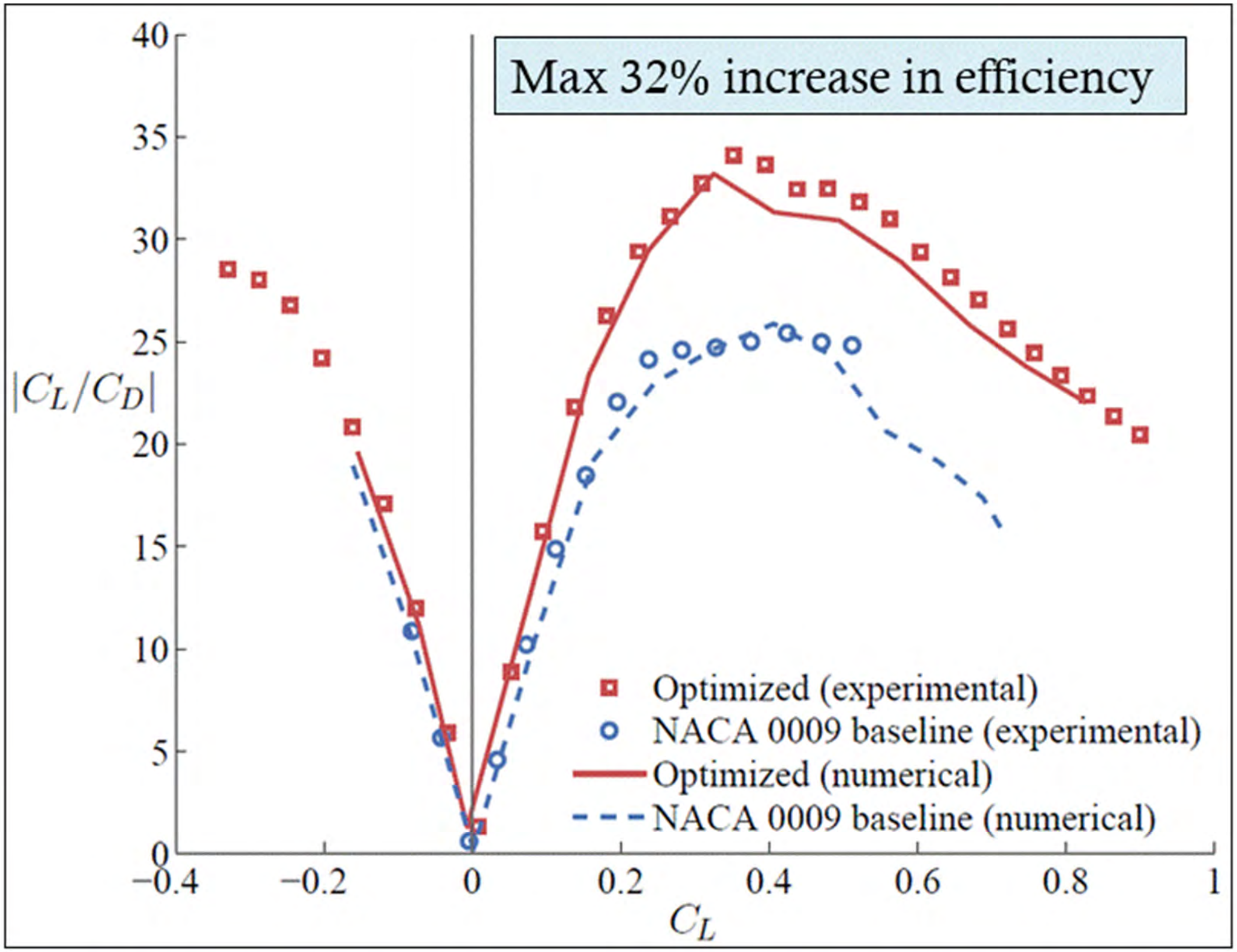

Experimental Result: Optimized hydrofoil is able to significantly delay cavitation inception, and yield much higher overall efficiency than the baseline hydrofoil.

Multi-functional Marine Structures

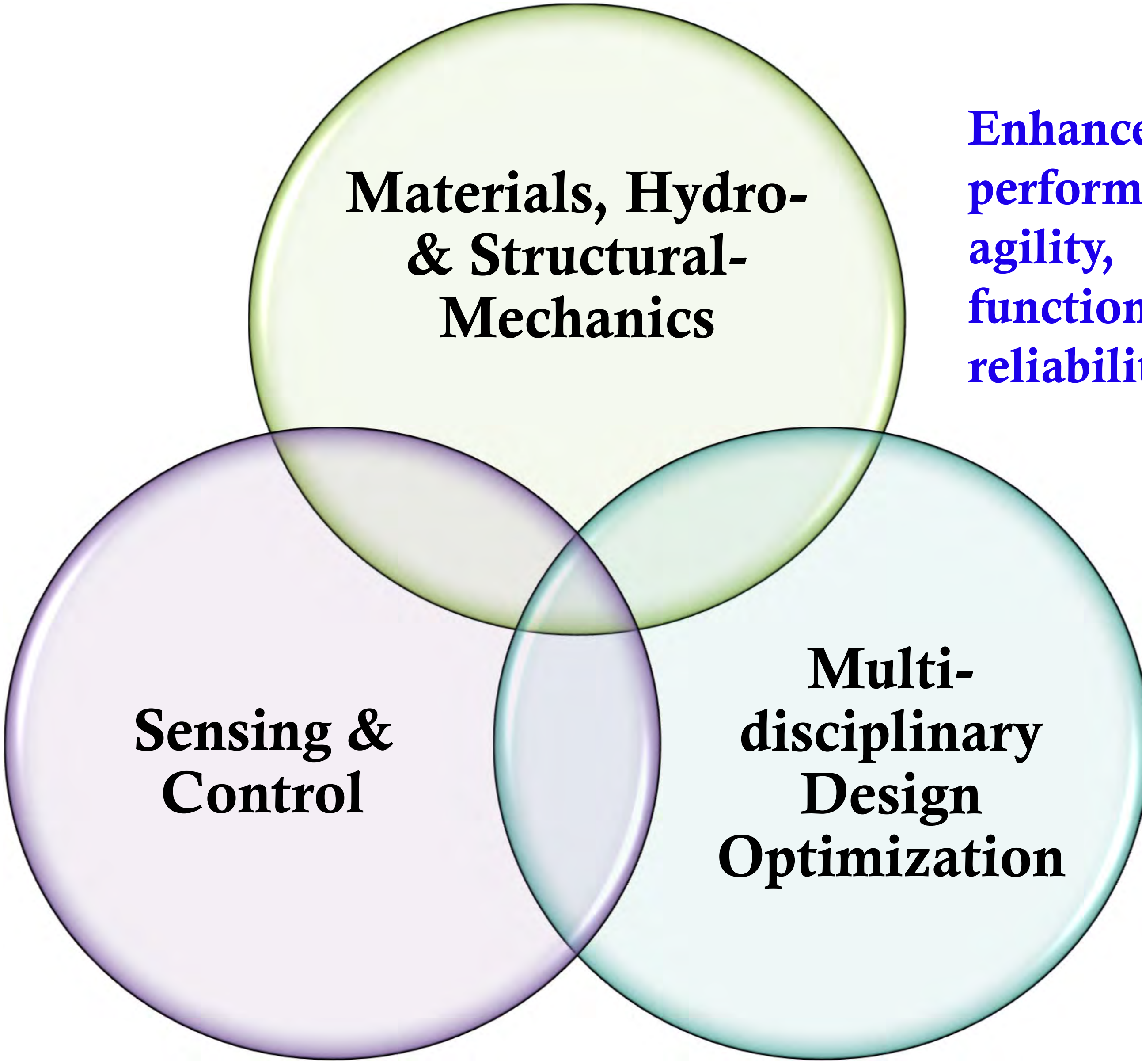

Enhance performance, agility, functionality, and reliability

Thank You!

Office of Naval Research Science & Technology

MICHIGAN

Marine Technology Research Institute INSEAN

Australian Government
Department of Defence
Defence Science and Technology Group

UNIVERSITY of TASMANIA

AMC Australian Maritime College

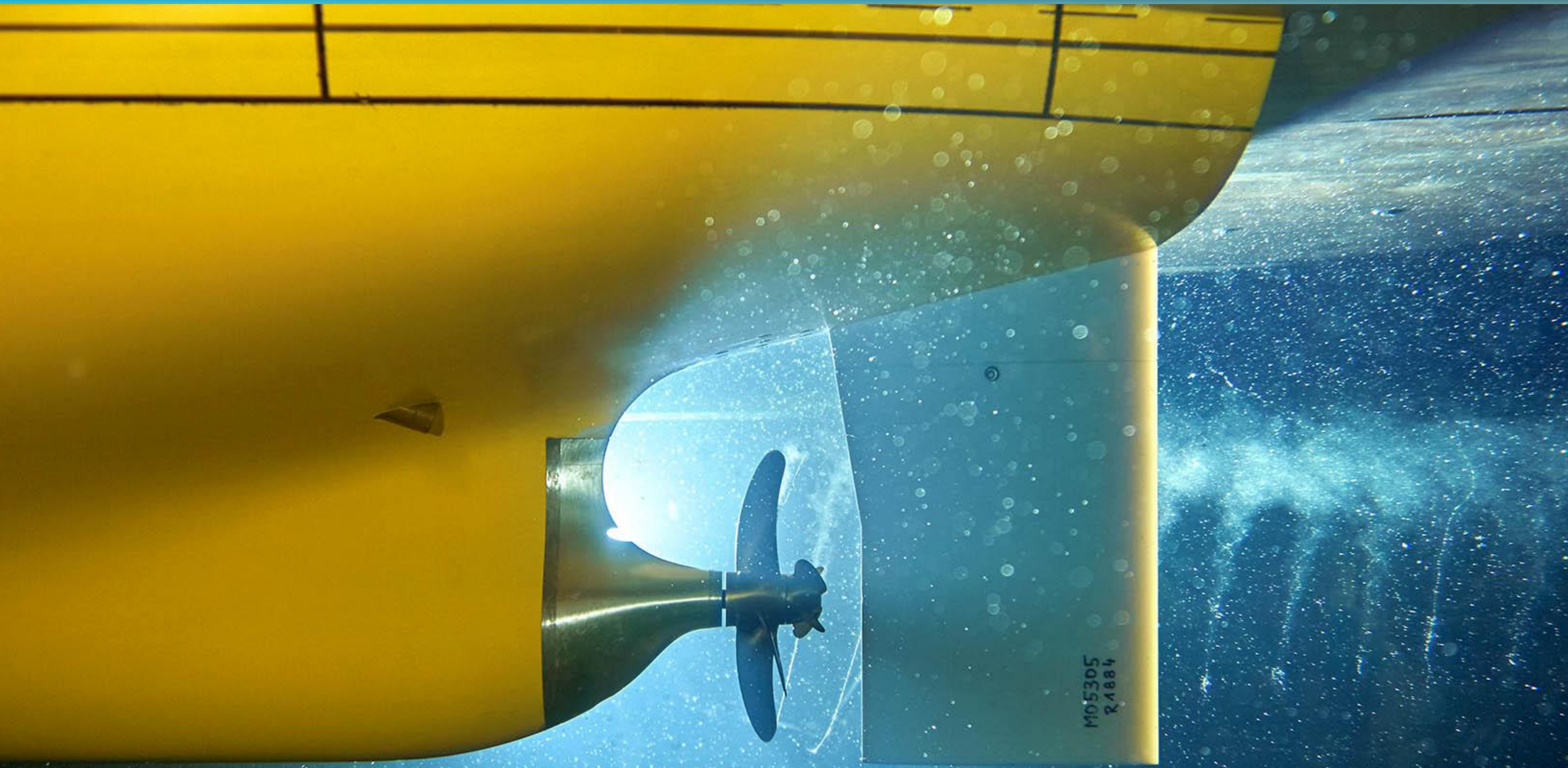

Propulsion Testing in HYKAT

Christian Johannsen, Hamburg Ship Model Basin (HSVA)

A. Yücel Odabaşi Colloquium Series
Istanbul, November 15, 2018

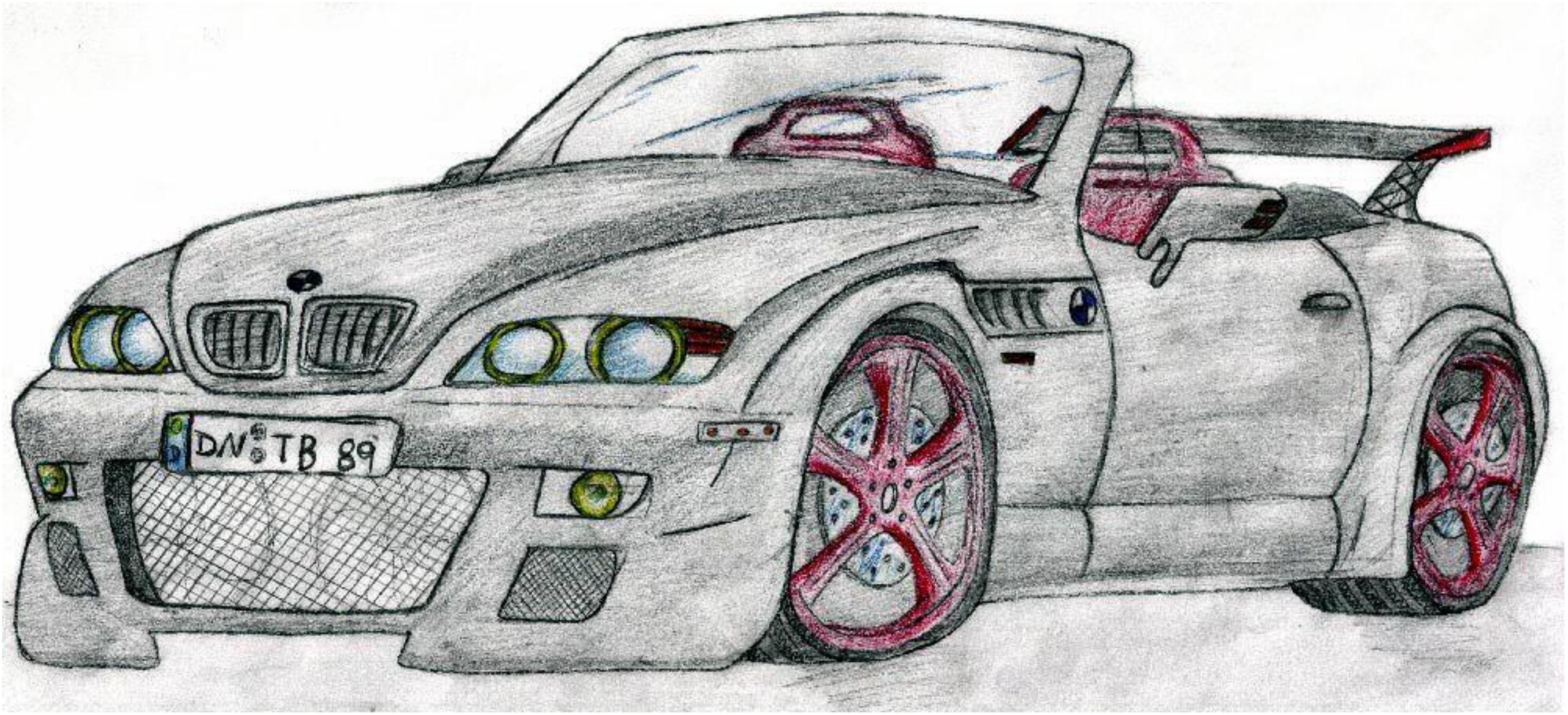
DN TB 89

The Claim: **More speed at same power** or respectively **Less fuel at same speed**

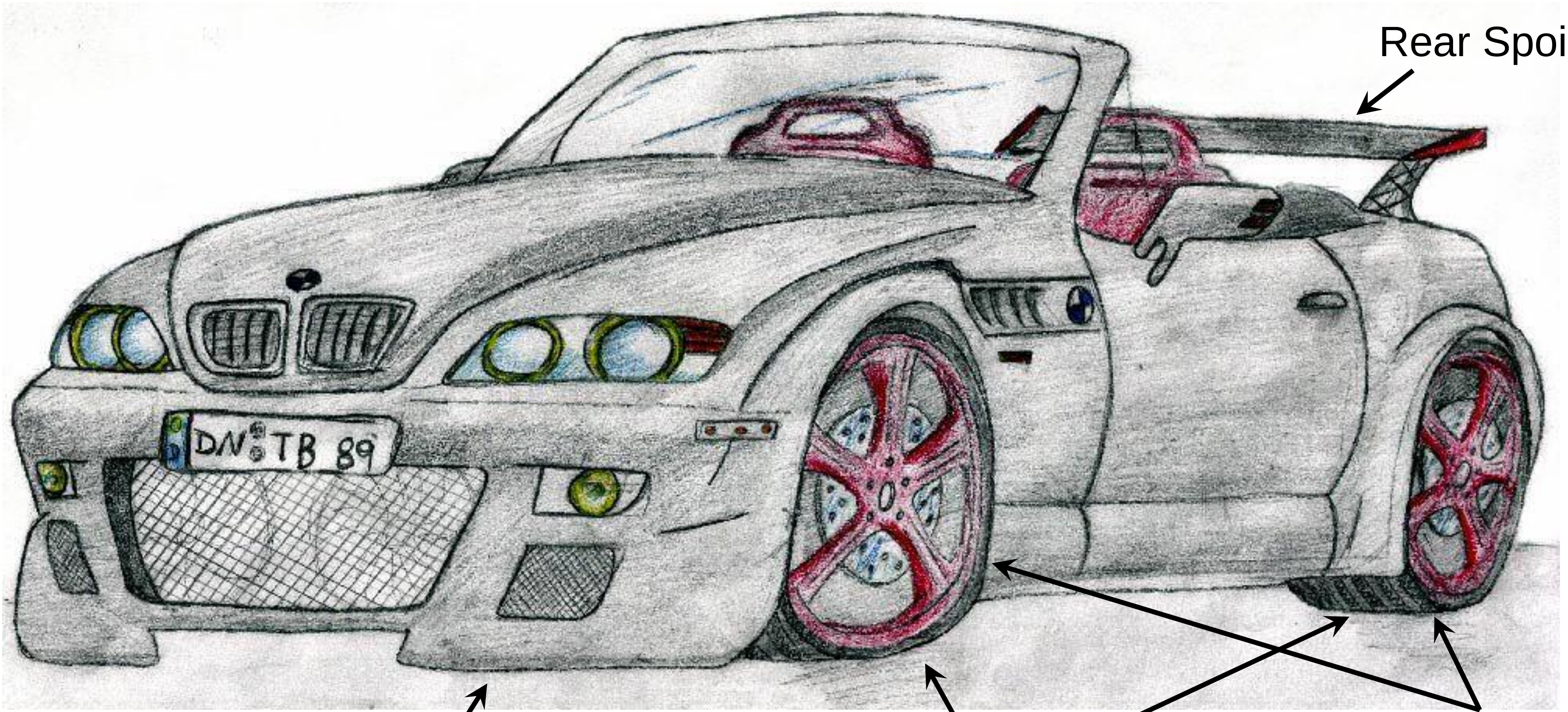

Rear Spoiler

Front Spoiler

Sporting Wheel Suspension

Racing Tires

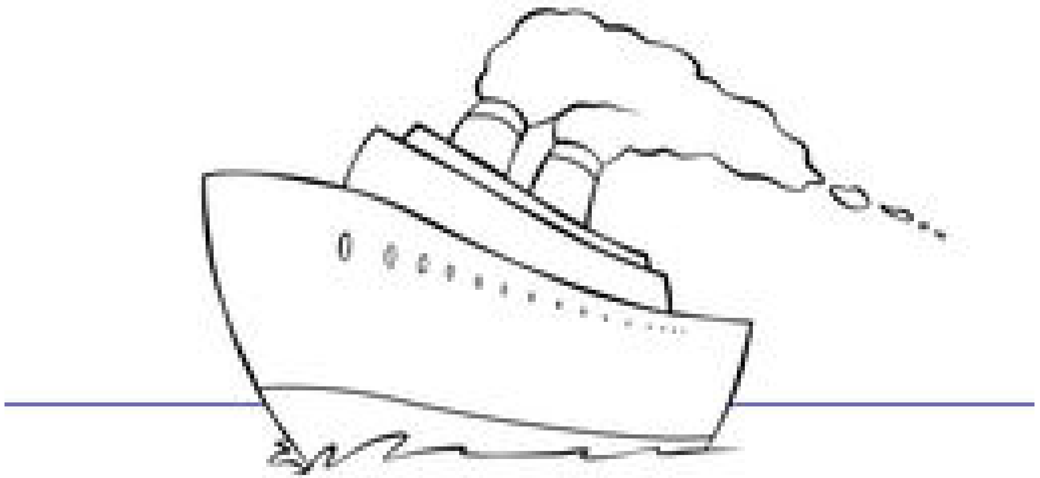

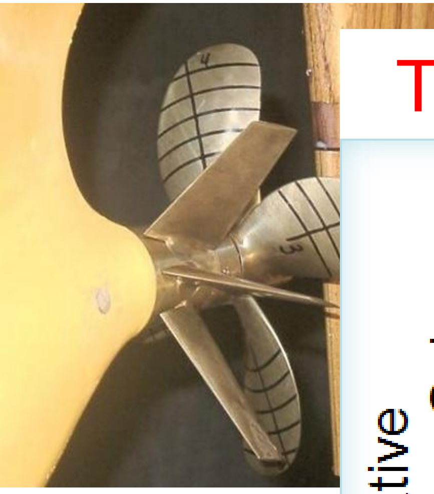

The Claim: Less Fuel Consumption

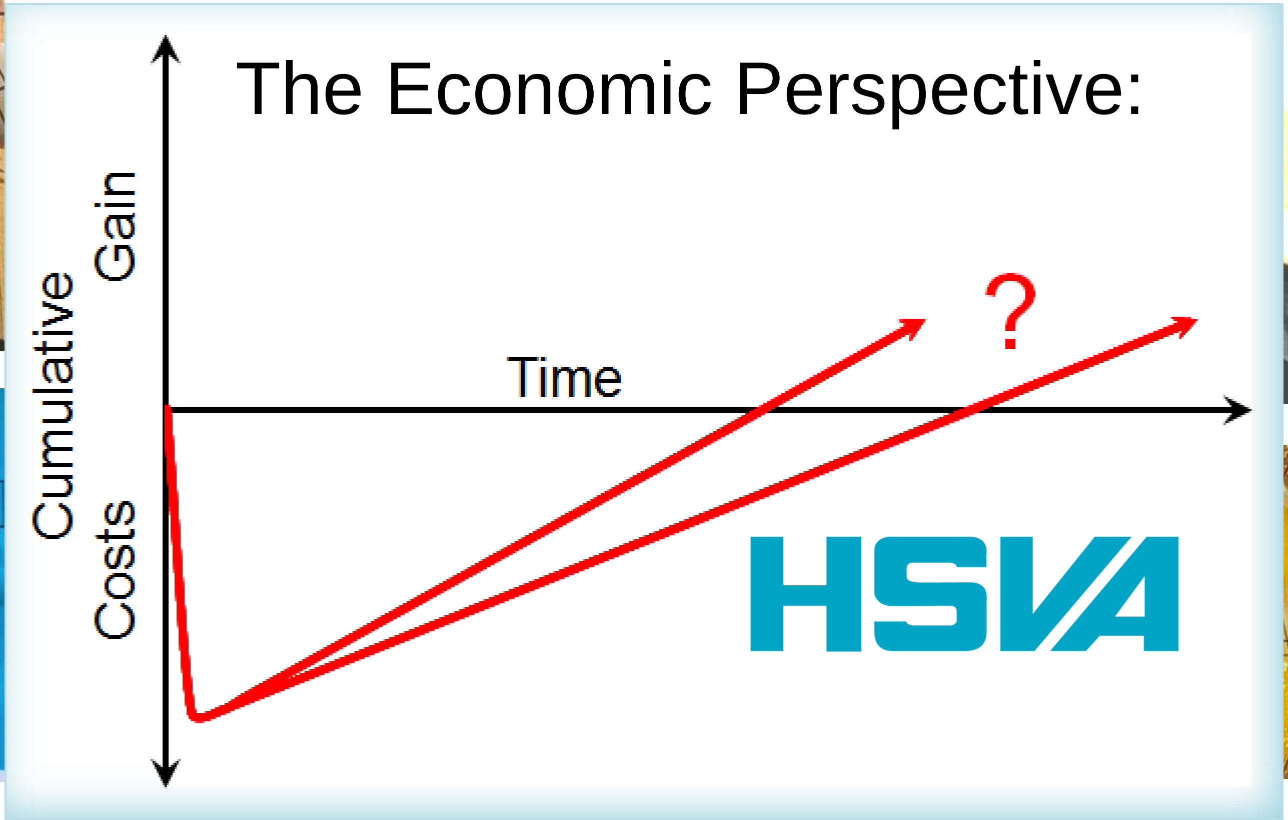

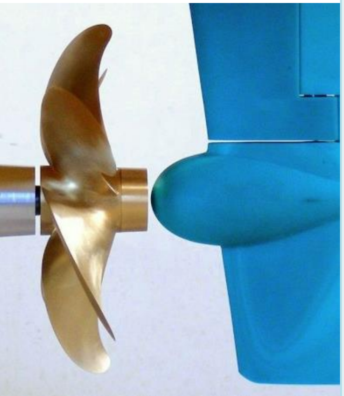

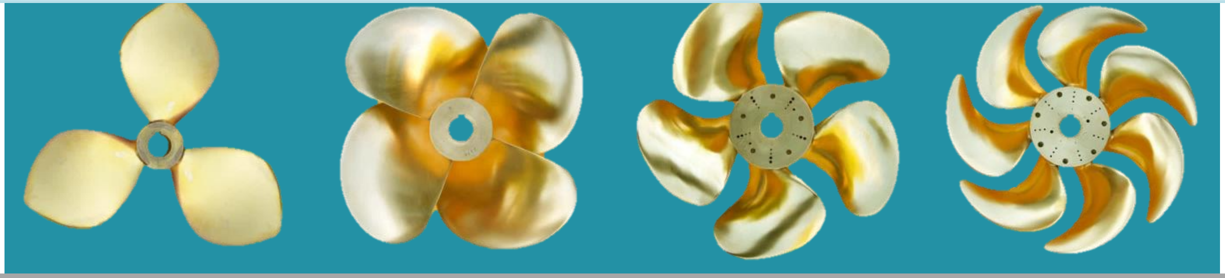

Contents

- Introduction ✓

Contents

- Introduction ✓
- The Problem with Scale Effects with Propulsion Improving Devices in a Towing Tank

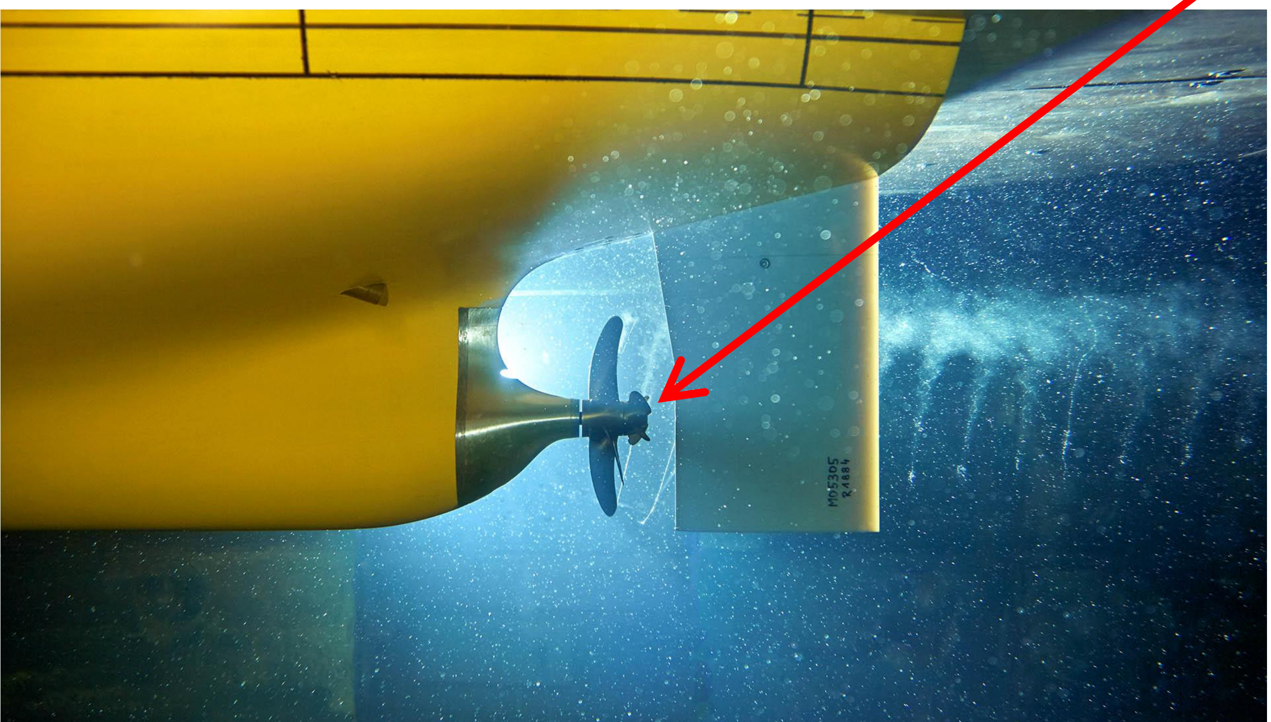

Propeller Cap Fins

Propeller Cap Fins

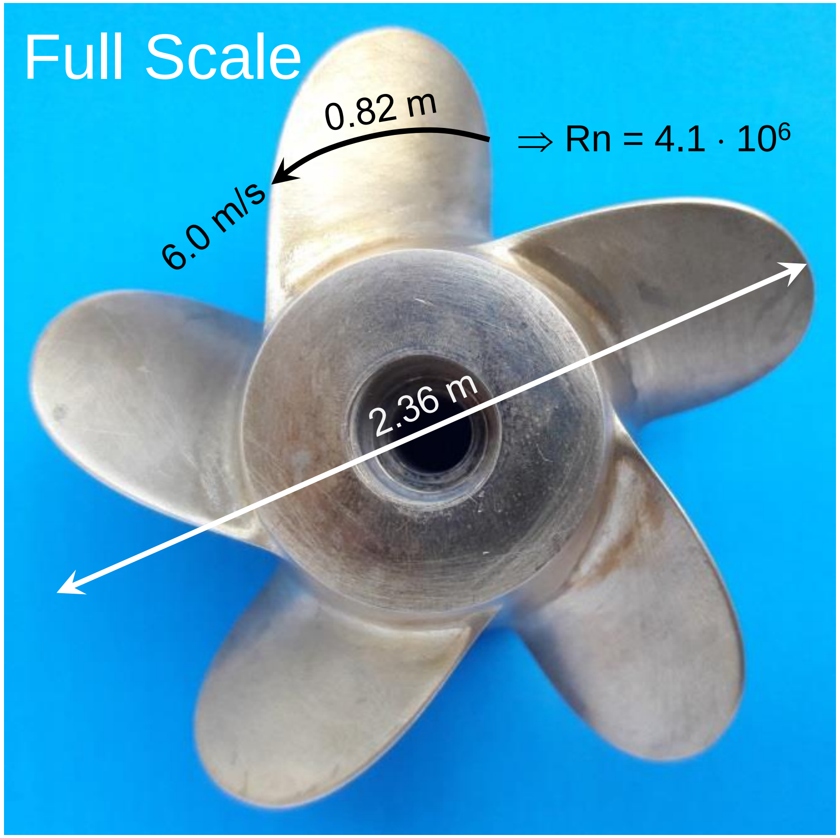

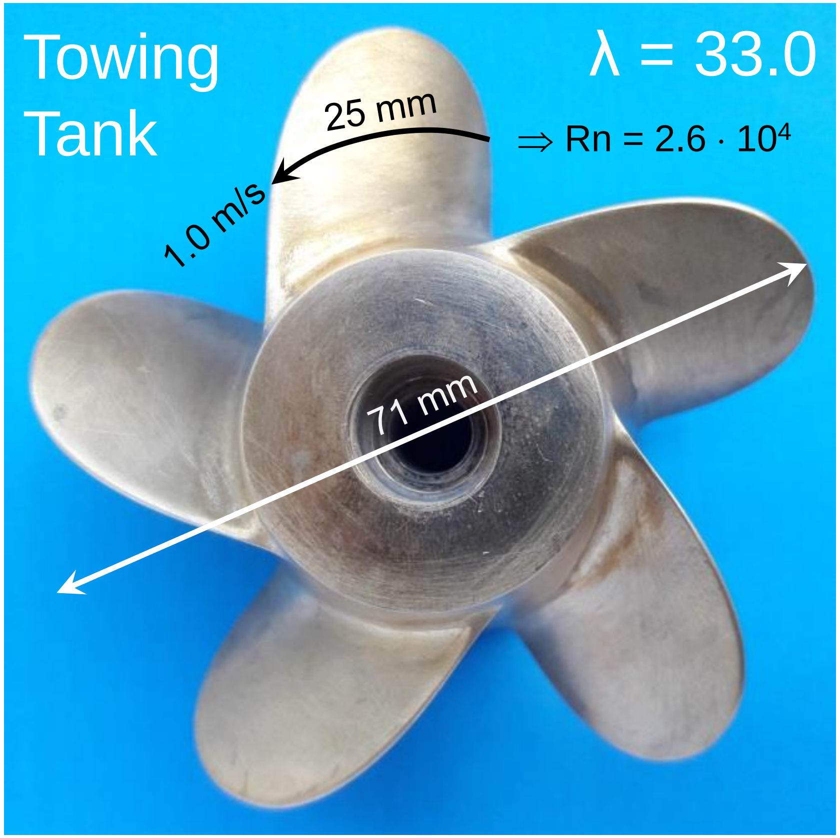

Fin Cap of a 4500 TEU Container Vessel

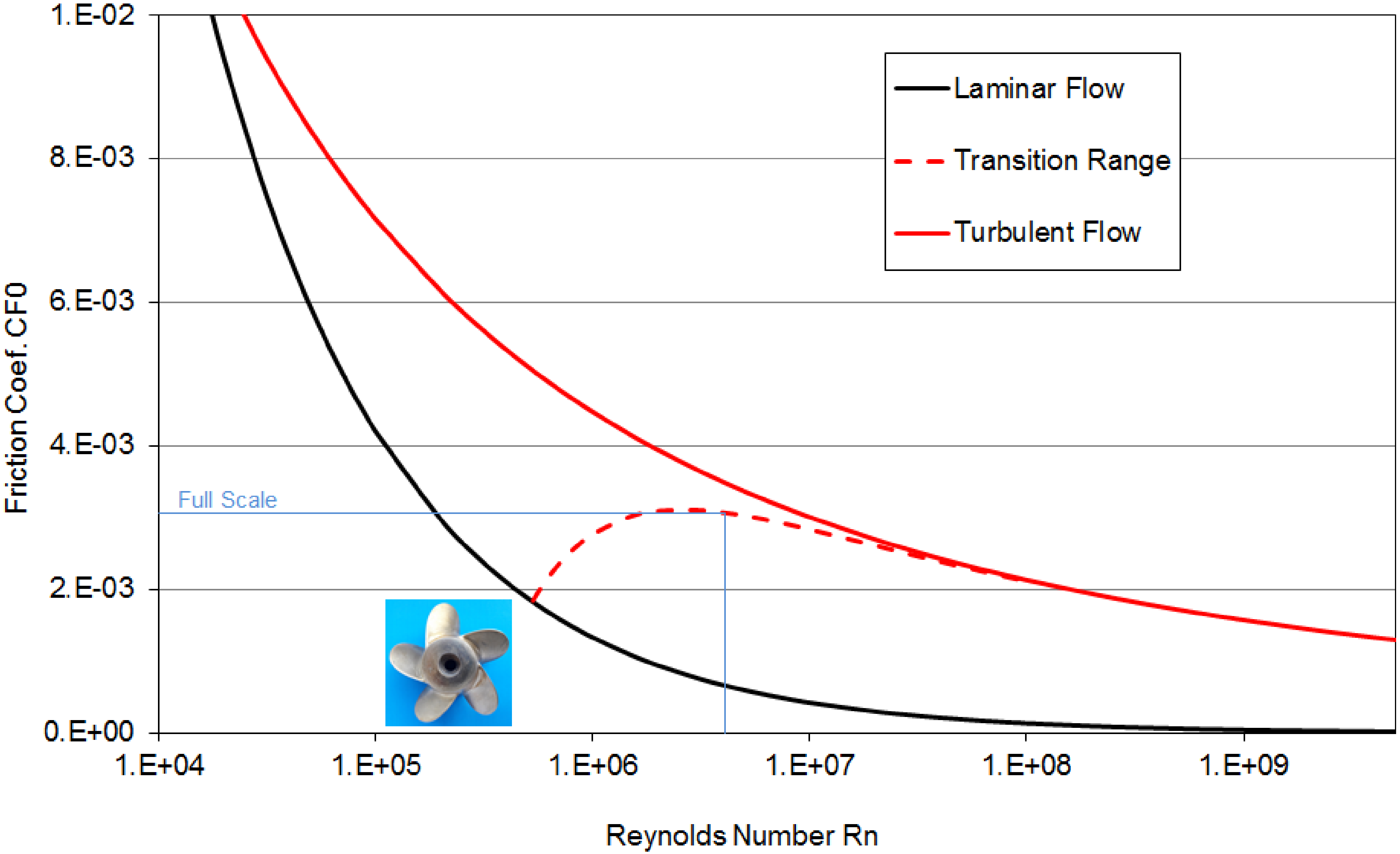

Friction Coefficients of a Flate Plate (Prandtl-Schlichting)

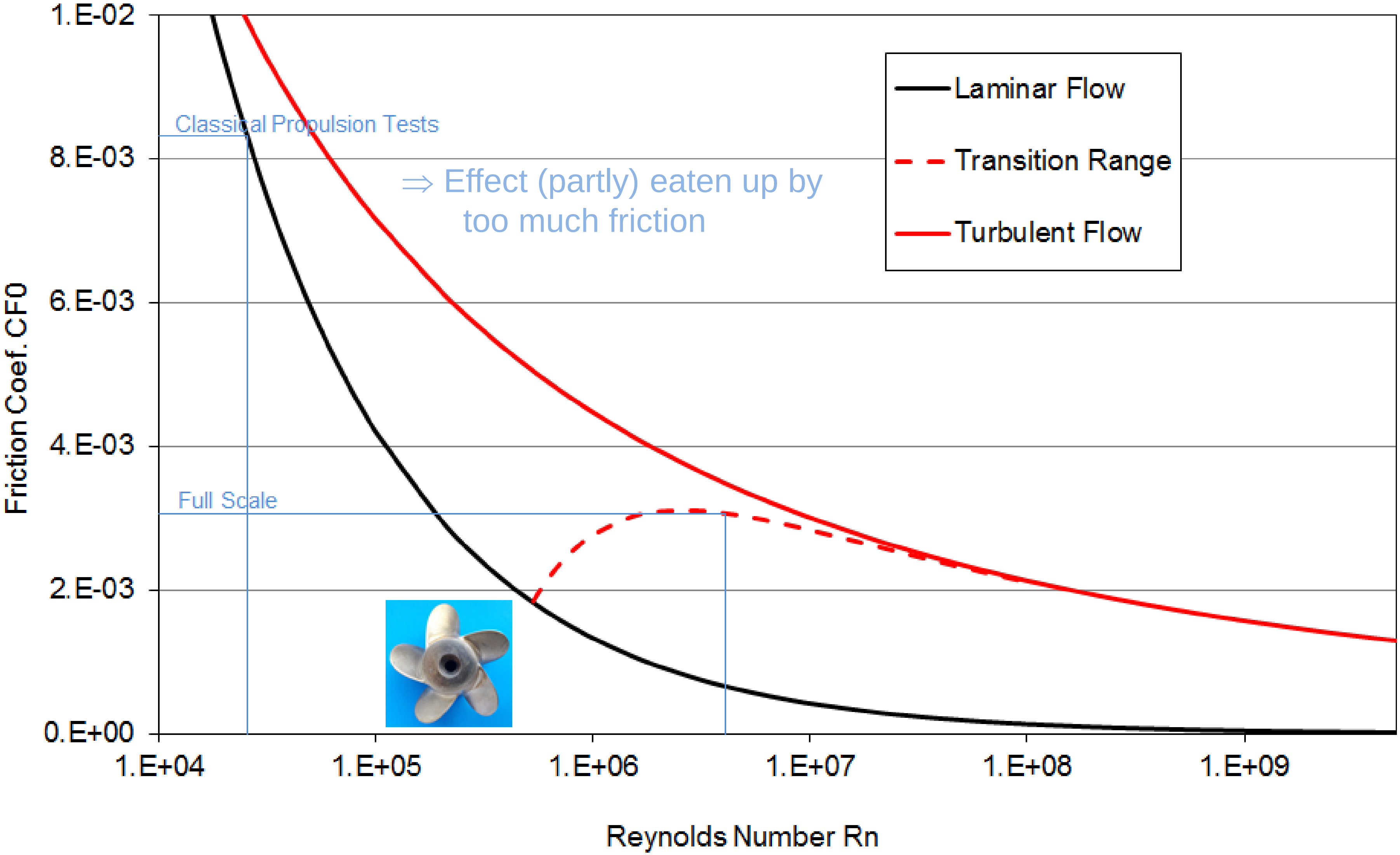

Friction Coefficients of a Flate Plate (Prandtl-Schlichting)

Alternative Towing Tank Set-Up

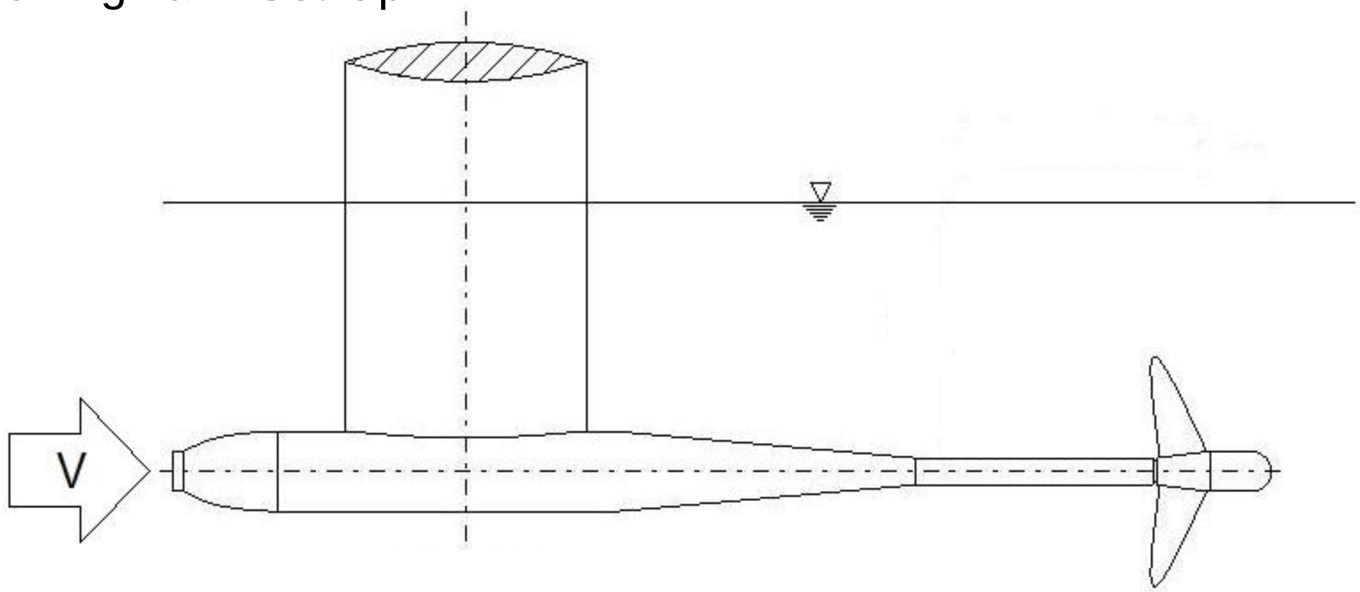

Alternative Towing Tank Set-Up

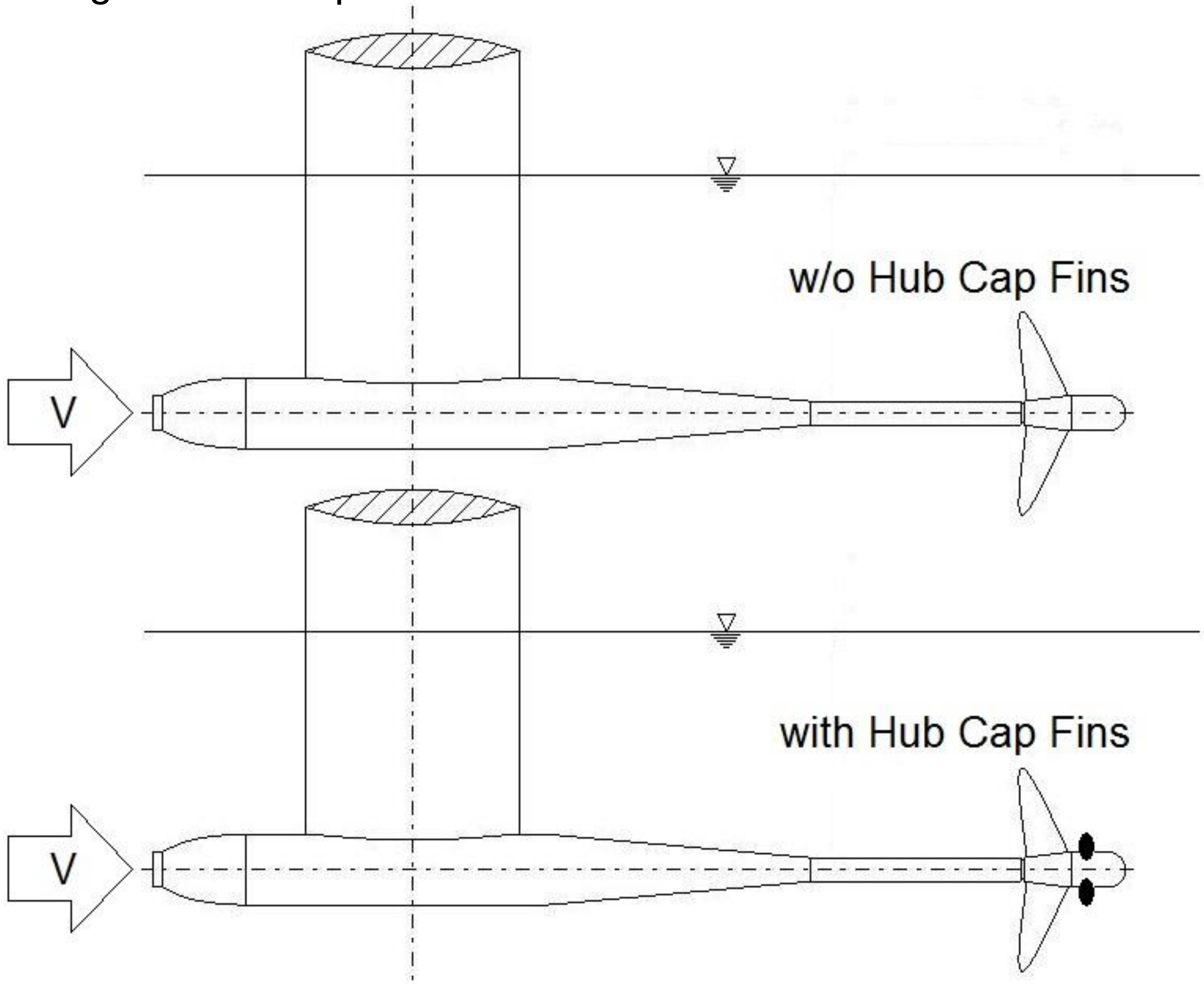

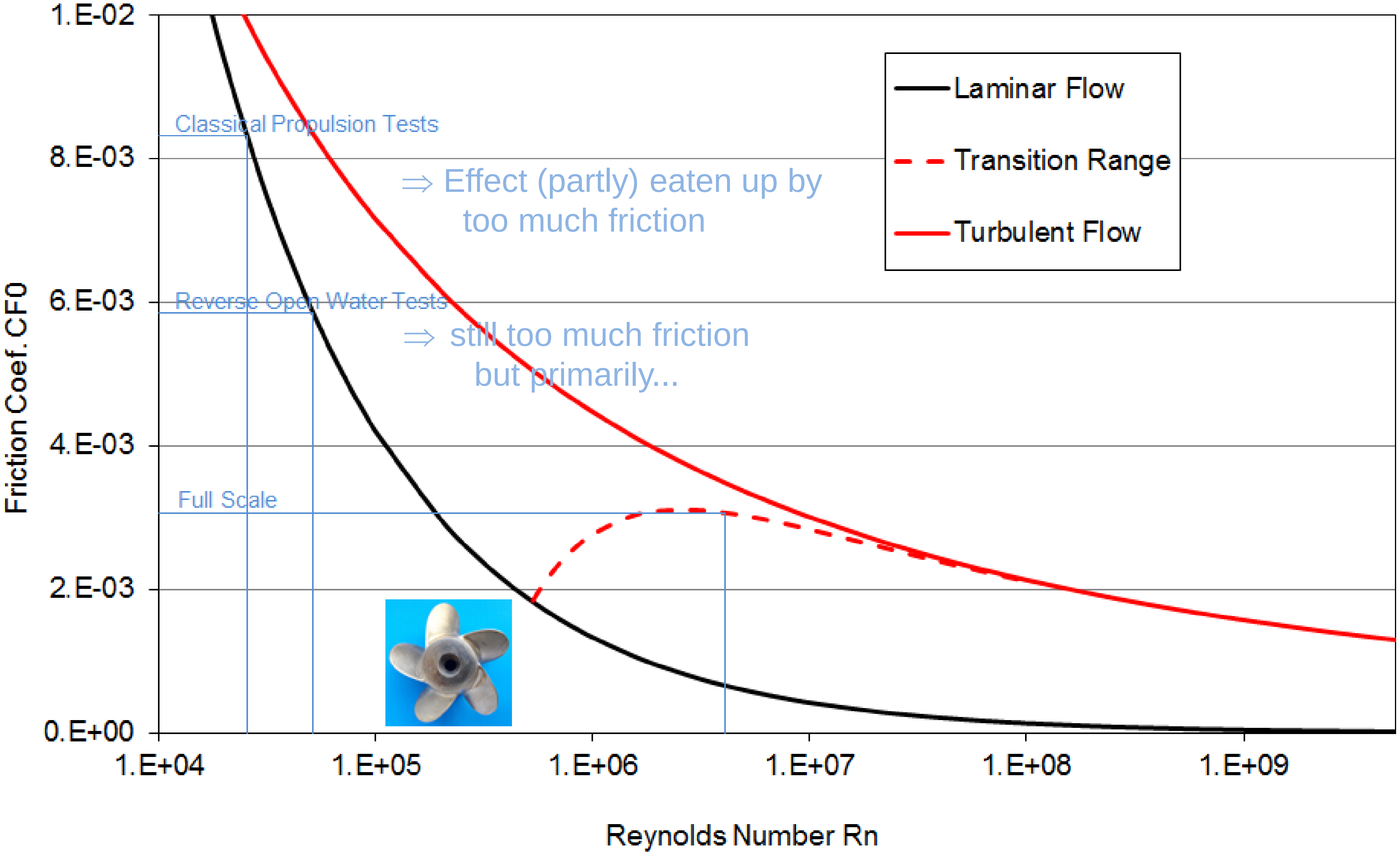

Friction Coefficients of a Flate Plate (Prandtl-Schlichting)

...the wake field is missing:

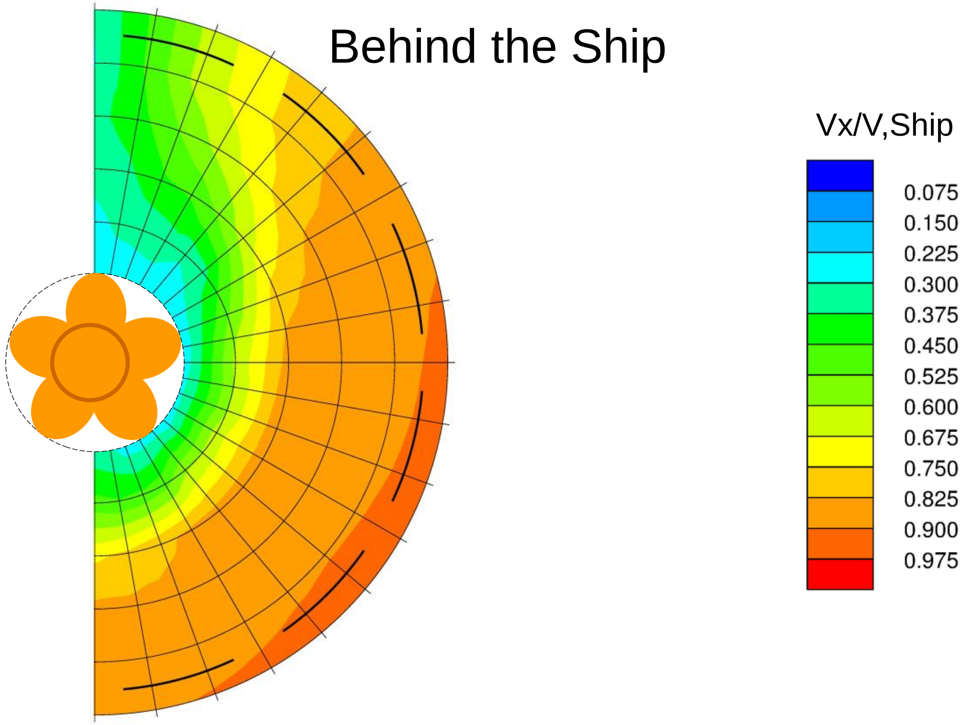

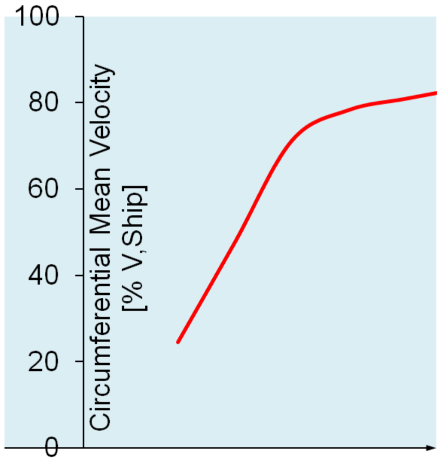

...the wake field is missing:

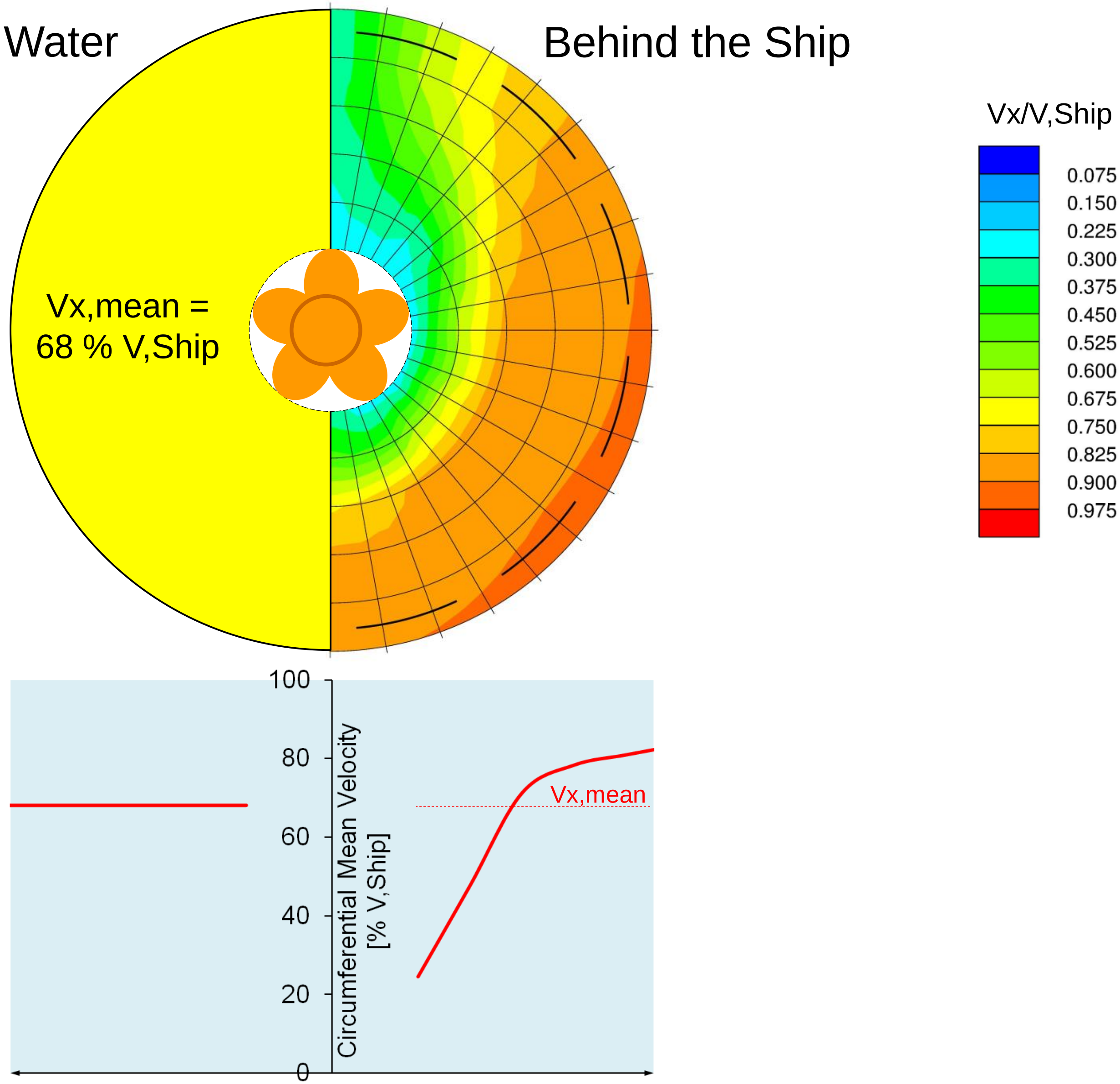

...the wake field is missing:

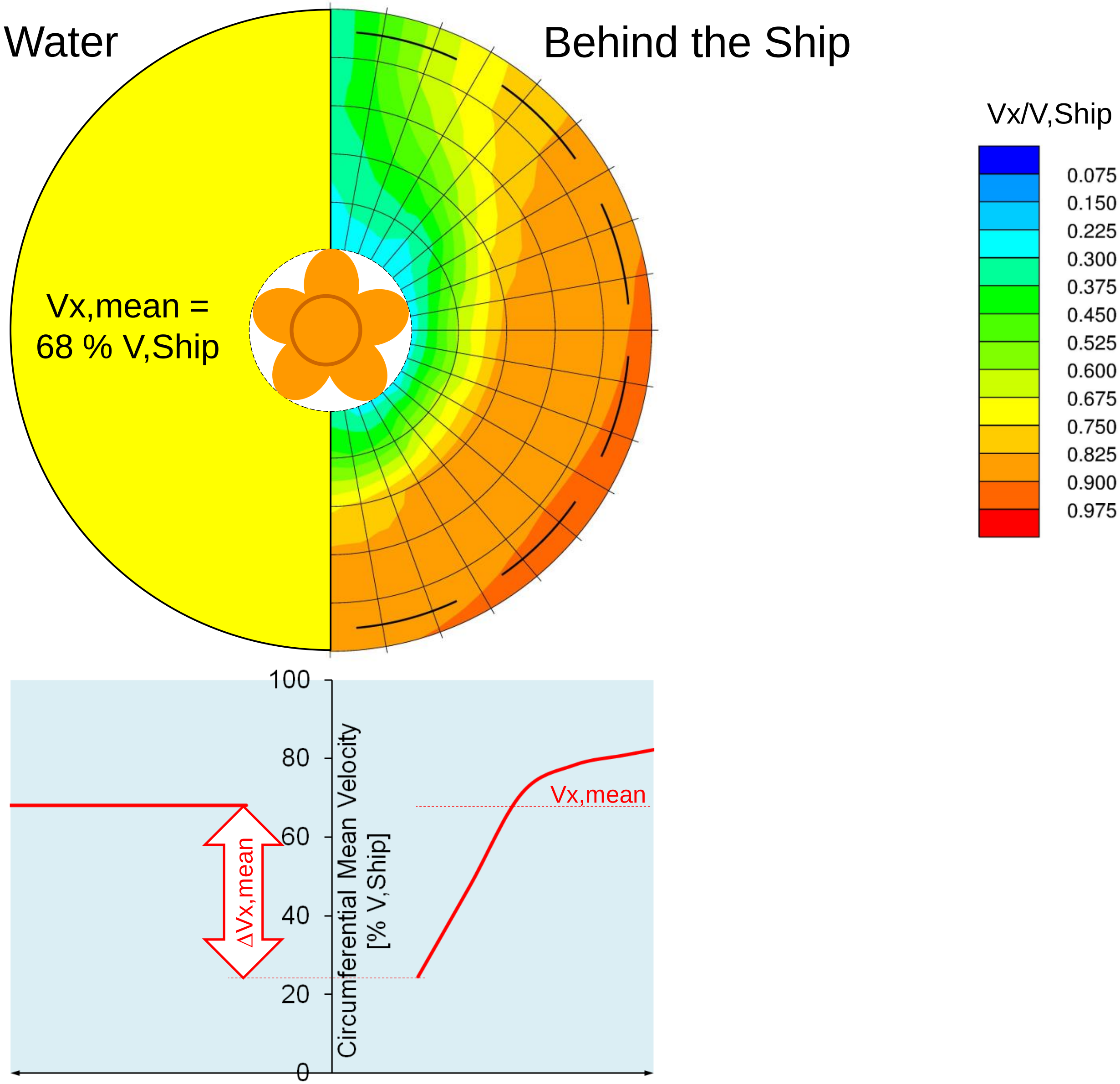

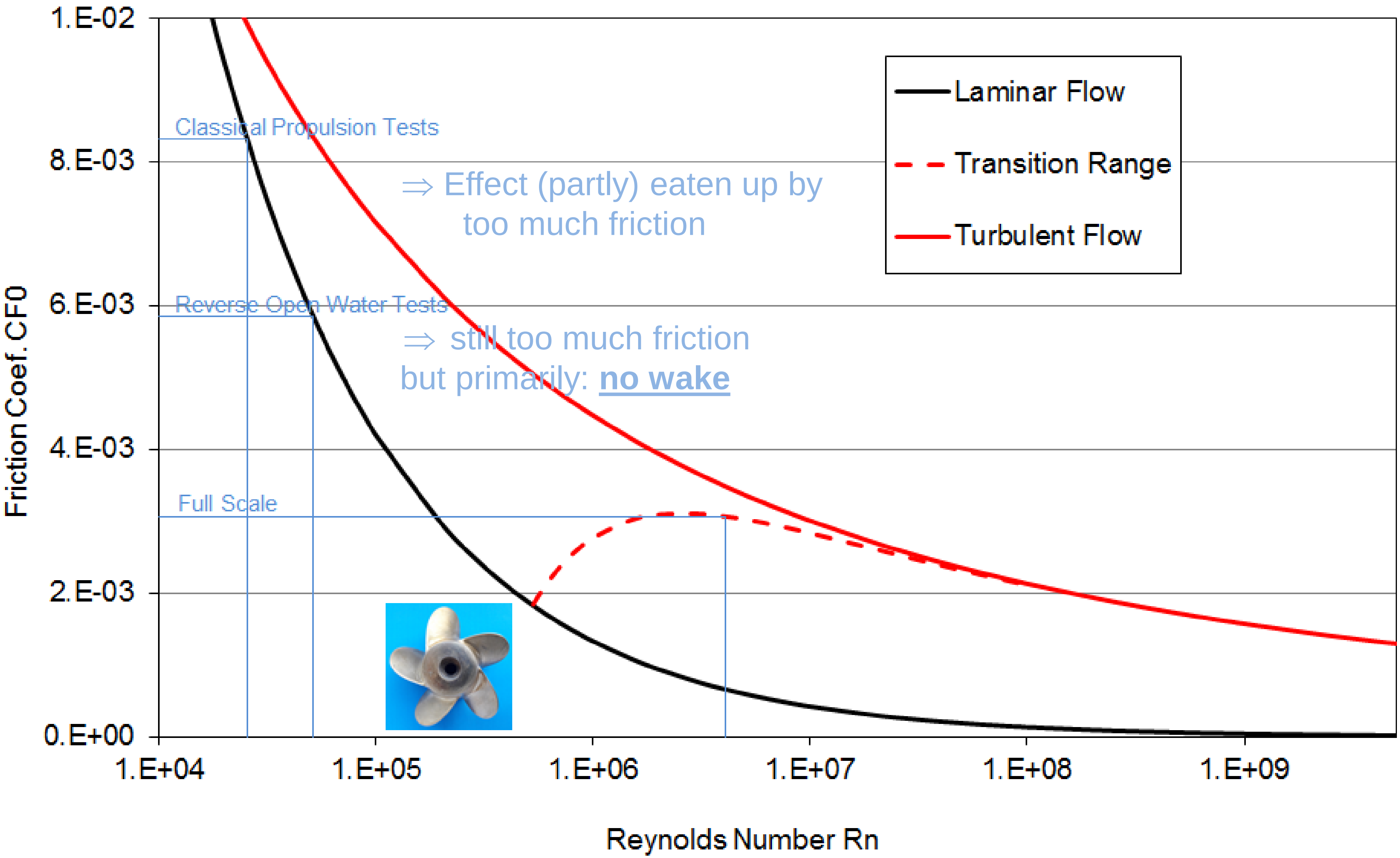

Friction Coefficients of a Flate Plate (Prandtl-Schlichting)

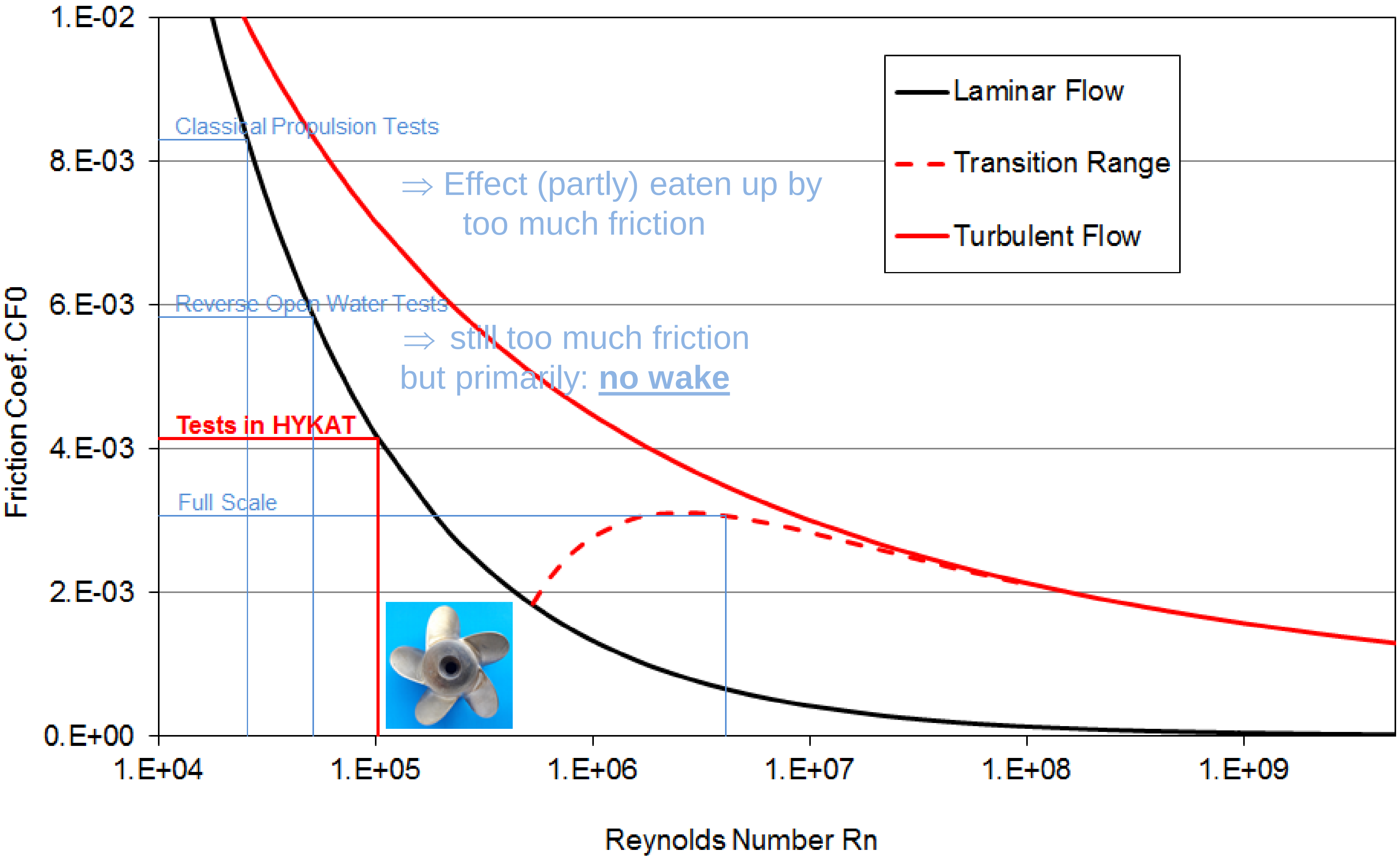

Friction Coefficients of a Flate Plate (Prandtl-Schlichting)

Contents

- Introduction ✓
- The Problem with Scale Effects with Propulsion Improving Devices in a Towing Tank

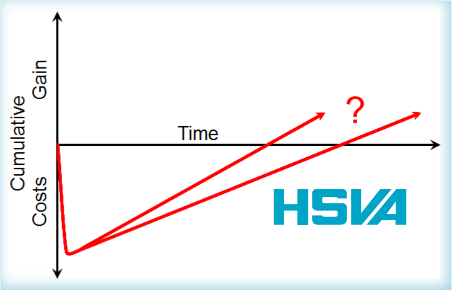

HYKAT Cavitation Tunnel

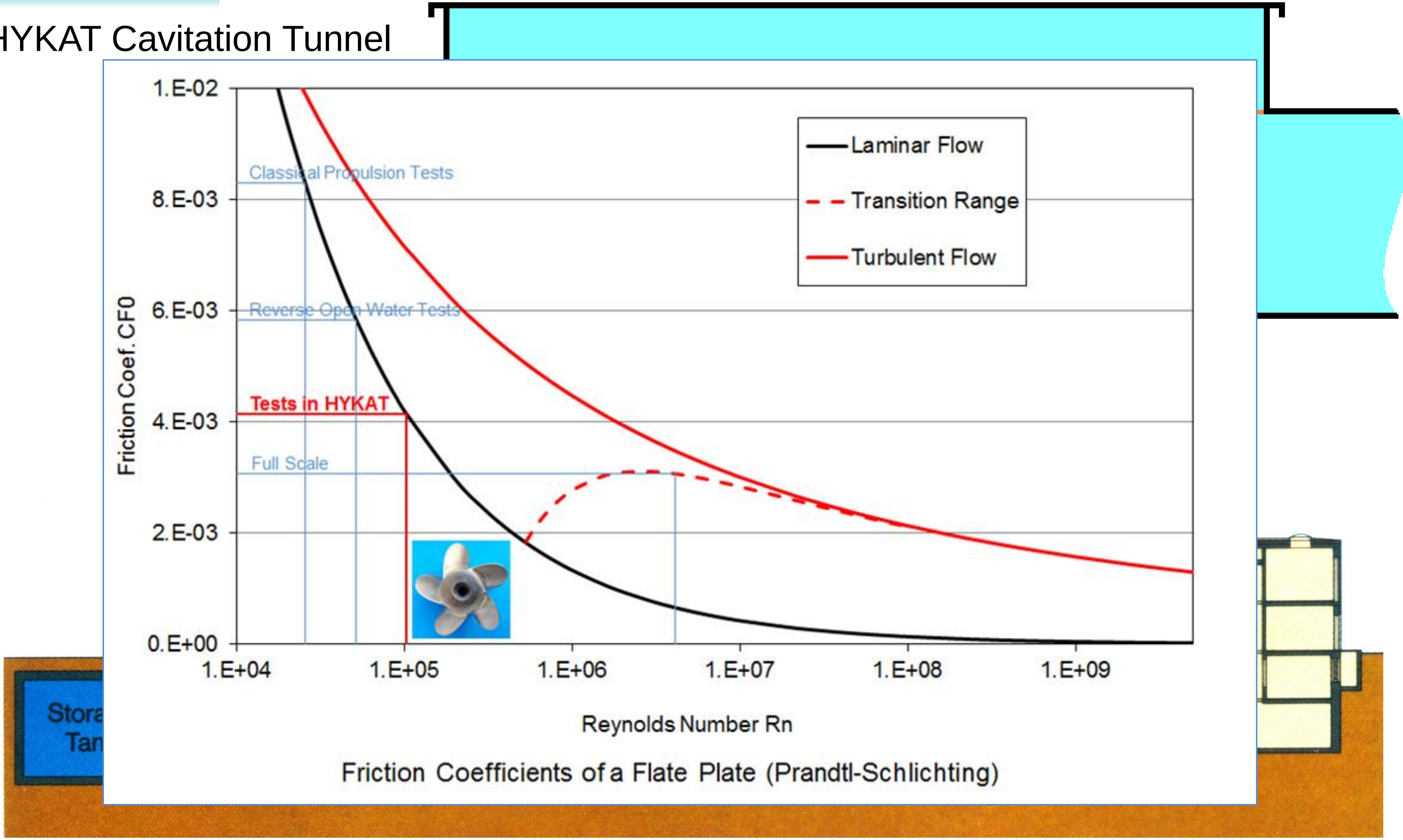

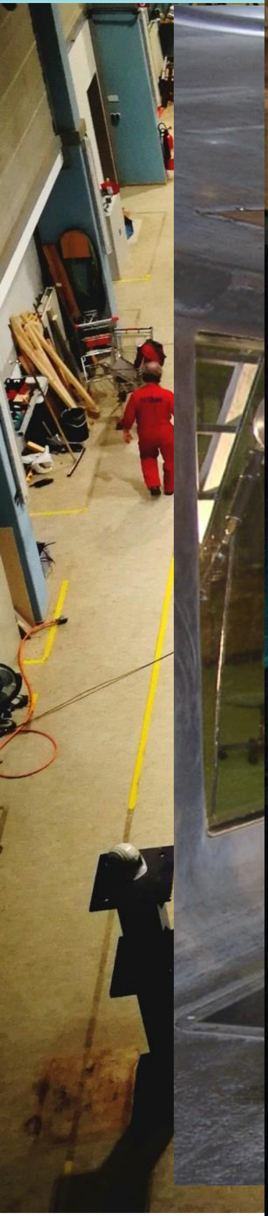

Test Procedure in HYKAT

Reference

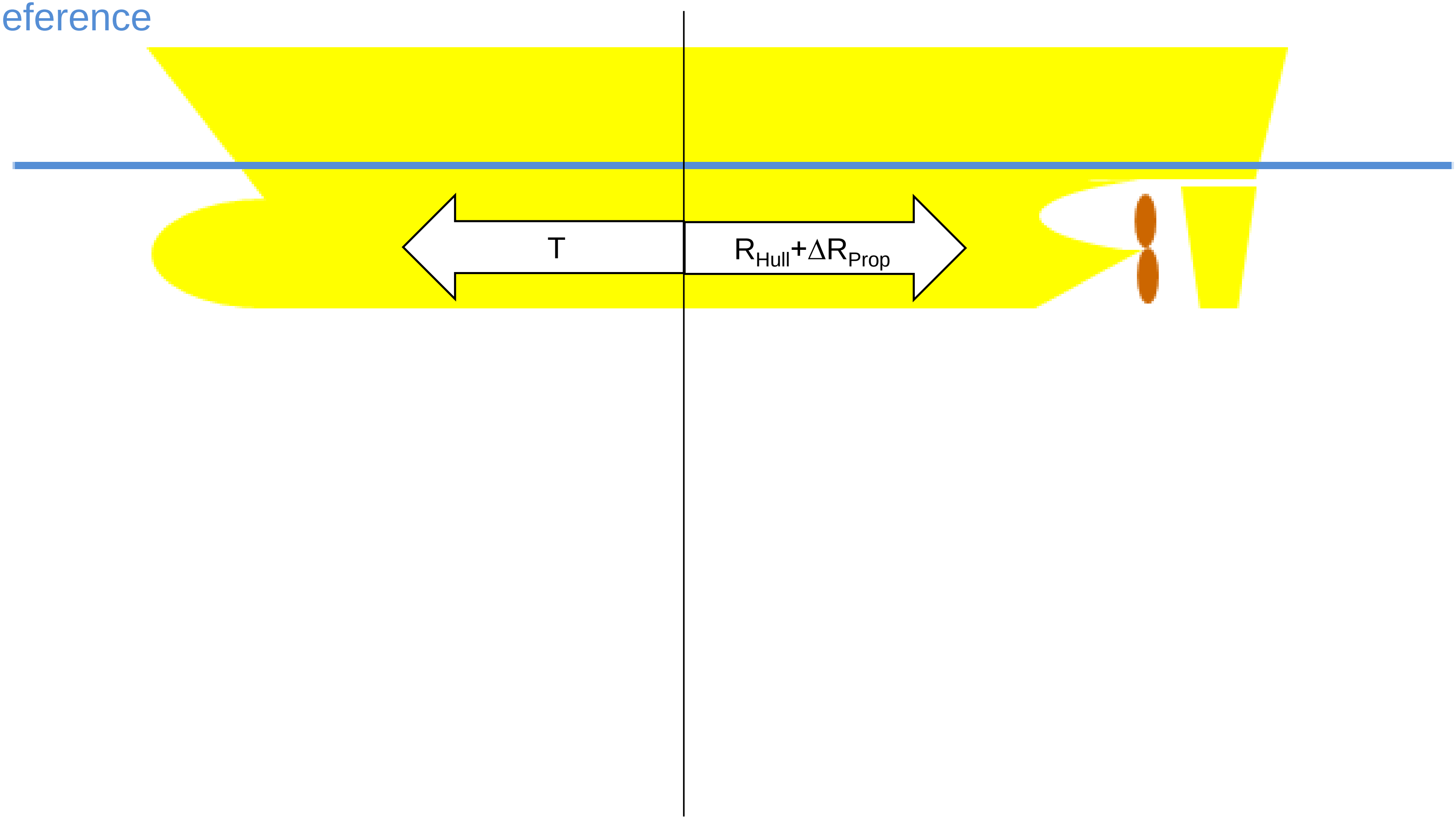

Test Procedure in HYKAT

Reference

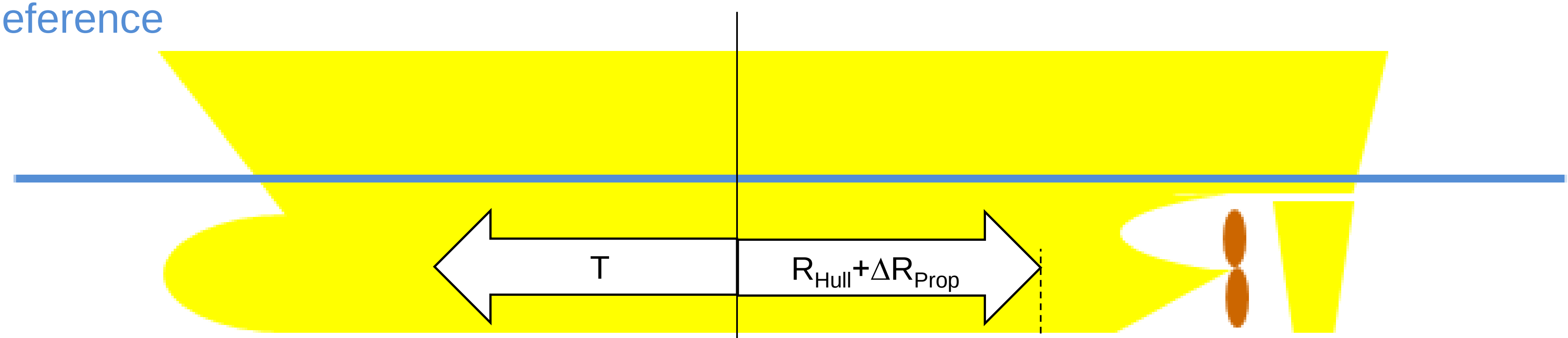

Propeller with Cap Fins

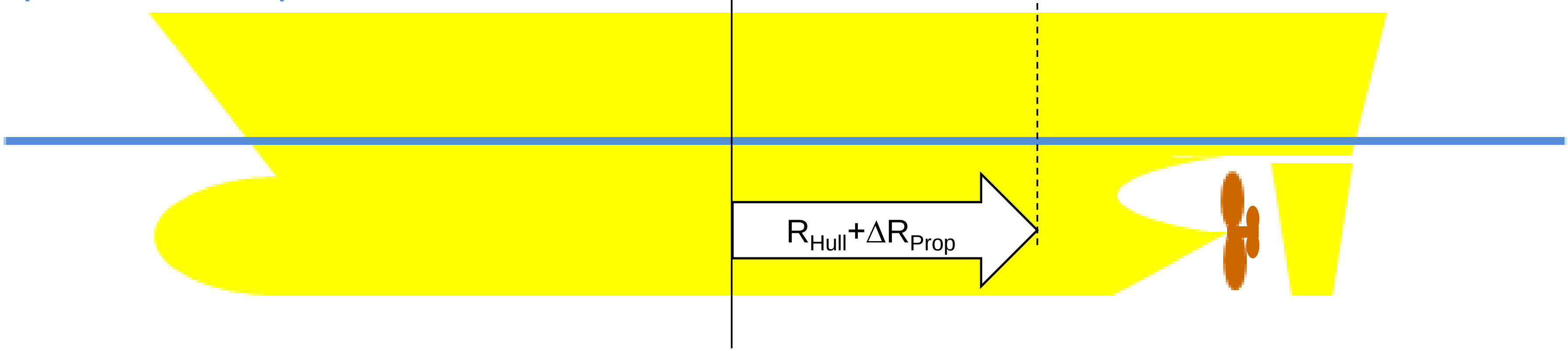

Test Procedure in HYKAT

Reference

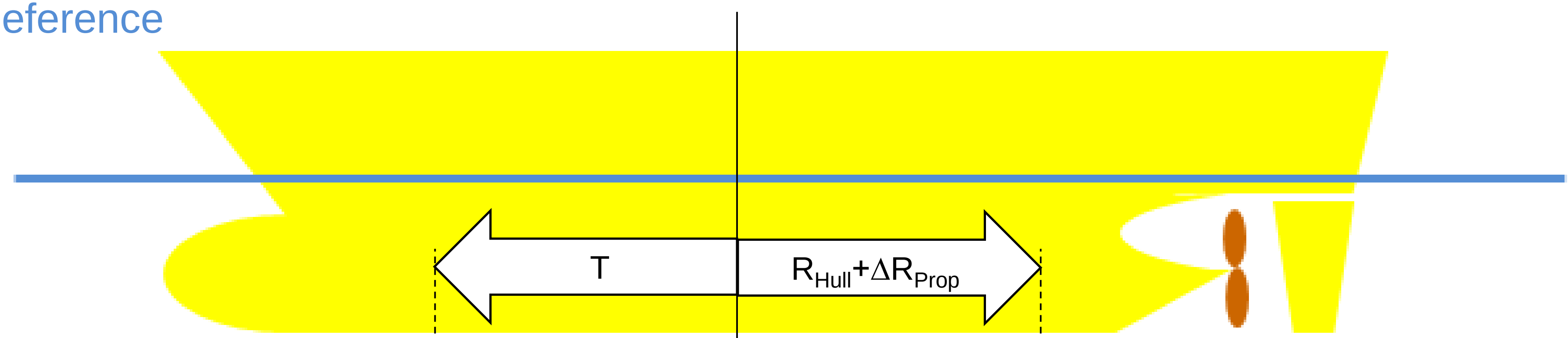

Propeller with Cap Fins

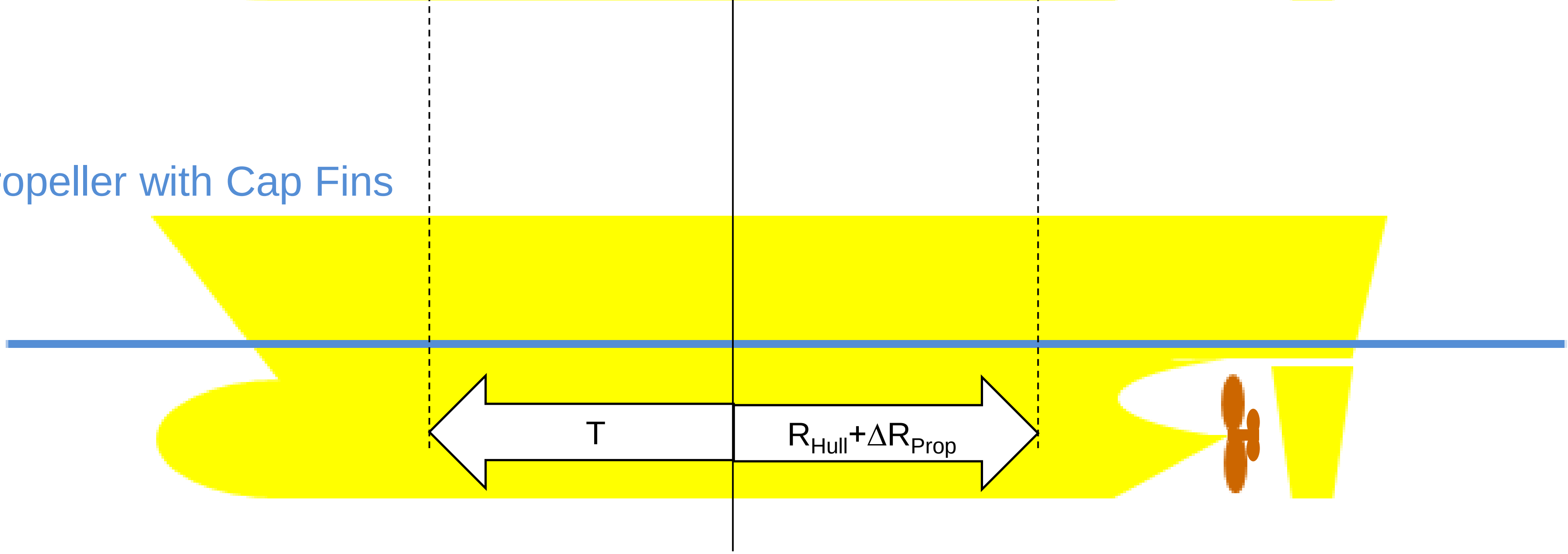

Test Procedure in HYKAT

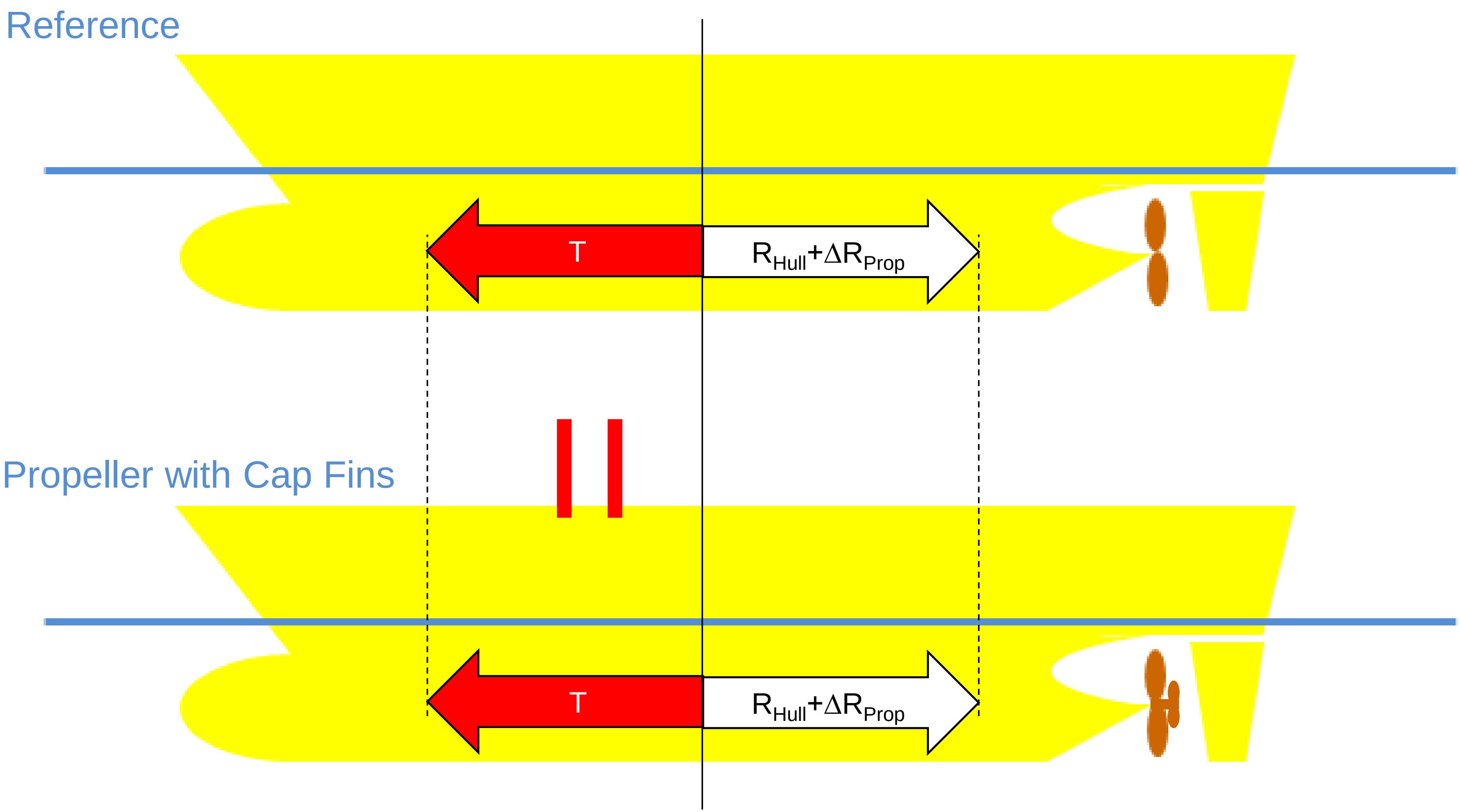

Test Procedure in HYKAT

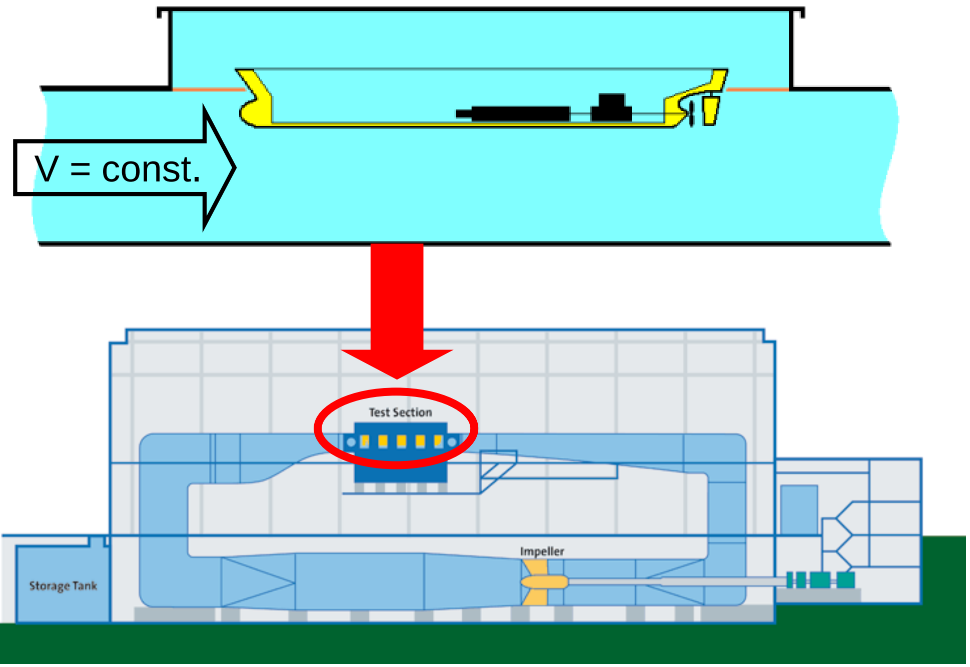

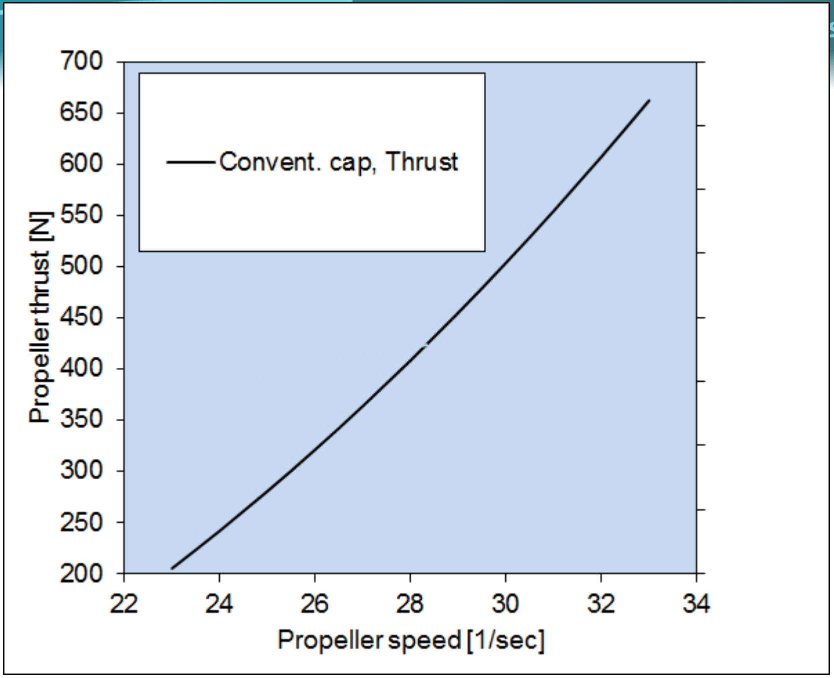

Test Procedure in HYKAT

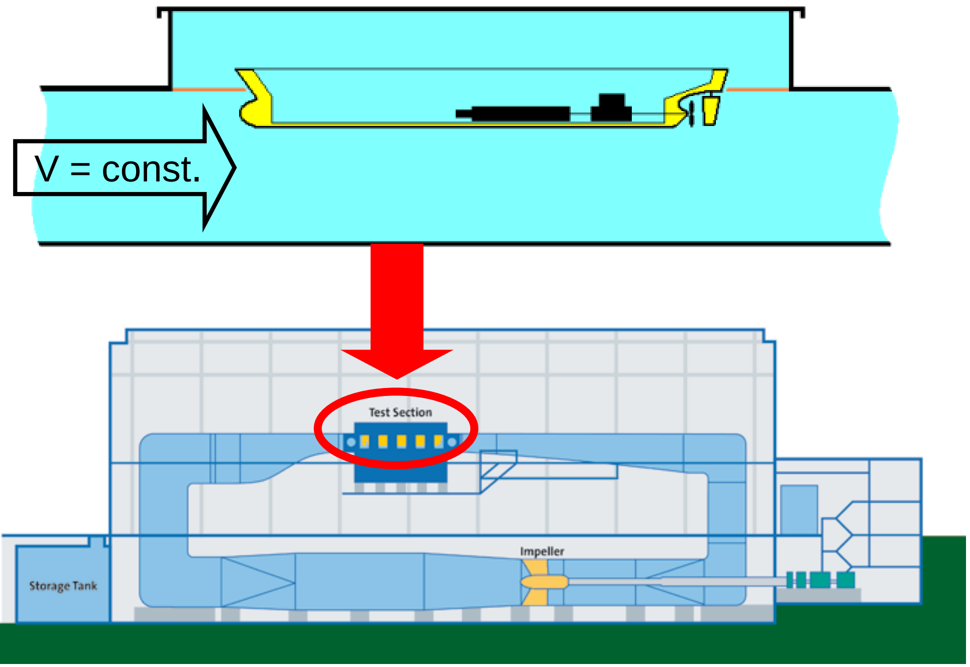

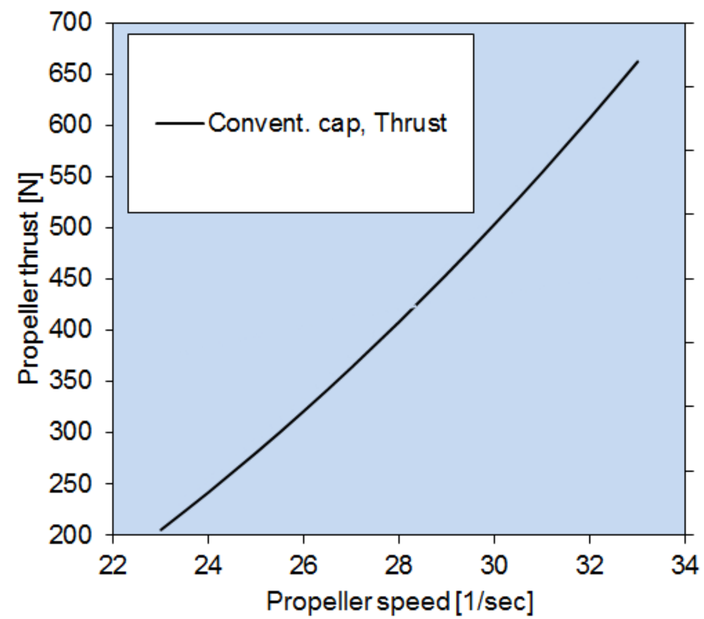

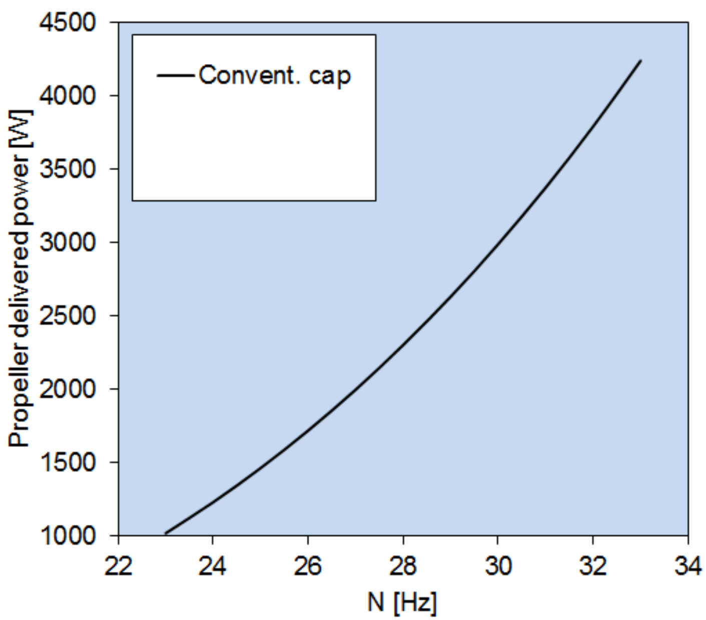

Test Procedure in HYKAT

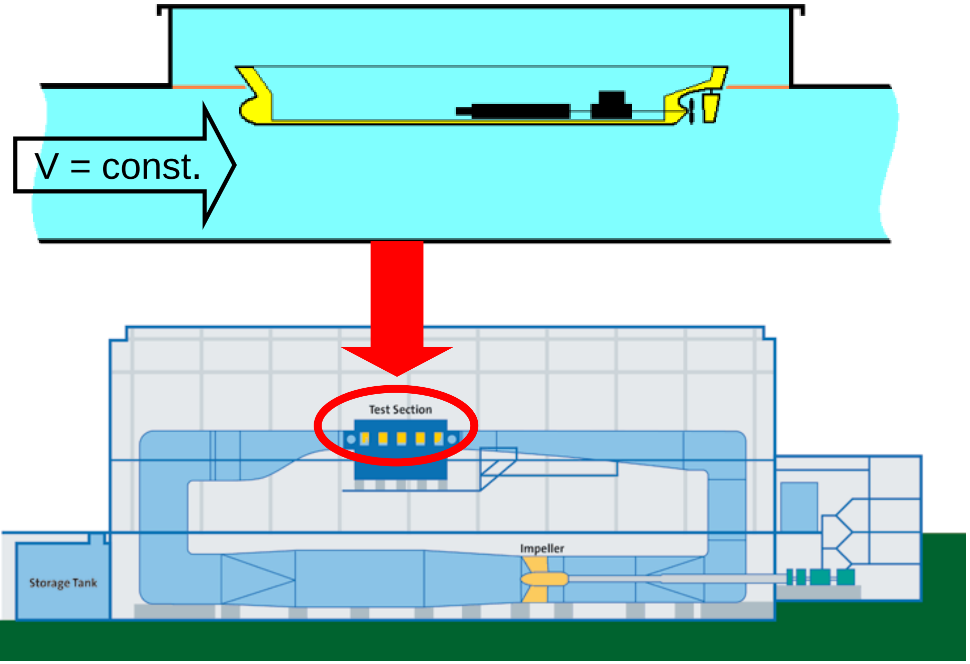

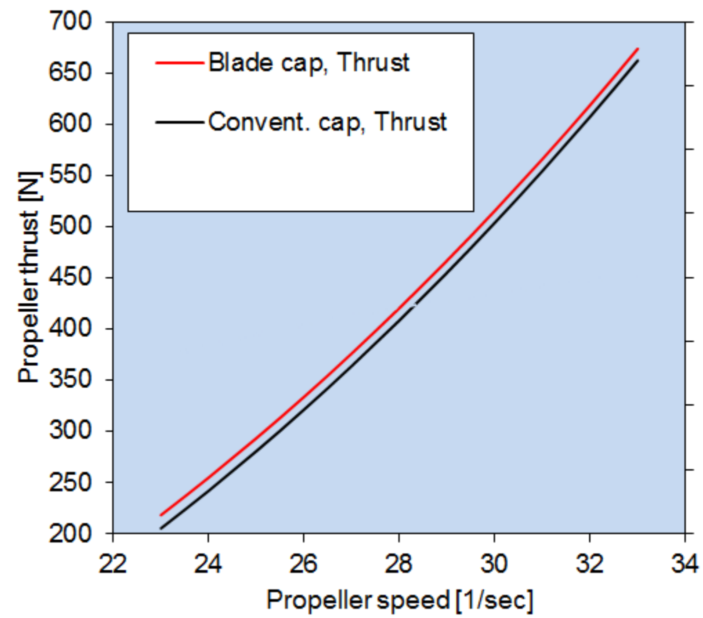

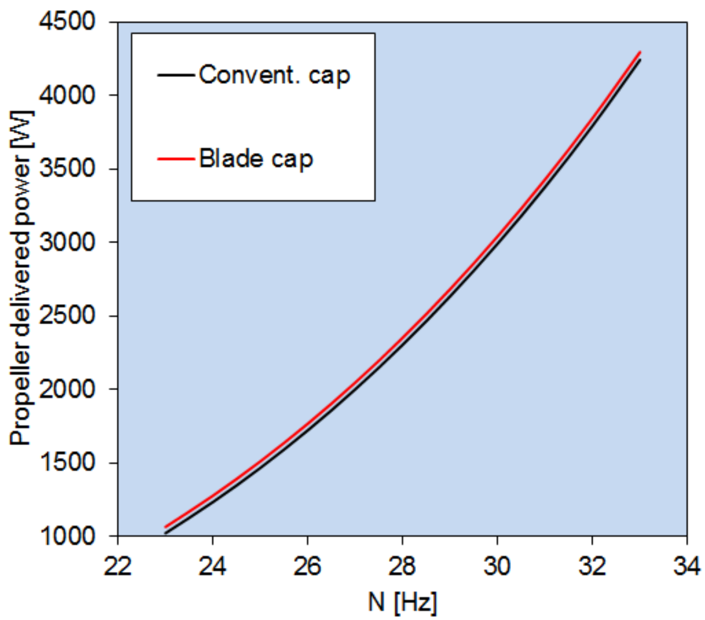

Test Procedure in HYKAT

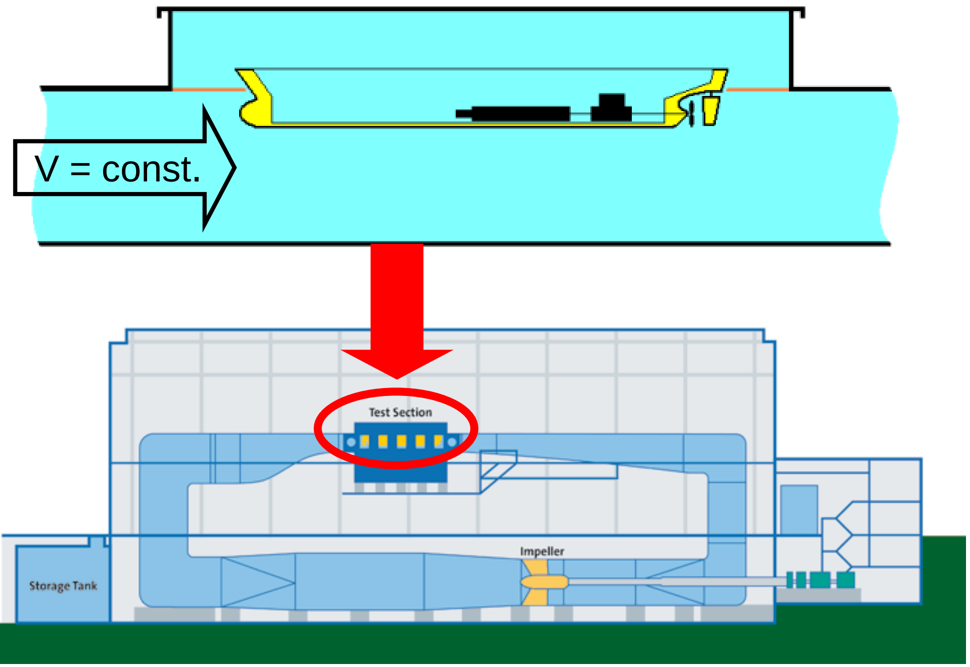

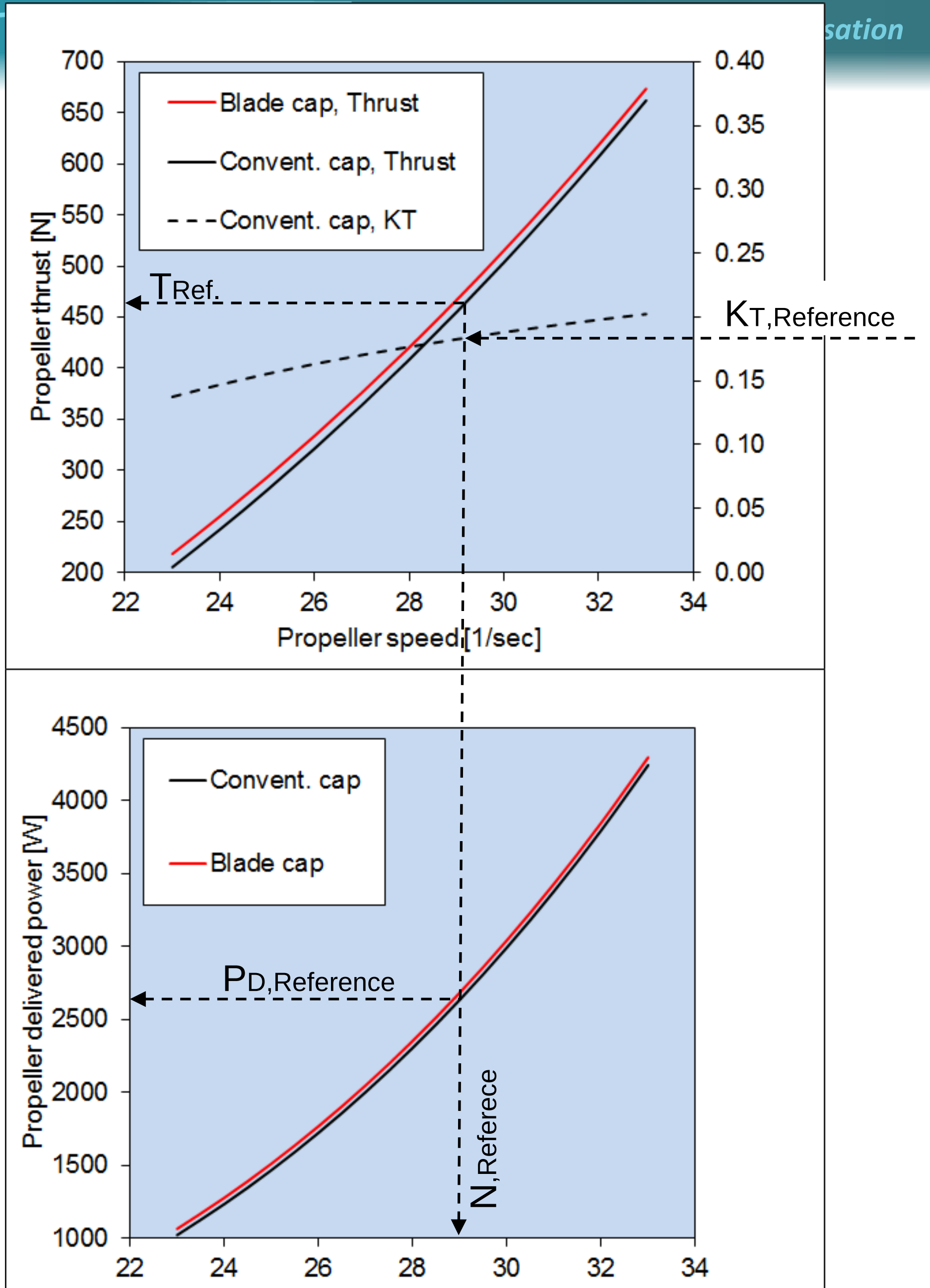

Test Procedure in HYKAT

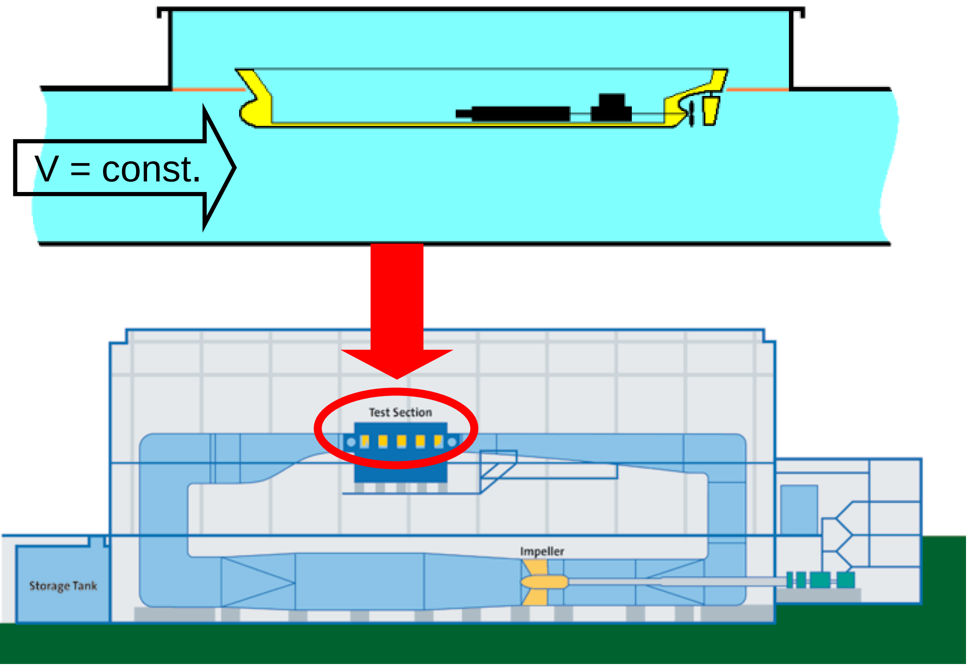

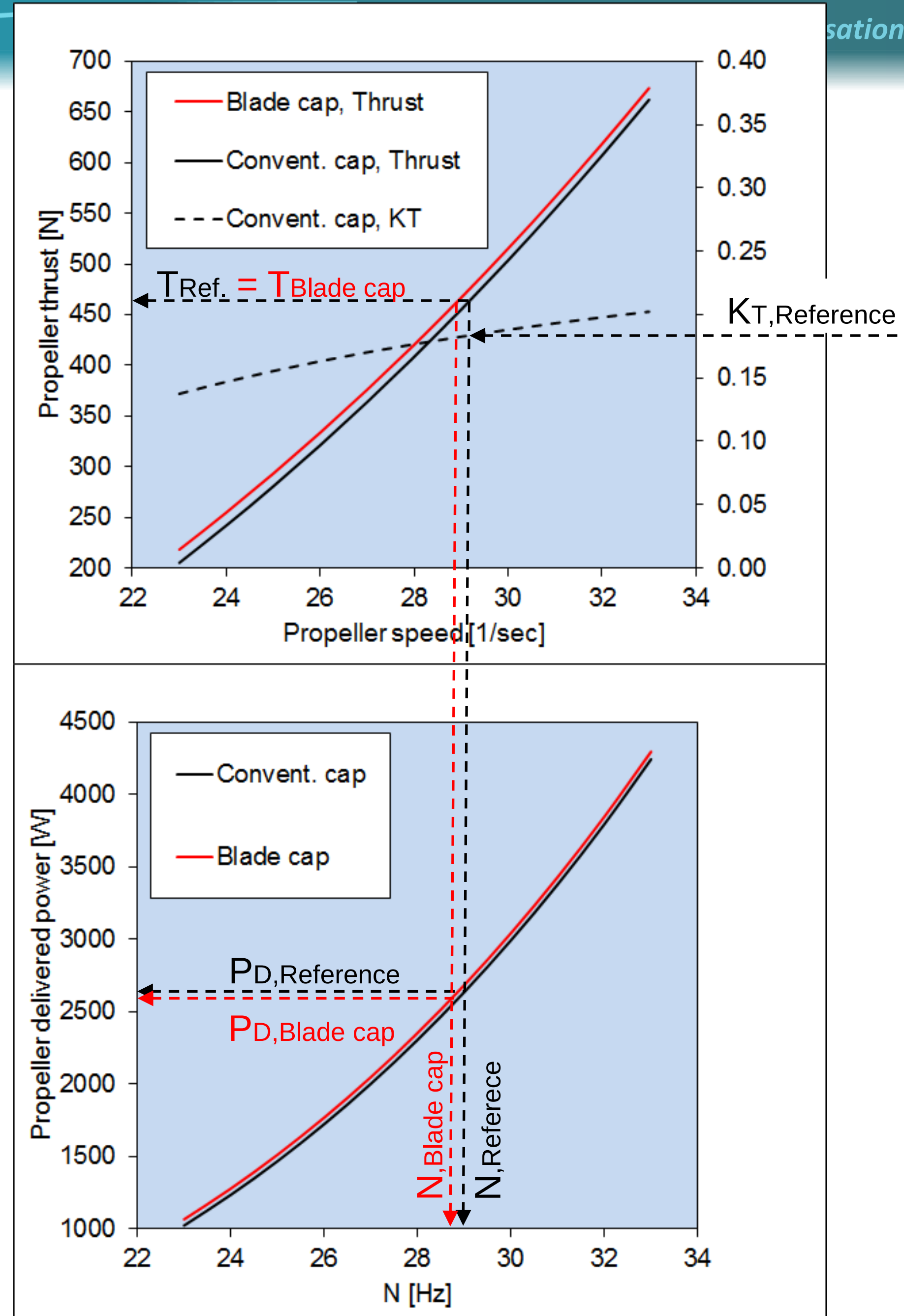

Test Procedure in HYKAT

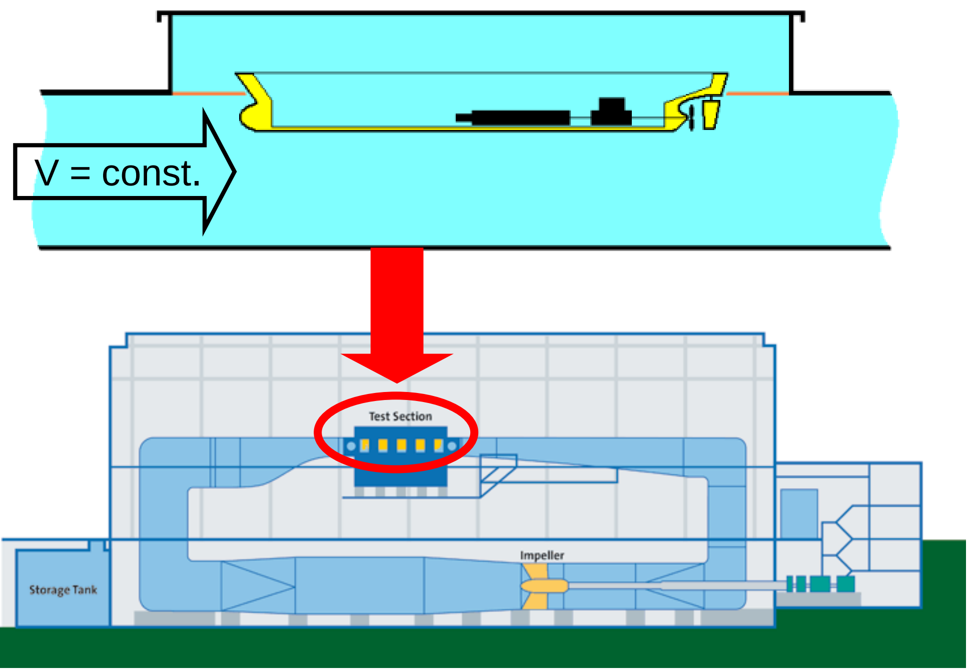

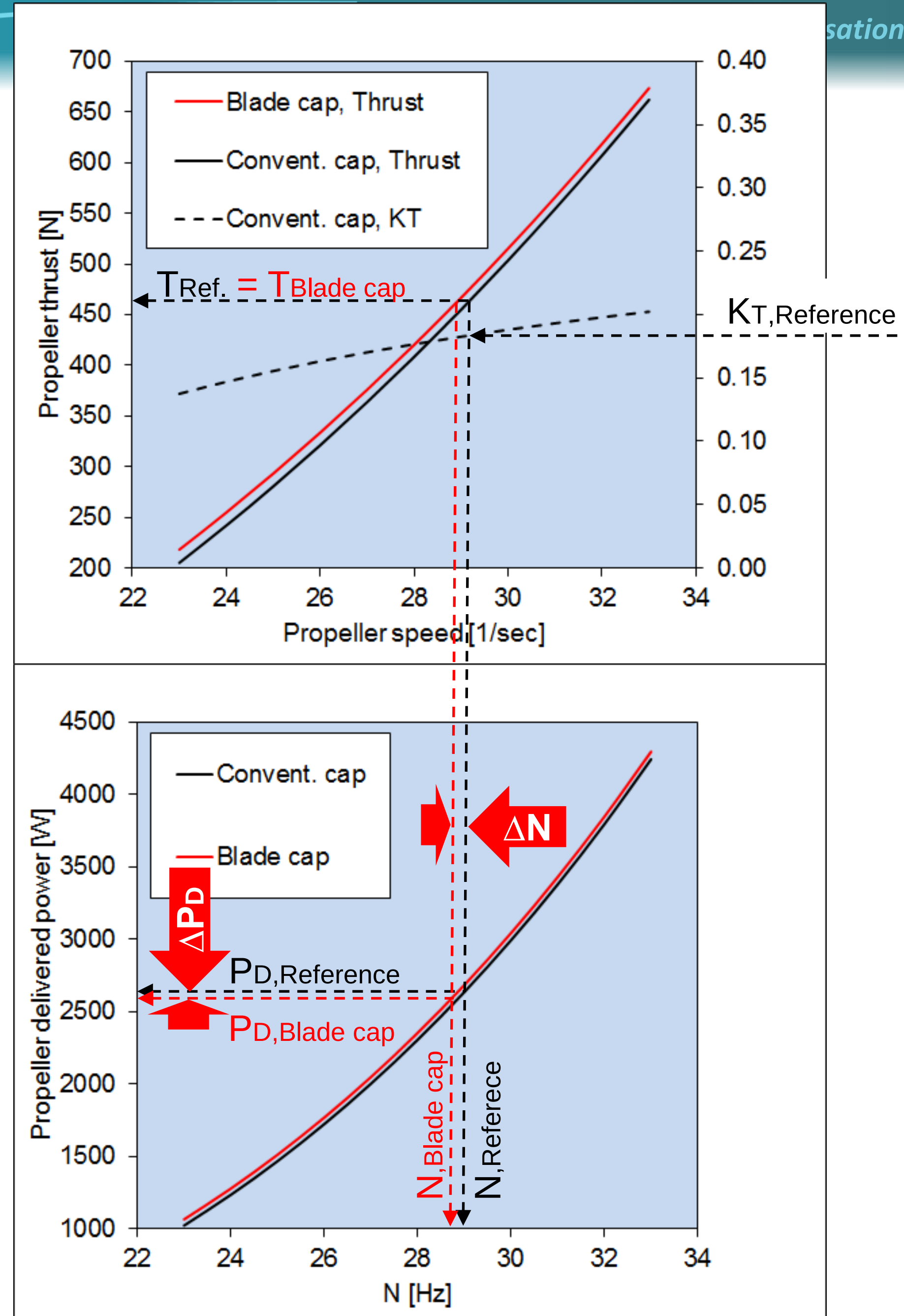

Contents

- Introduction ✓
- The Problem with Scale Effects with Propulsion Improving Devices in a Towing Tank ✓
- The Solution: Comparative Propulsion Testing in a Large Cavitation Tunnel

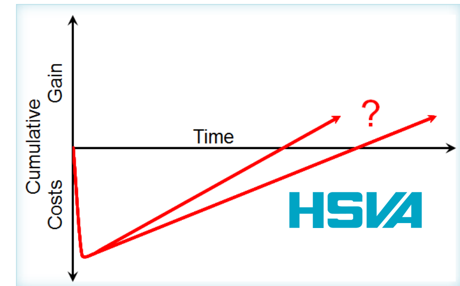

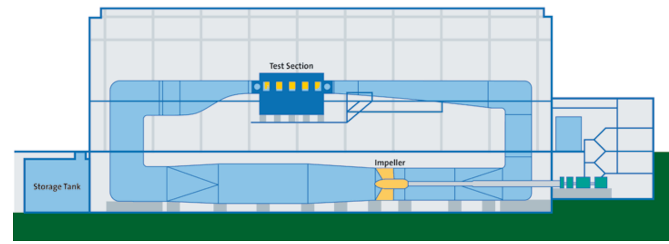

Results Gathered in HYKAT

Results Gathered in HYKAT

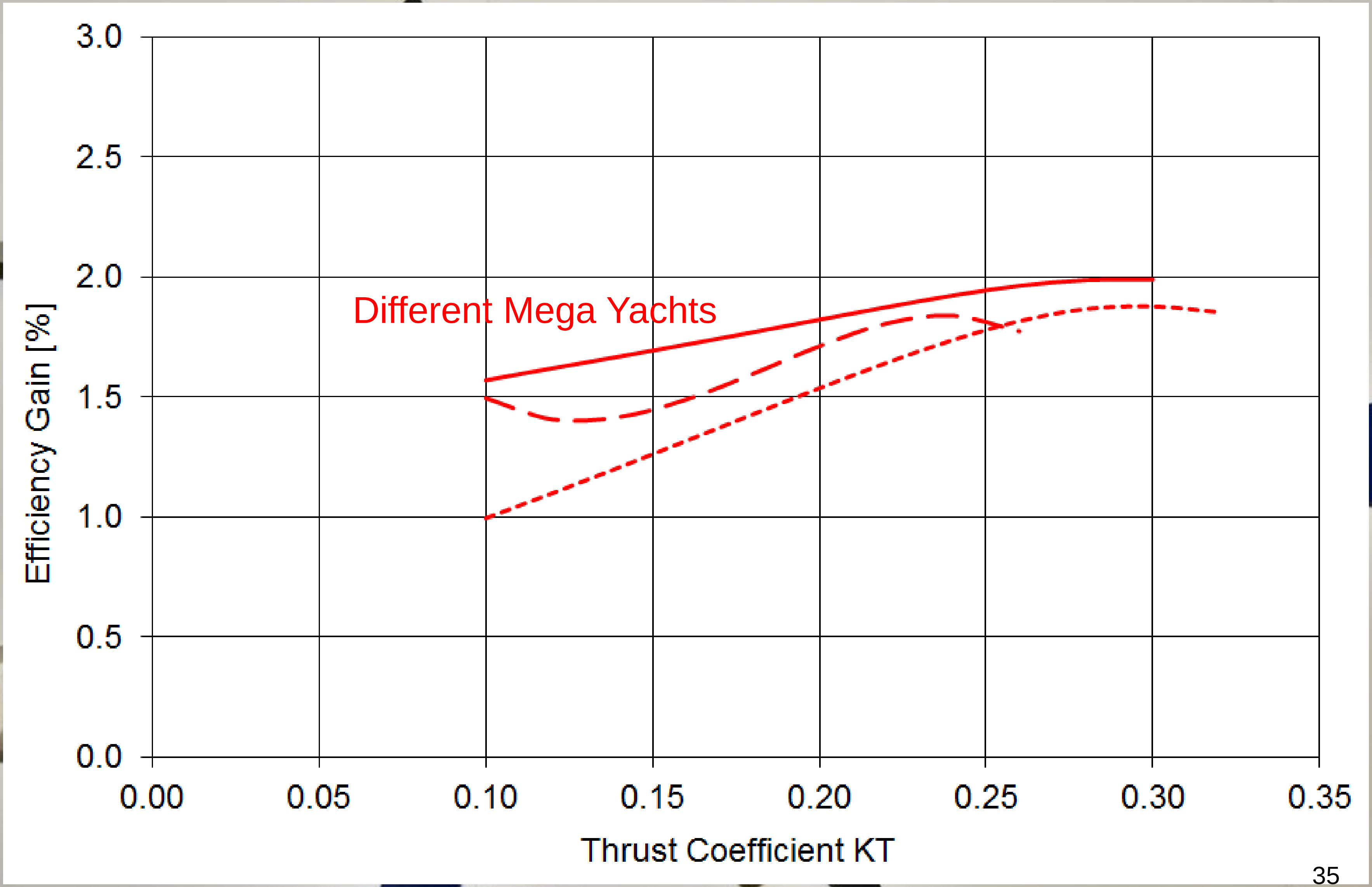

Results Gathered in HYKAT

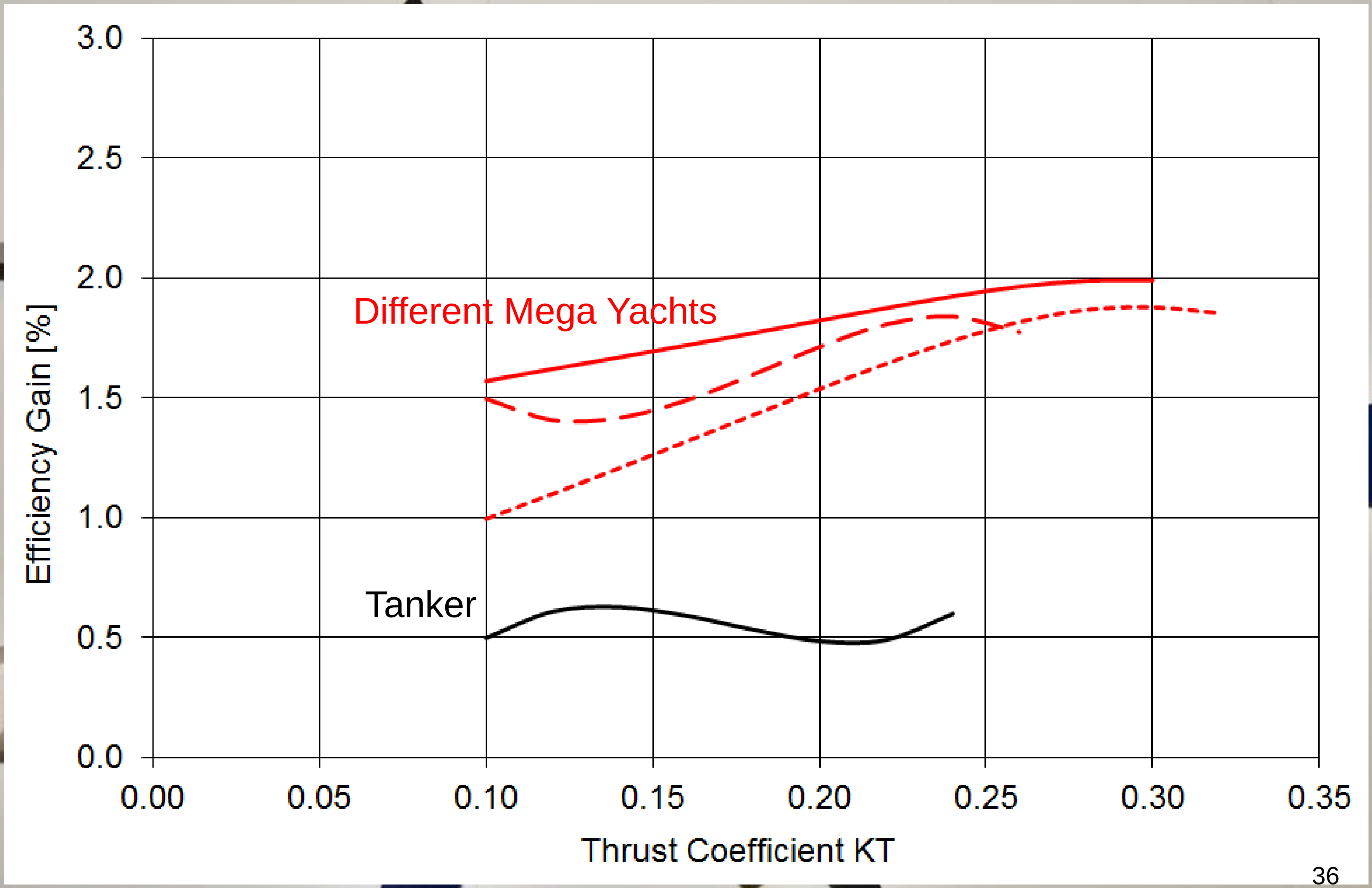

Results Gathered in HYKAT

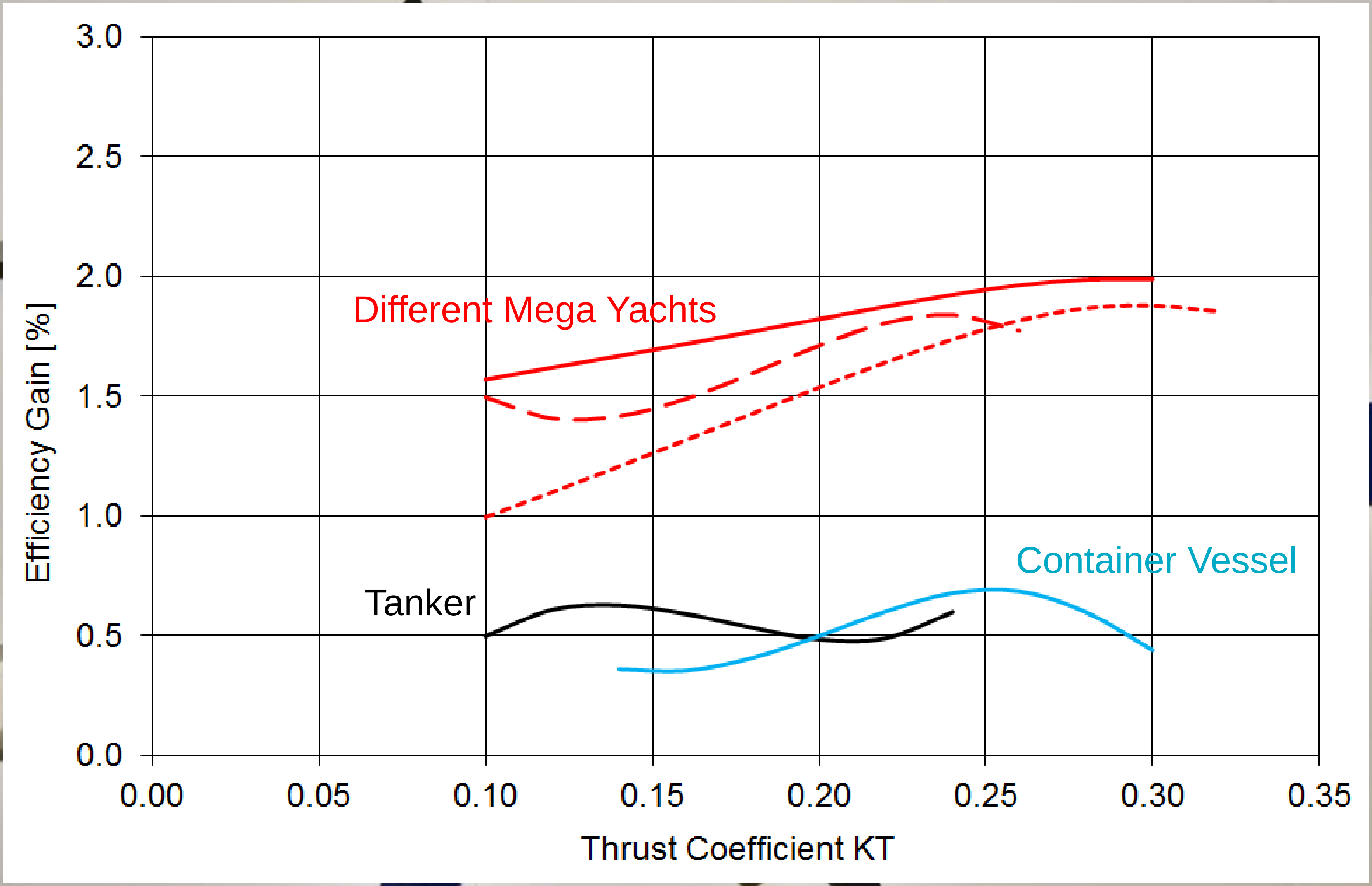

Why so different effectiveness?

Tanker or Container Vessel

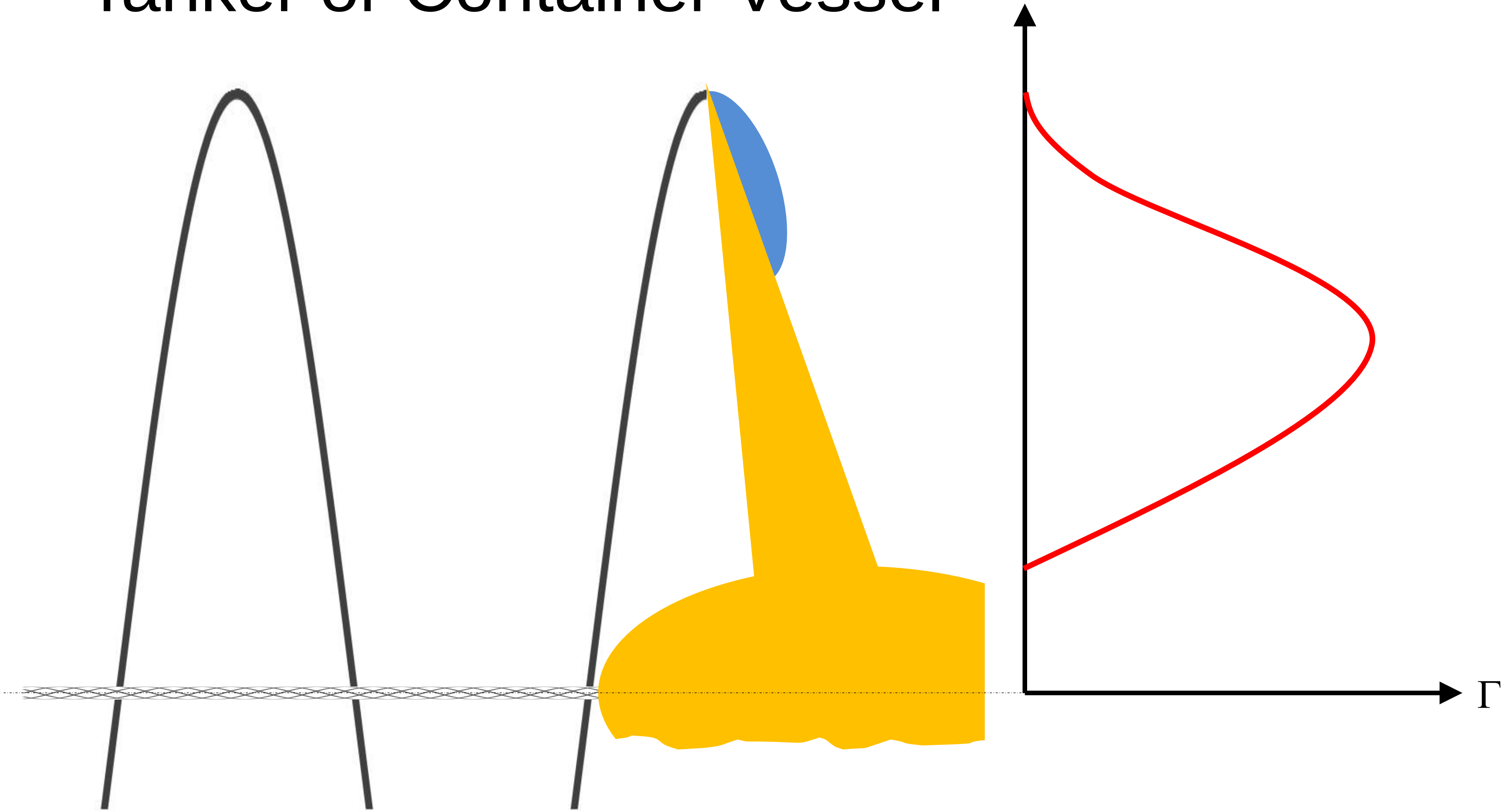

Why so different effectiveness?

Mega Yacht

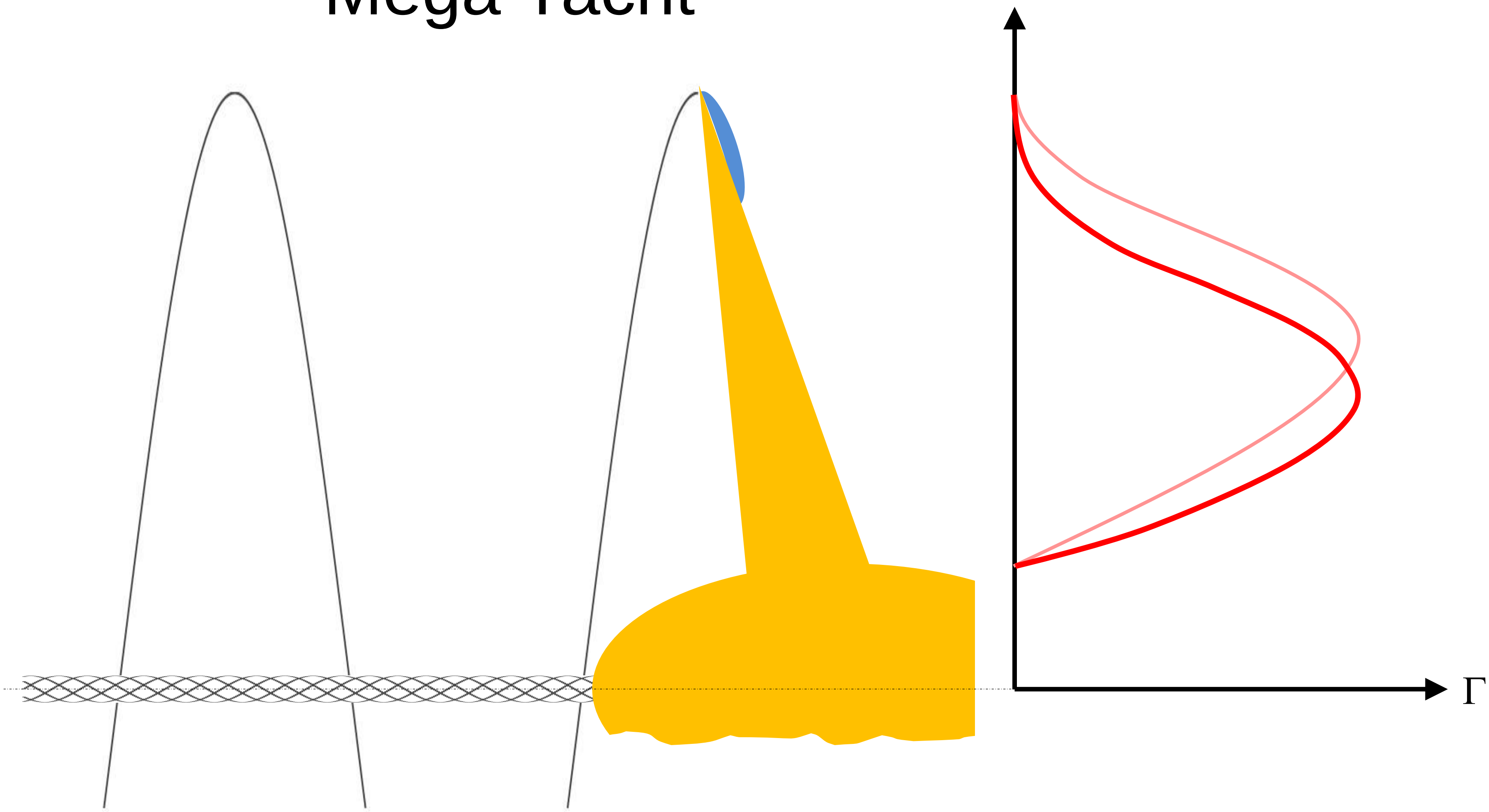

Why so different effectiveness?

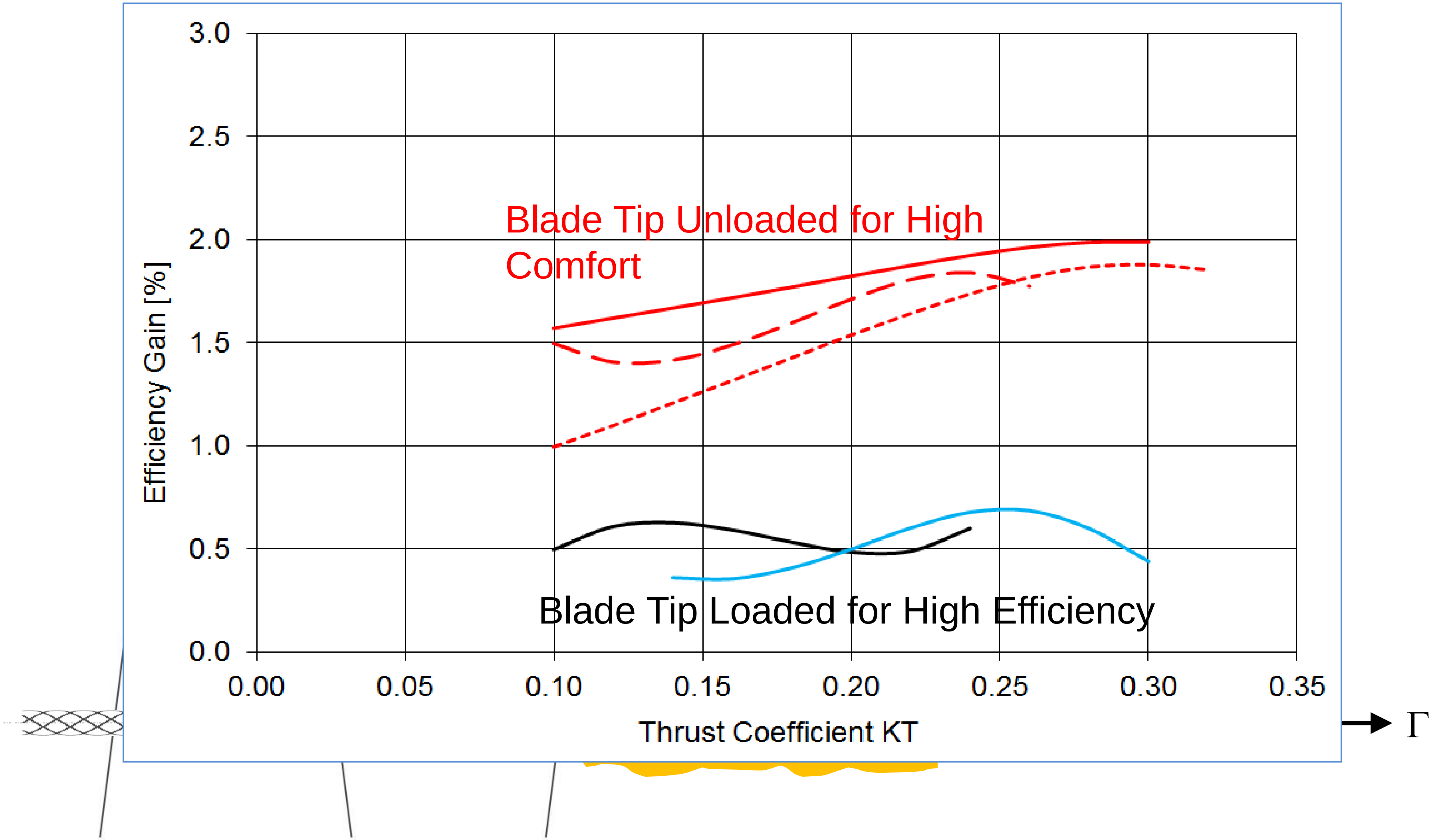

Contents

- Introduction ✓

- The Problem with Scale Effects with Propulsion Improving Devices in a Towing Tank ✓

- The Solution: Comparative Propulsion Testing in a Large Cavitation Tunnel ✓

- Results Gathered in HYKAT ✓

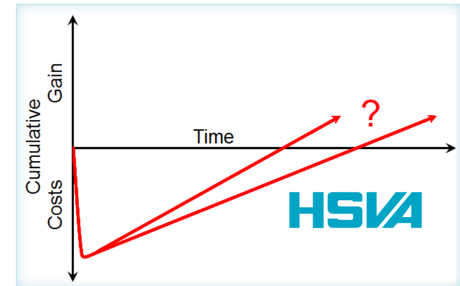

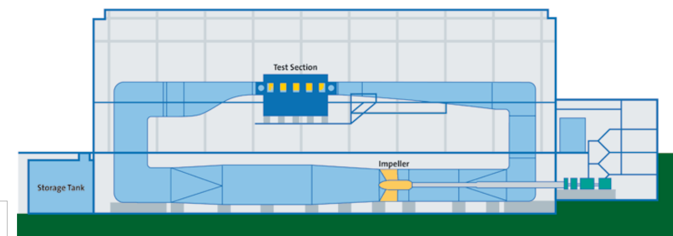

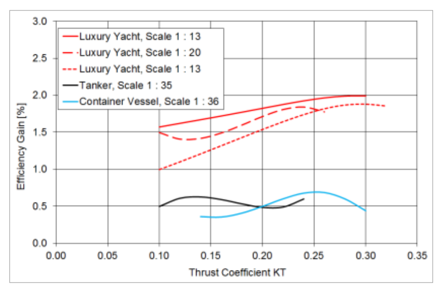

Enhancement for Unconventional Rudders

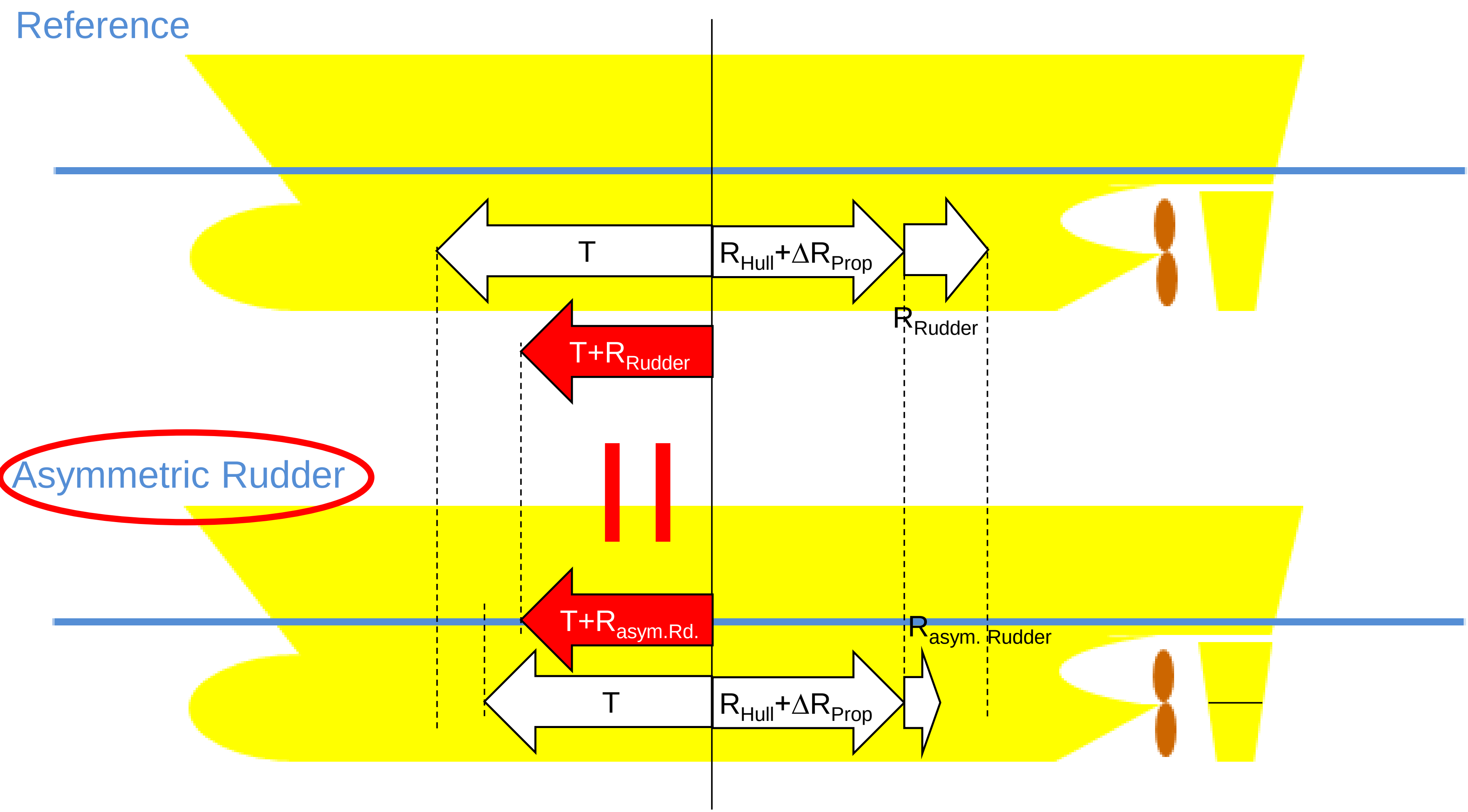

Enhancement for Unconventional Rudders

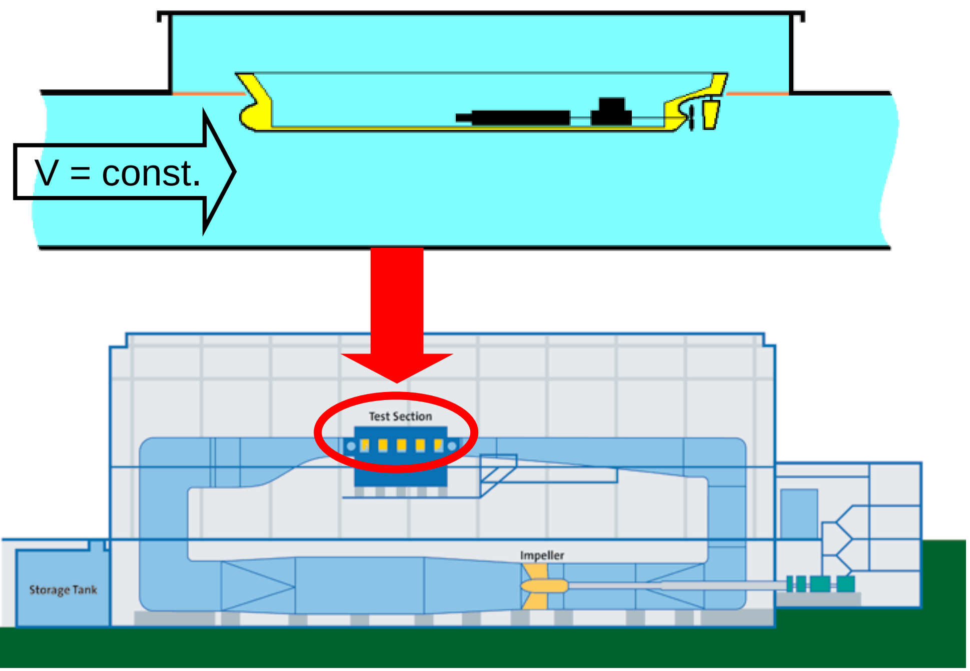

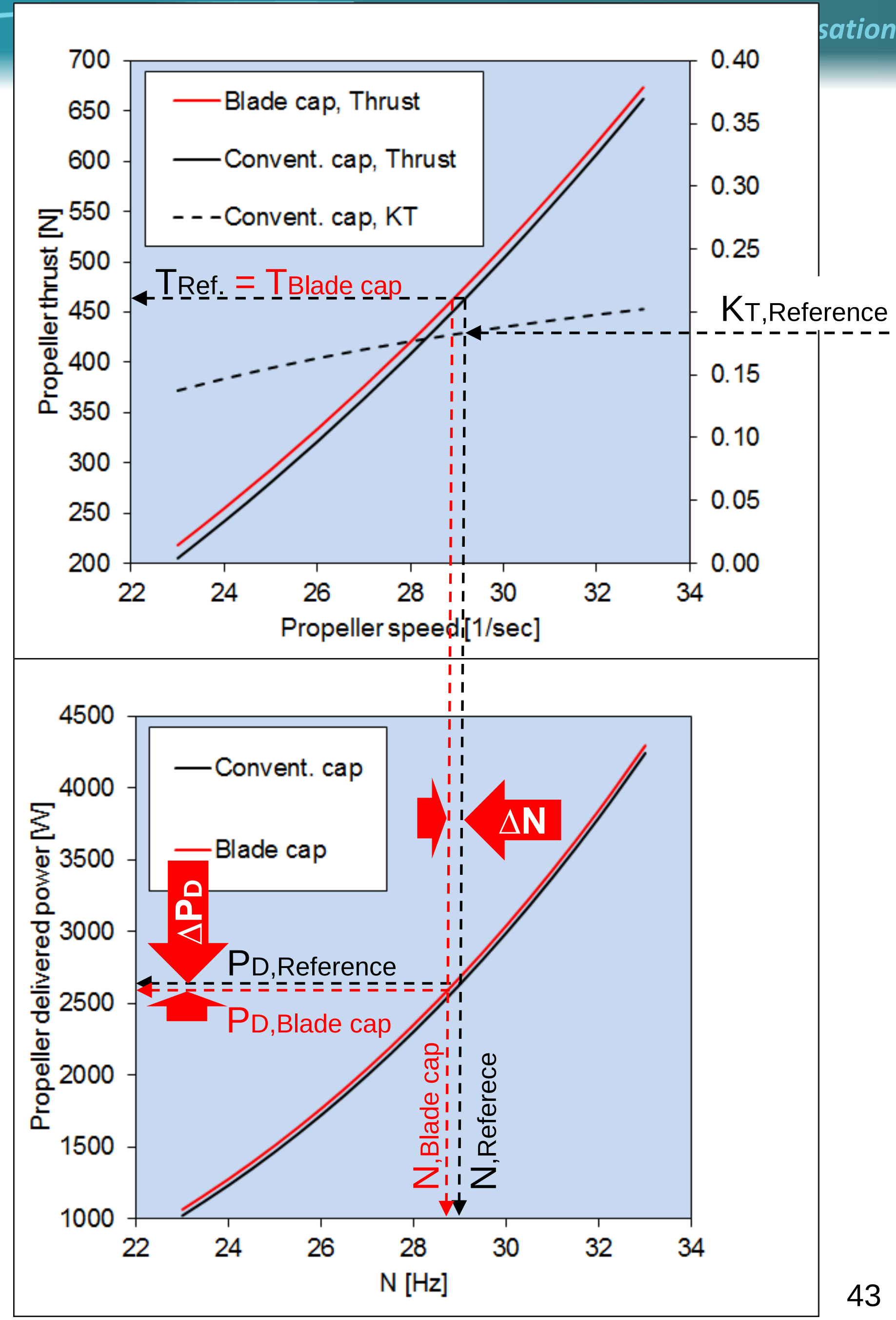

Enhancement for Unconventional Rudders

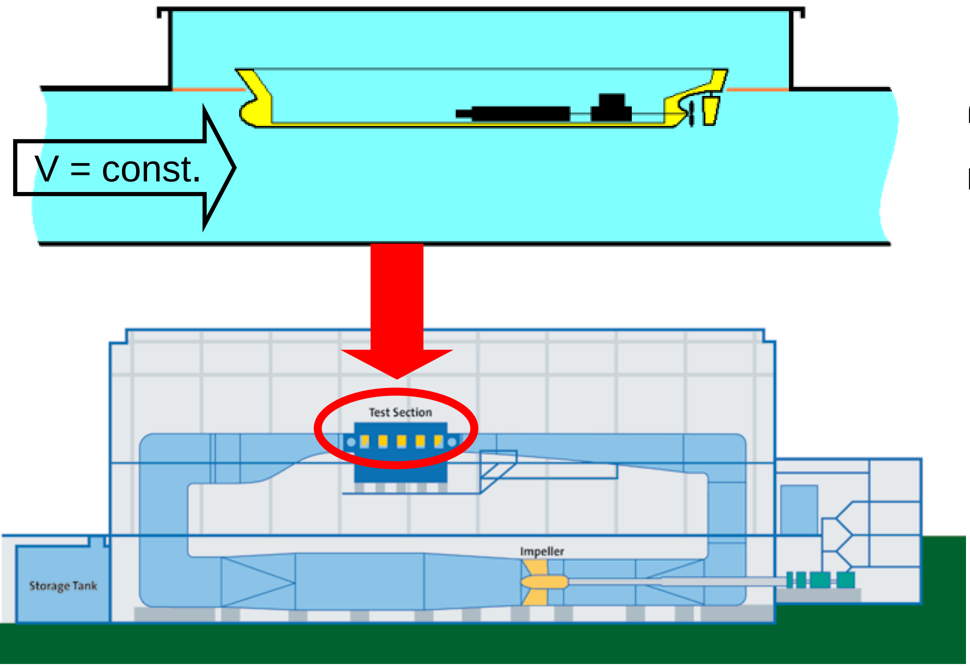

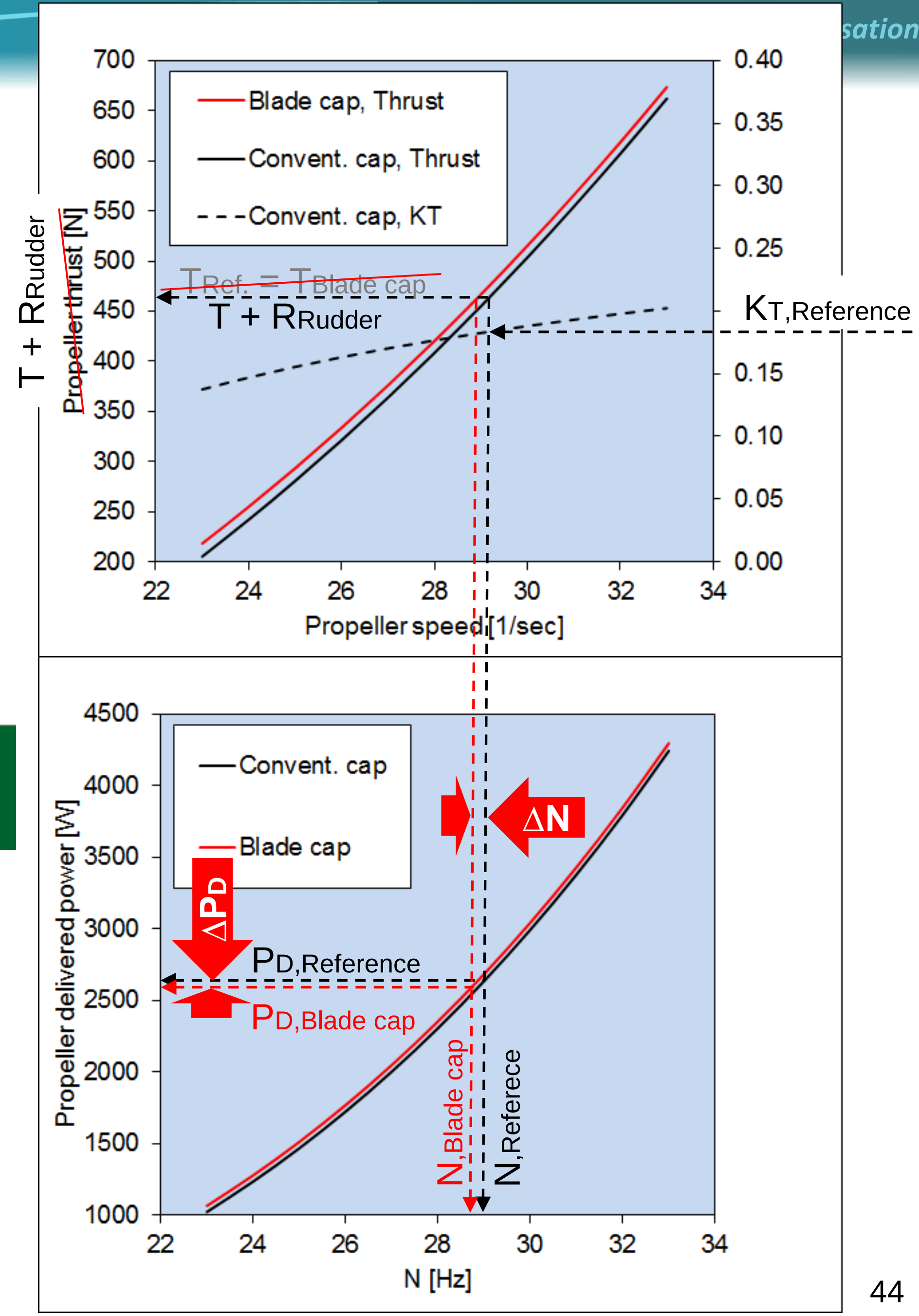

Enhancement for Unconventional Rudders

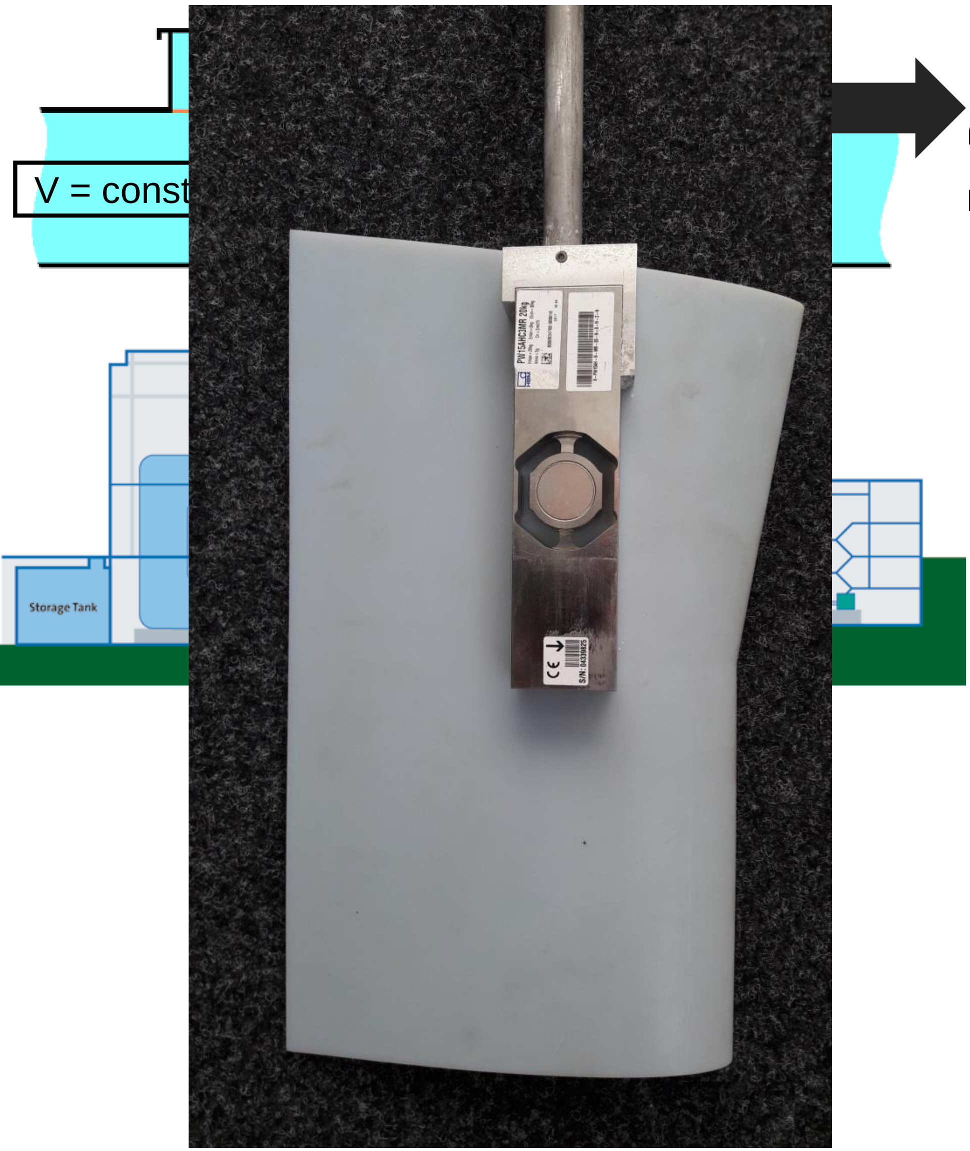

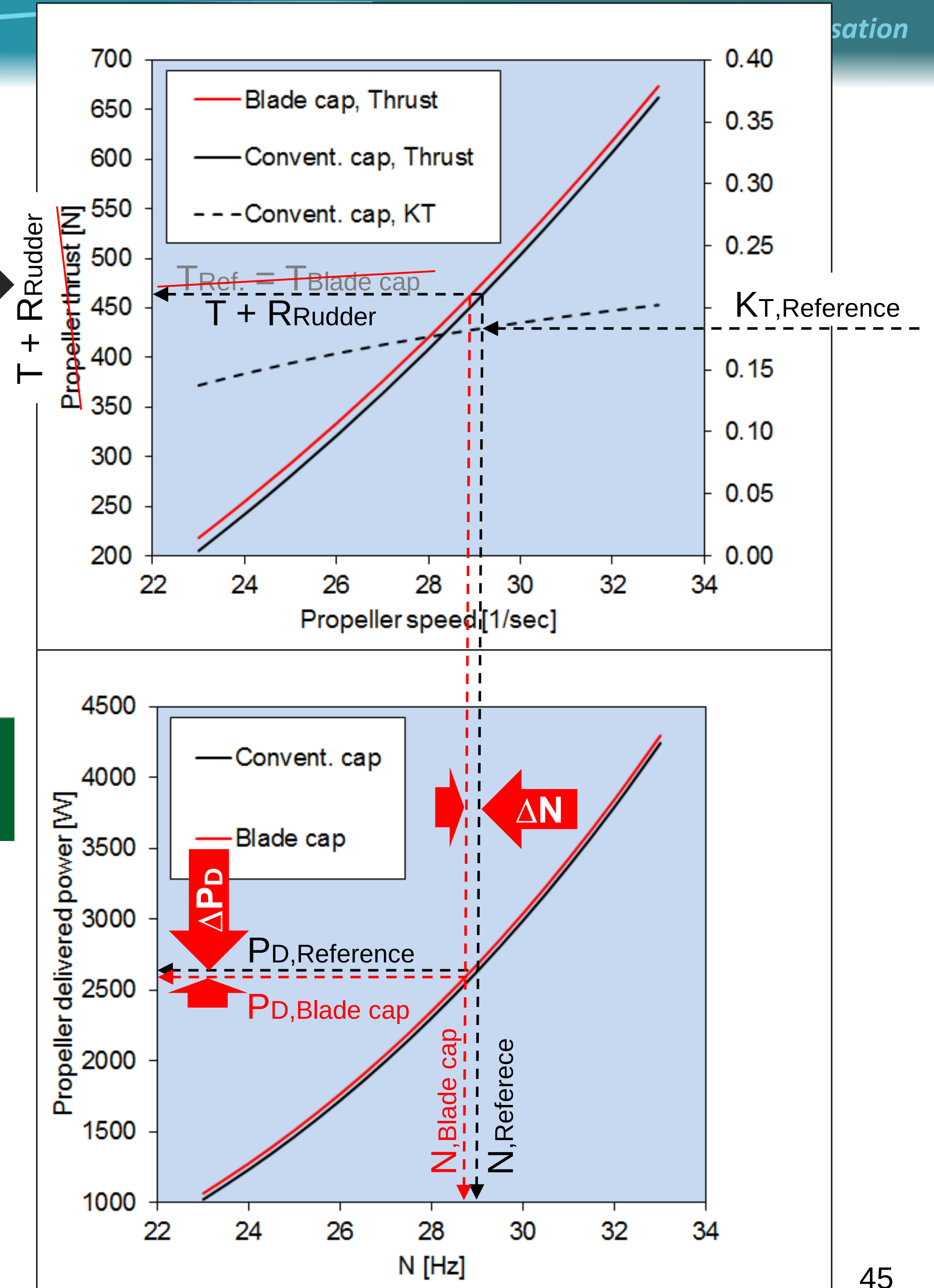

What to keep in mind?

What to keep in mind?

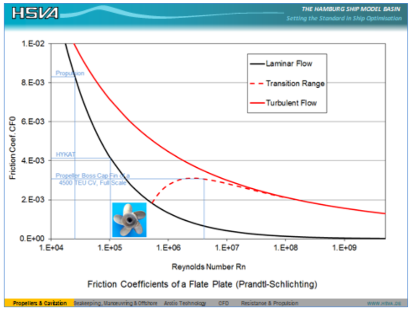

- Propeller cap fins (or other local propeller modifications) can be investigated in HYKAT very precisely.

What to keep in mind?

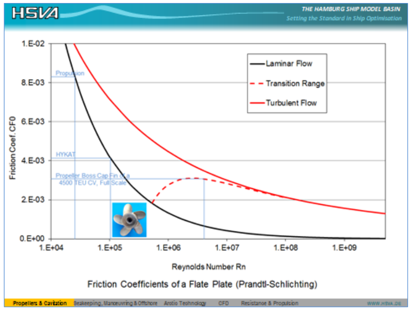

- Propeller cap fins (or other local propeller modifications) can be investigated in HYKAT very precisely.

- Propeller design philosophy has influence on the potential of propeller cap fins

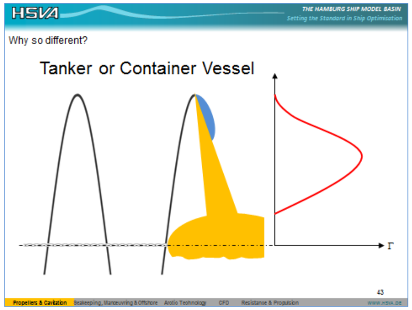

What to keep in mind?

- Propeller cap fins (or other local propeller modifications) can be investigated in HYKAT very precisely.
- Propeller design philosophy has influence on the potential of propeller cap fins.
- Since recently the new method also works for rudder modifications.

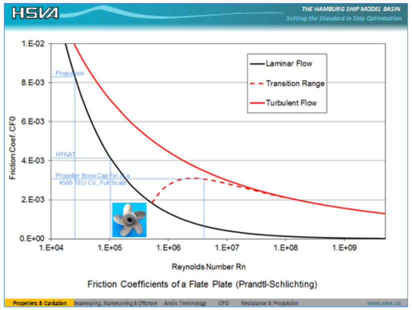

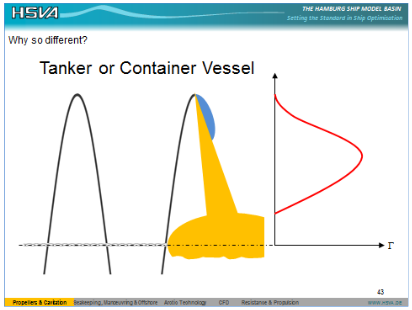

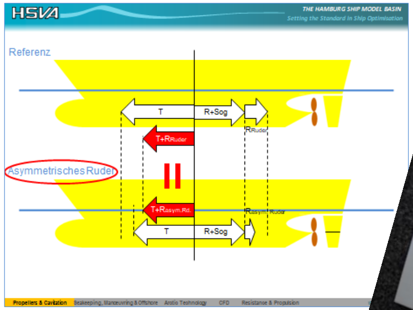

What to keep in mind?

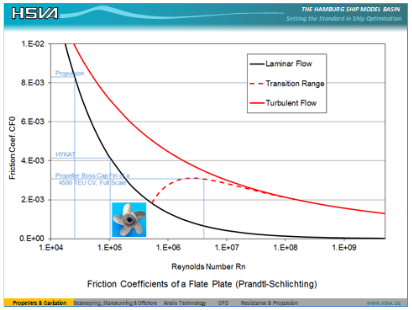

- Propeller cap fins (or other local propeller modifications) can be investigated in HYKAT very precisely.

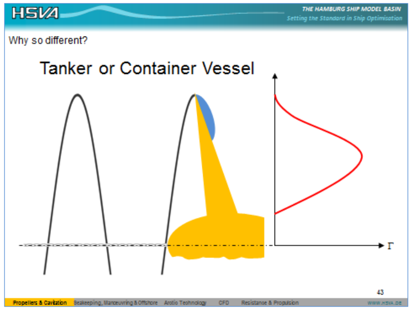

- Propeller design philosophy has influence on the potential of propeller cap fins.

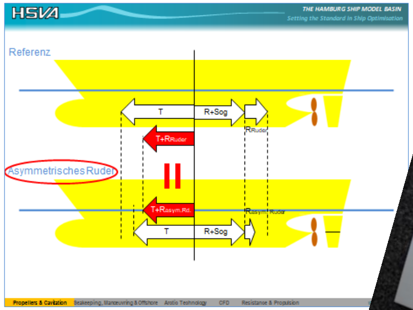

- Since recently the new method also works for rudder modifications.

- If a cavitation test is performed anyway, this requires just small additional money.

PROPELLER EFFECTS ON MANEUVERING OF A SUBMERGED BODY

S. Duman[1], S. Sezen[1] and S. Bal[2]

[1], Yildiz Technical University

[2], Istanbul Technical University

TABLE OF CONTENTS

INTRODUCTION

- Nowadays, CFD method have become very popular in predicting hydrodynamic characteristics of both surface ships and underwater vehicles.

- Turbulence models developed to mimic the real fluid flows in nature have shown great progress.

- Besides the conventional straight-ahead towing simulations, complex problems such as dynamic maneuverings have successfully been analzed by CFD method.

INTRODUCTION

- Un-appended DARPA Suboff (AFF-1) model is chosen due to available comparison data.
- A V&V study has been conducted.
- Oblique towing simulations of AFF-1 have been carried out.
- Body force propeller method has been implemented.

MAIN PARTICULARS

- Principal parameters of AFF-1:

L_{OA} (m)	**4.356**
L_{PP} (m)	4.261
D_{max} (m)	0.508
S (m^2)	5.989
(m^3)	0.699

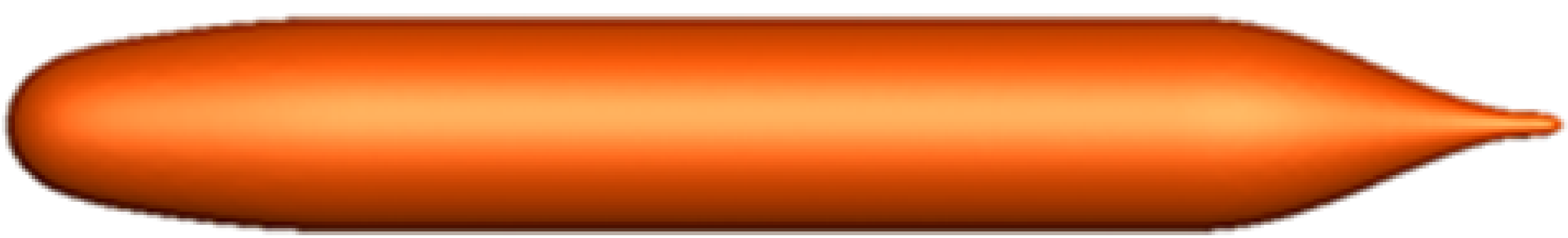

MATHEMATICAL BACKGROUND

- Continuity equation:

$$\frac{\partial U_i}{\partial x_i} = 0$$

- Momentum equations:

$$\frac{\partial \mathrm{U_i}}{\partial \mathrm{t}} + \frac{\partial \left(\mathrm{U}_i \mathrm{U}_j \right)}{\partial \mathrm{x_j}} = -\frac{1}{\rho} \frac{\partial \mathrm{P}}{\partial \mathrm{x_i}} + \frac{\partial}{\partial x_j} \left[\nu \left(\frac{\partial U_i}{\partial \mathrm{x_j}} + \frac{\partial U_j}{\partial \mathrm{x}_i} \right) \right] - \frac{\partial \overline{\mathrm{u_i^{'} u_j^{'}}}}{\partial \mathrm{x_j}}$$

COMPUTATIONAL RESULTS

- Simulation cases:

Method	Drift angle (β°)	Drift angle (β°)
Re	$12*10^6$	$14*10^6$
w/o propeller	0, 4, 8, 12, 16, 18	0, 4, 8, 12, 16, 18
with propeller	0, 4, 8, 12, 16, 18	0, 4, 8, 12, 16, 18

COMPUTATIONAL RESULTS

- Frictional resistance coefficient on the longitudinal symmetry line:

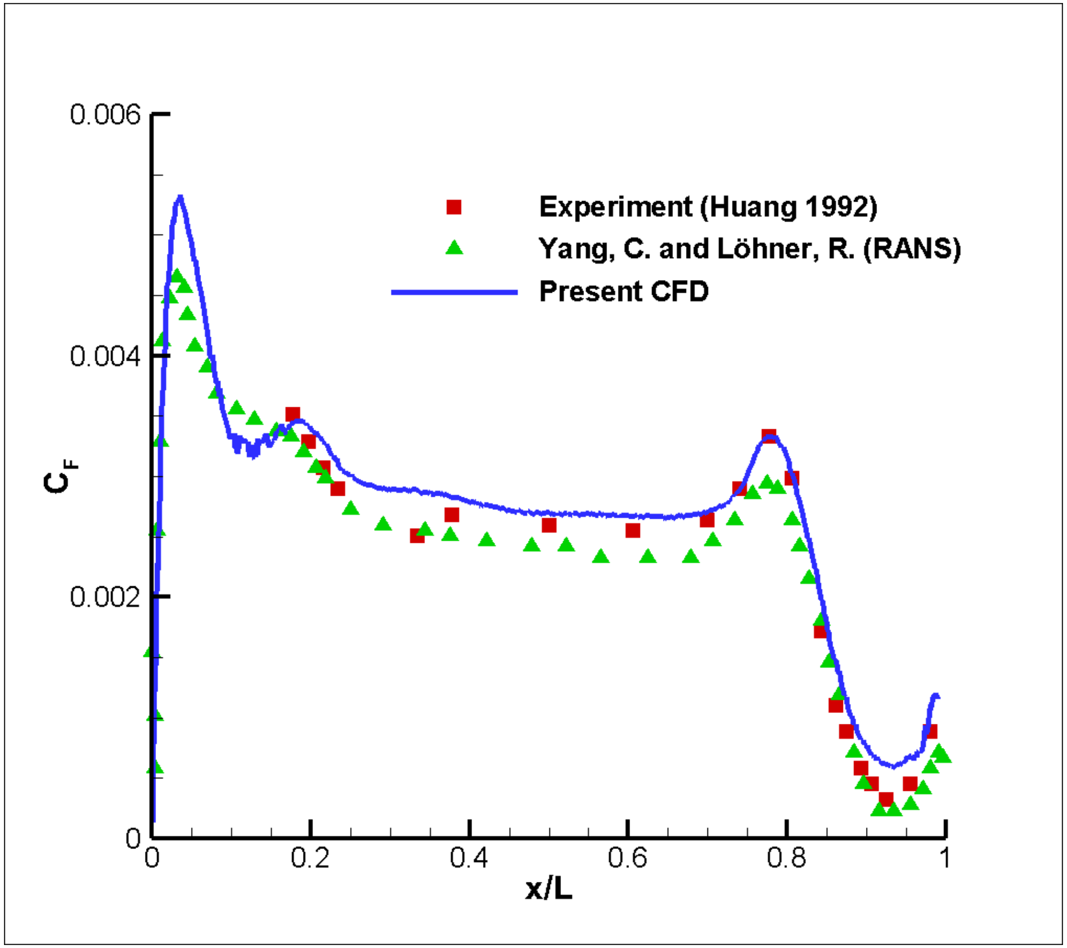

COMPUTATIONAL RESULTS

- Pressure coefficient on the longitudinal symmetry line:

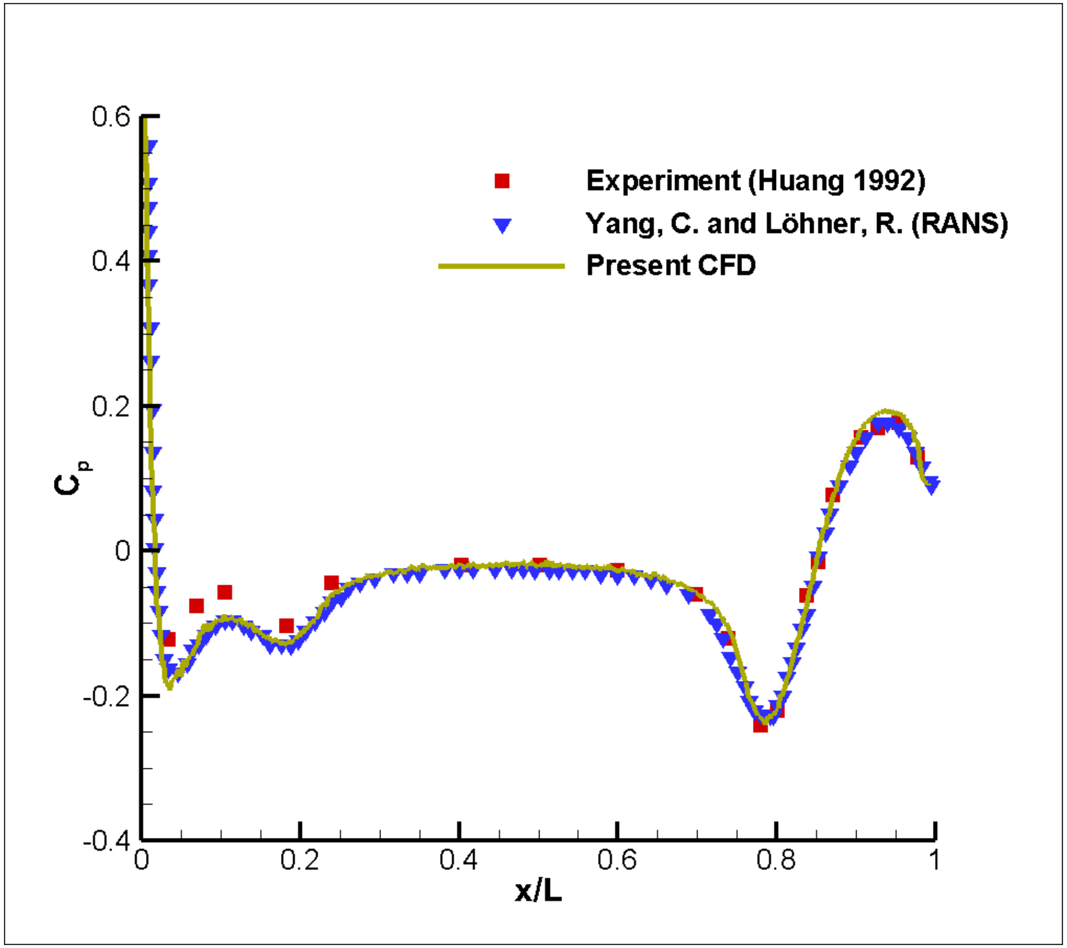

COMPUTATIONAL RESULTS

- Open-water propeller data:

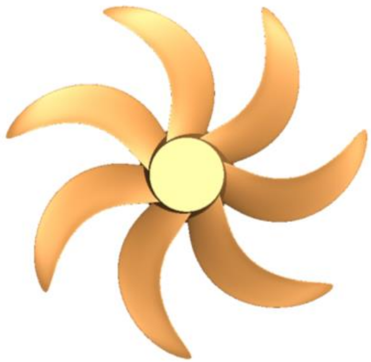

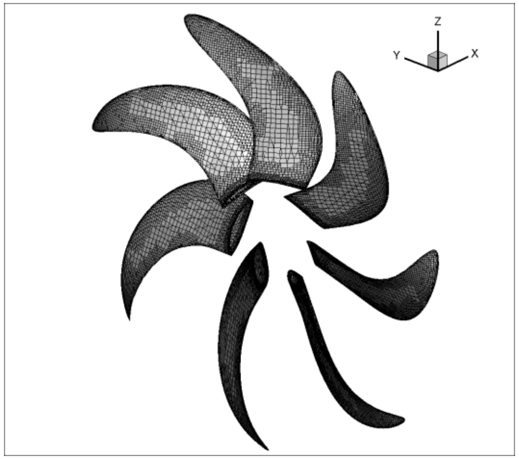

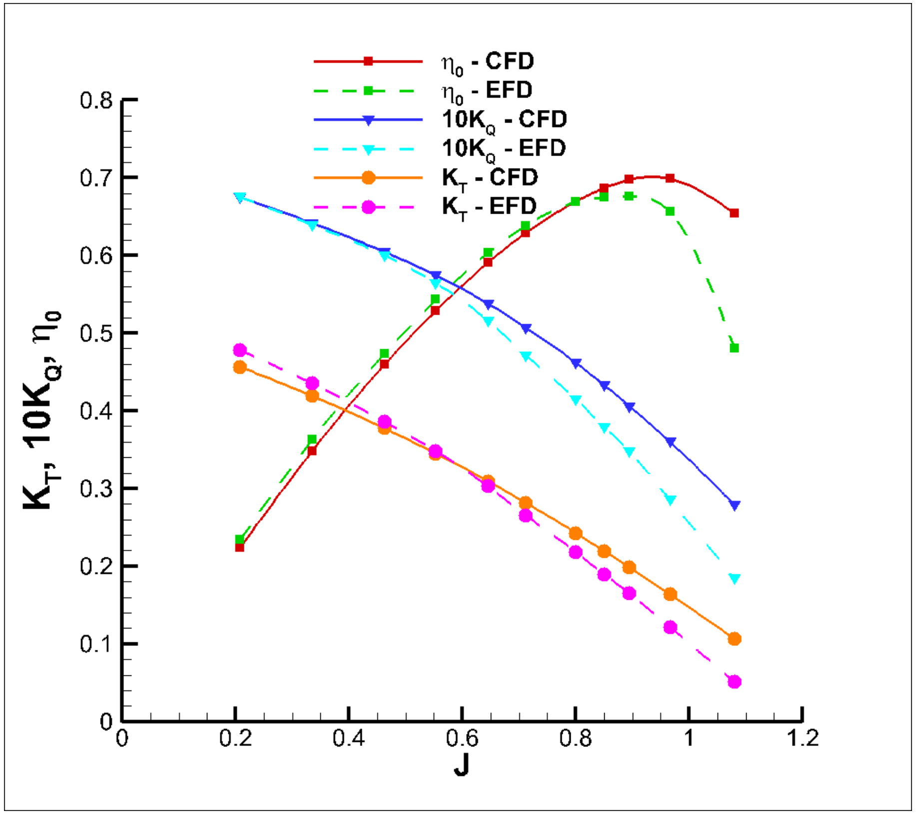

COMPUTATIONAL RESULTS

- Longitudinal (left) and lateral (right) forces are compared with the experimental results.

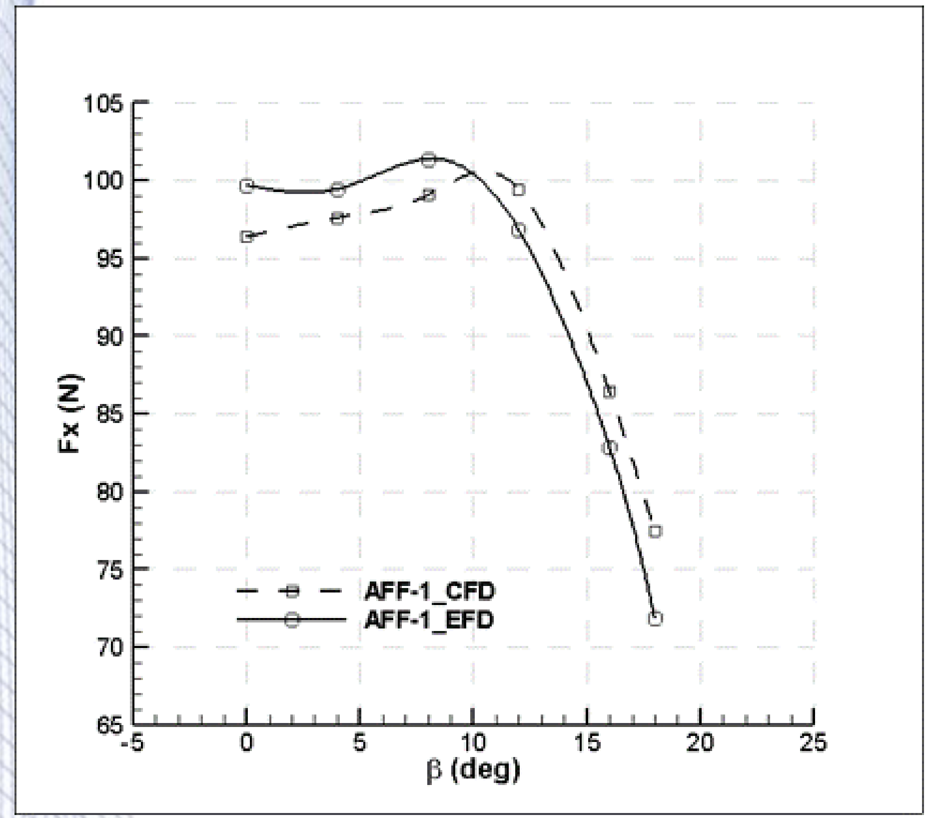

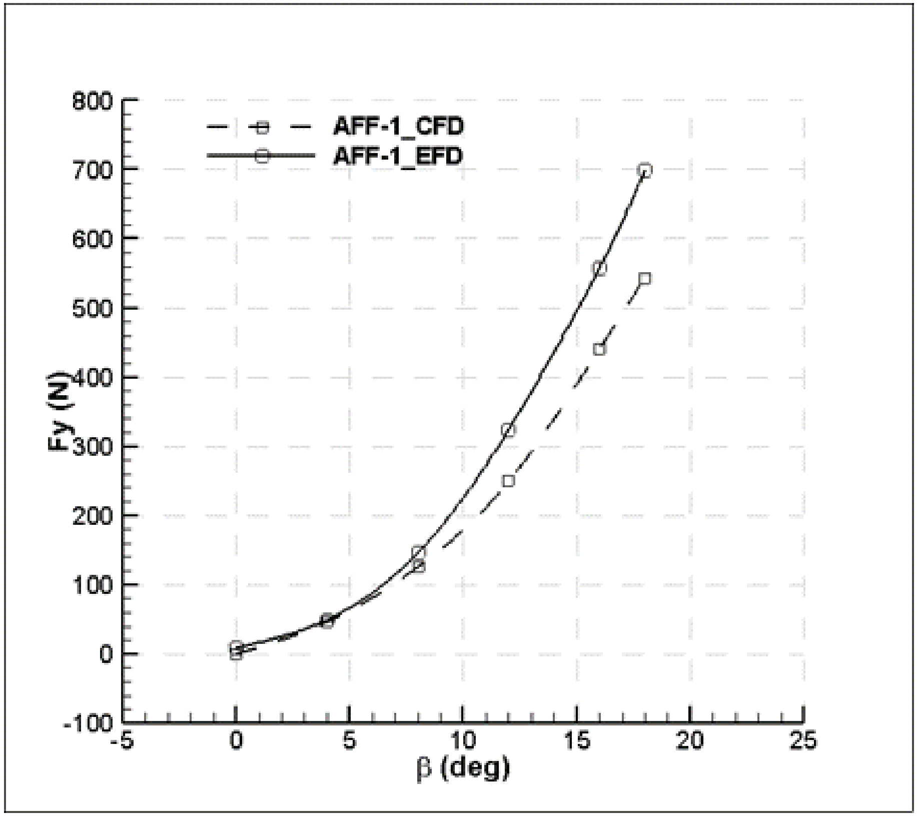

COMPUTATIONAL RESULTS

- Yaw-moment is compared with the experimental data.

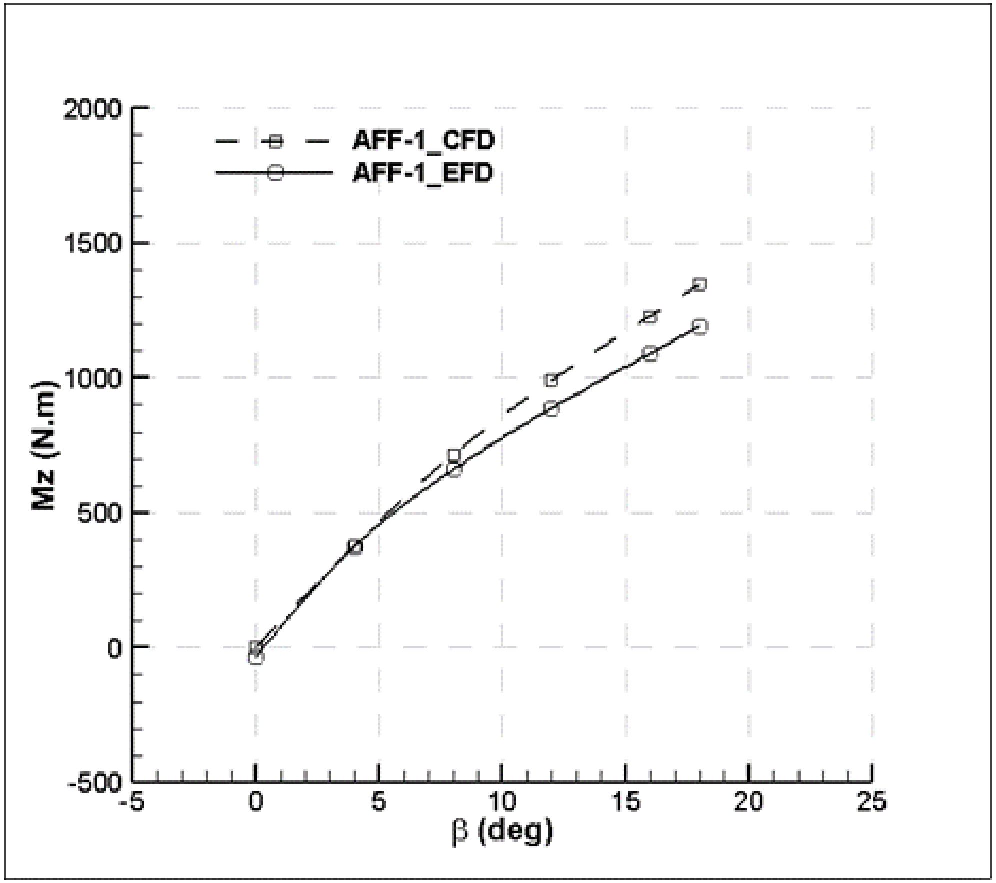

COMPUTATIONAL RESULTS

- Comparison of surge force coefficients with experiment and another numerical method (multiplied by 10^3).

β°	Present study	Toxopeus 2008	X_{EFD}	$(1+k)_{CFD}$	$(1+k)_{ITTC}$	$\varepsilon\text{-}_{present}$ %	$\varepsilon\text{-}_{Toxopeus}$ %	$\varepsilon\text{-}_{(1+k)}$ %
0	1.021	1.046	1.056	1.124	1.131	3.32	0.95	0.55
4	1.034	1.143	1.054	-	-	1.85	8.50	-
18	0.820	1.376	0.761	-	-	7.82	80.79	-

COMPUTATIONAL RESULTS

- Comparison of sway force (top) and yaw moment coefficients (bottom) with experiment and another numerical method (multiplied by 10^3).

β°	Present	Toxopeus 2008	Y_{EFD}	ε-$_{present}$ %	ε-$_{Toxopeus}$ %
4	0.485	0.410	0.520	6.77	21.21
18	5.744	6.322	7.397	22.34	14.53

β°	Present	Toxopeus 2008	Mz_{EFD}	ε-$_{present}$ %	ε-$_{Toxopeus}$ %
4	0.942	0.897	0.930	1.34	3.54
18	3.345	3.260	2.963	12.92	10.04

COMPUTATIONAL RESULTS

- The effects of propeller on maneuvering forces:

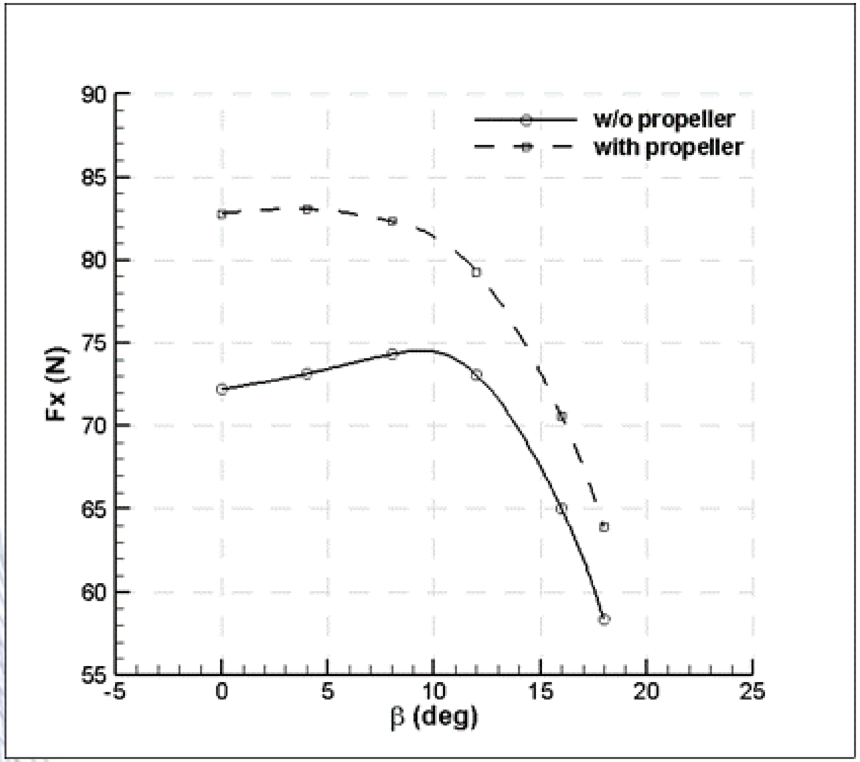

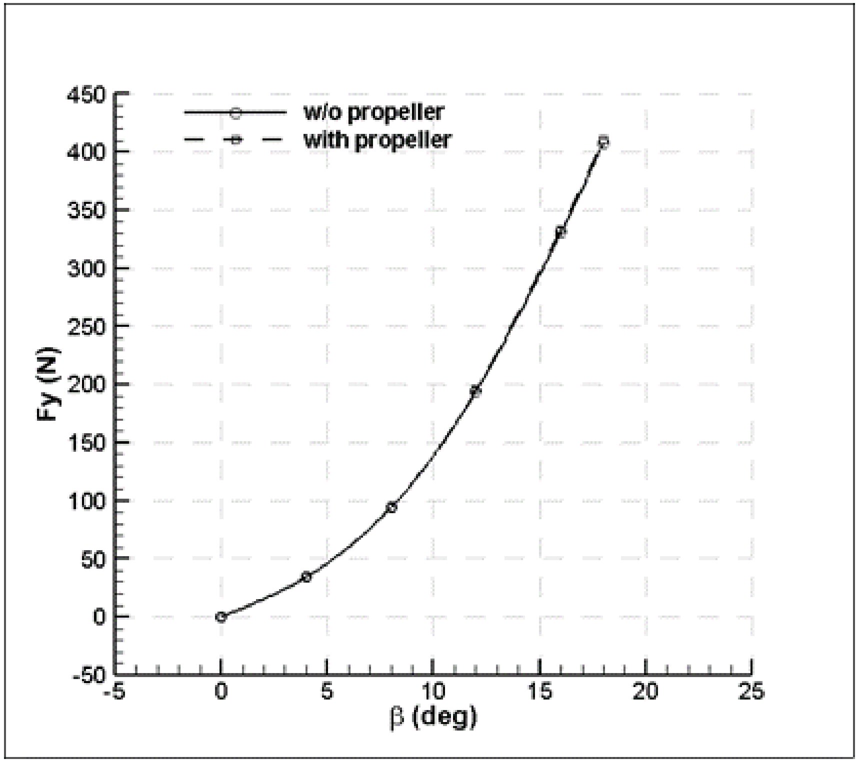

COMPUTATIONAL RESULTS

- The effects of propeller on maneuvering forces:

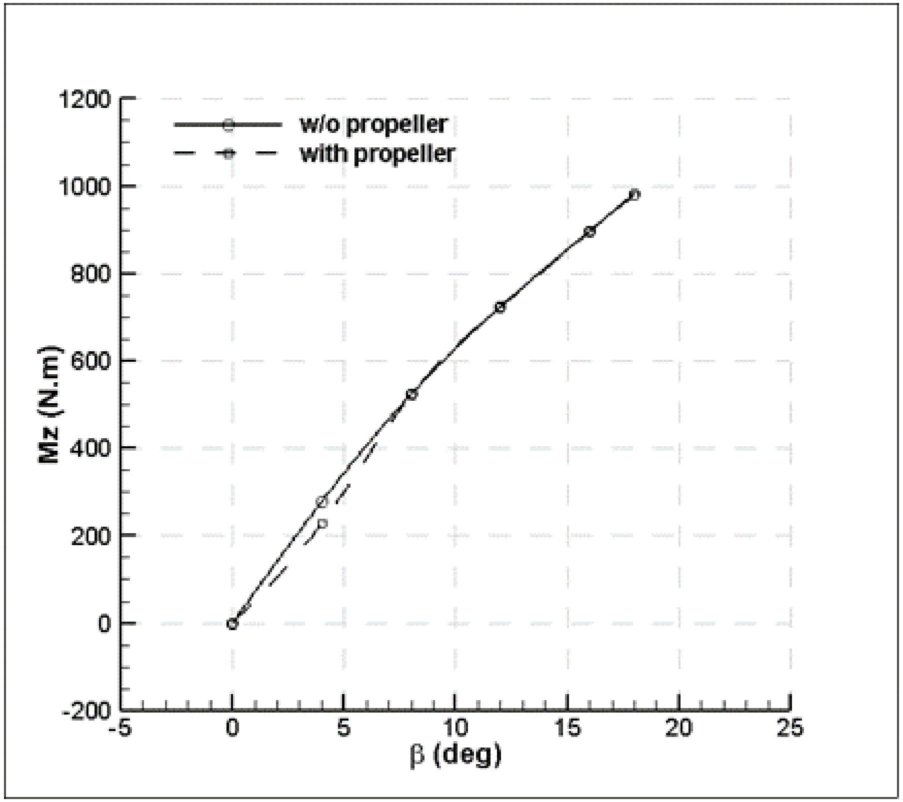

COMPUTATIONAL RESULTS

- The effects of propeller on maneuvering forces:

	$Re=12 \times 10^6$		$Re=14 \times 10^6$		
Derivative	w/o propeller	with propeller	w/o propeller	with propeller	experimental
Y_v	-0.0087	-0.0087	-0.0087	-0.0086	-0.0059
N_v	-0.0543	-0.0543	-0.0545	-0.0545	-0.0127

CONCLUSIONS

- It is found that accurate results can be obtained by CFD method for hydrodynamic forces and moment predictions.
- The integral values are in good agreement with the experiments.
- An offset almost the same in all drift angles is observed between the numerical and experimental longitudinal forces.
- It is also found that propeller does not affect the sway forces and yaw moments while there is a considerable difference in longitudinal forces at relatively small drift angles.
- An original propeller working behind the body may have different effects than the propeller modelled by body force method. This issue will be investigated in further studies.

Thank you
for your kind attention!

An Experimental Investigation into PressurePores™ Technology to Mitigate Propeller Cavitation and Underwater Radiated Noise

B. Aktas[1,*], N. Yilmaz[1], N. Sasaki[1], M. Atlar[1], G. Tani[2], F. Miglianti[2], M. Viviani[2] and D. Taylor[3]

[1]University of Strathclyde, Glasgow, UK

[2]University of Genova, Genova, ITALY

[3]OSCAR Propulsion, West Sussex, UK

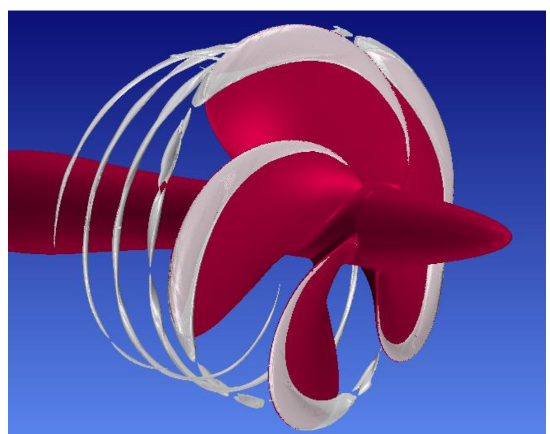

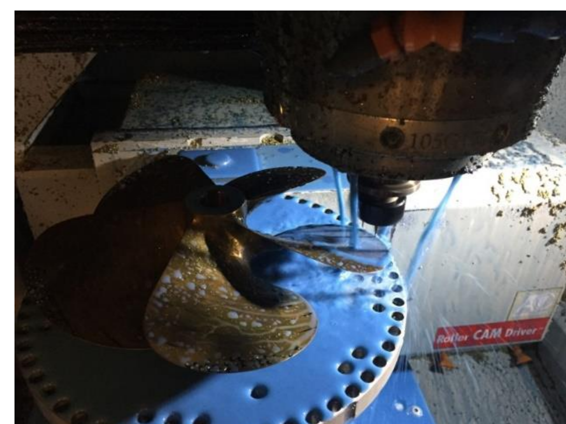

Presentation Layout

- Introduction
- Aims & Objectives
- Background
- Test Case
- Numerical Simulations
- Experimental Setup
    - Cavitation Observations
    - Radiated Noise Measurements
- Propeller Performance Tests
- Conclusions

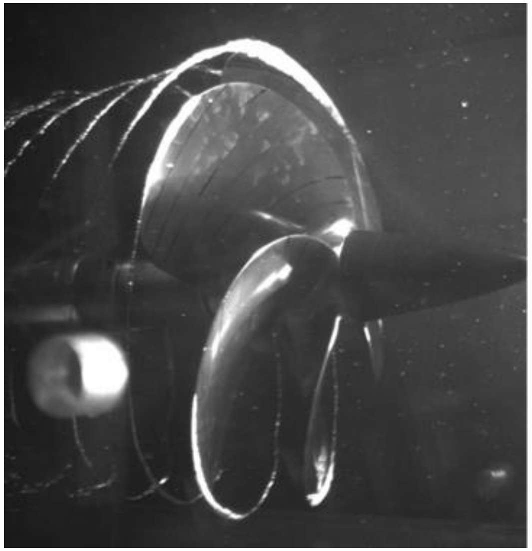

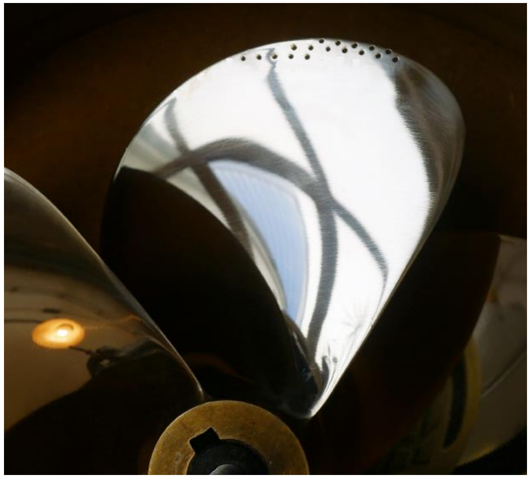

Introduction

- The first interest due to Naval Warfare
- Flagged up by IMO /MEPC
- Various Projects has been initiated
- Guidelines to IMO for potential enforcement of limits to Radiated Noise Levels

SONIC SEA Documentary

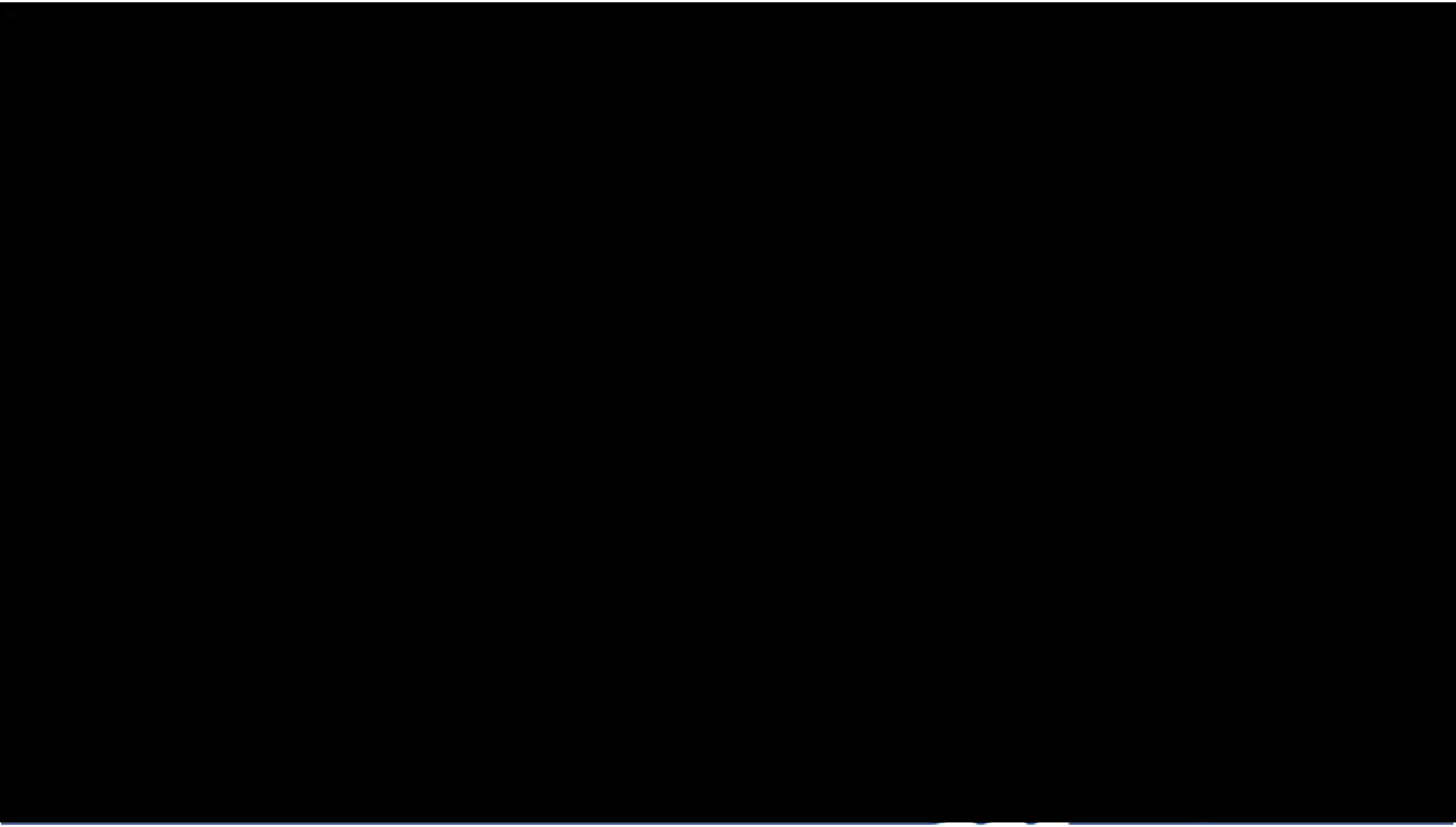

Introduction

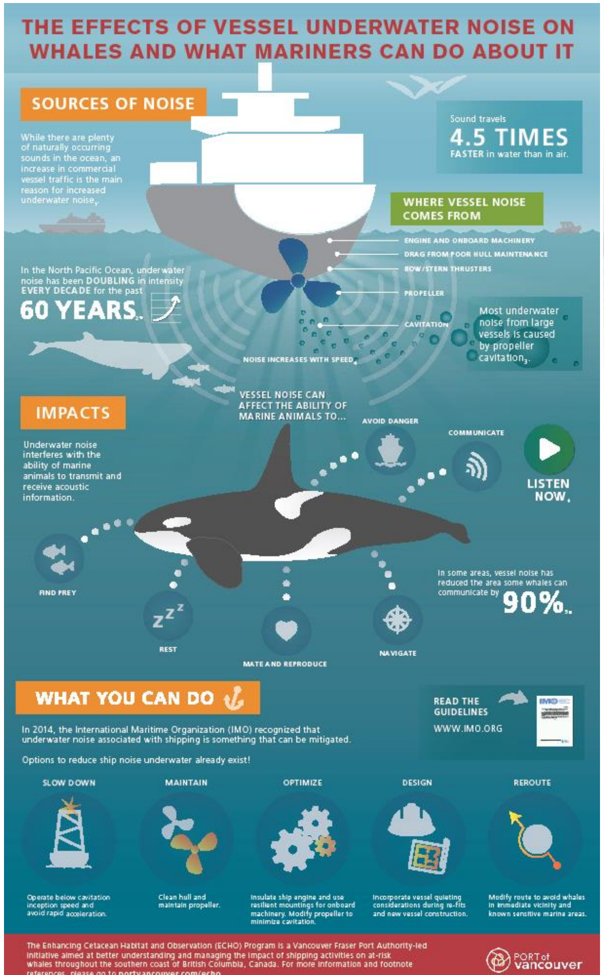

[The Effects of Underwater Noise]

Vancouver Fraser Port Authority harbour due rates, effective January 1, 2017, per gross registered tonne (GRT) in Canadian funds, are as follows:

- GOLD $0.050/GRT
- SILVER $0.061/GRT
- BRONZE $0.072/GRT
- BASIC $0.094/GRT

NEW for 2017

Underwater noise reduction criteria

Underwater noise created from shipping activities can impact whales' ability to navigate, communicate, and find prey. With a number of at-risk whale species frequenting our waters, reducing underwater noise from vessels is a priority for the Vancouver Fraser Port Authority.

We are proud to be the first port in the world to recognize vessels who are doing their part to reduce underwater noise.

Eligible options for reduced rates:

- Ship classification society quiet vessel notations
  - Bureau Veritas Underwater Radiated Noise (URN)
  - DNV-GL Silent-Environmental (E)
  - RINA DOLPHIN
- Cavitation/wake flow reduction technologies
  - Becker Mewis duct
  - Propeller Boss Cap Fins (PBCF)
  - Schneekluth duct

Aims & Objectives

Aim

- The aim of the project is to demonstrate the potential of the pressure relieving holes concept to reduce cavitation and hence to mitigate the Underwater Radiated Noise of a marine propeller

Objectives

- Comprehensive CFD investigations were conducted to aid strategical implementation of PressurePores^{TM}
- Confirmation of the numerical simulations through experimental cavitation tunnel and towing tank tests to confirm effectiveness of PressurePores^{TM}

Background

Literature Review

Sharma's Results for modified propellers;

- Drilling holes were adopted in the blade tip area extending radially in the leading edge area.
- Propeller A and B were modified by drilling 300 holes (with 0.3 mm diameter) that were adopted closely and uniformly spaced.
- There was no measurable influence in terms of performance characteristics of the basic propellers.
- On the other hand, it can be seen that the tip vortex cavitation is reduced due to propeller modifications.

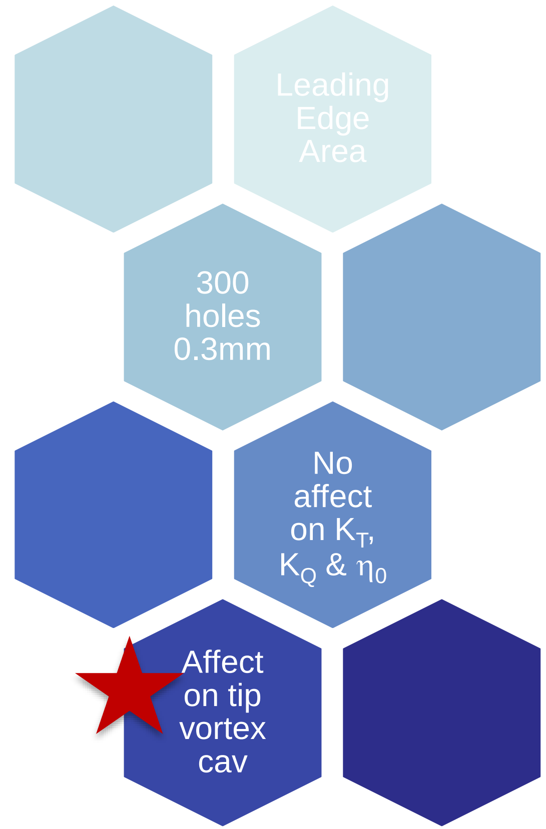

Background

Literature Review

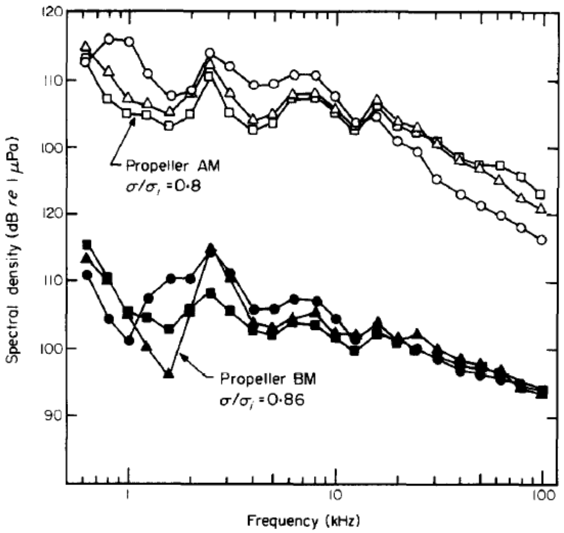

- For the modified propeller AM and BM, there was no dominant spectral peak as found for the basic propeller A and B.

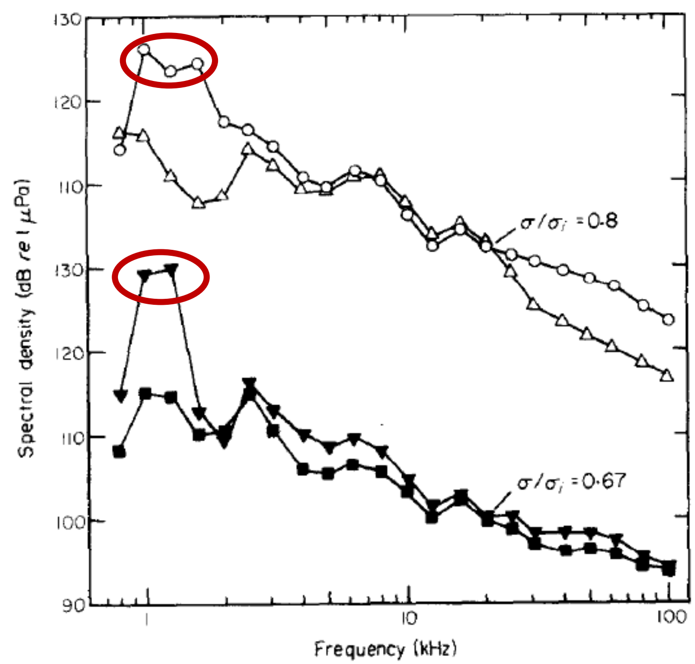

- At low J values, tip vortex cavitation delayed due to propeller modification, comparison of noise levels from the basic and modified propellers will be of practical significance.
- When the figure was examined, it can bee seen that the modification has suppressing effect of the low frequency peaks on the both propellers.

Background

Propeller Performance Characteristics

Base Tip Sheet

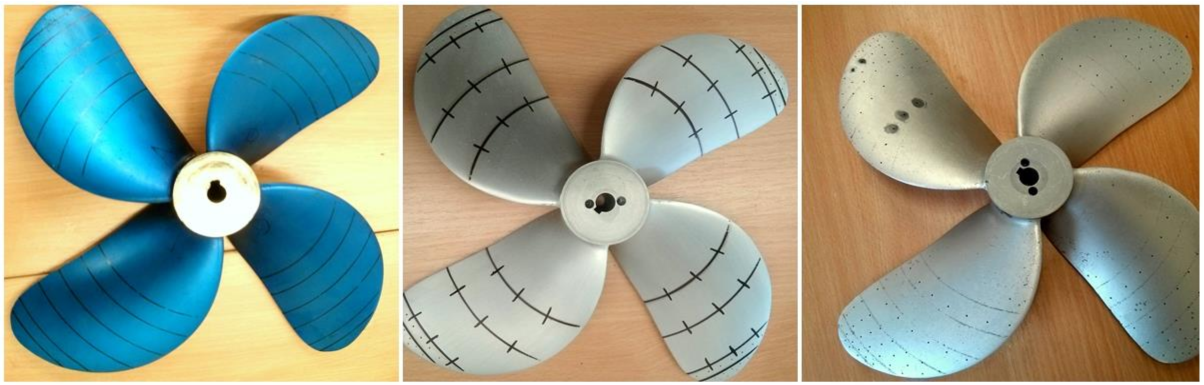

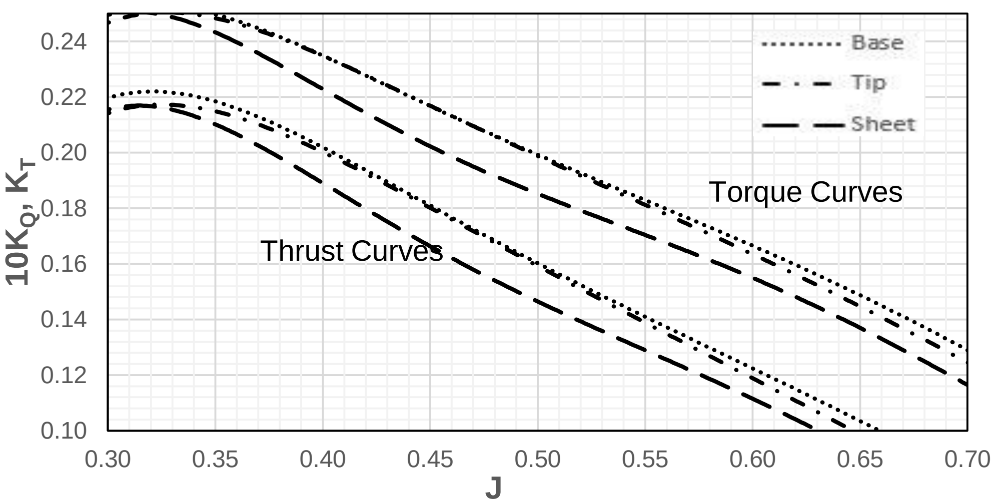

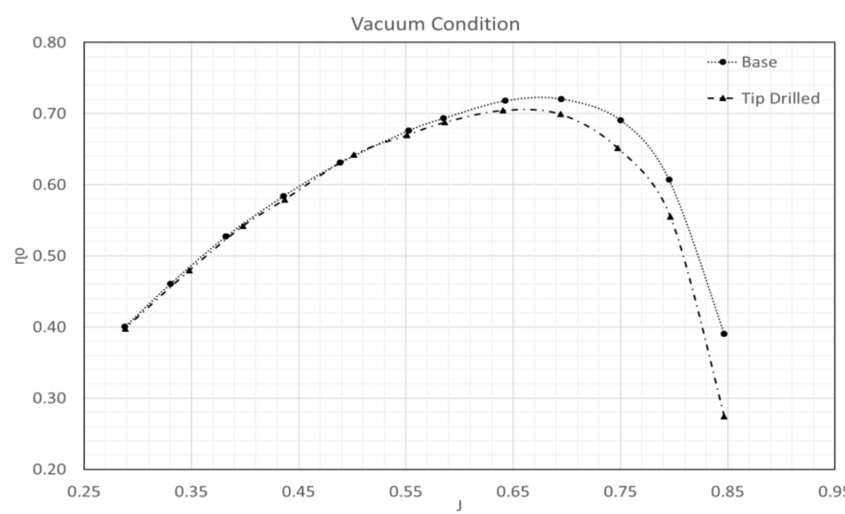

Background

Guardian Noise Data Comparison

17 Holes

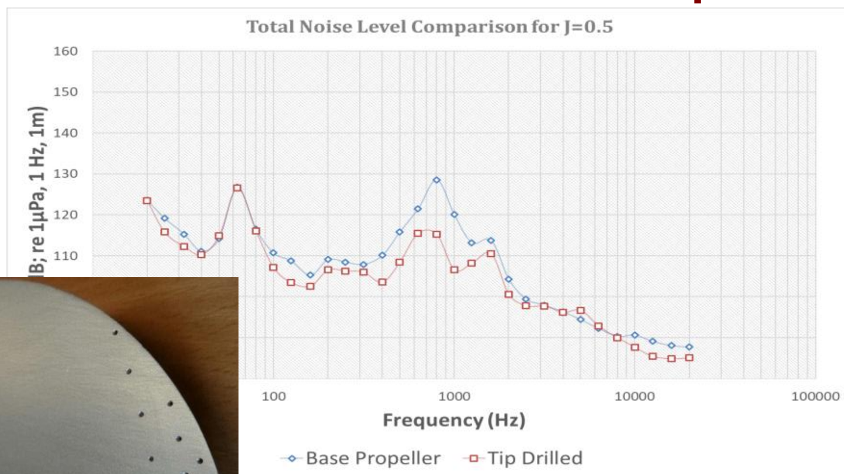

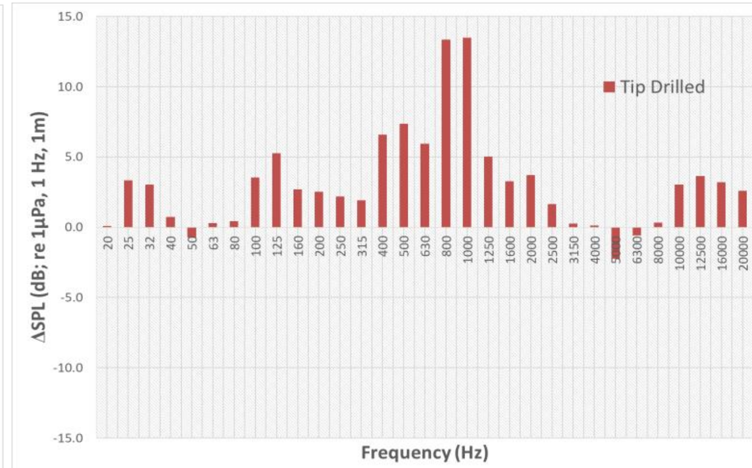

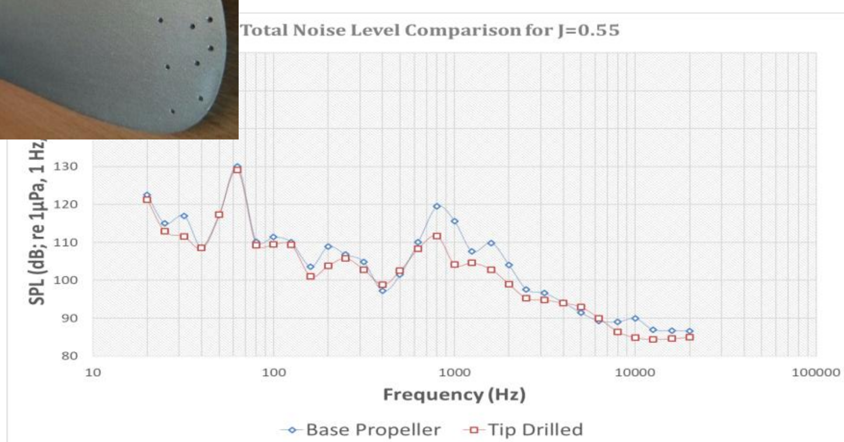

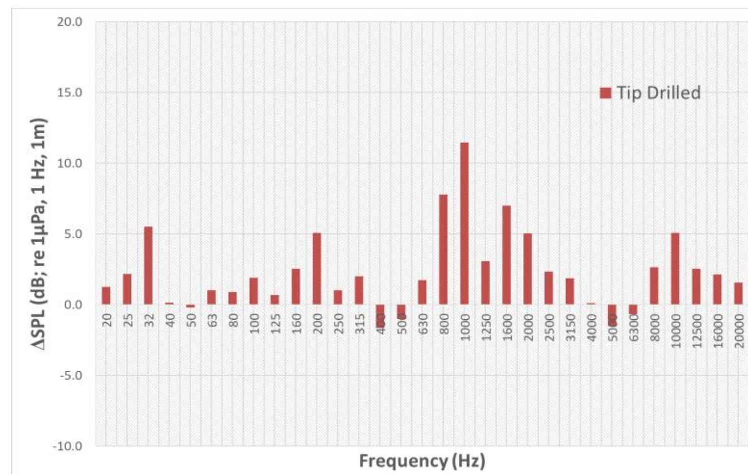

Background

Guardian propeller CFD simulations

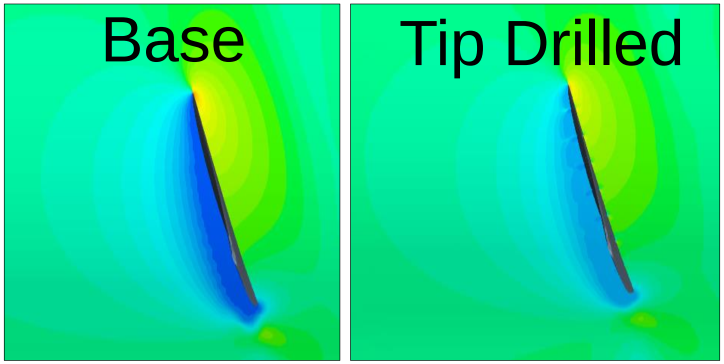

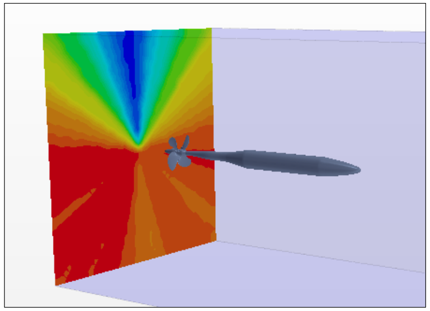

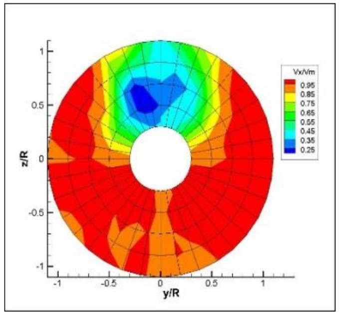

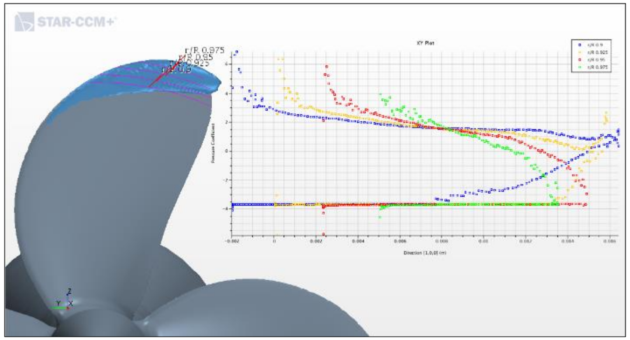

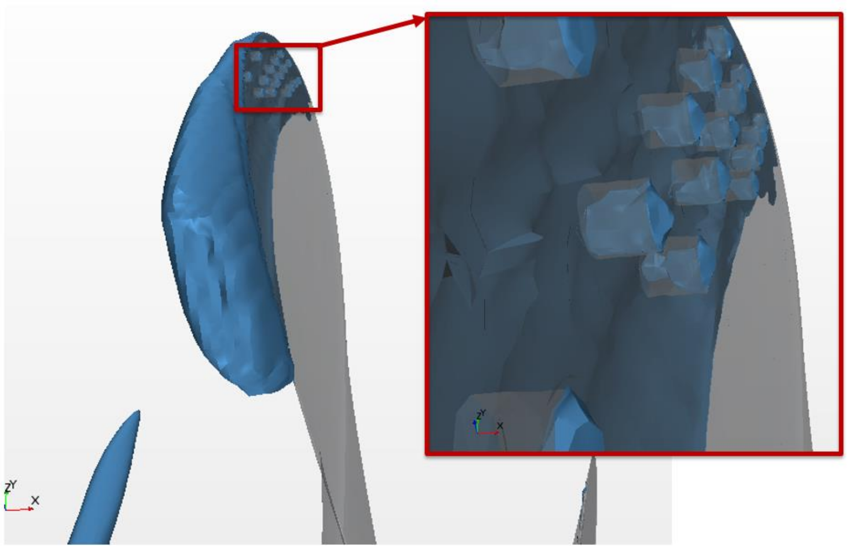

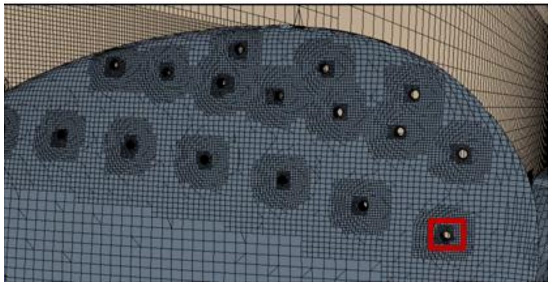

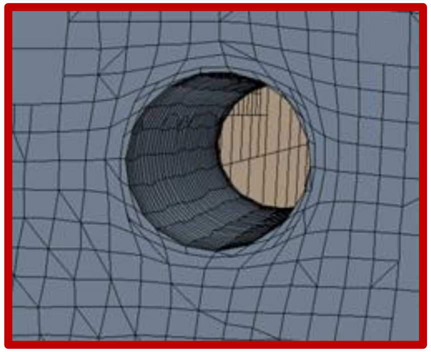

Test Case

➢ Validation with Princess Royal propeller

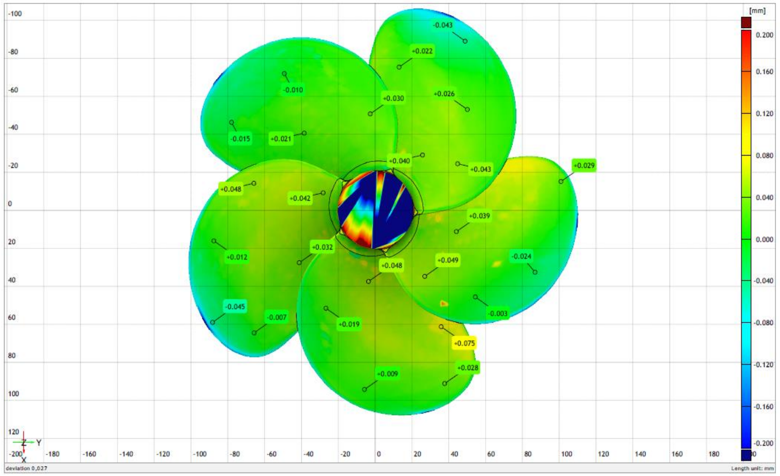

- It is a sub-cavitating propeller (i.e. majority part of the blades operate in cavitating condition and hence more noise prone)
- Readily available in-house data on the PR propeller including the full-scale noise/cavitation data.
- Possibility to do full scale-trials by drilling holes
- Recognised by the ITTC and now has become the benchmark propeller.

Numerical Simulations

➤ MARCS Application for tip vortex cavitation

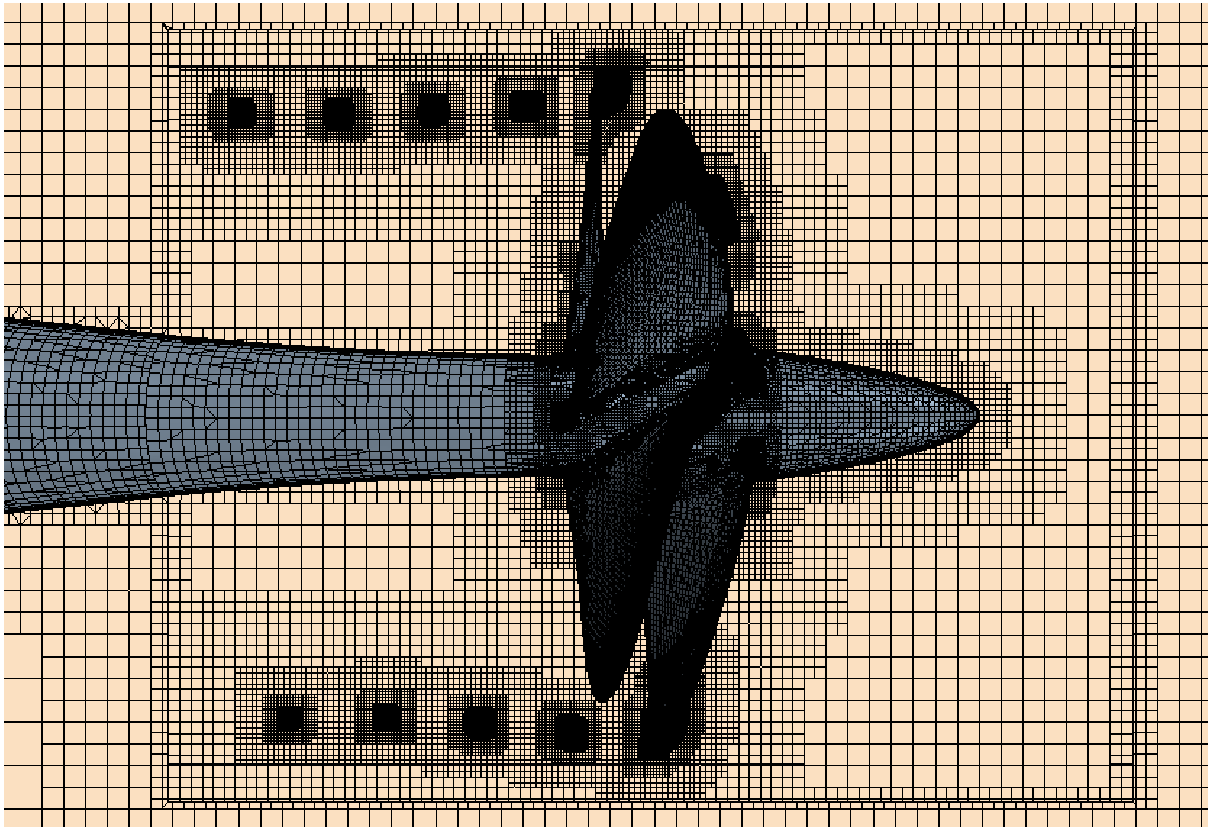

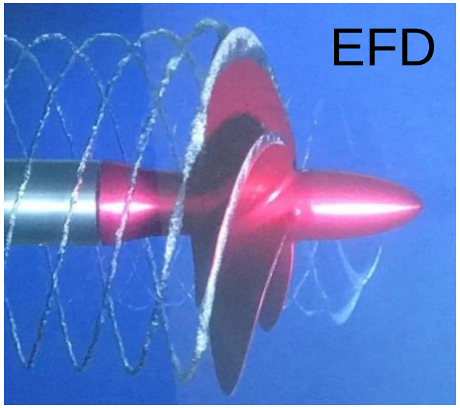

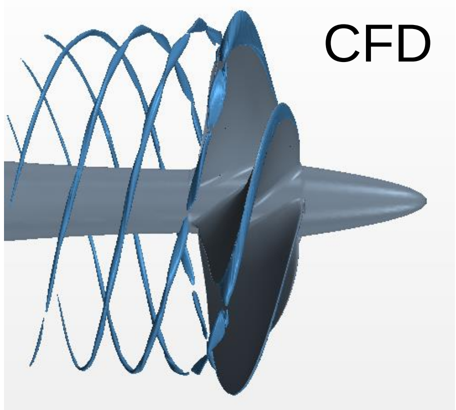

Numerical Simulations

➢ Strategic Hole Application

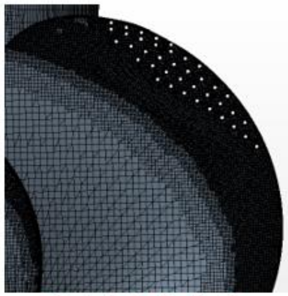

Strategic Application 1

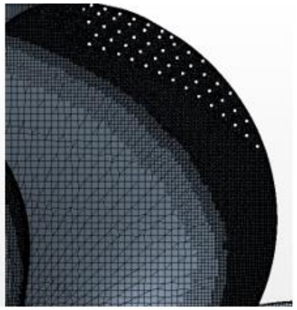

Strategic Application 2

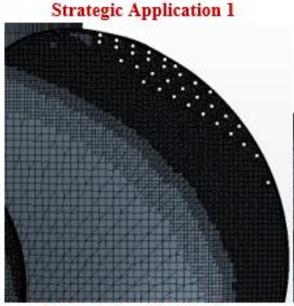

Strategic Application 3

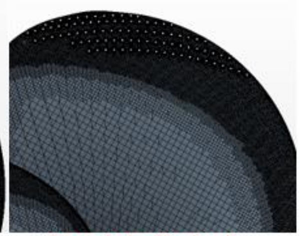

Strategic Application 4

Strategic Application 5

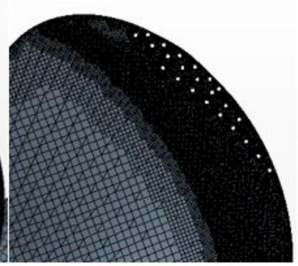

Strategic Application 6

PR_SA1	41-1mm holes
PR_SA2	60-1mm holes
PR_SA3	33-1mm holes
PR_SA4	92-0.6mm holes
PR_SA5	17-1mm holes
PR_SA6	23-1mm holes

- ❖ **Constant Drilled hole area per blade**
- ❖ **Constant Drilled hole area per propeller**

Numerical Simulations

University of Strathclyde

- Strategic Hole Application

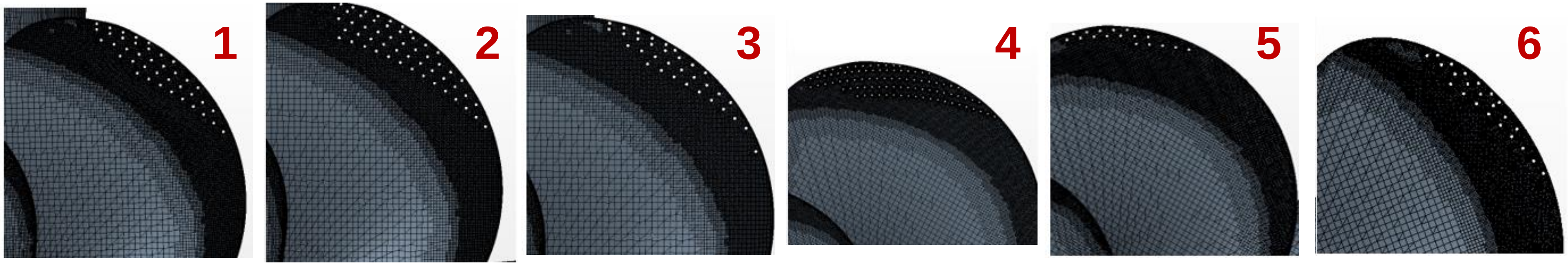

	PR_BASE	PR_SA1	PR_SA2	PR_SA3	PR_SA4	PR_SA5	PR_SA6
Thrust (N)	586.64	578.71	574.94	578.86	579.59	582.04	580.96
Torque (Nm)	17.11	17.95	18.16	17.79	17.77	17.47	17.60
Cavitation Volume (m^3)	8.11E-06	6.02E-06	5.14E-06	6.47E-06	6.17E-06	7.18E-06	6.89E-06
Efficiency	61.38%	57.73%	56.69%	58.24%	58.41%	59.67%	59.09%
KT	0.2254	0.2223	0.2209	0.2224	0.2227	0.2236	0.2232
Δ%Thrust		-1.35%	-1.99%	-1.33%	-1.20%	-0.78%	-0.97%
Δ%Torque		4.89%	6.11%	3.99%	3.82%	2.06%	2.87%
Efficiency Loss (%)		5.95%	7.64%	5.11%	4.84%	2.79%	3.73%
Δ%Cavitation Volume		-25.77%	-36.67%	-20.19%	-23.97%	-11.5%	-15.04%
CT	2.19	2.16	2.15	2.16	2.16	2.17	2.17
Δ%CT		-1.35%	-1.99%	-1.33%	-1.20%	-0.78%	-0.97%

Experimental Setup

Propeller models for Experimental Tests

Without Holes

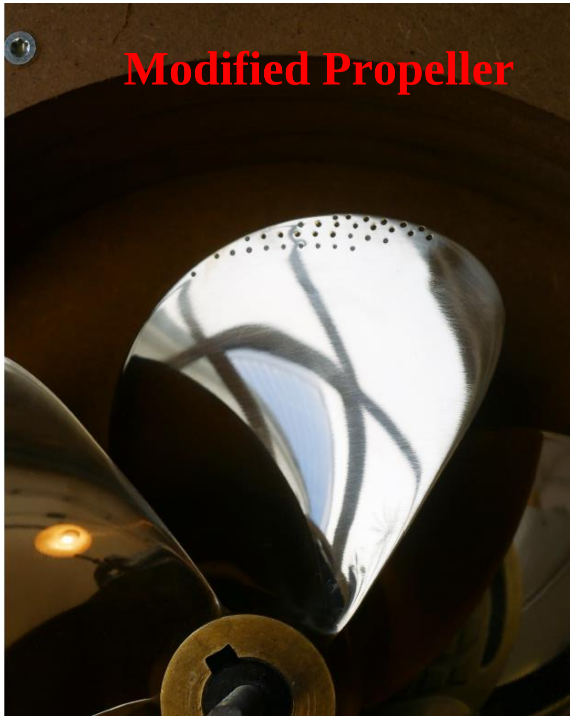

33 Holes

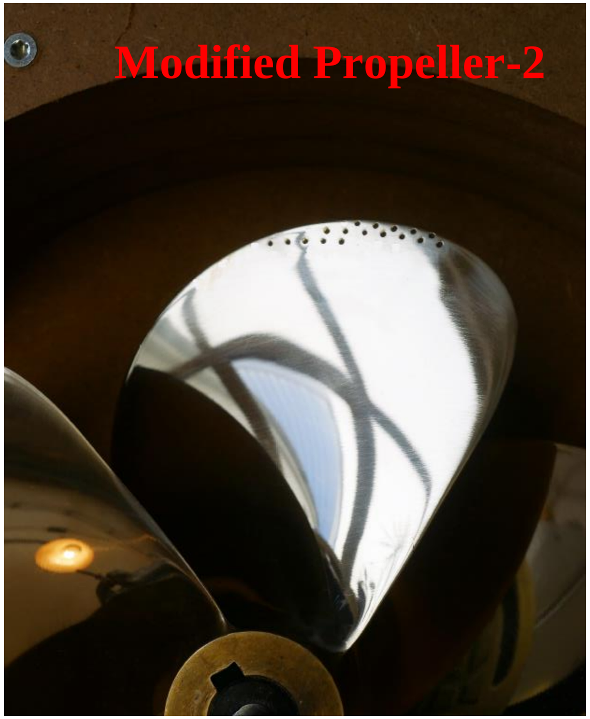

17 Holes

Experimental Setup

Cavitation Tests at University of Genova Cavitation Tunnel

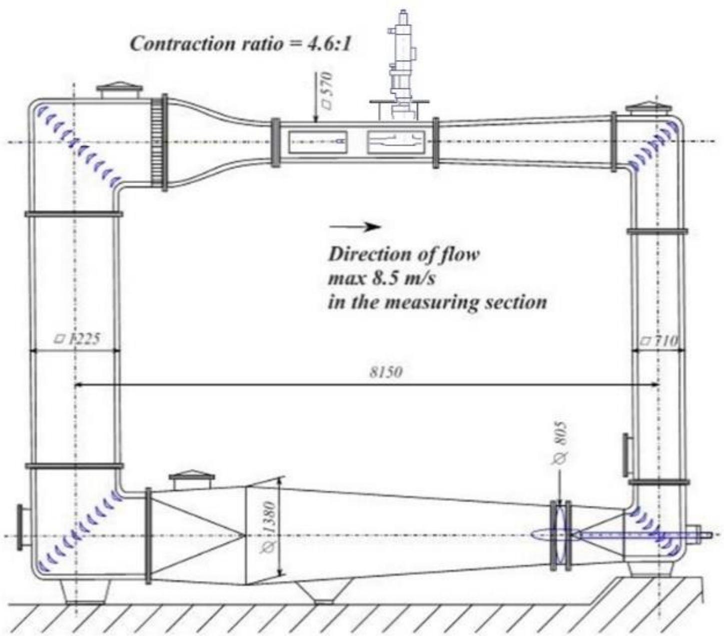

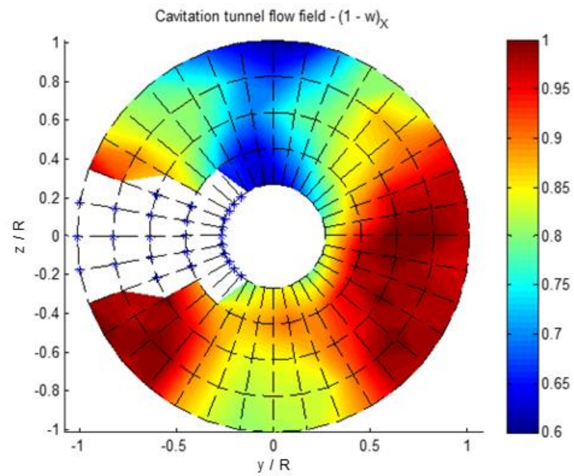

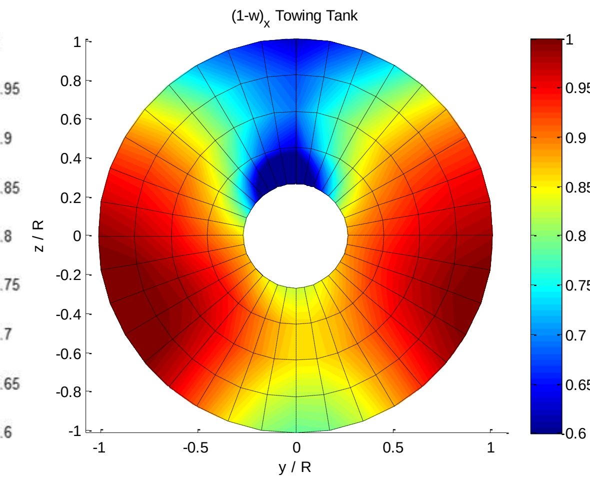

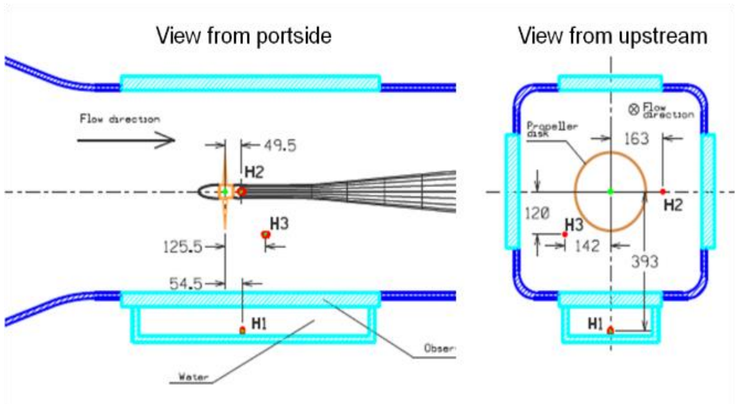

Condition	Engine [RPM]	Shaft [rps]	STW (kn)	K_T	10KQ	σ_N (nD)
V1	1500	14.3	10.5	0.211	0.323	1.91
V2	2000	19.0	15.1	0.188	0.318	1.07

Cavitation Observations

Cavitation Tests at University of Genova Cavitation Tunnel (V1)

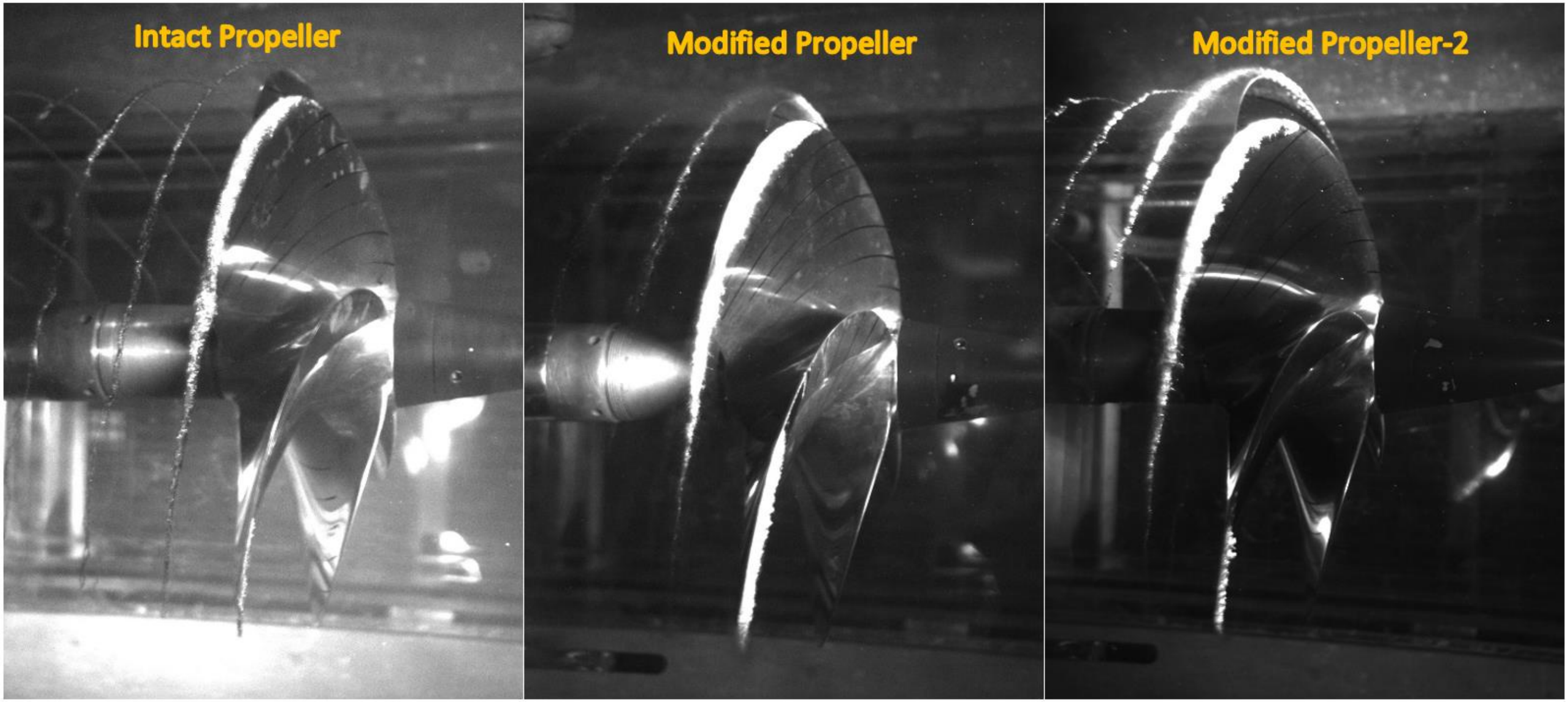

Without Holes | 33 Holes | 17 Holes

Cavitation Observations

Cavitation Tests at University of Genova Cavitation Tunnel (V2)

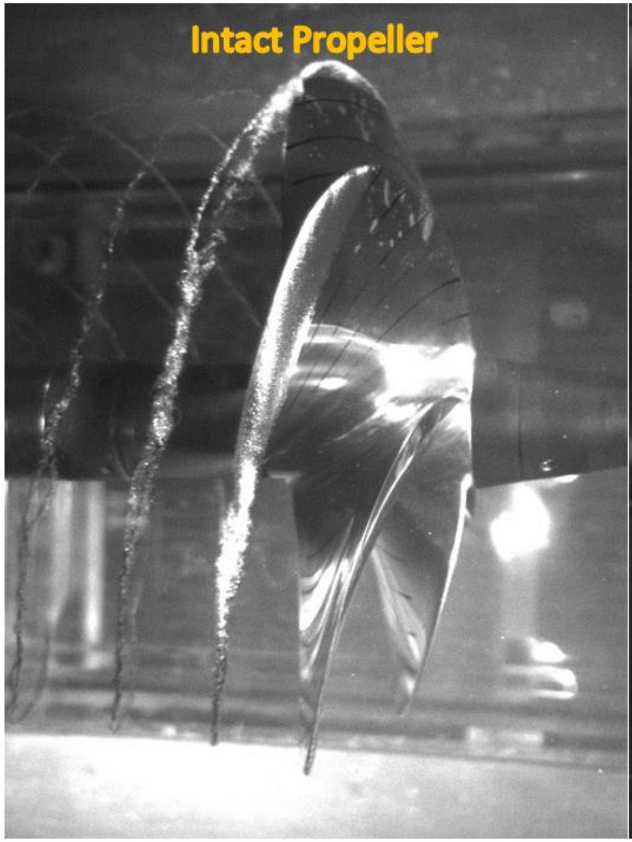

Without Holes

33 Holes

17 Holes

Procedure Validation

CFD and EFD Comparisons in terms of tip vortex cavitation (with and without holes)

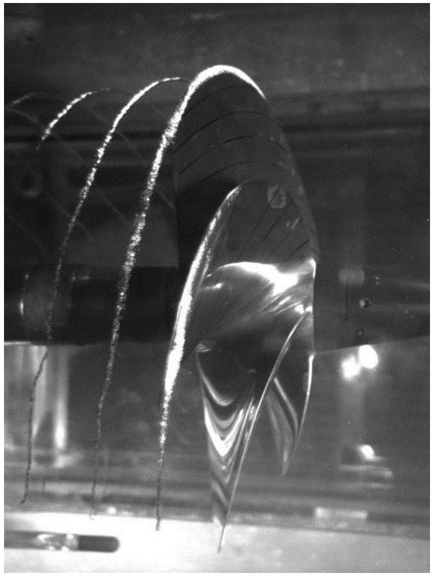

Without Holes

With 33 Holes

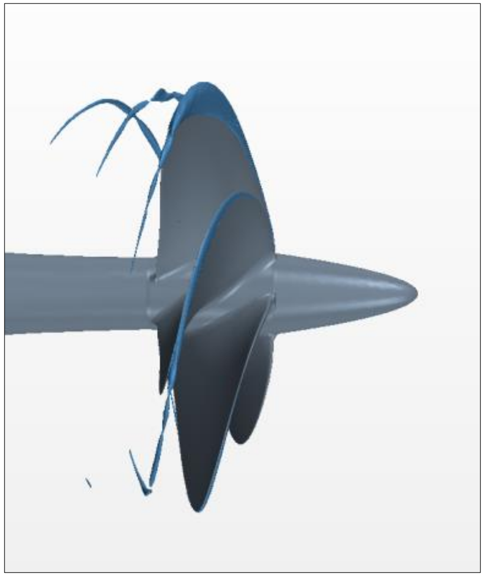

Without Holes

With 33 Holes

Test Results
V3 : 10.5 knot, 1500 rpm

CFD Results
C2 Condition @ SJTU

Radiated Noise Measurements

3rd Octave Noise Data Comparison between Intact, Modified and Modified 2 Propellers

10-knot

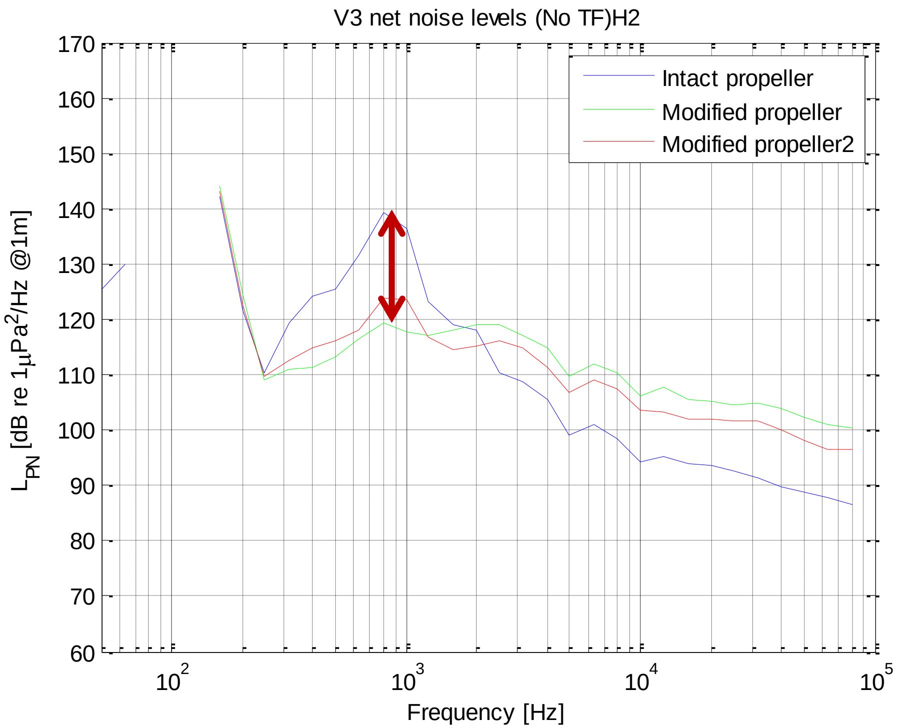

15-knot

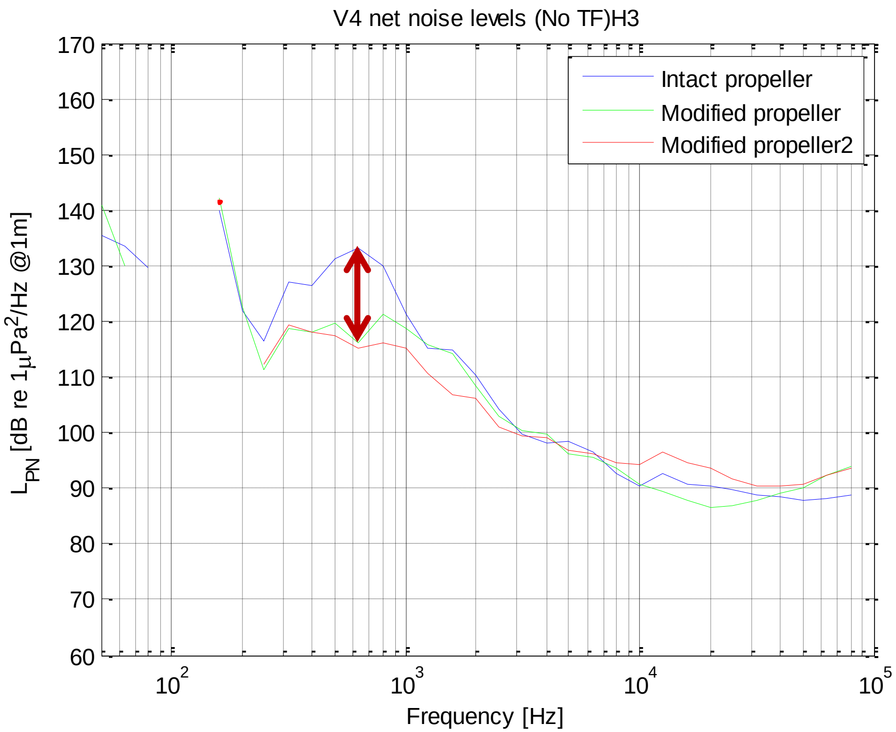

Radiated Noise Measurements

Narrowband Noise Data Comparison between Intact, Modified and Modified 2 Propellers

10-knot

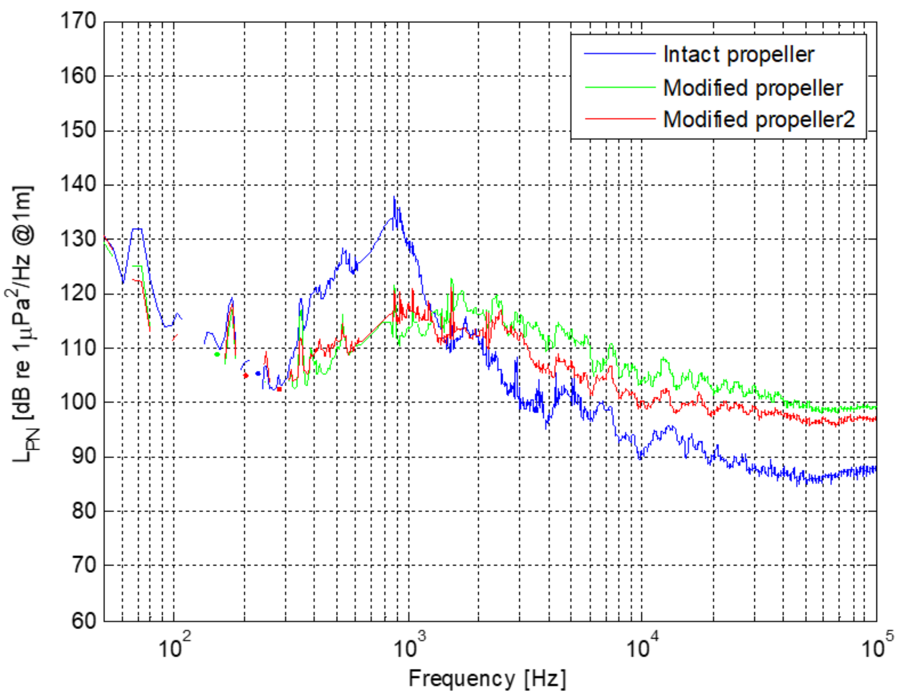

15-knot

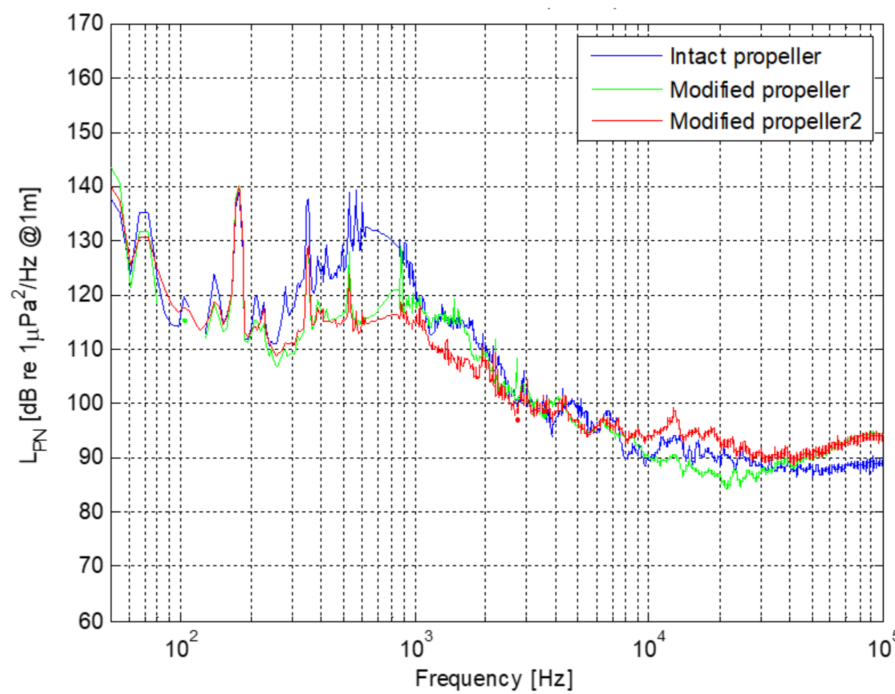

Radiated Noise Measurements

University of Strathclyde

Noise Data Comparison between Modified and Modified 2 Propellers

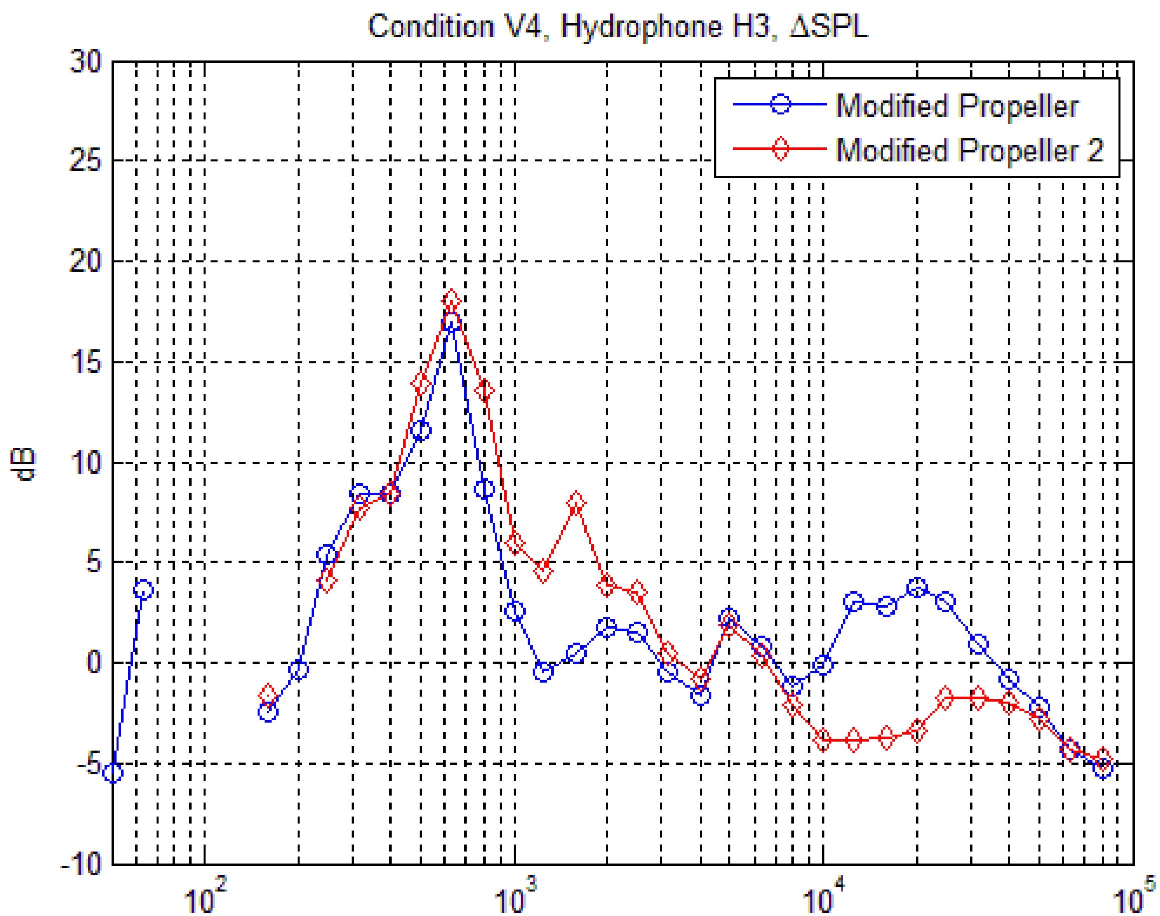

15-knot

Propeller Performance Tests

CTO Towing Tank Tests

For Modified Propeller-2 case (17-1mm Holes), there is a 0.1% loss of thrust and 2.2% gain in torque which consequently results in an overall loss of 2.3% from efficiency.

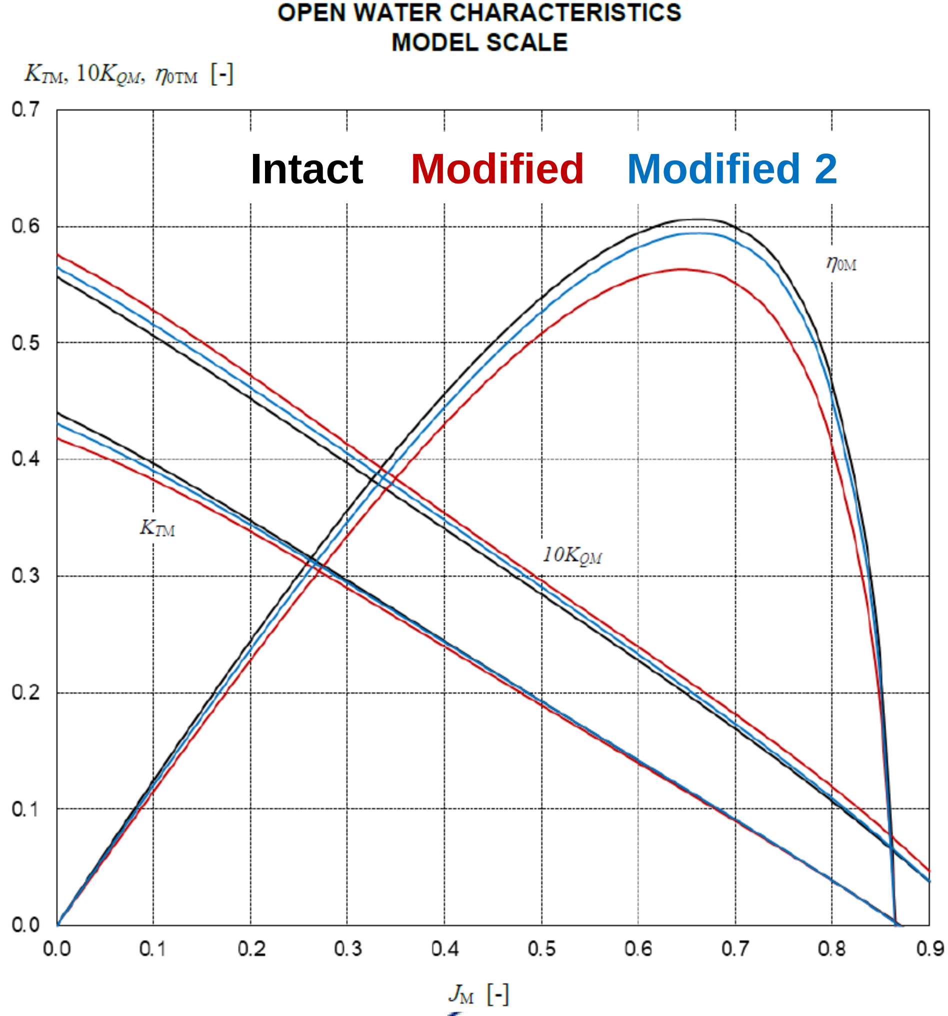

Conclusions

- ✓ State of the art Adaptive mesh refinement (MARCS) applied for Guardian propeller simulations. The adopted method enhanced the cavitation predictions and results has shown up to 11.5% cavitation volume reduction for Modified Propeller-2 case with only 2.5% loss from the efficiency.
- ✓ The experimental results with Princess Royal propeller model have shown significant reduction in terms of cavitation noise (up to 17dB) for Modified Propeller-2 with 17-1mm holes case particularly in the frequency regions that are utmost important for marine fauna whilst only loosing 2% from the efficiency.
- ✓ Available two sets of CFD and Experimental data from Guardian and Princess Royal propeller, a pressure relief hole number determination procedure is established based on major hydrodynamic non-dimensional coefficients and propeller design parameters.

Thank you for listening

Any Questions?

University of Strathclyde Glasgow

Computational investigation of hydroacoustic propeller performances for non-cavitating case

BY

SAMIR E. BELHENNICHE – *ORAN UNIVERSITY OF SCIENCE AND TECHNOLOGY*

OMAR IMINE – *ORAN UNIVERSITY OF SCIENCE AND TECHNOLOGY*

OMER KEMAL KINACI – *ISTANBUL TECHNICAL UNIVERSITY*

Introduction

Noise is an unwanted physical phenomenon!

Neither in our daily lives, nor in war conditions; humans would not prefer noisy machines.

A noisy washing machine is definitely unsettling!

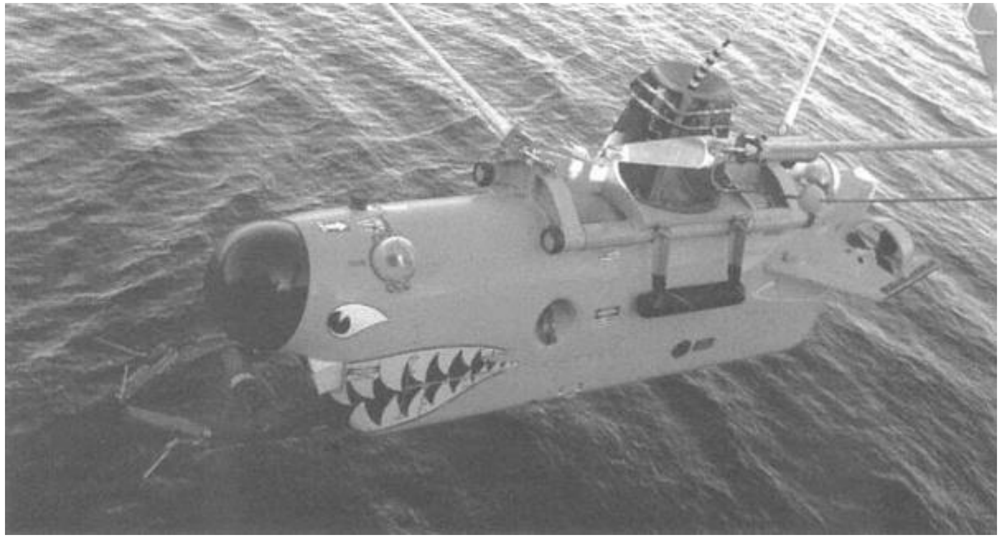

A noisy submarine during war can be fatal!

Introduction

Every mechanical device should be optimized in terms of noise generation. Noise should be actively controlled if possible.

For active noise control, the basics of the underlying physics of noise should first be understood.

Aeroacoustics is a large field which is studied intensively. That is why some devices that we use in our daily lives are optimized in terms of acoustics.

Can we say the same thing for under the water?

Hydroacoustics vs aeroacoustics

Why is the hydroacoustic field less developed than the aeroacoustic field?

We do not live under the water. We do not have the intuition of it.

Marine environment is challenging. Experiments are harder to conduct.

Theoretical background is also harder. Different physical incidents that may happen underwater (such as cavitation) complicate computations.

There is very little work on hydroacoustics. Studies devoted to ship hydroacoustics are even lesser.

Why do we need to work on hydroacoustics?

Hydroacoustics is very important for warfare in seas. A warship propagating too much sound may easily be targeted by a torpedo.

Ships are disturbing marine habitat in seas. It has been identified by many researchers that the low frequency sound generated by ships are disturbing communication of whales and dolphins. IMO has attempts to restrict noise emanating from ships.

However, attempts of IMO reverted back due to insufficient knowledge on underwater acoustics.

Lack of knowledge in state of the art can only be removed by developments in state of research.

A video from Arctic WWF (https://arcticwwf.org/newsroom/the-circle/underwater-noise/)

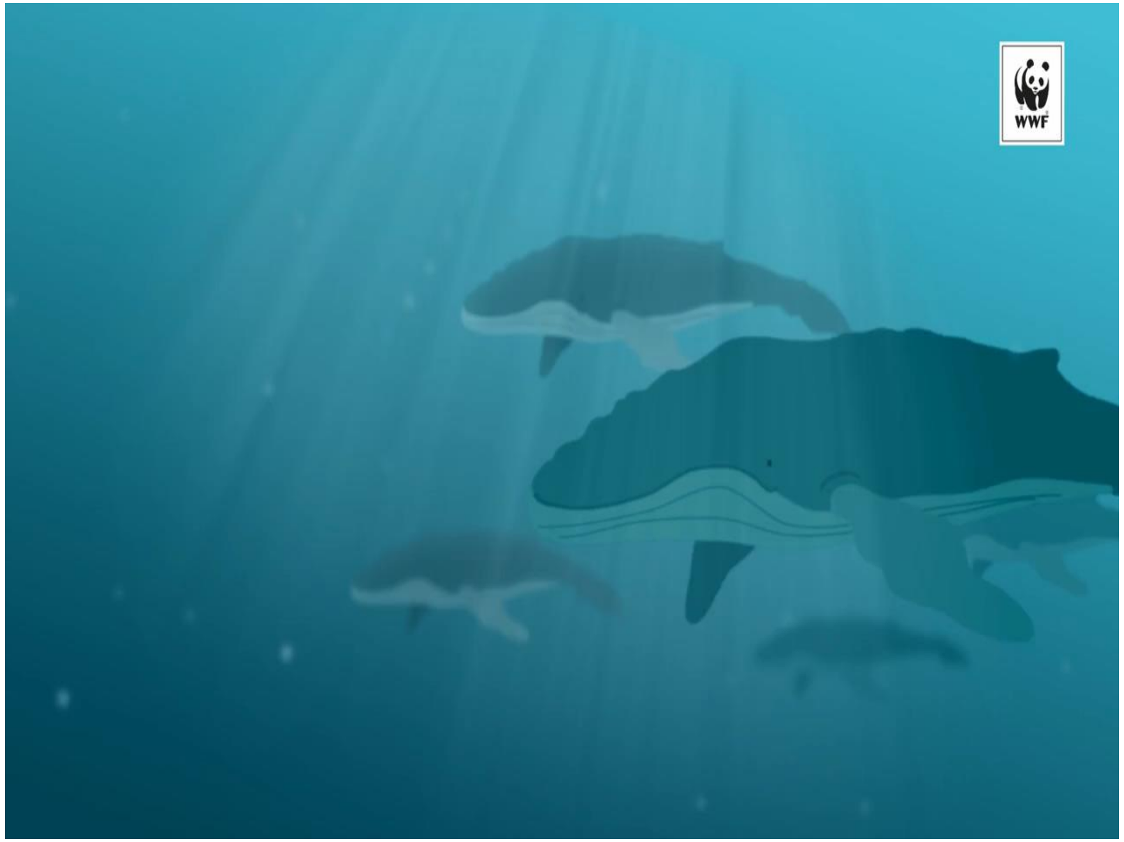

To limit noise in seas, we have to be able to calculate it first!

Method of the study

The aim of this study is to carry out numerical simulations to assess the hydroacoustic performance of Seiun Maru highly skewed marine propeller for non-cavitating case.

Hydrodynamical aspects of the propeller are first validated with experiments for open-water and behind-the-hull cases.

Then, hydroacoustic properties of the propeller was obtained by coupling the hydrodynamic solver with the hydroacoustic solver.

Propeller Geometry

Seiun Maru propeller is highly skewed and has considerable rake.

It has five blades and its full scale diameter is D=3.6m.

r/R	r	C	Skew	P/D	Rake
[-]	[mm]	[mm]	[mm]	[-]	[mm]
0.20	360	743.0	-2.4	0.945	-11.2
0.30	540	897.5	-53.6	0.987	50.2
0.40	720	1030.6	-47.3	1.010	65.1
0.50	900	1133.1	-1.2	1.015	59.4
0.60	1080	1191.9	91.9	0.993	39.5
0.70	1260	1185.3	265.7	0.944	1.7
0.80	1440	1076.8	533.5	0.871	-42.9
0.90	1620	820.8	893.2	0.780	-80.1
0.95	1710	587.6	1105.0	0.727	-91.2
1.00	1800	0.0	1336.7	0.668	-95.2

The offset data of the propeller

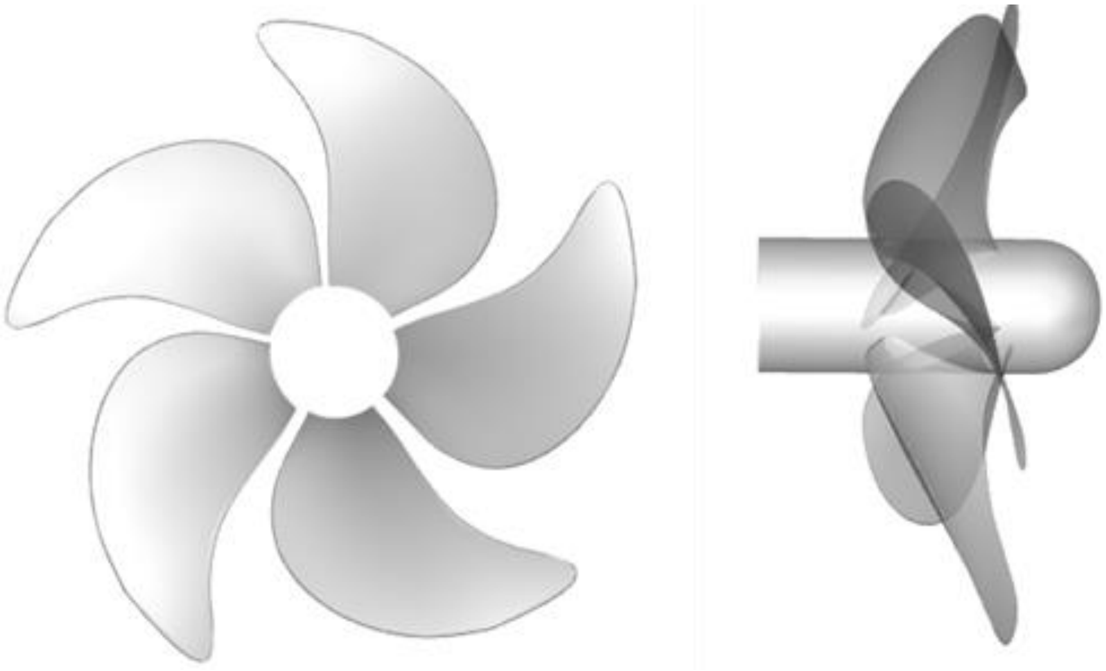

The geometry of the propeller

Numerical Implementation

Hydrodynamic pressure is obtained by RANSE. k – omega turbulence model is used.

Hydroacoustic pressure is calculated by FWH. Farassat’s impermeable formulation is adopted.

To control element sizes, computational domain was divided into 18 blocks which consists of 3 inner and 15 outer blocks.

Blocks	Mesh	Distribution	No. of elements
Inner block 3 (Propeller block)	Tetra	Start size : 0.0056D Max size : 0.0208D	1 246 228
Inner block 1 (Aft of propeller)	Tetra	Start size : 0.0208D	202 439
Inner block 2 (Forward of propeller)	Tetra	Start size : 0.0208D	58 287
Exterior blocks 4, 7, 10, 13 and 16 (Forward of propeller)	Hexa	Exponent distribution 12 x 25 x 25	37 500
Exterior blocks 5, 8, 11, 14 and 17	Hexa	Exponent distribution 12 x 25 x 33	49 500
Exterior blocks 6, 9, 12, 15 and 18 (Aft of propeller)	Hexa	Exponent distribution 12 x 25 x 45	67 500

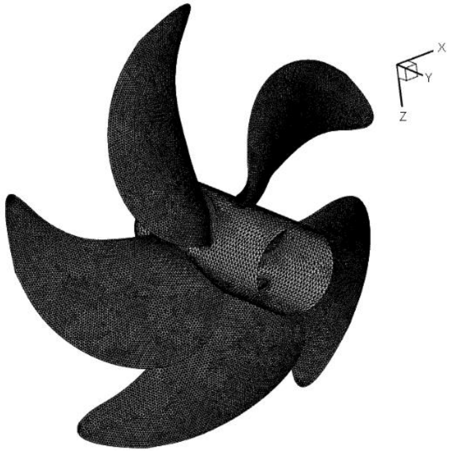

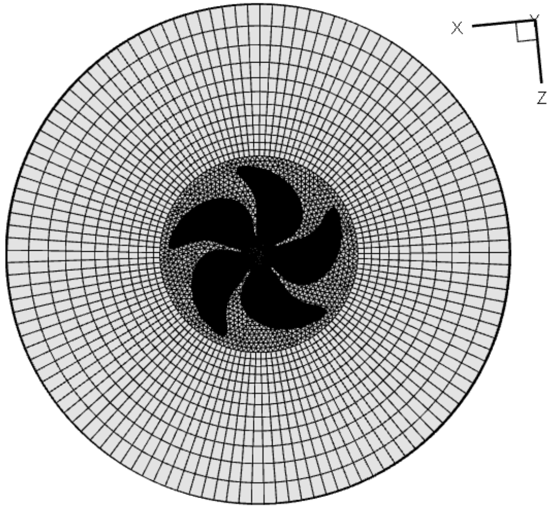

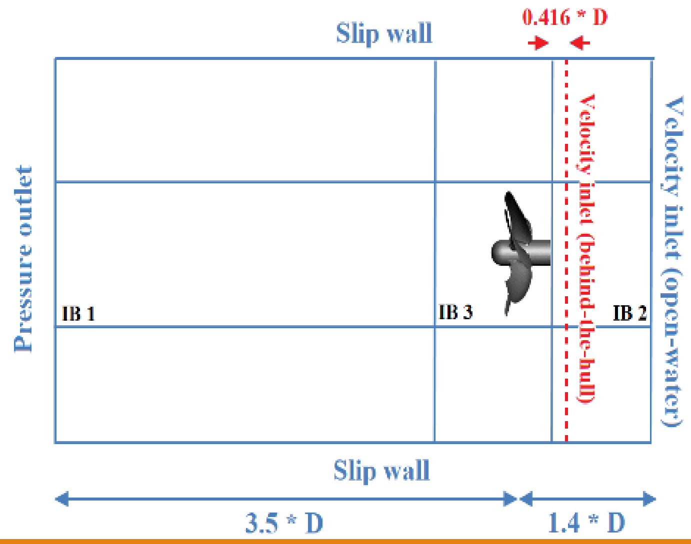

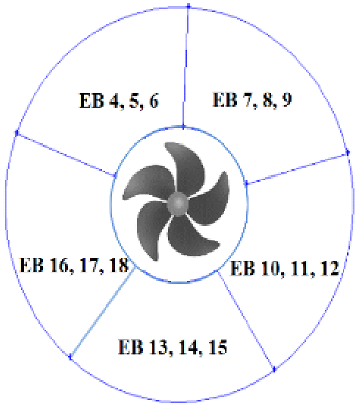

Selection of Time Step Size

Steady solver was used for open-water case but behind-the-hull condition was solved by the unsteady solver of the software.

Sound pressure levels (SPL) in frequency domain for a specific position depends on correct approximation of pressures at those points.

The existence of a rotating propeller creates oscillations in pressure and a good estimation of pressure fluctuations heavily relies on the selection of time step size.

Selection of Time Step Size

Let us assume a propeller having one blade Z=1 rotating at n=1rps.

In this case, the blade passage frequency is BPF=1.

The pressure fluctuations usually look like a sine curve.

This pressure curve which is formed by only one rotation of the propeller can only be represented by some amount of points in time.

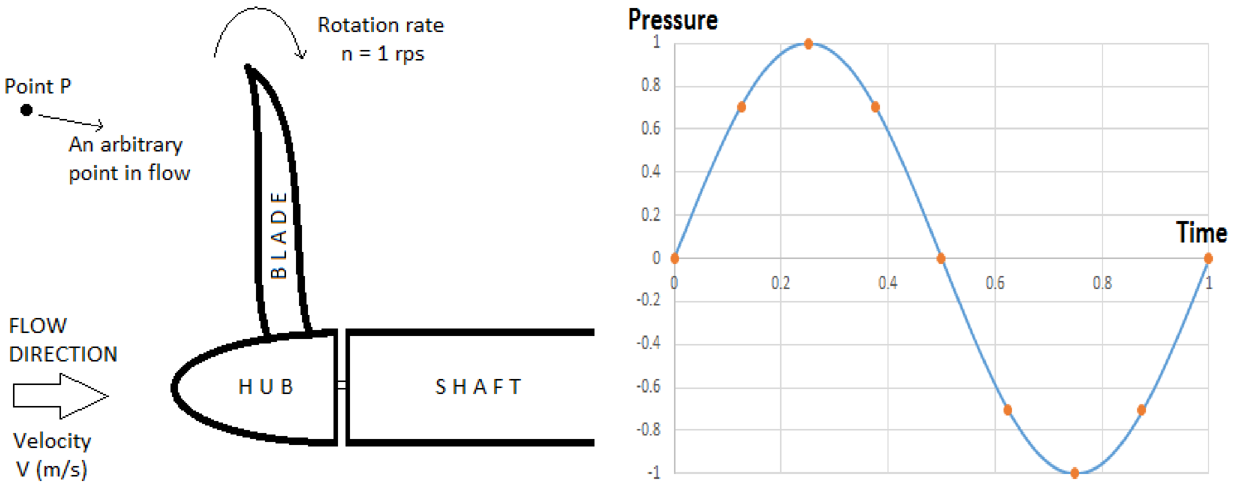

Selection of Time Step Size

Blade passage frequency of the propeller BPF=n*Z.

Let k denote the number of representation points for the pressure curve.

In this case the time step size should be;

$$\Delta t \leq \frac{1}{k \cdot Z \cdot n}$$

Number of representation points is considered to be at least k=9.

Therefore; the time step size becomes $\Delta t \leq 1/9s$.

Selection of Time Step Size

A Fast Fourier Transform (FFT) is made to convert the data from the time domain to the frequency domain in acoustic problems.

While doing FFT, the number of data points should be a power of 2; therefore, for 1 second of hydroacoustic simulation the time step size should be;

$$\Delta t = \frac{1}{2^m}$$

where m is an integer.

Using these two equations for Δt, we get;

$$m \geq \log_2 kZn$$

Selection of Time Step Size

In our simple example; k=9, Z=1 and n=1rps.

Solving $m \geq \log_2 kZn$ equation we get $m \geq 4$. The time step size for this case should be $\Delta t \leq 1/16s$.

In our study; k=13, Z=5 and n=1.512rps for behind the hull condition. This makes $\Delta t \leq$0.0108s which corresponds to a rotation angle of $\theta = 5.54°$ per time step.

Uncertainty of Numerical Simulations

Numerical simulation of uncertainty was carried out at a low advance coefficient, J = 0.3.

Due to steady solver implementation for the open-water case, time step size uncertainty was neglected, $U_T = 0$.

Iterative uncertainty was very low as compared to the grid uncertainty; therefore, $U_I \approx 0$.

Total numerical uncertainty becomes $U_N \approx U_G \approx 0$.

Three different grids were used to calculate the thrust coefficient which was taken as the integral variable.

	Exp	Grid 1	Grid 2	Grid 3
No. of elem.	-	708k	1662k	3787k
K_T	0.357	0.347	0.352	0.353

Uncertainty of Numerical Simulations

Total numerical uncertainty was found as $U_G = 0.0122 = 3.47\% S_{G_2}$.

The error of grid 2 was $E = 0.005 = 1.4\% S_{G_2}$.

The error of grid 2 remains in uncertainty region of the simulation. $E < U_G$ and the numerical simulation was validated.

Open-water condition

The open water simulation was performed for Seiun Maru model scale with a diameter of $D = 0.4m$ and a propeller revolution of $n = 3.63rps$.

Computational results were compared with the experimental data obtained by Ukon et al. (1989; 1990) for an advance coefficient range of $0.1 \leq J \leq 1$.

Open-water propeller performance predicted numerically were generally better for lower J. The discrepancy in results were higher as the advance ratio increased.

J	K_T Exp	K_T RANS	$10K_Q$ Exp	$10K_Q$ RANS
0.1	0.440	0.420	0.596	0.588
0.2	0.401	0.391	0.553	0.553
0.3	0.357	0.352	0.504	0.509
0.4	0.308	0.308	0.454	0.459
0.5	0.258	0.262	0.396	0.408
0.6	0.210	0.216	0.336	0.357
0.7	0.160	0.167	0.276	0.301
0.8	0.106	0.115	0.214	0.238
0.9	0.051	0.056	0.140	0.164
1	-	-	0.064	0.079

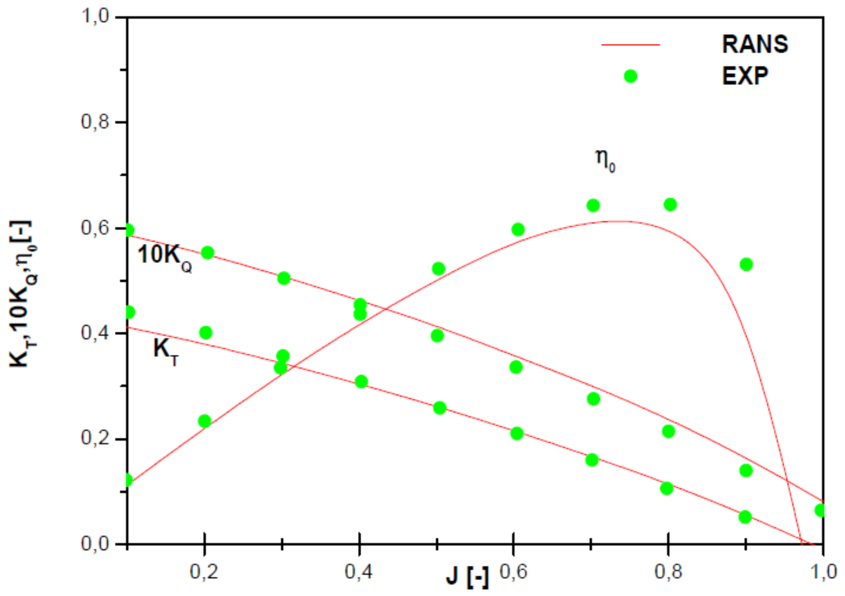

Open-water condition

C_P contours at the suction side for $J = 0.5$ (left) and $J = 0.7$ (right).

Pressure coefficients in this figure lie between $-1.9 < C_P < 0.846$.

There was a dramatic pressure decrease at the tips of the blades in low advance coefficients. This is accounted to higher propeller rotation rates which resulted in higher flow velocities; decreasing the pressure especially in these regions and leading to cavitation.

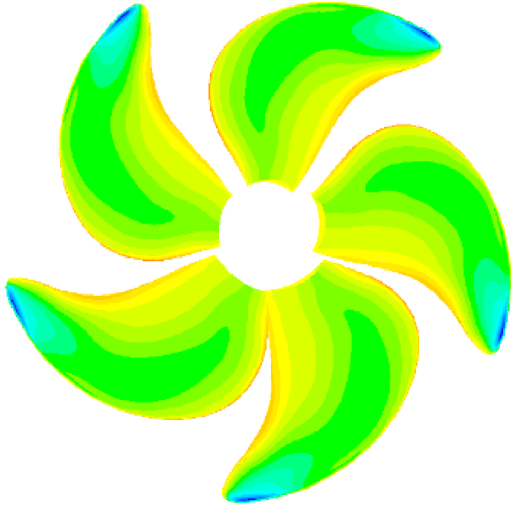

Behind-the-hull condition

Behind-the-hull propeller simulations were initialized by introducing the axial velocities calculated from the measured nominal wake by (Ukon et al., 1989; 1990) in towing tank.

Prediction of thrust agrees with (Nakatake et al., 2002).

It is worthy to note that thrust coefficient per blade in five blades case is lower than one blade case. This is due to:

- Each blade is at a different position producing a different thrust coefficient.
- The interactions between blades lower the total thrust.

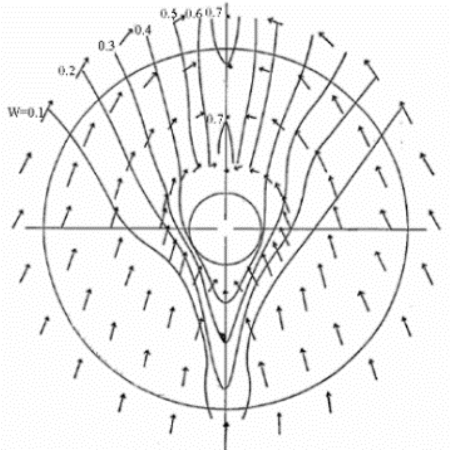

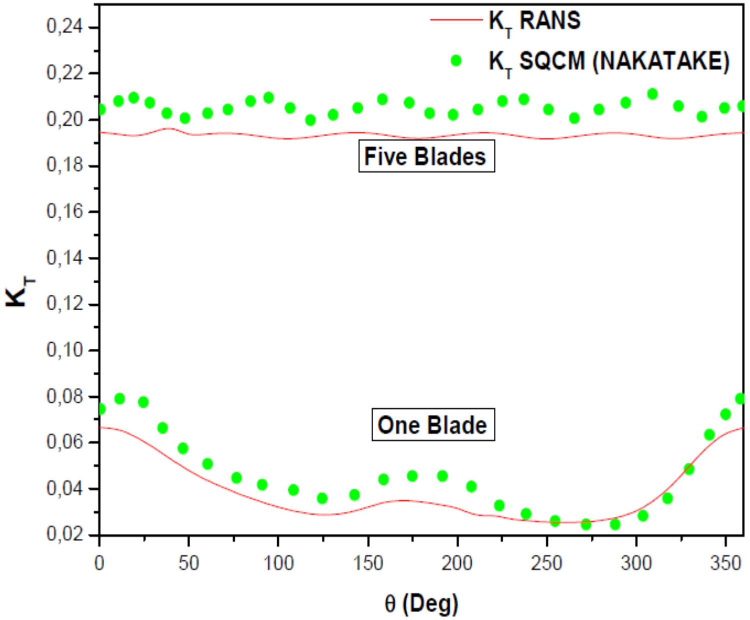

	n (rpm)	σ (-)	J (-)
Simulation in non uniform ship wake (Non cavitating flow)	90.7	6.08	0.85

Behind-the-hull condition

Contours of pressure coefficients on blade suction side for different angle positions.

The legend lies between $-1.95 < C_P < 1.03$. The angle of 0° corresponds to the top position.

This figure notes the differences in pressure at each angle. This is due to the propeller being subjected to a non-uniform flow.

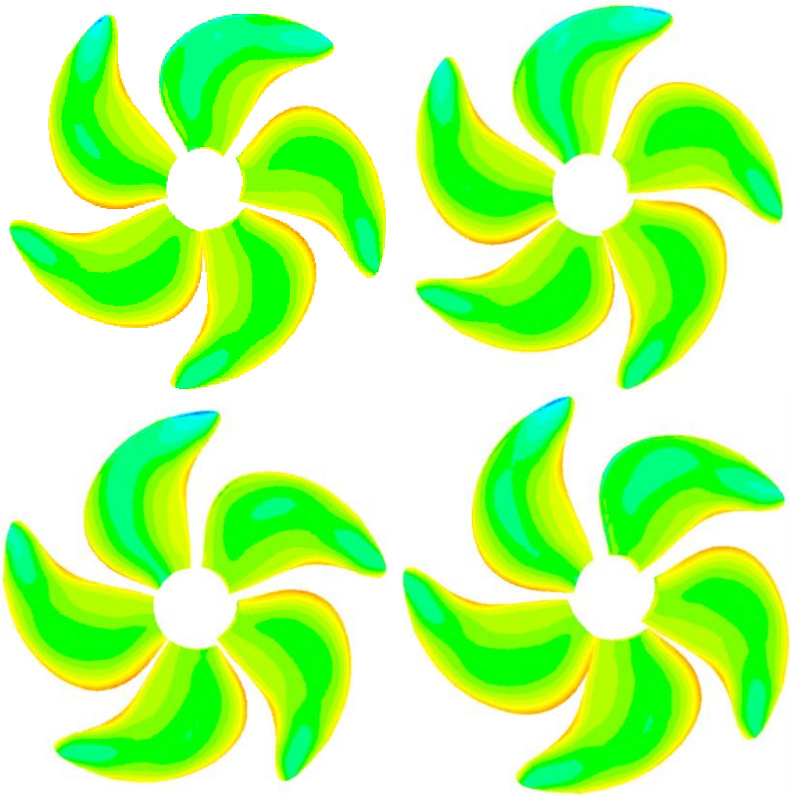

Hydroacoustic results

Hydroacoustic calculations were performed for the propeller operating at $n = 90.7 rpm$ in non-uniform ship wake (behind a ship hull).

Reference pressure for Sound Pressure Level calculations was taken as $1 \mu Pa$, density was $\rho = 998.2 kg/m^3$ and the velocity of sound in the undisturbed medium was $c = 1500 m/s$.

Simulations were conducted for 8 rounds of propeller rotations.

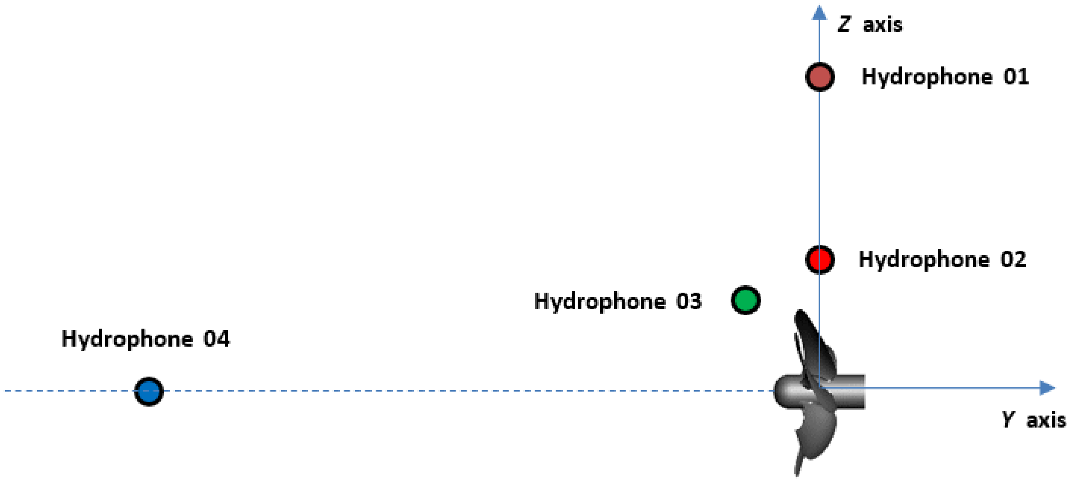

Hydrophones	X	Y	Z
1	0	0	3.3R
2	0	0	1.5R
3	0	-0.5R	R
4	0	10R	0

Hydroacoustic results

Acoustic pressure fluctuations in time at hydrophones 2 and 3 for the last rotation.

5 peaks in pressure graph correspond to 5 blades existing in Seiun Maru propeller.

Acoustic pressures for hydrophones 1 and 4 were not presented because pressure peaks could not be identified at these locations.

The underlying reason for this is the acoustic signal vanishing in the far field which is probably due to the insufficiency in grid resolution.

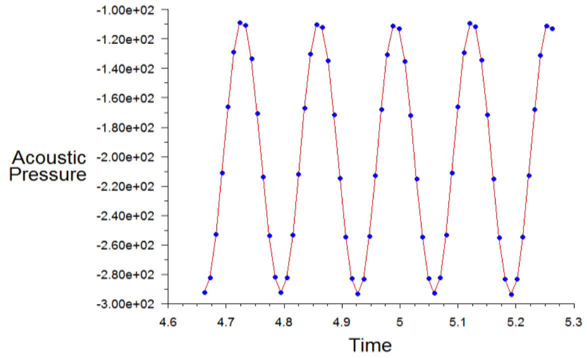

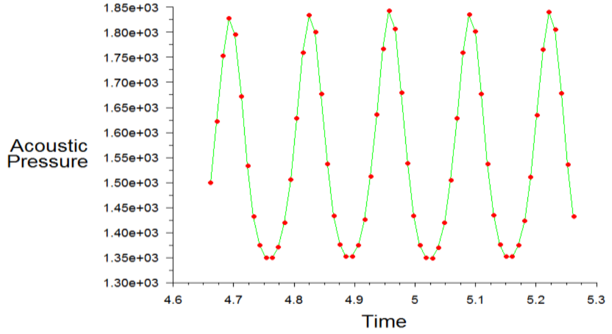

Hydroacoustic results

Noise spectra in dB for hydrophones 2 and 3 up to 50 Hz.

Sound pressure level (SPL) peaks of these graphs are in accordance with the blade passage frequency (BPF).

$$BPF = n * Z = 5 * 1.512 = 7.56Hz$$

Other harmonics should be seen at 15.12Hz, 22.67Hz, 30.23Hz, 37.79Hz and 45.35Hz.

We can only see the first harmonic in Hydrophone 2. Numerical simulation could not resolve the other harmonics. Mesh refinement in this zone is needed.

The first four harmonics are visible in Hydrophone 3. Accuracy in higher frequencies require mesh refinement as well as a reduction in time step size.

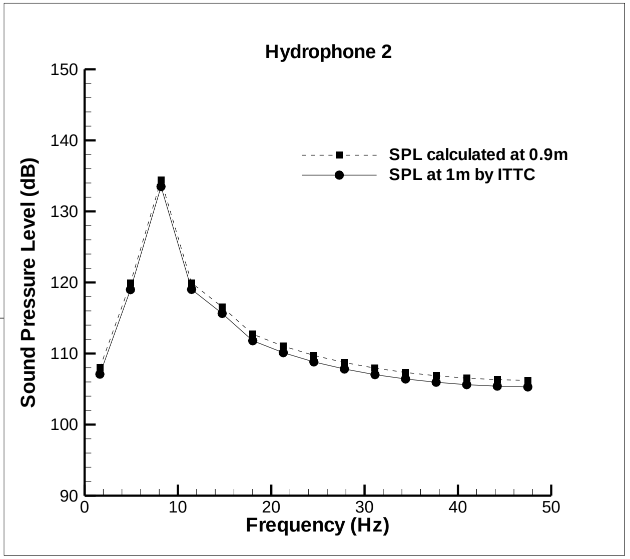

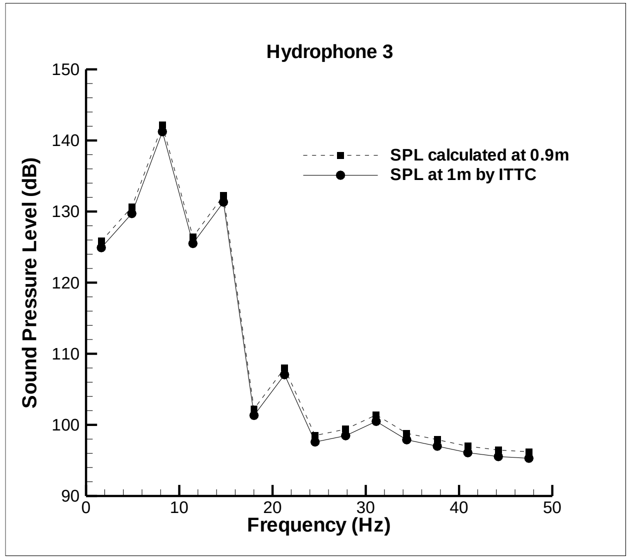

Conclusions

Hydroacoustic performance of the benchmark Seiun Maru propeller was numerically solved in the near field.

Numerical approach was first validated with experiments for open-water and behind-the-hull cases.

Validation of the numerical approach with hydrodynamic propeller performance could only return partially satisfactory results in the near-field.

Grid refinement in unsatisfactory zones are necessary. Time step size reduction may also be an issue depending on the refinement.

THANK YOU FOR YOUR ATTENTION!

ANY QUESTIONS?

NATIONAL RESEARCH COUNCIL OF ITALY

Effectiveness of Boundary Element Method Hydrodynamic Data for Propeller Hydroacoustics

A. Yücel Odabaşı Colloquium Series
3rd International Meeting on Propeller Noise and Vibration
17th – 18th November 2018, Istanbul, Turkey

Claudio Testa
Luca Greco
Roberto Muscari

INM Institute of Marine engineering

Federico Porcacchia

ROMA TRE UNIVERSITÀ DEGLI STUDI

Outline of the Talk

THE PROBLEM

To shed light on capabilities and drawbacks of **potential-based hydrodynamic data** for the prediction of the **tonal noise** generated by marine propellers in **open water**.

GUIDELINES FROM PREVIOUS RESEARCH

Sound from propeller shape & kinematics (thickness noise) and blade pressure distribution (loading noise) are significant only close to the propeller disk, decreasing rapidly respect to the volume terms contribution (**quadrupole noise**) induced by the hydrodynamic sources of sound like vortex released at the blade tip, vorticity, turbulence, etc…, which can be very intense and persisting around/downstream the propeller *(27th and 28th ITTC).*

HOW TO COMPUTE PROPELLER SIGNATURE

The notable know-how gained through 30 years of research activities on Aeroacoustics proves that the **Ffowcs Williams and Hawking Equation** (FWH) is the most powerful approach to tackle the hydroacoustic analysis of rotary-wing devices. Since propeller hydroacoustics is an inherently **nonlinear problem,** it requires a very accurate description of the hydrodynamic field by **CFD solutions**.

UNSOLVED QUESTIONS

Tonal noise components may play an important role in both prediction and alleviation of the overall sound spread out from ships powered by propellers. In order to detect the sources of sound inherently associated to the blades and vorticity convected downstream, a potential-based hydrodynamic theory for unsteady three-dimensional flows around lifting bodies might be used, at reasonable computational costs. However…..

- Which is the **range of applicability** of Boundary Element Method *(BEM)* hydrodynamic data for propeller hydroacoustics?

- Which is the **degree of confidence in the accuracy** of such predictions respect to those based on *RANSE*, *DES*, *LES* hydrodynamic data commonly used in propeller performance analysis?

AIM OF THE PAPER

To gain a better insight on the capability of propeller BEM hydrodynamic analysis in the detection of the hydrodynamic sources of tonal noise generated by marine propellers in open water.

OUTCOME OF THE WORK

Assessment of a numerical procedure based on the solution of the FWH for permeable surfaces coupled with DES and BEM hydrodynamic data.

NUMERICAL RESULTS

The investigation is addressed both in the time and frequency domain to get a deep insight into the quality of the predicted signals in terms of waveform and harmonic content. The four-bladed propeller model **INSEAN E779A** is considered in open water; hydrodynamic data for hydroacoustics assure comparable thrust and torque predictions between DES and BEM as well as a coherent wake flow description.

Sound Generation by Flow – Lighthill's Acoustic Analogy

- The question of how precisely to identify the real origins of a sound wave was not successfully addressed until Lighthill, in 1951, developed his theory of hydrodynamic sound in response to the emerging need to control the noise of a jet propelled aircraft;

- The Lighthill equation represents a **rearrangement** of the fundamental conservation laws of mass and momentum into an inhomomogeneus wave equation:

$$\Box^2 p' = \frac{1}{c_0^2}\frac{\partial^2 p'}{\partial t^2} - \nabla^2 p' = \frac{\partial^2 T_{ij}}{\partial x_i \partial x_j}$$

where:

- ◇ p' is the *acoustic pressure*, that is the (isentropic) fluctuation of pressure with respect to p_0 (fluid at rest);
- ◇ $T_{ij} = \rho u_i u_j - S_{ij} + (p' - c_0^2 \rho')\delta_{ij}$ is the *Lighthill tensor*, where $\mathbf{u}$, ρ are the fluid velocity and density and $\mathbf{S}$ the viscous stress tensor;
- ◇ $c_0^2 = \left.\frac{\partial p}{\partial \rho}\right|_{s_0}$ is the (isentropic) *sound speed*.

(…Cont'd)

$$\Box^2 p' = \frac{1}{c_0^2}\frac{\partial^2 p'}{\partial t^2} - \nabla^2 p' = \frac{\partial^2 T_{ij}}{\partial x_i \partial x_j} \qquad (1)$$

where:

- ◇ p' is the *acoustic pressure*, that is the (isentropic) fluctuation of pressure with respect to p_0 (fluid at rest);
- ◇ $T_{ij} = \rho u_i u_j - S_{ij} + (p' - c_0^2 \rho')\delta_{ij}$ is the *Lighthill tensor*, where $\mathbf{u}$, ρ are the fluid velocity and density and $\mathbf{S}$ the viscous stress tensor;
- ◇ $c_0^2 = \left.\frac{\partial p}{\partial \rho}\right|_{s_0}$ is the (isentropic) *sound speed*.

The RHS of (1) includes all possible noise source mechanisms taking place in the flow:

- * the convective term, represented by the Reynolds tensor $\rho u_i u_j$;
- * the possible deviation from isentropic behavior $p' - c_0^2 \rho'$;
- * viscous stresses S_{ij}.

Since no approximation has been made, equation (1) is exact and its solution *is not easier* than original equations of motion.

The Ffowcs Williams and Hawkings Equation

- The Ffowcs Williams-Hawkings equation is an *extension* of Lighthill work, accounting for the possible presence of a **body moving in the fluid**.
- Such a presence is described by representing the surface $f(\mathbf{x},t)=0$ (on which $u_n = v_n$) as a moving *discontinuity* in the flow and, then, re-writing the same conservation laws in terms of *generalized functions*:

$$\boxed{\bar{\Box}^2 p'} = \frac{1}{c_0^2}\frac{\partial^2 p'}{\partial t^2} - \nabla^2 p' = \boxed{\frac{\bar{\partial}}{\partial t}\left[\rho_0 v_i \frac{\partial f}{\partial x_i}\delta(f)\right]} - \boxed{\frac{\bar{\partial}}{\partial x_i}\left[\tilde{P}_{ij}\frac{\partial f}{\partial x_j}\delta(f)\right]} + \boxed{\frac{\bar{\partial}^2}{\partial x_i \partial x_j}\left\{\left[\rho u_i u_j - S_{ij} + \left(p' - c_0^2\rho'\right)\delta_{ij}\right]H(f)\right\}}$$

Sound

Noise due to the displacement of the fluid forced by the body passage

Effect due to the pressure distribution upon the body surface

Acoustic contributions from sources of noise in the flow-field

where:

* $\dfrac{\partial f}{\partial x_i} = \left|\dfrac{\partial f}{\partial x_i}\right| n_i$;

* $\tilde{P}_{ij} = P_{ij} - p_0\delta_{ij}$ (being $P_{ij} = p\delta_{ij} - S_{ij}$);

* $H(f)$ is the *Heaviside* function.

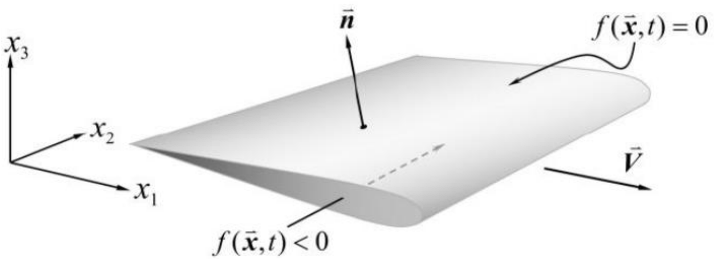

- Compared to Lighthill equation and the original **flow** 3D term, two additional **surface** 2D terms appear, known as *thickness* and *loading* noise components.

(…Cont'd)

Main advantages:
- **Identification of noise generated by well-defined source terms**
- **Hybrid approach based on the fundamental conservation laws for compressible flows**
- **Time domain solutions**
- **Standard and validated formulation in aeronautical applications**

In *compact* form, the FWH equation for **impermeable surfaces** reads:

$$\bar{\Box}^2 p' = \frac{\bar{\partial}}{\partial t}\left[\rho_0 \, \mathbf{v} \cdot \nabla f \; \delta(f)\right] - \overline{\nabla} \cdot \left[\mathbf{P} \; \nabla f \; \delta(f)\right] + \overline{\nabla} \cdot \left\{\overline{\nabla} \cdot \left[\mathbf{T} \; H(f)\right]\right\}$$

Disturbance Acoustic Pressure	$p' = c_0^2 \left(\rho - \rho_0\right)$
Generalized Wave Operator	$\bar{\Box}^2 = (1/c_0^2)(\bar{\partial}^2/\bar{\partial}t^2) - \overline{\nabla}^2$
Compressive Stress Tensor	$\mathbf{P} = \left[(p - p_0)\,\mathbf{I} + \mathbf{V}\right]$
Lihgthill Stress Tensor	$\mathbf{T} = \left[\rho(\mathbf{u} \otimes \mathbf{u}) + (p - p_0)\mathbf{I} - c_0^2(\rho - \rho_0)\mathbf{I} + \mathbf{V}\right]$

The use of the standard **Green function approach** yields the following **Boundary-Field Solution** for the acoustic pressure, in a space rigidly connected to S (*SRC*):

(…Cont'd)

"quadrupole" "loading"

$$p'(\mathbf{x},t) = \int_V \left[\hat{G}\,\nabla\cdot\nabla\cdot(\mathbf{T}\,H)\right]_\vartheta \mathrm{d}V(\mathbf{y}) - \int_S \left[(\mathbf{P}\mathbf{n})\cdot\nabla\hat{G} - (\mathbf{P}\mathbf{n})^{\cdot}\cdot\nabla\vartheta\,\hat{G}\right]_\vartheta \mathrm{d}S(\mathbf{y})$$
$$- \rho_0 \int_S \left[\mathbf{v}\cdot\mathbf{n}\,\mathbf{v}\cdot\nabla\hat{G} + \Big(\mathbf{v}\cdot\mathbf{n}\,(1-\mathbf{v}\cdot\nabla\vartheta)\Big)^{\cdot}\,\hat{G}\right]_\vartheta \mathrm{d}S(\mathbf{y})$$

"thickness"

$$\hat{G}(\mathbf{x},\mathbf{y},t) = \frac{-1}{4\pi}\left[\frac{1}{r\,(1-M_r)}\right]_{\mathrm{ret}}$$

$(\,)^{\cdot}$ **denotes time derivative computed In the *SRC***

θ **denotes compressibility delay**

ϑ , $[\;]_{\mathrm{ret}}$ **denotes evaluation at emission time**

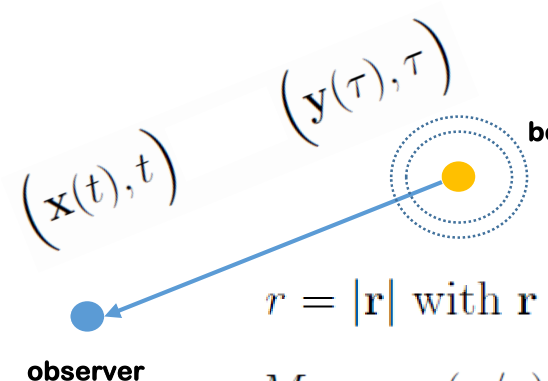

body source emitting at the emission time $\tau = t - \theta$

$$r = |\mathbf{r}| \text{ with } \mathbf{r} = \mathbf{x}(t) - \mathbf{y}(\tau)$$

$$M_r = \mathbf{v}\cdot(\mathbf{r}/r)/c$$

BIR fully equivalent to the Farassat formulation

The solver is based on a **backward-in-time** integration scheme (for each source point and at each observer time step ***t*** the procedure determines the corresponding retarded time ***τ***) and a **zero-order BEM** formulation.

(…Cont’d)

At the usual rotational speed occurring underwater, the FWH surface terms **decay** very rapidly (few diameters from the propeller hub, thickness and loading noise effects are pratically ineffective) → volume terms may play a relevant role in the overall noise prediction → Lighthill tensor **can never be left** out of consideration → **direct volume integration becomes mandatory** → **significant increase of the computation burden.**

To compute efficiently noise effects induced by nonlinear sources of sound in the flowfield, the so called ***porous FWH formulation (FWH-P)***, introduced by Difrancescantonio in 1997, allow to remove the need for a volume integration, significantly decreasing CPU time.

Turbulence, vorticity & cavitating phenomena occur inside the porous surface. They represent the acoustic noise sources forcing the wave operator at the LHS

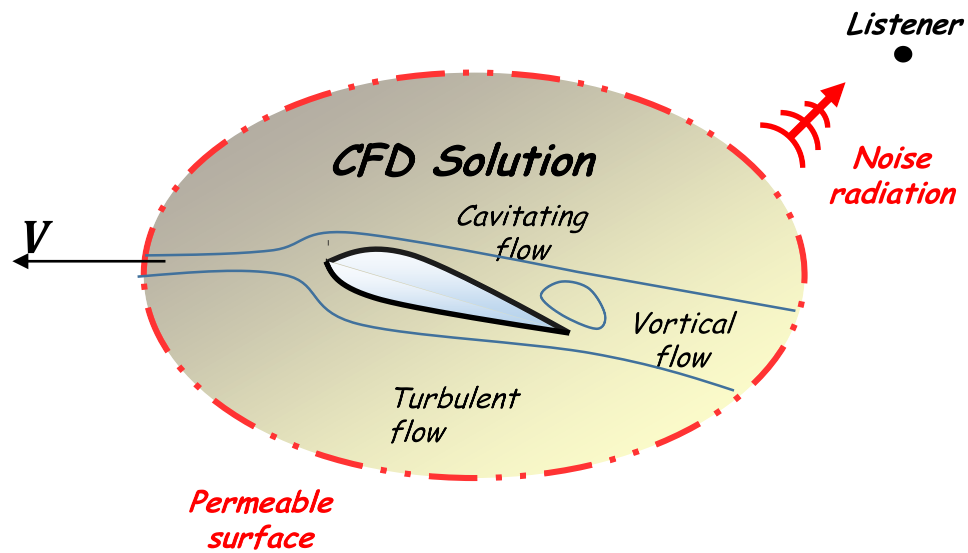

The Porous FWH Equation

The FWH-P solution yields the noise field outside a permeable surface S_p starting from the knowledge of:

i) the hydrodynamic flowfield ***upon it****;*
ii) the nonlinear sources of sound ***outside it****.*

However, if the permeable surface is such to embed "all" the nonlinear sources of noise, the last contribution is zero and the noise outside S_p is due to the radiation of acoustic contributions from S_p that account for all the sources of sound enclosed by it.

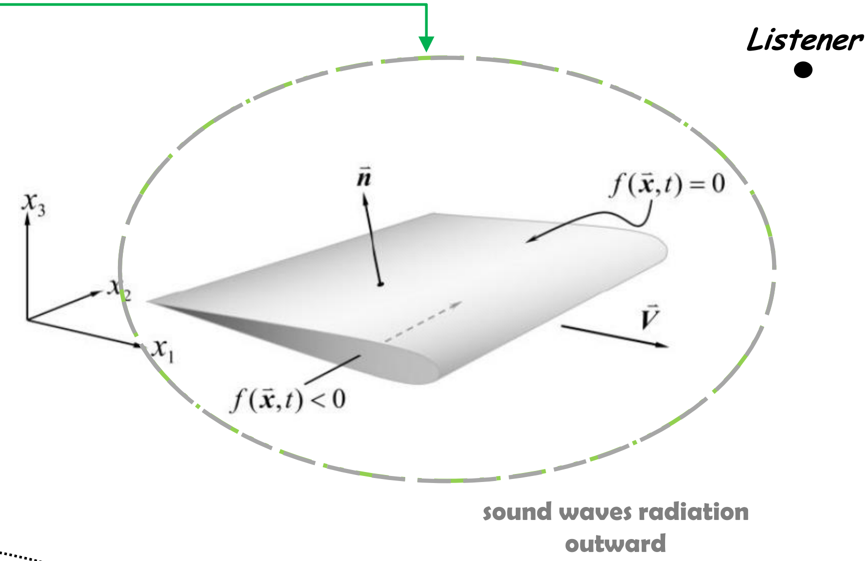

$$\bar{\Box}^2 p' = \frac{\bar{\partial}}{\bar{\partial} t}\left[\rho_0\, \mathbf{v}\cdot\nabla f\, \delta(f)\right] + \frac{\bar{\partial}}{\bar{\partial} t}\left[\rho\,(\mathbf{u}-\mathbf{v})\cdot\nabla f\, \delta(f)\right] - \bar{\nabla}\cdot\left[\mathbf{P}\,\nabla f\,\delta(f)\right] - \bar{\nabla}\cdot\left[\rho\,\mathbf{u}\otimes(\mathbf{u}-\mathbf{v})\,\nabla f\,\delta(f)\right] + \bar{\nabla}\cdot\bar{\nabla}\cdot\left[\mathbf{T}\,H(f)\right]$$

PROS

1- It has become the standard solving approach for the FWH equation
2 - Complete solution of the problem provided
3 - Demanding 3D integral calculations avoided
4 - Easy to be coded
5 – Suited to be included in hydrodynamic tools to avoid the management of huge databases

Altho oise
embe ose.

(…Cont'd)

Akin to the FWH for impermeable surfaces, the use of the standard **Green function approach** yields the following **Boundary Integral Representation** for the acoustic pressure, in a space rigidly connected to S_p (SRC):

Noise effects captured by surface terms

BIR

$$
\begin{aligned}
p'(\mathbf{x},t) \;=\; & -\int_S \Big[(\mathbf{P}\mathbf{n})\cdot\nabla\hat{G} - (\mathbf{P}\mathbf{n})^{\boldsymbol{\cdot}}\cdot\nabla\vartheta\,\hat{G}\Big]_\vartheta \,\mathrm{d}S(\mathbf{y}) \\
& - \rho_0\int_S \Big[\mathbf{v}\cdot\mathbf{n}\,\mathbf{v}\cdot\nabla\hat{G} + \big(\mathbf{v}\cdot\mathbf{n}\,(1-\mathbf{v}\cdot\nabla\vartheta)\big)^{\boldsymbol{\cdot}}\,\hat{G}\Big]_\vartheta \,\mathrm{d}S(\mathbf{y}) \\
& - \int_S \Big[\rho\mathbf{u}^-\cdot\mathbf{n}\,\mathbf{u}^+\cdot\nabla\hat{G} + \big(\rho\mathbf{u}^-\cdot\mathbf{n}\,(1-\mathbf{u}^+\cdot\nabla\vartheta)\big)^{\boldsymbol{\cdot}}\,\hat{G}\Big]_\vartheta \,\mathrm{d}S(\mathbf{y})
\end{aligned}
$$

Transpiration terms on the porous surface $\quad \mathbf{u}^- = (\mathbf{u}-\mathbf{v}) \quad \mathbf{u}^+ = (\mathbf{u}+\mathbf{v})$

Numerical Results

E779A Insean Propeller in OW

Hydroacoustics

Hydrodynamics

Simulation parameters

$J = \frac{|v_0|}{nD} = 0.88$ D= 0.22727 [m] n= 25 [Hz]

The (3D unsteady) RANSE simulation is based on a **finite volume** approach exploiting the **Chimera** technique to achieve a very effective grid clustering

INSEAN E779A model	
Number of blades	4
Diameter	0.227
Expanded area ratio	0.689
Pitch ratio (0.7R)	1.1
Hub ratio	0.2
Turning rate	25 rps
Nominal advance coefficient	0.88
Reynolds	1.781 x 10^6

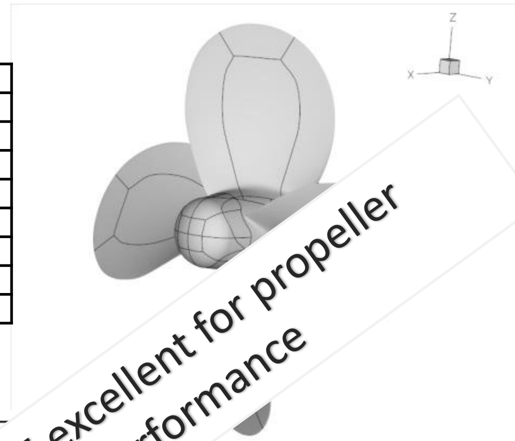

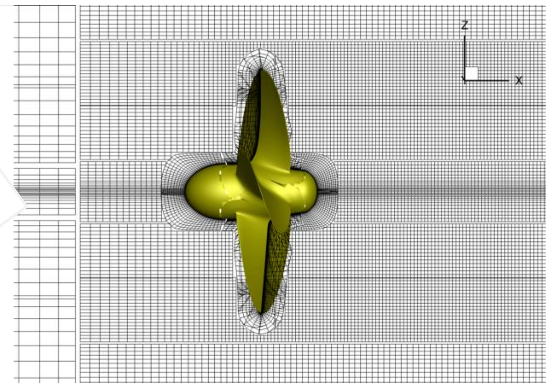

RANSE excellent for propeller performance

Open water characteristics

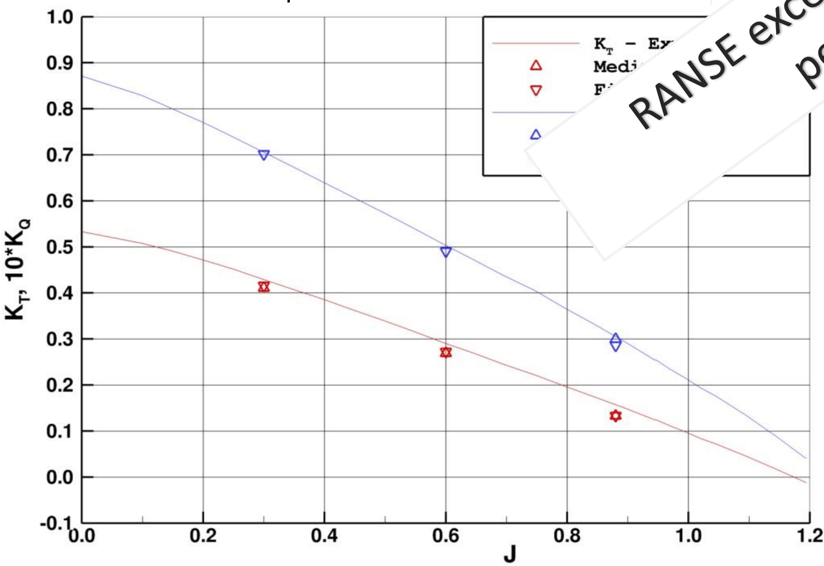

Y-component of **vorticity** (*J=0.88*)

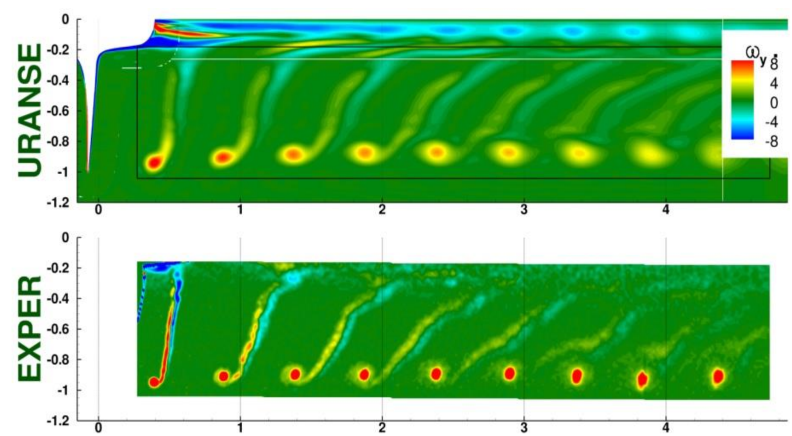

S. Ianniello, R. Muscari, A. Di Mascio, Ship underwater noise assessment by the Acoustic Analogy. Part I: nonlinear analysis of a marine propeller in an uniform flow, JSMT, 18, 2013

BEM simulation based on a three-dimensional **free-wake unsteady** hydrodynamics for subsonic potential flows around lifting bodies.

Detached Eddy Simulation (**DES**) is a modification of a RANSE model that switches to a subgrid scale formulation in regions fine enough for Large Eddy Simulation (LES) calculations. Regions near solid boundaries and where the turbulent length scale is less than the maximum grid dimension are assigned the **RANSE** mode of solution. As the turbulent length scale exceeds the grid dimension, the regions are solved as a **LES**.

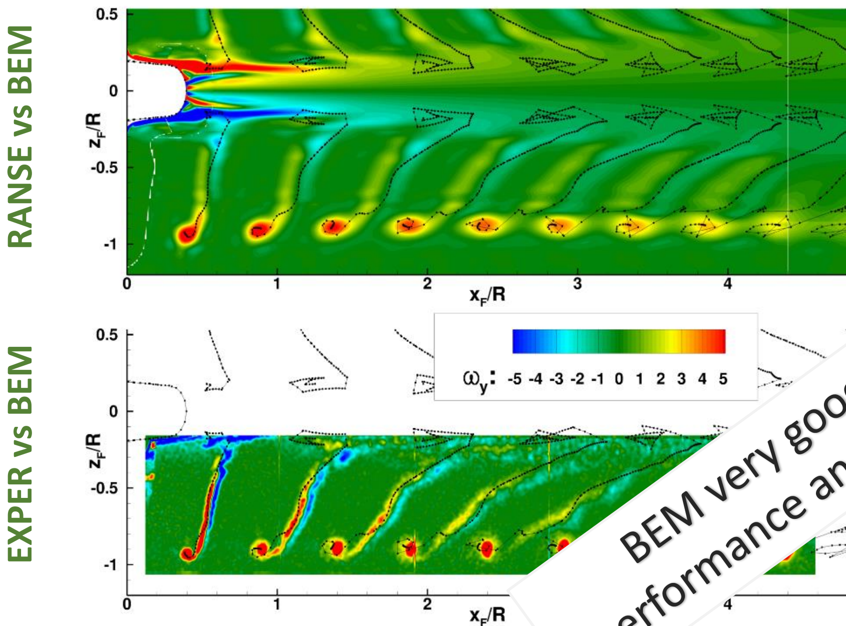

Y-component of the vorticity field along the Y axis predicted by Experiments, RANSE and DES-averaged simulations compared to trailing wake location by BEM (black lines)

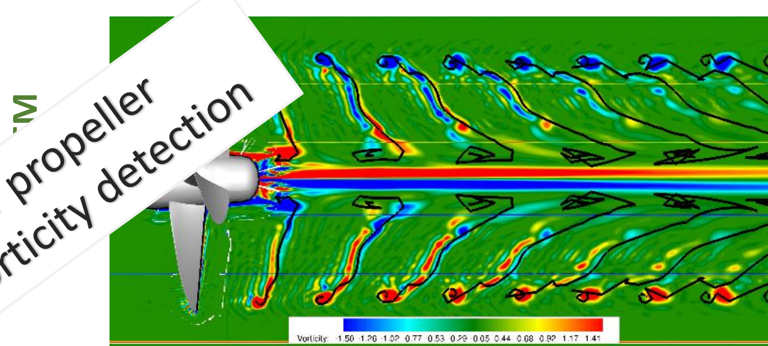

BEM very good for propeller performance and vorticity detection

RANSE	BEM	EXPER	DES running averaged
KT = 0.133	KT = 0.1407	KT = 0.157	KT = 0.1335
10KQ = 0.286	10KQ = 0.2971	10KQ = 0.305	10KQ = 0.2843

Di Felice F., Di Florio D. And FELLI M. et al. Experimental investigation of the propeller wake at different loading conditions by particle image velocimetry[J]. Journal of Ship Research, 2004, 48(2): 168-190.

Greco, L., Muscari, R., Testa, C., and Di Mascio, A. (2014). 'Marine Propellers Performance and Flow-Field Features Prediction by a Free-Wake Panel Method'. J. Hydrod., Ser. B (English Ed.) 26(5), pp. 780-795.

RANSE vs DES Sources of Sound Detection

DES may be well suited for capturing the hydrodynamic sources of noise. Why?

Hydrodynamics:

DES/RANSE simulations

Muscari R., Di Mascio A., Verzicco R., "Modeling of vortex dynamics in the wake of a marine propeller", Computer & Fluids, 73, 2013, pp. 65–79

J=0.71 ***J=0.38***

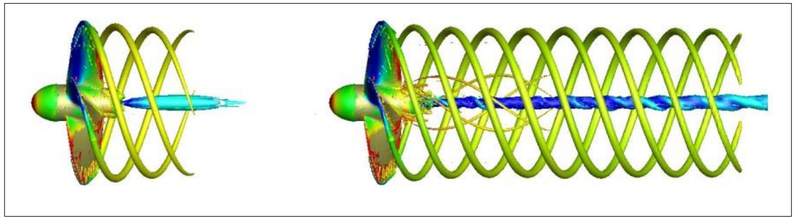

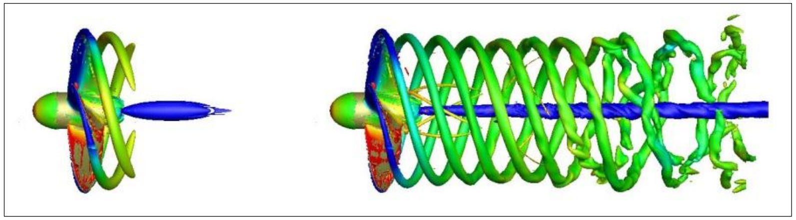

RANSE DES RANSE DES

Measurement points

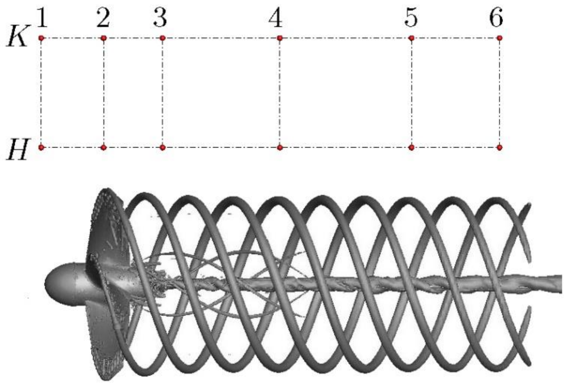

Hydroacoustics:

1 Linear Farassat *formulation 1A*

2 RANSE – DES direct calculations

(…Cont'd)

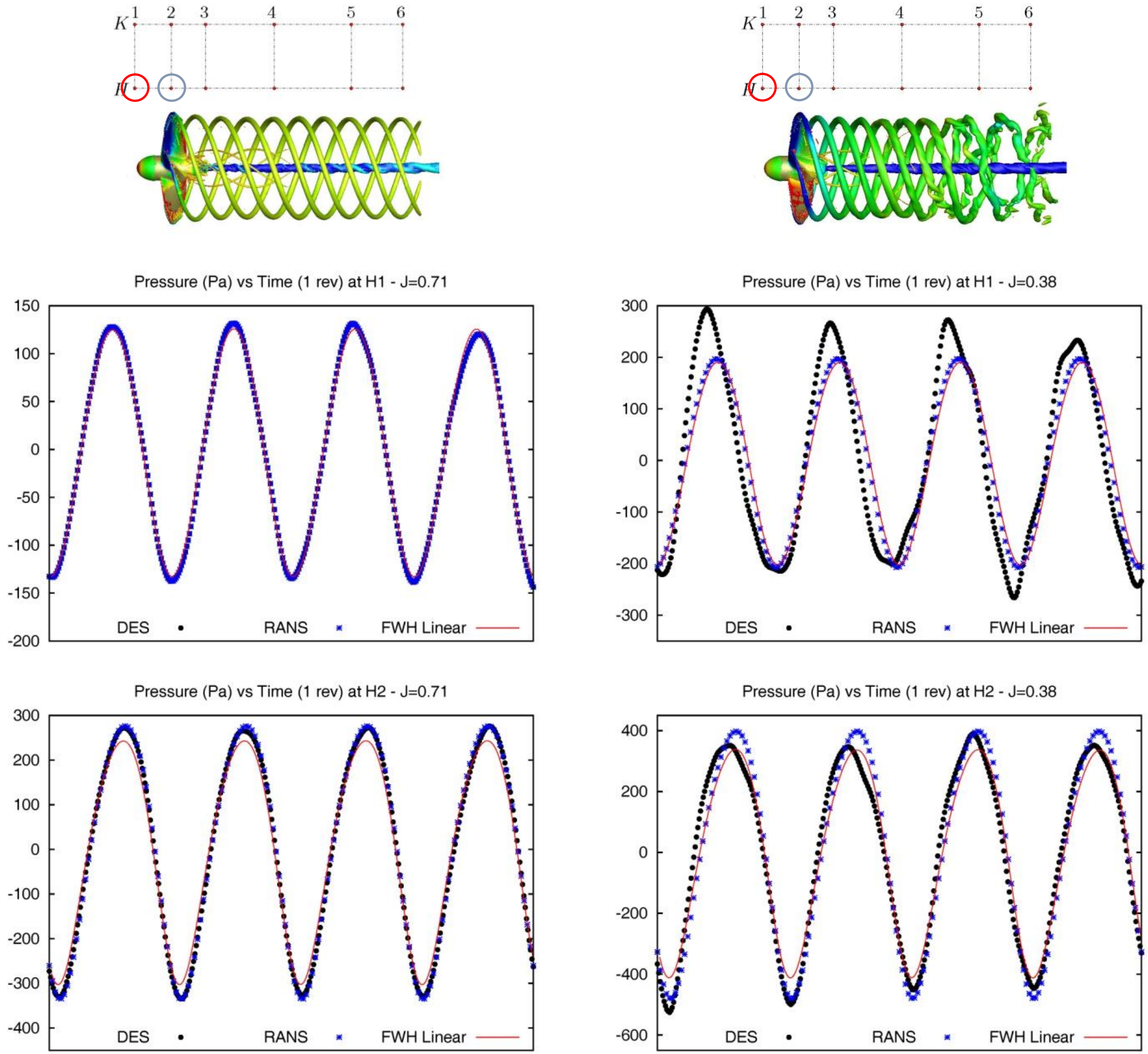

S.Ianniello, E. De Bernardis. 2015 Farassat's formulations in marine propeller hydroacoustics. Intl J. Aeroacoust. 14 (1-2), 87-103

Linear FWH and RANSE solutions show a good agreement ‘everywhere’ in the field, even when they are clearly unrealistic! Even though RANSE solution is wrong from a hydroacoustic standpoint, the FWH linear solution is correct ! In fact, it only depends on blade kinematics and hydrodynamic loads successfully validated by experimental data

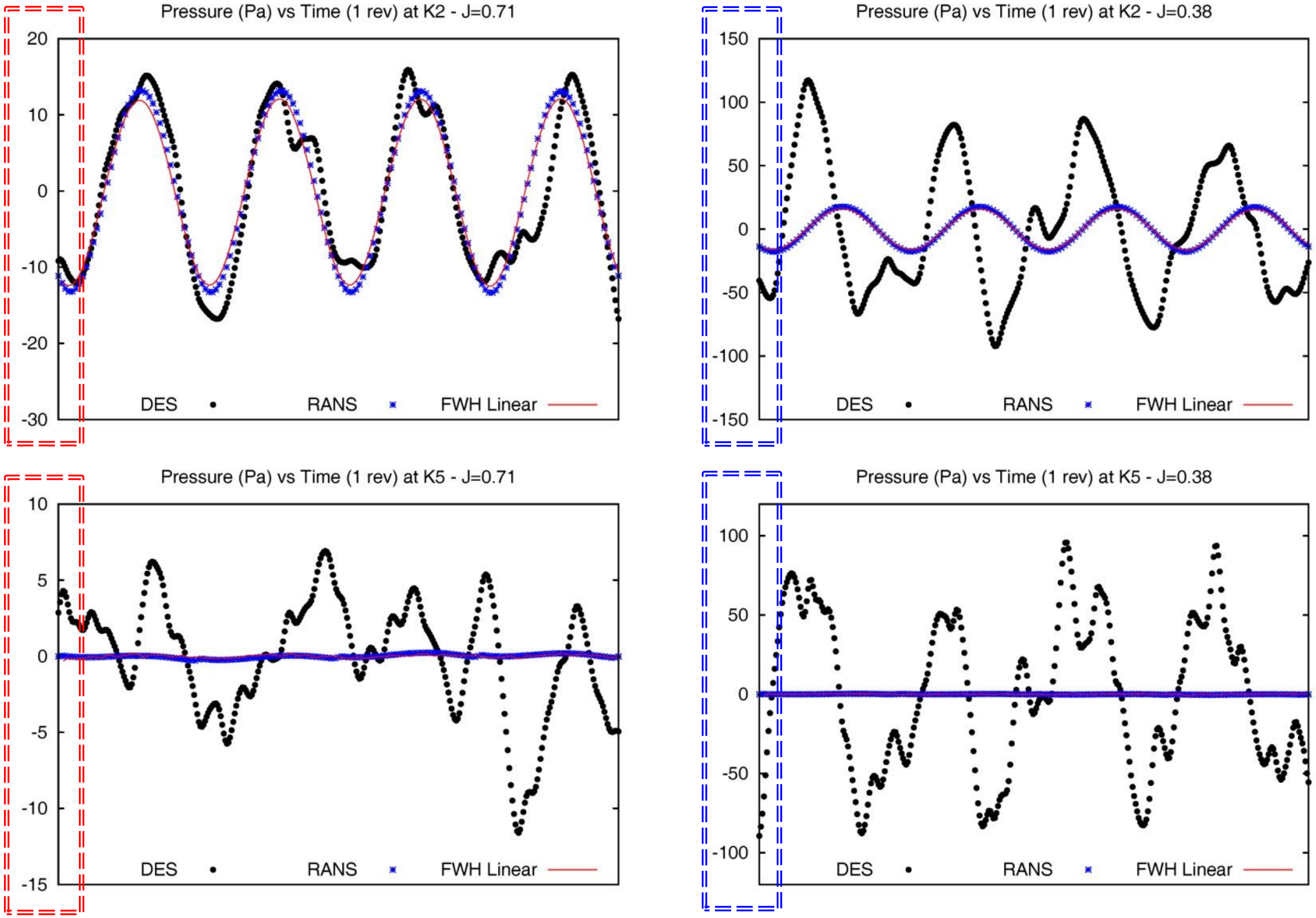

S.Ianniello, E. De Bernardis. 2015 Farassat’s formulations in marine propeller hydroacoustics. Intl J. Aeroacoust. 14 (1-2), 87-103

Hydroacoustics by FWH-P

Choice of the porous cylindrical surface:
 - the radius size assures that, just outside the cylinder, the Lighthill stress tensor ***T*** is negligible at any time of DES simulation;
 - longitudinally, the cylinder length guarantees that the end-closure is placed where the magnitude of ***T*** *i*s bounded (in time) within the smallest values it assumes in the slipstream of the propeller

Obs	[x/D]	[y/D]	[z/D]
1	-1	0	0.75
2	-0.5	0	0.75
3	0	0	0.75
4	0.5	0	0.75
5	1	0	0.75
6	1.5	0	0..75
7	2	0	0.75

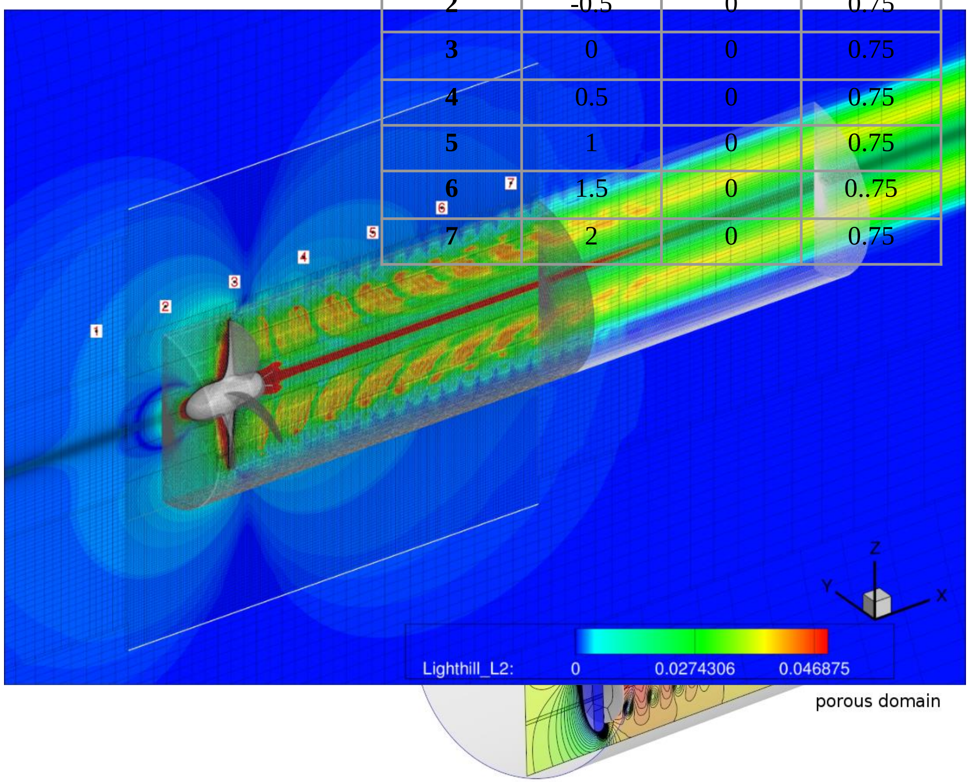

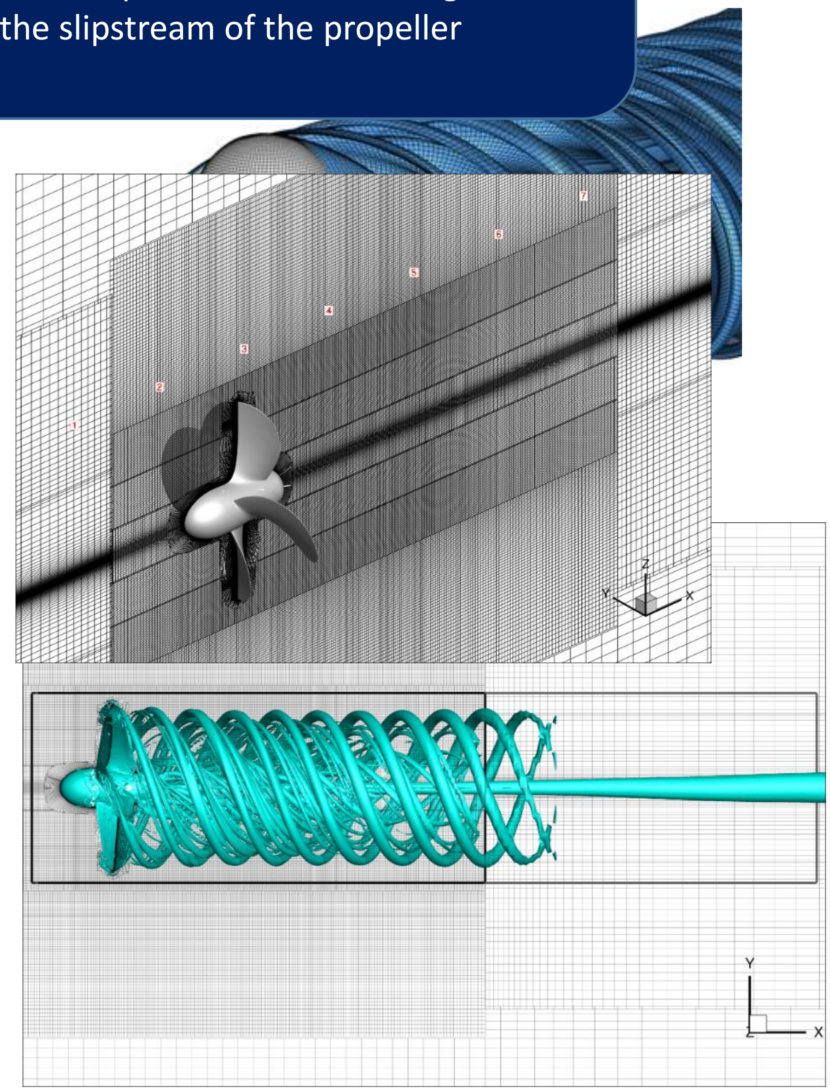

Genesis of FWH-P Hydrodynamic data

- **CFD & BEM** based on **incompressible solvers**. Well suited to yield input data on the porous surface

- **CFD pressure signatures** are **NOT SOUND** in that determined by the overlapping of signals emitted istantaneously by the hydrodynamic sources on the blades and in the flowfield. However, [1] and [2] demonstrate how the numerical differences are totally negligible in the near field

- **Running-averaged solution:** phase-locked averaging process of the unsteady hydrodynamic flowfield, yielding a vortical flow filtered by any turbulence-induced effect

- **DES averaged** solution is **different** from the RANSE one because of the inherently different solution strategy

- **DES averaged** field may detect important vorticity contributions due to **complex interactions among vortices** occurring during propeller revolution (if any) that, locally, may give rise to stronger vortex structures inducing higher level of noise behind the propeller disk

[1] Testa C., Ianniello S., Salvatore F., Gennaretti M., "Numerical Approaches for Hydroacoustic Analysis of Marine Propellers", JSR-10-06-0049.R1, Journal of Ship Research, 2007.

[2] Ianniello, S., Muscari, R., Di Mascio, A. (2013). 'Ship underwater noise through the acoustic analogy Part I: Nonlinear analysis of a marine propeller in a uniform flow", J. Mar. Sci. Tech., 18, pp. 547-570.

(…Cont'd)

Comparison among noise signals predicted by **DES, FWH-P/BEM** and **FWH-P/DES** computations during a propeller revolution. Running-averaged DES data are here considered.

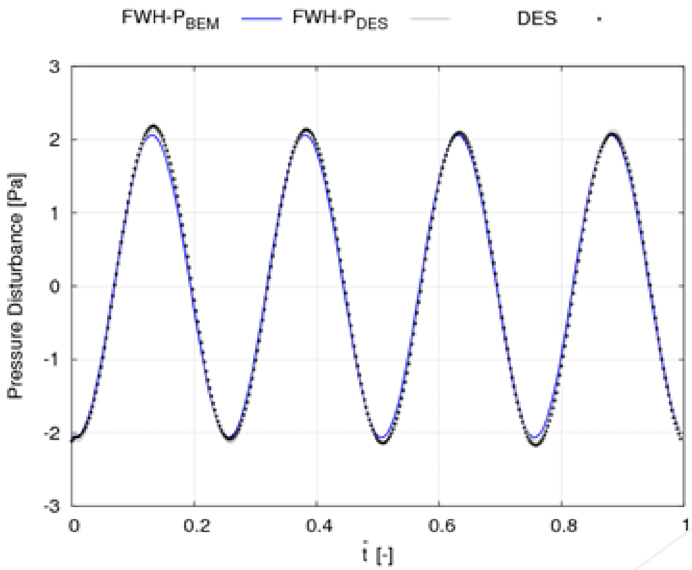

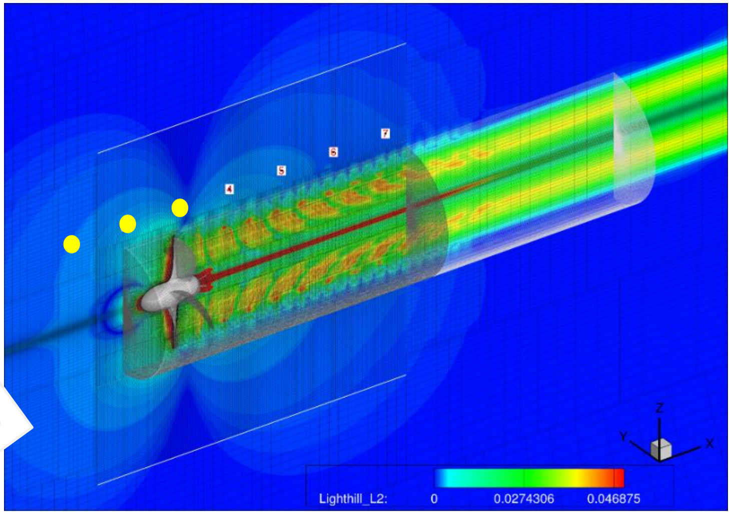

Averaged DES Data

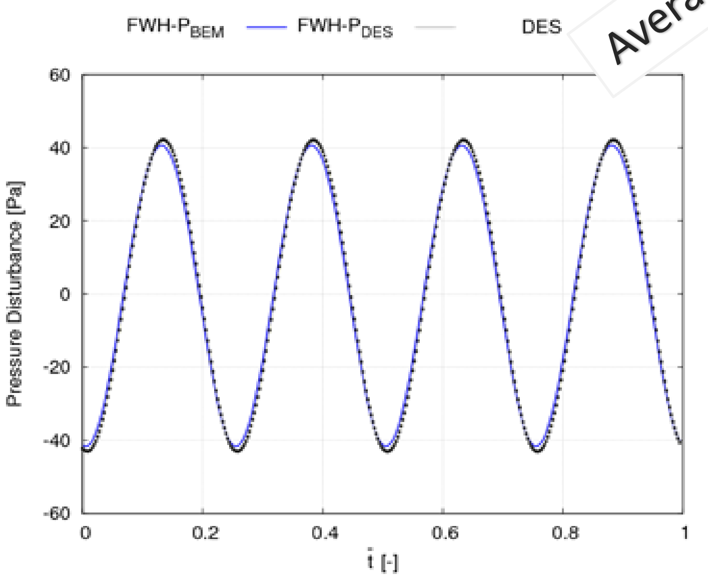

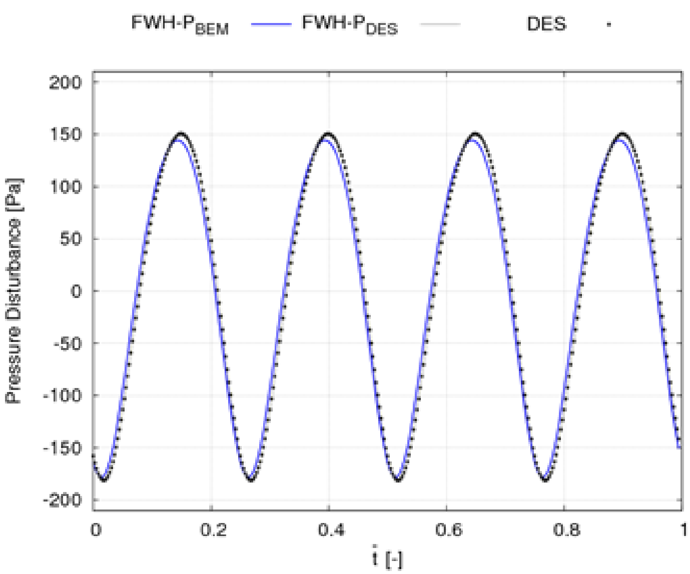

(…Cont'd)

Comparison among noise signals predicted by DES, FWH-P/BEM and FWH-P/DES computations during a propeller revolution. Running-averaged DES data are here considered.

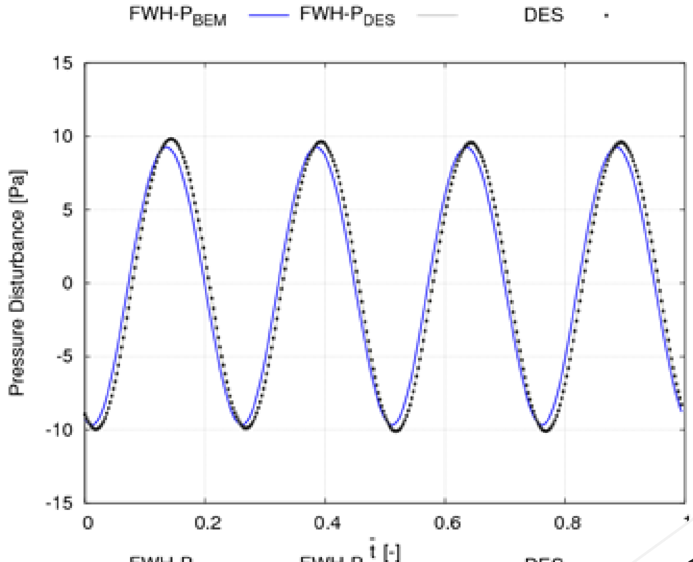

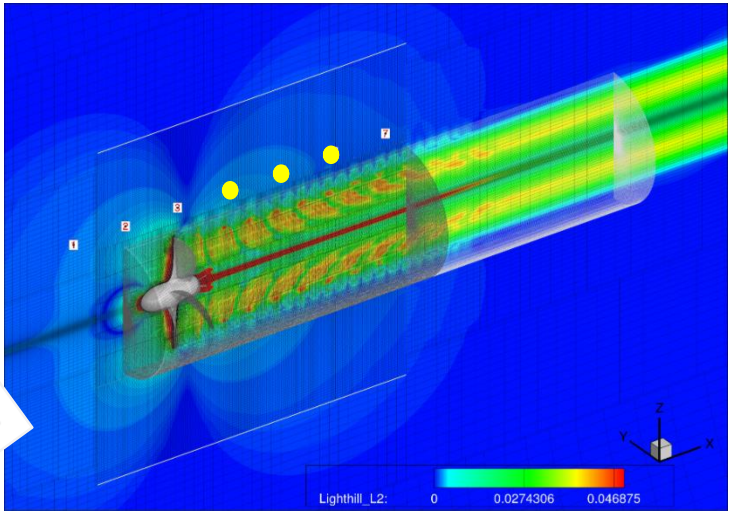

Averaged DES Data

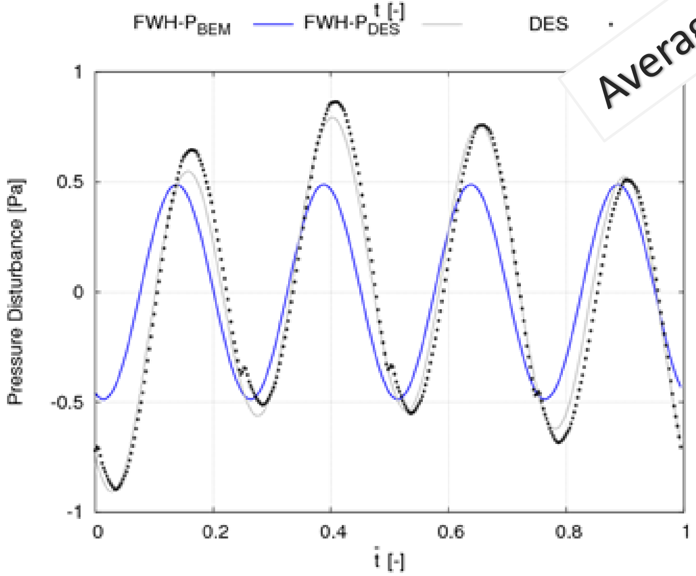

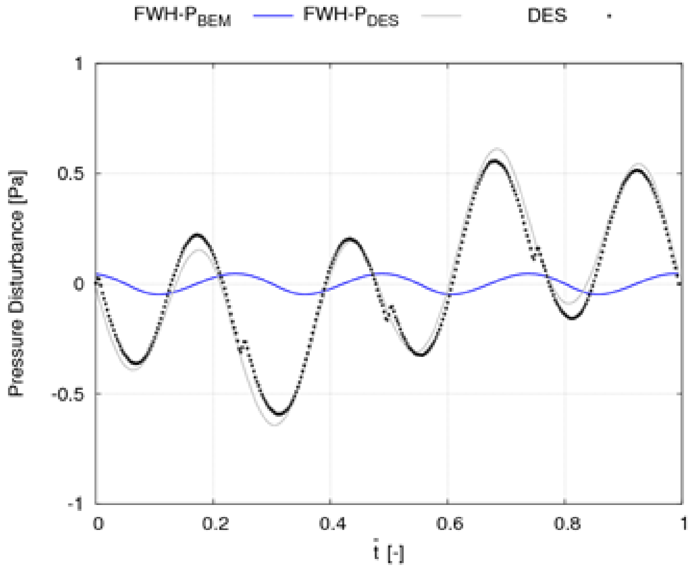

(…Cont'd)

Comparison among noise signals predicted by DES, FWH-P/BEM and FWH-P/DES computations during a propeller revolution. Running-averaged DES data are here considered

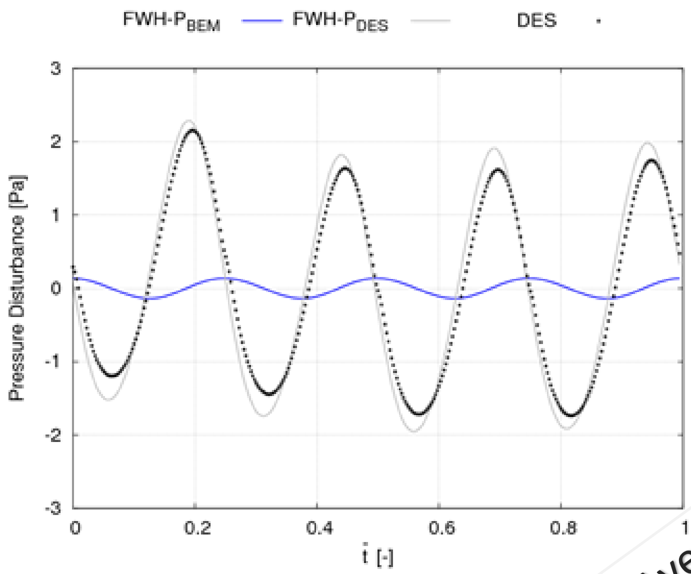

Averaged DES Data

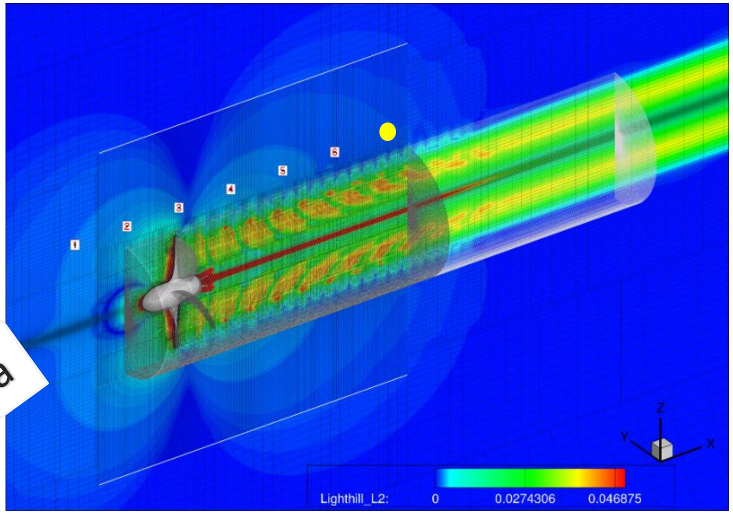

- *Within a longitudinal distance of 0.5 ÷1D from the hub, propeller hydroacoustics is dominated by potential wake vorticity effects ➤ BEM ☺*
- *However, moving downstream, the DES averaged field detects important vorticity contributions that deeply modify the overall sound*
- *Although averaged, these contributions are the results of complex interactions among vortices occurring during propeller revolution, that, locally, may give rise to stronger vortex structures inducing higher level of noise behind the disk*
- *Look at Obs7 where the noise magnitude is almost 5 times greater than at Obs6 located one radius upstream*

(…Cont'd)

Comparison among noise spectra predicted by DES, FWH-P/BEM and FWH-P/DES computations

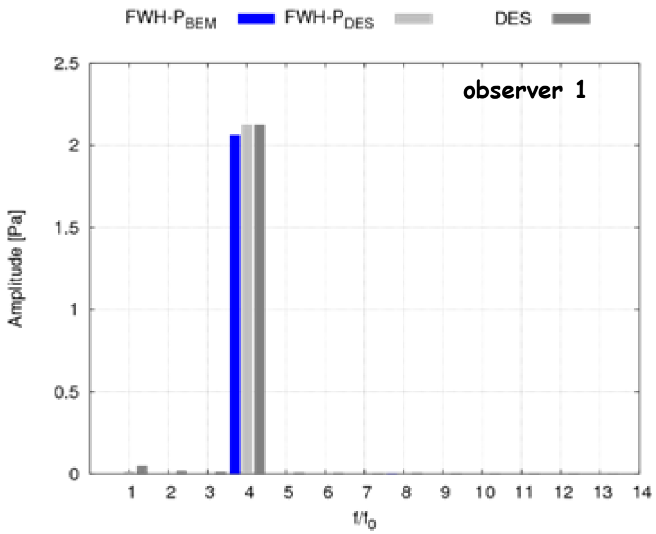

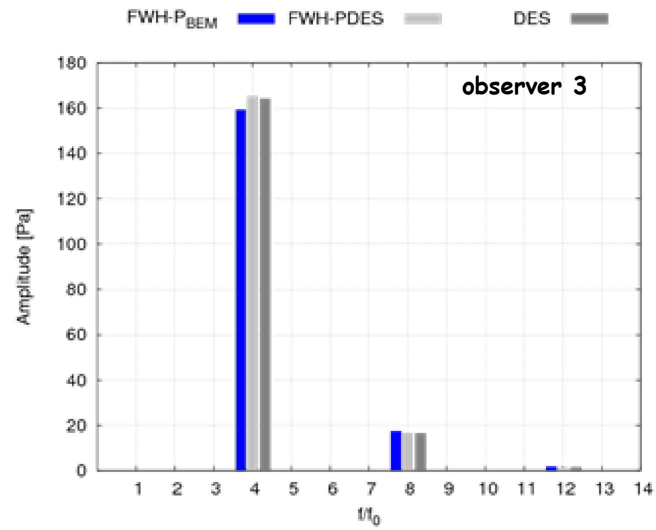

Tonal behaviour

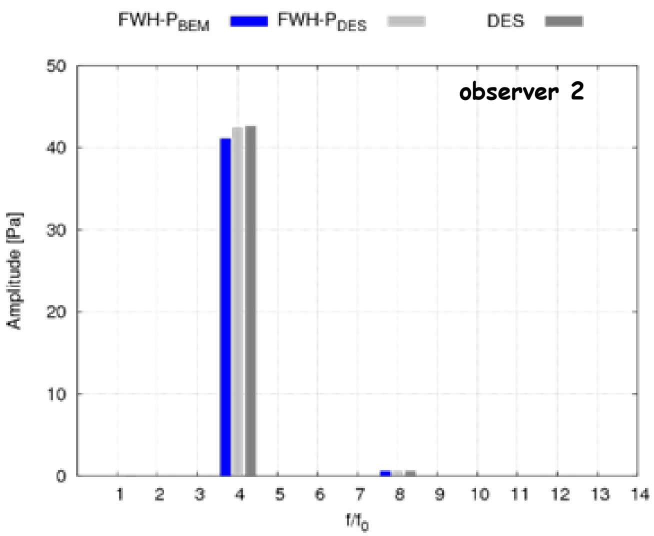

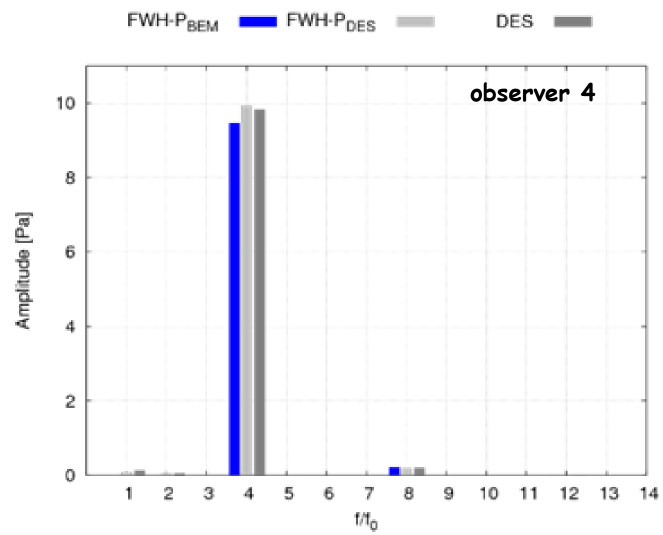

Comparison among noise spectra predicted by DES, FWH-P/BEM and FWH-P/DES computations

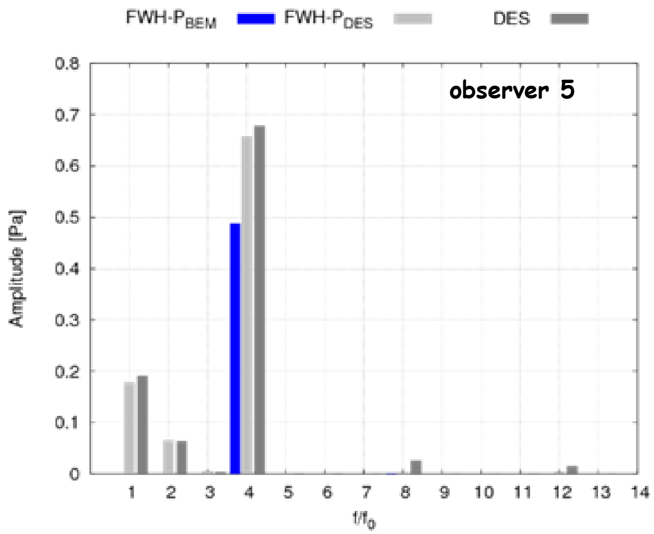

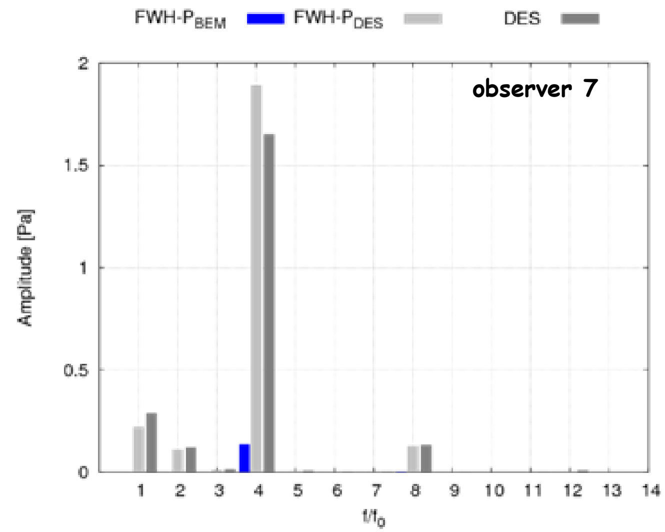

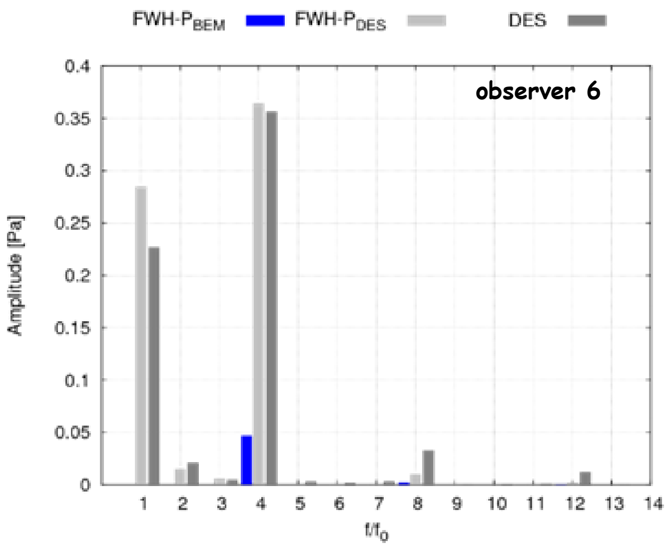

Relevant contribution from the shaft frequency f_0

Comparison among noise signals predicted by DES, FWH-P/BEM and FWH-P/DES computations during a propeller revolution. Unsteady DES data are used

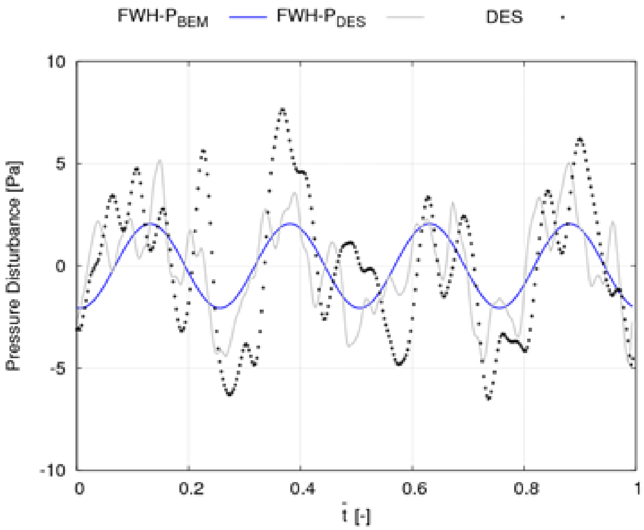

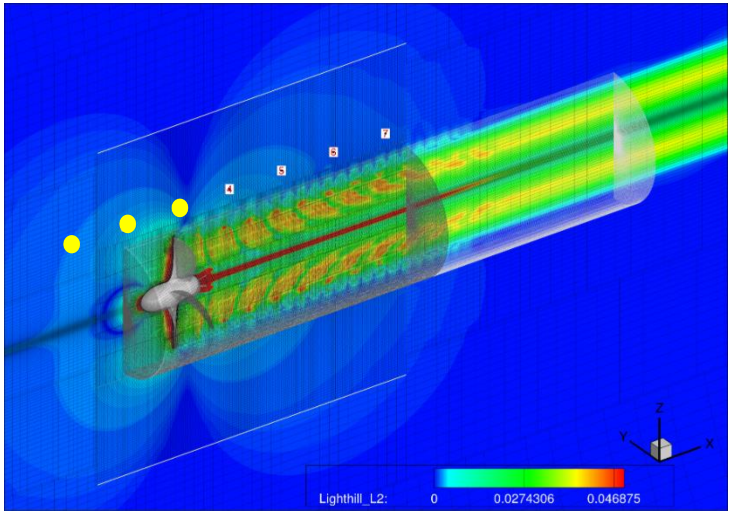

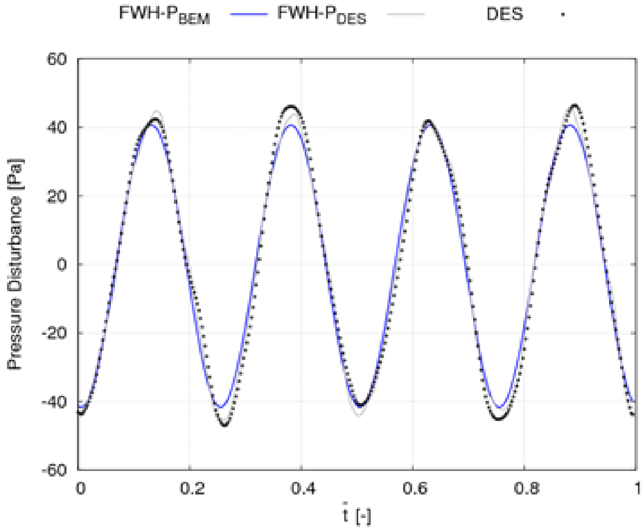

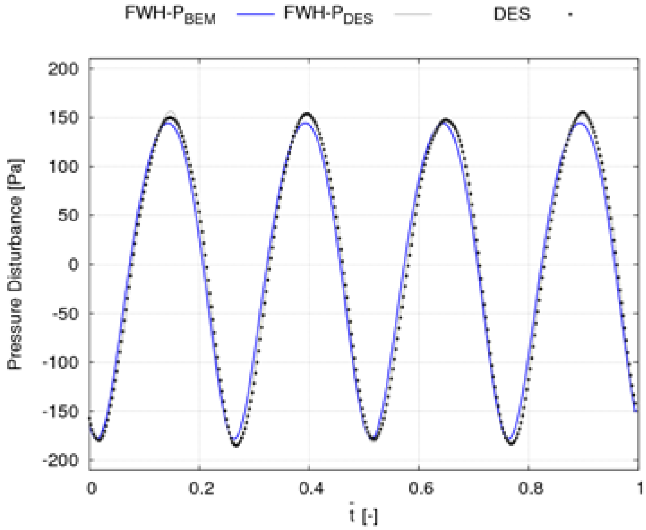

Comparison among noise signals predicted by DES, FWH-P/BEM and FWH-P/DES computations during a propeller revolution. Unsteady DES data are used

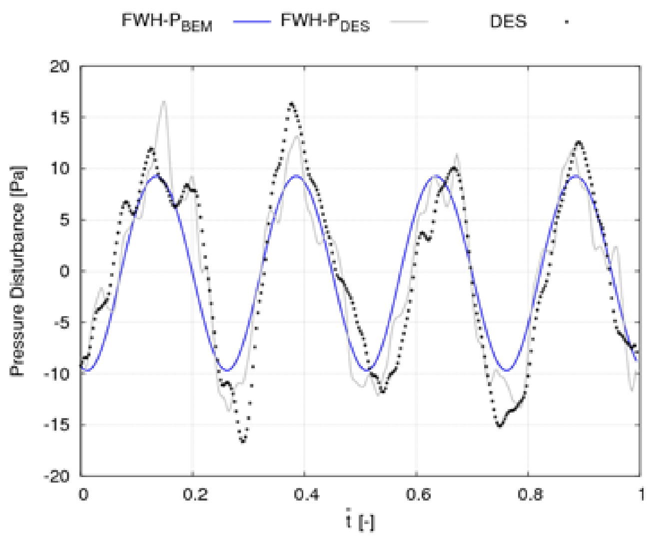

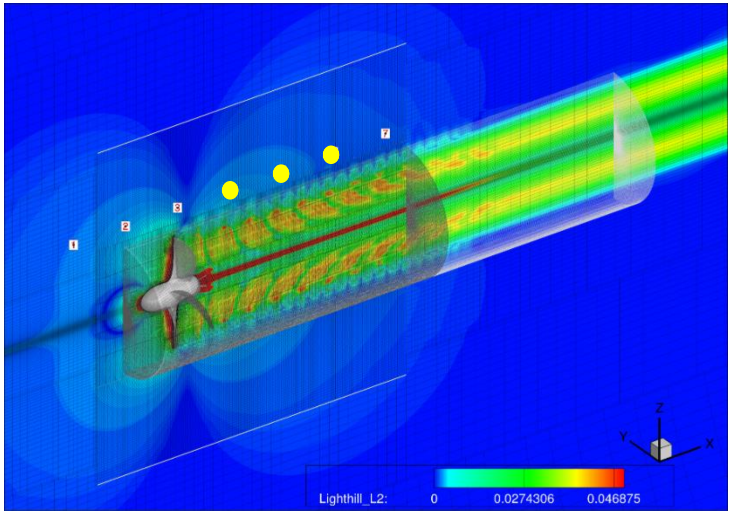

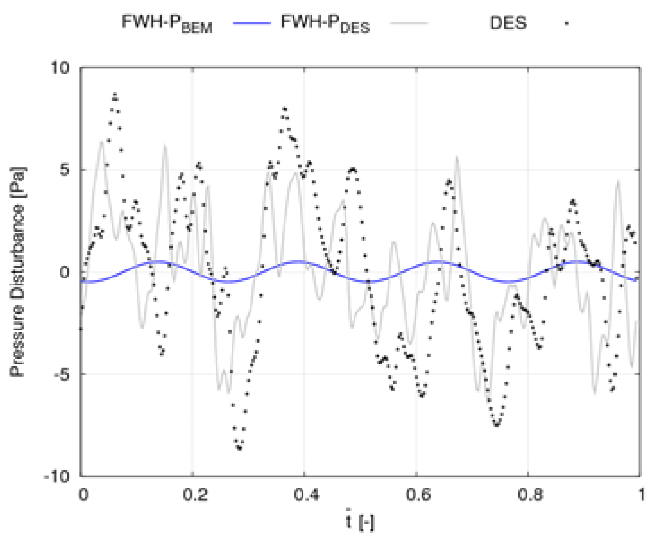

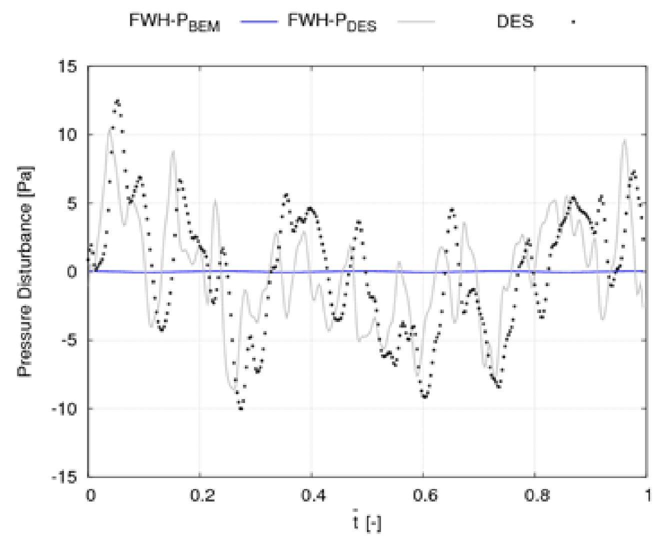

(…Cont'd)

Comparison among noise signals predicted by DES, FWH-P/BEM and FWH-P/DES computations during a propeller revolution. Unsteady DES data are used

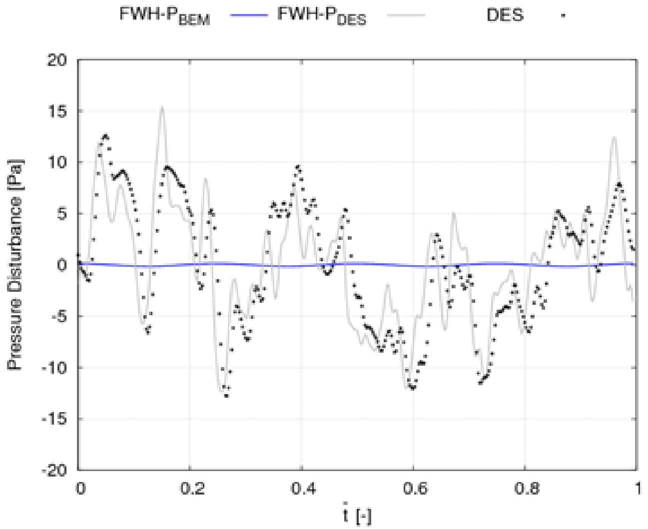

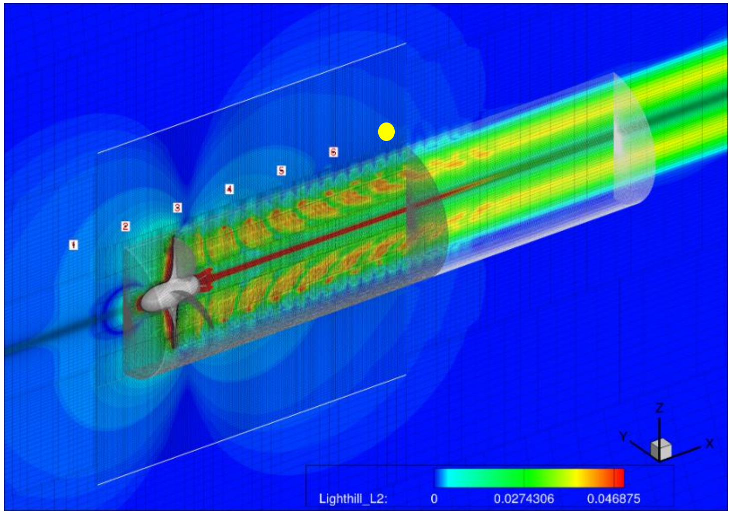

- *FWH-P/DES computations include turbulence-induced noise effects; they are consistent with or oscillate about FWH-P/BEM predictions, at least up to Obs4 ▶ BEM ☺*
- *At Obs1 and Obs5, the low level of pressure fluctuations from the direct DES simulation emphasizes the effects caused by reflections of disturbances from the boundaries of the numerical domain ▶ hard issue for CFD (incompr) solvers oriented to performance*
- *At Obs2 and Obs3, turbulence-induced noise is almost negligible, since the waveforms, noise levels and frequency content of the overall sound are very similar to those predicted by the running averaged technique*
- *At Obs4, turbulence sources of sound determine a distortion of the signal; differently form Obs2 and Obs3, the spectrum highlights acoustic energy spread out over all the harmonics herein analyzed. Nevertheless, the FWH-P/BEM signal captures the main features of the noise and provides a sort of average signature about which the FWH-P/DES prediction oscillates*
- *Akin to the running-averaged case, from Obs5 on, the comparison between signals is no more reasonable; broadband noise due to flowfield vorticity and turbulence is exhibited and the 1BPF is also not well captured by the FWH-P/BEM approach ☹*

(…Cont’d)

Comparison among noise spectra predicted by DES, FWH-P/BEM and FWH-P/DES computations

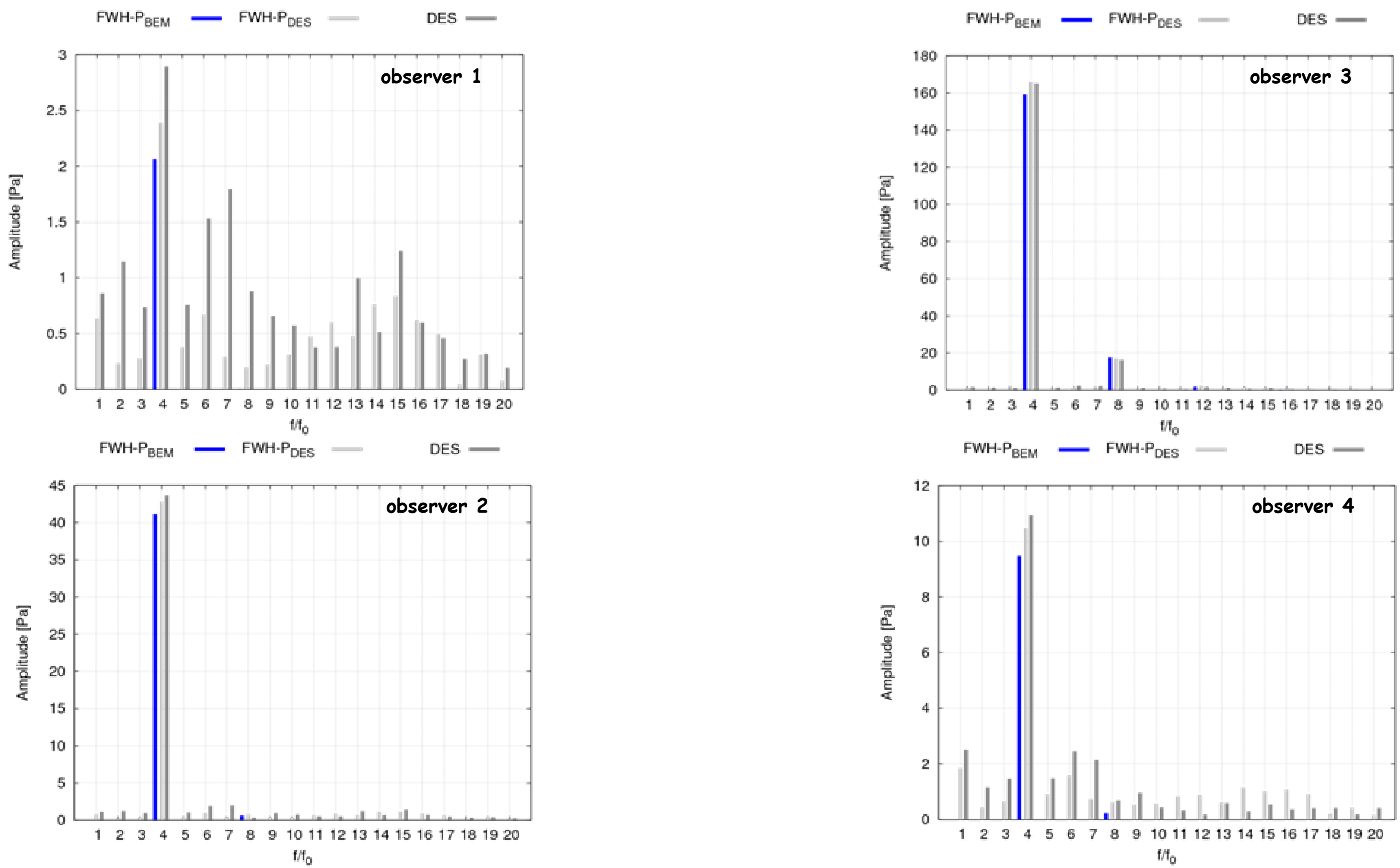

(…Cont’d)

Comparison among noise spectra predicted by DES, FWH-P/BEM and FWH-P/DES computations

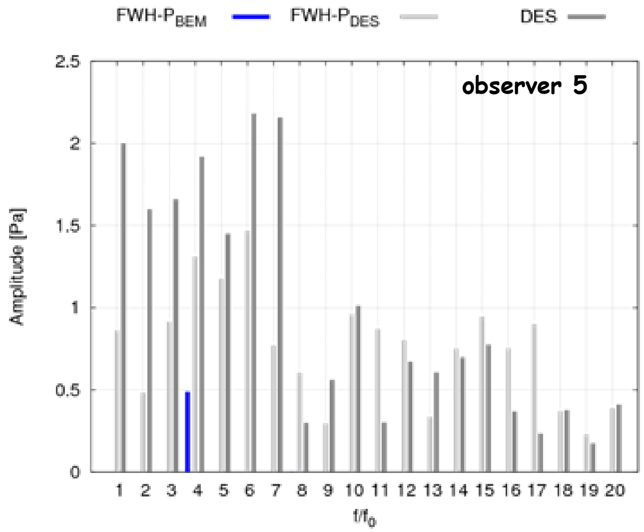

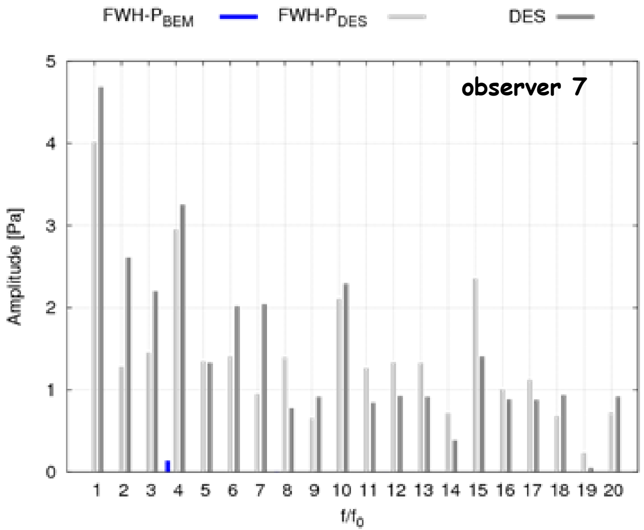

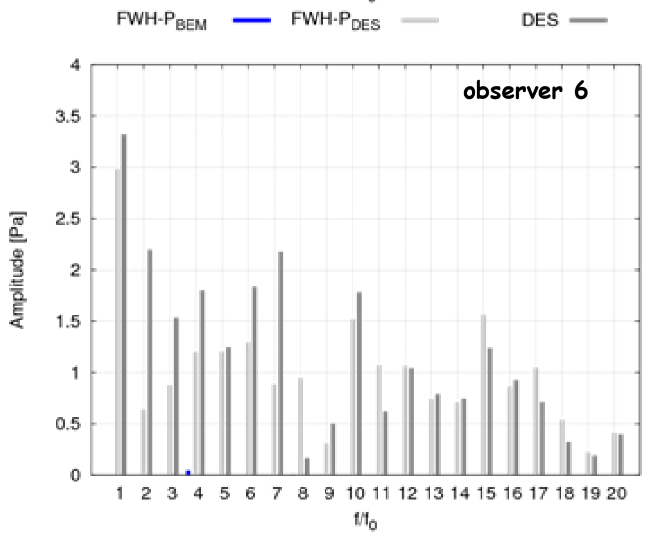

Concluding Remarks & Future Work

- BEM hydrodynamics is adequate to capture the tonal sources of sound due to cyclic blade passages and trailing vortices convected downstream. Limiting to observers placed **upstream and downstream up to 0.5÷1 diameter far from the disk,** FWH-P/BEM signatures well match FWH-P/DES results obtained by a running-average post-processing of the DES solution.

- Since this technique inherently filters out any turbulence-induced effect by the definition of a mean-vorticity field, it is proven that **propeller hydroacoustics is dominated by potential wake vorticity effects**.

- **Moving downstream**, DES averaged field detects important **vorticity contributions** that deeply modify the overall sound. These **are completely lost** by the BEM-based detection.

- Within the same range, **similar conclusions hold** for the comparison between FWH-P/BEM signatures and FWH-P/DES results obtained by an **unsteady DES simulation**.

- It is shown that, in presence of turbulence-induced noise effects, FWH-P/BEM predictions **are in good agreement** with FWH-P/DES outcomes or represent **a sort of mean noise signal** for FWH-P/DES predictions.

- Moving **downstream**, the not modeled turbulent structures, evolving in the wake, make the use of **BEM hydrodynamics data inadequate** for any hydroacoustic investigation.

- The above results are **preliminary.** More advancing ratios should be investigated to define a sort of admissible distance from the hub where BEM hydrodynamics is able to detect the sources of tonal noise generated by a propeller.
- In view of the higher blade(s) load and more intense wake, **it is expected a a crucial role of the turbulent structures** and, in turns, a **more limited range of BEM hydrodynamics data validity**.

Thanks for your Attention

A. Yücel Odabaşı Colloquium Series

3rd International Meeting

15-16 November 2018
Istanbul, Turkey

Progress in Propeller Cavitation and its Consequences: Experimental and Computational Methods for Predictions

in conjuction with

The Inauguration of ITU Cavitation Tunnel (ITU-CAT)

Parametric Study of a Pre-swirl Stator for a Tanker

Zeynep TACAR & Emin KORKUT
Istanbul Technical University

Nov. 16, 2018

Layout

1. Introduction
2. Objectives
3. Specifications of the Ship and the Propeller
4. Design Parameters of the PSS
5. Computational Study
6. Results & Discussion
7. Conclusion

Introduction

Pre-swirl stators are the passive fin systems located before the propeller to generate a swirling flow opposite to the rotation direction of the propeller in order to reduce the rotational losses.

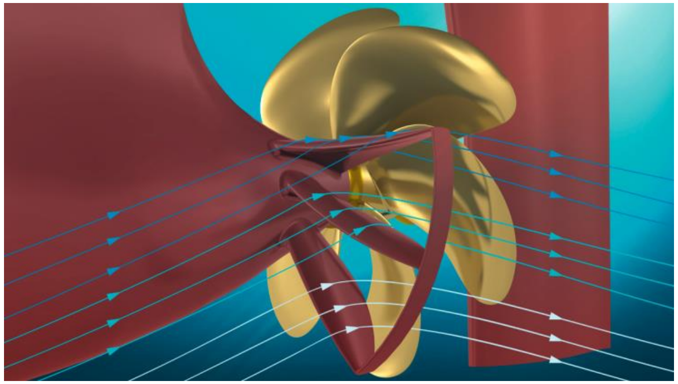

EnergoFlow (Wartsila)

Biased Pre-swirl Stator Attached to 300K KVLCC model (Pusan University)

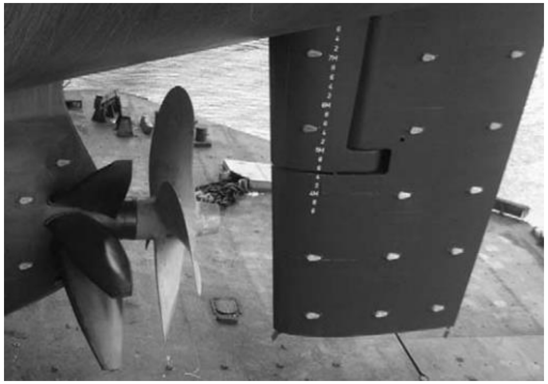

Bulk Carrier with the PSS (MARIN & HSVA)

Objectives

- To improve the flow characterictics at the propeller plane
- Increase the quasi proulsive coefficient, QPC
- Compare relatively the effects of design parameters of PSS :
    - number of the stator blades,
    - angular position of the stator blades
    - the pitch angles of the stator blades

  on the propulsive coefficients and try to get some insight into the phenomenon.

Our Study

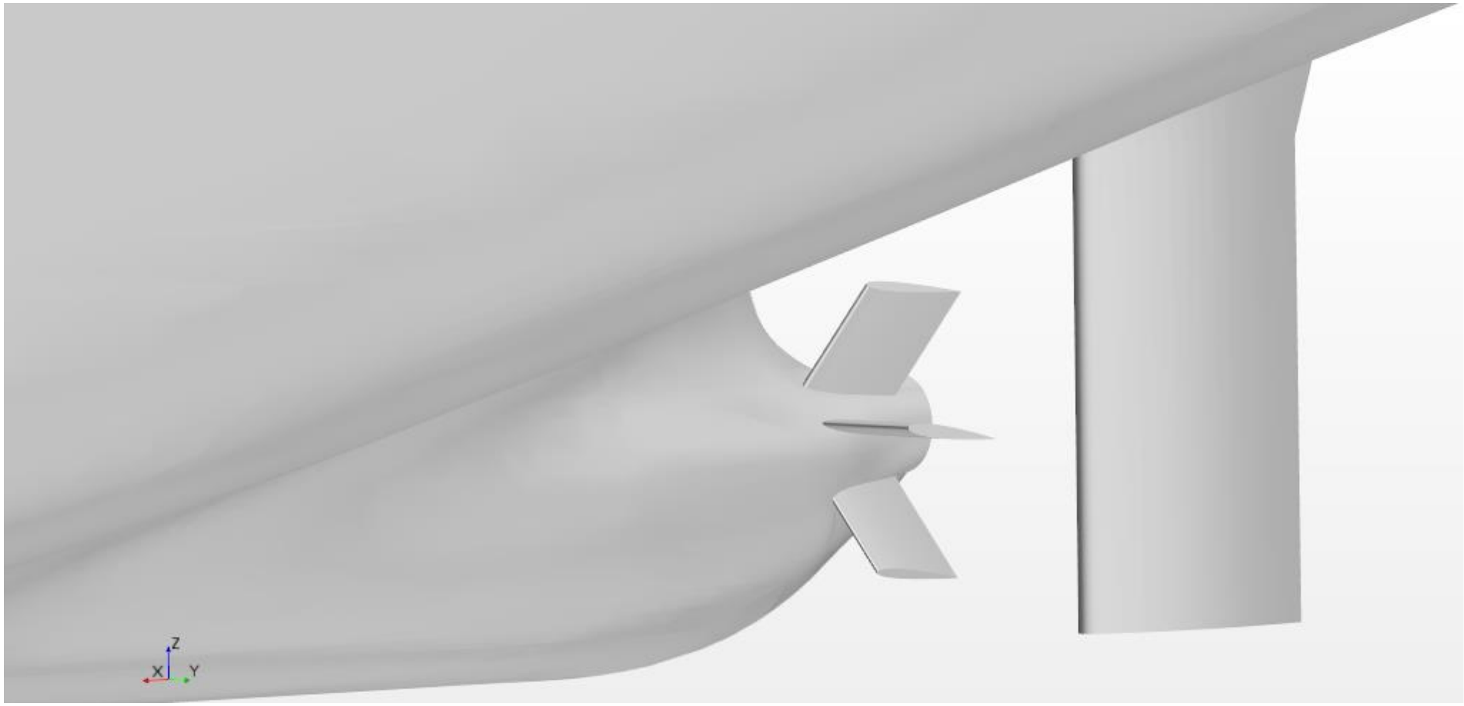

This study is part of a Ph.D. study of the principal author and the paper presents the preliminary results of the parametric study of an Pre-swirl stator.

Specifications of the Ship

Specifications of the INSEAN 7000DWT Tanker

Specification	Full Scale	Model Scale (λ = 16.5)
Length between perpendicular, LPP [m]	94.0	5.697
Length of waterline, LWL [m]	96.753	5.864
Beam, overall, BOA [m]	15.422	0.935
Draft [m]	6.005	0.364
Displacement, ∇ [m^3]	6820.6	1.518
Block coefficient, C_B	0.762	0.762
Number of propellers	1	1
Service speed, V_s	14 knots	1.773 m/s
Froude Number	0.23	0.23
Reynolds Number	6.123×10^8	9.136×10^6

Specifications of the Ship

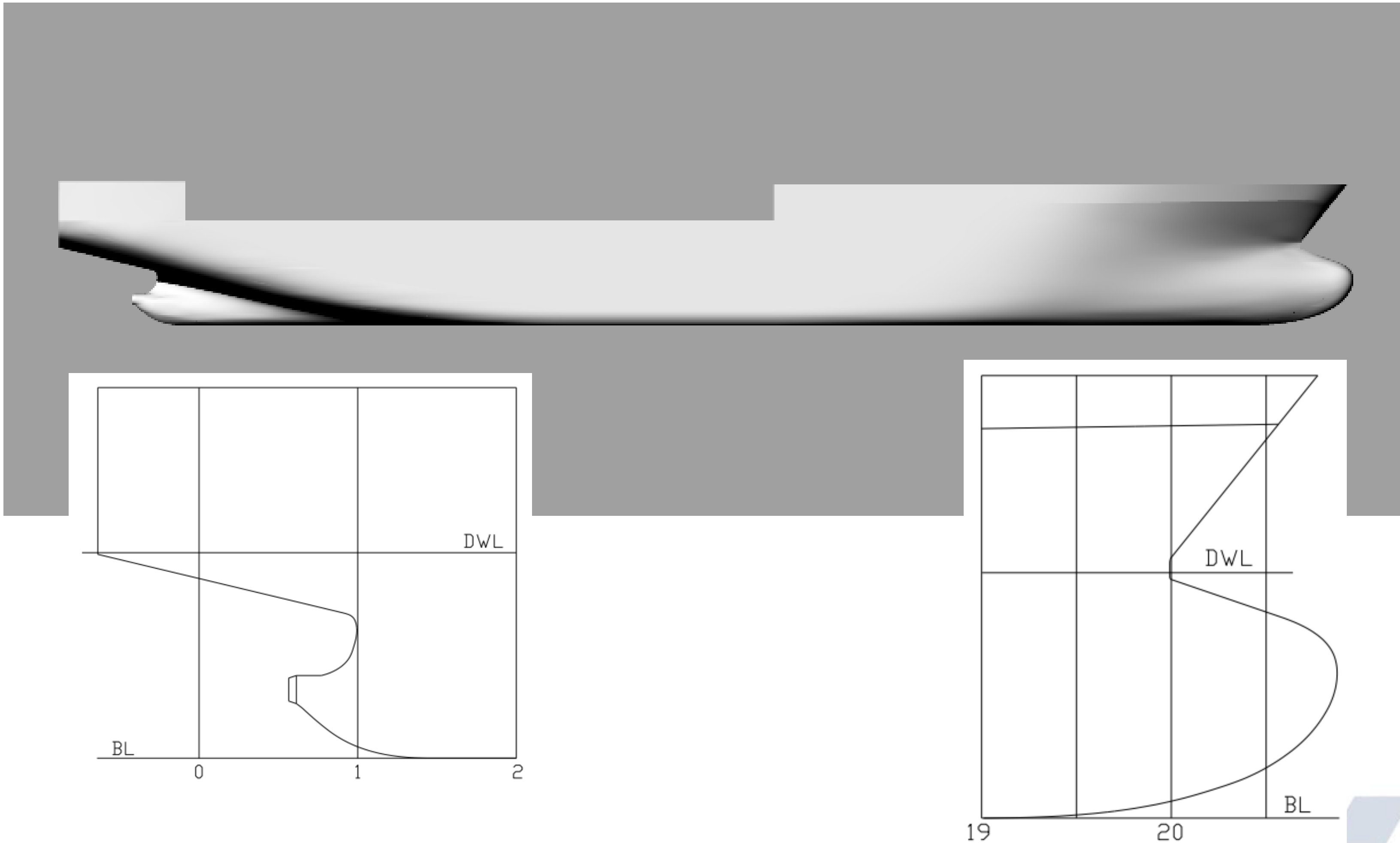

Specifications of the Propeller

İTÜ

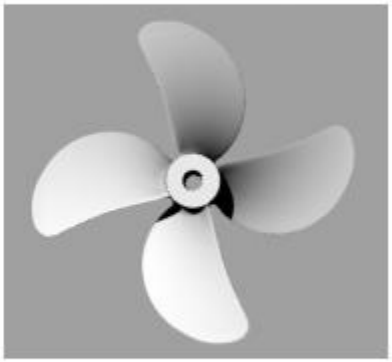

E1637 Propeller
Tests: CNR-INSEAN (towing tank)
220m x 9m x 3.8 m
Kempf & Remmers type H29 dynamometer

Property	Full Scale	Model Scale
Diameter [m]	3.85	0.233
Number of Blades	4	4
Nominal Pitch Ratio (P/D 0.75R)	1.0	1.0
Skew Angle [deg]	3.0	3.0
Expanded Area Ratio (EAR)	0.58	0.58
Boss Diameter Ratio (DH/DP)(at propeller disc)	0.168	0.168

PSS Design

Parameter	
Diameter	0.9Dp
Chord Length of the blade section	0.25Dp
X-Location	0.3Dp upstream of the propeller plane
Blade Section	NACA 0012

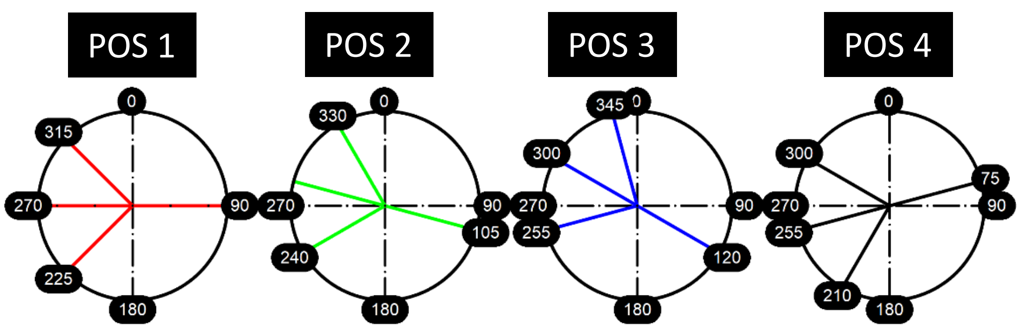

Case	Blade Pitch Angle (°)					
	PU	PC	PL	SC		Angular Position
1	0	0	0	0	all blades	POS 1
2	0	0	0	-	wo SC	
3	0	0	0	0	half SC	
4	-	0	0	0	wo PU	
5	0	0	0	-	wo SC	POS 2
6	0	0	0	-	wo SC	POS 3
7	0	0	0	-	wo SC	POS 4
8	4	0	0	-	wo SC	POS 1
9	-4	0	0	-	wo SC	
10	-8	0	0	-	wo SC	
11	-8	4	0	-	wo SC	
12	-8	-4	0	-	wo SC	
13	-8	-8	0	-	wo SC	
14	-8	-8	-4	-	wo SC	
15	-8	-8	-4	-	wo SC	
16	-8	-8	-8	-	wo SC	

Computational Study-1

Domain Used In The CFD Analyses

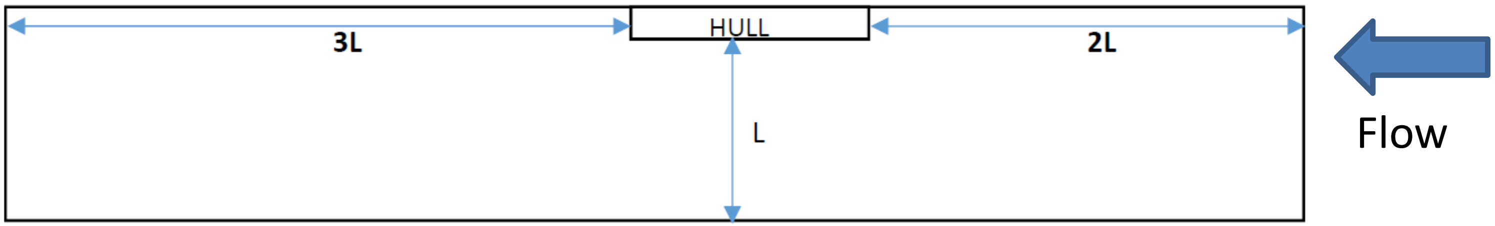

Profile View of the Domain

Methods Used In The Following CFD Analyses

- Double body (ignoring free surface effects)
- RANS equations, segregatedly solved
- SST k-ω turbulence model
- Virtual Disk Model (in self-propulsion analyses)

Computational Study-2

Grid Generation

- Cartesian cut cell method
- y+ < 5
- 8 prism layers, 1.45 stretching ratio
- 1.82 M cells

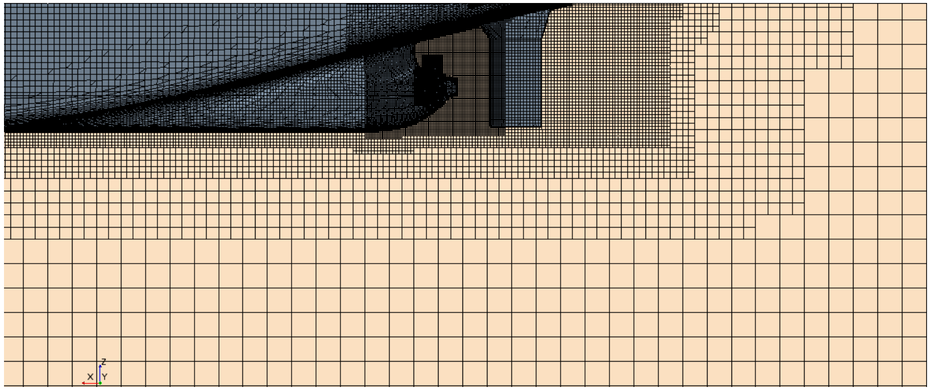

General Mesh View

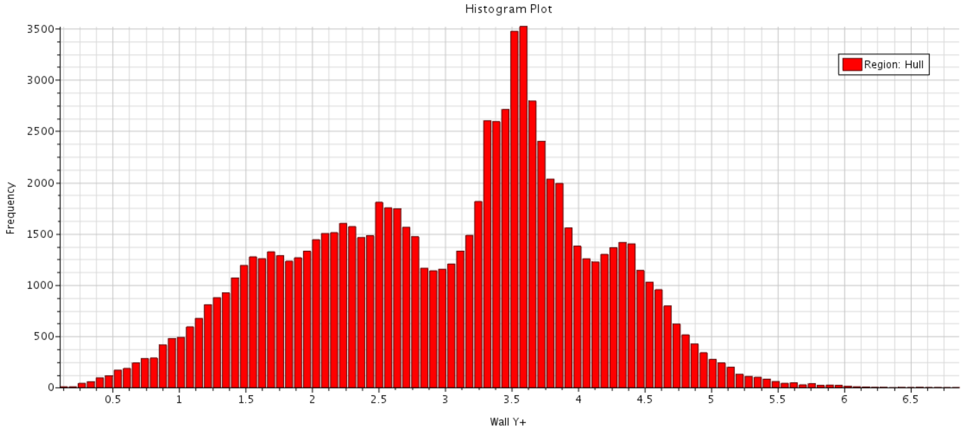

y+ Distribution on the Hull Surface

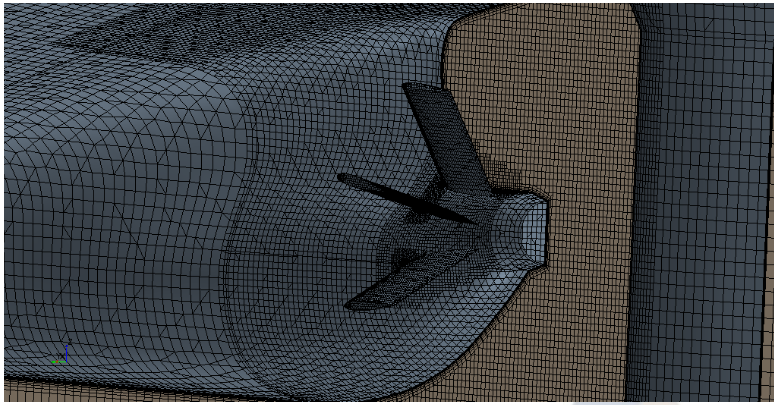

Aft Part of the Hull

Computational Study-3

Analysis of the Bare Hull (without propeller and stator)

$$C_R = C_{TM} - C_{VM} = C_{TM} - (1+k)C_{FM}$$

$$R_R = \frac{1}{2}\rho_M V_M^{\ 2} S_M C_R$$

$$R_{VM} = R_{TM} - R_{RM}$$

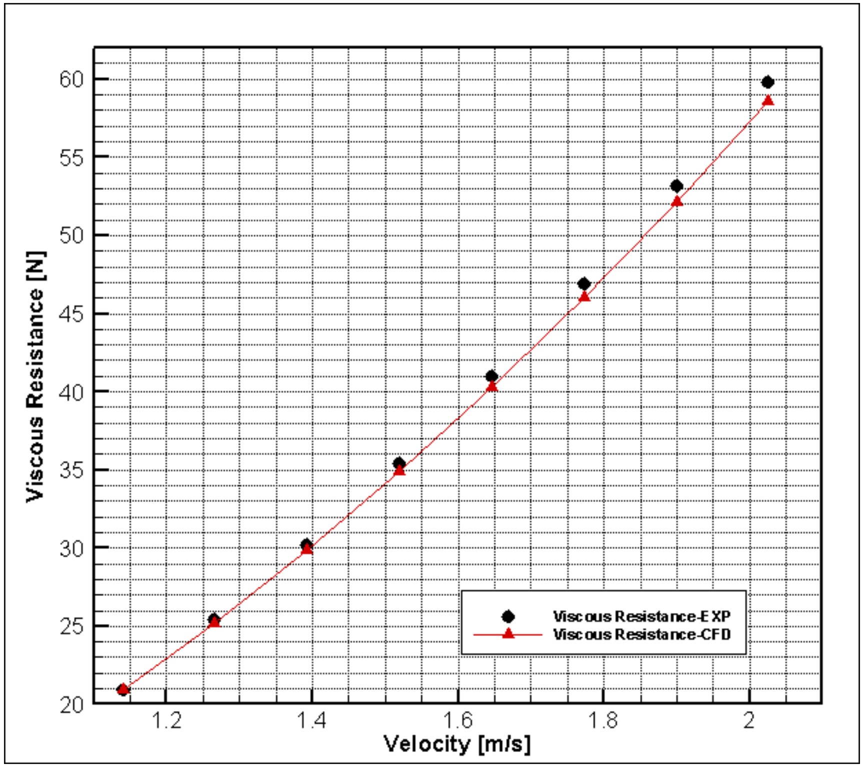

Max % difference with experimental results is 2.08% at the highest speed (Vm=2.026 m/s)

Computational Study-4

Resistance Analysis of the Hull with stator

- 2.2 M cells were used in the resistance analyses with stator blades
- Stator blades caused 0.92-3.73% increment in towed resistance comparing to the bare hull condition

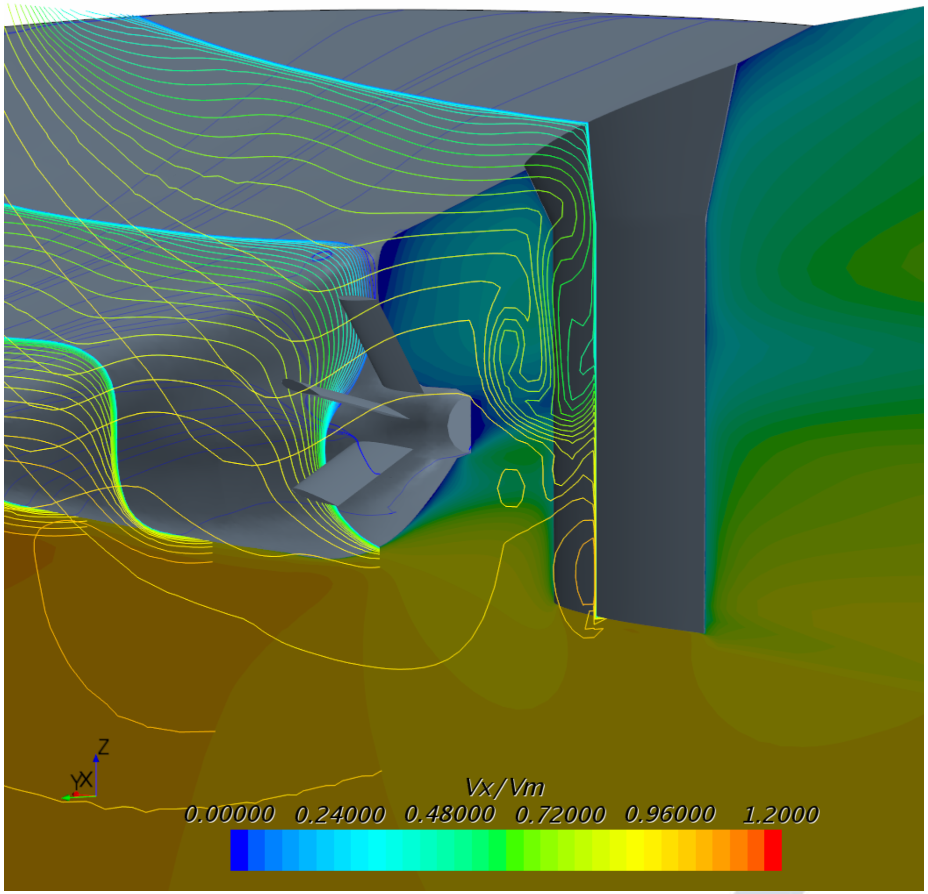

Axial Velocity Distribution at the Frames in the Aft Region

Computational Study-5

Self-Propulsion Analyses

- Actuator disk (virtual disk) was used
- 3 different rate of revolutions (n= 8, 8.2, 8.4 rps)
- Body Force Propeller Method was used
- Open water curves obtained from open water tests were used
- Rotation rate at self-propulsion point was determined by linear regression

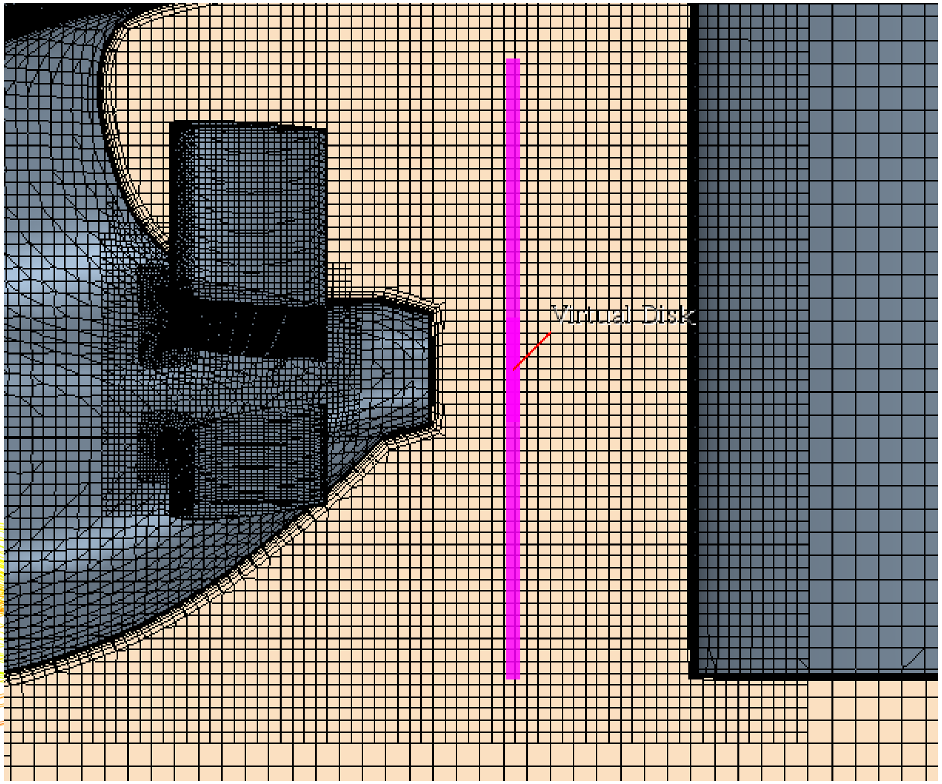

Representation of Virtual Disk at the Propeller Plane

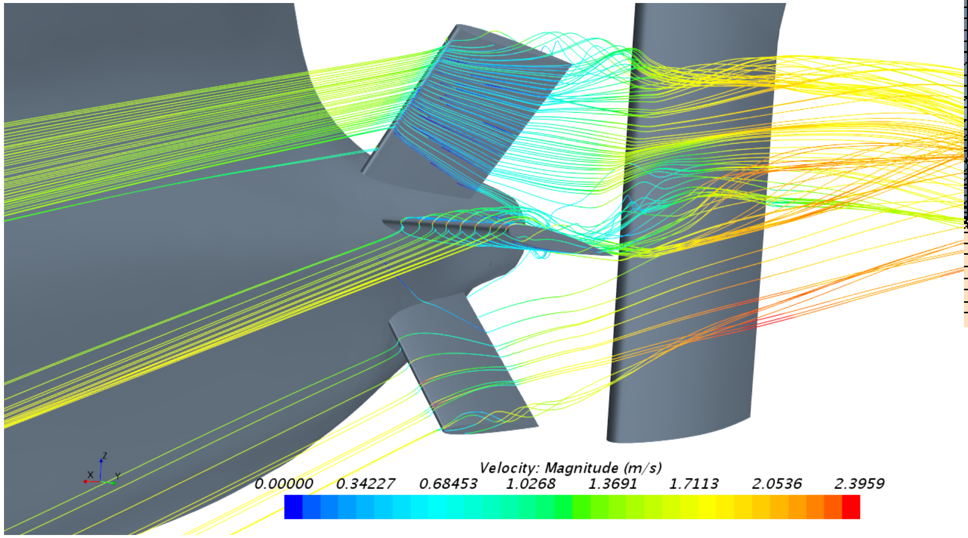

Streamlines on Stator Blades for the Optimum PSS Configuration

Computational Study-6

Velocity Vectors at 0.06 Dp Upstream of the Propeller Plane- with stator

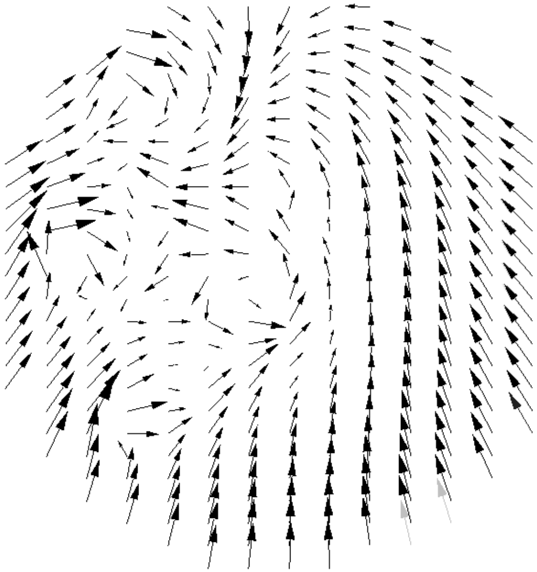

Velocity Vectors at 0.06 Dp Upstream of the Propeller Plane- without stator

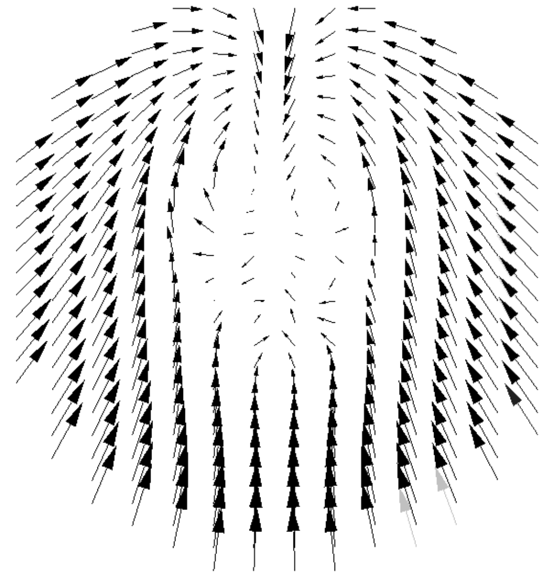

Velocity Vectors at 0.06 Dp Downstream of the Propeller Plane- with stator

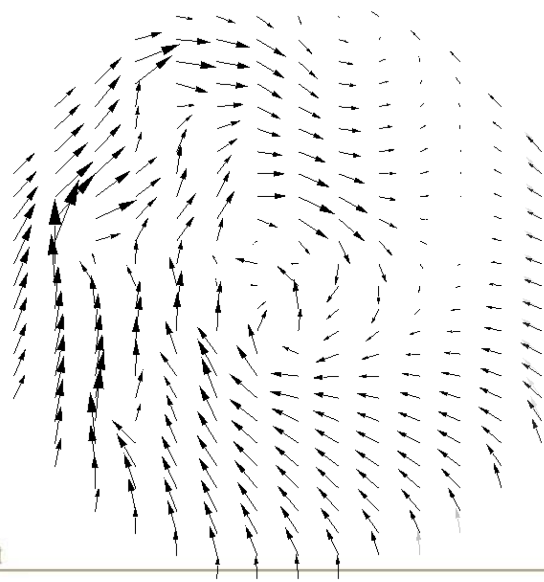

Velocity Vectors at 0.06 Dp Downstream of the Propeller Plane- without stator

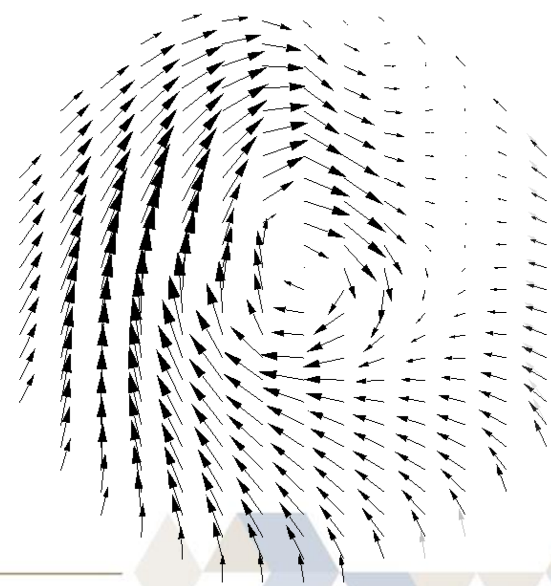

Results & Discussion

Effect of the number of the blades on efficiencies in Position 1

Case	n [rps]	η_{0T}	w_{tT}	t	η_H	η_R	η_D	$\%\eta_D$	
no PSS	8.245	0.650	0.206	0.181	1.031	0.9880	0.662		
1	8.241	0.649	0.209	0.174	1.045	0.9880	0.670	1.22	**all blades**
2	8.209	0.649	0.212	0.174	1.048	0.9880	0.672	1.59	**wo SC**
3	8.214	0.649	0.211	0.174	1.047	0.9880	0.672	1.48	**half SC**
4	8.247	0.650	0.207	0.174	1.042	0.9880	0.669	1.00	**wo PU**

Results & Discussion

Effect of the angular blade positions on efficiencies

Case	n [rps]	η_{0T}	w_{tT}	t	η_H	η_R	η_D	$\%\eta_D$	
no PSS	8.245	0.650	0.206	0.181	1.031	0.988	0.662		
2	8.209	0.649	0.212	0.174	1.048	0.988	0.672	1.59	**woSC POS1**
5	8.209	0.650	0.211	0.174	1.048	0.988	0.673	1.60	**woSC POS2**
6	8.210	0.650	0.211	0.174	1.046	0.988	0.671	1.45	**woSC POS3**
7	8.213	0.649	0.211	0.173	1.048	0.988	0.672	1.60	**woSC POS4**

Results & Discussion

Effect of the blade pitch angles on efficiencies

Case	n [rps]	η_{0T}	w_{tT}	t	η_H	η_R	η_D	$\%\eta_D$	
no PSS	8.245	0.650	0.206	0.181	1.031	0.988	0.662		
2	8.209	0.649	0.212	0.174	1.048	0.988	0.672	1.59	**initial**
8	8.209	0.650	0.211	0.174	1.048	0.988	0.672	1.57	**PU4**
9	8.218	0.649	0.213	0.175	1.048	0.988	0.672	1.54	**PU-4**
10	8.225	0.648	0.215	0.175	1.051	0.989	0.673	1.69	**PU-8**
11	8.223	0.648	0.215	0.177	1.048	0.989	0.671	1.44	**PC4**
12	8.229	0.647	0.215	0.173	1.053	0.989	0.674	1.86	**PC-4**
13	8.237	0.646	0.218	0.172	1.060	0.989	0.678	2.36	**PC-8**
14	8.244	0.646	0.219	0.174	1.058	0.989	0.676	2.06	**PL4**
15	8.243	0.646	0.218	0.174	1.056	0.989	0.675	1.95	**PL-4**
16	8.239	0.646	0.218	0.170	1.061	0.990	0.678	2.50	**PL-8**

Conclusion

- The numerical method, RANS method with SST k-ω turbulence model applied here predicts well the resistance and propulsive factors with a reasonable accuracy.
- The optimum PSS was determined as the 3-bladed stator (without SC blade) located in Position 1 and with the blade pitch angle of -8°. The optimum PSS configuration indicates an increase in the propulsive efficiency, hence reduction in the fuel consumption of the ship.
- In order to obtain an increase in the propulsive efficiency of the ship the PSS should be installed around 0.3Dp before the propeller plane with a diameter of 0.9 Dp and 3 blades on port side with blade pitch angles of -8°.
- A further increase in the propulsive efficiency may be obtained by the combination of PSS with an energy saving duct, which requires a further study.
- A further study to include scale effect issues for the full-scale is recommended.

THANK YOU

A.Yücel ODABAŞI Colloquium Series
3rd International Meeting

The Effect of Extreme Trim Operation on Propeller Cavitation in Self-Propulsion Conditions

Authors: M. Maasch, O. Turan, S. Day

Matthias Maasch
Matthias.Maasch@strath.ac.uk

Agenda

- **Motivation**
- **Extreme Trim Concept**
- **Simulation Setup**
- **Loading Conditions**
- **Propulsion Results**
- **Cavitation Results**

Matthias Maasch
Matthias.Maasch@strath.ac.uk

Extreme Trim Concept: Motivation

- **LNG SHIP IS 300 M LONG**
- **72000 DWT capacity, 40,000 tonnes of Ballast and 20,000 tonnes Ballast even in fully laden condition**
- **Pressure to reduce GHG emissions through design and operations**
- **Study is sponsored by Shell Shipping and LR**
- **Main Focus is reduction of fuel consumption without affecting the reliability of ship structure and propulsion system**

Matthias Maasch
Matthias.Maasch@strath.ac.uk

Extreme Trim Concept

- **Extreme bow-up trim is applied to an LNG Carrier in ballast loading conditions (empty tanks)**

- **A minimum amount of ballast water is carried to submerge the propulsor**
- **Zero draft at the bow**

Matthias Maasch
Matthias.Maasch@strath.ac.uk

Extreme Trim Concept

- **Experimental model tests have shown a nominal resistance reduction of 25% at a moderate speed**

- **Experimental model tests in waves have shown an acceptable seakeeping performance at low and moderate speeds**

➢ **The present numerical study investigates the performance in self-propulsion conditions**

Kelvin Hydrodynamics Laboratory Glasgow

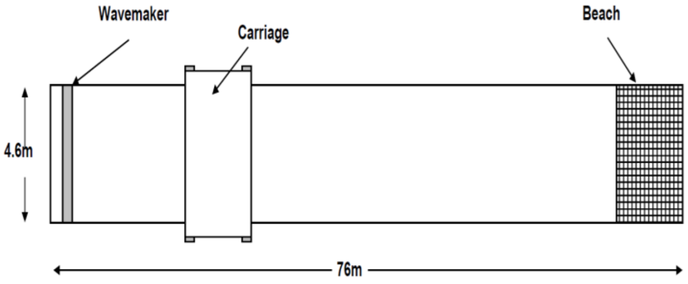

Matthias Maasch
Matthias.Maasch@strath.ac.uk

Simulation Setup

- **Various numerical marine applications were coupled for an automated simulation setup**

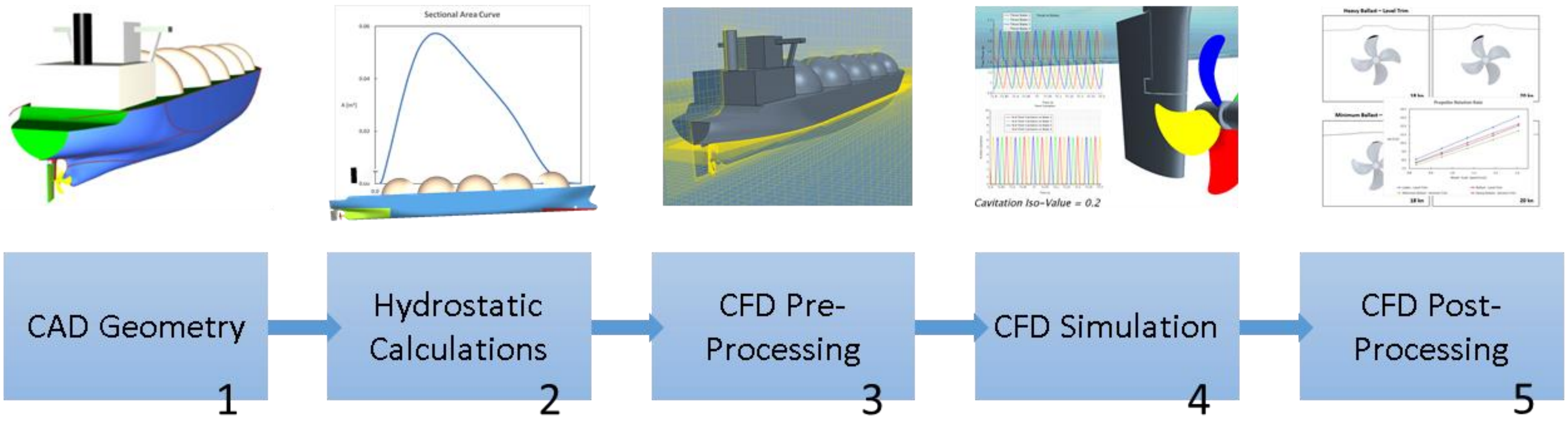

Matthias Maasch
Matthias.Maasch@strath.ac.uk

Simulation Setup

- **Box-shaped numerical domain with the ship in its centre**
- **Hexahedral cells in the static domain to properly capture the free surface**
- **Automatically adapting refinement regions around the hull and along the free surface**
- **7 million cells in total**

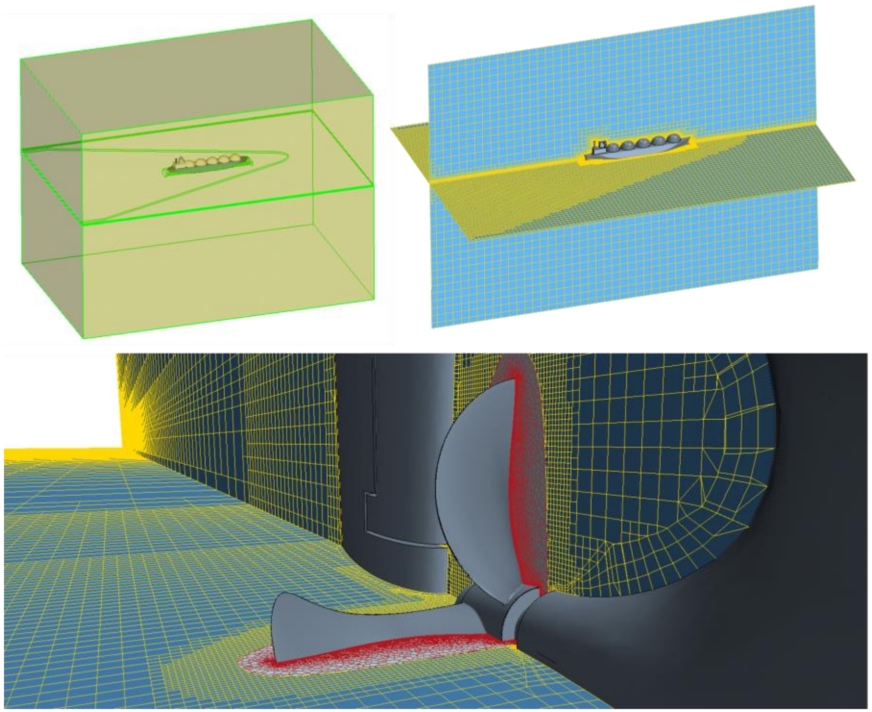

Matthias Maasch
Matthias.Maasch@strath.ac.uk

Simulation Setup

- **Polyhedral cells in the rotating domain**
- **4.3 million cells**
- **Very small cells at the propeller surface to capture cavitation**
- **Larger cells at the domain interface for better blend into static mesh**

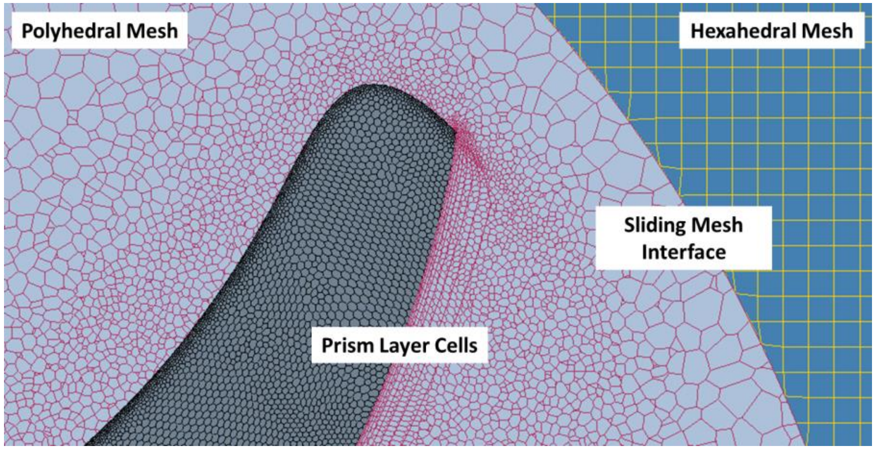

Matthias Maasch
Matthias.Maasch@strath.ac.uk

Simulation Setup

- **To ensure appropriate mesh and time step conditions for the flow solver, the Y+ and the Courant number were monitored**

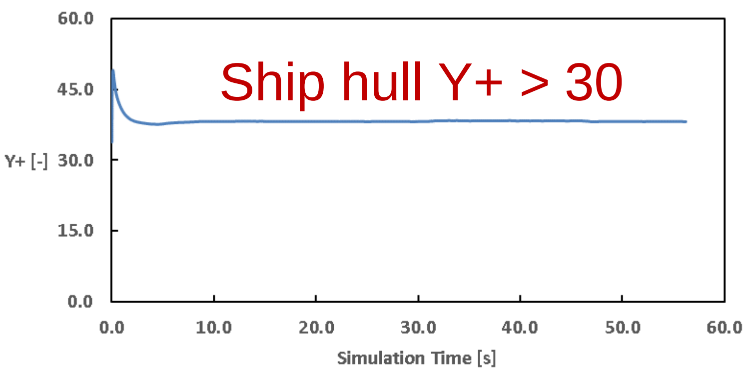

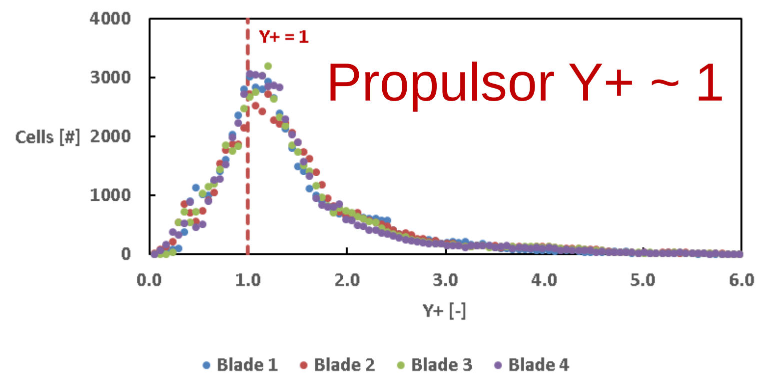

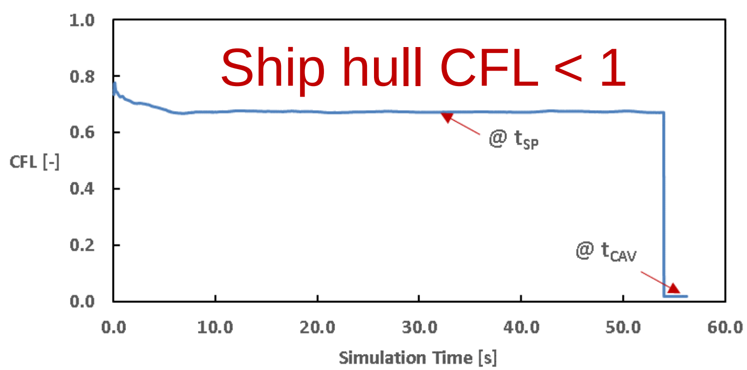

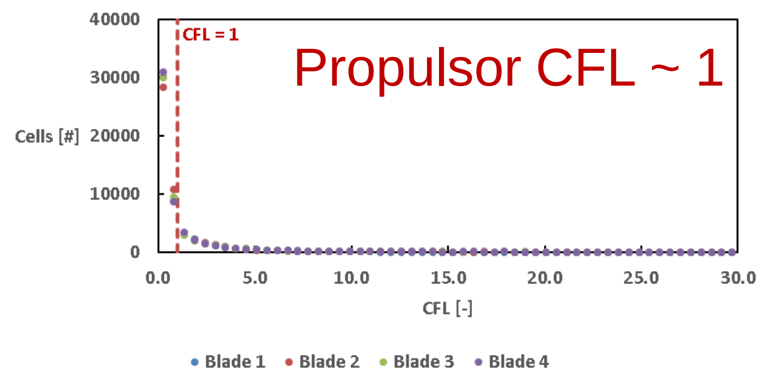

Matthias Maasch
Matthias.Maasch@strath.ac.uk

Loading Conditions

- **Four loading conditions were investigated**

1. **Laden Level Trim (Standard loadcase in fully laden conditions; 11 m draft)**
2. **Heavy Ballast Level Trim (Standard loadcase in unladen conditions; 9 m)**
3. **Minimum Ballast Extreme Trim (1st proposed loadcase in unladen conditions; 2 Degrees or 9 m bow up)**
4. **Heavy Ballast Extreme Trim (2nd proposed loadcase in unladen conditions; 2.4 degrees of 11 m)**

Matthias Maasch
Matthias.Maasch@strath.ac.uk

Numerical Self-Propulsion Results

Measurements include

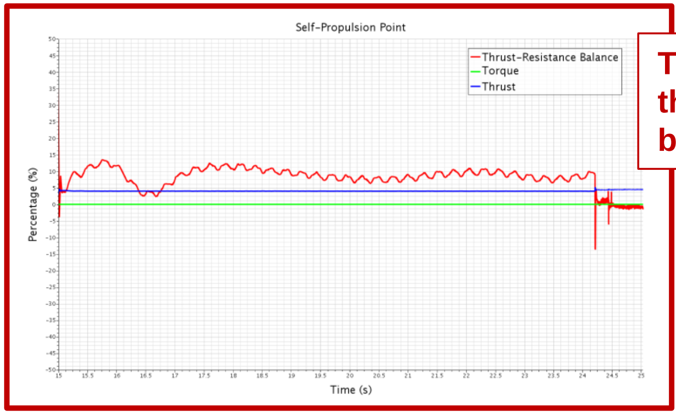

Thrust, torque & thrust-resistance balance

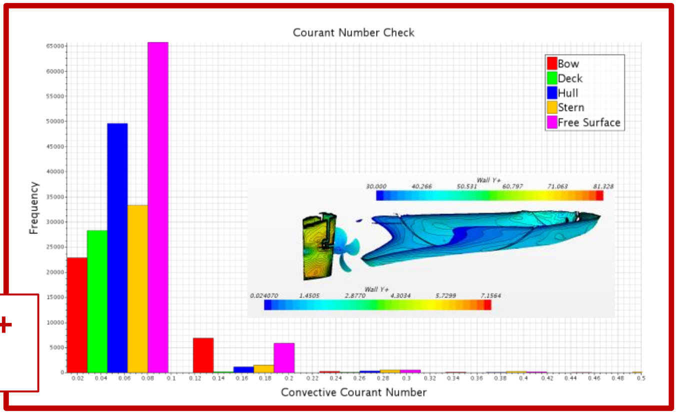

CFL and Y+ check

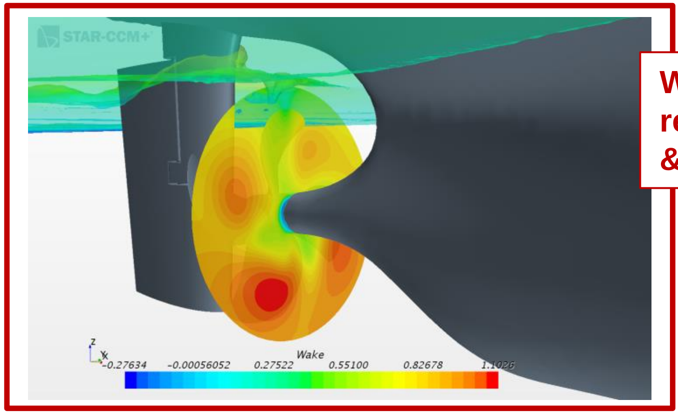

Wake field recording & analysis

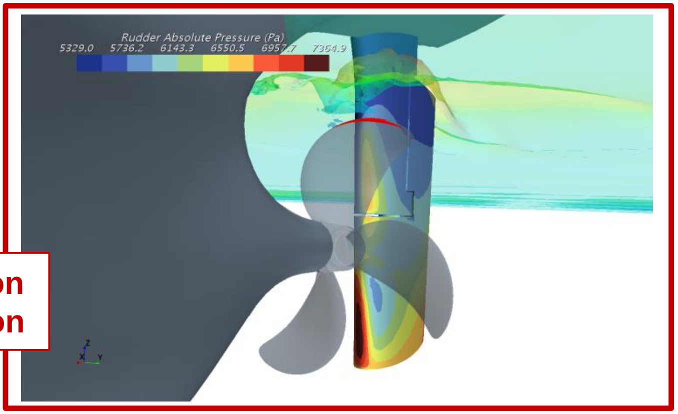

Cavitation prediction

Matthias Maasch
Matthias.Maasch@strath.ac.uk

Propulsion Results

- The full scale self-propulsion point was simulated
- Delivered Power to the propeller PD = 2 π rps Q

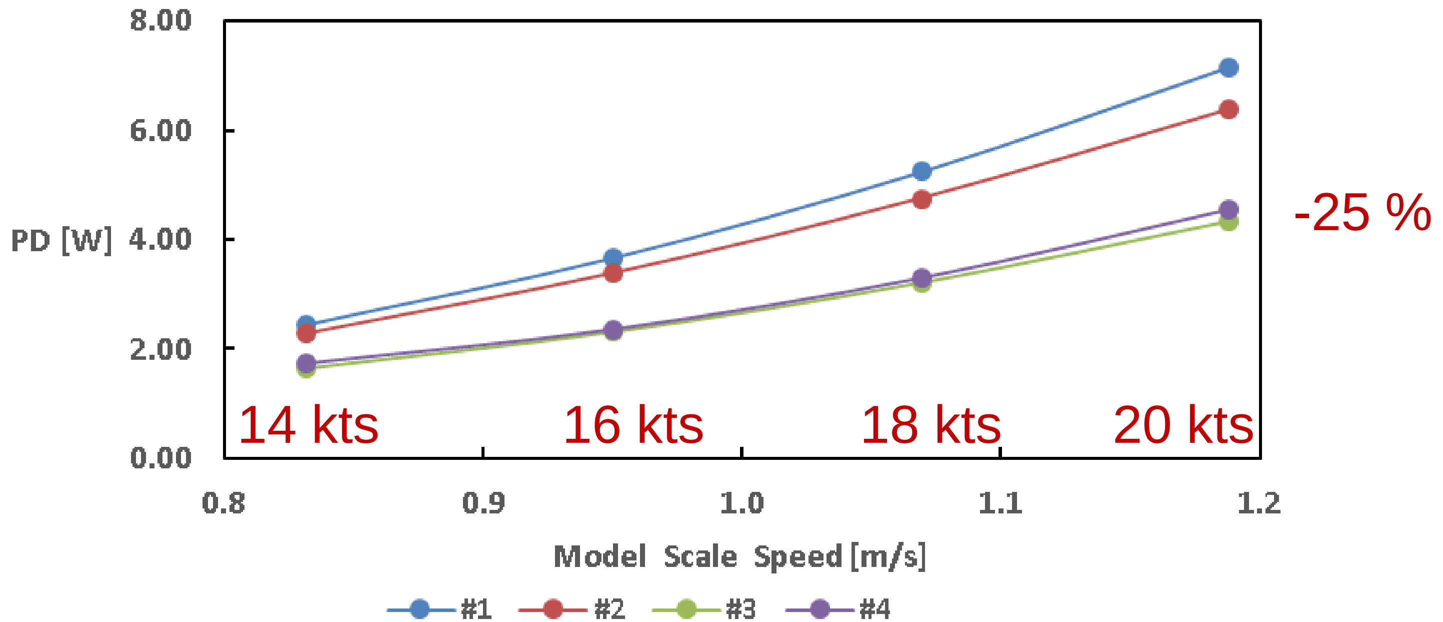

Matthias Maasch
Matthias.Maasch@strath.ac.uk

Numerical Self-Propulsion Results

Level & Extreme Trim Results

Level Trim

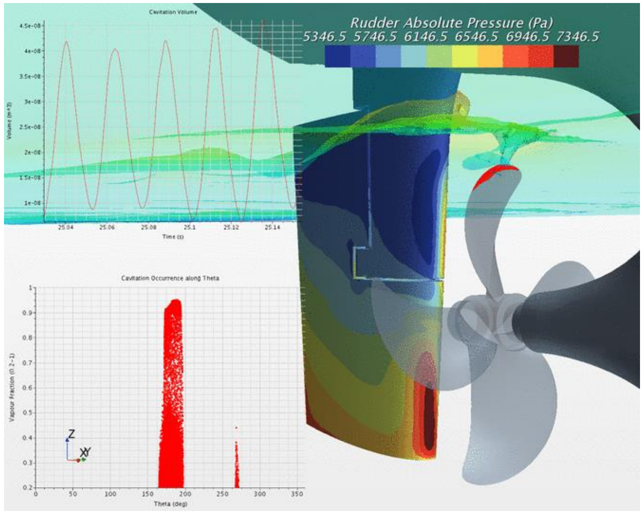

Cavitation Analysis

Maximum Cavitation Volume

4.8e-8 m^3	2.8e-8 m^3
48 mm^3	28 mm^3
	- 42%

Extreme Trim

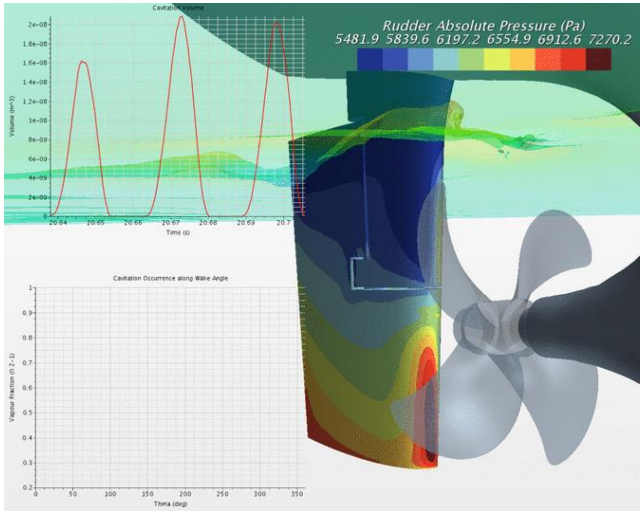

Matthias Maasch
Matthias.Maasch@strath.ac.uk

Cavitation Results

- **Propeller rotation per numerical solver time step: 1.8° (of 360°)**

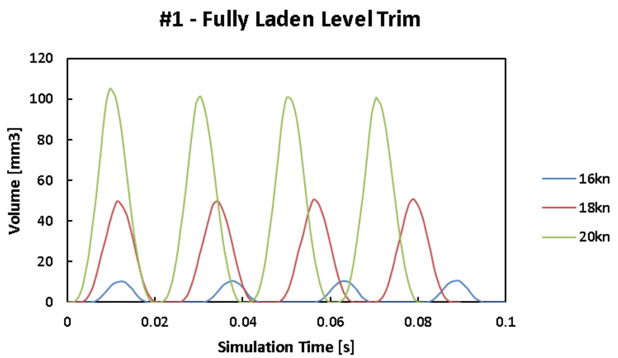

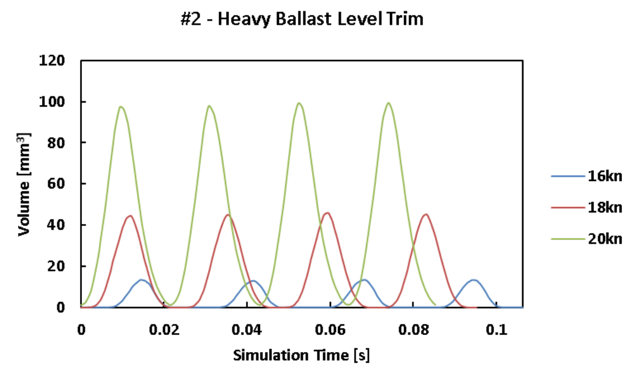

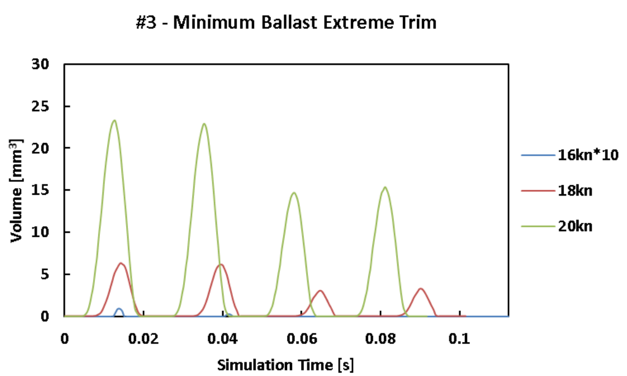

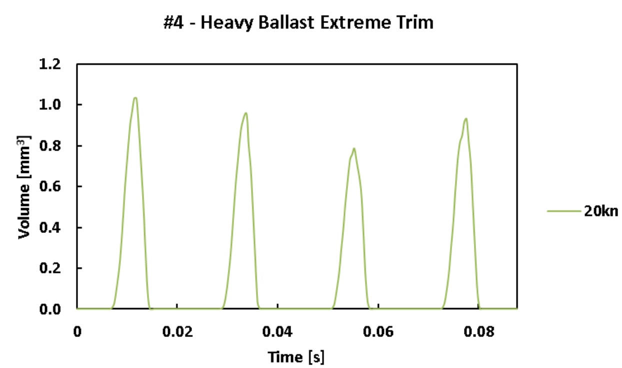

Matthias Maasch
Matthias.Maasch@strath.ac.uk

Cavitation Results

- **Animation for 20 kts full scale speed**

Fully Laden Level Trim

Heavy Ballast Level Trim

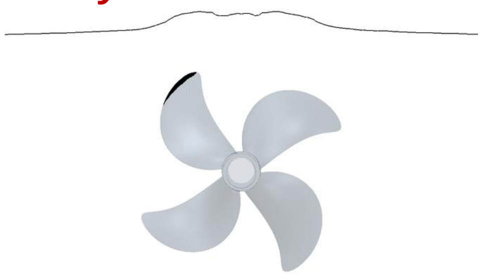

Min. Ballast Extreme Trim

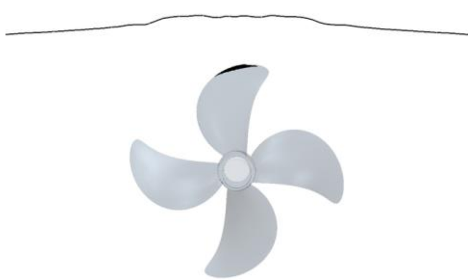

Heavy Ballast Extreme Trim

Matthias Maasch
Matthias.Maasch@strath.ac.uk

Conclusion

- **Delivered power to the propeller reduced by around 25% for both extreme trim conditions**
  - **Since condition #4 provides a higher displacement and thus a better seakeeping performance it should be the preferred loadcase**

- **Occurrence of cavitation largely reduced for both extreme trim conditions**
  - **Condition #4 results in the best cavitation performance due to a deeper submerged propeller**

Matthias Maasch
Matthias.Maasch@strath.ac.uk

7. Acknowledgement

- The authors would like to thank SHELL SHIPPING and LLOYD’S REGISTER for sponsoring this PhD Study.
- Numerical RANSE results were obtained using the EPSRC funded ARCHIE-WeSt High Performance Computer (www.archie-west.ac.uk). EPSRC grant no. EP/K000586/1.

Matthias Maasch
Matthias.Maasch@strath.ac.uk

University of
Strathclyde
Glasgow